



HAL
open science

Identification and functional characterization of novel genes implicated in congenital myopathies

Xavière Lornage

► **To cite this version:**

Xavière Lornage. Identification and functional characterization of novel genes implicated in congenital myopathies. Rheumatology and musculoskeletal system. Université de Strasbourg, 2019. English. NNT : 2019STRAJ067 . tel-02900858

HAL Id: tel-02900858

<https://theses.hal.science/tel-02900858>

Submitted on 16 Jul 2020

HAL is a multi-disciplinary open access archive for the deposit and dissemination of scientific research documents, whether they are published or not. The documents may come from teaching and research institutions in France or abroad, or from public or private research centers.

L'archive ouverte pluridisciplinaire **HAL**, est destinée au dépôt et à la diffusion de documents scientifiques de niveau recherche, publiés ou non, émanant des établissements d'enseignement et de recherche français ou étrangers, des laboratoires publics ou privés.

ÉCOLE DOCTORALE DES SCIENCES DE LA VIE ET DE LA SANTÉ (ED 414)

IGBMC, INSERM, UNIVERSITÉ DE STRASBOURG

THÈSE

Présentée par :

Xavière LORNAGE

Soutenue le 13 Septembre 2019

En vue d'obtenir le grade de : **Docteur de l'Université de Strasbourg**

Discipline : Aspects moléculaires et cellulaires de la biologie

Identification and functional characterization of novel genes implicated in congenital myopathies

THÈSE dirigée par :

Mme Valérie BIANCALANA

MCU-PH, Université de Strasbourg, IGBMC

RAPPORTEURS :

M. Helge AMTHOR

PU-PH, Université Versailles Saint-Quentin-en-Yvelines

Mme Catherine COIRAULT

DR INSERM, Institut de Myologie

AUTRES MEMBRES DU JURY :

Mme Amélie PITON

MCU-PH, Université de Strasbourg, IGBMC

MEMBRES INVITES :

M. Jocelyn Laporte

DR INSERM, Université de Strasbourg, IGBMC

M. Johann Böhm

CR INSERM, Université de Strasbourg IGBMC

ACKNOWLEDGEMENTS

I would like to thank Catherine Coirault, Helge Amthor, and Amélie Piton for accepting to be part of the jury, and to read and evaluate my work.

I am very grateful to Jocelyn Laporte, Johann Böhm, and Valérie Biancalana for giving me the chance to work in their team. By sharing your advice and knowledge, you helped me a lot to become closer to the scientist I want to be.

I would like to express my gratitude to all the collaborators for this work, and especially to Norma Romero for sharing her very inspiring knowledge and her enthusiasm.

I am also very grateful to all present and former MAD team members. Thanks a lot for the dynamic, friendly, and positive atmosphere, the discussions, the outings, and the friendships! Valentina, Raphaël, Kirsley, thanks a lot for your significant technical assistance. Special thanks to Elodie, Inès, Mégane and Laurine, it was a pleasure to supervise your work and discuss all your exciting results! Johann, danke für deinen Geduld, besonders bei den Korrekturen. Dank Dir habe ich viele Wissenschaftler, Ärzte, und auch Patienten kennengelernt!

This work was made much easier thanks to all people from the molecular biology, microscopy, and antibody production platforms, and from the animal and cell culture facilities. Thanks to all of you!

Papa et maman, merci beaucoup de m'avoir toujours encouragée à tenter ce que je considérais impossible.

TABLE OF CONTENT

1	INTRODUCTION.....	6
1.1	The congenital myopathies	7
1.1.1	Normal and abnormal skeletal muscle function and structure	7
1.1.2	The classification of congenital myopathies	11
1.2	Diagnosis of congenital myopathies	17
1.2.1	DNA sequencing in diagnostic laboratories.....	17
1.2.2	Rationale.....	19
1.2.3	The MYOCAPTURE project.....	19
1.2.4	Aims of the project.....	21
2	RESULTS.....	22
2.1	Mutations in known myopathy genes in patients with classical phenotypes	22
2.1.1	Publication 1: Loss of sarcomeric scaffolding as a common baseline histopathologic lesion in titin-related myopathies (Avila-Polo et al. 2018)	23
2.1.2	Publication 2: Common and variable clinical, histological, and imaging findings of recessive <i>RYR1</i> -related centronuclear myopathy patients (Abath Neto et al. 2017).....	25
2.2	Mutations in known myopathy genes with new phenotypes	27
2.2.1	Publication 3: Novel <i>SPEG</i> mutations in congenital myopathy without centralized nuclei (Lornage et al. 2018)	28
2.2.2	Publication 4: HSPB8 haploinsufficiency causes dominant adult-onset axial and distal myopathy (Echaniz-Laguna et al. 2017).....	30
2.2.3	Publication 5: Expanding the spectrum of congenital myopathy linked to recessive mutations in <i>SCN4A</i> (Mercier et al. 2017)	32
2.2.4	Publication 6: <i>CASQ1</i> mutations impair calsequestrin polymerization and cause tubular aggregate myopathy (Bohm et al. 2018).....	33
2.2.5	Publication 7: <i>HNRNPDL</i> -related muscular dystrophy: expanding the clinical, morphological and MRI phenotypes (Berardo et al. 2019).....	35

2.2.6	Publication 8: Dihydropyridine receptor (DHPR, CACNA1S) congenital myopathy (Schartner et al. 2017)	36
2.2.7	Publication 9: Affected female carriers of MTM1 mutations display a wide spectrum of clinical and pathological involvement: delineating diagnostic clues (Biancalana et al. 2017)	38
2.2.8	Publication 10: Sarcomeric disorganization and nemaline bodies in muscle biopsies of patients with EXOSC3-related type 1 pontocerebellar hypoplasia (Pinto et al. 2018).....	40
2.2.9	Publication 11: Discordant manifestations in Italian brothers with GNE myopathy (Dotti et al. 2018)	41
2.3	Mutations in novel genes.....	42
2.3.1	Publication 12: Recessive MYPN mutations cause cap myopathy with occasional nemaline rods (Lornage et al. 2017).....	43
2.3.2	Publication 13: ACTN2 mutations cause “Multiple structured Core Disease” (MsCD) (Lornage et al. 2019).....	45
2.3.3	Investigation of the pathogenicity of the <i>ACTN2</i> c.302A>G p.(Asn101Ser) mutation	47
	DISCUSSION	58
2.4	<i>MYPN</i> and <i>ACTN2</i> – two novel congenital myopathy genes	58
2.4.1	<i>MYPN</i> mutations in human disease	58
2.4.2	<i>ACTN2</i> mutations in human disease.....	63
2.4.3	<i>ACTN2</i> - and <i>MYPN</i> -related myopathies: conclusion	69
2.5	MYOCAPTURE: contributions and future prospects	70
2.5.1	Global analysis of the MYOCAPTURE project	70
2.5.2	Significance of the MYOCAPTURE project	72
2.5.3	Future prospects: identification of the missing myopathy genes	73
3	FRENCH SUMMARY	81
4	REFERENCES.....	86

LIST OF FIGURES AND TABLES

Table I1: Main clinical features of NMDs with primary muscle involvement	6
Fig I1: Overall skeletal muscle organization.....	7
Fig I2: Overall sarcomere organization.....	8
Table I2: Properties of type 1 and type 2 muscle fibers.....	10
Fig I4: Type 1 fiber predominance in a patient with congenital myopathy	11
Fig I5: Histological anomalies of CNM patients	12
Fig I6: Histological and ultrastructural characteristics of nemaline rods.....	13
Fig I7: Histological and ultrastructural hallmarks of cap myopathy.....	14
Fig I8: Presence of cap and rods in the same muscle biopsy	14
Fi I9: Oxidative staining anomalies in the biopsies of patients with CCD and MmD.....	16
Table I3: Main features associated with different congenital myopathies.....	18
Fig R1: Schematic representation of SPEG isoforms and protein domains.....	28
Fig R2: <i>ACTN2</i> mutation and segregation, and localization of the affected residue	48
Fig R3: Impact of the <i>ACTN2</i> c.302A>G p.(Asn101Ser) mutation on alpha-actinin-2 localization	49
Fig R4: Impact of the Asn101Ser mutation on actin recruitment and localization.....	50
Fig R5: Impact of the Asn101Ser mutation on alpha-actinin-2 dimerization	51
Fig R6: Impact of the AAV-mediated Asn101Ser alpha-actinin-2 expression on the TA alpha-actinin-2 level and muscle force.....	52
Fig R7: Impact of intramuscular AAV-mediated Asn101Ser alpha-actinin-2 expression on TA muscle histology.....	53
Fig R8: Impact of systemic AAV-mediated Asn101Ser alpha-actinin-2 expression on TA muscle force.....	54
Fig R9: Impact of the systemic injection of an AAV encoding Asn101Ser alpha-actinin-2 on TA muscle histology.....	54
Fig R10: Normal heart weight and structure in mice systemically expressing Asn101Ser alpha-actinin-2.....	56
Fig D1: Myopalladin protein domains and reported mutations	58
Table D1: Genetic, histological and clinical features of patients with <i>MYPN</i> mutations	59
Table D2: Myopalladin myopathy patients, biopsied muscles and main histological defects.....	60
Table D3: <i>MYPN</i> cardiomyopathy mutations, type of mutations and frequency.....	61
Fig D2: Myopalladin protein domains and reported cardiomyopathy mutations	62

Fig D4: Alpha-actinin-2 protein domains and mutations.....	65
Table D5: ACTN2 cardiomyopathy mutations, frequency, and segregation.....	65
Fig D5: Alpha-actinin-2 protein domains and cardiomyopathy mutations.....	66
Fig D6: Alpha-actinin-2 protein domains, mutations and known interactors.....	67
Fig D7: Overall diagnostic rate for families included in MYOCAPTURE.....	72
Fig D8: Venn diagram showing the genetic overlap between different neuromuscular diseases.....	74
Table D7: Correlation between gene expression and involvement in muscle and cardiac diseases.....	76
Fig D9: Venn diagram showing the genetic overlap between human diseases and mouse models.....	77
Table D8: List of 153 candidate myopathy genes.....	78
Fig S1 : Caractéristiques histologiques des principales classes de myopathies congénitales.....	81
Fig S2 : Caractéristiques histologiques des patients souffrant d'une myopathie liée au gène <i>MYPN</i>	83
Fig S3 : Caractéristiques histologiques des patients souffrant d'une myopathie liée au gène <i>ACTN2</i>	84
Fig S3 : Morphologie des poissons exprimant l'alpha-actinine-2 humaine sauvage et mutée.....	84
Fig S3 : Caractéristiques histologiques des muscles de souris exprimant l'alpha-actinine-2 mutée.....	85

1 INTRODUCTION

Skeletal muscle is the most abundant tissue of the human organism, and accounts for around 40% of the total body mass of an adult (Janssen et al. 2000). Around 600 skeletal muscles have been described and they play a crucial role in locomotion, maintaining posture, as well as metabolite equilibrium and thermogenesis (Frontera and Ochala 2015; Periasamy et al. 2017; Pant, Bal, and Periasamy 2016).

Functional or structural anomalies of skeletal muscles result in a lower force generation, ranging from mild muscle weakness to more severe conditions such as paralysis, swallowing difficulties or respiratory failure, which are potentially lethal (Braun, Arora, and Rochester 1983; Willig et al. 1994).

Neuromuscular diseases (NMDs) embrace different human disorders impairing skeletal muscle function, either by inducing dysfunction of nerves, of the neuromuscular junction, and/or of muscles (Morrison 2016). At the time of the writing of this thesis, the gene table of neuromuscular diseases (<http://muscle.genetable.fr>) classifies the inherited muscle diseases into 16 groups, encompassing 955 diseases involving 533 different genes, reflecting a large genetic and phenotypic heterogeneity. The inherited NMDs primarily affecting skeletal muscle can be sub-grouped into four main classes: muscular dystrophies, metabolic myopathies, mitochondrial myopathies. The different muscle disorders are characterized by the presence of specific phenotypical features (**Table I1**).

Muscular dystrophies	Metabolic myopathies
<ul style="list-style-type: none"> • Progressive muscle weakness • Loss of muscle mass 	<ul style="list-style-type: none"> • Exercise intolerance • Episodes of fatigue • Myalgia
Mitochondrial myopathies	Congenital myopathies
<ul style="list-style-type: none"> • Muscle weakness • Exercise intolerance • Cardiac involvement • Hearing loss • Seizures 	<ul style="list-style-type: none"> • Early-onset muscle weakness • Slow progression of the disease • Dymorphic facial features: Elongated face High-arched palate

Table I1: Main clinical features of NMDs with primary muscle involvement

Muscular dystrophies, metabolic myopathies, mitochondrial myopathies, and congenital myopathies all cause muscle weakness. The additional commonly encountered features are summarized (Pfeffer and Chinnery 2013; Berardo, DiMauro, and Hirano 2010; Emery 2002; Cassandrini et al. 2017).

1.1 The congenital myopathies

Congenital myopathies define a heterogeneous group of rare hereditary muscle diseases with an estimated incidence of around 1:25000 (Tubridy, Fontaine, and Eymard 2001). They are characterized by a non-progressive or slowly progressive muscle weakness usually starting from birth or early childhood, but the age at onset can significantly vary, even within families (Colombo et al. 2015; North et al. 2014). Congenital myopathies interfere with the muscle contractile function and the fiber type composition, and they can be distinguished from other NMDs by the presence of particular histopathological anomalies on the muscle biopsy (Jungbluth et al. 2018; Cassandrini et al. 2017).

1.1.1 Normal and abnormal skeletal muscle function and structure

Aberrant contractile skeletal muscle function in myopathic muscles

Skeletal muscles is attached to the bones through a tendon and is composed of several fascicles. Each fascicle is surrounded by the perimysium, a structure containing nerves and capillaries, with essential function for the synchronized contraction of the fibers within the fascicle. The muscle fibers are composed of myofibrils which contain repeating contractile structures called sarcomeres (**Fig 11**).

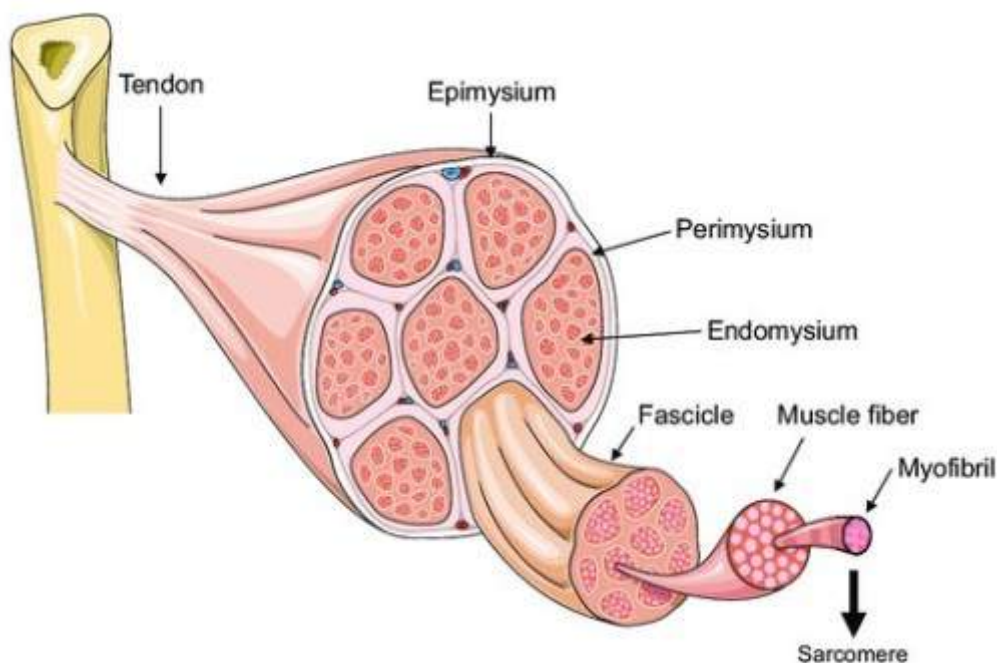


Fig 11: Overall skeletal muscle organization

Skeletal muscles are attached to the bones via tendons. They are composed of muscle fascicles surrounded by a connective tissue called endomysium. These fascicles contain muscle fibers composed of myofibrils. The myofibrils are made of a succession of sarcomeres, the basic unit of skeletal muscle. Adapted from Basic and Applied Bone Biology – 2nd Edition.

The sarcomeres are mainly composed of actin and myosin filaments, also known as thin and thick filaments (**Fig I2**). At rest, tropomyosin is bound to actin, and prevents the myosin from attaching to the actin filaments. During contraction, calcium released from the sarcoplasmic reticulum binds to troponin and initiates a chain reaction that causes the displacement of tropomyosin and unmasking of the myosin-binding sites on actin. This enables the binding of the molecular motor myosin to actin, and the relative movement of the thin and thick filaments powered by ATP hydrolysis. This shortens the sarcomeres and thereby generates force (Gordon, Homsher, and Regnier 2000).

Pathogenic variants in genes encoding various components of the thin and thick filaments such as *ACTA1*, *TPM2*, *TPM3*, *MYH7* (Laing et al. 2009; Marttila et al. 2014; Pajusalu et al. 2016), disrupt the function, assembly, or stability of the myofilament proteins, and cause abnormal sarcomeric structures leading to myopathies.

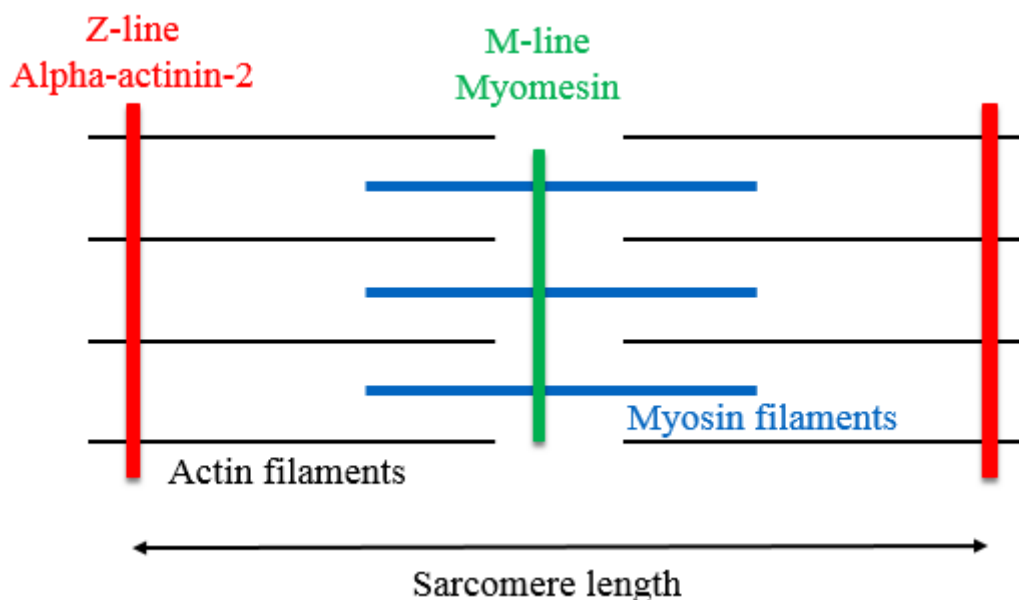


Fig I2: Overall sarcomere organization

The sarcomeres are delimited by Z-lines, and they are mainly composed of actin and myosin filaments. Myomesin crosslinks myosin filaments at the M-line and alpha-actinin-2 crosslinks actin filaments at the Z-line. Numerous other structural proteins are implicated in the organization and maintenance of the sarcomeres.

Specific myopathy mutations do not cause major defects in the sarcomeric structures, but induce an impaired excitation-contraction coupling (ECC) instead. After a neuronal stimulus, the neurotransmitter acetylcholine is released by the axon terminal, and the activation of the acetylcholine receptors leads to a depolarization of the motor endplate of the sarcolemma. This results in the propagation of an action potential along the muscle fiber and into deep membrane invaginations called T-tubules. The action potential activates the calcium channel DHPR located on the T-tubule, which undergoes a conformational change enabling its physical

interaction with the sarcoplasmic reticulum Ca^{2+} channel ryanodine receptor (RyR1), and finally induces Ca^{2+} release from the sarcoplasmic reticulum (Block et al. 1988). Ca^{2+} release finally triggers shortening of the contractile unit, the sarcomere (**Fig I3**) (reviewed by Kuo and al., 2015).

Impairment of ECC at different levels can severely impact on muscle physiology and give rise to different congenital myopathies. Defective calcium handling results from mutations in diverse genes encoding key regulators of ECC such as *DHPR* and *RYR1* (Schartner et al. 2017; Avila, O'Brien, and Dirksen 2001). Structural defects of triads and misorientation of t-tubules, and in some cases impaired localization of DHPR and RyR1 are caused by mutations in *MTM1*, *BINI1*, *DNM2*, *SPEG*, *CCDC78* encoding membrane-bound proteins (Al-Qusairi et al. 2009; Toussaint et al. 2011; Majczenko et al. 2012; Huntoon et al. 2018).

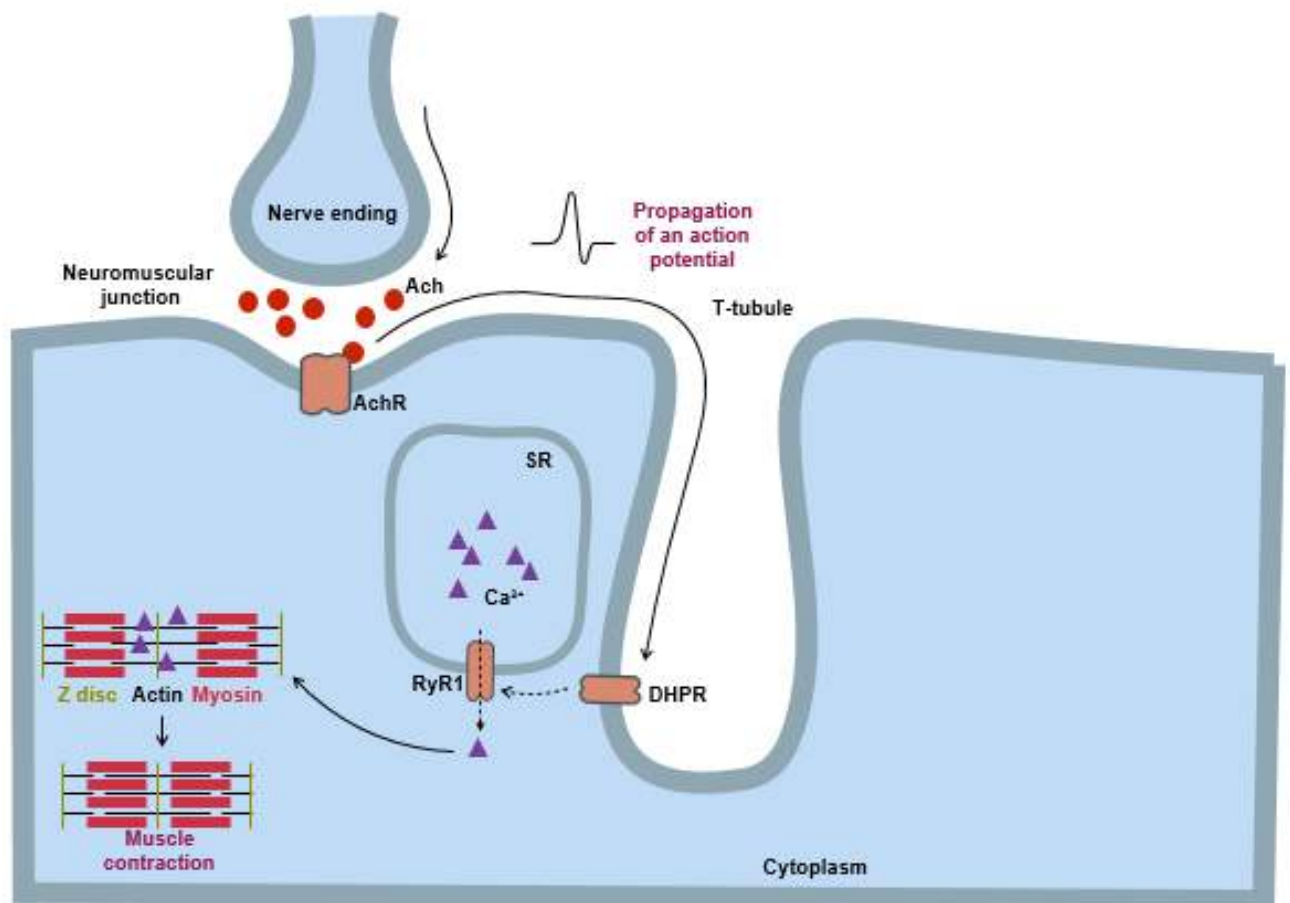


Fig I3: Overview of skeletal muscle contraction

After a neuronal stimulus, the neurotransmitter acetylcholine (ACh) is released to the neuromuscular junction (NMJ). The activation of the neurotransmitter receptors (AChR) at the muscle membrane induces an action potential that propagates to the T-tubule, and activates DHPR, which interacts and activates RyR1 and induces Ca^{2+} release from the sarcoplasmic reticulum (SR) to the cytoplasm. Thereby, cytoplasmic Ca^{2+} enables myosin-actin binding and subsequent force generation. ACh: acetylcholine; AChR: acetylcholine receptors; SR: sarcoplasmic reticulum.

Overall, congenital myopathies are muscle disorders impairing excitation-contraction coupling and/or muscle organization, and leading to dysfunctional sarcomere contractility, an important contributor to muscle weakness (Joureau et al. 2018).

Changes in fiber type composition

Skeletal muscle is composed of bundles of different types of muscle fibers, based on their histochemical, morphological, and metabolic properties.

Human adult skeletal muscle is primarily composed of type 1 and type 2 muscle fibers expressing different myosins. Myosin is a large protein complex composed of two heavy chains, and two pairs of light chains, and different combinations of heavy and light chains are possible and define specific fiber types. While type 1 fibers express a definite pattern of heavy and light chains, type 2 fibers can be further divided based on different combinations of myosin heavy chain gene expression (reviewed by (Schiaffino and Reggiani 2011; Stuart et al. 2016). Other proteins also have a fiber type-specific program of gene expression. As an example, the sarcomeric component alpha-actinin-3, and the Ca²⁺ buffer calsequestrin, are both mainly expressed in type 2 fibers (North and Beggs 1996; Lambole et al. 2013). Furthermore, type 1 and type 2 muscle fibers have distinct metabolic properties. Type 1 fibers have numerous mitochondria and high level of glycolytic enzymes, and primarily rely on oxidative phosphorylation to generate ATP. They are thus suitable to produce energy under aerobic conditions for sustained muscle activity. On the contrary, type 2 fibers mainly use glycogen to produce ATP, and fatigue occurs quickly upon glycogen store depletion (Vollestad, Tabata, and Medbo 1992) (**Table 2**).

	Type 1	Type 2
Myosin ATPase activity (pH 9,4)	Low	High
Twitch	Slow	Fast
Oxidative capacity	High	From Low to High
Glycolytic capacity	Low	High
Fatigability	Low	High

Table I2: Properties of type 1 and type 2 muscle fibers

Type 1 and type 2 fibers use different sources of energy to initiate muscle contraction, resulting in a different metabolism and fatigability.

Type 1 fiber predominance or uniformity is common to all congenital myopathies (Cassandrini et al. 2017; North et al. 2014; Luo et al. 2011; Oh and Danon 1983), and can be revealed on the

muscle biopsies based on a histochemical reaction for myosin adenosine triphosphatase (ATPase) (Guth and Samaha 1969) (**Fig I4**).

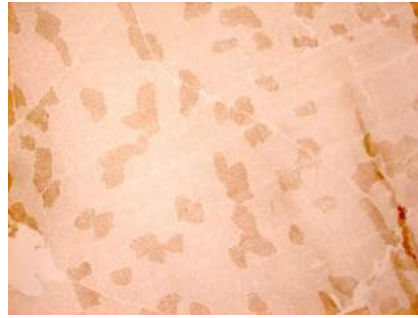


Fig I4: Type 1 fiber predominance in a patient with congenital myopathy

Type 1 fiber predominance revealed with histochemical reactions for ATPase at pH 9.4. Type 1 fiber predominance is characterized by a high proportion of lighter type 1 fibers.

Little is known about the clinical significance of type 1 fiber predominance, since alterations of fiber types also occur through life in response to external stimuli, including exercise and hormones (Zhang et al. 2014; Fitzsimons et al. 1990). However, knockout experiments in mice demonstrated that a tight regulation of myosin heavy chain expression is required for proper muscle physiology (Acakpo-Satchivi et al. 1997), suggesting that the imbalanced fiber type proportion in patients with congenital myopathy might contribute to muscle weakness. Furthermore, whether the transcriptional program of type 1 fibers found in patients with congenital myopathy is different or equivalent to “healthy” type 1 fibers, remains to be determined.

1.1.2 The classification of congenital myopathies

The classification of congenital myopathies relies on a range of particular morphological abnormalities observed in muscle biopsies of patients, including abnormal centralization of myonuclei (centronuclear myopathy), rod-like protein aggregates (nemaline myopathies), or well-delimited foci devoid of oxidative activity in myofibers (central and multi-minicore myopathy).

Centronuclear myopathy

As the name suggests, biopsies from patients with centronuclear myopathy (CNM) manifest abnormal central localization of nuclei, and additional features include irregularities in oxidative stains and type 1 fiber hypotrophy (Romero and Clarke 2013; Nance et al. 2012) (**Fig I5**).

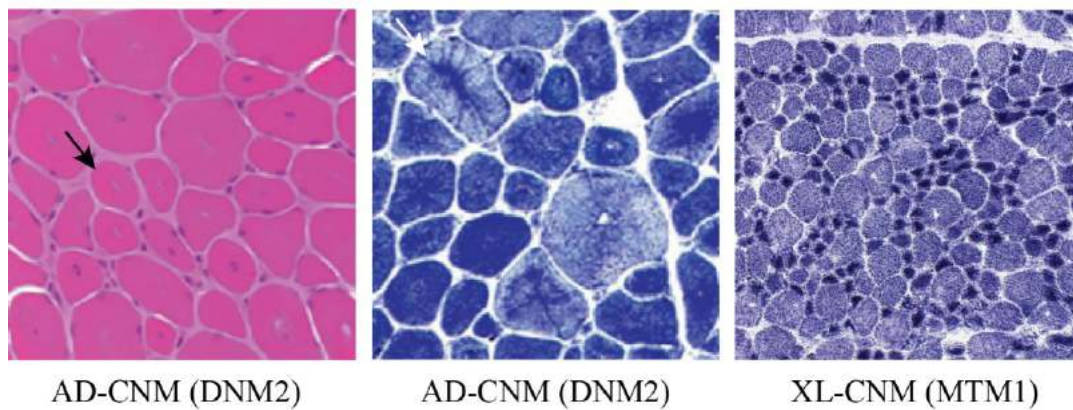


Fig I5: Histological anomalies of CNM patients

Muscle sections of patients with CNM stained with H&E and NADH. H&E staining reveals an increased number of fibers with central nuclei (black arrow). NADH reaction shows radial arrangements of sarcoplasmic strands (white arrow), and highlights type 1 fiber predominance and hypotrophy. Adapted from Romero and Clarke 2013.

The severity and onset of CNM significantly vary depending on the implicated gene and the causative mutation, and ranges from the appearance of antenatal signs with polyhydramnios and reduced fetal movements, to mild adult-onset cases. The most severe patients have hypotonia at birth and are unable to breathe spontaneously, and they usually die within the first year of life due to respiratory insufficiency or aspiration pneumonia (Annoussamy et al. 2019). Less affected patients with childhood-onset hypotonia and proximal and distal muscle weakness, may achieve independent walking. Facial muscle weakness, ptosis, and ophthalmoparesis are frequent features in both severe and milder patients. Adult-onset cases exhibit a slowly progressive distal and axial muscle weakness, sometimes causing loss of ambulation (Cassandrini et al. 2017; Catteruccia et al. 2013).

Common forms of CNM are caused by X-linked recessive mutations in *MTM1*, autosomal dominant mutations in *DNM2* and *BINI*, and autosomal recessive mutations in *SPEG*, *BINI*, *CCDC78*, *RYR1* and *TTN* (Bitoun et al. 2005; Nicot et al. 2007; Laporte et al. 1996; Agrawal et al. 2014; Bohm et al. 2014; Majczenko et al. 2012; Zhou et al. 2006; Wilmshurst et al. 2010; Ceyhan-Birsoy et al. 2013). Investigations of the pathomechanisms primarily revealed impaired triad morphology, abnormal excitation-contraction coupling, and defects in membrane trafficking including autophagy (Jungbluth and Gautel 2014; Dowling, Lawlor, and Dirksen 2014). Whether and to what extent these defects are linked to the nuclear centralization in the muscle fibers of patients remains to be determined.

Two compounds currently undergo clinical trials for the treatment of CNMs, and both involve a different approach. The AT132 gene replacement therapy from Audentes Therapeutics is designed to treat patients with *MTM1*-related myopathy. It uses a viral vector to introduce a

working copy of *MTM1* in the patients, which encodes a functional MTM1 protein able to compensate for the absence or strong reduction of the endogenous MTM1 protein. The DYN101 antisense oligonucleotide approach from Dynacure aims to reduce the DNMT2 protein level, and will be used to treat patients with *MTM1*- and *DNMT2*-related myopathies. It has indeed previously been shown that the increased level and/or over-activity of DNMT2 is responsible for the muscle weakness in *MTM1* and *DNMT2*-related CNM (Tasfaout et al. 2017; Buono et al. 2018).

Nemaline myopathy

Nemaline myopathy (NM) owes its name to the presence of rod-like structures in the muscle fibers of patients appearing as characteristic purple staining inclusions on Gomori trichrome stain (mGT) (Romero and Clarke 2013; Nance et al. 2012) (**Fig I6**).

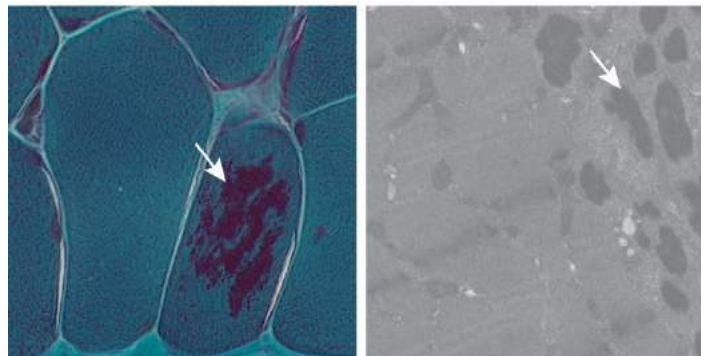


Fig I6: Histological and ultrastructural characteristics of nemaline rods
Muscle sections of a patient with nemaline myopathy stained with mGT, and showing clusters of purple stained bodies called nemaline rods (left arrow). On electron microscopy, rods appear as electron-dense material (right arrow).

NM is clinically variable, and the seriousness of the disease varies from mild to severe depending on the implicated gene as well as on the type of mutation (Wallgren-Pettersson et al. 2011). Obstetric complications such as polyhydramnios and decreased fetal movements occur in half of the severe congenital NM cases. At birth, patients present with sucking and swallowing difficulties, and frequently encounter additional features encompass arthrogryposis and cardiomyopathy. Death usually occurs within the first year of life due to respiratory insufficiency. Patients with milder congenital NM present with hypotonia at birth, delayed motor milestones, trunk and facial muscle weakness, and most are able to walk independently. The facial muscle weakness is associated with dysphagia resulting in feeding difficulty. Respiratory insufficiency is often severe and the mortality is due to respiratory failure in most of the cases (Ryan et al. 2001; Cassandrini et al. 2017; Wallgren-Pettersson, Beggs, and Laing 1998; Gonorazky et al. 2019).

Cap myopathy is a rare form of NM, in which muscle fibers exhibit sharply demarcated subsarcolemmal inclusions located at the periphery of the fibers. Ultrastructural studies showed that caps contain disorganized thin filaments, and are devoid of thick filaments (Phadke 2019; North et al. 2014; Fidzianska et al. 1981) (**Fig I7**). The proportion of fibers containing caps varies between 4 and 100%, and correlates with the disease severity. The clinical features of cap myopathy are early-onset proximal and axial muscle weakness with prominent neck muscle involvement. Scoliosis and respiratory insufficiency are also found in most of the patients. Overall, the pattern of affected muscles and the respiratory involvement overlap with the clinical features of typical NM. Furthermore, caps and rods may be encountered in the same muscle biopsy, suggesting that both histological lesions are signatures of the same disease (**Fig I8**) (Kiiski et al. 2019; Tasca et al. 2013).

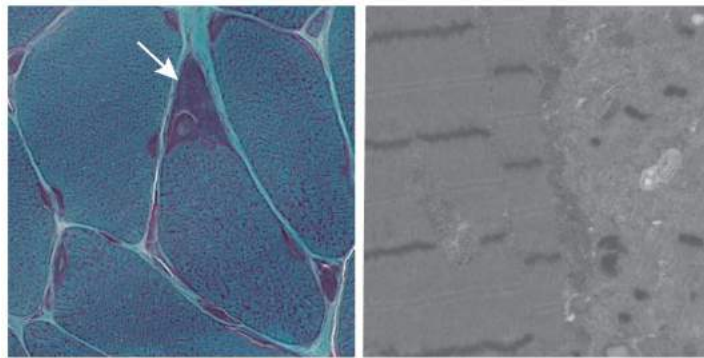


Fig I7: Histological and ultrastructural hallmarks of cap myopathy

Muscle sections of a patient with cap myopathy stained with mGT, and showing purple staining in subsarcolemmal regions of muscle fibers (arrow). On electron microscopy, caps appear to be well-demarcated areas of filament disorganization with disruption of the sarcomeric organization.

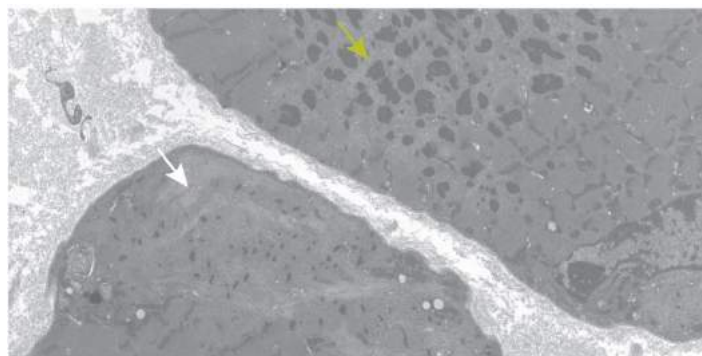


Fig I8: Presence of cap and rods in the same muscle biopsy

Ultrastructural analysis of a patient's muscle biopsy showing coexistence of caps (white arrow) and rods (yellow arrow) in neighboring fibers.

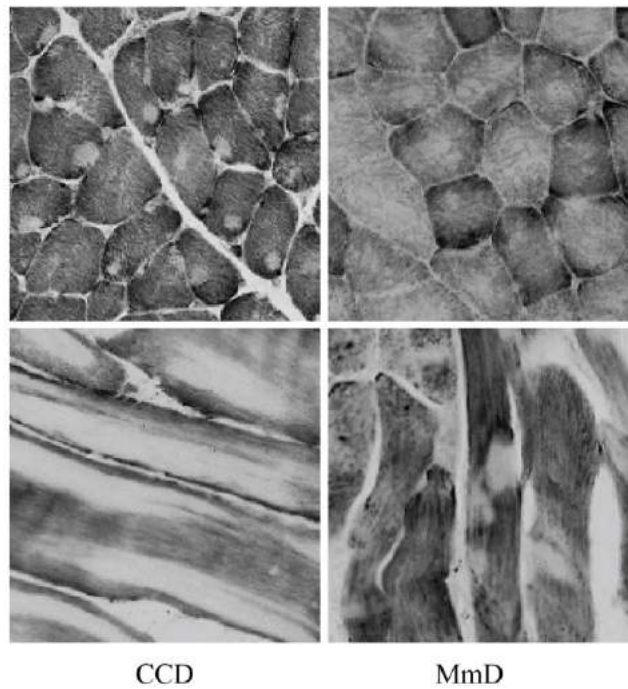
To date, mutations in over ten different genes have been reported in patients with NM. This includes autosomal dominant mutations in *ACTA1*, *TPM2*, *TPM3*, *KBTBD13*, and autosomal recessive mutations in *NEB*, *MYO18B*, *TNNT1*, *KLHL40*, *KLHL41*, *KBTBD13*, *LMOD3*, *CFL2*

(Laing et al. 2004; Donner et al. 2002; Laing et al. 1995; Pelin et al. 1999; Malfatti et al. 2015; Alazami et al. 2015; Johnston et al. 2000; Ravenscroft et al. 2013; Gupta et al. 2013; Sambuughin et al. 2010; Agrawal et al. 2007). Most of these genes encode components of the thin filaments, proteins contributing to the stability or turnover of thin filaments, or proteins involved in cross-bridge kinetics. NM mutations lead to changes in the muscle ultrastructure, and result in impaired muscle contractility (de Winter and Ottenheijm 2017).

Up to now, no specific therapy is available for NM and the treatments mainly rely on physical therapy to slow down disease progression and on ventilatory support to prevent respiratory failure. NM mutations cause muscle weakness, partially by decreasing the Ca^{2+} sensitivity of muscle contractility. Troponin activators slow down the dissociation rate of Ca^{2+} from the troponin complex, and thereby unblock the myosin-binding sites on actin at lower Ca^{2+} concentrations, and thus facilitates contraction. This approach showed promising results and improved muscle weakness in muscle cells from patients (de Winter et al. 2013).

Core myopathy

Core myopathy is the most common histopathological subtype of congenital myopathy, with an estimated prevalence of 1:80 000 (Amburgey et al. 2011). Two types of core myopathy exist, central core myopathy (also known as central core disease or CCD) and multi-minicore disease (MmD). Histologically, CCD is characterized by extensive areas devoid of oxidative staining, called cores, and running along the longitudinal axis of the muscle fiber, as opposed to MmD, where cores are more numerous and less extended along the fibers (Romero and Clarke 2013; Nance et al. 2012) (**Fig I9**).



Fi 19: Oxidative staining anomalies in the biopsies of patients with CCD and MmD

Transverse muscle sections (upper panel) and longitudinal muscle sections (lower panel) of muscle biopsies of patients with CCD and MmD, and stained with oxidative enzyme reactions. Central cores are well-delimited and can be central or located beneath the sarcolemma, while multimimicores are restricted areas of disorganization. Adapted from Jungbluth et al., 2011.

The clinical presentation of CCD patients can be heterogeneous, even within families. Most of them present with delayed motor development, proximal and axial symmetric muscle weakness, and scoliosis. Of note, the onset of the disease may be in adulthood with exertional rhabdomyolysis and myalgia (Dlamini et al. 2013; Voermans, Snoeck, and Jungbluth 2016). While CCD patients have a relative sparing of the respiratory muscles, MmD patients are recognizable by an early onset spinal rigidity and a severe scoliosis leading to trunk deformations resulting in a severe respiratory insufficiency. A subset of patients additionally display ophthalmoplegia (Lawal, Todd, and Meilleur 2018; Jungbluth, Sewry, and Muntoni 2011; Ferreiro et al. 2000).

Genetically, CCD is most commonly caused by dominant mutations in the *RYR1* gene, encoding a Ca^{2+} release channel of the sarcoplasmic reticulum. MmD is mainly caused by recessive mutations in *RYR1* and *SEPNI*, coding for the selenoprotein N, a protein with crucial function in redox and Ca^{2+} homeostasis (Lawal, Todd, and Meilleur 2018).

Elevated oxidative stress is believed to be a pathological feature of *RYR1* and *SEPNI*-related myopathies (Durham et al. 2008; Moghadaszadeh et al. 2013; Lawal, Todd, and Meilleur 2018), and might contribute to the mitochondrial dysfunction in the muscle of patients with core myopathies (Cui, Kong, and Zhang 2012). In a *Ryr1* mouse model, food supplementation with

the antioxidant N-acetylcysteine (NAC) resulted in a decreased formation of cores, increased muscle force, and reduced mitochondrial damage (Michelucci et al. 2017). The safety and efficacy of NAC antioxidant therapy in *RYR1*- and *SEPNI*-related myopathy patients has been tested in two separate clinical trials (NCT02505087 and NCT02362425). The Phase I/II clinical trial for *RYR1*-related myopathy has recently been completed but the results are not yet publicly available (Lawal, Todd, and Meilleur 2018).

Other congenital myopathies

Besides the main congenital myopathy subtypes, additional rare forms of CM with distinct histopathological features exist, including tubular aggregate myopathy characterized by abnormal accumulations of densely packed membrane tubules on muscle biopsies, myosin storage myopathy characterized by slow myosin aggregates in type 1 muscle fibers, and congenital fiber type disproportion characterized by significantly smaller type 1 fibers compared to type 2 fibers (Romero and Clarke 2013).

1.2 Diagnosis of congenital myopathies

1.2.1 DNA sequencing in diagnostic laboratories

The diagnosis of congenital myopathy is established based on the clinical and histological features of the patient. The inclusion into clinical trials however requires a molecular diagnosis. In France, screening of known genes for congenital myopathies is mainly performed in accredited diagnostic laboratories.

Sanger sequencing

Over decades, the identification of causative mutations relied on Sanger sequencing of known myopathy genes, requiring the individual amplification of each exon of the gene of interest. In general, the phenotypic presentation of the patients directs molecular diagnosis, and only selected genes compatible with the disease picture were sequenced. The selection of candidate genes was particularly challenging for heterogeneous disorders such as congenital myopathies, and the clinical phenotype of the patients and the histological anomalies on the muscle biopsies are often not sufficient to reliably indicate the causative gene. This is partially due to the overlapping histopathological features in the different congenital myopathy classes. For example, patients with core myopathy may frequently also present with central nuclei or more rarely with rods, and in turn, patients with CNM may also display cores. In addition, none of

the known genes associated with congenital myopathies give rise to distinct clinical signs (**Table I3**).

Sanger sequencing as a diagnostic approach covered only a limited number of genes, and the exon-by-exon and gene-by-gene analysis is time-consuming. The time to diagnosis has been greatly accelerated with the development of next generation sequencing.

Feature	Core myopathy		CNM				NM		
	<i>RYR1</i> autosomal dominant	<i>RYR1</i> autosomal recessive	<i>SEPN1</i>	<i>TTN</i>	<i>MTM1</i>	<i>DNM2</i>	<i>NEB</i>	<i>ACTA1</i>	<i>KLHL40</i>
Epidemiology									
Frequency of mutations	+++	+++	++	++	++	+	++	++	+
Onset									
Infancy	++	+++	+	+++	+++	+	+++	++	+++
Childhood	+++	++	+++	+	+	+	+	++	+
Adulthood	++	+	–	–	–	+++	–	–	–
Clinical features									
Extraocular muscle involvement	+	+++	–	–	+++	+++	–	–	++
Bulbar involvement	+	+++	++	++	+++	++	++	++	+++
Distal involvement	–	+	–	++	+	+++	++	+	+
Respiratory involvement	+	++	+++	++	+++	+	++	++	+++
Cardiac involvement	–	+	+ ^a	+++ ^b	–	–	–	+	–
Contractures	+	+	+	+++	+++	++	++	++	+++
Histopathology									
Cores	+++	+++	+++	++	–	+	+	+	–
Central nuclei	++	++	–	+++	+++	+++	–	–	–
Nemaline rods	+	+	–	+	–	–	+++	+++	+++
Fibre type disproportion	+	+++	+	+	+	–	–	+	–
Connective tissue and/or fat infiltration	++	++	++	+++	–	+	–	–	–
Imaging									
Muscle MRI (specificity for genetic defect)	+++	++	++	–	+	+++	+++	+	–

Table I3: Main features associated with different congenital myopathies

Frequency of the main features associated with genes mutated in congenital myopathies, highlighting the clinical and histological heterogeneity. CNM: centronuclear myopathy; NM: nemaline myopathy. – : not reported; +: infrequent; ++: common; +++: very common. Adapted from Jungbluth et al., 2018.

Next generation panel sequencing

Next generation sequencing enables the simultaneous sequencing of all genomic regions of interest. The genomic DNA is fragmented, the targeted sequences are captured by hybridization to complementary probes, and amplified before being sequenced. The commercialized NGS technologies vary depending on the template preparation, and on the amplification and sequencing approaches. Illumina is the most widely used platform, and the sequencing relies on

the cyclic incorporation of fluorescently labelled nucleotides containing reversible terminators temporarily blocking DNA synthesis. The fluorescence of the incorporated nucleotide is recorded at each cycle, allowing reconstruction of the sequence. The sequence of each fragment is called a read. The reads are aligned to the reference genome and the variants are extracted based on the differences between the index genome and the reference genome (Head et al. 2014; Ambardar et al. 2016). Next generation sequencing appeared in 2005 (Margulies et al. 2005), and progressively replaces Sanger sequencing in the French diagnostic laboratories. Panel sequencing is an approach used to sequence a subset of genes of interest, by the design of specific probes for the capture. For congenital myopathies, the national standards include the sequencing of the coding region of 12 genes for patients with NM, and the sequencing of 32 genes for other types of congenital myopathies (Krahn et al. 2019). Overall, panel sequencing offers a reliable and robust strategy to simultaneously verify the presence of mutations in several genes at a limited cost. This approach is adequate to facilitate the quick discovery of known or novel mutations in known myopathy genes. At the Strasbourg diagnostic laboratory, the diagnosis rate for patients with myopathies approximates 40%.

1.2.2 Rationale

Panel sequencing revealed that half of the patients with congenital myopathy do not carry mutations in the known genes. This suggests that the mutations in the undiagnosed patients affect genes that were not captured, and thereby highlight the presence of a large number of yet unidentified myopathy genes.

1.2.3 The MYOCAPTURE project

In order to identify novel genes implicated in congenital myopathies, Jocelyn Laporte's group coordinated the MYOCAPTURE project, a French consortium encompassing seven research teams, with the aim to sequence a total of 1000 exomes from families with NMDs. Patients with muscular dystrophy, myasthenia, or congenital myopathy were assembled into homogeneous cohorts and exome-sequenced. Exome sequencing is a next generation sequencing approach to investigate the coding regions encompassing 1-2% of the human genome, and believed to harbor about 80% of the disease-causing mutations. It is therefore an unbiased and straightforward strategy with a high probability to identify the causative mutations.

In average, 20 000 variants are identified in each exome. In order to efficiently (1) filter and (2) prioritize pathogenic variants, we developed a robust bioinformatics pipeline.

- (1) The filters used to reduce the number of candidate genes include the quality of detection of the variation, the frequency of the variation in the general population, and the inheritance scenario. The quality of the variation is evaluated by the depth of sequencing, corresponding to the number of reads aligned at a given position. With our pipeline, we discard variations with a depth of sequencing lower than 5. Furthermore, we assess the frequency of each variation in the public gnomAD database containing 125 748 exomes and 15 708 genomes. Since congenital myopathies are rare diseases, variants found in more than 1% of the general population are filtered out from the analysis. The inheritance scenario takes into account the transmission of the disease within the family. For dominant families, we focus on heterozygous variations present in all affected individuals, and absent in unaffected family members. For consanguineous families, we specifically look at the homozygous variations present in all affected individuals, and absent or at the heterozygous state in healthy family members. The analysis of sporadic cases takes into account dominant, recessive and X-linked modes of inheritance, and the simultaneous sequencing of the exomes of both healthy parents is useful to restrict the total number of candidate variants and to uncover *de novo* and compound heterozygous mutations.
- (2) Variant prioritization mainly relies on the type of variation and on the muscle gene expression.

Variations are usually classified into the following five categories depending on their predicted impact at the protein or RNA level:

Synonymous: a nucleotide substitution which does not change the encoded amino acid, due to the redundancy of the genetic code.

Missense: a nucleotide substitution which changes the encoded amino acid

Nonsense: a nucleotide substitution which induces the appearance of a premature stop codon. Nonsense mutations usually activate nonsense-mediated mRNA decay and mostly result in the absence of the encoded protein.

Indel: a small nucleotide insertion or deletion which can be in-frame or generate a frameshift. Frameshift mutations usually result in the appearance of a premature stop codon and activate nonsense-mediated mRNA decay.

Splice: a nucleotide substitution which disrupts an essential splice site or activates cryptic splice acceptor or donor sites. Synonymous and missense mutations can also have a deleterious impact on splicing.

To complement the bioinformatics analysis, and to validate the pathogenicity of the identified variations, functional experiments are carried out. The patients included in the MYOCAPTURE project underwent a muscle biopsy, and myoblast and fibroblast cell lines have been established in a few cases. This biological material can be used to evaluate the impact of the candidate variations *in vivo*. RNA extraction enables the detection of splicing aberrations and of nonsense-mediated mRNA decay through RT-qPCR. Muscle and cell extracts are useful to verify the expression of the proteins, and immunostaining on muscle sections and cells might indicate a potential impact on the localization of the protein. If no biological material is available, additional approaches such as minigene experiments, transfections in cells, or modeling of the disease in animal models are performed.

1.2.4 Aims of the project

Congenital myopathies are rare muscle diseases characterized by early-onset hypotonia and muscle weakness. These monogenic diseases were previously linked to mutations in around 30 different genes. However, 50% of the patients are still awaiting molecular diagnosis even after routine screening of the known genes, suggesting the implication of yet unidentified genes.

This thesis project aimed to identify and to functionally validate new congenital myopathy genes, and was divided into three work packages:

- **Data analysis**: analysis of exome sequencing data of patients with congenital myopathy generated through the MYOCAPTURE project, and filtering of the variations in order to identify new candidate genes.
- **Segregation studies**: validation of the presence of the genetic variations in affected individuals and verification of the segregation within the family.
- **Functional experiments**: investigations to prove the pathogenicity of the mutations. Study of the impact of the putative mutations at the RNA and protein level, on protein function in cellular or animal models, and study of the pathomechanism of the disease *in vivo*.

The characterization of the genetic bases of congenital myopathies is essential to improve molecular diagnosis and genetic counselling. Novel genes will contribute to the understanding of normal and pathological muscle physiology, and may unravel novel pathways and suitable targets for therapeutic approaches.

2 RESULTS

2.1 Mutations in known myopathy genes in patients with classical phenotypes

A few years ago, genetic investigations on patients with congenital myopathy were performed using targeted Sanger sequencing of individual genes. Primer sets were designed in order to amplify and sequence each exon of the gene. *TTN* and *RYR1* are large genes, respectively composed of 363 and 106 exons. Due to their giant size and complexity, only selected exons of the genes were screened by Sanger sequencing.

The MYOCAPTURE project was designed to identify novel genes mutated in myopathies and patients enrolled in the study were excluded for the main known genes. However, at the start of the project, large genes such as *TTN* and *RYR1* were not entirely screened by routine methods.

Analysis of the MYOCAPTURE cohort pointed out new *TTN* and *RYR1* mutations. They were included into two publications in order to underline the correlation between mutation type and localization, disease severity, and histopathological hallmarks.

2.1.1 Publication 1: Loss of sarcomeric scaffolding as a common baseline histopathologic lesion in titin-related myopathies (Avila-Polo et al. 2018)

Background

TTN is a gene composed of 364 exons and encoding titin, the largest described human protein (Labeit et al. 1990). This giant protein extends from the M-line to the Z-line and is believed to have multiple roles in skeletal muscle including assembly and length of thick filaments (Labeit et al. 1992; Houmeida et al. 1995), maintenance of the sarcomere integrity (Gregorio et al. 1998) and cell signaling through its autocatalytic serine kinase domain (Mayans et al. 1998; Lange et al. 2005). *TTN* mutations have been reported in a wide spectrum of diseases and can lead to a pure cardiac phenotype, a pure skeletal muscle phenotype, or to a mixed phenotype (Chauveau, Rowell, and Ferreiro 2014). The large size of the gene and the high number of isoforms challenge the assessment of the pathogenicity of *TTN* variations (Granzier et al. 2000; Savarese, Jonson, et al. 2018) and the interpretation requires the combination of data from different sources such as the evaluation of the clinical phenotype and study of the RNA (Savarese, Maggi, et al. 2018).

Aim of the study

The aim of the study was to identify *TTN* patients in the MYOCAPTURE cohort and to give a thorough description and classification of the histopathological and ultrastructural skeletal muscle lesions caused by *TTN* mutations.

Results

The patients were clinically divided into four groups and the histological and ultrastructural hallmarks of each group were analyzed by light and electron microscopy (Table 2). The first group encompassed ten patients with congenital myopathy, the second group four patients with Emery-Dreifuss-like myopathy and the third group four patients with adult-onset distal myopathy. All carried compound heterozygous or homozygous *TTN* mutations. The fourth group reported patients with hereditary myopathy with early respiratory failure, and we identified heterozygous or homozygous *TTN* mutations in exon 344. Despite the high clinical heterogeneity, patients of all groups presented with internalized nuclei on muscle biopsies, and ultrastructural analyses revealed myofibrillar anomalies characterized by M-band disruption and intact Z-lines, a combination of ultrastructural features previously undescribed in patients with myopathies.

Conclusion

We reported 15 new patients harboring *TTN* mutations and described and compared the skeletal muscle histopathology and ultrastructure of a total of 23 *TTN* patients, including eight previously reported cases (Carmignac et al. 2007; De Cid et al. 2015; Hackman et al. 2008; Evila et al. 2016). This study showed that there is no clear genotype/phenotype correlation between the type and location of mutations, and the severity of the disease. However, the comprehensive histological and ultrastructural characterization is expected to provide additional clues for the interpretation of the pathogenicity of *TTN* variations, especially for patients carrying *TTN* variations of unknown significance and presenting typical histological findings of titinopathy.

Contribution

I identified *TTN* mutations in nine patients and confirmed the segregation in the families by Sanger sequencing. I summarized the genetic information and wrote the genetic part of the publication.

Loss of Sarcomeric Scaffolding as a Common Baseline Histopathologic Lesion in Titin-Related Myopathies

Rainiero Ávila-Polo, MD, Edoardo Malfatti, MD, PhD, Xavière Lornage, MSc, Chrystel Cheraud, MD, Isabelle Nelson, PhD, Juliette Nectoux, PharmD, PhD, Johann Böhm, PhD, Raphaël Schneider, MSc, Carola Hedberg-Oldfors, PhD, Bruno Eymard, MD, PhD, Soledad Monges, MD, Fabiana Lubieniecki, MD, Guy Brochier, PhD, Mai Thao Bui, BSc, Angeline Madelaine, BSc, Clémence Labasse, BSc, Maud Beuvin, MSc, Emmanuelle Lacène, MSc, Anne Boland, PhD, Jean-François Deleuze, PhD, Julie Thompson, PhD, Isabelle Richard, PhD, Ana Lía Taratuto, MD, PhD, Bjarne Udd, MD, PhD, France Leturcq, PharmD, Gisèle Bonne, PhD, Anders Oldfors, MD, PhD, Jocelyn Laporte, PhD, and Norma Beatriz Romero, MD, PhD

From the Neuromuscular Morphology Unit, Myology Institute, GHU Pitié-Salpêtrière, Paris, France (RÁ-P, EM, GB, MTB, AM, CL, MB, EL, NBR); FISEVI-UGC Anatomía Patológica-HU Virgen del Rocío, Sevilla, Spain (RÁ-P); University of Granada, Granada, Spain (RÁ-P); Sorbonne University, INSERM UMR5974, GHU Pitié-Salpêtrière, Paris, France (IN, MB, GB, NBR); AP-HP, GHU Pitié-Salpêtrière, Centre de Référence des Maladies Neuromusculaires Nord/Est/Ile de France, Paris, France (EM, BE, EL, NBR); Department of Translational Medicine, IGBMC, INSERM U1258, UMR7104, Strasbourg University, Illkirch, France (XL, CC, JB, RS, JL); Assistance Publique-Hôpitaux de Paris (AP-HP), GH Cochin-Broca-Hôtel Dieu, Laboratoire de Biochimie et Génétique Moléculaire, Paris, France (JN, FL); Department of Pathology and Genetics, Institute of Biomedicine, University of Gothenburg, Gothenburg, Sweden (CHO, AO); Hospital Nacional de Pediatría J.P. Garrahan and Instituto de Investigaciones Neurológicas FLENI, Buenos Aires, Argentina (SM, FL, ALT); Neuromuscular Research Center, Tampere University and University Hospital, Tampere, Finland (BU); Folkhalsan Institute of Genetics, Helsinki University, Helsinki, Finland (BU); Centre National de Recherche en Génétique Humaine (CNRGH), Institut de Biologie François Jacob, CEA, Evry, France (AB, JFD); Genethon Institute, Evry, France (IR); and Complex Systems and Translational Bioinformatics, ICube, Strasbourg University, CNRS UMR7357, Illkirch, France (RS, JT)

Send correspondence to: Norma Beatriz Romero, MD, PhD, Myology Institute, Sorbonne University, GHU La Pitié-Salpêtrière, 75013 Paris, France; E-mail: nb.romero@institut-myologie.org

Rainiero Ávila-Polo and Edoardo Malfatti contributed equally to this work.

This study was financially supported by Association Française contre les Myopathies (AFM-Telethon, 20323, 21267), AIM Association Institut de Myologie, the Assistance Publique-Hôpitaux de Paris, the Institut National de la Santé et de la Recherche Médicale, the Sorbonne Université, the University of Strasbourg, the Centre National de la Recherche Scientifique, the Instituto de Salud Carlos III (M-AES 2015), the Fundación Pública Andaluza para la Gestión de la Investigación en Salud en Sevilla (FISEVI), the University of Granada (PhD International Mobility Programme 2014/2015), the France Génomique National infrastructure, funded as part of the Investissements d'Avenir program managed by the Agence Nationale pour la Recherche (ANR-10-INBS-09), and by Fondation Maladies Rares within the frame of the "Myocapture" sequencing project, the ANR-10-LABX-0030-INRT under the frame program Investissements d'Avenir ANR-10-IDEX-0002-02, and the Swedish Research Council.

The authors have no duality or conflicts of interest to declare.

Abstract

Titin-related myopathies are heterogeneous clinical conditions associated with mutations in *TTN*. To define their histopathologic boundaries and try to overcome the difficulty in assessing the pathogenic role of *TTN* variants, we performed a thorough morphological skeletal muscle analysis including light and electron microscopy in 23 patients with different clinical phenotypes presenting pathogenic autosomal dominant or autosomal recessive (AR) mutations located in different *TTN* domains. We identified a consistent pattern characterized by diverse defects in oxidative staining with prominent nuclear internalization in congenital phenotypes (AR-CM) ($n = 10$), \pm necrotic/regenerative fibers, associated with endomysial fibrosis and rimmed vacuoles (RVs) in AR early-onset Emery-Dreifuss-like (AR-ED) ($n = 4$) and AR adult-onset distal myopathies ($n = 4$), and cytoplasmic bodies (CBs) as predominant finding in hereditary myopathy with early respiratory failure (HMERF) patients ($n = 5$). Ultrastructurally, the most significant abnormalities, particularly in AR-CM, were multiple narrow core lesions and/or clear small areas of disorganizations affecting one or a few sarcomeres with M-band and sometimes A-band disruption and loss of thick filaments. CBs were noted in some AR-CM and associated with RVs in HMERF and some AR-ED cases. As a whole, we described recognizable histopathological patterns and structural alterations that could point toward considering the pathogenicity of *TTN* mutations.

Key Words: Congenital myopathies, Electron microscopy, M-line disruption, Muscle histopathology, Sarcomere disorganizations, Titin, *TTN*-related myopathies.

INTRODUCTION

Titin is the largest human protein (33 000 amino acids) (1, 2) and is encoded by the *TTN* gene (OMIM *188840) on chromosome 2q31 (3–5). Titin is expressed in both skeletal and cardiac muscles (6–8) and is located in the sarcomere extending from the Z-disc to the M-line (9). Its amino-terminal

domain is anchored to the Z-disc interacting with many proteins at this level (10–12). The I-band region is responsible of the elastic property of the protein (13, 14) whereas the A-band region represents the largest part of the protein and is a rigid portion tightly associated to myosin, providing stabilization to the sarcomere (5). The carboxy-terminal domain contains a kinase domain. At this level, titin filaments from the adjacent half-sarcomere overlap and connect with other protein elements such as myomesin (15) and calpain 3 (16). Titin has a critical role in the maintenance of the sarcomere structure during the contraction (17–19).

Next generation sequencing (NGS) approaches have led to an exponential increase in the number of identified mutations, either pathogenic mutations or changes of unknown significance, in *TTN*. To date, mostly through NGS methods, *TTN* mutations have been associated with a large spectrum of clinical conditions ranging from isolated dilated or hypertrophic cardiomyopathies (MIM #604145; MIM #613765) (20–23) to numerous skeletal muscle myopathies (MIM #600334, MIM #608807, MIM #603689, MIM #611705) (24–26). However, not all rare *TTN* variants are associated with a disease and in this respect a recent study by Savarese et al highlighted how challenging is the assignment of new mutations to a plausible titinopathy (27) and that, in all likelihood, new phenotypes may emerge in the future. For this reason, histopathological phenotype and genotype correlations are of critical importance, particularly because functional studies are possible only for some mutations located in specific *TTN* domains (28).

Histopathological changes in *TTN*-related myopathies are markedly variable as reported in muscle biopsies from patients with tibial muscular dystrophy ([TMD]; MIM #600334) and limb-girdle muscular dystrophy 2J ([LGMD2J]; MIM #608807) with rimmed vacuoles (RVs) (29, 30), or hereditary myopathy with early respiratory failure ([HMERF]; MIM #603689) with cytoplasmic bodies (CBs) (31–35). Moreover, increased nuclear internalization and deficits in oxidative staining described as minicores/minicore-like lesions have been reported in early-onset myopathies (28, 36, 37). Nevertheless, to date, a systematic and exhaustive skeletal muscle histopathologic and ultrastructural analysis have not been performed in large cohorts of *TTN*-related conditions.

In order to define histopathologic boundaries of *TTN*-related myopathies and help both clinicians and geneticists supporting the pathogenic role of *TTN* variants, we report a systematic histopathological and ultrastructural analysis of 23 patients with *TTN* mutations presenting different clinical phenotypes.

MATERIALS AND METHODS

Patients

Twenty-three patients (14 male and 9 female) of various ethnic backgrounds were included in the present study. Patients P1 to P10, P14, and P17 to P20 (n = 15) are reported herein for the first time. Part of the clinical, pathologic or genetic data from patients P11 to P13, P15, P16, and P21 to P23 (n = 8) have been previously reported (35, 38–41). Clinical

data of these patients were systematically retrieved and retrospectively analyzed (Table 1). Patients were classified into 4 groups according to their clinical features as follows: Group 1: Autosomal recessive congenital myopathy (AR-CM) (n = 10); Group 2: Autosomal recessive early-onset Emery-Dreifuss-like myopathy without associated cardiomyopathy (AR-ED) (n = 4); Group 3: Autosomal recessive young or early-adult onset distal myopathy (AR-DM) (n = 4); and Group 4: HMERF (n = 5). All patients underwent open biopsy for morphological and histochemical analyses of fresh-frozen skeletal muscle tissue.

Mutation Analysis

Patients or parents gave informed consent for the genetic analysis and DNA storage according to French legislation (Comité de Protection des Personnes Est IV DC-2012-1693). Genomic DNA was extracted from blood or frozen skeletal muscle by standard methods. DNA was studied by direct sequencing of exons of *TTN* gene or exome sequencing. Exome sequencing was performed for patients P1, P2, P3, P4, P5, P7, P8, P9, P10, P17, P18, and P19 with the SureSelect Human All Exon 50 Mb Capture Library v5, P6 and P14 with SureSelect Human All Exon Capture Library v6 (Agilent, Santa Clara, CA) and paired-end sequenced on a HiSeq 2500 (Illumina, San Diego, CA). Confirmation of variants and segregation was performed by Sanger sequencing of genomic DNA and cDNA (Transcript variant IC, References Sequences NM_001267550.2), with standard techniques. P20 mutations were determined by Sanger sequencing. Sequencing primers are available on request. PCR was performed with DreamTaq DNA polymerase according to standard protocol (Fermentas, Waltham, MA). PCR products were sequenced on an ABI3730xl DNA Analyzer (Applied Biosystems, Foster City, CA), using the Big-Dye Terminator v3.1 kit and analyzed with Sequencher 5.0 software (Gene Codes Corp., Ann Arbor, MI).

Morphological Studies

Open muscle biopsy was performed for all patients after informed consent. Age at biopsy varied from 1 month (P9) to 71 years (P20). The biopsied muscle is reported in Table 2. Samples were analyzed either in our research laboratory at the Myology Institute in Paris, France, or at the Neuropathology laboratory of FLENI-Institute and J.P. Garrahan Hospital in Buenos Aires, Argentina, or at the Department of Pathology, Sahlgrenska University Hospital in Gothenburg, Sweden. For conventional histochemical techniques, 10- μ m-thick cryostat sections were stained with hematoxylin and eosin (H&E), modified Gomori trichrome, periodic acid Schiff technique, Oil red O, reduced nicotinamide adenine dinucleotide dehydrogenase-tetrazolium reductase (NADH-TR), succinic dehydrogenase, cytochrome c oxidase, menadione-nitro blue tetrazolium and adenosine triphosphatase preincubated at pH 9.4, 4.63, 4.35. Digital photographs of each biopsy were obtained with a Zeiss AxioCam HRc linked to a Zeiss Axio-plan Bright Field Microscope and processed with the Axio Vision 4.4 software (Zeiss, Oberkochen, Germany).

TABLE 1. Clinical Phenotypes and Genetic Data

Patient	Sex, Onset	Clinical Phenotype	Family Affected	TTN Mutation (Ref Seq NM_001267550.2): Nucleotide Change/Isoform Modification	Exon	Inheritance	Titin Domain	Reference
Group 1								
P1 ^{‡,§}	M (Childhood)	Congenital myopathy	None	c.2137C>T/p.(Arg713*)	14	AR	Z-line	PA
				c.95562G>C/p.(Trp31854Cys)	345		A-band	
P2 ^{‡,§}	M, 3 years	Congenital myopathy	Yes [†]	c.56200_56215dup/p.(Asn18739Ilefs*2)	290	AR	A-band	PA
				c.23444G>A/p.(Arg7815Gln)	82		I-band	
P3 ^{‡,§}	F, Birth	Congenital myopathy	None	c.79070_79071del/p.(Tyr26357Cysfs*55)	327	AR	A-band	PA
				c.76502T>C/p.(Val25501Ala)	327		A-band	
				c.10045A>G/p.(Thr3349Ala)	43		I-band	
				c.4078G>A/p.(Gly1360Arg)	24		Z-line	
P4 ^{‡,§}	M, <1 year	Congenital myopathy	None	c.64688C>G/p.(Pro21563Arg)	311	AR	A-band	PA
				c.97218_97221dupTATT/p.(Lys32408Tyrfs*2)	350		A-band	
P5 ^{*,§}	M, Birth	Congenital myopathy	None	c.35713+1G>A/Intron 162 (not in N2A isoform)	—	AR	—	PA
				c.53918del/p.(Gly17973Gluifs*18)	281		A-band	
P6 [‡]	F, Birth	Congenital myopathy, mainly distal	None	c.95867G>A/p.(Trp31956*)	346	AR	A-band	PA
				c.99415A>G/p.(Lys33139Glu)	356		A-band	
P7 ^{‡,§}	M, 2	Congenital myopathy with severe dilated cardiomyopathy (11 y)	None	c.99833dup/p.(Val33278Serfs*2)	356	AR	A-band	PA
				c.71993G>C/p.(Arg23998Pro)	327		A-band	
P8 ^{*,§}	F, Birth	Congenital myopathy with early diffuse contractures and cardiomyopathy (23 y)	None	c.107425del/p.(Asp35809Thrfs*35)	363 (Mex5)	AR	M-line	PA
				c.97417del/p.(Arg32473Valfs*19)	350		A-band	
P9 ^{‡,§}	M, Birth	Severe congenital myopathy with arthrogrypotic features	None	c.17009G>A/p.(Trp5670*)	59	AR	A-band	PA
				c.19715-1G>C/splice	68		A-band	
P10 ^{‡,§}	M, Birth	Congenital myopathy with early diffuse contractures	None	c.29621_29624del/p.(Glu9874Glyfs*28)	105	AR	I-band	PA
				c.102214T>C/p.(Trp34072Arg)	359 (Mex1)		M-line	
Group 2								
P11 ^{*,§}	M, 10	Early-onset recessive Emery-Dreifuss-like without cardiomyopathy	None	c.106959T>A/p.(Tyr35653*) (homozygous)	361 (360 [‡]) (Mex2)	AR	M-line	(38) (P1)
P12 ^{*,§}	F, Childhood	Early-onset recessive Emery-Dreifuss-like without cardiomyopathy	None	c.106050del/p.(Glu35351Asnfs*54)	359 (358 [‡]) (Mex1)	AR	M-line	(38) (P2)
				c.106978C>T/p.(Gln35660*)	361 (360 [‡]) (Mex3)		M-line	
P13 ^{*,§}	F, 19 months	Early-onset recessive Emery-Dreifuss-like without cardiomyopathy	None	c.105910_105914del/p.(Thr35304Cysfs*3)	359 (358 [‡]) (Mex1)	AR	M-line	(38) (P3)
				c.106422del/p.(Phe35475Serfs*3)	360 (359 [‡]) (Mex2)		M-line	
P14 ^{‡,§}	M, 20 years	Young adult recessive proximal weakness with mild contractures without cardiomyopathy	None	c.26877G>A/p.(Trp8959*)	94	AR	I-band	PA
				c.107387A>C/p.(Glu35796Ala)	363 (Mex5)		M-line	
Group 3								
P15 ^{*,}	M, 20 years	Young adult onset recessive distal titinopathy	Yes ²	c.100558_100561dup/p.(Gly35521Aspfs*25)	358 (357 [‡])	AR	A-band	(5, 39A)
				c.107647del/p.(Ser35883Glnfs*10)	363 (362 [‡]) (Mex5)		M-line	(40) (C1)
P16 [*]	F, 30 years	Young adult onset recessive distal titinopathy	Yes ³	c.98105del/p.(Pro32702Leufs*15)	353 (352 [‡])	AR	A-band	(41) (B)
				c.107647del/p.(Ser35883Glnfs*10)	363 (362 [‡]) (Mex5)		M-line	(5, 39B)
							A-band	(40) (C2)

(continued)

TABLE 1. Continued

Patient	Sex, Onset	Clinical Phenotype	Family Affected	TTN Mutation (Ref Seq NM_001267550.2): Nucleotide Change/Isoform Modification	Exon	Inheritance	Titin Domain	Reference
P17* [§]	M, 20 years	Young adult recessive proximal & distal myopathy	Yes ⁴	c.107867del/p.(Leu35956Argfs*16) c.52021C>T/p.(Arg17341*)	364 (Mex6) 274	AR	M-line A-band	(41) (C) PA
P18* [§]	F, 30 years	Young adult recessive proximal & distal myopathy	Yes ⁵	c.107867del/p.(Leu35956Argfs*16) c.52021C>T/p.(Arg17341*)	364 (Mex6) 274	AR	M-line A-band	PA
Group 4								
P19*	F, 10 years	HMERF	Yes ⁶	c.95185T>C/p.(Trp31729Arg)	344	AD	A-band	PA
P20*	M, 50 years	HMERF	None	c.95187G>C/p.(Trp31729Cys)	344	AD	A-band	PA
P21*	F, 54 years	HMERF	Yes ⁷	c.95195C>T/p.(Pro31732Leu)	344 (343 [¶])	**	A-band	(35) (L; II-1)
P22*	M, 25 years	HMERF	None	c.95195C>T/p.(Pro31732Leu) (homozygous)	344 (343 [¶])	**	A-band	(35) (K; II-1)
P23*	M, 38 years	HMERF	Yes ⁸	c.95134T>C/p.(Cys31712Arg)	344 (343 [¶])	AD	A-band	(35) (G; II-2)

All listed variations are heterozygous and predicted to affect N2A mature skeletal muscle isoform except otherwise stated.
[¶]Patients are carriers of truncating mutations or of mutations previously reported.
[†]Patients are carriers of 1 truncating mutation and 1 missense mutation found in an exon already reported as mutated in the disease.
[‡]Patients are carriers of 1 truncating mutation and 1 missense mutation found in an exon never reported as mutated in the disease.
[§]Segregation in the family was confirmed.
[¶]Numbered as firstly published, according to the old numbering (before October 2013); AR: Autosomal recessive; AD: Autosomal dominant.
^{**}Described in the original paper as semirecessive or semidominant (34); M: Male; F: Female; Ref Seq: Reference Sequence; PA: Present Article; HMERF: Hereditary Myopathy with Early Respiratory Failure; ¹: sisters; ²: his mother (P16); ³: her son (P15); ⁴: his sister (P18); ⁵: her brother (P17); ⁶: her father; ⁷: her brother; ⁸: his mother.

Electron Microscopy (EM)

Detailed EM analysis was performed in 19 patients (Table 2). For ultrastructural studies, small muscle samples were fixed in 2.5% glutaraldehyde, pH 7.4, postfixed in 2% osmium tetroxide for 2 hours, dehydrated and embedded in epoxy resin. At least 3 blocks from each patient were studied, including longitudinal and transverse-oriented samples. Semi-thin sections were stained by toluidine blue and examined in light microscopy to select pathological areas. Ultrathin sections were stained with uranyl acetate and lead citrate. The grids were observed using a Philips CM120 electron microscope (80kV; Philips Electronics NV, Eindhoven, The Netherlands).

RESULTS

Clinical Findings

Clinical summary and laboratory features of all patients are provided in Table 1.

Group 1: AR-CM patients, P1–P10, showed congenital hypotonia or early onset diffuse muscle weakness, with congenital arthrogryposis or early development of contractures (P8, P9, and P10); associated cardiomyopathy was found in P7 and P8.

Group 2: AR-ED patients, P11–P13 have been recently reported (38) and P14 is firstly described in this report.

Group 3: AR-DM patients, P15–P18, showed distal or proximal-distal early severe muscle weakness of the 4 limbs. P15 and P16 were described elsewhere (39, 41). P17 and P18 are reported here for the first time.

Group 4: HMERF group included patients P19–P23. Most of them had adult onset weakness with diaphragmatic respiratory failure. Earlier onset (10 years) has been observed in P19. Patients P21–P23 were previously reported (35).

Molecular Data

To identify the mutations in patients without a genetic diagnosis, we performed exome sequencing on genomic DNA from the patients and their parents. Exome sequencing allows a fast and parallel screening of most human genes, and is suitable and efficient for the diagnosis of neuromuscular diseases and the analysis of large genes such as *TTN* (42). This approach also covers any newly discovered gene for the disorder.

For all patients, we found known or novel mutations in *TTN* (Table 1). These changes were confirmed by Sanger sequencing, and their familial segregation validated when parental DNA was available. Parents of patients P1, P2, P3, P4, P5, P7, P8, P9, P10, P11, P12, P13, P14, P17, and P18 were screened to confirm the segregation of the mutations and to verify that *TTN* mutations are on opposite alleles (in trans position). Most of the patients harbored compound heterozygous mutations (21 patients), at least one of them was a truncating mutation (frameshift, nonsense mutation or mutation affecting an essential splice site) leading to a predicted protein truncation or degradation (Table 1). The second mutations were either truncating mutations or rare missense mutations. Two cases carried homozygous mutations: P11 (AR-ED) and

TABLE 2. Patient Data and Summarized Histological Findings

Patient	Age at Biopsy	Muscle Biopsied	Method	Light Microscopy	Electron Microscopy	Reference
Group 1						
P1	8 y; 13 y	NR	LM, EM	Well-defined areas of defective oxidative staining, some nuclear internalizations, type 1 fiber predominance	Focal and short areas of myofibrillar disorganization, nuclear internalizations; some clear areas with myofilaments loss, M-line disruption and almost intact Z-line	PA
P2	7 y	Vastus lateralis	LM, EM	Multiple and well-delimited areas of uneven oxidative staining, centralized nuclei, type 1 fiber predominance	Focal and multiple areas of myofibrillar disarray resembling minicores, nuclear internalizations	PA
P3	3 y	Deltoid	LM, EM	Multiple and well-delimited areas of uneven oxidative staining, prominent nuclear centralizations, type 1 fiber uniformity	Foci of myofibrillar disorganization with Z-band streaming running over few sarcomeres, some large clear areas with myofilaments loss, M-line disruption and almost intact Z-line	PA
P4	7 y	Vastus lateralis	LM, EM	Type 1 fiber predominance, internalized nuclei, uneven oxidative staining	Focal and multiple areas of myofibrillar disarray resembling minicores, nuclear internalizations, Z-line streaming spanning all along the sarcomere resembling “pennants”	PA
P5	31 y	Deltoid	LM, EM	Uneven oxidative staining, numerous internalized nuclei, type 1 fiber predominance	Z-line streaming spanning all along the sarcomere or as small “pennants”, rare focal areas of myofibrillar disorganization	PA
P6	49 y	Deltoid	LM, EM	Type 1 fiber predominance, numerous internalized nuclei, uneven oxidative staining, increased interstitial fat and connective tissue, occasional COX negative fibers.	Z-line streaming spanning all along the sarcomere or as small “pennants”, internalized nuclei in rows, small RVs, focal areas of myofibrillar disorganization	PA
P7	12 y	Deltoid	LM, EM	Multiple and well-delimited areas of uneven oxidative staining, prominent nuclear centralizations, type 1 fiber uniformity	Focal and multiple areas of myofibrillar disarray resembling minicores, granular streaming spanning all along the sarcomere or as small “pennants”, internalized nuclei	PA
P8	23 y	Deltoid	LM, EM	Prominent nuclear centralizations, type 1 fiber uniformity, presence of rare areas of uneven oxidative staining	Z-line streaming spanning along the sarcomere or as small “pennants”, internalized nuclei	PA
P9	1 m	Vastus lateralis	LM, EM	Fiber caliber variation, many small fibers, internalized nuclei, uneven oxidative staining, fuchsinophilic protein inclusions	Focal and multiple areas of myofibrillar disarray resembling minicores, clear areas with loss of myofilaments with almost intact Z-line, CBs, numerous fibers with marked sarcomere disorganization	PA
P10	4 m; 4 y	Vastus lateralis	LM, EM	Fuchsinophilic protein inclusions, uneven oxidative staining, nuclear internalizations	CBs, nuclear filamentous inclusions, atrophic fibers with degenerated myofibrils, duplication of triads	PA

(continued)

TABLE 2. Continued

Patient	Age at Biopsy	Muscle Biopsied	Method	Light Microscopy	Electron Microscopy	Reference
Group 2						
P11	7 y	Deltoid	LM, EM	Necrotic/regenerating fibers, some nuclear internalizations, and type 1 fiber predominance	Clear areas with loss of myofilaments with almost intact Z-line, internalized nuclei	(38) (P1)
P12	43 y; 52 y	Deltoid	LM, EM	Rare necrotic/regenerating fibers, nemaline bodies, RVs, uneven oxidative staining, and some nuclear internalizations	CBS, sometimes with dense material in the peripheral halo, nemaline bodies, nuclear tubulo-filamentous inclusions, RVs/AV, clear areas with loss of myofilaments with almost intact Z-line, internalized nuclei	(38) (P2)
P13	9 y	Vastus lateralis	LM, EM	Type 1 fiber predominance, rods, RVs, uneven oxidative staining, internalized nuclei, necrotic and regenerative fibers	CBS, sometimes with dense material in the peripheral halo, nemaline bodies, tubulo-filamentous material, RVs, and filamentous nuclear inclusions, focal Z-line streaming spanning all along the sarcomere or as small “pennants”.	(38) (P3)
P14	47 y	Deltoid	LM, EM	Uneven oxidative staining, internalized nuclei, increased interstitial connective tissue, occasional COX negative fibers	Z-line streaming spanning all along the sarcomere or as small “pennants”, mini-cores, internalized nuclei, nemaline rods in some fibers, mitochondrial abnormalities	PA
Group 3						
P15	42 y	Deltoid	LM, EM	Uneven oxidative staining, internalized nuclei	Clear areas with loss of myofilaments with almost intact Z-line, Z-line streaming spanning all along the sarcomere or as small “pennants”, large areas of protein material and myofibrillar loss, internalized nuclei	(39) (5A) (40) (C1) (41) (B)
P16	69 y	Deltoid	LM, EM	Uneven oxidative staining, internalized nuclei	Z-line streaming spanning all along the sarcomere or as small “pennants”, large areas of accumulated protein material with myofibrillar loss.	(39) (5B) (40) (C2) (41) (C)
P17	54 y	Deltoid	LM	Necrotic fibers, few RVs, internalized nuclei, mild uneven oxidative staining, Type 1 fiber predominance, mild endomysial fibrosis	NA	PA
P18	NS	NR	LM	Few internalized nuclei (only H&E staining available)	NA	PA
Group 4						
P19	10 y	Deltoid	LM, EM	CBS, uneven oxidative staining, internalized nuclei	CBS sometimes with dense protein aggregates in the peripheral halo, RVs, Z-line streaming as small “pennants”, large areas of protein material and myofibrillar loss, atrophic fibers with disorganized internal structure with thin-filaments and small segments of dense material	PA

(continued)

TABLE 2. Continued

Patient	Age at Biopsy	Muscle Biopsied	Method	Light Microscopy	Electron Microscopy	Reference
P20	71 y	Peroneus longus	LM	Rods, CBs fuchsinophilic protein inclusions, slight increase in endomysial fibrosis, type 1 fiber predominance, internalized nuclei	NA	PA
P21	55 y	Deltoid	LM, EM	Type 1 fiber predominance, CBs, RVs, uneven oxidative staining, internalized nuclei	CBs sometimes with dense material in peripheral halo, protein inclusions, RVs, large areas of protein material and myofibrillar loss, internalized nuclei	(35) (L: II-1)
P22	27 y	Deltoid	LM	CBs, RVs, uneven oxidative staining, internalized nuclei	NA	(35) (K: II-1)
P23	48 y	Deltoid	LM EM	CBs, RVs, regenerative fibers, internalized nuclei	CBs, large areas of protein material and myofibrillar loss, atrophic fibers with disorganized internal structure with thin-filaments and small segments of dense material	(35) (G: II-2)

Abbreviations: y: years; m: months; NR: not referred; LM: light microscopy; EM: electron microscopy; PA: present article; CBs: cytoplasmic bodies; RVs: rimmed vacuoles; NA: not available; H&E: hematoxylin and eosin.

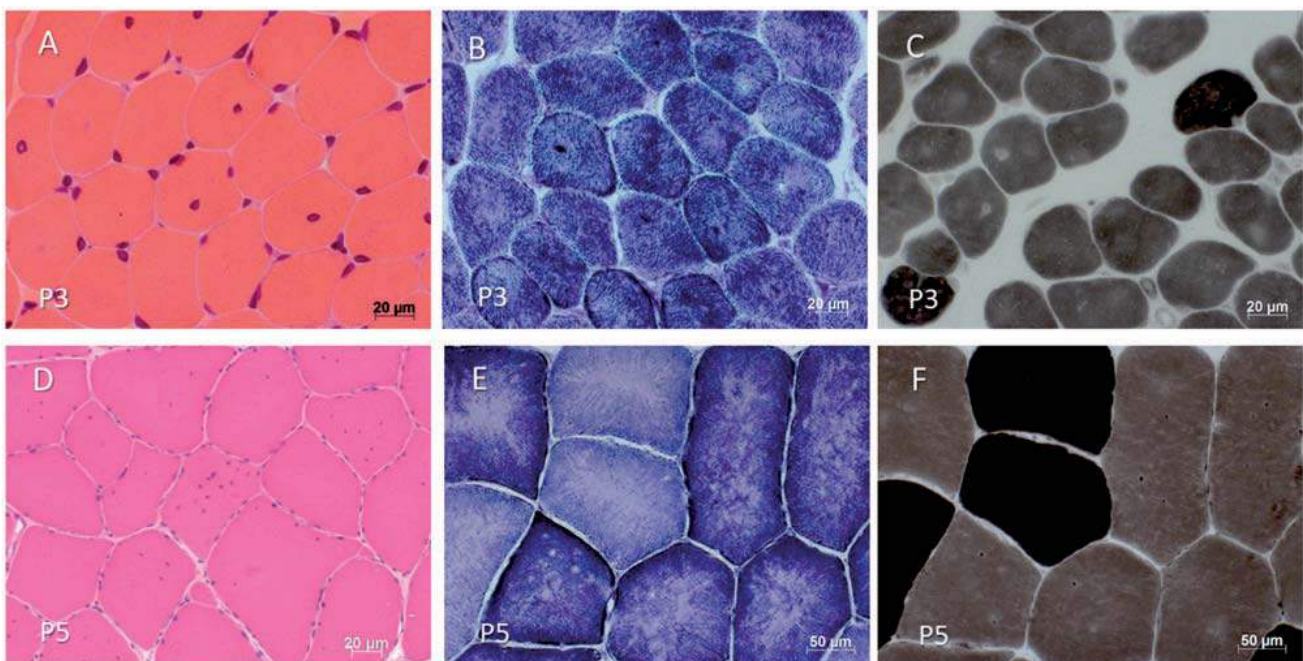


FIGURE 1. Histochemistry from group 1 patients (AR-CM). P3 **(A–C)**: **(A)** H&E. Presence of numerous fibers harboring centralized nuclei. **(B)** NADH. The majority of muscle fibers show multiple and irregular areas of defective oxidative reaction. **(C)** ATPase 9.4. Type 1 fiber predominance. P5 **(D–F)**: **(D)** H&E. Great fiber size diameter variation and presence of multiple nuclear internalization in numerous fibers. **(E)** NADH. Multiple and irregular centrally placed areas of defective oxidative reaction. **(F)** ATPase 9.4. Type 1 fiber predominance.

P22 (HMETF). Several mutations were previously known or affected exons already mutated in the disease. The mutations were located in different protein domains (Table 1). Patients from Group 1 (AR-CM) had the most heterogeneous results. Although variants were distributed all along

the protein, they mostly were located within the A-band (9 of 10 cases). I-band was involved in 3 of 10 cases, and both M-line and Z-line in 2 of 10 cases, respectively. As recently reported, patients P11–P13 from Group 2 (AR-ED) had *TTN* mutations located in exons coding for the M-line domain

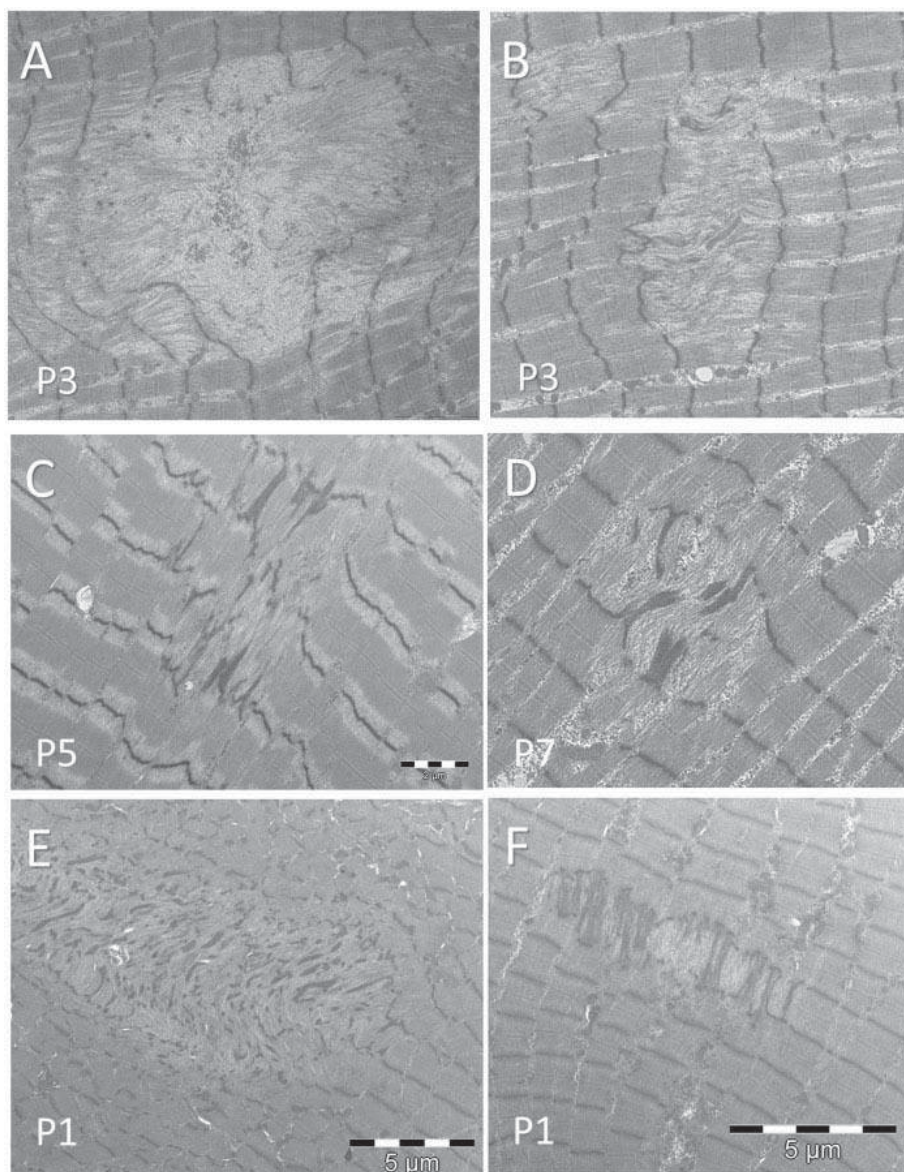


FIGURE 2. Electron microscopy studies from Group 1 patients (AR-CM). **(A, B)** P3. Characteristic lesions showing evident loss of thick myofilaments with M-line and A-line dissolution and slight fragmentation of Z-line involving a few or several sarcomeres and myofibrils. **(C, D)** P5 and P7. Small areas of myofibrillar disarray involving one or few sarcomeres with dispersion of Z-line material resembling small “pennants”. **(E)** P1. Focal and large area of myofibrillar disorganization with Z-line streaming and paucity of mitochondria. **(F)** P1. Small area of sarcomeric disarray with accumulation of Z-line material spanning one sarcomere. Areas of myofibrillar disorganization extended through the adjacent myofibrils.

(Mex1–Mex3) (38). P14 showed a similar phenotype with severe proximal weakness mainly in lower limbs and limitation in abduction of the arms due to mild contracture of the shoulder, but mutations were located in exons 363/Mex5 and 94 (I-band). In Group 3 (AR-DM), a combination of Mex5/Mex6 mutations and a second mutation involving A-band domain was present in all patients (39–41). Finally, HMERF patients carried several reported mutations in exon 344 (35). We studied Calpain 3 on Western blot in 5 patients (P6, P11, P12, P13, and P14). Four patients (P11, P12, P13, and P14) harboring at least one mutation in

different *TTN* exons coding for M-line domain (Mex) had calpain deficiency without mutations in *CAPN3*.

Morphological Findings

Detailed histopathologic analysis is reported in Table 2. Group 1: AR-CM (P1–P10) (Figs. 1 and 2). Muscle biopsies from all cases showed multiple small irregular and randomly distributed areas of reduced/absent oxidative activity or better-defined core areas (P1, P2, P3, P7) associated with mild fiber size variability, type 1 fiber predominance and increased

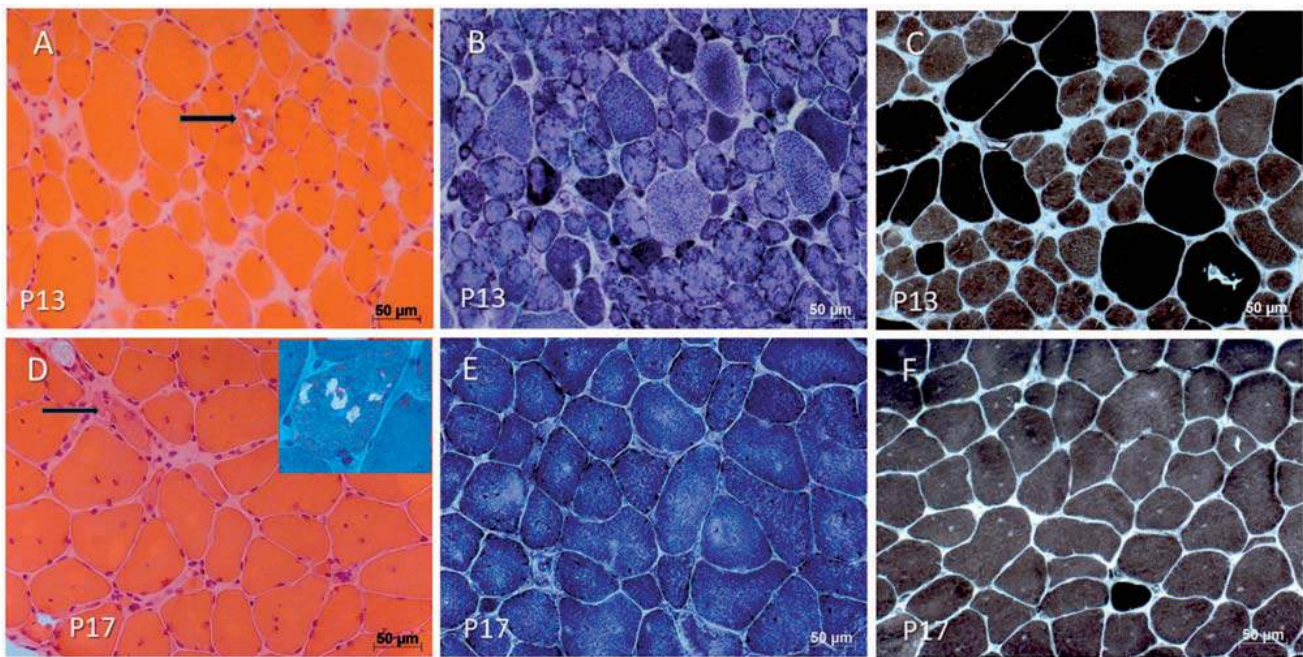


FIGURE 3. Histochemistry from Group 2 (AR-ED) and Group 3 patients (AR-DM). **(A–C)** P13 (AR-ED): **(A)** H&E. Presence of great round fibers size variation with numerous atrophic fibers, some necrotic fibers, rimmed vacuoles (arrow), internalized nuclei and endomysial fibrosis. **(B)** NADH. Numerous fibers showing diffuse alterations of oxidative staining conferring a lobulated aspect to smaller fibers. **(C)** Type 1 fiber predominance. **(D–F)** P17 (AR-DM). **(D)** H&E. Fibers type variation, prominent nuclear internalizations and mild endomysial fibrosis, necrotic/regenerative fibers (arrow). Presence of some rimmed vacuoles (GT in top right corner). **(E)** NADH. Irregular areas of uneven oxidative staining. **(F)** ATPase 9.4. Marked type 1 fiber predominance.

nuclear internalizations (Fig. 1A–F). Increased frequency of nuclear centralizations was evident in 4 cases (P2, P3, P7, P8). In addition, P9 and P10 displayed numerous CBs in atrophic fibers. Using EM, we identified variable length sarcomere disorganizations characterized by (i) clear small areas of M-line dissolution by subsequent disintegration of thick filaments, running along one or a few sarcomeres with preservation of the Z-line structure (P1, P3, P7, P9) (Fig. 2A, B); some areas of myofibrillar disorganization extended through the adjacent myofibrils; (ii) focal areas of diffusion of Z-line material resembling small “pennants” starting from the Z-line (P4, P5, P6, P7, P8) (Fig. 2C, D); sometimes, the electron dense material appeared to span the full width of a sarcomere (Fig. 2F); (iii) many focal areas of sarcomeric disruption affecting a few sarcomeres with Z-line streaming and sharp limits from the adjoining normal sarcomeres with paucity of mitochondria, evoking classical minicores (P1, P2, P3, P4, P6, P7, P9) (Fig. 2E). Moreover, P9 and P10 showed additional changes as CBs (P9, P10), nuclear inclusions corresponding to tubulofilamentous aggregates (P10), duplication of triads (P10) or atrophic fibers showing disorganized internal structure with thin filaments and small segments of dense Z material (P9, P10). Internalized/centralized nuclei were common in most of the cases.

Group 2: AR-ED (P11–P14) (Figs. 3A–C, 4). Muscle biopsies showed a dystrophic pattern with marked fiber size variability, necrotic and regenerative fibers, endomysial fibrosis, numerous RVs and sometimes rods or CBs (Fig. 3A–C). In addition, irregularities in oxidative staining were also evident in

most of the cases. Ultrastructural study showed also the presence of clear small and focal areas of sarcomere M-line dissolution spanning one or a few sarcomeres with almost complete preservation of the Z-line (P11, P12) (Fig. 4A, B), and dense Z-line material disrupted (Fig. 4C), or resembling small “pennants” (P13, P14). CBs were observed in P12 and P13; some of them showed small segments of dense material among the thin filaments in the peripheral halo. Moreover, nemaline bodies (P12, P13, P14) with the characteristic square lattice structure (Fig. 4D), RVs containing degradation products (P13, P14), tubulofilamentous sarcoplasmic (P13) and nuclear inclusions (P12, P13) were also observed.

Group 3: AR-DM (P15–P18) (Figs. 3D–F, 5A–C). Muscle biopsies showed mild irregular disorganizations at oxidative staining associated with mild to moderate myopathic changes (Fig. 2D–F). Few necrotic and regenerative fibers, as well as RVs in sparse fibers were evident in P17. By EM, we showed the presence of small and focal areas involving one sarcomere as clear areas with loss of myofilaments including M-line dissolution with almost intact Z-line (P15) (Fig. 5A), Z-line diffusion spanning all along the sarcomere (Fig. 5B) or resembling small “pennants” (P15, P16), or large areas of accumulated dark protein material and myofibrillar striation loss (P15, P16) (Fig. 5C).

Group 4: HMERF (P19–P23) (Figs. 5D–F, 6). All biopsies showed internalized nuclei (Fig. 6A), and numerous fuchsinophilic inclusions corresponding to CBs, presenting a remarkable circular disposition in some fibers in P19 and P21 (Fig. 6B–D). By EM some CBs showed small electron dense

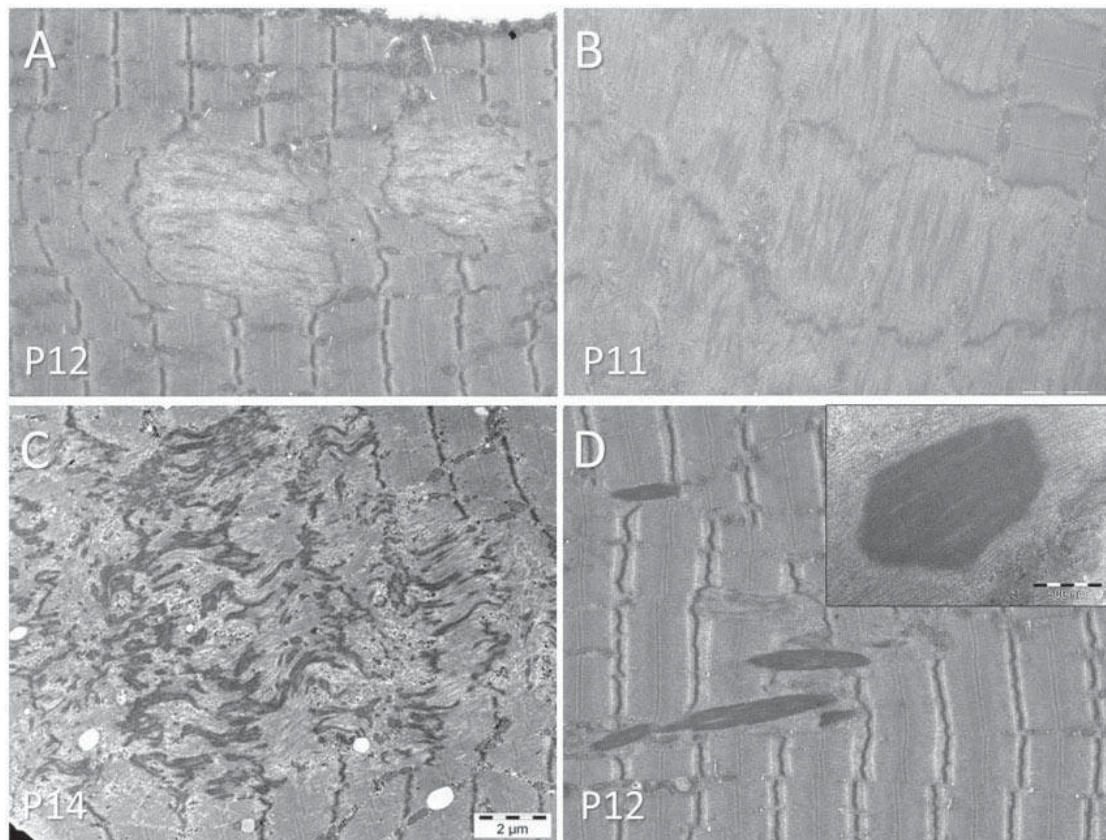


FIGURE 4. Electron microscopy from Group 2 (AR-ED) **(A)** P12. Distinctive lesion showing loss of myofilaments with M-line dissolution, disintegration of thick filament and almost preserved Z-line, involving a few sarcomeres and myofibrils; **(B)** Clear areas of myofibrillar disintegration extending to the adjacent sarcomeres corresponding to dissolution of M-band structure, with almost intact Z-line. **(C)** P14. Small areas of disorganization of the structure with Z-line material accumulation occasionally reminding a classical minicore. **(D)** P12. Cytoplasmic elongated nemaline bodies (rods), with the characteristic square lattice structure (in top right corner).

amorphous inclusions among the thin filaments in the peripheral halo (P19 and P21) (Fig. 5D, E). Widespread abnormal areas corresponding to accumulated filamentous material and damage of myofibrils with loss of striations were frequently observed (P19, P21, P23). Furthermore, we rarely found focal sarcomere disruptions with small “pennants” starting from the Z-line (P19, P23). Eventually, we encountered some atrophic fibers with completely disorganized internal structure and rods (P19), and rimmed/autophagic vacuoles (P19, P21, P23) (Fig. 5F).

Summary

Overall, Group 1 (AR-CM) was characterized by multiple and small particular areas of sarcomere disorganization distributed through the muscle fibers. In AR-ED and AR-DM, sarcomere disruptions were associated with mild myopathic changes or moderate dystrophic pattern \pm RVs. In HMERF patients, CBs were the main feature, with a typical but not constant circular peripheral distribution.

As a whole, in all muscle biopsies we identified variable sarcomere disruptions suggesting a loss of sarcomeric

scaffolding as common histopathologic lesions associated with *TTN* pathogenic mutations.

DISCUSSION

TTN-related myopathies comprise a large group of different clinical entities (24–26). The relatively recent employment of NGS techniques has led and probably will continue to lead to increased numbers of genetic variants described in *TTN* as well as new associated clinical phenotypes (28, 38, 43, 44). Our study focuses on the description of recessive *TTN* cases and HMERF cases. Interestingly, while HMERF is usually a dominant disorder, P22 presented with homozygous p.Pro31732Leu mutation. This mutation (initially described as p.Pro30091Leu) was reported by Palmio et al in 2014 as a semirecessive mutation since some heterozygous carriers don't develop a disease and some do (37). An outstanding diagnostic challenge is the assignment of a pathogenic value to the already huge and still increasing number of *TTN* sequence variants identified with NGS (27). Moreover, reliable functional tests for the interpretation of single variants are lacking. However, considering the high number of variants of uncertain significance in the *TTN* gene, confrontation of molecular,

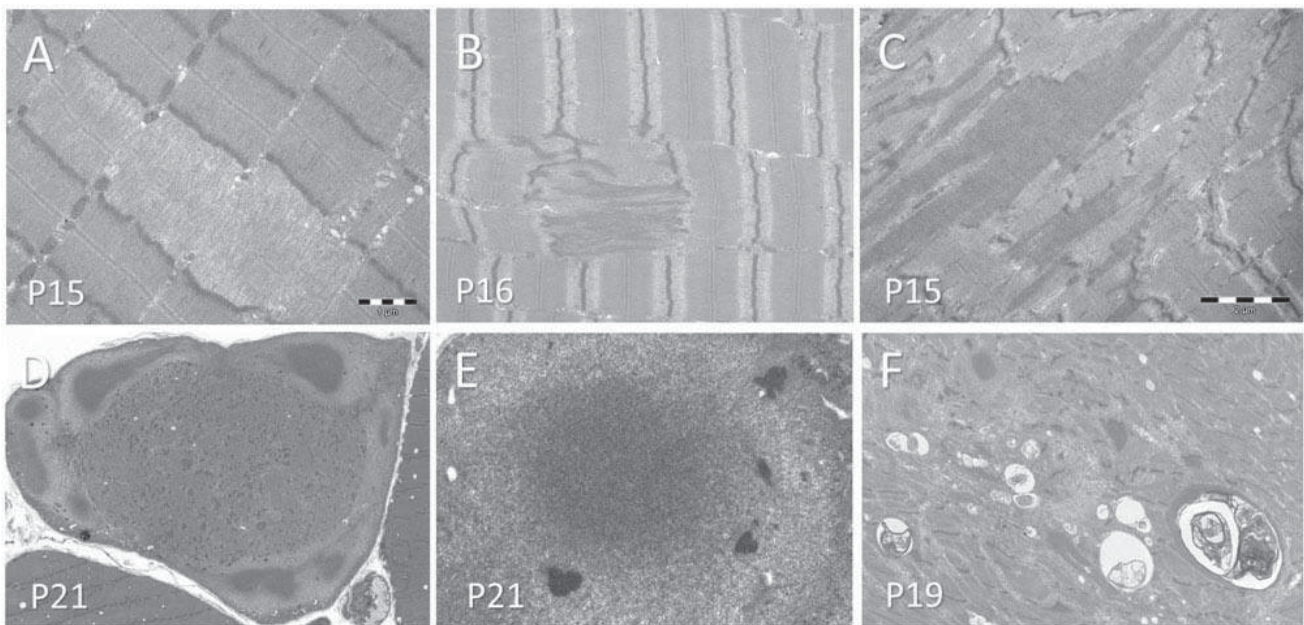


FIGURE 5. Electron microscopy studies from Group 3 (AR-DM). **(A)** P15. Loss of myofilaments with M-line dissolution (in the central area of the image) and preserved Z-line involving one sarcomere; and in a small part are noted reminiscent of M-band. **(B)** P16. Streaming of dark material starting from the Z-line and spanning all along the sarcomere; **(C)** P15. Large areas of accumulated filamentous/granular material and myofibrillar striation loss. EM studies from Group 4 (HMETF). **(D)** P21. Muscle fiber with subsarcolemmal cytoplasmic bodies disposed in a circle. **(E)** P21. Compact central area of a cytoplasmic body harboring small electron-dense structures in the peripheral region. **(F)** P19. Autophagic material and cellular debris.

clinical and morphological data is crucial for the establishment of the molecular diagnosis.

With the morphological studies of 23 *TTN* mutated patients, we intended to correlate specific histopathological lesions with each different clinical group of patients. AR-CM patients (P1–P10) from Group 1 presented a typical congenital myopathy phenotype (Table 1). Cardiomyopathy was present in 2 cases (P7 and P8) and was reported in a clinically affected sister of P2. All patients harbored recessive compound heterozygous mutations in different exons of *TTN* involving different domains but predominantly located in the A-band. Muscle biopsies showed disorganizations of the mesh of the intermyofibrillar network at oxidative staining as predominant findings, associated with type 1 fiber predominance, internalized or centralized nuclei, corresponding to some extent to previously described pathological spectrum of the disorder (28, 36, 37). Nevertheless, ultrastructural studies (Table 2) consistently revealed common and relevant features: (1) small clear areas of focal myofibrillar disintegration with loss of thick filament corresponding to dissolution of M-band structure, and sometimes also A-band, with almost intact Z-line (Figs. 2A, B, 7A, B); (2) areas with Z-line diffusion spanning all along the sarcomere, or resembling small “pennants” (Fig. 2C, D, F); and (3) focal myofibrillar disorganizations with Z-line streaming and paucity of mitochondria, involving a few sarcomeres (Fig. 2E).

Patients from Group 2 with AR-ED (P11–P14) harbored compound heterozygous (P12, P13, P14) or homozygous (P11) mutations involving M-line protein domains. Muscle biopsies had a variably severe dystrophic pattern with RVs, rods and CBs. Our detailed ultrastructural analysis allowed

disclosing the presence of distinctive small and focal areas of sarcomere disorganizations with M-line dissolution in all patients (Fig. 4A, B). Some of CBs had an atypical aspect with small dense material in the peripheral halo (Table 2).

Group 3 patients P15 and P16 were originally considered as severe early-onset TMD with proximal involvement (39), and shared a mutation in exon 363/Mex5 but harbored different second truncating mutations that explained their more severe phenotype (39–41) allowing them to be redefined as AR-DM. P17 and P18 harbored the same 2 mutations in exons 364/Mex6 and 274. Muscle biopsies revealed multiple nuclear internalization and uneven oxidative staining. Mild variability in the size of the fibers, slight increase in endomyocardial connective tissue and some RVs were evident in P17. EM mainly showed both focal and large areas of disorganizations with myofibrillar/filaments loss (Fig. 5A–C) (P15 and P16).

Group 4 included HMETF patients (P19–P23) characterized by severe early respiratory insufficiency with variable degree of muscular involvement. P19 showed uncommon early-onset at 10 years old. All the patients harbored missense *TTN* mutations in the same *TTN* exon 344 (35). Presence of CBs was the common and most prominent histological feature (Fig. 6). CBs were preferentially subsarcolemmal, sometimes with a circular peripheral distribution of CBs as described (45). EM disclosed that some of them harbored the presence of short segments of dense material in the peripheral halo (Fig. 5D, E). Variable length of sarcomere disorganizations has also been reported in biopsies from HMETF patients (34, 45–47). Our cases showed mainly large areas of protein material deposit (P19, P21, P23) and Z-line streaming

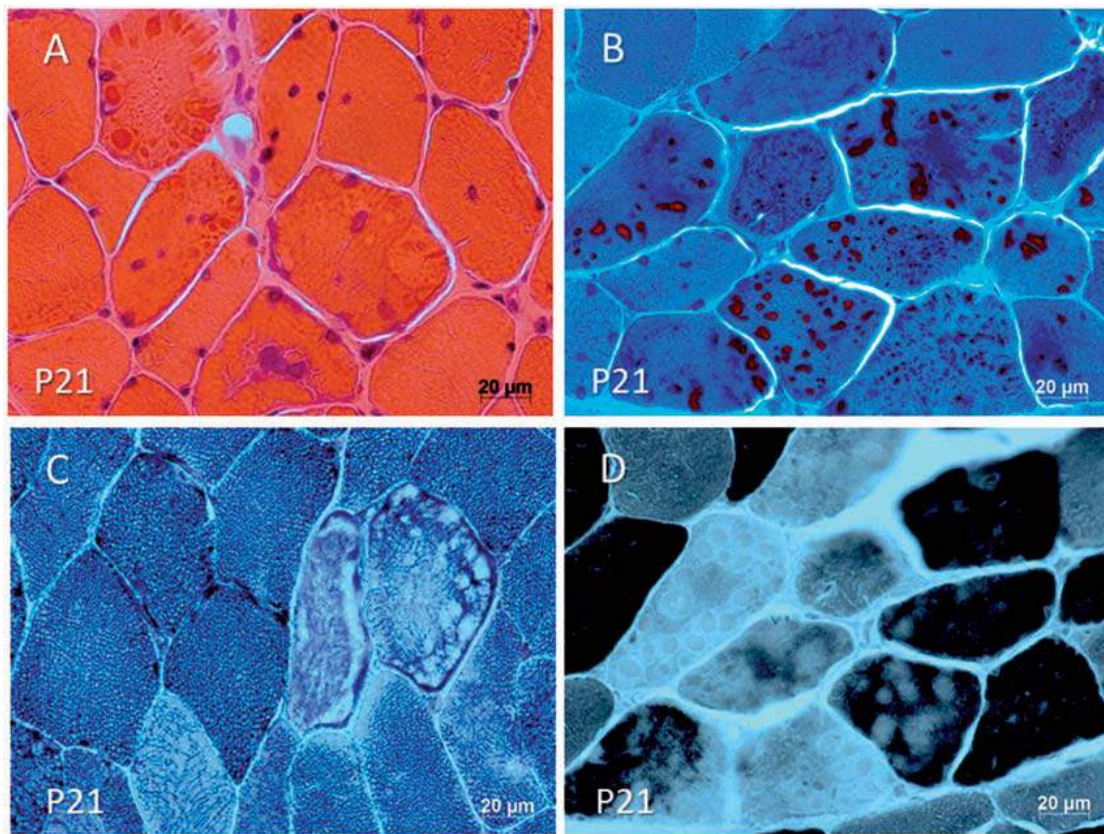


FIGURE 6. Histochemistry from P21, Group 4 (HMERF). **(A)** H&E. Fibers size variability and internalized nuclei. Presence of fibers with cytoplasmic bodies. **(B)** Modified Gomori trichrome. Fibers show numerous and multiple fuchsinophilic rounded inclusions corresponding to cytoplasmic bodies. **(C)** NADH. Areas of defective oxidative staining corresponding to the zone occupied by the cytoplasmic bodies with particular circular and peripheral distribution. **(D)** ATPase 9.4 Some fibers harbor areas devoid of reactions corresponding to the cytoplasmic bodies.

resembling small “pennants” (P19, P23). Atrophic fibers showed complete sarcomere disorganization, rods and rimmed/autophagic vacuoles (P19, P21).

As a whole, we identified here that *TTN* pathogenic mutations cause a large spectrum of histopathologic lesions always associated with particular sarcomere disruptions. Although one could imagine that the presence of sarcomeric pathology is as an expected finding related to the loss of titin intrinsic properties, the above mentioned particular sarcomeric disruption presented common elements such as focal myofibrillar disintegration with loss of thick filament corresponding to dissolution of M-band structure, with almost intact Z-line, that we have never observed in the EM analyses of muscle biopsies from other congenital diseases. The sarcomere disruption observed initially on the band M as shown in Figure 7A–D, then in Figures 2B and 5A, can be extended later on the whole of the sarcomere structure, as shown in Figures 2A and 4A. The dissolution of M line with almost intact Z line could be considered as an early lesion (Fig. 7) and, clearly, there may be different degrees of disruption of the sarcomere. Thus, these lesions might be considered as a common and priming myofibrillar damage that successively lead to the development of multiple and variable histopathological alterations.

Of note, these restricted and focal sarcomere abnormalities identified in *TTN*-related myopathies appear different from classical cores or minicores lesions as observed in myopathies related to *RYR1* (OMIM *180901) and *SEPN1* (OMIM *606210) genes. Indeed, ultrastructurally, typical cores found in *RYR1* mutated patients correspond to wide areas of compacted and disorganized myofibrils, with Z-line streaming and absence of mitochondria extending over numerous sarcomeres or almost along the full length of the fibers; they are sharply demarcated from the normally structured zones of the muscle fibers (48). However, mostly in *RYR1* recessives, the core areas frequently occupied the whole myofiber cross sectional and extended to a moderate number of sarcomeres in length (49). In contrast, the classical minicores as found in *SEPN1*-related myopathies have poorly defined borders and are characterized by the presence of multiple foci of myofibrillar disorganization, with Z-line streaming running over a few sarcomeres, even if occasionally they are longer; mitochondria are absent from the altered areas (48). Additionally, and this is a key point in our work, these “minicore” lesions never appear as focal clear areas of myofibrillar disruption involving one or few sarcomeres, with M-line disintegration and some loss of filaments in the central part of the abnormal areas associating

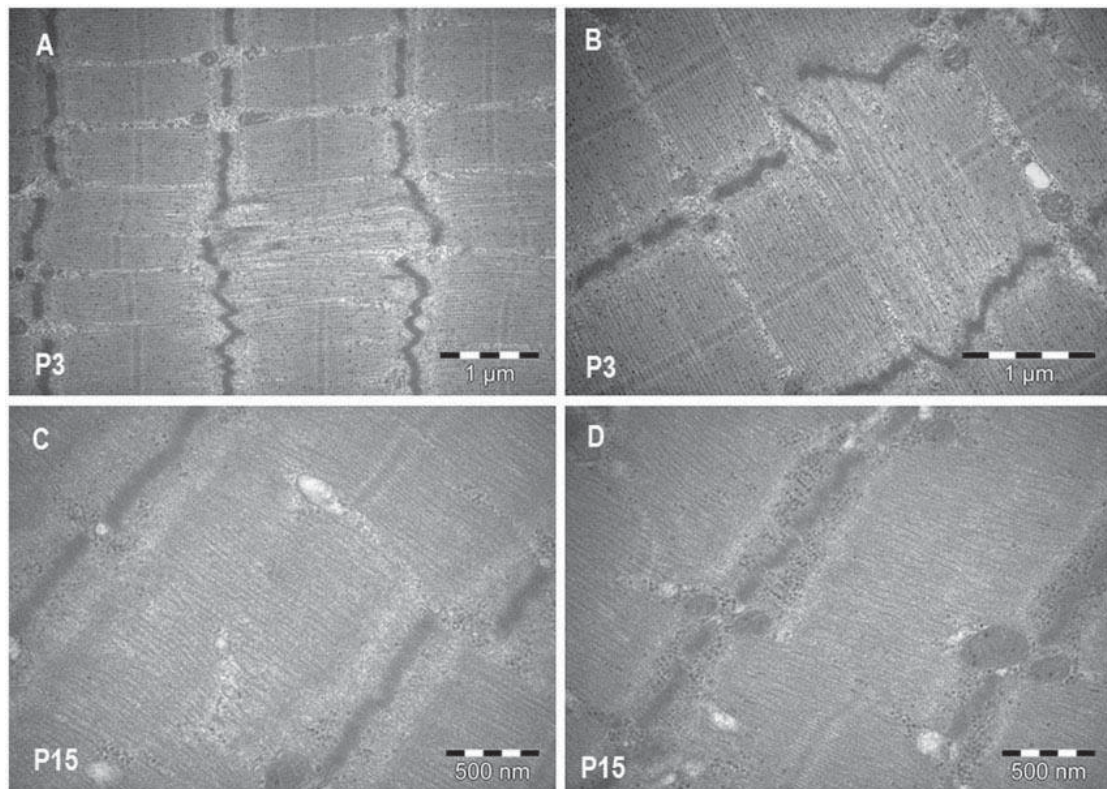


FIGURE 7. High-magnification electron microscopy studies from P3 (AR-CM) (**A, B**), and P15 (AR-DM) (**B, C**). These images show slight abnormalities, only identified by especially M-band disruption, without A-band alterations, which could be considered as initial or early changes.

with almost intact Z-line, as we observed in *TTN*-related myopathies (Figs. 2A, B, 4A, B, 5A).

On the basis of our findings, we aimed at establish a strong correlation between histopathologic phenotype and genotype that would explain the mechanism underlying the loss of sarcomere scaffolding. Unfortunately, this was hindered by the lack of tools for functional studies of the mutations. Further studies will also be required to better characterize the *TTN* isoforms and their role for muscle function.

In conclusion, our morphological analysis of the muscle biopsies from 23 patients carrying *TTN* pathogenic mutations suggest a recognizable pattern of myofibrillar alteration that could help in the diagnosis of titinopathies in a complicated scenario where functional studies are still lacking. Further histopathological analyses are needed to assess the exact specificity of these lesions.

ACKNOWLEDGMENTS

The authors thank Pr. M. Fardeau for his invaluable contribution, F. Levy-Borsato and N. Haslin for secretarial assistance, and Valérie Biancalana for suggestions. This article presents part of the results of the main author Rainiero Ávila Polo to achieve the PhD degree in the PhD program in Biomedicine at the University of Granada, Spain.

REFERENCES

1. Maruyama K, Kimura S, Yoshidomi H, et al. Molecular size and shape of beta-connectin, an elastic protein of striated muscle. *J Biochem* 1984;95:1423–33
2. Kurzban GP, Wang K. Giant polypeptides of skeletal muscle titin: Sedimentation equilibrium in guanidine hydrochloride. *Biochem Biophys Res Commun* 1988;150:1155–61
3. Labeit S, Barlow DP, Gautel M, et al. A regular pattern of two types of 100-residue motif in the sequence of titin. *Nature* 1990;345:273–6
4. Rossi E, Faiella A, Zeviani M, et al. Order of six loci at 2q24-31 and orientation of the HOXD locus. *Genomics* 1994;24:34–40
5. Bang ML, Centner T, Fornoff F, et al. The complete gene sequence of titin, expression of an unusual approximately 700-kDa titin isoform, and its interaction with obscurin identify a novel Z-line to I-band linking system. *Circ Res* 2001;89:1065–72
6. Wang K. Titin/connectin and nebulin: Giant protein rulers of muscle structure and function. *Adv Biophys* 1996;33:123–34
7. Maruyama K. Connectin/titin, giant elastic protein of muscle. *FASEB J* 1997;11:341–5
8. Gregorio CC, Granzier H, Sorimachi H, et al. Muscle assembly: A titanic achievement? *Curr Opin Cell Biol* 1999;11:18–25
9. Fürst DO, Osborn M, Nave R, et al. The organization of titin filaments in the half-sarcomere revealed by monoclonal antibodies in immunoelectron microscopy: A map of ten nonrepetitive epitopes starting at the Z line extends close to the M line. *J Cell Biol* 1988;106:1563–72
10. Young P, Ferguson C, Bañuelos S, et al. Molecular structure of the sarcomeric Z-disk: Two types of titin interactions lead to an asymmetrical sorting of alpha-actinin. *EMBO J* 1998;17:1614–24
11. Witt CC, Burkart C, Labeit D, et al. Nebulin regulates thin filament length, contractility and Z-disk structure in vivo. *EMBO J* 2006;25:3843–55

12. Labeit S, Lahmers S, Burkart C, et al. Expression of distinct classes of titin isoforms in striated and smooth muscles by alternative splicing, and their conserved interaction with filamins. *J Mol Biol* 2006;362:664–81
13. Witt CC, Olivieri N, Centner T, et al. A survey of the primary structure and the interspecies conservation of I-band titin's elastic elements in vertebrates. *J Struct Biol* 1998;122:206–15
14. Linke WA, Kulke M, Li H, et al. PEVK domain of titin: An entropic spring with actin-binding properties. *J Struct Biol* 2002;137:194–205
15. Obermann WM, Gautel M, Weber K, et al. Molecular structure of the sarcomeric M band: Mapping of titin and myosin binding domains in myomesin and the identification of a potential regulatory phosphorylation site in myomesin. *EMBO J* 1997;16:211–20
16. Kinbara K, Sorimachi H, Ishiura S, et al. Muscle-specific calpain, p94, interacts with the extreme C-terminal region of connectin, a unique region flanked by two immunoglobulin C2 motifs. *Arch Biochem Biophys* 1997;342:99–107
17. Horowitz R, Kempner ES, Bisher ME, et al. A physiological role for titin and nebulin in skeletal muscle. *Nature* 1986;323:160–4
18. Linke WA, Rudy DE, Centner T, et al. I-band titin in cardiac muscle is a three-element molecular spring and is critical for maintaining thin filament structure. *J Cell Biol* 1999;146:631–44
19. Helmes M, Trombitás K, Granzier H. Titin develops restoring force in rat cardiac myocytes. *Circ Res* 1996;79:619–26
20. Gerull B, Gramlich M, Atherton J, et al. Mutations of TTN, encoding the giant muscle filament titin, cause familial dilated cardiomyopathy. *Nat Genet* 2002;30:201–4
21. Herman DS, Lam L, Taylor MR, et al. Truncations of titin causing dilated cardiomyopathy. *N Engl J Med* 2012;366:619–28
22. Arimura T, Bos JM, Sato A, et al. Cardiac ankyrin repeat protein gene (ANKRD1) mutations in hypertrophic cardiomyopathy. *J Am Coll Cardiol* 2009;54:334–42
23. Lopes LR, Zekavati A, Syrris P, et al. Genetic complexity in hypertrophic cardiomyopathy revealed by high-throughput sequencing. *J Med Genet* 2013;50:228–39
24. Savarese M, Sarparanta J, Vihola A, et al. Increasing role of titin mutations in neuromuscular disorders. *J Neuromuscul Dis* 2016;3:293–308
25. Hackman P, Udd B, Bönnemann CG, et al. Database Consortium. 219th ENMC International Workshop Titinopathies International database of titin mutations and phenotypes, Heemskerk, The Netherlands, 29 April–1 May 2016. *Neuromuscul Disord* 2017;27:396–407.
26. Oates EC, Jones KJ, Donkervoort S, et al. Congenital titinopathy: Comprehensive characterisation and pathogenic insights. *Ann Neurol* 2018;83:1105–24
27. Savarese M, Maggi L, Vihola A, et al. Interpreting genetic variants in titin in patients with muscle disorders. *JAMA Neurol* 2018;75:557–65
28. Chauveau C, Bönnemann CG, Julien C, et al. Recessive TTN truncating mutations define novel forms of core myopathy with heart disease. *Hum Mol Genet* 2014;23:980–91
29. Udd B, Rapola J, Nokelainen P, et al. Nonvacuolar myopathy in a large family with both late adult onset distal myopathy and severe proximal muscular dystrophy. *J Neurol Sci* 1992;113:214–21
30. Partanen J, Laulumaa V, Paljärvi L, et al. Late onset foot-drop muscular dystrophy with rimmed vacuoles. *J Neurol Sci* 1994;125:158–67
31. Edström L, Thornell LE, Albo J, et al. Myopathy with respiratory failure and typical myofibrillar lesions. *J Neurol Sci* 1990;96:211–28
32. Chinnery PF, Johnson MA, Walls TJ, et al. A novel autosomal dominant distal myopathy with early respiratory failure: Clinico-pathologic characteristics and exclusion of linkage to candidate genetic loci. *Ann Neurol* 2001;49:443–52
33. Pfeffer G, Elliott HR, Griffin H, et al. Titin mutation segregates with hereditary myopathy with early respiratory failure. *Brain* 2012;135:1695–713
34. Ohlsson M, Hedberg C, Brådvik B, et al. Hereditary myopathy with early respiratory failure associated with a mutation in A-band titin. *Brain* 2012;135:1682–94
35. Carmignac V, Salih MA, Quijano-Roy S, et al. C-terminal titin deletions cause a novel early-onset myopathy with fatal cardiomyopathy. *Ann Neurol* 2007;61:340–51
36. Ceyhan-Birsoy O, Agrawal PB, Hidalgo C, et al. Recessive truncating titin gene, TTN, mutations presenting as centronuclear myopathy. *Neurology* 2013;81:1205–14
37. Palmio J, Evilä A, Chapon F, et al. Hereditary myopathy with early respiratory failure: Occurrence in various populations. *J Neurol Neurosurg Psychiatry* 2014;85:345–53
38. De Cid R, Ben Yaou R, Roudaut C, et al. A new titinopathy: Childhood-juvenile onset Emery-Dreifuss like phenotype without cardiomyopathy. *Neurology* 2015;85:2126–35
39. Hackman P, Marchand S, Sarparanta J, et al. Truncating mutations in C-terminal titin may cause more severe tibial muscular dystrophy (TMD). *Neuromuscul Disord* 2008;18:922–8
40. Evilä A, Vihola A, Sarparanta J, et al. Atypical phenotypes in titinopathies explained by second titin mutations. *Ann Neurol* 2014;75:230–40
41. Evilä A, Arumilli M, Udd B, et al. Targeted next-generation sequencing assay for detection of mutations in primary myopathies. *Neuromuscul Disord* 2016;26:7–15
42. Vasli N, Laporte J. Impacts of massively parallel sequencing for genetic diagnosis of neuromuscular disorders. *Acta Neuropathol* 2013;125:173–85
43. Chauveau C, Rowell J, Ferreira A. A rising titan: TTN review and mutation update. *Hum Mutat* 2014;35:1046–59
44. Fernández-Marmiesse A, Carrascosa-Romero MC, Alfaro Ponce B, et al. Homozygous truncating mutation in prenatally expressed skeletal isoform of TTN gene results in arthrogyrosis multiplex congenital and myopathy without cardiac involvement. *Neuromuscul Disord* 2017;27:188–92
45. Uruha A, Hayashi YK, Oya Y, et al. Necklace cytoplasmic bodies in hereditary myopathy with early respiratory failure. *J Neurol Neurosurg Psychiatry* 2015;86:483–9
46. Pfeffer G, Joseph JT, Innes AM, et al. Titinopathy in Canadian family sharing the British founder haplotype. *Can J Neurol Sci* 2014;41:90–4
47. Toro C, Olivé M, Dalakas MC, et al. Exome sequencing identifies titin mutations causing hereditary myopathy with early respiratory failure (HMERF) in families of diverse ethnic origins. *BMC Neurol* 2013;13:29
48. Romero NB, Clarke NF. Congenital myopathies. *Handb Clin Neurol* 2013;113:1321–36
49. Bevilacqua JA, Monnier N, Bitoun M, et al. Recessive RYR1 mutations cause unusual congenital myopathy with prominent nuclear internalisation and large areas of myofibrillar disorganization. *Neuropathol Appl Neurobiol* 2011;37:271–84

2.1.2 Publication 2: Common and variable clinical, histological, and imaging findings of recessive *RYR1*-related centronuclear myopathy patients (Abath Neto et al. 2017)

Background

RYR1 encodes the ryanodine receptor 1, a large intracellular Ca²⁺ channel specifically expressed in skeletal muscle, and mediating the Ca²⁺ release from the sarcoplasmic reticulum required to induce muscle contraction (Franzini-Armstrong and Protasi 1997; Fleischer and Inui 1989). *RYR1* mutations have previously been associated with various muscle disorders including dominantly inherited central core disease (CCD), and recessive multi-minicore disease (MmD) and centronuclear myopathies (CNM) (Wilmshurst et al. 2010; Ferreira et al. 2002; Lynch et al. 1999). Functional studies have shown that dominant CCD mutations generate a leaky channel, while recessive MmD and CNM mutations cause a reduction of the ryanodine receptor protein level (Witherspoon and Meilleur 2016).

Aim of the study

This study aimed to identify *RYR1* patients in the MYOCAPTURE cohort, and to provide a comprehensive clinical, histological, and genetic characterization of patients with *RYR1*-related CNM.

Results

We described 21 new patients from 18 families with autosomal recessive *RYR1*-related CNM. 15 families showed a common mutational pattern: a missense mutation on one parental allele, and a truncating mutation on the other allele. These mutations were evenly distributed on the gene with no obvious hotspot. The disease typically manifested with hypotonia at birth, and with a relatively stable proximal muscle weakness at later stages. All patients presented either with ocular defects (ptosis or ophthalmoparesis), facial weakness, or both. Additional skeletal deformities and respiratory involvements were also reported. MRI of six patients revealed that the vastus lateralis muscle was selectively more affected than the other muscles of the thigh. Muscle biopsy analyses showed a high number of centralized nuclei, predominance of type 1 fibers, and irregularities resembling cores as the major histopathological hallmarks. Electron microscopy disclosed that the cores correspond to areas with disruption of the myofibrillar architecture. Our study did not reveal a clear genotype/phenotype correlation with regard to type or location of the mutations since the clinical presentation of patients with one truncating and one missense mutation were as severe as patients carrying two missense mutations.

Conclusion

In this study, we showed that *RYR1*-related CNM is mainly characterized by a relatively stable early-onset proximal and facial/ocular muscle weakness. Dominant *RYR1* mutations are mainly found in the C-terminal region, believed to be a mutational hotspot in patients with *RYR1*-related CCD (Davis et al. 2003). In contrast, we reported 24 novel recessive mutations evenly distributed on the gene, and we confirmed that mutations in a large gene like *RYR1* can efficiently be diagnosed with NGS techniques.

Contribution

I identified and verified the segregation of *RYR1* mutations in one third of the reported patients.



Common and variable clinical, histological, and imaging findings of recessive *RYR1*-related centronuclear myopathy patients

Osorio Abath Neto ^{a,b,c}, Cristiane de Araújo Martins Moreno ^a, Edoardo Malfatti ^d, Sandra Donkervoort ^c, Johann Böhm ^b, Júlio Brandão Guimarães ^e, A. Reghan Foley ^c, Payam Mohassel ^c, Jahannaz Dastgir ^c, Diana Xerxes Bharucha-Goebel ^c, Soledad Monges ^f, Fabiana Lubieniecki ^f, James Collins ^g, Līvijā Medne ^h, Mariarita Santi ⁱ, Sabrina Yum ^j, Brenda Banwell ^j, Emmanuelle Salort-Campana ^k, John Rendu ^l, Julien Fauré ^l, Uluc Yis ^m, Bruno Eymard ⁿ, Chrystel Cheraud ^b, Raphaël Schneider ^{b,o}, Julie Thompson ^o, Xaviere Lornage ^b, Lilia Mesrob ^p, Doris Lechner ^p, Anne Boland ^p, Jean-François Deleuze ^p, Umbertina Conti Reed ^a, Acary Souza Bulle Oliveira ^q, Valérie Biancalana ^{b,r}, Norma B. Romero ^d, Carsten G. Bönnemann ^c, Jocelyn Laporte ^b, Edmar Zanoteli ^{a,*}

^a Departamento de Neurologia, Faculdade de Medicina da Universidade de São Paulo (FMUSP), São Paulo, Brazil

^b Department of Translational Medicine and Neurogenetics, IGBMC, INSERM U964, CNRS UMR7104, University of Strasbourg, Illkirch, France

^c Neuromuscular and Neurogenetic Disorders of Childhood Section, National Institutes of Health, Bethesda, MD, USA

^d Center for Research in Myology, Sorbonne University, Pitié-Salpêtrière Hospital Group, Paris, France

^e Department of Radiology, DASA Laboratory, São Paulo, Brazil

^f Servicio de Neurología y Servicio de Patología, Hospital de Pediatría Garrahan, Buenos Aires, Argentina

^g Department of Neurology, Cincinnati Children's Hospital Medical Center, Cincinnati, OH, USA

^h Individualized Medical Genetics Center, Division of Human Genetics, Department of Pediatrics, Children's Hospital of Philadelphia, Philadelphia, PA, USA

ⁱ Department of Pathology, The Children's Hospital of Philadelphia, Philadelphia, PA, USA

^j Department of Pediatrics, Division of Neurology, The Children's Hospital of Philadelphia, Philadelphia, PA, USA

^k APHM, Dept. Neurology, Neuromuscular & ALS Reference Center, La Timone Univ. Hospital, France Aix Marseille Université, INSERM, GMGF, Marseille, France

^l Dept. Biochemistry, Molecular Biochemistry & Genetics, Toxicology & Pharmacology, Grenoble Alpes University, GIN Inst. Neurosciences, Grenoble, France

^m Division of Child Neurology, Department of Pediatrics, School of Medicine, Dokuz Eylül University, İzmir, Turkey

ⁿ Paris-Est Neuromuscular Center, APHP – GH Pitié-Salpêtrière, Paris, France

^o Department of Computer Science, ICube, UMR 7357, CNRS, Strasbourg, France

^p Centre National de Génotypage, Institut de Génomique, CEA, Evry, France

^q Setor de Doenças Neuromusculares, Departamento de Neurologia, Universidade Federal de São Paulo (UNIFESP), São Paulo, Brazil

^r Faculté de Médecine, Laboratoire de Diagnostic Génétique, Nouvel Hopital Civil, Strasbourg, France

Received 19 December 2016; received in revised form 10 May 2017; accepted 25 May 2017

Abstract

Mutations in *RYR1* give rise to diverse skeletal muscle phenotypes, ranging from classical central core disease to susceptibility to malignant hyperthermia. Next-generation sequencing has recently shown that *RYR1* is implicated in a wide variety of additional myopathies, including centronuclear myopathy. In this work, we established an international cohort of 21 patients from 18 families with autosomal recessive *RYR1*-related centronuclear myopathy, to better define the clinical, imaging, and histological spectrum of this disorder. Early onset of symptoms with hypotonia, motor developmental delay, proximal muscle weakness, and a stable course were common clinical features in the cohort. Ptosis and/or ophthalmoparesis, facial weakness, thoracic deformities, and spinal involvement were also frequent but variable. A common imaging pattern consisted of selective involvement of the vastus lateralis, adductor magnus, and biceps brachii in comparison to adjacent muscles. In addition to a variable prominence of central nuclei, muscle biopsy from 20 patients showed type 1 fiber predominance and a wide range of intermyofibrillary architecture abnormalities. All families harbored compound heterozygous mutations, most commonly a truncating mutation combined with a missense mutation. This work expands the phenotypic characterization of patients with recessive *RYR1*-related centronuclear myopathy by highlighting common and variable clinical, histological, and imaging findings in these patients.

© 2017 Elsevier B.V. All rights reserved.

Keywords: *RYR1*; Centronuclear myopathy; Congenital myopathies

* Corresponding author. Departamento de Neurologia, Av. Dr. Enéas de Carvalho Aguiar 255, 5 andar, sala 5131, Cerqueira Cesar, Sao Paulo 05403-900, Brazil.
E-mail address: edmar.zanoteli@usp.br (E. Zanoteli).

1. Introduction

Centronuclear myopathy (CNM) is a form of congenital myopathy, a heterogeneous group of primary hereditary skeletal muscle disorders characterized by congenital or early onset of manifestations, relatively stable course (i.e. absence of overt progression or at the most slow progression over prolonged periods), normal or slightly elevated serum creatine kinase (CK) levels, and characteristic structural abnormalities in skeletal muscle biopsies [1]. Prominence of centralized nuclei in a large number of muscle fibers distinguishes CNM from other typical congenital myopathies. However, typical pathologic features of congenital myopathy such as type 1 fiber predominance, and other specific findings such as necklace-fibers and radiating sarcoplasmic strands may also be seen [2]. It has classically been grouped into autosomal dominant (AD), X-linked recessive (XLR), and autosomal recessive (AR) forms, but most often it is found in a sporadic fashion, leaving the mode of inheritance unclear in an individual patient until a firm molecular diagnosis is established. AD CNM is associated with *DNM2* (MIM *602378), *BINI* (MIM *601248), and *CCDC78* (MIM *614666); XLR CNM, also called myotubular myopathy (MTM), has *MTM1* (MIM *300415) as the implicated gene, while some AR forms are caused by *BINI* (MIM *601248) or *SPEG* (MIM *615950).

Before the advent of next-generation sequencing, *RYR1* (MIM *180901) mutations were found in some sporadic AR cases of CNM. *RYR1* mutations cause several phenotypes such as central core disease, King–Denborough syndrome, and susceptibility to malignant hyperthermia and rhabdomyolysis. *RYR1* codes for the ryanodin calcium channel, which is located on the sarcoplasmic reticulum and is involved in the excitation–contraction coupling. Upon membrane depolarization, conformational changes of the dihydropyridine channel (DHPR) on the T-tubule trigger calcium release through the ryanodine receptor and subsequent contraction. In 2010, a definite association of CNM with *RYR1* was established [3], while a parallel study demonstrated a novel histopathological pattern showing muscle fibers with large, poorly defined areas of myofibrillar disorganization and internal nuclei associated with recessive *RYR1* mutations [4]. In both studies, patients showed an intermediate severity between MTM and AD CNM. After the introduction of high-throughput sequencing technology, which made it possible to routinely sequence all 106 exons of *RYR1*, mutations in this gene have been found with increasing frequency in neuromuscular disorder cohorts [5,6].

In this work, we characterize a large series of patients with a histological diagnosis of CNM who were found to harbor recessive mutations in *RYR1*. This new series in AR *RYR1*-related CNM shows a wider phenotypic and genotypic variability than previously reported, and supports histological and imaging findings associated with this diagnosis.

2. Patients and methods

To assemble a cohort of recessive *RYR1*-related patients with a clinical diagnosis of congenital myopathy and histological features compatible with CNM, an international collaboration

of multiple centers was established. In Brazil, patients were recruited after muscle biopsy reports between January 2008 and December 2013, and totaling around 2500 patient samples in two large referral neuromuscular centers in the city of Sao Paulo were screened for the presence of CNM. An expert muscle biopsy pathologist then reviewed the slides and noted the salient features. The patients were then recruited for an initial outpatient consultation and parents were invited to participate in the study after informed consent was obtained. Blood samples were taken from patients and parents for DNA extraction, and patients were Sanger sequenced to evaluate *DNM2*, *MTM1*, and *BINI*. Families not harboring pathogenic variants in these genes were subjected to whole exome sequencing (WES) and analyzed within the scope of the Myocapture project, a collaborative ongoing effort aiming to uncover new gene associations via whole exome sequencing of 1000 individuals from families with myopathy without a molecular diagnosis after excluding commonly implicated genes with Sanger sequencing.

Along with Brazilian patients, additional families from France and Turkey were found in the Myocapture project to be affected with recessive *RYR1*-related CNM and were included in this study. From the National Institutes of Health (NIH), Bethesda, MD, USA, we incorporated patients who were diagnosed through targeted *RYR1* gene screening after clinical and histological assessments, including two patients (L.1 and N.1) who were previously published in a cohort of early onset *RYR1*-related myopathies, focusing on the characterization of phenotypes [7].

2.1. Clinical evaluation

Patients were evaluated either directly via enrollment in the study or their clinical notes were obtained and reviewed. Data included medical history (gestational, neonatal, and developmental history), and general physical and neurological examination. Motor strength was graded using the Medical Research Council (MRC) scale. Results of ancillary exams such as CNS imaging, nerve conduction studies and electromyography, serum CK levels, pulmonary function tests, polysomnography, EKG and echocardiogram, when available, were noted. Informed consent and age appropriate assent was obtained from all participants. Blood samples and tissue were obtained as part of the standard clinical evaluation of patients.

2.2. Histological analysis

All biopsies had been collected using an open technique in the biceps brachii, deltoid or quadriceps muscles, and had the following staining and histochemistry studies available: hematoxylin and eosin (HE), modified Gömöri trichrome (GO), periodic acid–Schiff (PAS), oil-red O (ORO), NADH tetrazolium reductase (NADH-TR), cytochrome C oxidase (COX), succinate dehydrogenase (SDH), and ATPase in three different pH values: 9.4, 4.6 and 4.3. Slides were reviewed by an expert muscle pathologist to note the following histological aspects: fiber size variability, amount of endomysial and perimysial connective tissue (graded into mild, moderate or marked); proportion of

fibers with nuclear centralization or internalization, and fiber type distribution (graded in percentages); slides were also evaluated for the presence or absence of fiber type disproportion, radiating sarcoplasmic strands (RSS), necklace fibers, connective tissue alterations and/or intermyofibrillar network abnormalities.

2.3. Muscle imaging

Some patients had select muscles evaluated by neuromuscular experts via muscle ultrasound, using a Philips ACUSON S2000 Ultrasound System, with settings adjusted for optimal skeletal muscle visualization, which are available upon request. Muscles were graded using the Heckmatt scale of muscle echogenicity from 1 (normal) to 4 (severely affected): deltoids, biceps, triceps, quadriceps (rectus femoris and vastus lateralis), gracilis, adductors, hamstrings, tibialis anterior, soleus, gastrocnemius, and paraspinal muscles [8].

Muscle MRI was available for six patients. Images were acquired in the axial plane, with STIR and T1-weighted FSE sequences. Areas of interest were studied in seven regions: right and left arms (TR = 450 ms; TE = minimal; FOV = 20 cm; width = 7 mm; gap = 0.5 cm), right and left forearms (TR = 450 ms; TE = minimal; FOV = 16 cm; width = 7 mm; gap = 0.5 cm), and hips, thighs and legs (TR = 600 ms; TE = minimal; FOV = 35 cm; gap = 1 cm), with a total estimated exam time of one hour. Muscles were evaluated by an expert neuromuscular radiologist and graded in a scale of fatty replacement of muscle [9] from 1 (normal appearance) to 4 (severe involvement). One patient had computed tomography scan of upper and lower limbs, and relative muscle involvement was also subjectively graded based on the degree of fatty degeneration by a radiologist on a scale from 1 (normal) to 4 (severely affected).

2.4. Sanger sequencing

Patients included in the Myocapture project had all exons of the *DNM2*, *MTM1* and *BIN1* genes Sanger-sequenced. Exons were PCR amplified using oligonucleotides and protocols that are available upon request, and the resulting PCR product was sequenced using an ABI 3130 Genetic Analyzer (Applied Biosystems, Foster City, CA). Sequences obtained were analyzed using the software *Mutation Surveyor Demo V3.20*, in comparison with the wild type sequence of the genes. Variants identified were compared to the *DNM2*, *MTM1*, and *BIN1* gene variant databases, curated in a Leiden Open Variation Database (LOVD) system (available at <http://www.dmd.nl/>), as well as the Human Gene Mutation Database (HGMD), public version (available at <http://www.hgmd.org/>). To exclude novel variants as possible polymorphisms, these were compared to human variant frequency databases, such as EVS (<http://evs.gs.washington.edu/EVS/>) and ExAC (<http://exac.broadinstitute.org/>), as well as to historical data on the sequencing of these genes in more than 100 individuals at the lab where the sequencing was performed.

2.5. Next-generation sequencing

Diagnosis of four US patients followed at NIH was carried out via targeted *RYR1* sequencing using a high-throughput

sequencing approach. All other patients were initially excluded for the most common known genes implicated in CNM and then included in the Myocapture project. Subsequently they underwent whole exome sequencing using methods with details available upon request. In short, after quality control, 4 µg of genomic DNA was degraded into 200 base pair fragments via sonication, capture was done using an Agilent SureSelect All Exon V5 kit from Agilent (Santa Clara, CA), and sequencing was performed in HiSeq 2000 sequencers from Illumina (San Diego, CA). FASTQ sequences were mapped against the hg19/GRCh37 reference genome using the bwa tool (<http://bio-bwa.sourceforge.net>), nomenclature coherence control and elimination of duplicates in BAM files was done using the SamTools (<http://samtools.sourceforge.net>) and PicardTools (<http://picardtools.sourceforge.net>) software suites. Variant calling was performed using GATK (<http://www.broadinstitute.org/gatk/>), and annotation of variants used SnpEff (<http://snpeff.sourceforge.net>) and SnpSift (<http://snpeff.sourceforge.net/SnpSift.html>). For the analysis and filtering of variants, the primary author developed a solution using perl scripts to parse VCF files into MySQL databases, and subsequently used SQL scripts in a database management system. A minimum allele frequency (MAF) of 0.5% in the Exome Aggregate Consortium dataset (<http://exac.broadinstitute.org>) was used as the threshold for polymorphisms. Pathogenic mutations identified after exome analysis were confirmed in the proband and tested for allelic segregation in parents via Sanger sequencing.

3. Results

A total of 21 patients from 18 families were included in this study. Twelve patients from 9 Brazilian families were diagnosed with AR *RYR1*-related CNM after WES in the Myocapture project. Analysis of around 400 exomes from the Myocapture project yielded another 5 sporadic *RYR1*-CNM cases, of which two families were from Argentina, two from France, and one from Turkey. The remaining 4 cases, also sporadic, were US cases evaluated at the NIH.

3.1. Clinical aspects

There was a wide variability in the clinical presentation of patients in this cohort, but a few common aspects can be highlighted (Table 1). In almost all patients hypotonia and/or motor delay were observed either during the first year of life or in early childhood. Only one individual (patient I.1) presented with frequent falls as their initial symptom. Patients tended to eventually achieve all motor milestones and followed a stable clinical course, albeit with a propensity to slightly worsen in motor function over time. This was more readily seen in older patients (C.1). Patient ages in Table 1 correspond to the most recent clinical visit reported in their notes or the age at which they were examined by the primary investigators of this study upon enrollment. All adult patients had clinical notes available from their teenage years. On the most severe end of the spectrum, two female patients were never able to stand or walk (M.1 and R.1), one was never able to walk independently (K.1), and another was the only one to lose independent ambulation at

Table 1
Clinical features of compound *RYR1*-related CNM patients.

Patient	Sex/Age (years)	Origin	Presentation	Motor function	P/O	Fac/Bulb	Neck/Resp	Thor/Sp	Other signs
A.1	M/5	Brazil	H, MD	Walking	Y/N	Y/Y	Y/N	PE/N	Mild heel contractures
A.2	F/12	Brazil	H, MD	Walking	Y/N	N/N	N/N	N/N	No
B.1	M/12	Brazil	H, MD	Walking	N/N	Y/N*	Y/N	PE/K,L,WS	Calf hypertrophy
B.2	F/7	Brazil	H, MD	Walking	N/N	Y/N	Y/Y	N/L,WS	Calf hypertrophy
C.1	M/51	Brazil	MD	Support	N/Y	Y/Y	Y/N	N/S	Calf hypertrophy, multiple contractures
C.2	F/43	Brazil	MD	Walking	N/Y	Y/Y	Y/Y	D/S,L	Multiple contractures
D.1	M/16	Brazil	H, MD	Walking	N/Y	Y/N	N/Y	PE/RS,WS	Multiple contractures
E.1	F/6	Brazil	H, MD	Walking	N/Y	N/N	N/N	PE/N	No
F.1	F/10	Brazil	H, MD	Walking	N/N	Y/Y	Y/Y	D/K,WS	No
G.1	F/5	Brazil	H, MD	Walking	Y/N	Y/Y	Y/Y	N/N	No
H.1	F/40	Brazil	MD	Walking	N/Y	N/N	N/N	N/N	No
I.1	M/26	Brazil	Frequent falls	Walking	N/Y	Y/N	N/Y	D,PE/RS,S	No
J.1	M/8	Argentina	H, MD	Walking	Y/Y	N/N	Y/N	PE/N	No
K.1	F/8	Argentina	H, MD	Never walked	Y/Y	Y/N	N/N	N/RS	Calf hypertrophy
L.1	F/6	USA	H, MD	Walking	Y/Y	Y/N	Y/Y	N/RS,L,WS	Lower extremities contractures
M.1	F/26	USA	H	Never walked	Y/Y	Y/N	Y/Y	N/RS	Multiple contractures
N.1	F/4	USA	H	Walking	N/N	Y/Y	Y/N	N/RS,S	Multiple contractures
O.1	F/1	USA	H	Sits without support	Y/N	Y/Y	Y/Y	PC/K,S	Tracheostomy, nasogastric tube, distal hyperlaxity
P.1	M/54	France	MD	Walking	Y/Y	Y/N	Y/N	N/L	No
Q.1	F/29	France	MD	Wheelchair at 9 years	N/Y	Y/N	Y/Y	N/S	Diffuse hyperlaxity, hip luxation
R.1	F/3	Turkey	H	Never walked	N/Y	Y/Y	Y/Y	D,PE/S	Tracheostomy, nasogastric tube, multiple contractures

M: male, F: female, Bulb: bulbar weakness; D: depression/flattening of thorax; Fac: facial weakness; H: hypotonia; K: kyphosis; L: lordosis; MD: motor delay; Neck: neck flexor weakness; O: ophthalmoparesis; P: ptosis; PC: pectus carinatum; PE: pectus excavatum; Resp: respiratory involvement; RS: rigid spine; S: scoliosis; Sp: spine deformities; Thor: thoracic deformities; WS: winged scapulae; y: years.

* Only during infancy.

9 years of age (Q.1), after starting to walk. While O.1 remains non-ambulant at 19 months of age, it is still early to conclude that she will not achieve that milestone.

All patients had predominantly proximal muscle weakness. Although most had some additional involvement of distal muscle groups, distal weakness was as severe as proximal weakness in only 4 (M.1, O.1, Q.1, and R.1). Interestingly, these were overall severely affected, non-ambulant patients. Muscle strength comparison in agonist/antagonist groups showed that biceps brachii was more involved than triceps, quadriceps was weaker than knee flexors, and hip abductors were weaker than adductors in most patients. Hip extension and hip flexion involvement did not follow a consistent pattern, and different distal muscle groups tended to be affected to the same degree. For example, wrist extension was as weak as wrist flexion, or foot dorsiflexion was as weak as plantar flexion.

Facial and ocular muscles were also frequently involved. Of the 21 patients in the cohort, 9 had ptosis, 13 showed different degrees of ophthalmoparesis, and 17 were found to have facial weakness. All patients had either ocular or facial involvement. Nine reported difficulties swallowing, with varying degrees of severity, ranging from mild dysphagia restricted to the first year of life (B.1) to a patient who, in spite of improving strength otherwise, still requires a nasogastric tube for feeding at 3 years of age (R.1).

Thoracic deformities of varying degrees of severity were observed in 10 patients (Fig. 1). Seven had pectus excavatum, two had unilateral flattening of the chest, and one had both signs.

Spine involvement was variable, but consistent within families. While family A had no changes, both patients from family B had lordosis and scapular winging, and both from family C had scoliosis. Six patients did not have spinal deformities or scapular winging, while the remaining had various combinations of spine involvement: a total of 5 had lordosis, 7 had scoliosis, and 6 had a rigid spine. Five patients showed scapular winging (Fig. 1B). Calf hypertrophy was seen in 4 patients, while varying degrees of contractures were noted in 8. Most patients (15) had neck muscle weakness predominantly characterized by neck flexion weakness.

Respiratory compromise was found in 11 patients, of which 4 had clinical nocturnal hypoventilation symptoms. Patients with pulmonary function tests showing a decrease in forced vital capacity to less than 70% of age and sex-matched controls were considered to have respiratory compromise. There was no direct correlation between the presence of respiratory compromise and age, and the presence of thoracic or spine deformities.

Normal to slightly elevated serum CK level was a consistent feature in the cohort. No patient had cardiac abnormalities detected on EKG or echocardiogram, when results were available.

3.2. Histological aspects

All patients except for B.2 had a muscle biopsy performed as part of their diagnostic workup, the main features of which are summarized in Table 2. The age at which biopsies were done



Fig. 1. Clinical features of *RYRI*-related CNM patients. Skeletal involvement can be present in various forms and combinations in different patients. Patient F.1 had flattening of right hemithorax (A), associated with scapular winging (B) and thoracic kyphosis (C). Patient D.1 showed pectus excavatum (E) and rigid spine (F), which was also found in Patient I.1 (H). Lumbar lordosis could be observed in Patient B.1 (G). Ocular findings are frequent, most often ptosis and ophthalmoparesis, illustrated in Patient L.1 as restricted left eye abduction on leftward gaze, with normal right eye adduction (D).

ranged from the neonatal period up to late adult life. Muscles chosen as biopsy sites were roughly evenly distributed among patients, and there did not seem to be an association between histology findings and the individual choice of sites. Of samples

on which histochemical reactions that differentiate fiber types were available, all but one (A.2) had type 1 fiber predominance, and all but two (A.2 and G.1) had fiber type disproportion, where type 1 fibers were smaller than type 2 fibers. All samples

Table 2
Muscle biopsy features of compound *RYRI*-related CNM patients.

Patient	Age at biopsy (years)	Biopsied muscle	% centralization/internalization	% type 1 fibers	Fiber type disproportion	Variability	Fatty/Connective tissue	IMA abnormalities
A.1	0.5	Deltoid	30	70	Yes	Moderate	No	No
A.2	6	Deltoid	30	50	No	Mild	No	Yes
B.1	5	Deltoid	40	70	Yes	Moderate	Mild	Yes
C.1	44	Deltoid	90	80	Yes	Marked	Moderate	Yes
C.2	37	Deltoid	90	80	Yes	Marked	Moderate	Yes
D.1	13	Biceps brachii	70	70	Yes	Marked	Moderate	Yes
E.1	3	Biceps brachii	40	70	Yes	Mild	Mild	Yes
F.1	2	Biceps brachii	50	90	Yes	Moderate	No	No
G.1	2.5	Deltoid	30	60	No	No	Mild	Yes
H.1	38	Biceps brachii	70	70	Yes	Mild	No	Yes
I.1	12	Biceps brachii	50	70	Yes	Marked	Mild	Yes
J.1	1	Vastus lateralis	20	80	Yes	Mild	Moderate	Yes
K.1	2.8	Vastus lateralis	60	80	Yes	Mild	Mild	No
L.1	2.5	Biceps brachii	20	90	Yes	Mild	Mild	Yes
M.1	0.5	Vastus lateralis	NA	NA	NA	Marked	Marked	No
N.1	0.1	Biceps brachii	30	80	Yes	Marked	Marked	Yes
O.1	0.04	Vastus lateralis	NA	NA	NA	Marked	Mild	NA
P.1	8	Deltoid	20	100	Yes	Moderate	Mild	Yes
Q.1	NA	NA	70	100	Yes	Mild	Mild	Yes
R.1	1	Vastus lateralis	70	NA	NA	NA	Marked	NA

IMA: intermyofibrillary network, NA: not available.

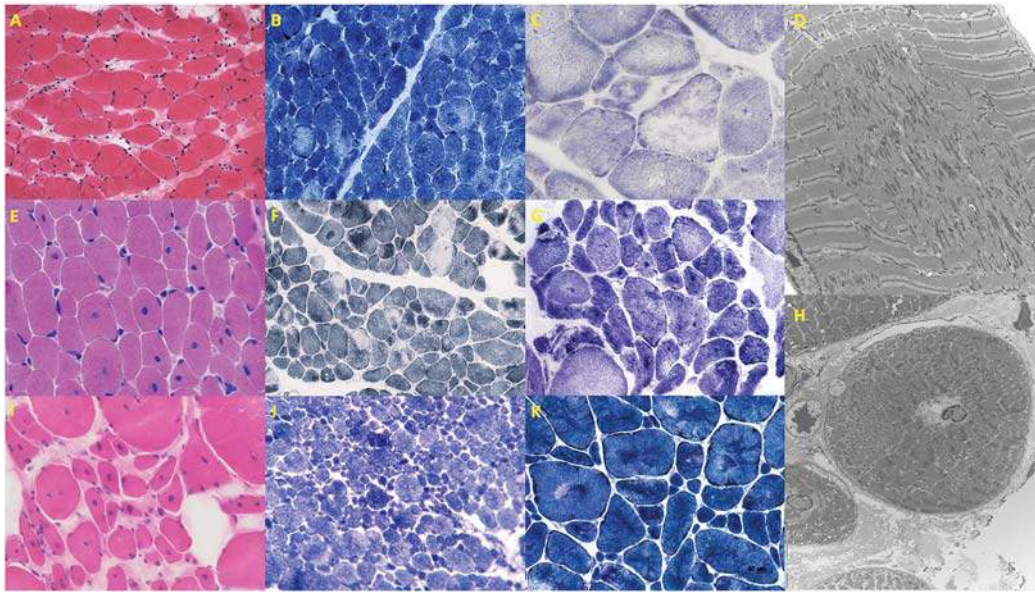


Fig. 2. Muscle histology of *RYR1*-related CNM patients. Histochemistry of biopsies showed, in addition to prominent nuclear centralization and internalization that tended to increase with age of biopsy (A, E, I), the presence of oxidative activity irregularities (B, C, F, G, and K), suggesting intermyofibrillary architectural disorganization. Electron microscopy showed complete sarcomeric disarray in areas corresponding to the oxidative activity abnormalities (D, H). A: HE, 20× objective; B, G, and K: NADH, 40×; C: SDH, 40×; E and I: HE, 40×; F: SDH, 20×; J and K: NADH, 20×; A and F: patient L.1; B and E: patient E.1; C: patient C.2; D, H, and K: patient P.1; G: patient I.1; I: patient C.1; J: patient J.1.

had an increase in the proportion of fibers with nuclear centralization or internalization, ranging from 20 to 90% of the total amount of fibers in muscle sections. We did not find RSS or necklace fibers, histological markers typical of other forms of CNM, in this muscle biopsy series.

Eleven samples had at least moderate increase in the variability of fiber size and seven showed moderate proliferation of fatty and/or connective tissue. The degree of fiber size variability and extent of connective tissue, as well as the percentage of fibers with centralized nuclei, tended to increase with age at which biopsy was taken. Fig. 2 illustrates the percentage of fibers with centralized nuclei and connective tissue content at different ages (Fig. 2, A, D, and G: ages 2.5 years, 3 years, and 44 years, respectively, for patients L.1, E.1, and C.1).

Intermyofibrillar network abnormalities (IMA), demonstrated in oxidative stains as irregular areas sometimes reminiscent of minicore, moth-eaten fibers, or core-like structures, were observed in most biopsies (14/20, but in two biopsies the data were unavailable). There was a slight increase in number and distinctiveness of the abnormalities with increasing age at the time of biopsy. While patient J.1's biopsy, done at 1 year of age, shows sparse rare disruptions in the IMA (Fig. 2, H), P.1's biopsy at 8 years and I.1's biopsy at 12 years shows frequent core/targetoid areas (Fig. 2, F and I). However, biopsies of patients C.2 (Fig. 2, C) and L.1 (Fig. 2, E) showed a very similar proportion of fibers with washed-out internal architecture, despite having been sampled at ages 37 and 2.5 years, respectively. Electron microscopy in a French patient showed that areas with disruptions of the IMA corresponded to a complete disarray of normal sarcomeric structures (Fig. 2, D and H).

3.3. Imaging aspects

Skeletal muscle imaging data were available for 10 patients, and results can be found in Table 3. Six patients had skeletal muscle magnetic resonance imaging (MRI), 3 had muscle ultrasound (US) imaging, and 1 had computerized tomography (CT).

With the exception of patient F.1, with mild to moderate and almost uniform involvement of different muscle groups, and patient M.1, with near complete fibro-fatty replacement of several muscle groups, a few common patterns of muscle involvement emerged, despite variable severity among various patients.

Vastus lateralis was the muscle that tended to be the most involved overall, and in particular it was systematically more affected than the rectus femoris in all patients but F.1 and M.1 (Fig. 3). Rectus femoris was prone to be less affected distally. In the medial compartment of the thigh, the adductor magnus was more affected than the adductor longus and gracilis in seven patients. Anterior and posterior compartments of the leg showed similar changes in most patients, but the soleus seemed to be more affected than the gastrocnemii in only a few (B.2, D.1, and F.1, Fig. 3). The biceps brachii was at least as involved, and often consistently more so than the triceps, except for patient L.1.

3.4. Molecular aspects

Analyses of high throughput sequencing data revealed compound heterozygous mutations in *RYR1* in all 18 families (Table 4). Sixteen families had compound heterozygous

Table 3

Muscle imaging severity chart for selected patients. Scores vary from 1 to 4, where 1 is least affected and 4 markedly affected. For US, the Heckmatt scale was used. For MRI and CT, muscles were graded according to Mercuri et al. (2002) [9].

Patient	Exam	Rectus femoris	Vastus lateralis	Sartorius	Adductor magnus	Adductor longus	Gracilis	Tibialis anterior	Soleus	Gastrocnemius lateralis	Biceps brachii	Triceps	Deltoids	Hamstrings	Paraspinals
B.1	MRI	3	4	4	4	3	3	3	3	3	3	2	3	3	3
B.2	MRI	3	4	3	4	3	3	3	4	3	3	2	2	3	3
D.1	MRI	3	4	2	4	3	2	3	4	3	3	2	2	3	3
F.1	MRI	2	2	2	2	2	2	2	3	2	2	1	2	2	2
G.1	MRI	3	4	4	4	3	3	3	3	3	2	2	2	3	3
I.1	US	2	3	1	3	2	1	2	3	3	3	2	3	3	3
L.1	US	3	4	3	4	3	2	3	3	3	1	2	2	3	4
M.1	MRI	4	4	4	4	4	4	4	4	4	4	4	3	4	4
N.1	US	3	4	4	4	4	4	1	3	3	3	3	4	3	4
P.1	CT	2	3	2	3	2	2	2	3	3	3	2	2	3	2

MRI: magnetic resonance imaging; US: ultrasound; CT: computed tomography.

mutations involving a truncating variant (frameshift, stop gain, or splice site disrupting) in addition to a missense variant. Of note, in two of these families, one missense variant was shown to also disrupt adjacent primary splice sites using splice effect predictor tools: p.Arg1075Gln creates a new acceptor in exon 25 in families F and I and p.Gly2343Ser affects the donor

splicing site at the end of exon 43 in family E. The remaining 2 families harbored two missense variants. Sanger sequencing of additional family members confirmed that each variant segregated from a heterozygous parent. Patient P.1 was the only one to have a *de novo* mutation (the splice site mutation c.6891 + 1G>T).

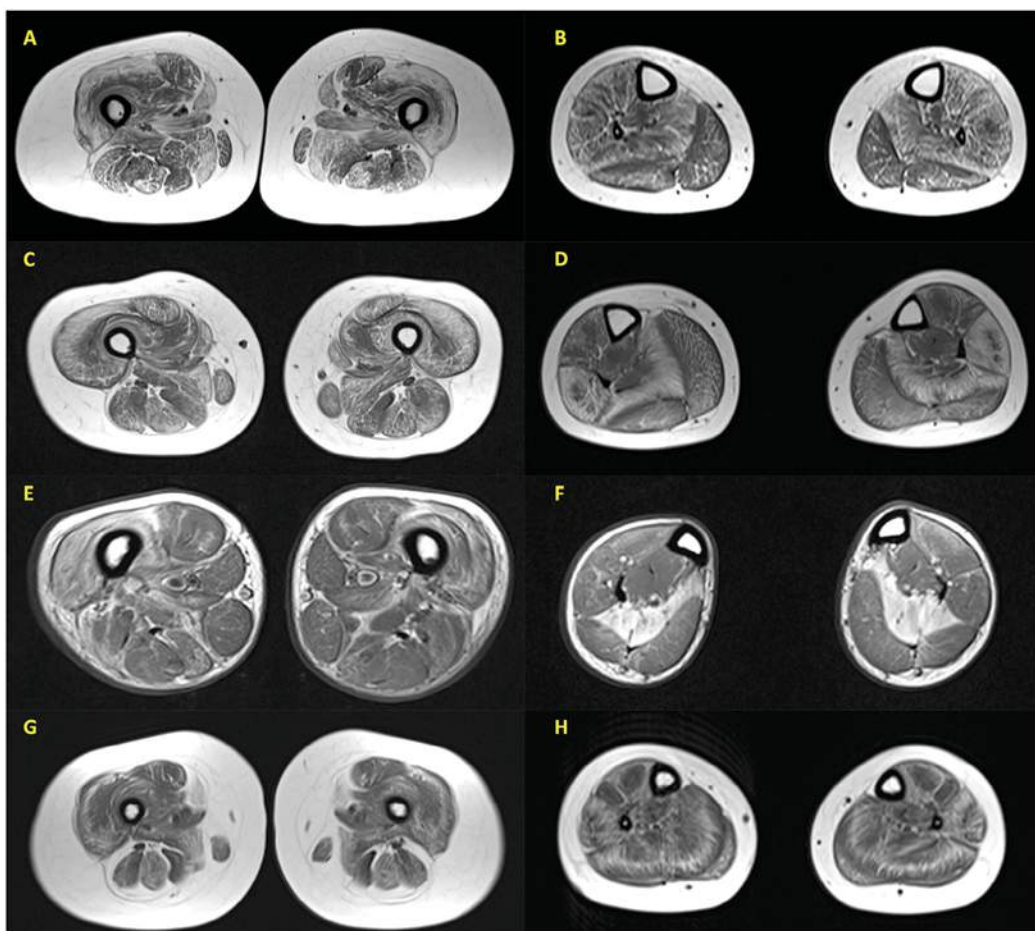


Fig. 3. MRI imaging of the lower limbs of *RYR1*-related CNM patients. At the level of the thighs, in the four patients shown, vastus lateralis is selectively more affected than the rectus femoris (A, C, E, and G). At the level of the legs, anterior and posterior compartments seemed to be affected in a similar degree, but the soleus muscle was selectively more involved in a few patients (D, F). T1-weighted FSE sequence MRI at the level of the thighs (A, C, E, G) and legs (B, D, F, H); patients B.1 (A, B), B.2 (C, D), D.1 (E, F) and G.1 (G, H).

Table 4
Mutations in *RYR1* identified in the CNM cohort.

Family	Exon/Intron	cNomen	pNomen	Type	Effect
A	14	c.1576 + 1G>A		Novel	ss
	44	c.7093G>A	p.Gly2365Arg	Novel	mis
B	42	c.6797-6_6798del		Novel	ss
	66	c.9892G>A	p.Ala3298Thr	Novel	mis*
C	33	c.4837C>T	p.Gln1613*	Novel	stop
	26	c.3523G>A	p.Glu1175Lys	Novel	mis
D	65	c.9611C>T	p.Ala3204Val	Novel	mis
	101	c.14545G>A	p.Val4849Ile	Known [10–16]	mis
E	43	c.7027G>A	p.Gly2343Ser	Novel	mis, ss
	94	c.13672C>T	p.Arg4558Trp	Novel	mis
F	25	c.3224G>A	p.Arg1075Gln	Novel	mis, ss
	74	c.10882C>G	p.Arg3628Gly	Novel	mis
G	8	c.725G>A	p.Arg242Lys	Novel	mis
	69	c.10348-6C>G		Known [15]	ss
H	42	c.6797-6_6798del		Novel	ss
	13	c.1342A>T	p.Ile448Phe	Novel	mis
I	25	c.3224G>A	p.Arg1075Gln	Novel	mis
	26	c.3523G>A	p.Glu1175Lys	Novel	mis
J	93–100			Novel	md
	101	c.14524G>A	p.Val4842Met	Known [3,4,15,17]	mis
K	53	c.8372del	p.Leu2791Argfs*23	Novel	fs
	101	c.14545G>A	p.Val4849Ile	Known [10–16]	mis
L	39	c.6295_6351dup	p.Ser2099-Val2117dup	Known [7]	if
	85	c.11763C>A	p.Tyr3921*	Known [7,13,17]	stop
M	101	c.14524G>A	p.Val4842Met	Known [3,4,15,17]	mis
	75	c.10946_10947insC	p.Cys3650Metfs*2	Novel	fs
N	12	c.1201C>T	p.Arg401Cys	Known [7,18–20]	mis
	47	c.7463_7475del	p.Pro2488Hisfs*39	Known [7]	fs
O	100	c.14416A>G	p.Asn4806Asp	Known [17]	mis
	28	c.3866G>C	p.Arg1289Pro	Novel	mis
P	4	c.325C>T	p.Arg109Trp	Known [13,17]	mis
	42	c.6891 + 1G>T		Novel	ss
Q	26	c.3523G>A	p.Glu1175Lys	Novel	mis
	34	c.5444del	p.Leu1815Argfs*36	Novel	fs
R	20	c.2500_2501dup	p.Pro836Glyfs*49	Novel	fs
	50	c.8024C>A	p.Thr2675Lys	Novel	mis

cNomen: cDNA nomenclature; pNomen: protein nomenclature; fs: frameshift variant; if: in-frame variant; md: macrodeletion; mis: missense variant with pathogenic prediction; ss: primary splice site disrupting variant; stop: stop gain variant.

* Unclear pathogenicity.

Variants were either not present in ExAC or were found with MAFs lower than 0.001, and none occurred in a homozygous state. Missense variants had strong pathogenicity prediction in tools such as PolyPhen-2 (<http://genetics.bwh.harvard.edu/pph2/>), SIFT (<http://sift.jcvi.org>), and CADD (<http://cadd.gs.washington.edu>), except for variant p.Ala3298Thr, found in family B, where pathogenicity prediction tools had conflicting results. Population frequency of this variant was extremely low (MAF of 0.0001).

The total number of unique variants found in the families was 30, of which 9 were known pathogenic mutations causative of congenital myopathies related to *RYR1* and the remaining were previously unreported. Of the known mutations, one (p.Arg401Cys, in family N) had been previously implicated in susceptibility to malignant hyperthermia, but neither she nor her family has a history of such episodes, albeit there was no exposure of immediate family members to anesthesia with halogenated anaesthetics or neuromuscular blocking agents. Mutations found in more than one family included the novel

variants c.6797-6_6798del (families B and H), p.Glu1175Lys (C, I, and Q), p.Arg1075Gln (F and I), as well as the known variants p.Val4849Ile (D and K) and p.Val4842Met (J and M).

Mutations were found throughout the entire length of *RYR1*, spanning exons 4 up to 101.

4. Discussion

This study was instituted as an international collaborative effort to characterize a cohort of AR *RYR1*-related CNM patients. Two patients (L.1 and N.1) had been previously reported in a series of initially severely affected *RYR1*-related cases [7]. The remaining patients have never been reported before. All patients were found to be compound heterozygous for *RYR1*, with at most one null or hypomorphic mutation (stop gain, frameshift, or splice disrupting). This is consistent with reports of lethality or extreme severity in patients with bi-allelic null mutations in *RYR1* [15], and of previous cohorts of recessive *RYR1*-related patients with biopsies showing irregularities in the intermyofibrillary network with compound

heterozygous mutations in *RYR1* with a null mutation and a missense change [6]. While several different types of mutation have been reported in *RYR1*, a noteworthy variant found in the cohort consisted of a macrodeletion in the C-terminal region of *RYR1*, spanning exons 93–100. This is a rare type of mutation in *RYR1*, which has been reported infrequently [21].

A report on genotype–phenotype correlations on *RYR1* [6] identified three hot spot regions enriched for mutations in recessive *RYR1*-related myopathies: An N-terminal region encompassing exons 2–17, a central region including exons 39–46, and a C-terminal hot spot that included exons 85–103. In our cohort, 6 mutations are found in the N-terminal, 5 mutations in the central, and 7 mutations in the C-terminal hot spot regions, respectively. The remaining 14 mutations were found in other exons, thus we could not observe a strong enrichment of these hot spots. As genetic tests become cheaper, it may be more reasonable to sequence the entire coding region of *RYR1* in suspected cases instead of focused targeting of groups of exons.

The cohort of this work was fairly homogeneous concerning the overall clinical course, with early symptom onset, a relatively stable course and predominance of proximal weakness. Other clinical features and severity were more variable. Facial and ocular findings were frequent, but there was inconsistent skeletal and respiratory involvement. Variability seemed to be the rule when comparing individual clinical features in the cohort, even among patients from the same family. For example, in the mildly affected family A, the younger boy (Patient A.1) had dysphagia, facial and neck flexor weakness, and pectus excavatum, while his sister (Patient A.2) is only mildly affected, having a history of early hypotonia and showing mild ptosis. In family B, the older male (Patient C.1) has a significant motor phenotype with difficulty walking, while his younger sister (Patient C.2) has milder motor impairment but is significantly limited in her respiratory function owing to marked thoracic and spine deformities.

Consistent with another report [17], no definite genotype–phenotype correlation could be established in this cohort, especially since patients were all found to have compound heterozygous variants. In particular, compound null/missense mutations do not seem to cause more severe disease compared to compound missense/missense mutations. Another study suggested that mutations in the C-terminal hot spot region are associated with a more severe clinical phenotype [6]. However, we could not confirm this effect in this cohort; this could be due to the extensive variability in clinical presentation that occurs in single *RYR1* mutations. Some of these mutations are also known to demonstrate variability not only in clinical severity, but also within the phenotypic spectrum of diseases related to *RYR1*. For example, heterozygous p.Val4849Ile mutations have been associated with exercise-induced myalgia, myopathic muscle biopsies, or asymptomatic individuals [16]. The same variant is associated with recurrent rhabdomyolysis [16] or central core disease [14] in a compound heterozygous state and it has been reported with central core disease and nonspecific congenital myopathy in a homozygous state [10,11,13]. Functional studies showed it to be unlikely to cause malignant hyperthermia [11]. In our cohort, p.Val4849Ile was found in two sporadic Latin

American patients with *RYR1*-related CNM with different clinical features in association with different variants. The first (Patient D.1) is a 16-year-old male with an axial-predominant phenotype with thoracic and spinal involvement, while the second (Patient K.1) is an 8-year-old girl with no axial involvement who never achieved independent ambulation.

RYR1 is also implicated in susceptibility to malignant hyperthermia (MH) and exertional rhabdomyolysis [18,22,23]. Even though one of the mutations found in the cohort (p.Arg401Cys) had been previously associated with MH [12,18], none of the patients or other members of their families have had such events. Adding to the complex picture of phenotypical presentation, this MH-causing mutation has also been reported in patients with bona fide myopathy [19,20]. Predicting MH susceptibility based on software tools is unreliable [24]. A definite, albeit intricate and not cost-effective solution to establish MH risk is to perform functional *in vitro* tests in muscle samples of patients affected with *RYR1*-related myopathy. In the absence of functional ryanodine channel activity tests for each specific mutation, all *RYR1*-related myopathy patients should be considered at risk of MH and carry a note advising against depolarizing neuromuscular blocking agents and halogenated inhaled anesthetics.

Skeletal muscle imaging may also help in clinical diagnosis of patients with pathogenic variants in *RYR1*. Previous reports refer to what is considered the typical pattern for muscle involvement of the lower limbs in *RYR1* (including AD and not necessarily CNM patients): 1) selective involvement of the vastus lateralis with relative sparing of the rectus femoris; 2) increased involvement of the adductor magnus compared to adductor longus; 3) Selective involvement of sartorius compared to gracilis; and 4) Increased involvement of soleus compared to the gastrocnemii [25]. A more recent study performed a blinded analysis of a larger cohort and found the typical pattern to be associated with AD *RYR1*-related myopathies and less so with AR *RYR1*-related myopathies, especially in the subgroup of patients who also presented with ophthalmoparesis [26].

In our cohort, the selective involvement of the vastus lateralis and adductor magnus in the thigh was very consistent, with 8 and 7 out of 10 patients showing this pattern. However, we could not observe a more uniform involvement of the sartorius as opposed to the gracilis, and of the soleus compared to the gastrocnemii, both of which occurred in only 3 out of 10 patients. We could also not observe a difference in pattern between patients who presented with ophthalmoparesis and those without this sign.

Our assessment was limited by the small number of patients who had muscle imaging data available. Moreover, two patients in the cohort displayed very homogeneous imaging findings, without any differential involvement or pattern: patient F.1 was mildly and M.1 severely affected in nearly all muscle groups.

In addition to lower limbs, we were able to assess upper limbs in all patients who had imaging studies, which showed the biceps to be more affected than the triceps in 6 out of 10 patients. Triceps was more affected than the biceps in only one patient. The differential involvement of the biceps may be

added to the clinical features of *RYR1*-related myopathies in general, and AR CNM in particular, pending confirmation from larger studies.

The more pronounced involvement of the vastus lateralis with relative rectus femoris sparing, while not specific, is suggestive of *RYR1*-related myopathies in general and can be easily evaluated with muscle ultrasound. This exam has the benefit of being a less expensive and faster exam than MRI that can also be performed in small infants without sedation and represents a reasonable approach in evaluation of a patient with suspected *RYR1*-related myopathy.

Histologically, in addition to the predominance and disproportionately reduced size of type 1 fibers and variable increase in nuclear centralization and internalization, the main feature of the cohort is the presence of irregularities in the oxidative activity, suggesting a disruption of the normal intermyofibrillary architecture (IMA). These do not fit the classical description of well-delineated central cores and can occur in different forms, from sparse mini-core or moth-eaten like areas to core/targetoid areas. They do not seem to correlate with phenotypic severity. Biopsies that did not display these alterations were performed at ages 2 years or less. Age at biopsy in our cohort seemed to be relevant for the magnitude of alterations found in microscopy slides, confirming what has been observed before in serial biopsies of an adult patient [27]. While there are exceptions, proportion of nuclear centralization, IMA abnormalities, and connective tissue content all tend to increase with age at biopsy. Concerning IMA abnormalities specifically, in a previous study on a mouse model of *RYR1*-related MH, investigators observed that localized mitochondrial defects lead to focal disruption of adjacent sarcoplasmic reticulum and T tubules, followed by progressive formation of cores in sequential biopsies [28]. We can only speculate whether, given enough time, all patients with *RYR1* mutations eventually develop IMA abnormalities. In the age of fast and comprehensive molecular tests, it is worth re-evaluating the utility of very early muscle biopsies, especially in mild cases. If the reason for the muscle biopsy is to establish pathological confirmation in cases with unclear genetic test results, it may be recommended to wait a few years until late childhood for a better diagnostic yield. Alternatively, imaging can potentially guide the choice of biopsy site on selectively more involved muscles, such as the vastus lateralis. Interestingly, in this series the muscle selected as the biopsy site was not important to determine the severity of histopathologic changes. However, in this case series a large portion of muscle biopsies was taken from biceps or deltoid muscles. In other cohorts quadriceps is generally the preferred site. This discrepancy may explain the increased uniformity of findings in our series. Moreover, we do not have imaging and clinical data matching age at biopsy to properly assess this result.

In summary, the main features of AR *RYR1*-related CNM patients are 1) the onset of hypotonia and delayed motor milestones in infancy, predominant proximal muscle weakness with a relatively stable clinical course, 2) relative sparing of rectus femoris on imaging with more involvement of vastus lateralis, biceps brachii, and adductor magnus muscles, and 3) type 1 fiber predominance and increase in nuclear centralization/

internalization with age with presence of intermyofibrillary architecture abnormalities on oxidative stains on muscle biopsy.

RYR1 genetics is complex and the gene is implicated in different, overlapping diseases. As genetic tests become cheaper and more widespread, we may be able to precisely determine a patient's diagnosis based on genetic testing alone, precluding the need for a muscle biopsy to establish a histological diagnosis in the first instance. Until then, however, histology and imaging will continue to be useful to inform the diagnosis, to aid pathogenicity ascertainment of unclear *RYR1* variants, and to expand genotype–phenotype correlations.

Acknowledgments

We would like to thank Dr. O. Hank Mayer from the Children's Hospital of Philadelphia for the continuing respiratory care of patients L.1 and N.1.

Funding: This work was supported by the Institut National de la Santé et de la Recherche Médicale (INSERM), the France Génomique National infrastructure funded as part of the Investissements d'Avenir program managed by the Agence Nationale pour la Recherche (ANR-10-INBS-09) and by Fondation Maladies Rares within the frame of the "Myocapture" sequencing project, Association Française contre les Myopathies (AFM-17088), Muscular Dystrophy Association (MDA-186985), Myotubular Trust and Sparks the Children's medical research charity; OAN was supported by a fellowship from CAPES Foundation, Ministry of Education of Brazil, process number 1286/51-2.

References

- [1] Jungbluth H, Voermans NC. Congenital myopathies: not only a paediatric topic. *Curr Opin Neurol* 2016;29:642–50.
- [2] Romero NB. Centronuclear myopathies: a widening concept. *Neuromuscul Disord* 2010;20:223–8.
- [3] Wilmshurst JM, Lillis S, Zhou H, et al. *RYR1* mutations are a common cause of congenital myopathies with central nuclei. *Ann Neurol* 2010;68:717–26.
- [4] Bevilacqua JA, Monnier N, Bitoun M, et al. Recessive *RYR1* mutations cause unusual congenital myopathy with prominent nuclear internalization and large areas of myofibrillar disorganization. *Neuropathol Appl Neurobiol* 2011;37:271–84.
- [5] Vasli N, Böhm J, Le Gras S, et al. Next generation sequencing for molecular diagnosis of neuromuscular diseases. *Acta Neuropathol* 2012;124:273–83.
- [6] Amburgey K, Bailey A, Hwang JH, et al. Genotype-phenotype correlations in recessive *RYR1*-related myopathies. *Orphanet J Rare Dis* 2013;8:117.
- [7] Bharucha-Goebel DX, Santi M, Medne L, et al. Severe congenital *RYR1*-associated myopathy: the expanding clinicopathologic and genetic spectrum. *Neurology* 2013;80:1584–91.
- [8] Heckmatt JZ, Leeman S, Dubowitz V. Ultrasound imaging in the diagnosis of muscle disease. *J Pediatr* 1982;101:656–60.
- [9] Mercuri E, Pichiecchio A, Counsell S, et al. A short protocol for muscle MRI in children with muscular dystrophies. *Eur J Paediatr Neurol* 2002;6:305–7.
- [10] Jungbluth H, Muller CR, Halliger-Keller B, et al. Autosomal recessive inheritance of *RYR1* mutations in a congenital myopathy with cores. *Neurology* 2002;59:284–7.
- [11] Ducreux S, Zorzato F, Ferreiro A, et al. Functional properties of ryanodine receptors carrying three amino acid substitutions identified in

- patients affected by multi-minicore disease and central core disease, expressed in immortalized lymphocytes. *Biochem J* 2006;395:259–66.
- [12] Robinson R, Carpenter D, Shaw MA, Halsall J, Hopkins P. Mutations in RYR1 in malignant hyperthermia and central core disease. *Hum Mutat* 2006;27:977–89.
- [13] Zhou H, Jungbluth H, Sewry CA, et al. Molecular mechanisms and phenotypic variation in *RYR1*-related congenital myopathies. *Brain* 2007;130:2024–36.
- [14] Kossugue PM, Paim JF, Navarro MM, et al. Central core disease due to recessive mutations in RYR1 gene: is it more common than described? *Muscle Nerve* 2007;35:670–4.
- [15] Monnier N, Marty I, Faure J, et al. Null mutations causing depletion of the type I ryanodine receptor (RYR1) are commonly associated with recessive structural congenital myopathies with cores. *Hum Mutat* 2008;29:670–8.
- [16] Kraeva N, Heytens L, Jungbluth H, et al. Compound RYR1 heterozygosity resulting in a complex phenotype of malignant hyperthermia susceptibility and a core myopathy. *Neuromuscul Disord* 2015;25:567–76.
- [17] Klein A, Lillis S, Munteanu I, et al. Clinical and genetic findings in a large cohort of patients with ryanodine receptor 1 gene-associated myopathies. *Hum Mutat* 2012;33:981–8.
- [18] Davis M, Brown R, Dickson A, et al. Malignant hyperthermia associated with exercise-induced rhabdomyolysis or congenital abnormalities and a novel *RYR1* mutation in New Zealand and Australian pedigrees. *Br J Anaesth* 2002;88:508–15.
- [19] Pietrini V, Marbini A, Galli L, Sorrentino V. Adult onset multi/minicore myopathy associated with a mutation in the RYR1 gene. *J Neurol* 2004;251:102–4.
- [20] Duarte ST, Oliveira J, Santos R, et al. Dominant and recessive RYR1 mutations in adults with core lesions and mild muscle symptoms. *Muscle Nerve* 2011;44:102–8.
- [21] Monnier N, Laquerrière A, Marret S, et al. First genomic rearrangement of the RYR1 gene associated with an atypical presentation of lethal neonatal hypotonia. *Neuromuscul Disord* 2009;19:680–4.
- [22] Dlamini N, Voermans NC, Lillis S, et al. Mutations in RYR1 are a common cause of exertional myalgia and rhabdomyolysis. *Neuromuscul Disord* 2013;23:540–8.
- [23] Snoeck M, Treves S, Molenaar JP, Kamsteeg EJ, Jungbluth H, Voermans NC. “Human stress syndrome” and the expanding spectrum of *RYR1*-related myopathies. *Cell Biochem Biophys* 2016;74:85–7.
- [24] Schiemann AH, Stowell KM. Comparison of pathogenicity prediction tools on missense variants in RYR1 and CACNA1S associated with malignant hyperthermia. *Br J Anaesth* 2016;117:124–8.
- [25] Jungbluth H, Davis MR, Müller C, et al. Magnetic resonance imaging of muscle in congenital myopathies associated with RYR1 mutations. *Neuromuscul Disord* 2004;14:785–90.
- [26] Klein A, Jungbluth H, Clement E, et al. Muscle magnetic resonance imaging in congenital myopathies due to ryanodine receptor type I gene mutations. *Arch Neurol* 2011;68:1171–9.
- [27] Snoeck M, van Engelen BG, Küsters B, et al. RYR1-related myopathies: a wide spectrum of phenotypes throughout life. *Eur J Neurol* 2015;22:1094–112.
- [28] Boncompagni S, Rossi AE, Micaroni M, et al. Characterization and temporal development of cores in a mouse model of malignant hyperthermia. *Proc Natl Acad Sci USA* 2009;106:21996–2001.

2.2 Mutations in known myopathy genes with new phenotypes

At the start of the project, genetic screening in patients with congenital myopathies mainly relied on the sequencing of single genes, compatible with the clinical and histological presentation of the patients.

Within the MYOCAPTURE project, mutations in *SPEG*, *SCN4A*, *HNRNPDL*, *MTM1*, *EXOSC3*, and *GNE* were found in patients with uncommon clinical or histological features, and novel *HSPB8*, *CASQ1*, and *CACNA1S* mutations involving different pathomechanisms were found to cause new subtypes of neuromuscular diseases.

These findings, summarized in the next nine publications, highlight the clinical and genetic heterogeneity, and enlarge the phenotypic and genetic spectrum of congenital myopathies.

2.2.1 Publication 3: Novel *SPEG* mutations in congenital myopathy without centralized nuclei (Lornage et al. 2018)

Background

Centronuclear myopathies (CNM) involve muscle weakness and atrophy, and are characterized by the presence of numerous centralized nuclei in the muscle fibers (Jungbluth, Wallgren-Pettersson, and Laporte 2008). Mutations in *MTM1*, encoding myotubularin, cause a severe X-linked form of the disease usually associated with neonatal hypotonia and respiratory distress (Laporte et al. 1996). *SPEG* was recently identified as an interacting partner of myotubularin. *SPEG* mutations were previously found in patients with CNM and associated cardiomyopathy (Agrawal et al. 2014). *SPEG* pre-mRNA is spliced into multiple isoforms with a predominant expression of *SPEG* α and *SPEG* β in skeletal muscle and heart (Hsieh et al. 2000) (**Fig R1**).

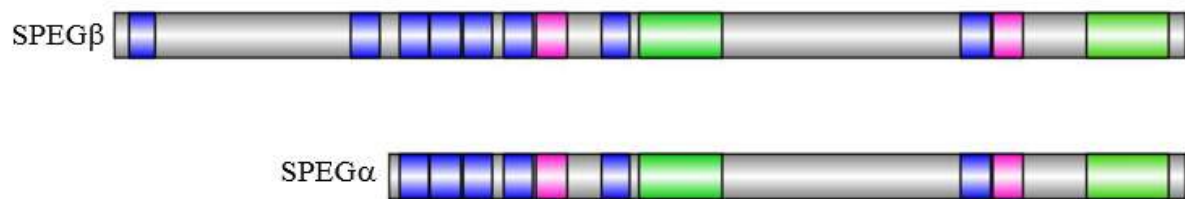


Fig R1: Schematic representation of *SPEG* isoforms and protein domains.

SPEG β and *SPEG* α are both highly expressed in adult heart and skeletal muscle. *SPEG* β is a 3262 amino acid protein, while *SPEG* α lacks the 854 most N-terminal amino acids. In blue: Ig-like domains. In pink: Fibronectin type III domains. In green: kinase domains.

Aim of the study

The aim of the study was to characterize a patient with an undefined myopathy at the clinical, histological and genetic level.

Results

Our patient presented with hypotonia at birth, delayed motor milestones and subsequently developed proximal, distal and facial muscle weakness. The muscle biopsy revealed a mild fiber size heterogeneity. Exome sequencing uncovered the presence of compound heterozygous truncating *SPEG* mutations. One mutation affected *SPEG* α and *SPEG* β , and the other was found in a *SPEG* β -specific exon and does therefore not affect the *SPEG* α isoform. Unlike our patient, previously reported *SPEG* patients all presented with CNM and numerous rounded muscle fibers.

Conclusion

SPEG mutations were initially considered to cause CNM, and our results illustrate that *SPEG* mutations can be found in patients without typical histological features of CNM. To date, nine patients with recessive truncating *SPEG* mutations are reported in the literature (Lornage et al. 2018; Qualls et al. 2019; Wang et al. 2017; Wang et al. 2018; Agrawal et al. 2014). Three patients carried a mutation that only affected *SPEG* β , and none of these three patients was diagnosed with a cardiomyopathy. We may thus hypothesize that the expression of *SPEG* α is sufficient to protect from cardiomyopathy.

Contribution

I identified the *SPEG* mutations and wrote the publication with inputs from the other authors.

Novel SPEG Mutations in Congenital Myopathy without Centralized Nuclei

Xavière Lornage^{a,b,c,d}, Pascal Sabouraud^e, Béatrice Lannes^{d,f}, Dominique Gaillard^g, Raphaël Schneider^{a,b,c,d,h}, Jean-François Deleuzeⁱ, Anne Bolandⁱ, Julie Thompson^{d,h}, Johann Böhm^{a,b,c,d}, Valérie Biancalana^{a,b,c,d,j} and Jocelyn Laporte^{a,b,c,d,*}

^a*Institut de Génétique et de Biologie Moléculaire et Cellulaire (IGBMC), Illkirch, France*

^b*INSERM U1258, Illkirch, France*

^c*CNRS, UMR7104, Illkirch, France*

^d*Université de Strasbourg, Strasbourg, France*

^e*Service de Pédiatrie A – Neurologie pédiatrique, CHU Reims, Reims, France*

^f*Department of Pathology, Strasbourg University Hospital, Strasbourg, France*

^g*Service de Génétique, CHU Reims, UFR médecine, Reims, France*

^h*ICube – UMR7357, CSTB Complex Systems and Translational Bioinformatics, Faculté de Médecine, Strasbourg, France*

ⁱ*Centre National de Recherche en Génomique Humaine (CNRGH), Institut de Biologie François Jacob, CEA, Evry, France*

^j*Laboratoire Diagnostic Génétique, Faculté de Médecine, CHRU, Strasbourg, France*

Abstract. Congenital myopathies are clinically and genetically heterogeneous, and are classified based on typical structural abnormalities on muscle sections. Recessive mutations in the striated muscle preferentially expressed protein kinase (*SPEG*) were recently reported in patients with centronuclear myopathy (CNM) associated in most cases with dilated cardiomyopathy. Here we report the identification of novel biallelic truncating *SPEG* mutations in a patient with moderate congenital myopathy without clinical and histological hallmarks of CNM and without cardiomyopathy. This study expands the phenotypic spectrum of *SPEG*-related myopathy and prompts to consider *SPEG* for congenital myopathies without specific histological features.

Keywords: Centronuclear myopathy, myotubular myopathy, MTM1, myotubularin, *SPEG*, congenital myopathy

INTRODUCTION

Congenital myopathies define a group of clinically and genetically heterogeneous rare muscle diseases. They cause neonatal or early onset hypotonia and/or muscle weakness, and the muscle biopsies of affected individuals exhibit characteristic structural defects [1, 2]. Recessive mutations in the *SPEG* gene, encoding the striated muscle preferentially expressed protein kinase (*SPEG*), were previously reported in five families with centronuclear myopathy (CNM)

and dilated cardiomyopathy [3, 4]. *SPEG* interacts with myotubularin (MTM1), mutated in X-linked CNM (also called myotubular myopathy), but its cellular functions are barely understood. In this report, we describe a peculiar case with biallelic truncating *SPEG* mutations, but without histopathological CNM hallmarks and without cardiomyopathy, demonstrating that recessive *SPEG* mutations can give rise to myopathies with non-specific features on muscle biopsy.

CASE REPORT

The proband is a 10-year-old girl born to non-consanguineous healthy parents. The pregnancy was

*Correspondence to: Dr. Jocelyn Laporte, IGBMC, 1 rue Laurent Fries, 67404 Illkirch, France. Tel.: +33 3 88 65 34 12; Fax: +33 3 88 65 32 01; E-mail: jocelyn@igbmc.fr.

uneventful. At birth, the patient had hypotonia without respiratory distress, and poor sucking. Motor milestones were delayed with independent sitting at 11 months and walking at 30 months of age. Cognitive development was normal. The patient developed a scoliosis around age 4 treated since with a back brace. Reduced myocardial contraction without ventricular dilatation appeared at age 5 and progressively normalized with digoxin and captopril treatment. At the age of 6 years, non-invasive ventilation was started to treat obstructive sleep apnea and alveolar hypoventilation. No supraclavicular, intercostal, subcostal or intercostal retractions were observed. Forced vital capacity was above 70%. Clinical investigation at 9 years of age revealed proximal and distal muscle weakness, positive Gowers' sign and facial weakness without ptosis or external ophthalmoplegia (Fig. 1A). The patient showed hypotonic pes planus and complained about difficulties climbing stairs. Maximal walking distance was 300 meters. Retractions were not noted. Swallowing was normal, but chewing difficulties required an enteral gastrostomy feeding from age 9 years and 10 months to prevent malnutrition. Serum creatine kinase levels were repeatedly normal. MRI scans of the thighs and lower legs was performed twice at age 3 and 5 years, and revealed a mild and non-progressive atrophy of the vastus lateralis, the gastrocnemius, and the soleus muscles (Fig. 1B). EMG at 1 year of age did not reveal any abnormalities. Motor examination was performed for the median, ulnar, common peroneal and tibial nerves, and sensory examination was performed for the median and ulnar nerves. Conduction velocities, amplitudes and distal latencies were normal, and intramuscular EMG from the tibialis anterior muscles showed an interferential pattern. A quadriceps muscle biopsy was performed at 16 months, and histological analyses of H&E, NADH-TR, SDH, PAS, Oil Red O, ATPase stains revealed hypotrophy of both fiber types and discrete fiber size heterogeneity (Fig. 1C). Typical CNM features such as centralized nuclei, necklace fibers, or type I fiber predominance were not observed.

Genetic counselling was provided, and informed consent was obtained for genetic analysis. The patient's DNA was sequenced for a targeted panel of 136 genes implicated in neuromuscular disorders, but no causative mutation was identified. Thus, exome sequencing was performed for the affected child and her healthy parents. Variants were filtered based on their frequency in gnomAD and an in-house control database composed of 1550 exomes, and ranked with

our in-house bioinformatics pipeline. Data analysis revealed compound heterozygous *SPEG* mutations segregating with the disease. We identified an out-of-frame duplication of 4 nucleotides in exon 4 (c.1071_1074dup; p.Lys359Valfs*35), predicted to induce a premature stop codon on the maternal allele, and a nonsense mutation in exon 20 (c.4399C>T; p.Arg1467*) on the paternal allele (Fig. 1D). None of these variants was listed in the gnomAD and ClinVar databases.

DISCUSSION

To date, *SPEG* mutations were reported in five families with severe neonatal hypotonia and muscle weakness [3, 4]. A single patient deceased shortly after birth, while all others exhibited delayed motor milestones. Facial weakness and eye involvement were noted in the majority of patients, and abnormal respiration requiring ventilation was reported in 2 families [3, 4]. A dilated cardiomyopathy was diagnosed in the surviving patients with exception of the youngest patient of 3 years of age. Histologically, all biopsies of the published cases revealed prominent central nuclei and some showed necklace fibers. Overall, both clinical and histological findings were similar to X-linked centronuclear myopathy resulting from *MTM1* mutations [5, 6], with the exception of the cardiac involvement.

Our patient is the oldest and mildest reported patient with *SPEG* mutations. Although presenting with neonatal hypotonia and delayed motor milestones, she reached independent walking before the age of three, did not show eye involvement and did not develop a dilated cardiomyopathy. Noteworthy, her muscle biopsy did not reveal internal or central nuclei nor necklace fibers. Similarly, one previously reported *MTM1* patient displayed no central nuclei on muscle biopsy, highlighting that mutations in CNM genes might cause an atypical muscle morphology [7].

MRI revealed a similar pattern for the published and new *SPEG* patients with predominant involvement of the anterior compartment of the thigh and of the posterior compartment of the lower legs [4]. Our patient shows a mild picture compared to previously described *SPEG* cases, correlating with the mild phenotypic presentation.

All *SPEG* mutations previously associated with the severe CNM-like muscle disorder are evenly distributed nonsense or frameshift mutations predicted

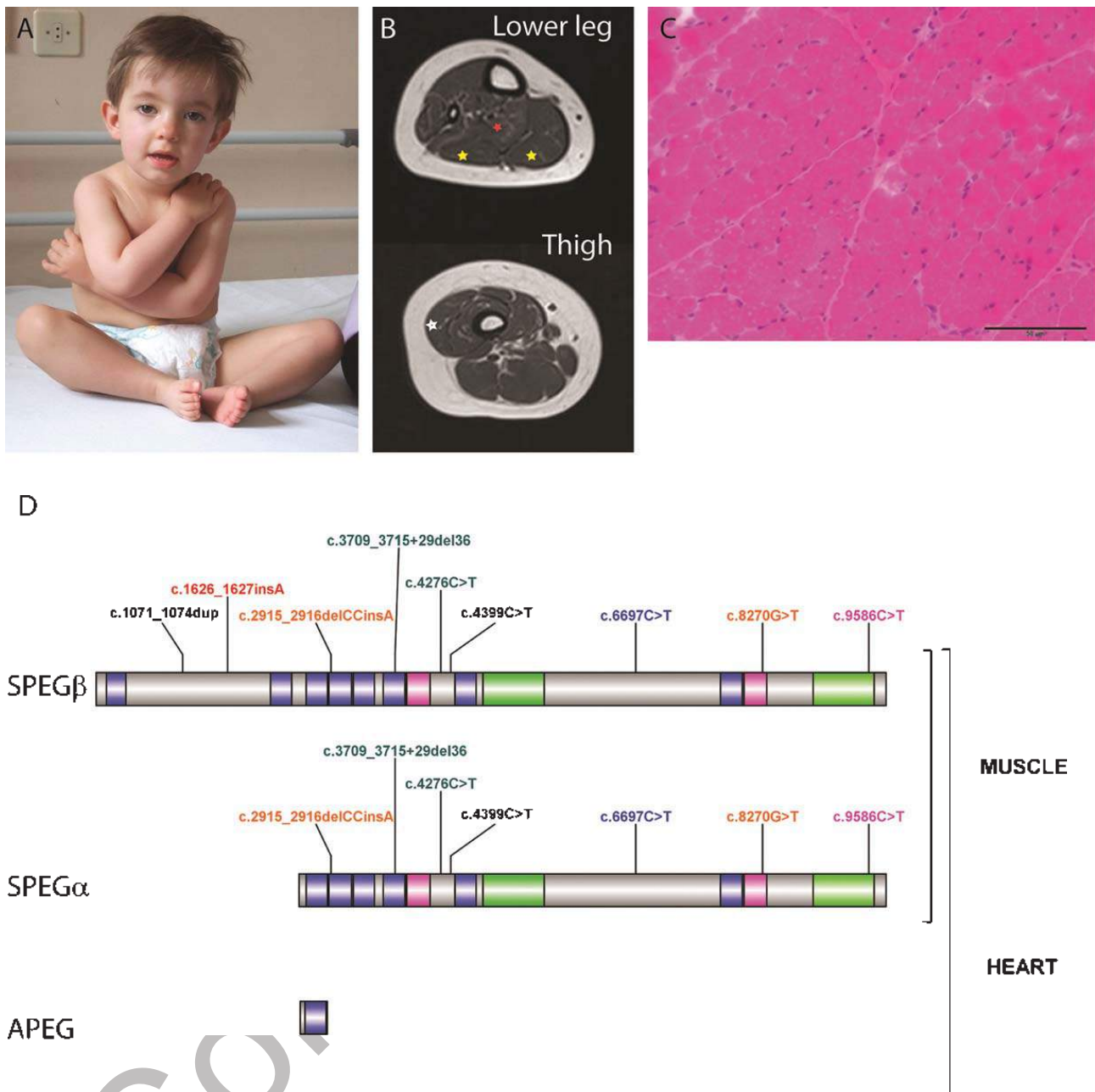


Fig. 1. (A) Facial features of the patient with compound heterozygous disrupting *SPEG* mutations. The picture was taken at 27 months of age (Permission was granted by the patient's parents). (B) T1-weighted MRI of the patient at the level of lower leg and of the thigh revealed involvement of the vastus lateralis muscle (white star), the soleus muscle (red star) and the gastrocnemius muscle (yellow star). (C) Haematoxylin-eosin staining on a muscle section displaying mild fiber size heterogeneity and normal nuclei position. NADH-TR, SDH, PAS, Oil Red O and ATPase stains did not reveal additional abnormalities. (D) *SPEG* protein domains and reported pathogenic mutations. Representation of *SPEG* domains (Illustrator for Biological Sequences) and isoforms predominantly expressed in human muscle and heart using murine nomenclature. SPEG β (ENST00000312358), SPEG α (ENST00000485813), and APEG (ENST00000396689). Ig-like domains are in blue, Fibronectin type III domains are depicted in pink and protein kinase domains in green. Previously reported mutations are multicoloured, and novel mutations identified in our study are depicted in black.

to induce a premature stop codon resulting in nonsense-mediated mRNA decay or alternatively the translation of a truncated protein. Both mutations found in our patient have not yet been described and involve a premature stop codon, predicted to remove

the myotubularin binding domain located between the *SPEG* residues 2530 and 2674 [3].

The *SPEG* locus encodes at least four differentially expressed isoforms [8]. Among the murine *SPEG* protein isoforms, SPEG α and SPEG β were

shown to be the main isoforms present in skeletal and cardiac muscles. The only reported patient without cardiomyopathy carries a homozygous truncating mutation in exon 4, predicted to affect SPEG β but not SPEG α thereby suggesting that the presence of SPEG α might be sufficient to protect from the development of a cardiomyopathy. Accordingly, our patient carries one of the truncating mutations in exon 4 and did not develop a cardiomyopathy. However, murine and human isoforms might be different, and this is substantiated by the human gene expression databases (www.gtexportal.org/). To better understand the pathomechanisms of *SPEG* mutations, further characterization of the human *SPEG* isoforms in human muscle and heart is necessary. It is nevertheless possible that patients with the milder phenotype will develop a dilated cardiomyopathy at later stages.

Strikingly, the muscle biopsy of our patient is the only one without central nuclei, potentially correlating with the disease severity. Of note, the mutation in exon 20 (c.4399C>T; p.Arg1467*) is one of the most distal mutation reported and might impact differently on protein stability and thereby explain the comparably milder phenotype in our patient.

Overall, our study expands the phenotype of congenital myopathies associated with recessive *SPEG* mutations. Specific *SPEG* mutations can induce a severe CNM-like or, as described in this study, a rather moderate congenital myopathy without central nuclei. This is of major diagnostic importance, as *SPEG* mutations should be considered in patients with congenital hypotonia even in the absence of central nuclei.

ACKNOWLEDGMENTS

The authors thank the family who participated in this study, Nicolas Dondaine who analyzed the results of the MYOdiagHTS panel and Gratiela Mac-Caby who performed MRI studies. This work was supported by the Institut National de la Santé et de la Recherche Médicale (INSERM), Centre National

de la Recherche Scientifique (CNRS), University of Strasbourg, the France Génomique National infrastructure, funded as part of the Investissements d'Avenir program managed by the Agence Nationale pour la Recherche (ANR-10-INBS-09) and by Fondation Maladies Rares within the frame of the "Myocapture" sequencing project, ANR-10-LABX-0030-INRT under the frame program Investissements d'Avenir ANR-10-IDEX-0002-02, Fondation pour la Recherche Médicale, and AFM-16992 and CREGEMES for the MYOdiagHTS project.

CONFLICTS OF INTEREST

The authors have no conflict of interest to report.

REFERENCES

- [1] Romero NB, Clarke NF. Congenital myopathies. *Handb Clin Neurol.* 2013;113:1321-36.
- [2] Nance JR, Dowling JJ, Gibbs EM, Bonnemann CG. Congenital myopathies: An update. *Curr Neurol Neurosci Rep.* 2012;12(2):165-74.
- [3] Agrawal PB, Pierson CR, Joshi M, Liu X, Ravenscroft G, Moghadaszadeh B, et al. SPEG interacts with myotubularin, and its deficiency causes centronuclear myopathy with dilated cardiomyopathy. *Am J Hum Genet.* 2014;95(2):218-26.
- [4] Wang H, Castiglioni C, Kacar Bayram A, Fattori F, Pekuz S, Araneda D, et al. Insights from genotype-phenotype correlations by novel SPEG mutations causing centronuclear myopathy. *Neuromuscul Disord.* 2017;27(9):836-42.
- [5] Laporte J, Hu LJ, Kretz C, Mandel JL, Kioschis P, Coy JF, et al. A gene mutated in X-linked myotubular myopathy defines a new putative tyrosine phosphatase family conserved in yeast. *Nat Genet.* 1996;13(2):175-82.
- [6] Bevilacqua JA, Bitoun M, Biancalana V, Oldfors A, Stoltenburg G, Claes KG, et al. "Necklace" fibers, a new histological marker of late-onset MTM1-related centronuclear myopathy. *Acta Neuropathol.* 2009;117(3):283-91.
- [7] de Goede CG, Kelsey A, Kingston H, Tomlin PI, Hughes MI. Muscle biopsy without centrally located nuclei in a male child with mild X-linked myotubular myopathy. *Dev Med Child Neurol.* 2005;47(12):835-7.
- [8] Hsieh CM, Fukumoto S, Layne MD, Maemura K, Charles H, Patel A, et al. Striated muscle preferentially expressed genes alpha and beta are two serine/threonine protein kinases derived from the same gene as the aortic preferentially expressed gene-1. *J Biol Chem.* 2000;275(47):36966-73.

2.2.2 Publication 4: *HSPB8* haploinsufficiency causes dominant adult-onset axial and distal myopathy (Echaniz-Laguna et al. 2017)

Background

Myofibrillar myopathies are hereditary muscle disorders characterized by protein aggregates, rimmed-vacuoles, and disorganization of the intermyofibrillar network on muscle biopsies (Olive, Kley, and Goldfarb 2013). The main causative genes are *DES*, *FLNC*, *MYOT*, *CRYAB*, *ZASP*, *BAG3*, encoding for components of the sarcomere/cytoskeleton or for proteins involved in the protein quality control (Behin et al. 2015). About half of the patients with myofibrillar myopathy do not have a molecular diagnosis, suggesting the implication of additional genes (Kley et al., 2016).

Aim of the study

The aim of the study was to identify the causative mutation(s) in three families with myofibrillar myopathy.

Results

We studied patients from three families with an adult-onset myopathy characterized by the appearance of camptocormia as the first clinical sign. Foot drop and proximal muscle weakness were observed at later stages. The muscle biopsies revealed fiber necrosis and regeneration, internal nuclei, fibrosis, rimmed vacuoles and protein aggregates, compatible with myofibrillar myopathy. Exome sequencing uncovered a heterozygous *HSPB8* frameshift mutation in the last exon, and western blot analysis of muscle extracts revealed a 50% reduced HspB8 protein level.

Conclusion

Dominant *HSPB8* mutations were previously shown to cause neuropathy (Irobi et al. 2004; Nakhro et al. 2013; Tang et al. 2005) or neuropathy with associated myopathy (Ghaoui et al. 2016; Cortese et al. 2018). These gain-of-function mutations cause the formation of toxic aggregates (Kwok et al. 2011; Bouhy et al. 2018). Here we demonstrated that HspB8 haploinsufficiency causes myofibrillar myopathy with no peripheral nerve involvement, and we described a new pathomechanisms for *HSPB8*-related diseases.

Contribution

I identified the *HSPB8* mutation in one family, confirmed the segregation by Sanger sequencing, and assessed the HspB8 protein level in the muscle extracts. The same mutation

was subsequently identified in two additional families by the diagnostic laboratory of the Strasbourg university hospital. I also wrote the publication with inputs from the other authors.

CORRESPONDENCE

HSPB8 haploinsufficiency causes dominant adult-onset axial and distal myopathy

Andoni Echaniz-Laguna¹ · Xavière Lornage² · Béatrice Lannes³ · Raphaël Schneider⁴ · Guillaume Bierry⁵ · Nicolas Dondaine⁶ · Anne Boland⁷ · Jean-François Deleuze⁷ · Johann Böhm² · Julie Thompson⁴ · Jocelyn Laporte² · Valérie Biancalana^{2,6}

Received: 30 March 2017 / Revised: 4 May 2017 / Accepted: 9 May 2017
© Springer-Verlag Berlin Heidelberg 2017

HSPB8 encodes the heat shock protein beta-8 (HSPB8) implicated in the chaperone-assisted selective autophagy complex, which is crucial for cellular protein quality control in mechanically strained tissues [1]. Autosomal dominant *HSPB8* mutations have been reported in distal hereditary motor neuropathy and axonal Charcot-Marie-Tooth disease [2, 4–6]. Here, we report five patients from three unrelated families with a myopathy caused by *HSPB8* haploinsufficiency.

Families A and B have a history of a muscle phenotype segregating as a dominant disease, and patient CIII is a

sporadic case (Fig. 1a, Supplementary Table 1). Mean age at onset was 39 years and camptocormia, i.e., a marked anteroflexion of the spine corrected by reclining, was the first symptom in all cases. The progression of the disease was slow with bilateral foot drop appearing around age 40 and proximal lower and upper limbs weakness around age 50 (Fig. 1b). Four patients with a disease duration of less than 24 years were still able to walk and patient CIII with a disease duration of more than 30 years became wheelchair dependent. In all cases, deep tendon reflexes were present in all limbs and vibration sense was normal in the ankles. Pes cavus, skeletal dysplasia, scapular winging, respiratory insufficiency, and cranial nerves involvement were not observed. No pyramidal, extrapyramidal and cerebellar signs were observed, suggesting the absence of central nervous system involvement. Electrophysiological examination showed normal muscle action potentials and normal sensory nerve action potentials in all cases, demonstrating the absence of polyneuropathy (Supplementary Table 2). EMG studies revealed myopathic abnormalities in deltoid, tibialis anterior, paraspinal and vastus lateralis muscles. No pathological spontaneous activity was observed using EMG.

CK levels were mildly increased in 4 patients (Supplementary Table 3). Pulmonary function tests, EKG and echocardiography were normal in all cases. In patients BIII1 and CII1, MRI and CT studies demonstrated a pattern of muscle involvement similar to the one reported by Ghaoui et al. in their patient III-2 with a *HSPB8* mutation [3]. Additionally, patients BIII1 and CII1 both demonstrated severe fatty infiltrations in the paraspinal muscles (Fig. 1c).

Muscle biopsies showed dystrophic features with atrophy, necrosis and regeneration, internal nuclei, fibrosis, fibre splitting and rimmed vacuoles (Fig. 1d 1–3). No

Andoni Echaniz-Laguna and Xavière Lornage contributed equally to this work.

Jocelyn Laporte and Valérie Biancalana contributed equally to this work.

Electronic supplementary material The online version of this article (doi:10.1007/s00401-017-1724-8) contains supplementary material, which is available to authorized users.

✉ Andoni Echaniz-Laguna
andoni.echaniz-laguna@chru-strasbourg.fr

¹ Department of Neurology, Neuromuscular Disease Centre (CERNEST), CHRU, Strasbourg, France

² Institut de Génétique et de Biologie Moléculaire et Cellulaire (IGBMC), INSERM U964, CNRS UMR7104, Fédération de Médecine Translationnelle de Strasbourg, Université de Strasbourg, Illkirch, France

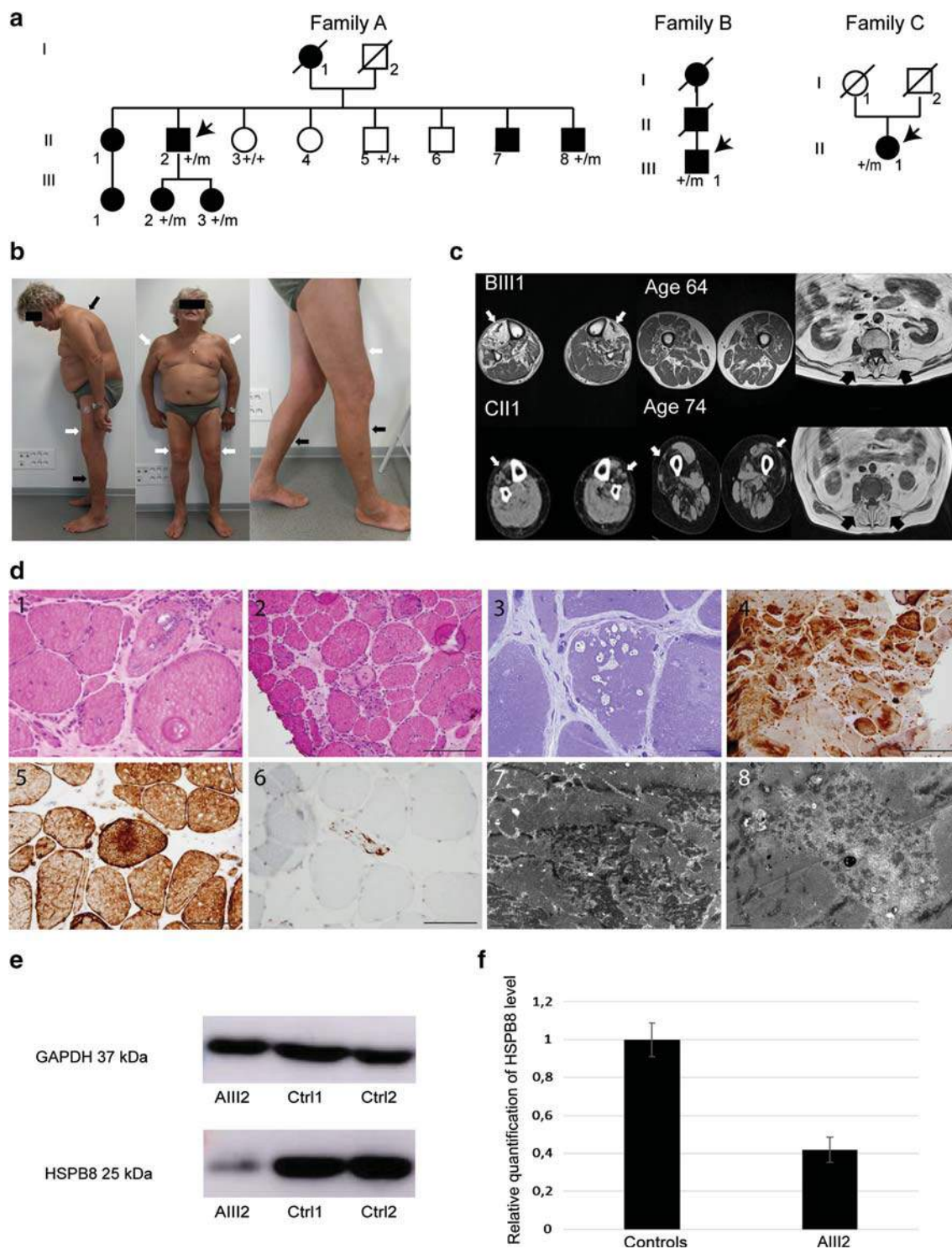
³ Department of Pathology, CHRU, Strasbourg, France

⁴ ICube-UMR7357, Strasbourg, France

⁵ Department of Radiology, CHRU, Strasbourg, France

⁶ Laboratoire Diagnostic Génétique, CHRU, Strasbourg, France

⁷ CNG, Evry, France



neurogenic aspect was seen. Protein aggregations were revealed using ubiquitin and desmin antibodies (Fig. 1d 4–5). TDP-43 antibody revealed coarse cytoplasmic aggregation and linear sarcolemmal expression (Fig. 1d 6). EM studies showed focal disruption of the myofibrillar network, Z lines streaming and areas lacking myofibrils containing granulo-filamentous material (Fig. 1d 7–8). NADH-TR and

ATPase pH 9.4 showed features compatible with myofibrillar myopathy (Supplementary Fig. 1).

Targeted exons sequencing using a custom panel of 136 genes implicated in neuromuscular disorders was performed for patients BIII1 and CII1 and exome sequencing was performed for individuals AII2, AII8, AIII2, AIII3. Following variants filtering, the same heterozygous two

Fig. 1 Clinical, histopathological and molecular features of patients with *HSPB8* mutations. **a** Pedigree of families A–C. **b** Patient BIII1: camptocormia and bilateral foot drop (*black arrows*), proximal lower and upper limb atrophy (*white arrows*). **c** Upper panel: MRI revealed generalized fatty replacements in the anterior compartment of the lower legs of patients BIII1 (*white arrows*) while soleus and thigh muscles were less affected. Massive muscle alterations with fatty infiltration were observed in paraspinal muscles (*black arrows*). Lower panel: Patient CIII1 presents fatty infiltrations in extensor digitorum longus and tibialis anterior muscles (*white arrows*), vastus muscles (*white arrows*), and paraspinal muscles (*black arrows*). Soleus muscles remained unaffected. **d** Histochemical, immunohistochemical and ultrastructural analysis of tibialis anterior muscle biopsy of patient AIII8 (1, 2) and deltoids of patients AIII2 (4), AIII3 (5, 6) and CIII1 (3, 7, 8). H&E (1, 2) and toluidine blue (3) ubiquitin (4), desmin (5), TDP-43 (6), and electron microscopy (7, 8). Magnification: Bar = 100 μ m (2, 4), 50 μ m (1, 5, 6), 20 μ m (3), 1 μ m (7, 8). Histological findings demonstrated a dystrophic pattern as well as features consistent with myofibrillar myopathy. **e** SDS-Page of controls and patient AIII2 muscle protein extracts revealed with antibodies against GAPDH and HSPB8. **f** Relative quantification of the level of HSPB8 in AIII2 compared to controls demonstrates a significant HSPB8 reduction in the patient

base-pair deletion in the *HSPB8* gene c.508_509delCA (NM_014365.2) was found in all affected. No other candidate gene was found in common within the studied families. The *HSPB8* variant was not listed in the gnomAD database and is predicted to induce a frameshift from aminoacid 170 (p.Gln170Glyfs*45) leading to the modification of the last 27 aminoacids and to 17 additional aminoacids compared to the normal length of the protein. Sanger sequencing confirmed the segregation of the mutation with the disease and none of the available healthy family members carried the mutation. Analysis confirmed the presence of the variant in patient AIII3 presenting with camptocormia, elevated CK levels and vacuolar myopathy. The impact of the variant on the protein was tested by western blot (Fig. 1e). Quantification revealed that the level of HSPB8 protein was decreased by 60% in the patient compared to healthy controls (Fig. 1f). Nor elongated or truncated protein was detected with this antibody targeting the N-terminal part of the protein, suggesting that *HSPB8* mutation induces nonsense-mediated mRNA decay or protein degradation and that the disease is caused by HSPB8 haploinsufficiency.

In conclusion, our study expands the knowledge on HSPB8-related disorders. All patients carried a heterozygous *HSPB8* frameshift mutation causing an adult-onset myopathy with camptocormia as the first clinical sign. These five cases confirm the involvement of the gene in a muscle disease as recently described in two patients with motor neuropathy and distal myofibrillar myopathy [3]. It is the first time that a *HSPB8* mutation is shown to cause a “pure” myopathy without associated motor neuropathy and it highlights that *HSPB8* mutations should be considered

in families with myopathy, even in the absence of motor neuropathy.

Acknowledgements We thank the families who participated in this study. This work was supported by the Institut National de la Santé et de la Recherche Médicale, Centre National de la Recherche Scientifique, University of Strasbourg, the France Génomique National infrastructure, funded as part of the Investissements d’Avenir program managed by the Agence Nationale pour la Recherche (ANR-10-INBS-09), and by Fondation Maladies Rares within the frame of the “Myocapture” sequencing project, AFM-16992 and CREGEMES for the MYOdiagHTS project, ANR-10-LABX-0030-INRT under the frame program Investissements d’Avenir ANR-10-IDEX-0002-02, Association Française contre les Myopathies (AFM-17088).

Compliance with ethical standards

Conflict of interest The authors declare that they have no conflict of interest.

Statement of human rights All procedures involving human participants were in accordance with the ethical standards of the institutional and/or national research committee and with the 1964 Helsinki declaration and its later amendments or comparable ethical standards.

Informed consent Informed consent was obtained from all individual participants included in the study. Additional informed consent was obtained from all individual participants for whom identifying information is included in this article.

References

- Arndt V, Dick N, Tawo R, Dreiseidler M, Wenzel D, Hesse M, Furst DO, Saftig P, Saint R, Fleischmann BK et al (2010) Chaperone-assisted selective autophagy is essential for muscle maintenance. *Curr Biol* 20:143–148. doi:10.1016/j.cub.2009.11.022
- Echaniz-Laguna A, Geuens T, Petiot P, Pereon Y, Adriaenssens E, Haidar M, Capponi S, Maissonobe T, Fournier E, Dubourg O et al (2017) Axonal neuropathies due to mutations in small heat shock proteins: clinical, genetic, and functional insights into novel mutations. *Hum Mutat* 38:556–568. doi:10.1002/humu.23189
- Ghaoui R, Palmio J, Brewer J, Lek M, Needham M, Evila A, Hackman P, Jonson PH, Penttila S, Vihola A et al (2016) Mutations in HSPB8 causing a new phenotype of distal myopathy and motor neuropathy. *Neurology* 86:391–398. doi:10.1212/WNL.0000000000002324
- Irobi J, Van Impe K, Seeman P, Jordanova A, Dierick I, Verpoorten N, Michalik A, De Vriendt E, Jacobs A, Van Gerwen V et al (2004) Hot-spot residue in small heat-shock protein 22 causes distal motor neuropathy. *Nat Genet* 36:597–601. doi:10.1038/ng1328
- Nakhro K, Park JM, Kim YJ, Yoon BR, Yoo JH, Koo H, Choi BO, Chung KW (2013) A novel Lys141Thr mutation in small heat shock protein 22 (HSPB8) gene in Charcot–Marie–Tooth disease type 2L. *Neuromuscul Disord* 23:656–663. doi:10.1016/j.nmd.2013.05.009
- Tang BS, Zhao GH, Luo W, Xia K, Cai F, Pan Q, Zhang RX, Zhang FF, Liu XM, Chen B et al (2005) Small heat-shock protein 22 mutated in autosomal dominant Charcot–Marie–Tooth disease type 2L. *Hum Genet* 116:222–224. doi:10.1007/s00439-004-1218-3

2.2.3 Publication 5: Expanding the spectrum of congenital myopathy linked to recessive mutations in *SCN4A* (Mercier et al. 2017)

Background

SCN4A encodes a voltage-gated sodium channel that is required for the generation and propagation of action potentials in muscle (Trimmer et al. 1989). *SCN4A* mutations have been linked to several diseases including hyperkalemic periodic paralyses, myasthenia, and myotonia congenita (Lerche et al. 1993; Ackerman and Clapham 1997; Tsujino et al. 2003). More recently, recessive loss-of-function mutations were reported in a cohort of 11 patients among which 7 died pre- or perinatally (Zaharieva et al. 2016).

Aim of the study

The aim of the study was to characterize the clinics, histology and genetics of three brothers with an undefined congenital myopathy.

Results

The three siblings presented with hypotonia at birth and delayed motor milestones, and clinical improvement was noted within the first decade of life. The muscle biopsy revealed aspecific anomalies including dystrophic features and abnormal mitochondria. Through exome sequencing, I identified compound heterozygous *SCN4A* mutations in all three affected brothers. A missense mutation affecting a conserved residue was found on the paternal allele and a splice mutation on the maternal allele. Muscle RNA analysis showed that the splice mutation leads to the use of a cryptic donor splice site followed by exon skipping and ultimately generating a shorter transcript with an in-frame deletion of 183 nucleotides.

Conclusion

This study expanded the clinical, histological and genetic spectrum of *SCN4A*-related myopathy, and highlighted that next-generation sequencing is an efficient approach to molecularly diagnose patients with unspecific myopathic features.

Contribution

I identified the *SCN4A* mutations in the family and confirmed segregation and contributed to the manuscript writi

Sandra Mercier, MD,
PhD*
Xavière Lornage, MS*
Edoardo Malfatti, MD,
PhD
Pascale Marcorelles, MD,
PhD
Franck Letournel, MD,
PhD
Cécile Boscher, MD
Gaëlle Caillaux, MD
Armelle Magot, MD
Johann Böhm, PhD
Anne Boland, PhD
Jean-François Deleuze,
PhD
Norma Romero, MD,
PhD
Yann Péréon, MD, PhD‡
Jocelyn Laporte, PhD‡

EXPANDING THE SPECTRUM OF CONGENITAL MYOPATHY LINKED TO RECESSIVE MUTATIONS IN *SCN4A*



Congenital myopathies are phenotypically and genetically heterogeneous.¹ While *SCN4A* mutations were previously described in hypokalemic or hyperkalemic periodic paralysis, paramyotonia, myotonia congenita, or myasthenic syndrome,²⁻⁶ loss-of-function recessive mutations in *SCN4A* were recently identified in 11 individuals with severe fetal hypokinesia or congenital myopathies.⁷ Among them, 7 died in the perinatal period and 4 had congenital hypotonia, significant respiratory and swallowing difficulties, and spinal deformities.

We report on 3 brothers presenting a peculiar clinical and histopathologic phenotype characterized by facial weakness with ptosis and a mild dystrophic pattern associated with recessive *SCN4A* mutations.

Cases. The 3 probands, including monozygous twins, were born to nonconsanguineous parents (figure, A). Detailed clinical features are presented in table e-1 at Neurology.org. Family history was unremarkable. Both pregnancies were complicated by polyhydramnios and premature birth. All patients had severe neonatal hypotonia and cryptorchidism. The twins showed severe swallowing difficulties, necessitating Nissen fundoplication surgery. Parenteral gastrostomy feeding was set up from the age of 6 and 14 months until 4, 5 years of age, respectively. The firstborn developed severe scoliosis. Motor skills were delayed. The patients acquired independent ambulation at 2 years of age. Cognitive development and cerebral MRIs were normal. Clinical examination revealed proximal and axial weakness, elongated face with dolichocephaly, and facial hypotonia with high-arched palate (table e-1). The twins had bilateral nonfluctuant ptosis and global amyotrophy with thin muscular bulk (figure, B–D). There was no myotonia, fluctuating muscle weakness, or fatigability. The 3 brothers experienced a significant clinical improvement over time as they now have normal gait and no problem with jumping or climbing stairs (table e-1). Serum creatine kinase levels were repeatedly normal. The firstborn underwent EMG at age 6 years, revealing a myopathic pattern associated with increased duration of the CMAP and decreased

muscle fiber conduction velocity (rectus femoris muscle [RF]: 1.9 m/s; normal range 2.8–4.1 m/s). Nerve conduction velocities were normal and there was no decrement after repetitive nerve stimulation. EMG, performed at 3 months of age, only showed reduction of muscle fiber conduction velocity (left and right RF: 0.9 m/s and 1.0 m/s, respectively).

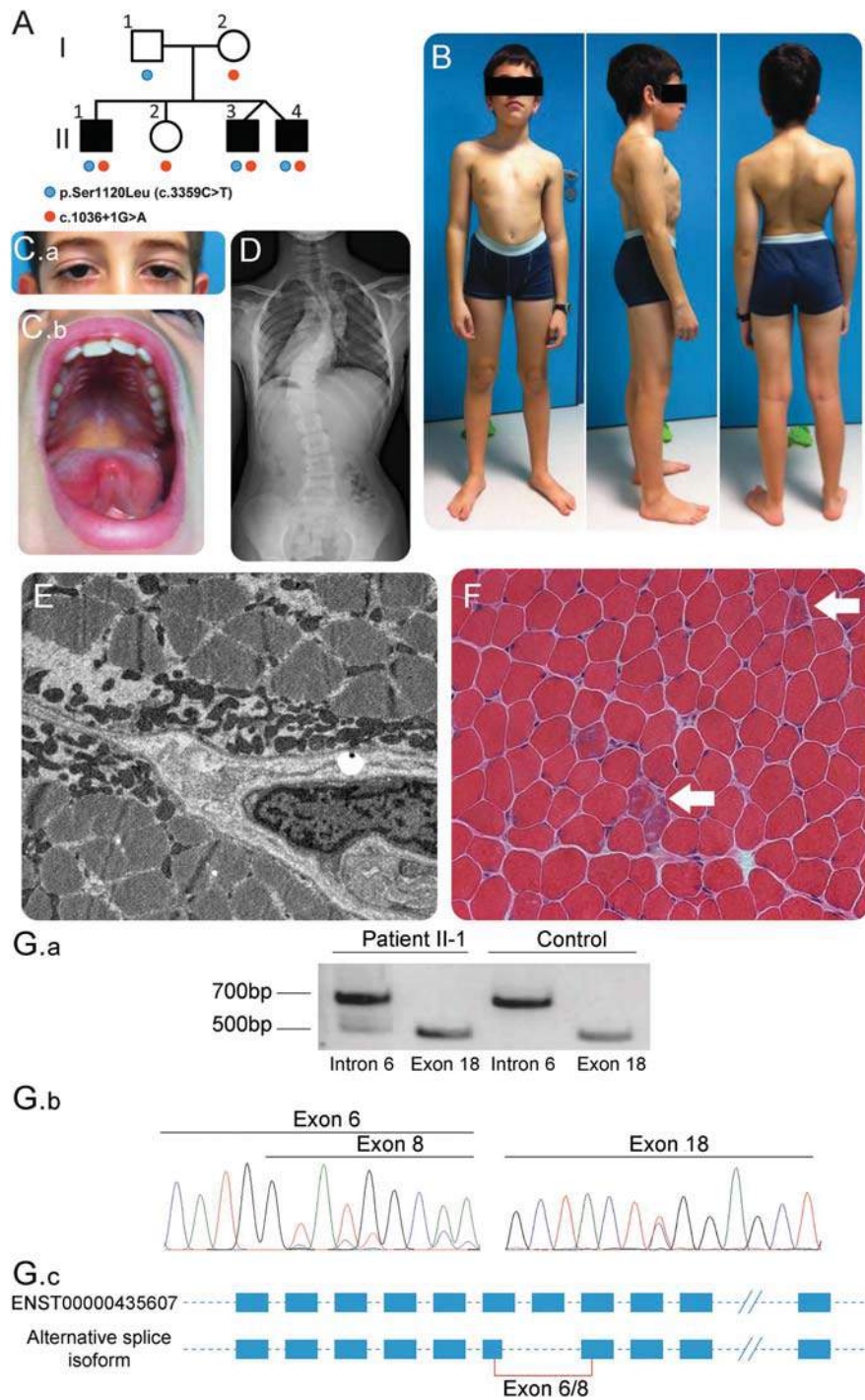
Muscle biopsy was performed in the firstborn at age 3 years. Electron microscopy study revealed abnormal subsarcolemmal collection of mitochondria that appeared abnormal in both shape and size (figure, F). Muscle biopsy performed in one of the twins at 5 years of age revealed a mild dystrophic pattern characterized by the presence of scattered necrotic-regenerating fibers presenting immunoreactivity with utrophin, CD68, and MHCd (developmental myosin heavy chain) antibodies (not shown). Mild fiber size diameter variation, increased nuclear internalization, and slight type I fiber predominance were also observed (figure, F).

Exome sequencing was performed for all 6 members of the family. Variants calling and filtering for rare variants compared to ExAC database and an in-house database of 1,550 exomes led to the identification of compound heterozygous mutations in *SCN4A* in the 3 affected members. Neither of those 2 mutations was found in the public variant or the in-house databases. The father carried a missense mutation p.Ser1120Leu (c.3359C > T) affecting a conserved amino acid encoded by exon 18 of *SCN4A* located close to the previously described p.Arg1135Cys found in the adjacent charged transmembrane domain.⁷ The mother carried a single nucleotide exchange in intron 6 (c.1036+1 G > A) in the essential donor splice site. Reverse transcription PCR analysis from patient II-1's muscle showed that this mutation leads to the use of a cryptic donor site in exon 6 and skipping of exon 7, producing a shorter RNA with an in-frame deletion (figure, G).

Discussion. Our study contributes to expanding the phenotypes of congenital myopathies associated with recessive mutations in *SCN4A* by the report of 3 additional cases to the 4 surviving individuals recently described.⁷ The patients were compound heterozygous for 2 novel mutations: an essential splice site variation and a missense variation in *SCN4A*. This led to severe

Supplemental data
at Neurology.org

Figure Clinical, pathologic, and molecular data of patients with compound heterozygous mutations in *SCN4A*



(A) Pedigree of the family with *SCN4A* mutations indicated compared to reference NM_000334. The 3 affected brothers are represented by shaded symbols. Segregation of the mutations was confirmed by Sanger sequencing. Clinical images of patient II-1: (B) bilateral scapular winging, scoliosis, and lumbar hyperlordosis, (C.a) ptosis in patient II-3, (C.b) high-arched palate in patient II-1. (D) Thoracolumbar spine X-ray shows a severe thoracic scoliosis with double curve in patient II-1 (Cobb angles of 59° for the upper curve and 51° for the lower curve). (E) Muscle biopsy analyses (electron microscopy, $\times 10,000$) presence of an abnormal subsarcolemmal collection of mitochondria with irregular shape and size in patient II-1. (F) Light microscopy (hematoxylin & eosin, $\times 20$) shows the presence of scattered basophilic bona fide regenerating fibers in patient II-2 (white arrows). (G) RNA analysis of patient II-1 muscle. (G.a) Agarose gel electrophoresis of reverse transcription PCR amplification product reveals an additional splice product generated by the mutation in intron 6. (G.b) Chromatophoregrams show that the impact of the mutation in intron 6 leads to the use of a cryptic donor site in exon 6 and skipping of exon 7, producing a shorter RNA with an in-frame deletion of 183 nt (predicted 61aa deletion in the third extracellular loop of the first transmembrane domain) (left) and the presence of the mutation in exon 18 affecting a conserved amino acid located in the second extracellular loop of the third transmembrane domain (right). (G.c) Scheme of the new splice product created by the mutation in intron 6.

myopathic features at birth with a good prognosis and improvement in the first decade of life. Ptosis was not observed in any member of this first report whereas it was obvious in the twins. It demonstrated that ptosis could be a key feature of this pathology as observed in other congenital myopathies. Moreover, muscle biopsy showed an overlap between myopathic and dystrophic features, broadening the spectrum of histologic traits/specificities associated with mutations in *SCN4A*. This study shows that a multidisciplinary approach including clinical, histologic, electrophysiologic, and genetic description of patients can lead to the identification of the disease-causing mutation and expand the knowledge of myopathy-causing genes such as *SCN4A*.

*These authors contributed equally as co-first authors.

‡These authors contributed equally as co-last authors.

From CHU de Nantes (S.M., C.B., G.C., A.M., Y.P.); University of Nantes (S.M., Y.P.), INSERM UMR1089 (S.M.), IRS2, Nantes; Institut de Génétique et de Biologie Moléculaire et Cellulaire (IGBMC) (X.L., J.B., J.L.); Centre National de la Recherche Scientifique (X.L., J.B., J.L.), UMR7104; Institut National de la Santé et de la Recherche Médicale (X.L., J.B., J.L.), U964; Université de Strasbourg (X.L., J.B., J.L.), Illkirch; Sorbonne Universités (E.M., N.R.), UPMC Univ Paris 06, INSERM UMRS974, GH La Pitié-Salpêtrière; Assistance Publique-Hôpitaux de Paris (E.M., N.R.), GHU La Pitié-Salpêtrière (E.M., N.R.); CHRU Brest (P.M.); EA 4586 LNB (P.M.), Université de Bretagne Occidentale, Brest; IBS (PBH-IRIS) (F.L.), CHU, Angers; and CEA (A.B., J.-F.D.), Evry, France.

Author contributions: Dr. Mercier: acquisition of data, critical revision of the manuscript, study supervision. Dr. Lornage: acquisition, analysis and interpretation of molecular data, critical revision of the manuscript. Dr. Malfatti: acquisition of data, critical revision of the manuscript. Dr. Marcorelles: acquisition of data. Dr. Letournel: acquisition of data. Dr. Boscher: acquisition of data. Dr. Caillaux: acquisition of data. Dr. Magot: critical revision of the manuscript. Dr. Böhm: acquisition, analysis and interpretation of molecular data. Dr. Boland: genomic data generation. Dr. Deleuze: genomic data generation. Dr. Romero: acquisition of data, critical revision of the manuscript. Dr. Péréon: acquisition of data, critical revision of the manuscript, study supervision. Dr. Laporte: analysis and interpretation of genetic data, critical revision of the manuscript, study supervision.

Acknowledgment: The authors thank the family who participated in this study and the collaborators who contributed to this work: Julie Perrier, Raphaël Schneider, Valérie Biancalana, Vanessa Schartner, Christine Kretz, Antoine Hamel, Anne Dariel, Julie Thompson, Emmanuelle Fleurence, and Jean-Yves Mabé.

Study funding: This work was supported by Fondation pour la Recherche Médicale and the France Génomique National infrastructure and funded as part of the “Investissements d’Avenir” program managed by the Agence Nationale pour la Recherche (ANR-10-INBS-09) and by Fondation Maladies Rares within the frame of the “Myocapture” sequencing project.

Disclosure: S. Mercier reports no disclosures relevant to the manuscript. X. Lornage received research support from the Fondation pour la Recherche Médicale and the France Génomique National infrastructure and was funded as part of the “Investissements d’Avenir” program managed by the Agence Nationale pour la Recherche (ANR-10-INBS-09) and the Fondation Maladies Rares within the frame of the “Myocapture” sequencing project. E. Malfatti, P. Marcorelles, F. Letournel, C. Boscher, G. Caillaux, and A. Magot report no disclosures relevant to the manuscript. J. Böhm received research support from the Fondation pour la Recherche Médicale and the France Génomique National infrastructure and was funded as part of the “Investissements d’Avenir” program managed by the Agence Nationale pour la Recherche (ANR-10-INBS-09) and the Fondation Maladies Rares within the frame of the “Myocapture” sequencing project. A. Boland, F. Deleuze, N. Romero, and Y. Péréon report no disclosures relevant to the manuscript. J. Laporte received research support from the Fondation pour la Recherche Médicale and the France Génomique National infrastructure and was funded as part of the “Investissements d’Avenir” program managed by the Agence Nationale pour la Recherche (ANR-10-INBS-09) and the Fondation Maladies Rares within the frame of the “Myocapture” sequencing project. Go to Neurology.org for full disclosures.

Received May 17, 2016. Accepted in final form October 19, 2016.

Correspondence to Dr. Mercier: sandra.mercier@chu-nantes.fr

© 2016 American Academy of Neurology

1. Nance JR, Dowling JJ, Gibbs EM, Bönnemann CG. Congenital myopathies: an update. *Curr Neurol Neurosci Rep* 2012;12:165–174.
2. Plassart E, Reboul J, Rime CS, et al. Mutations in the muscle sodium channel gene (*SCN4A*) in 13 French families with hyperkalemic periodic paralysis and paramyotonia congenita: phenotype to genotype correlations and demonstration of the predominance of two mutations. *Eur J Hum Genet* 1994;2:110–124.
3. Ptáček LJ, Tawil R, Griggs RC, et al. Sodium channel mutations in acetazolamide-responsive myotonia congenita, paramyotonia congenita, and hyperkalemic periodic paralysis. *Neurology* 1994;44:1500–1503.
4. Sternberg D, Maisonobe T, Jurkat-Rott K, et al. Hypokalemic periodic paralysis type 2 caused by mutations at codon 672 in the muscle sodium channel gene *SCN4A*. *Brain* 2001;124:1091–1099.
5. Magot A, David A, Sternberg D, Péréon Y. Focal and abnormally persistent paralysis associated with congenital paramyotonia. *BMJ Case Rep* 2014; pii: bcr2014204430.
6. Habbout K, Poulin H, Rivier F, et al. A recessive Nav1.4 mutation underlies congenital myasthenic syndrome with periodic paralysis. *Neurology* 2016;86:161–169.
7. Zaharieva IT, Thor MG, Oates EC, et al. Loss-of-function mutations in *SCN4A* cause severe foetal hypokinesia or “classical” congenital myopathy. *Brain* 2016;139:674–691.

2.2.4 Publication 6: CASQ1 mutations impair calsequestrin polymerization and cause tubular aggregate myopathy (Bohm et al. 2018)

Background

Tubular aggregate myopathy (TAM) is a progressive muscle disorder primarily affecting the proximal muscles of the lower limbs and is characterized by abnormal accumulations of membrane tubules in muscle fibers (Morgan-Hughes 1998). TAM arises from gain-of-function mutations in *STIM1* and *ORAI1*, both encoding key factors in the regulation of Ca^{2+} homeostasis (Bohm and Laporte 2018; Endo et al. 2015; Bohm et al. 2017; Bohm et al. 2013). A significant number of TAM patients do not carry mutations in *STIM1* and *ORAI1*, suggesting the implication of additional genes.

Aim of the study

The aim of the study was to identify the genetic cause of the disease in two families with molecularly undiagnosed TAM, and to characterize the pathomechanism of the disease.

Results

The patients described in this study belong to two unrelated families with slowly progressive adult-onset muscle weakness or myalgia predominantly affecting the lower limbs. Muscle biopsies revealed prominent tubular aggregates as the main histopathological hallmark. Exome sequencing identified heterozygous *CASQ1* missense mutations affecting conserved amino acids. Calsequestrin encoded by *CASQ1* and exclusively expressed in skeletal muscle, is the major Ca^{2+} -binding protein in the sarcoplasmic reticulum, and forms needle-like polymers with increasing Ca^{2+} -binding capacities. A single missense mutation in *CASQ1* has previously been shown to cause vacuolar myopathy, differing from tubular aggregate myopathy at both the clinical and histopathological level (Rossi et al. 2014). Our functional experiments in transfected cells demonstrated a reduced capacity of mutant calsequestrin to depolymerize upon Ca^{2+} store depletion, and ultracentrifugation and turbidity assays on recombinant proteins showed that the mutants display a reduced polymerization rates at rising Ca^{2+} concentrations.

Conclusion

Here we showed that specific *CASQ1* mutations cause mild TAM, and functional experiments revealed that the mutations impact on the polymerization/depolymerization dynamics of calsequestrin. In contrast, the vacuolar myopathy mutation led to calsequestrin aggregation, suggesting that TAM involves a different pathomechanism. A parallel study confirmed the


implication of *CASQ1* mutations in TAM, and the results showed reduced Ca^{2+} stores in patient myotubes, demonstrating that the *CASQ1* mutations impair proper Ca^{2+} storage (Barone et al. 2017).

Contribution

I performed the transfection experiments and their analysis.

CORRESPONDENCE

CASQ1 mutations impair calsequestrin polymerization and cause tubular aggregate myopathy

Johann Böhm¹ · Xavière Lornage¹ · Frederic Chevessier² · Catherine Birck¹ · Simona Zanotti³ · Paola Cudia⁴ · Monica Bulla⁵ · Florence Granger¹ · Mai Thao Bui⁶ · Maxime Sartori¹ · Christiane Schneider-Gold⁷ · Edoardo Malfatti⁶ · Norma B. Romero⁶ · Marina Mora³ · Jocelyn Laporte¹ 

Received: 7 September 2017 / Revised: 10 October 2017 / Accepted: 10 October 2017 / Published online: 16 October 2017
© Springer-Verlag GmbH Germany 2017

Tubular aggregate myopathy (TAM) is a rare muscle disorder characterized by abnormal accumulations of membrane tubules in muscle fibers, and marked by progressive muscle weakness, cramps, and myalgia [3]. Genetically, TAM has been assigned to mutations in *STIM1* [2] and *ORAI1* [7], both encoding key regulators of Ca²⁺ homeostasis. Through exome sequencing of molecularly undiagnosed TAM cases, we now identified *CASQ1* as the third TAM gene, and we support our findings by clinical, histological, genetic, and functional data.

Family 1 has an ancestral history of a muscle phenotype segregating as a dominant disease, and a partial clinical and histological description was reported earlier [8]. Patient 103901 from Family 2 is a singleton. Birth, early childhood, and motor milestones were normal for all affected members from both families. Disease onset was between early 20s and mid-40s with a slowly progressive muscle weakness mainly

involving the proximal muscles in the lower limbs for Family 1, and early 50s with post-exercise myalgia in the lower limbs for Family 2 (Supplementary Table 1). Histological and ultrastructural analyses of the muscle biopsies displayed tubular aggregates as the main histopathological hallmark in both families (Fig. 1a). Exome sequencing identified the heterozygous *CASQ1* missense mutations c.166A>T (N56Y) in exon 1 in Family 1, and c.308G>A (G103D) in exon 2 in Family 2. Both mutations affect highly conserved amino acids (Supp. Figure 1), none was found in the available healthy family members, and none was listed in the public or internal SNP databases. A single *CASQ1* missense mutation (D244G) has previously been associated with vacuolar myopathy involving protein aggregates [9]. *CASQ1* is primarily expressed in skeletal muscle and encodes calsequestrin, the major Ca²⁺ storage protein in the sarcoplasmic reticulum. Calsequestrin binds Ca²⁺ with moderate affinity and high capacity, and forms higher order polymers with increasing Ca²⁺-binding capacities [4].

Immunohistochemistry on a muscle biopsy from Family 2 revealed strong signals for calsequestrin, STIM1, and RyR1 in aggregated structures most likely corresponding to the tubular aggregates, while ORAI1 was not trapped (Fig. 1b). This conforms to the observations made on biopsies from *STIM1* and *ORAI1* patients and demonstrates that the trapped proteins are primarily of sarcoplasmic reticulum origin [1, 2]. These findings on a single muscle biopsy also suggest that aggregation of STIM1 appears to be a consequence of *CASQ1* mutations, providing a pathological link between *STIM1*- and *CASQ1*-related TAM. In transfected C2C12 myoblasts, WT and both TAM N56Y and G103D mutants formed calsequestrin networks of comparable complexity, while the vacuolar myopathy D244G mutant induced major calsequestrin aggregation (Fig. 1c). Calsequestrin polymerization and depolymerization are dynamic

Electronic supplementary material The online version of this article (doi:10.1007/s00401-017-1775-x) contains supplementary material, which is available to authorized users.

✉ Johann Böhm
johann@igbmc.fr

✉ Jocelyn Laporte
jocelyn@igbmc.fr

¹ IGBMC, Inserm U 964, CNRS UMR 7104, University of Strasbourg, Illkirch, France

² CureVac AG, Tübingen, Germany

³ IRCCS Istituto Neurologico C. Besta, Milan, Italy

⁴ IRCCS San Camillo Hospital, Venice, Italy

⁵ University of Geneva, Geneva, Switzerland

⁶ Institut de Myologie, Paris, France

⁷ Ruhr-University Bochum, Bochum, Germany

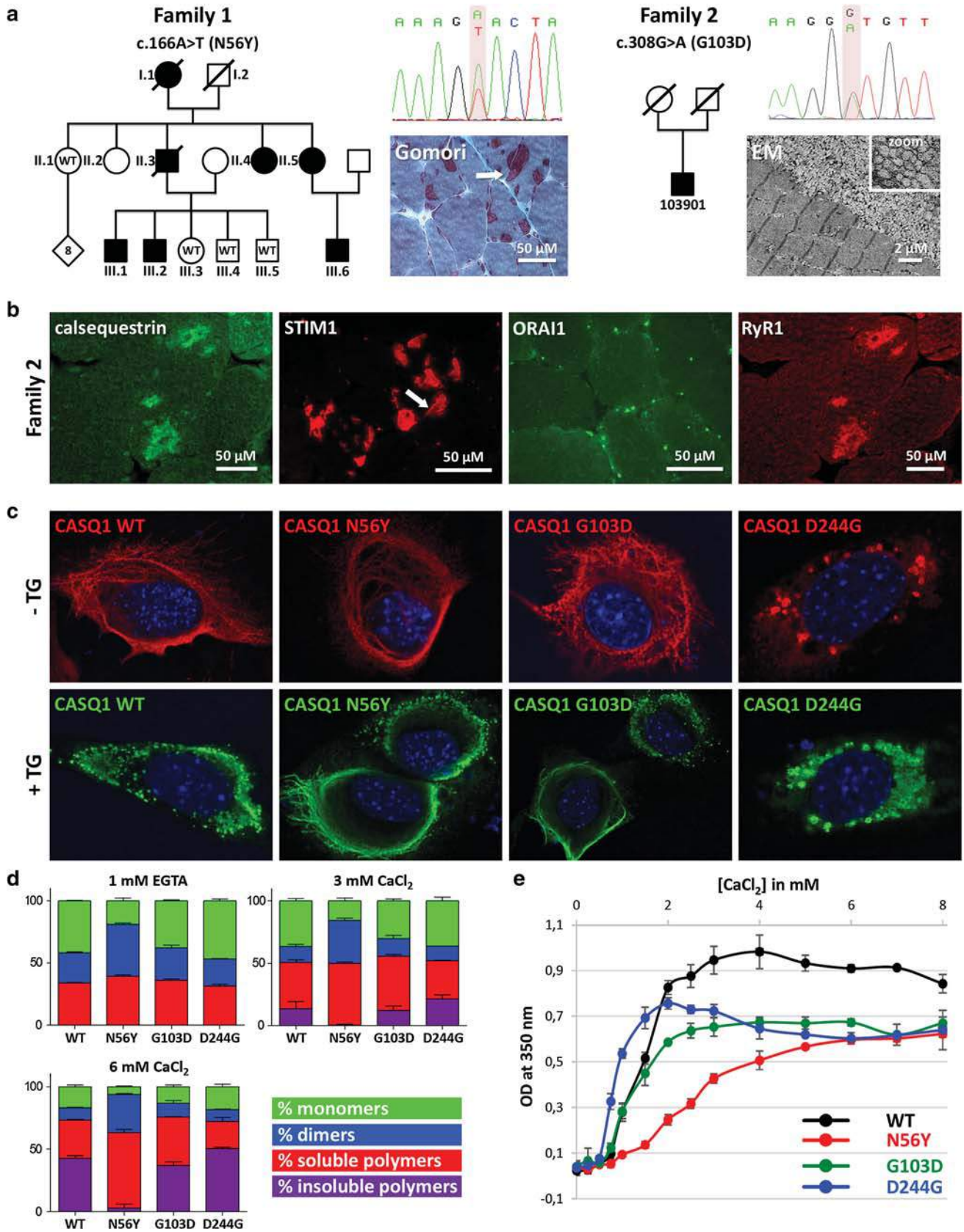


Fig. 1 Impact of the *CASQ1* mutations and immunohistochemistry on muscle biopsies. **a** Heterozygous *CASQ1* missense mutations segregating with the disease were identified in both families displaying tubular aggregates on muscle biopsies (arrow, zoom). **b** Immunohistochemistry on the biopsy from Family 2 revealed aggregation of calsequestrin, STIM1, and RyR1, but not of ORAI1. The STIM1 signals were thereby more pronounced in the periphery of the aggregated structures (arrow), while calsequestrin and RyR1 were also found in the center. **c** In Ca^{2+} -containing medium, WT calsequestrin and the N56Y and G103D mutants formed complex networks in transfected C2C12 myoblasts, while the D244G mutant aggregated. Ca^{2+} store depletion through addition of Thapsigargin (Tg) induced major monomerization of WT calsequestrin, while the N56Y and G103D mutants remained in large parts polymeric. **d** Analytical ultracentrifugation showed that especially the TAM N56Y mutant formed less insoluble higher order polymers at rising Ca^{2+} concentrations compared to the wild type, while the vacuolar myopathy D244G strongly polymerized. **e** Turbidity assays confirmed the reduced propensity of both TAM mutants to polymerize at rising Ca^{2+} concentrations

Ca^{2+} -dependent processes, and the depletion of the SR Ca^{2+} stores was shown to favor the monomeric form of calsequestrin [6]. To test whether the *CASQ1* mutations influence calsequestrin monomerization upon Ca^{2+} store depletion, we treated the transfected cells ($n > 300$ per condition) with the SERCA inhibitor Thapsigargin (Tg). Dot-like calsequestrin signals corresponding to monomers or minor oligomers were seen in the majority (76%) of the cells expressing the WT, but only in 49.4% and 42.5% of the cells, respectively, expressing N56Y or G103D. To investigate the impact of the *CASQ1* mutations on calsequestrin polymerization, we performed analytical ultracentrifugation in solution containing recombinant calsequestrin and rising Ca^{2+} concentrations (Fig. 1d). We found that especially the TAM N56Y mutant formed significantly less higher order polymers than the wild-type, while the vacuolar myopathy D244G mutant showed an increased propensity to form insoluble polymers. To follow the polymerization kinetics of WT and mutant calsequestrin, we next performed turbidity assays (Fig. 1e). G103D and especially N56Y calsequestrin show reduced polymerization rates, and produced significantly less polymers at maximal Ca^{2+} levels compared to the wild-type protein. Contrasting wild-type and TAM calsequestrin, the D244G mutant strongly polymerized at minimal Ca^{2+} levels, confirming the results obtained by a previous study [5].

Taken together, we demonstrate that specific *CASQ1* mutations are one of the genetic causes of TAM. We show that the tubular aggregates in our patients contain calsequestrin, STIM1, and RyR1, and we provide functional evidence that *CASQ1* mutations significantly impair calsequestrin polymerization and depolymerization, while the vacuolar myopathy mutation increases Ca^{2+} -dependent

polymerization. This suggests that the *CASQ1* mutations causing either TAM or vacuolar myopathy involve different pathomechanisms.

Acknowledgements We thank the members of the families for their interest in this study, Wolfram Kress, Michel Fardeau, and Daniel Hantai for material transfer, and Catherine Koch, Anaïs Chanut, and Raphaël Schneider for their valuable technical assistance. This work was funded by INSERM, CNRS, University of Strasbourg, Agence Nationale de la Recherche (ANR-11-BSV1-026, ANR-10-LABX-0030-INRT, ANR-10-IDEX-0002, and FRISBI ANR-10-INBS-05), Fondation Maladies Rares, Association Française contre les Myopathies (AFM-17088), the Muscular Dystrophy Association (MDA-186985), and the Swiss National Science Foundation (323530_158118 to MB). The EuroBioBank and Telethon Network of Genetic Biobanks (GTB12001F to MM) are gratefully acknowledged for providing biological samples.

References

- Bohm J, Bulla M, Urquhart JE, Malfatti E, Williams SG, O'Sullivan J, Szlauer A, Koch C, Baranello G, Mora M et al (2017) ORAI1 mutations with distinct channel gating defects in tubular aggregate myopathy. *Hum Mutat*. doi:10.1002/humu.23172
- Bohm J, Chevessier F, Maues De Paula A, Koch C, Attarian S, Feger C, Hantai D, Laforet P, Ghorab K, Vallat JM et al (2013) Constitutive activation of the calcium sensor STIM1 causes tubular-aggregate myopathy. *Am J Hum Genet* 92:271–278. doi:10.1016/j.ajhg.2012.12.007S0002-9297(12)00641-6
- Chevessier F, Bauche-Godard S, Leroy JP, Koenig J, Paturneau-Jouas M, Eymard B, Hantai D, Verdiere-Sahuque M (2005) The origin of tubular aggregates in human myopathies. *J Pathol* 207:313–323. doi:10.1002/path.1832
- Damiani E, Salvatori S, Margreth A (1990) Characterization of calsequestrin of avian skeletal muscle. *J Muscle Res Cell Motil* 11:48–55
- Lewis KM, Ronish LA, Rios E, Kang C (2015) Characterization of two human skeletal calsequestrin mutants implicated in malignant hyperthermia and vacuolar aggregate myopathy. *J Biol Chem* 290:28665–28674. doi:10.1074/jbc.M115.686261
- Manno C, Figueroa LC, Gillespie D, Fitts R, Kang C, Franzini-Armstrong C, Rios E (2017) Calsequestrin depolymerizes when calcium is depleted in the sarcoplasmic reticulum of working muscle. *Proc Natl Acad Sci USA* 114:E638–E647. doi:10.1073/pnas.1620265114
- Nesin V, Wiley G, Kousi M, Ong EC, Lehmann T, Nicholl DJ, Suri M, Shahrizaila N, Katsanis N, Gaffney PM et al (2014) Activating mutations in STIM1 and ORAI1 cause overlapping syndromes of tubular myopathy and congenital miosis. *Proc Natl Acad Sci USA* 111:4197–4202. doi:10.1073/pnas.1312520111
- Rohkamm R, Boxler K, Ricker K, Jerusalem F (1983) A dominantly inherited myopathy with excessive tubular aggregates. *Neurology* 33:331–336
- Rossi D, Vezzani B, Galli L, Paolini C, Toniolo L, Pierantozzi E, Spinozzi S, Barone V, Pegoraro E, Bello L et al (2014) A mutation in the *CASQ1* gene causes a vacuolar myopathy with accumulation of sarcoplasmic reticulum protein aggregates. *Hum Mutat* 35:1163–1170. doi:10.1002/humu.22631

2.2.5 Publication 7: *HNRNPDL*-related muscular dystrophy: expanding the clinical, morphological and MRI phenotypes (Berardo et al. 2019)

Background

HNRNPDL encodes the heterogeneous nuclear ribonucleoprotein D-like protein (hnRNPDL). This protein belongs to a family of ribonucleoproteins, controlling the maturation and splicing of nuclear hnRNAs/pre-mRNAs (Dreyfuss et al. 1993; Motta-Mena, Heyd, and Lynch 2010). Two distinct *HNRNPDL* mutations affecting the same amino-acid (p.(Asp378Asn), p.(Asp378His)) were previously reported in patients with adult-onset limb-girdle muscular dystrophy (Vieira et al. 2014; Sun et al. 2019).

Aim of the study

The aim of the study was to characterize two families with an adult-onset myopathy at the clinical, histological and genetic level.

Results

We described five patients from two families with a progressive muscle weakness starting in the third or fourth decade. The first signs of the disease are lower limb muscle weakness and scapular winging. Histological and ultrastructural studies revealed a high number of rimmed vacuoles and autophagic changes, and MRI investigations on three patients highlighted a selective sparing of rectus femoris and adductor longus muscles compared to other muscles of the thigh. All patients were found to carry a previously described *HNRNPDL* p.(Asp378His) missense mutation.

Conclusion

This study expands the clinical and histological spectrum of patients with *HNRNPDL* mutations. Detailed MRI analyses of three patients and comparison with a previously reported *HNRNPDL* case uncovered a specific pattern recognizable from early stages of the disease (Sun et al. 2019). All *HNRNPDL* cases described so far carry mutations affecting amino acid 378 with aspartic acid changed either to asparagine or histidine. The families are from different ethnic background, suggesting that the codon for Asp378 may represent a mutational hotspot.

Contribution

I identified the *HNRNPDL* mutation in one family, confirmed the segregation, and contributed to the writing of the manuscript.



HNRNPDL-related muscular dystrophy: expanding the clinical, morphological and MRI phenotypes

Andrés Berardo¹ · Xavière Lornage² · Mridul Johari^{3,4} · Teresinha Evangelista^{5,6} · Claudia Cejas⁷ · Fabio Barroso⁷ · Alberto Dubrovsky⁸ · Mai Thao Bui⁵ · Guy Brochier^{5,6} · Maria Saccoliti⁹ · Johann Bohm² · Bjarne Udd^{4,10} · Jocelyn Laporte² · Norma Beatriz Romero^{5,6} · Ana Lia Taratuto⁹

Received: 23 March 2019 / Revised: 16 June 2019 / Accepted: 18 June 2019
© Springer-Verlag GmbH Germany, part of Springer Nature 2019

Abstract

Autosomal dominant limb girdle muscular dystrophy D3 *HNRNPDL*-related is a rare dominant myopathy caused by mutations in *HNRNPDL*. Only three unrelated families have been described worldwide, a Brazilian and a Chinese carrying the mutation c.1132G>A p.(Asp378Asn), and one Uruguayan with the mutation c.1132G>C p. (Asp378His), both mutations occurring in the same codon. The present study enlarges the clinical, morphological and muscle MRI spectrum of AD-*HNRNPDL*-related myopathies demonstrating the significant particularities of the disease. We describe two new unrelated Argentinean families, carrying the previously reported c.1132G>C p.(Asp378His) *HNRNPDL* mutation. There was a wide phenotypic spectrum including oligo-symptomatic cases, pure limb girdle muscle involvement or distal lower limb muscle weakness. Scapular winging was the most common finding, observed in all patients. Muscle MRIs of the thigh, at different stages of the disease, showed particular involvement of adductor magnus and vastus besides a constant preservation of the rectus femoris and the adductor longus muscles, defining a novel MRI pattern. Muscle biopsy findings were characterized by the presence of numerous rimmed vacuoles, cytoplasmic bodies, and abundant autophagic material at the histochemistry and ultrastructural levels. *HNRNPDL*-related LGMD D3 results in a wide range of clinical phenotypes from the classic proximal form of LGMD to a more distal phenotype. Thigh MRI suggests a specific pattern. Codon 378 of *HNRNPDL* gene can be considered a mutation hotspot for *HNRNPDL*-related myopathy. Pathologically, the disease can be classified among the autophagic rimmed vacuolar myopathies as with the other multisystem proteinopathies.

Keywords LGMD D3 *HNRNPDL*-related · *HNRNPDL* gene · Rimmed vacuolar myopathy · Autophagy

✉ Norma Beatriz Romero
nb.romero@institut-myologie.org

¹ Neuropsychiatry Center Valencia Positiva, Córdoba, Argentina

² Department of Translational Medicine, Institut de Génétique Et de Biologie Moléculaire Et Cellulaire (IGBMC)INSERM U1258, UMR7104, Strasbourg University, Illkirch, France

³ Department of Medical Genetics, University of Helsinki, Medicum, Finland

⁴ Folkhälsan Research Center, Helsinki, Finland

⁵ Morphology Unit, Myology Institute, GHU Pitié-Salpêtrière, 75013 NeuromuscularParis, France

⁶ Sorbonne Université, AP-HP, INSERM, Centre de référence Des Maladies Neuromusculaires Nord/Est, Ile de France, Paris, France

⁷ Instituto de Investigaciones Neurológicas FLENI, Buenos Aires, Argentina

⁸ Fundación Favaloro, Buenos Aires, Argentina

⁹ Neuropathology and Neuromuscular Diseases Laboratory, Buenos Aires, Argentina

¹⁰ Neuromuscular Research Center, Tampere University and University Hospital, Tampere, Finland

Introduction

According to the recent definition established by a group of experts at the 229th European Neuromuscular Centre (ENMC) international workshop in 2017: ‘Limb girdle muscular dystrophy (LGMD) is a genetically inherited condition that primarily affects skeletal muscle leading to progressive, predominantly proximal muscle weakness at presentation’ [1]. Among LGMD, the autosomal dominant forms are relatively rare and represent 10% of all LGMD [2]. According to the new LGMD classification, autosomal dominant LGMD includes: LGMDD1 DNAJB6-related, LGMDD2 TNPO3-related, LGMDD3 HNRNPDL-related and LGMDD4 CAPN3-related myopathy [1].

LGMDD3 HNRNPDL-related, previously LGMD1G (OMIM #609115) was first described in 2004 in a dominant Brazilian-Caucasian family with 12 patients distributed over three generations [2]. The age at onset varied from 30 to 47 years. The slowly progressive disease started with proximal lower limbs involvement later followed by proximal upper limbs weakness. Progressive finger and toe flexion limitations and muscle cramps were present in most patients. Serum creatinekinase (CK) activity was normal or slightly increased. Muscle histology was available for one patient and described as a “myopathic pattern” with fibre size variability, necrotic fibres, groups of atrophic angulated fibres, and rimmed vacuoles [2]. In 2014, LGMDD3HNRNPDL-related was also reported in a Uruguayan family with 18 affected members [3]. The age of onset varied from 15 to 55 years of age. The clinical signs were similar to those of the Brazilian family, but in 8 patients the symptoms started with proximal upper limb weakness and difficulty to raise the arms. Additionally, some affected members presented early onset cataracts [3]. For both the Brazilian and Uruguayan families; the disease affected both sexes with incomplete penetrance. Genome sequencing identified two different missense mutations in *HNRNPDL* (on chromosome 4q21) encoding the heterogeneous nuclear ribonucleoprotein D-like (hnRNPDL). Both mutations were heterozygous and affected the same aminoacid: p.(Asp378Asn) in the Brazilian family and p.(Asp378His) in the Uruguayan family. Recently, a Chinese family with 10 affected individuals over three generations was reported to carry the original Brazilian p.(Asp378Asn) mutation [4]. While muscle morphology showed similar features with the presence of rimmed vacuoles, the clinical phenotype slightly differed from the previously reported families with half of the Chinese patient’s presenting distal as well as proximal limb weakness. Flexion limitation of fingers and toes, which was a typical feature in the other two reported families,

was not present, highlighting the broad clinical spectrum of the disease.

hnRNPDL acts as a regulator of pre-mRNA splicing and nuclear export. *HNRNPDL* mutations are thought to cause defects in mRNA biogenesis and metabolism [5]. This DNA/RNA-binding protein has been shown to localize in the cytoplasm and in the nucleus [6, 7]. Data from Vieira et al. 2014, suggested that the translocation of the protein from the cytoplasm to the nucleus might be impaired by the p.(Asp378Asn) mutation. This could prevent the protein to access to the nucleus to perform its function on pre-mRNA maturation. Many hnRNPs were linked to various diseases due to their crucial role in the regulation of gene expression [8]. Mutations in the prion-like domains (PrLD) of hnRNP A1 and hnRNP A2B1 cause a multisystem proteinopathy (MSP), an inherited pleiotropic degenerative disorder that can affect muscle, bone, and the nervous system. However, an isolated myopathy has also been described in association with hnRNP A1 mutations [9]. Affected tissues in multisystem proteinopathies present ubiquitin-positive inclusions that contain RNA-binding proteins, such as hnRNP A1 and hnRNP A2B1, and may stain positive for proteins that mediate ubiquitin-dependent autophagy [9]. Rimmed vacuolation is a key feature of the myopathology in MSP [10].

Here we describe two unrelated families from Argentina with LGMDD3 HNRNPDL-related at the clinical, muscle imaging, histopathological and ultrastructural level.

Materials and methods

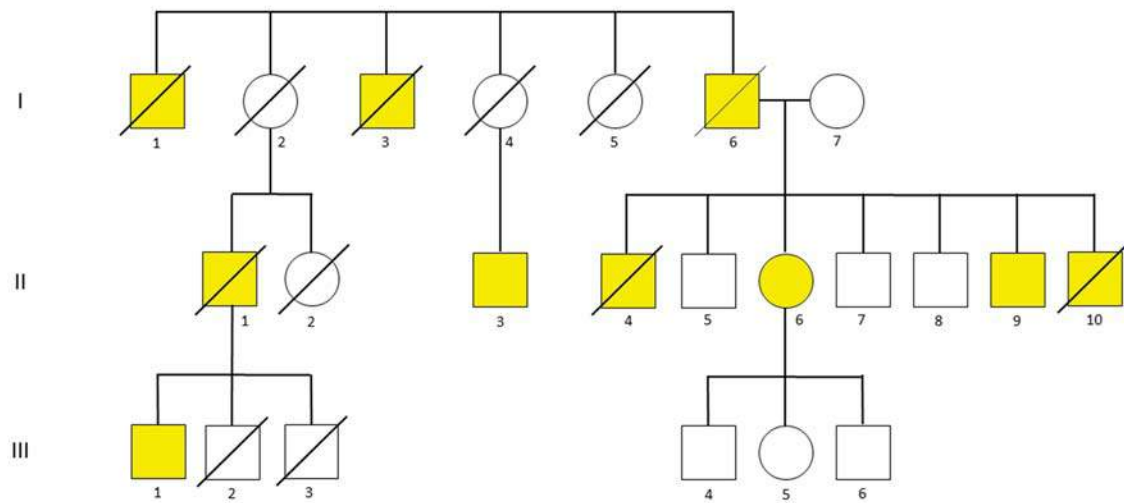
Patients

Two unrelated Argentinean families of European ancestry with history of adult-onset myopathy were included in the study (Fig. 1: family A and family B). All patients underwent detailed clinical examination summarized in Table 1.

Morphological studies

Open muscle biopsies of the quadriceps were obtained from four patients, three (III-1, II-6 and II-9) from family A (FA) and one (III-1) from family B (FB) (Fig. 1). For conventional histochemical techniques 10- μ m thick cryostat sections were stained with haematoxylin and eosin (HE), modified Gomori trichrome (mGT), Periodic-acid Schiff technique (PAS), Oil red O, nonspecific esterase, reduced nicotinamide adenine dinucleotide dehydrogenase-tetrazolium-reductase (NADH-TR), succinic dehydrogenase (SDH), cytochrome c oxidase (COX), menadione-nitro blue tetrazolium and adenosine triphosphatase (ATPase) pre-incubated at pH 9.4, 4.63, 4.35.

Family A



Family B

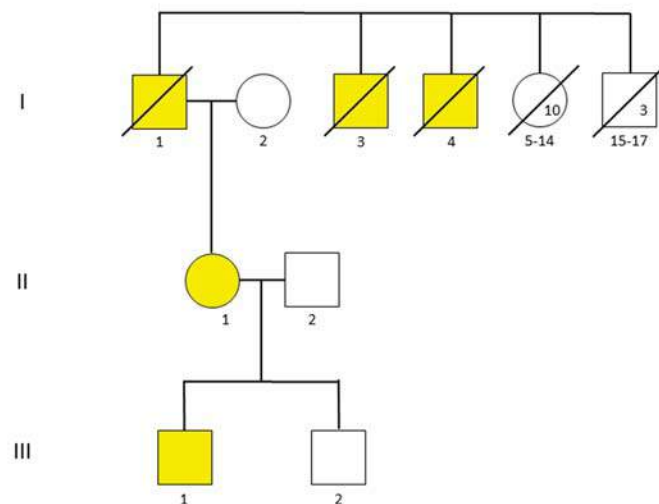


Fig. 1 Family A and Family B pedigrees

Immunohistochemistry (IHC)

IHC was performed in frozen muscle sections from patients III-1, II-6, II-9 from FA. Antibodies against Desmin (Anti-Human Desmin, Clone D33, Dako Laboratories, Denmark A/S), Myotilin (NCL-Myotilin, Novocastra Laboratories, Newcastle Upon Tyne, United Kingdom), α B-crystallin (CRYAB, GeneTex International Corporation, Irvine, USA), C5b9 (Dako), P62 (BD-Transduction Laboratories) and antibodies against dystrophin (Dys2, Leica), a, b, g, d sarcoglycans (Leica), alpha 2 laminin, dysferlin (Leica), were applied to 10 μ m thick cryosections and revealed using immunoperoxidase techniques.

Electron microscopy

Electron microscopy (EM) was performed in three cases (FA.III-1, FA.II-6 and FB.III-1). Small muscle samples were fixed in 2.5% glutaraldehyde, pH 7.4, post-fixed in 4% osmium tetroxide, dehydrated and embedded in araldite. Several blocks from each patient were studied, including longitudinally and transversally oriented samples. Semi-thin sections were stained with toluidine-blue and examined on light microscopy. Ultrathin sections were stained with uranyl acetate and lead citrate (Reynolds) and viewed with a Zeiss EM 109 T.

Table 1 Clinical, MRI and histological findings in the patients

Patient	FA.III-1	FA.II-6	FA.II-9	FB.II-1	FB.III-1
Age (y)	56	68	59	65	46
Age at onset (y)	38	48	38	63	41
Sex	M	F	M	F	M
Weakness	Early distal LL, then proximal LL and UL	Early proximal LL, then distal UL and LL	Early proximal LL, then distal UL and LL	Slight proximal LL	Proximal LL, proximal UL
Scapular winging	+	+	+	mild	+
Limitation of fingers flexors	+	+	+	-	-
Thigh atrophy	+	+	+	-	+
Early cataracts	-	+	-	-	-
MRI pattern	NP	RF/AL preserved Tibial anterior and soleus involvement	NP	RF/AL preserved No lower leg involvement	RF/AL preserved No lower leg involvement
Histology findings	Numerous rimmed vacuoles, cytoplasmic bodies and atrophic fibres	Rimmed vacuoles. Few necrotic/regenerative fibres. Some atrophic fibres and pyknotic nuclear clumps	Numerous rimmed vacuoles	NP	Scarce rimmed vacuoles Slight subsarcolemmal increase in oxidative activity was present. Isolated atrophic fibres
Electron microscopy findings	Abundant autophagic changes, cytoplasmic bodies, myofibrillar degeneration, filamentous bundles of Z-disc origin	Some autophagic changes with myofibrillar degeneration and filamentous accumulation	NP	NP	Clear autophagic material and filamentous structures
CK levels	42y: 1123–1800 IU/L 54y: 677 IU/L	300 IU/L	N.P	Normal	862 IU/L (upper normal limit) 150 IU/L
Echocardiogram	Normal	Normal	Normal	Normal	Normal
Spirometry	Normal	Normal	VI; diminished VC	Normal	Normal

NP not performed, LL lower limbs, UL upper limbs, RV rimmed vacuoles, Y year, CK creatine kinase, VC vital capacity, VI ventilatory insufficiency, RF rectus femoris muscle, AL adductor longus muscle

Genetic analysis

In family A (Fig. 1), exome sequencing was performed for individuals FA.II-6, FA.II-7 and FA.II-9 with the SureSelect Human All Exon 50 Mb capture library v5 (Agilent, Santa Clara, USA). Samples were paired-end sequenced on Illumina HiSeq 2500 (Illumina, San Diego, USA). In family B (Fig. 1), exome sequencing was performed on the index patient (FB.III-1) with Roche SeqCap EZ Human Exome v3 with 75 bp paired end reads and sequenced on Illumina NextSeq 550 (Illumina, San Diego, USA).

Alignment was performed on the GRCh37/hg19 reference genome and the variants were filtered using their frequency in gnomAD (<https://gnomad.broadinstitute.org/>) and in our in-house database containing over 1500 exomes. The variants with minor allele frequency over 0.01 were removed from analysis. The mutation was numbered according to the GenBank NM_031372.3 with +1 corresponding to the A of the ATG translation initiation codon.

In family A, confirmation of variants and segregation was performed with Sanger sequencing for four affected (FA.II-6, FA.II-9, FA.II-10, FA.III-1) and three healthy individuals (FA.II-5, FA.II-7, FA.III-2). In family B, the segregation was verified by Sanger sequencing in three other family members (FB.II-1, FB.II-2 and FB.III-2).

Magnetic resonance imaging (MRI)

Muscle MRI was performed in one member from family A (FA.II-6) and two from family B (FB.III-1, FB.II-1). Fast Spin Echo (FSE) T1 and T2-weighted STIR (Short-tau inversion recovery) images were acquired in axial and coronal planes of both thighs and legs. We analysed and classified all cases considering the type of involvement of each muscle: perifascial, concentric, mottled, muscle atrophy vs. hypertrophy, oedema vs. fatty infiltration, the muscles most affected in each compartment, using the Mercuri score [11, 12].

Results

Phenotypic presentation and clinical investigations

Family A (FA)

An Argentinean family originally from the province of Buenos Aires with Italian ancestry. There were 10 affected family members over 3 generations (Fig. 1). All affected individuals had a normal early motor development. The age at onset ranged from 38 to 48 years. The initial symptoms were proximal lower limb weakness in two patients (FA.II-6, II-9) associated with distal lower limb weakness in one of

them (FA.III-1). Scapular winging and anterior thigh atrophy were common findings in all patients (Fig. 2). Other symptoms and signs were muscle cramps (FA. I-6, II-6 and II-10) and early onset cataracts (FA. I6, II-4, II-6 and II-10). No additional clinical information was available from the deceased relatives.

FA.III-1

A 56-year-old male with asymmetric distal lower limb weakness from the age of 38, unable to walk on heels. Muscle weakness progressed to the proximal lower limb muscles, and to the shoulder and arm muscles. This resulted in frequent falls. Later on, he developed limitations of finger and toe flexors. At present he is unable to raise his arms, has marked bilateral scapular winging (Fig. 2b), symmetrical quadriceps atrophy and walks with a cane. No cataracts were observed. CK levels were variably increased at several determinations, with values between 677–1800 IU/l [normal values (nv): 55–170 IU/l]. Cardiovascular and pulmonary evaluation was unremarkable. He had two non-affected brothers that are deceased. His deceased father developed scapular winging during adulthood and cataracts at 70 years of age.

FA.II-6

A 68-year-old woman whose first symptom was early onset cataracts revealed at the age of 42 years. By the age of 48, she developed proximal lower limb weakness, progressive difficulty in climbing stairs and frequent falls. Later on, the weakness progressed to distal muscles with movement limitation affecting first the toes and later the finger flexors and small hand muscles. Scapular winging was also present (Fig. 2e). Currently she has both proximal and distal lower limb weakness (MRC 3/5), walks with a cane, and experiences frequent cramps in her feet, legs, and hands. She had a medical history of hypothyroidism controlled with medication. The CK levels were slightly elevated at 300 IU/l (nv: 30–135 IU/l). The EMG showed a “myopathic” pattern consistent with a distal involvement with normal nerve conduction studies (NCS).

FA. II-9

A 59-year-old man, started at the age of 38 with proximal and later on distal muscle weakness. Similar to the other patients he presented with limitation of toes and later finger flexors; and scapular winging (Fig. 2a). He has a normal cardiovascular evaluation; reduced forced vital capacity with ventilatory insufficiency.



Fig. 2 Scapular winging and vastus atrophy are common clinical findings. Scapular winging was a common finding in patients: FA.II-9 (a), FA.III-1 (b), FB.III-1 (c), FA.II-6 (e) and FB.II-1 (f). Severe thigh atrophy was present in all patients (patient B.III-1) (d, g). In case

B.II-1 (f) although she carries the mutation, slight symptoms were present. Marked atrophy of vastus muscles were observed with preservation of the rectus femoris (Patient B.III-1) (g)

Family B (FB)

An Argentinean family from the province of Entre Rios, with French-Basque ancestry with 5 affected members over three generations (Fig. 1). Age at onset varied from 41 to 63-year-old with progressive proximal lower limb muscle weakness. There was no history of early onset cataracts or restriction of finger and toe flexion with reduced range of movement in the interphalangeal joints.

FB.III-1

A 46-year-old man, semi-professional cyclist, started to experience progressive weakness and wasting of the quadriceps from the age of 41. He has difficulty standing from the crouched position, has occasional unexplained falls and some difficulty climbing stairs. Cardiopulmonary examination was normal. The maternal grandfather and three great uncles were affected by a similar, late onset, muscle condition. At the time of his first examination at age 41, he had no shoulder girdle or upper arm muscles weakness but a mild bilateral scapular winging; prominent atrophy of the vastus lateralis and medialis and a striking preservation of the rectus femoris (knee extension: MRC power grade 4-/5) (Fig. 2d,g). Atrophy of the posterior thigh compartment was noticed as well as abdominal weakness. Pelvic girdle weakness was present with hip adduction and abduction being

compromised (MRC power grade 4+/5). Muscle strength was preserved in the lower legs and there was calf hypertrophy. Five years after the first evaluation a more pronounced scapular winging (Fig. 2c) and shoulder weakness with no lower limb distal weakness was observed. No finger or toes flexion limitation was present. The CK levels were mildly elevated (862 U/l; nv: 55–170 UI/l) and the electromyography was consistent with a “myopathic” pattern.

FB.II-1 case

The mother of the proband, a 65-year-old woman, showed a slight weakness of the vastus muscles (Knee extension MRC 4+/5), mild and asymmetrical scapula displacement (Fig. 2f) and lumbar scoliosis. The patient reports occasional lower limb cramps and for the last 3 years some difficulties climbing stairs. The CK level was normal. There is no history of early onset cataracts.

Muscle biopsies

Histochemistry

Quadriceps muscle biopsies from patients FA.III-1, FA.II-6, FA.II-9, FB.III-1 at the age of 42, 55, 40 and 41 years-old, respectively, showed the presence of rimmed vacuoles, autophagic vacuoles and cytoplasmic bodies (Fig. 3). There

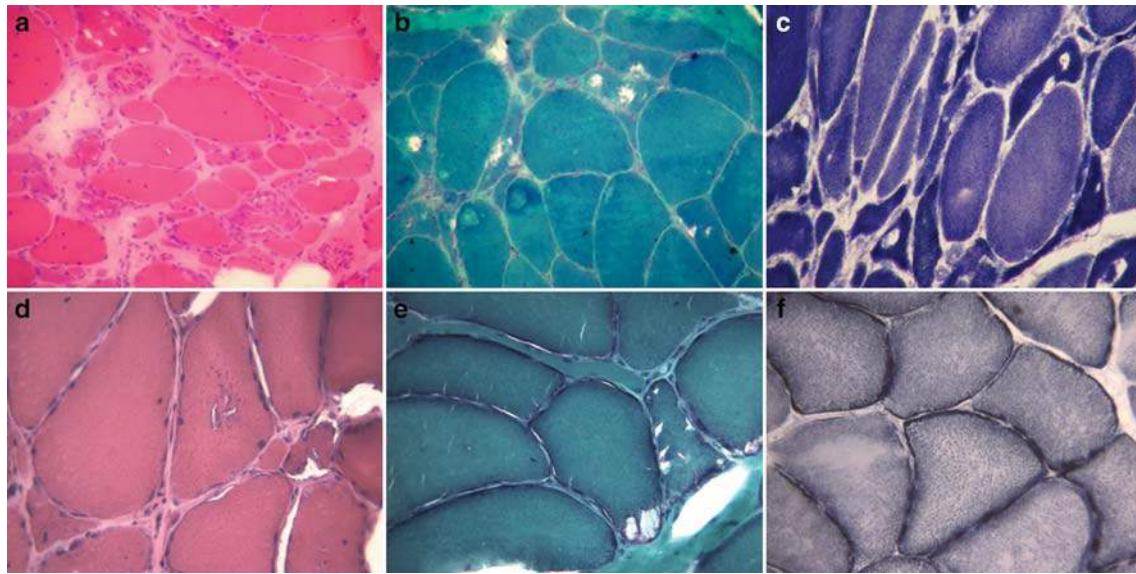


Fig. 3 Histochemistry. Frozen muscle sections from patients: FA.III-1 (**a–c**) and FB.III-1 (**d–f**). Marked variability of fibre size with some atrophic fibres. Numerous rimmed vacuoles and abundant

autophagy lesions were observed in many fibres: **a** (HE), **b** (GT), **d** (HE) and **e** (GT). Vacuoles and some areas of disorganized structure were also detected with oxidative techniques: **c** and **f** (NADH-TR)

was variability in muscle fibre size with the presence of atrophic fibres and a few pyknotic nuclear clumps. There was a moderate increase in the endomysial/perimysial connective tissue and in one case, some necrotic/regenerating fibres were observed.

Immunohistochemistry (IHC)

Dystrophin; laminin α -2; α , β , γ , and δ sarcoglycans labelling was preserved. For FA.II-9: Some of the vacuoles were labelled with antibodies for dystrophin, thus confirming the presence of sarcolemma membranes in the vacuoles as previously described. IHC study for desmin, myotilin, and α B-crystallin did not show any specificity, with only an inconsistent and unspecific immunostaining of a few degenerating fibres. Some vacuoles were labelled with the antibodies against C5b9 and dystrophin and a good number of muscle fibres presented accumulations of P62.

Ultrastructural study

Electron microscopy studies were performed in three muscle biopsies (FA.III-1, FA.II-6 and FB.III-1) (Fig. 4). All biopsies showed marked autophagic changes, particularly in patients FA.III-1 and FB.III-1 and less prominent in patient FA.II-6. We could observe numerous vacuoles containing membranous remnants, myeloid bodies, and cytoplasmic bodies (Fig. 4b, c, f). The myofibrils were regularly dissociated by amorphous material from the autophagy debris. Cytoplasmic areas with tubulofilamentous inclusions, a

structural marker of rimmed vacuoles, were detected in some muscle fibres (Fig. 4a, d). Additionally, remaining segments of disrupted sarcomeres were present in the disorganized regions of the fibres, and small areas of dispersed filamentous bundles of Z-disc origin were also noted (Fig. 4e). Of note that, neither granular filamentous aggregates nor nuclear tubulofilamentous inclusions were observed in these muscle biopsies.

Genetic analysis

By exome sequencing, we identified the same heterozygous *HNRNPDL* mutation in both families. This missense mutation, c.1132G>C p.(Asp378His), affects a conserved amino acid encoded by exon 6 of *HNRNPDL*. The mutation was not listed in gnomAD or in our in-house database containing over 1500 exomes and was previously reported as causing LGMD3. In family A, the presence of the *HNRNPDL* mutation in the patients and its absence in the healthy family members was confirmed by Sanger sequencing. In F.B, *HNRNPDL*: c.1132G>C p.(Asp378His) was found in the index patient as well as the mother, whereas the father and the healthy brother did not harbour the mutated allele.

MRI findings

MRI findings showed in the three cases analysed at the thighs, a selective pattern involving heavily adductor magnus and vastus muscles with preservation of rectus femoris and adductor longus (Fig. 5). Lower distal leg involvement

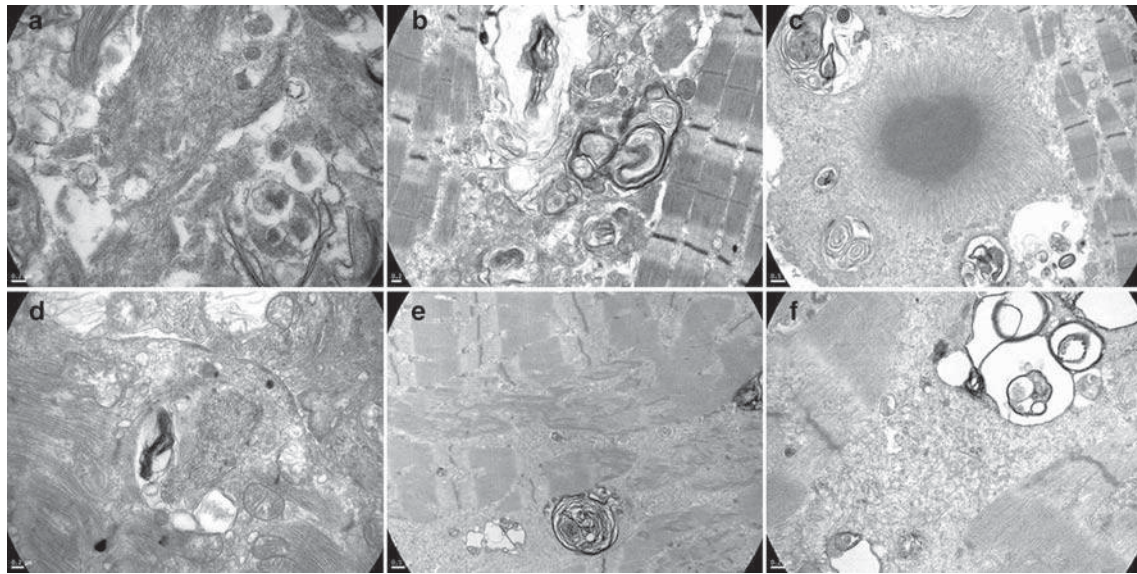


Fig. 4 Ultrastructural findings. Longitudinal muscle sections from patients: FA. III-1 (**a–c**) and FB. III-1 (**d–f**). The autophagic vacuoles containing membranous remnants, myeloid bodies and some glycogen granules (**b, f**) are observed among the myofibrils. Cytoplasmic

bodies (**c**) and few zones with spread filamentous bundles of Z-disc material (**e**) were also noted. Areas with tubulofilamentous inclusions, a structural marker of rimmed vacuoles, were detected in some muscle fibres (**a, d**)

was present only in one patient showing replacement of anterior compartment and soleus muscles.

FA. II-6

Muscle MRI shows a diffuse, symmetric, fatty infiltration of the gluteus minimus and ilio-psoas muscles; moderate fatty infiltration of the gluteus maximus predominantly on the right and of the tensor fascia lata with relative sparing of gluteus medium muscles. At the thighs, on the anterior compartment, a selective involvement of vastus medialis, intermedius and lateralis, sartorius, adductor magnus, with relative sparing of the rectus femoris and adductor longus muscles were observed (Fig. 5e). On the posterior compartment there was a severe involvement of the semitendinosus with relative sparing of the semimembranosus and long head of biceps femoris. At the lower legs the tibial anterior, extensor hallucis and soleus were affected (Fig. 5f).

FB.III-1

Thigh MRI showed severe fatty infiltration of all vastus muscles, sartorius and adductor magnus with relative sparing of gracilis, biceps femoris, semitendinosus, and semimembranosus muscles. Preservation of rectus femoris and adductor longus were observed with hypertrophy of rectus femoris (Fig. 5c). At the lower leg there was no evident muscle involvement (Fig. 5d).

FB. II-1

Severe fatty infiltration was observed in the vastus lateralis, adductor magnus and sartorius muscles with relative sparing of rectus femoris and the adductor longus (Fig. 5a). Semitendinosus, semimembranosus and biceps femoris were moderately affected. At the lower leg level, no evident involvement was detected (Fig. 5b).

Comparative MRI studies

Comparative MRI studies from both FA. II-6 and FB.III-1 patients were performed with an interval of 12 years and 4 years, respectively (Fig. 6).

Discussion

LGMDD3 HNRNPL-related is caused by heterozygous mutations in the *HNRNPDL* gene. Until now, only three families were described worldwide: a Brazilian-Caucasian, a Uruguayan, and a Chinese family [2-4]. The missense mutations in *HNRNPDL* affected the same amino acid in all families although the transition is different: p.(Asp378Asn) in the Brazilian and Chinese families and p.(Asp378His) in the Uruguayan family. The description of several families carrying the mutation in the same amino acid could define a mutational hotspot.

This study describes two unrelated Argentinian families with European ancestry (Italian/French-Basque) with

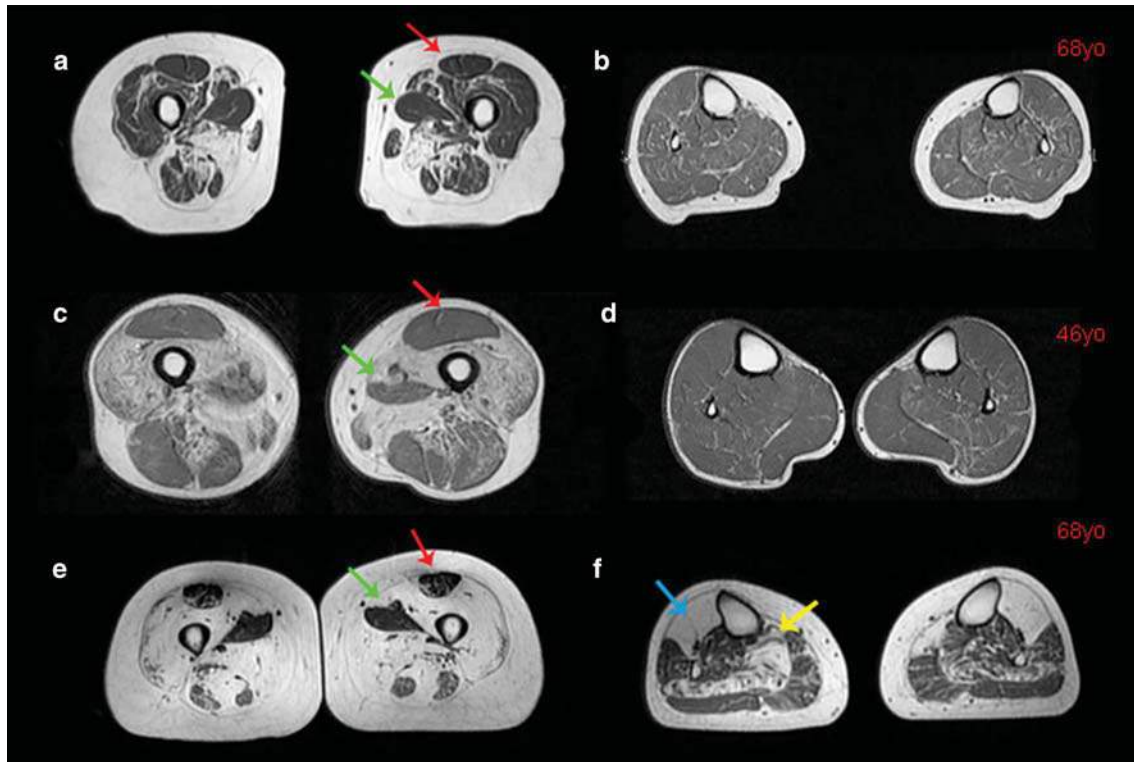


Fig. 5 MRI reveals a specific muscle pattern at the thigh. T1 weighted MRI sections shows preservation of adductor longus and rectus femoris as a common finding in all patients, even in different stages of the disease. **a** Thigh MRI Patient FB.II-1 performed at age 68; severe fatty infiltration was observed on the vastus lateralis, adductor magnus and sartorius muscles with relative sparing of rectus femoris (arrow) and the adductor longus (arrow). Semitendinosus, semimembranosus and biceps femoris were moderately affected. **b** At the leg level no evident involvement was observed. **c** Thigh MRI in patient FB.III-1 performed at age 46 showed severe fatty infiltration of vasti muscles, Sartorius and adductor magnus with relative sparing of gracilis, biceps femoris, semitendinosus and semimembrano-

muscles. Preservation of rectus femoris and adductor longus were observed with hypertrophy of rectus femoris. **d** At the leg level no evident involvement was observed. **e** Muscle MRI in patient FA.II-6 performed at 68-year-old. At the thigh level, almost complete fatty replacement is observed with selective involvement of vastus medialis, intermedius and lateralis, sartorius and adductor magnus with relative sparing of the rectus femoris and adductor longus. In the posterior compartment, severe involvement of semitendinosus was seen, with relative sparing of semimembranosus and long head of biceps femoris. **f** At the legs, tibial anterior (arrow), extensor hallucis and soleus (arrow) were also affected

LGMD3 HNRNPDL-related, histologically characterized by marked autophagy with numerous rimmed vacuoles associated with the p.(Asp378His) dominant *HNRNPDL* mutation. Moreover, we provide new clinical, histopathology and ultrastructural findings, as well as evidence of a selective muscle MRI involvement which seems to be specific in any stages of the disease, even in oligo-symptomatic patients.

In our two families, the disease manifested with two different initial phenotypes; a typical late onset limb girdle proximal weakness with atrophy of the thighs, and a distal asymmetric lower limb ankle dorsiflexion weakness. Whereas limitation of fingers flexors was a late manifestation in all members of one of our families, early onset cataracts were present in only four patients. Despite the variable presentation in both families, scapular winging was a regular clinical finding in all affected patients. The presence of a 65 years-old oligo-symptomatic patient reinforces previous

descriptions regarding variable clinical severity of the disease. In our cohort, as in previous reported series, the myopathy usually manifested as a late onset slowly progressive disorder, the age of onset ranging from 38 to 63 years. Normal cardiac and respiratory assessments in most of the studied patients could suggest that cardiac and respiratory insufficiency may not be a feature of this condition, however, the oldest patient in this series presents a reduction of the FVC over time with a pattern that may suggest the diaphragm is compromised. We, therefore, suggest that the respiratory function should be monitored in this condition. Some clinical similarities can be established between LGMD D3 HNRNPDL-related and myopathies associated with mutations in other genes coding for other heterogeneous nuclear ribonucleoproteins (hnRNPs) such as hnRNPA1. Rimmed vacuolar myopathy has been documented with mutations in hnRNPA1, causing a similar autosomal dominant, late onset

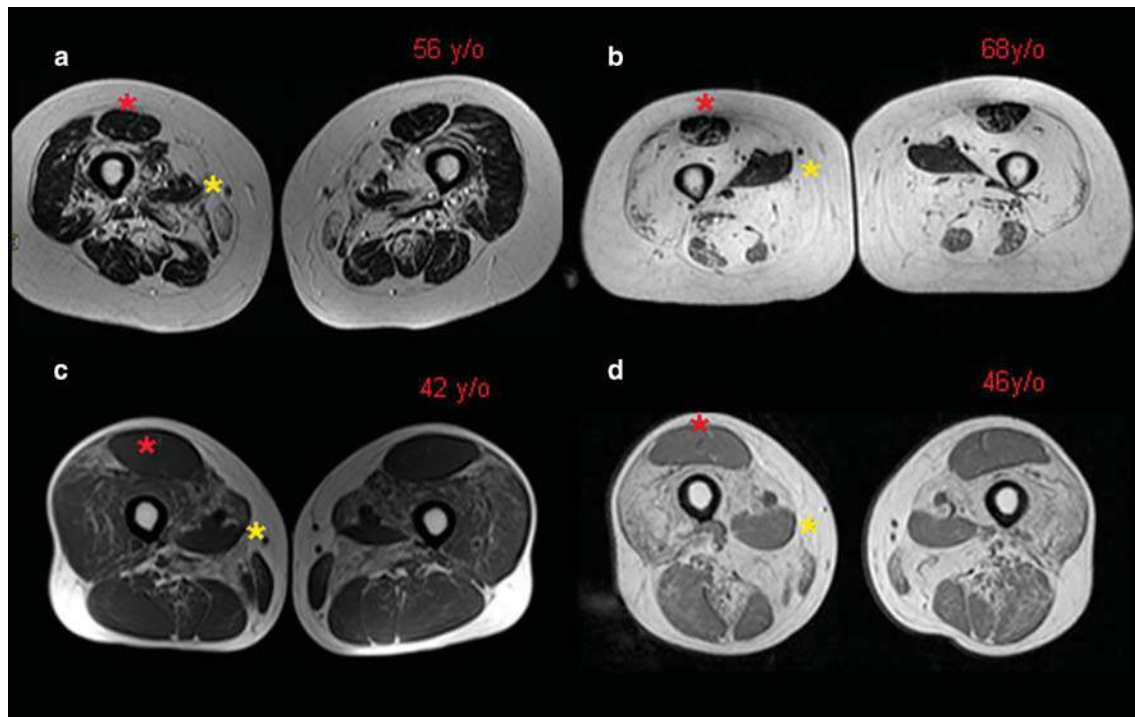


Fig. 6 Comparative thigh MRI in two different patients. T1 weighted comparative thigh MRI performed in patient FA.II-6 (56-year-old and 68-year-old) (a, b) and FB.III-1 (42-year-old and 46-year-old) (c, d) which illustrates selective sparing of rectus femoris (asterisk)

and adductor longus (asterisk) through the years with marked degeneration of vasti. Posterior compartment muscles in case FA.II-6 were severely affected with the exception of semimembranosus and biceps femoris whereas in FB.III-2 are less affected

myopathy with distal or proximal lower limb onset and no cardiac or respiratory involvement [9, 10, 13].

Our MRI findings allow us to postulate a specific and pathognomonic pattern of involvement of the thighs with preservation of the rectus femoris and adductor longus, even at late stages of the disease (Figs. 5, 6). These findings are in accordance with the previous description by Sun et al. (2019), showing a strikingly similar muscle MRI pattern. Vastus muscles seem to be early and particularly affected and probably may correlate with the early falls of the patients. In contrast, no leg-specific muscle involvement was observed. A similar muscle MRI pattern, with preservation of the rectus femoris was described previously in MSPs like hnRNPA1 and hnRNPA2B1 associated diseases [9]. The reason for the selective involvement of some particular muscles with relatively sparing of others remains unclear. We could speculate that a possible association of myotoxicity with the levels of mutant HNRNPDL in different muscles might be related with the selective muscle involvement, or some muscles being more dependent on correct mRNA-processing than others. Selective muscle involvement is not a specific finding of LGMD D3 HNRNPDL-related, but rather a common finding in muscular dystrophies. Previous reports demonstrated significant variations in isoform and gene expression levels in anatomically different muscles as

one of the possible explanations of this discrepancy [14]. Other factors remain to be clarified.

The muscle biopsy studies allowed us to demonstrate a particular morphological pattern characterized by fibres harbouring numerous autophagic rimmed vacuoles and cytoplasmic bodies. Electron microscopy, performed for the first time in HNRNPDL-related LGMD D3, demonstrated autophagic changes with numerous vacuoles containing membranous remnants, myeloid bodies, besides cytoplasmic bodies and some filamentous material. Myofibrils in dissolution were separated by amorphous autophagic debris material (Fig. 4).

The morphological and clinical aspects of the HNRNPDL-related myopathy, suggest that this entity should be included in the group of the “autophagic vacuolar myopathies” (AVM) instead of the LGMD. Of note, the cases previously reported of HNRNPDL-related muscular dystrophy in the literature did not include electron microscopy studies and the morphological description was very limited. These facts have led to the classification of this entity as an autosomal dominant muscular dystrophy mostly based on the clinical phenotype. With the new findings in electron microscopy that we report here, we postulate that the histological phenotype is compatible with an AVM and we suggest that the classification of this entity should be reconsidered.

HNRNPDL belongs to the subfamily of the heterogeneous nuclear ribonucleoproteins (hnRNPs) essential for the maturation of newly formed heterogeneous nuclear pre-mRNA into mRNA and the transport of mRNA. They are key proteins in the RNA metabolism and many hnRNP genes are known to cause degenerative diseases in particular with mutations in the prion-like domains (PrLD). Mutations in the PrLD of hnRNPA1 and A2B1 cause MSP [10]. Mutations in the PrLD of TIA1 cause rimmed vacuolar distal myopathies [15]. Mutations in the PrLD increase the tendency to self-aggregation.

In conclusion, HNRNPDL-related LGMD D3 results in a wide range of phenotypes from the classic proximal form of LGMD to a more distal phenotype. Codon 378 of HNRNPDL gene can be considered a mutation hotspot for HNRNPDL-related myopathy. Moreover, cataracts and limited fingers flexion may not be uniform findings. On the other hand, scapular winging is an important clinical key sign with similarity to VCP mutated MSP myopathy. The preservation of rectus femoris and adductor longus muscles is a common MRI feature at all stages of the disease. Pathologically the disease can be classified among the autophagic rimmed vacuolar myopathies as with the other MSP myopathies.

Acknowledgements This work has been financially supported by Association Française contre les Myopathies (AFM-Telethon), Association Institut de Myologie (AIM), Assistance Publique-Hôpitaux de Paris (AP-HP), Institut National de la Santé et de la Recherche Médicale (INSERM), Sorbonne Université, Centre National de la Recherche Scientifique (CNRS), University of Strasbourg, the France Génomique National infrastructure funded as part of the Investissements d'Avenir program managed by the Agence Nationale pour la Recherche (ANR-10-INBS-09) and by Fondation Maladies Rares within the frame of the "Myocapture" sequencing project, the Fondation pour la Recherche Médicale.

Compliance with ethical standards

Conflicts of interest All authors have reviewed the manuscript. Authors have no conflict of interest to declare.

Ethical standards The study was conducted after receiving written informed consent from patients in accordance to the declaration of Helsinki.

References

1. Straub V, Murphy A, Udd B, LGMD workshop study group (2018) 229th ENMC international workshop: Limb girdle muscular dystrophies—nomenclature and reformed classification Naarden, the Netherlands, 17–19 March 2017. *Neuromuscul Disord* 28:702–710. <https://doi.org/10.1016/j.nmd.2018.05.007>
2. Starling A, Kok F, Passos-Bueno MR, Vainzof M, Zatz M (2004) A new form of autosomal dominant limb-girdle muscular dystrophy (LGMD1G) with progressive fingers and toes flexion limitation maps to chromosome 4p21. *Eur J Hum Genet*. 12:1033–1040
3. Vieira NM, Naslavsky MS, Licinio L, Kok F, Schlesinger D, Vainzof M, Sanchez N, Kitajima JP, Gal L, Cavacana N, Serafini PR, Churtzman S, Vasquez C, Mimbacas A, Nigro V, Pavanello RC, Schuldiner M, Kunkel LM, Zatz M (2014) A defect in the RNA-processing protein HNRNPDL causes limb-girdle muscular dystrophy 1G (LGMD1G). *Hum Mol Genet* 23:4103–4110. <https://doi.org/10.1093/hmg/ddu127>
4. Sun Y, Chen H, Lu Y, Duo J, Lei L, OuYang Y, Hao Y, Da Y, Shen X-M (2019) Limb girdle muscular dystrophy D3 HNRNPDL related in a Chinese family with distal muscle weakness caused by a mutation in the prion-like domain. *J Neurol* 266:498–506. <https://doi.org/10.1007/s00415-018-9165-4>
5. Li RZ, Hou J, Wei Y, Luo X, Ye Y, Zhang Y (2019) hnRNPDL extensively regulates transcription and alternative splicing. *Gene* 687:125–134. <https://doi.org/10.1016/j.gene.2018.11.026>
6. Kawamura H, Tomozoe Y, Akagi T, Kamei D, Ochiai M, Yamada M (2002) Identification of the nucleocytoplasmic shuttling sequence of heterogeneous nuclear ribonucleoprotein D-like protein JKTBP and its interaction with mRNA. *J Biol Chem* 277:2732–2739
7. Kamei D, Yamada M (2002) Interactions of heterogeneous nuclear ribonucleoprotein D-like protein JKTBP and its domains with high-affinity binding sites. *Gene* 298:49–57
8. Geuens T, Bouhy D, Timmerman V (2016) The hnRNP family: insights into their role in health and disease. *Hum Genet* 135:851–867. <https://doi.org/10.1007/s00439-016-1683-5>
9. Izumi R, Warita H, Niihori T, Takahashi T, Tateyama M, Suzuki N, Nishiyama A, Shirota M, Funayama R, Nakayama K, Mitsuhashi S, Nishino I, Aoki Y, Aoki M (2015) Isolated inclusion body myopathy caused by a multisystem proteinopathy-linked hnRNPA1 mutation. *Neurol Genet* 1:e23. <https://doi.org/10.1212/NXG.0000000000000023>
10. Kim HJ, Kim NC, Wang YD, Scarborough EA, Moore J, Diaz Z, MacLea KS, Freibaum B, Li S, Molliex A, Kanagaraj AP, Carter R, Boylan KB, Wojtas AM, Rademakers R, Pinkus JL, Greenberg SA, Trojanowski JQ, Traynor BJ, Smith BN, Topp S, Gkazi AS, Miller J, Shaw CE, Kottlors M, Kirschner J, Pestronk A, Li YR, Ford AF, Gitler AD, Benatar M, King OD, Kimonis VE, Ross ED, Weihl CC, Shorter J, Taylor JP (2013) Mutations in prion-like domains in hnRNPA2B1 and hnRNPA1 cause multisystem proteinopathy and ALS. *Nature* 495:467–473. <https://doi.org/10.1038/nature11922>
11. Mercuri E, Cini C, Pichiecchio A, Allsop J, Counsell S, Zolkipli Z, Messina S, Kinali M, Brown SC, Jimenez C, Brockington M, Yuva Y, Sewry CA, Muntoni F (2003) Muscle magnetic resonance imaging in patients with congenital muscular dystrophy and Ullrich phenotype. *Neuromuscular Disord* 13:554–558
12. Mercuri E, Pichiecchio A, Allsop J, Messina S, Pane M, Muntoni F (2007) Muscle MRI in inherited neuromuscular disorders: past, present, and future. *J Magn Reson Imaging* 25:433–440
13. Kottlors M, Moske-Eick O, Huebner A, Krause S, Mueller K, Kress W, Schwarzwald R, Bornemann A, Haug V, Heitzer M, Kirschner J (2010) Late-onset autosomal dominant limb girdle muscular dystrophy and Paget's disease of bone unlinked to the VCP gene locus. *J Neurol Sci* 291:79–85. <https://doi.org/10.1016/j.jns.2009.12.008>
14. Huovinen S, Penttilä S, Somervuo P, Keto J, Auvinen P, Vihola A, Huovinen S, Pelin K, Raheem O, Salenius J, Suominen T, Hackman P, Udd B (2015) Differential isoform expression and selective muscle involvement in muscular dystrophies. *Am J Pathol* 185:2833–2842. <https://doi.org/10.1016/j.ajpath.2015.06.018>
15. Lee Y, Jonson PH, Sarparanta J, Palmio J, Sarkar M, Vihola A, Evilä A, Suominen T, Penttilä S, Savarese M, Johari M, Minot MC, Hilton-Jones D, Maddison P, Chinnery P, Reimann J, Kornblum C, Kraja T, Zierz S, Sue C, Goebel H, Azfer A, Ralston SH, Hackman P, Bucelli RC, Taylor JP, Weihl CC, Udd B (2018) TIA1 variant drives myodegeneration in multisystem proteinopathy with SQSTM1 mutations. *J Clin Invest* 128:1164–1177. <https://doi.org/10.1172/JCI97103>

2.2.6 Publication 8: Dihydropyridine receptor (DHPR, *CACNA1S*) congenital myopathy (Schartner et al. 2017)

Background

CACNA1S encodes a calcium channel subunit of the dihydropyridine receptor (DHPR), serving as voltage sensor at the T-tubule and playing a key role in excitation-contraction coupling (ECC) (Protasi 2002; Franzini-Armstrong and Kish 1995). Autosomal dominant *CACNA1S* mutations have been shown to cause hypokalemic periodic paralysis (Fontaine et al. 1994; Ptacek et al. 1994; Jurkat-Rott et al. 1994), a disease characterized by episodes of generalized muscle weakness associated with low serum potassium levels (Statland et al. 2018).

Aim of the study

The aim of the study was to unravel the genetic cause and the pathomechanism of a molecularly undiagnosed congenital myopathy in a homogeneous cohort of seven families.

Results

We reported 11 patients from seven unrelated families with a myopathy characterized by congenital or early-onset hypotonia and a progressive muscle weakness with facial involvement. Analyses of the muscle biopsies revealed an alveolar aspect of the intermyofibrillar network as the histopathological hallmark of the disease (Fig. 1 of the publication). Predominance of type 1 fibers and fiber size heterogeneity were also observed. Exome sequencing led to the identification of compound heterozygous *CACNA1S* mutations in four families and revealed heterozygous *CACNA1S* missense mutations in three families. Western blot analyses on muscle extracts revealed a strong decrease in *CACNA1S* protein level in both recessive and dominant families, and functional analyses in patients myotubes showed a decreased Ca^{2+} release upon KCl depolarization.

Conclusion

We identified *CACNA1S* mutations as the genetic cause of a novel congenital myopathy clinically characterized by early-onset hypotonia and facial weakness, and histologically characterized by an alveolar aspect on oxidative staining. Both recessive and dominant mutations led to a strong decrease in *CACNA1S* protein content in muscle, and to reduced Ca^{2+} release upon depolarization. DHPR is known to be active as a tetrad, and our results suggest that DHPR tetrads containing at least one subunit with dominant *CACNA1S* mutation are prone to degradation.

Contribution

I performed the skeletal muscle RNA extraction and amplification to evaluate the impact of the *CACNA1S* mutations on RNA splicing and expression.

Dihydropyridine receptor (DHPR, *CACNA1S*) congenital myopathy

Vanessa Schartner^{1,2,3,4} · Norma B. Romero^{5,6} · Sandra Donkervoort⁷ · Susan Treves^{8,9} · Pinki Munot¹⁰ · Tyler Mark Pierson^{11,12} · Ivana Dabaj^{13,14,15} · Edoardo Malfatti^{5,6} · Irina T. Zaharieva¹⁰ · Francesco Zorzato^{8,9} · Osorio Abath Neto^{1,7} · Guy Brochier^{5,6} · Xavière Lornage^{1,2,3,4} · Bruno Eymard¹⁶ · Ana Lía Taratuto¹⁷ · Johann Böhm^{1,2,3,4} · Hernan Gonorazky¹⁸ · Leigh Ramos-Platt¹⁹ · Lucy Feng¹⁰ · Rahul Phadke¹⁰ · Diana X. Bharucha-Goebel^{7,20} · Charlotte Jane Sumner^{21,22} · Mai Thao Bui^{5,6} · Emmanuelle Lacene^{5,6} · Maud Beuvin^{5,6} · Clémence Labasse^{5,6} · Nicolas Dondaine²⁶ · Raphael Schneider^{1,2,3,4,23} · Julie Thompson²³ · Anne Boland²⁴ · Jean-François Deleuze²⁴ · Emma Matthews¹⁰ · Aleksandra Nadaj Pakleza²⁵ · Caroline A. Sewry¹⁰ · Valérie Biancalana^{1,2,3,4,26} · Susana Quijano-Roy^{13,14,15,27} · Francesco Muntoni¹⁰ · Michel Fardeau^{5,6} · Carsten G. Bönnemann⁷ · Jocelyn Laporte^{1,2,3,4}

Received: 15 October 2016 / Revised: 9 December 2016 / Accepted: 11 December 2016
© Springer-Verlag Berlin Heidelberg 2016

Abstract Muscle contraction upon nerve stimulation relies on excitation–contraction coupling (ECC) to promote the rapid and generalized release of calcium within myofibers. In skeletal muscle, ECC is performed by the direct coupling of a voltage-gated L-type Ca^{2+} channel (dihydropyridine receptor; DHPR) located on the T-tubule with a Ca^{2+} release channel (ryanodine receptor; RYR1) on the sarcoplasmic reticulum (SR) component of the triad. Here, we characterize a novel class of congenital myopathy at the morphological, molecular, and functional levels. We

describe a cohort of 11 patients from 7 families presenting with perinatal hypotonia, severe axial and generalized weakness. Ophthalmoplegia is present in four patients. The analysis of muscle biopsies demonstrated a characteristic intermyofibrillar network due to SR dilatation, internal nuclei, and areas of myofibrillar disorganization in some samples. Exome sequencing revealed ten recessive or dominant mutations in *CACNA1S* ($\text{Ca}_v1.1$), the pore-forming subunit of DHPR in skeletal muscle. Both recessive and dominant mutations correlated with a consistent phenotype, a decrease in protein level, and with a major impairment of Ca^{2+} release induced by depolarization in cultured myotubes. While dominant *CACNA1S* mutations were previously linked to malignant hyperthermia susceptibility or

V. Schartner and N. B. Romero contributed equally.

Electronic supplementary material The online version of this article (doi:10.1007/s00401-016-1656-8) contains supplementary material, which is available to authorized users.

✉ Jocelyn Laporte
jocelyn@igbmc.fr

¹ Institut de Génétique et de Biologie Moléculaire et Cellulaire (IGBMC), 1, rue Laurent Fries, BP 10142, 67404 Illkirch, France

² INSERM U964, 67404 Illkirch, France

³ CNRS, UMR7104, 67404 Illkirch, France

⁴ Fédération de Médecine Translationnelle de Strasbourg (FMTS), Université de Strasbourg, 67404 Illkirch, France

⁵ Université Sorbonne, UPMC Univ Paris 06, INSERM UMRS974, CNRS FRE3617, Center for Research in Myology, GH Pitié-Salpêtrière, 47 Boulevard de l'hôpital, 75013 Paris, France

⁶ Centre de référence de Pathologie Neuromusculaire Paris-Est, Institut de Myologie, GHU Pitié-Salpêtrière, Assistance Publique-Hôpitaux de Paris, Paris, France

⁷ Neuromuscular and Neurogenetic Disorders of Childhood Section, Neurogenetics Branch, National Institute of Neurological Disorders and Stroke, National Institutes of Health, Bethesda, MD 20892-1477, USA

⁸ Department of Anesthesia, Universitätsspital Basel, 4031 Basel, Switzerland

⁹ Department of Biomedizin, Universitätsspital Basel, 4031 Basel, Switzerland

¹⁰ Dubowitz Neuromuscular Centre and MRC Centre for Neuromuscular Diseases, UCL Great Ormond Street Institute of Child Health, London WC1N 1EH, UK

¹¹ Departments of Pediatrics and Neurology, Cedars-Sinai Medical Center, 8700 Beverly Boulevard, Los Angeles, CA 90048, USA

¹² The Board of Governors Regenerative Medicine Institute, Cedars-Sinai Medical Center, 8700 Beverly Boulevard, Los Angeles, CA 90048, USA

hypokalemic periodic paralysis, our findings strengthen the importance of DHPR for perinatal muscle function in human. These data also highlight CACNA1S and ECC as therapeutic targets for the development of treatments that may be facilitated by the previous knowledge accumulated on DHPR.

Keywords DHPR · Congenital myopathy · Excitation–contraction coupling · Triad · Centronuclear myopathy · Core myopathy · Myotubular myopathy

Introduction

Excitation–contraction coupling (ECC) is the process by which an action potential triggered by nerve-induced muscle membrane depolarization causes the muscle fiber to contract. In skeletal muscle, ECC relies on a direct coupling between a Ca^{2+} release channel (the ryanodine receptor; RyR1) located on the sarcoplasmic reticulum (SR), and a voltage-gated L-type Ca^{2+} channel (the dihydropyridine receptor; DHPR) on the T-tubule [33]. ECC occurs at the triad, a specialized membrane structure formed by the apposition of a sarcolemma invagination (the T-tubule) and two SR saccules containing RyRs [10]. Upon depolarization, activation of the DHPR induces the opening of RyR1 and the release of Ca^{2+} from the SR stores, subsequently triggering muscle contraction.

The *CACNA1S* ($\text{Ca}_v1.1$) gene encodes the pore-forming subunit of DHPR in skeletal muscle. It is composed of 44 exons and has an embryonic splice variant lacking the in-frame exon 29. CACNA1S is a 1873 amino-acid protein with four transmembrane domains (I–IV), each with six

transmembrane segments (S1–S6) [40]. The loop between domains II and III is instrumental in mediating the activation of RyR1 [8, 21, 33]. The importance of CACNA1S in ECC has been demonstrated *in cellula* and also *in vivo*. Cells lacking CACNA1S have impaired ECC, and mice and drosophila with defective CACNA1S (*Dmca1D* ortholog in the fly) are embryonically lethal [5, 9, 18]. In adult mice, CACNA1S appears to control muscle mass as acute down-regulation of *Cacna1s* leads to massive atrophy, although ECC was functional [30].

Heterozygous dominantly acting *CACNA1S* mutations have previously been associated either with malignant hyperthermia susceptibility (MHS5; MIM#601887) triggered by volatile anaesthetics [25], hypokalemic periodic paralysis (HOKPP; MIM#170400) characterized by periodic attacks of muscle weakness associated with a decrease in the serum potassium level [16, 32], and thyrotoxic periodic paralysis (TTPP1; MIM#188580) [20]. Moreover, alternative splicing of exon 29 is repressed in patients with myotonic dystrophy and correlates with increased channel conductance and voltage sensitivity [38]. However, the link between mutations of DHPR and a myopathy is not yet fully established. More generally, triad defects due to mutations in other genes encoding for the ECC machinery have been reported in a sub-class of myopathies known as triadopathies, while secondary triad abnormalities may be observed in several other muscle diseases [1, 6].

In this study, we analyzed a cohort of patients with congenital myopathy, a clinically and genetically heterogeneous group of muscle diseases of variable severity, characterized by antenatal, neonatal, or early onset, ranging from severe fetal akinesia to milder forms of hypotonia

¹³ Assistance Publique des Hôpitaux de Paris (AP-HP), Service de Pédiatrie, Hôpital Raymond Poincaré, Hôpitaux Universitaires Paris-Ile-de-France Ouest, Garches, France

¹⁴ Centre de Référence de Maladies Neuromusculaires Garches-Necker-Mondor-Hendaye (GNMH), Garches, France

¹⁵ Réseau National Français de la Filière Neuromusculaire (FILNEMUS), Garches, France

¹⁶ Centre de Référence de Pathologie Neuromusculaire Paris-Est, Groupe Hospitalier Pitié-Salpêtrière, Paris, France

¹⁷ Consultant-Neuropathology Department, National Pediatric Hospital J-P-Garrahan and Institute for Neurological Research-FLENI, Buenos Aires, Argentina

¹⁸ Present Address: Division of Neurology, Department of Pediatrics, The Hospital for Sick Children, University of Toronto, Toronto, ON, Canada

¹⁹ Division of Neurology at Children’s Hospital of Los Angeles, Department of Pediatrics, Keck School of Medicine, University of Southern California, 4650 W. Sunset Blvd, Mailstop #34, Los Angeles, CA 90027, USA

²⁰ Division of Neurology, Children’s National Health System, Washington, DC 20010, USA

²¹ Department of Neurology, Johns Hopkins University School of Medicine, Baltimore, MD 21205, USA

²² Department of Neuroscience, Johns Hopkins University School of Medicine, Baltimore, MD 21205, USA

²³ Faculté de Médecine, ICube-UMR7357, CSTB Complex Systems and Translational Bioinformatics, 67000 Strasbourg, France

²⁴ Centre National de Génotypage, Institut de Génétique, CEA, Evry, France

²⁵ Centre de référence des maladies neuromusculaires Nantes/Angers, Service de Neurologie, CHU Angers, Angers, France

²⁶ Laboratoire de Diagnostic Génétique, Faculté de Médecine, Nouvel Hôpital Civil, 67000 Strasbourg, France

²⁷ Université de Versailles-St Quentin, U1179 UVSQ-INSERM, Montigny, France

and muscle weakness, in conjunction with the presence of characteristic morphological hallmarks on skeletal muscle biopsy [26, 35]. Histopathologically and ultrastructurally, they can be sub-classified into nemaline myopathies with rods inclusions and/or protein aggregates, core myopathies with well-defined muscle fiber areas devoid of oxidative enzyme activity, and centronuclear myopathy with several fibers with internal and centralized nuclei. Fiber-type disproportion with a bias toward smaller and more abundant type 1 fibers is a feature common in several forms of congenital myopathies [27]. Advances in recent genetic technologies combined with extensive studies of large families and well-defined cohorts led to the identification of approximately 30 causative congenital myopathy genes (<http://www.musclegenetable.fr>), of which a majority encodes proteins associated with the sarcomere structure or its stability [22, 23, 26, 35]. Despite these advances, approximately half of patients with congenital myopathies remain without a confirmed genetic diagnosis, which is essential for appropriate disease management, prognosis, genetic counseling, and development of therapies [2].

Here, we identified by exome sequencing both recessive and dominant *CACNA1S* mutations as a cause of a congenital myopathy characterized by peculiar morphological hallmarks in a cohort of 11 patients from 7 families.

Materials and methods

Patients

Eleven patients from seven unrelated families from Caucasian, Argentinean, or Vietnamese origin were included in this study. The cohort comprises 3 sporadic cases (patients P2, P5, and P9), 2 families with dominant inheritance (P6–8; P10, and P11), and 2 families with several affected siblings and recessive inheritance (P1; P3, and P4). All patients presented with a clinical history of a congenital myopathy and underwent detailed clinical examinations. Clinical, histopathological, and genetic features are summarized in Table 1. Sample collection was performed with written informed consent from the patients or parents according to the declaration of Helsinki.

Muscle imaging

CT scan for P1 and MRI for P2, P4, P5, P7, P8, P9, P10, and P11 were performed. T1-STIR was performed for P4, P5, P7, P8, P9, P10, and P11. P2 was scaled by the Mercury method.

Exome sequencing and analysis

Genomic DNA of patients and relatives was isolated from peripheral blood by phenol–chloroform extraction. DNA storage and usage was IRB approved (DC-2012-1693 and 12-N-0095 for NIH). Exome sequencing (ES) was performed for all living patients, the parents of families 1 and 6, the mother of P3 and P4 in family 3, and the father of P7 and P8 in family 5. ES was performed at CNG (Evry, France), at DeCode as part of Neuromics (Reykjavik, Iceland), at the Broad Institute (Cambridge, USA) and at the UCLA (Los Angeles, USA). Fragmented genomic DNA was enriched for exons using the SureSelect Human all Exon 50 Mb capture library v5 (Agilent, Santa Clara, USA) and sequenced 90nt paired-end on Illumina HiSeq 2000/2500 sequencers.

Sequence data were aligned to the GRCh37/hg19 reference genome using the Burrows–Wheeler aligner software (<http://bio-bwa.sourceforge.net>), and variant calling was performed with SAMtools or the UnifiedGenotyper (<https://www.broadinstitute.org/gatk>). The following databases were used for variant annotation and filtering: Exome Variant Server (<http://evs.gs.washington.edu/EVS/>), ExAC Browser (<http://exac.broadinstitute.org/>), dbSNP (<http://www.ncbi.nlm.nih.gov/projects/SNP/>), 1000 genomes (<http://www.1000genomes.org/>), as well as in-house exome databases. Variants ranking was performed with VaRank [13].

Confirmation of variants was performed by Sanger sequencing. Haplotype analysis between families 1 and 2 was performed using four (CA)_n microsatellites flanking the *CACNA1S* gene, which are localized 39- and 25-kb upstream and 3.5- and 18-kb downstream, respectively (coordinates, primers, and conditions are available on request).

Morphological studies

An open deltoid muscle biopsy was performed for patients P1, 2, 3, 6, 7, and 9 following informed consent. Age at muscle biopsy varied from 6 months to 60 years. A needle quadriceps biopsy was performed on patient 5 at 9 months and a bicep brachii biopsy was performed for P10 at 44 years of age. For the conventional histochemical techniques, 10- μ m cryostat sections were stained with haematoxylin and eosin (H&E), modified Gomori trichrome (mGT), periodic acid Schiff technique (PAS), oil red O, reduced nicotinamide adenine dinucleotide dehydrogenase-tetrazolium reductase (NADH-TR), succinic dehydrogenase (SDH), cytochrome oxidase (COX), the menadione-nitro blue tetrazolium, and adenosine triphosphatase (ATPase) preincubated at pH 9.4, 4.63, or 4.35.

Table 1 Molecular, clinical, and histopathological features of patients mutated in *CACNA1S*

Families	Family 1	Family 2	Family 3	Family 4	Family 5	Family 6	Family 7
Ethnicity	Caucasian	Argentinian	Vietnamese	Caucasian	Caucasian	Caucasian	Caucasian
Segregation	3 affected	Sporadic	2 affected	Sporadic	3 affected	Sporadic de novo	2 affected
Mutations	Compound heterozygous c.1189_1190del (exon 9) p.Ser397Profs*3; c.4967del (exon 40) p.Leu1656Argfs*67	Compound heterozygous c.4453C>T (exon 37) p.Gln1485*; c.4967del (exon 40) p.Leu1656Argfs*67	Compound heterozygous c.825C>A (exon 6) p.Phe275Leu; c.2371delC (exon 18) p.Leu791Cysfs*37	Compound heterozygous c.298G>T (exon 3) p.Glu100Lys; c.3795G>T (exon 30) p.Gln1265Hisfs*57	Compound heterozygous c.2225C>A (exon 16) p.Pro742Gln	Compound heterozygous c.2224C>T (exon 16) p.Pro742Ser	Compound heterozygous c.4099C>G (exon 33) p.Leu1367Val
Onset	Antenatal/neonatal	Antenatal/neonatal	Neonatal	Neonatal	Early childhood	Antenatal/neonatal	P10: early onset (6–7 months); P11: neonatal
Age at last examination (in years) and gender	P1: 60 (M)	P2: 16 (M)	P3: 15 (F); P4: 7 (F)	P5: 10 (M)	P6: 48 (F); P7: 19 (M); P8: 15 (M)	P9: 24 (M)	P10: 42 (M); P11: 5 (F)
Motor development	Delayed	Delayed	P3 and P4: delayed	Delayed	P6 and P8: normal; P7: delayed	Delayed	P10 and P11: delayed
Muscle weakness	Proximo-distal and major axial deficit	Limb girdle and axial	Stable diffuse (P > D) with preserved reflexes	Generalized with axial and proximal weakness; periodic weakness and loss of speech	Generalized	Generalized with axial weakness	Diffuse, slightly more severe at upper member and P > D at lower members
Facial involvement	Mild with high arched palate and ophthalmoplegia	Mild with high arched palate and ophthalmoplegia	Mild with high arched palate	Mild with high arched palate, ophthalmoplegia and ptosis	Mild with high arched palate	Mild with high arched palate and ophthalmoplegia	Mild with high arched palate
Respiratory involvement	Normal	Mild	Normal	Severe	Mild	Severe	Mild
Scoliosis	No	No	P3: mild	Mild	P7: Yes; P6 and P8: No	Yes	Yes
Feeding	Slight swallowing problem	Slight swallowing problem	P4: swallowing issues (G-tube)	Intermittent feeding difficulties	Normal	Occasional swallowing difficulties	Occasional swallowing difficulties
CK levels	Normal	Normal	Normal	Normal	Normal	Normal	Elevated (1000–2000)
Muscle MRI	Muscle atrophy	Fatty replacement and anterior muscle involvement in lower limb	P4: mild involvement of the anterior thigh, predominantly in the vastus lateralis	Marked atrophy involving all muscle groups of the upper leg bilaterally. Fatty infiltration, particularly of the extensor groups.	P7 and P8: muscle wasting of the anterior thigh, no fatty infiltration	Diffuse atrophy, more severe fatty infiltration in anterior compartment of the thigh and soleus-peroneal muscles in the leg	Severe changes in thigh (anterior > posterior); relative sparing of anterior compartment in the leg

Table 1 continued

Families	Family 1	Family 2	Family 3	Family 4	Family 5	Family 6	Family 7
Histology	Centralized nuclei; focal disorganization; fiber size variability; alveolar aspect of the intermyofibrillar network Uniformity of type I fibers	Centralized nuclei; minicore; alveolar aspect of the intermyofibrillar network Uniformity of type I fibers	No data	Fiber size variability endomyofibrillar connective tissue around most fibers. Predominance of type I fibers	Fiber size variability; alveolar aspect of the intermyofibrillar network Predominance of type I fibers	Rare internalized nuclei. Fiber size variability; alveolar aspect of the intermyofibrillar network Uniformity of type I fibers	P10: internalized nuclei; core-like structures; fiber size variability; endomyofibrillar network

Phenotypes are similar in the different affected from the same family, unless indicated otherwise. Antenatal onset based on delayed/decreased fetal movements

P Proximal, D distal

Digital photographs were obtained with a Zeiss AxioCam HRc linked to a Zeiss AxioPlan Bright Field Microscope and processed with the Axio Vision 4.4 software (Zeiss, Germany) for the majority of patients with exception of patient 5 where a digital Leica scanner was used.

Electron microscopy

Electron microscopy analysis was performed in patients P1, 2, 4, 6, 7, 9, and 10. Muscle specimens were fixed with glutaraldehyde (2.5%, pH 7.4), post fixed with osmium tetroxide (2%), dehydrated, and embedded in resin (EMBed-812, Electron Microscopy Sciences, USA). Ultra-thin sections from three blocks from each patient were stained with uranyl acetate and lead citrate. The grids were observed using a Philips CM120 electron microscope (80 kV; Philips Electronics NV, Eindhoven, The Netherlands) and were photo documented using a Morada camera (Soft Imaging System, France).

Immunohistochemistry and immunofluorescence

Frozen muscle samples for immunohistochemical and immunofluorescence analyses were available for five patients (P1, 5, 6, 7, and 9). Fast, slow, developmental, neonatal myosin heavy chain (NCL-MHCn, Novocastrol Laboratories, Newcastle Upon Tyne, UK) antibodies were applied to 10- μ m-thick cryosections, and revealed by immunoperoxidase techniques (ROCHE-Benchmark XT). In addition, immunofluorescence analyses were assessed on 8- μ m-thick cryosections overnight at 4 °C using different antibodies as Myosin alpha and beta-slow heavy chain, fast 2A heavy chain, and 2X myosin heavy chain (BA-D5, SC-71, and 6H1, Developmental Studies Hybridoma Bank, University of Iowa, Iowa City, USA), CACNA1S antibody (ab2862 mouse monoclonal, Abcam, Cambridge, UK), Ryanodine Receptor 1 (C-terminal rabbit polyclonal), and triadin (kind gift from Isabelle Marty, rabbit polyclonal) [34]. Subsequently, sections were incubated with appropriate conjugated secondary antibodies during 1 h. A set of control slides was prepared with omission of the primary antibodies and using aged-matched non-myopathic muscles.

RNA studies

RNA was extracted from muscle samples of P1 and P3 and from myotubes differentiated from fibroblasts infected by a MyoD expressing lentivirus for P5 using Tri-Reagent (Molecular Research Center, Inc., Cincinnati, USA) according to the manufacturer's instructions.

Reverse transcription was done using random and oligo-d(T) primers. Amplification of the regions of interest was performed with specific *CACNA1S* primers (Supplementary Table 1) and PCR products were Sanger-sequenced.

Western Blot

Cryostat sections of fresh frozen muscle tissue were lysed in a buffer containing 2% SDS, 5% beta-mercaptoethanol, and 62.5 mM Tris HCl pH 6.8 with a mix of protease inhibitors (Sigma). Samples were quickly micro-centrifuged. Laemmli buffer was added and samples were denatured at room temperature. Total protein extract were separated on 10% SDS-PAGE and transferred to nitrocellulose membranes, blocked with non-fat milk, and incubated overnight with anti-*CACNA1S* antibody. Immunoblots were visualized by Immobilon Western Chemiluminescent HRP Substrate (Millipore, Saint Quentin in Yvelines, France) on a G-Box system using the GeneSnap software (Ozyme, Montigny le Bretonneux, France).

Myotubes from patient P1 and from healthy controls were lysed in a buffer containing 50 mM Tris, 100 mM NaCl, 1 mM EGTA, 0.5% NP-40, 0.5% Triton-X100, 0.1% SDS, 1 mM DTT, 1 mM PMSF, and a mix of protease inhibitor (Complete EDTA-free, Roche), and denatured in Laemmli buffer at 95 °C. Total protein extracts were separated on 6% SDS-PAGE gel and transferred to a nitrocellulose membrane. Detection of *CACNA1S* was done with an antibody targeting the middle part of the protein (HPA048892, Sigma, St. Louis, USA). Loading control was verified with the use of a stain-free technique (Trichloroethylene, Sigma, St. Louis, USA) and imaged were acquired with the ChemiDoc Touch Imaging System (Bio-Rad).

Cell culture and imaging

Muscle cells were established from patient P1 by the Cochin Center (Paris, France). Cells were plated on a thin matrigel layer on 35 mm dishes (Ibidi, Martinsried, Germany) with proliferation medium [DMEM/HAMF10 (1:1), 20% FCS, HEPES 10 mM, penicillin 100 UI/mL, streptomycin 100 µg/mL], then differentiated into myotubes at 80% confluence by changing the medium (DMEM, 2% HS, Penicillin 100 UI/mL, streptomycin 100 µg/mL). The next day, an upper layer of matrigel was added and the differentiation medium was changed every 2 days for 10 days. Myotubes were fixed with 4% PFA and incubated with antibodies against *CACNA1S* (HPA048892, Sigma, St. Louis, USA) and *RYR1* (R129, Sigma, St. Louis, USA).

Intracellular calcium measurements

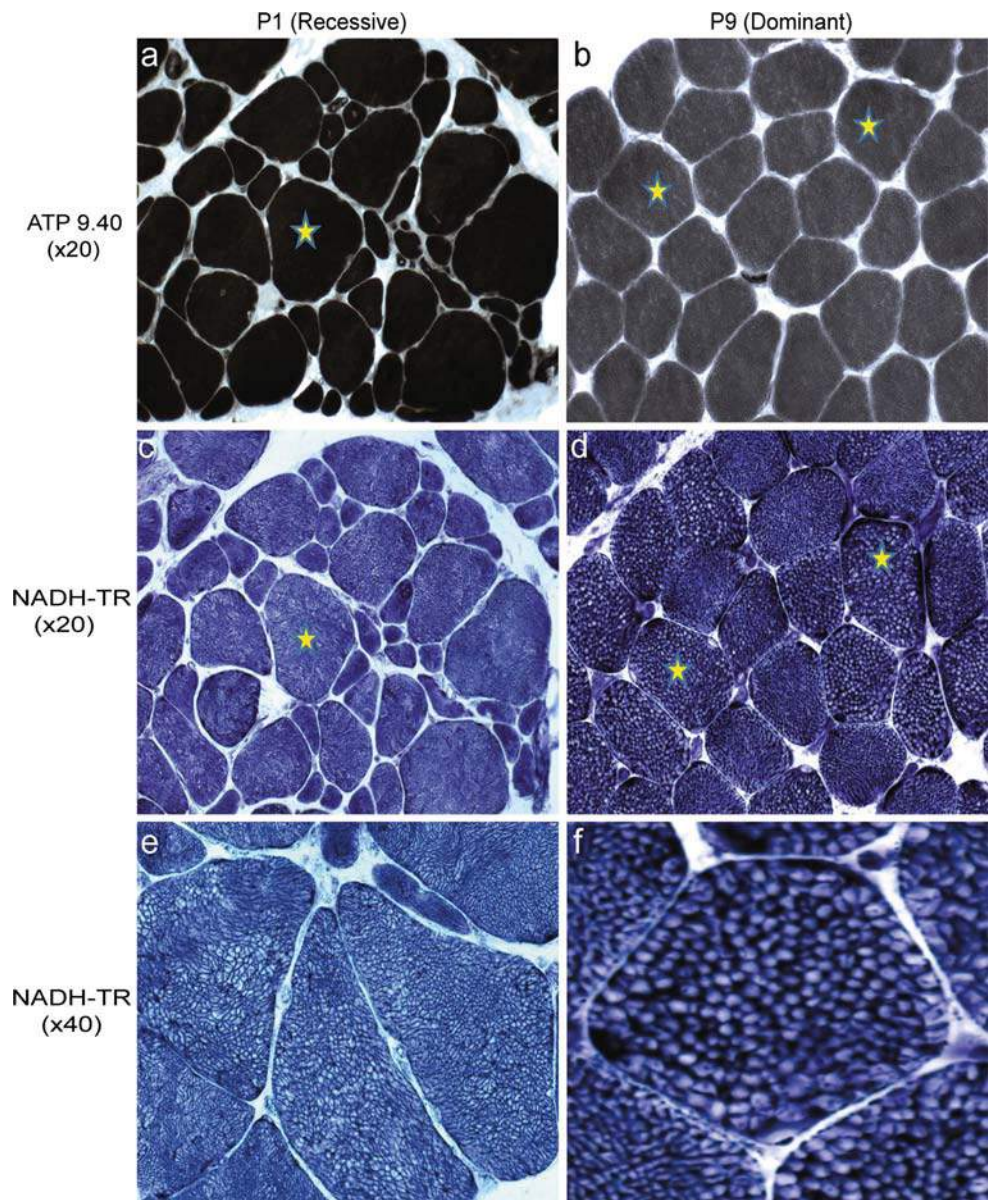
Patient P1, P10, and control muscle cells were transferred onto glass coverslips and allowed to proliferate in growth medium until visible groups of >10 cells were formed. The medium was then switched to differentiation medium, and Ca^{2+} measurements were performed 7–10 days later. Free cytosolic $[\text{Ca}^{2+}]$ was determined using the fluorescent Ca^{2+} indicator Fura-2 as described [4, 7, 36]. Coverslips were mounted onto a 37 °C thermostatted chamber which was continuously perfused with Krebs–Ringer medium. Individual cells were stimulated with different concentrations of KCl or 4-chloro-m-cresol, with a 12-way 100-mm-diameter quartz micromanifold computer-controlled micro-perfuser (ALA Scientific) as previously described [39]. On-line (340 nm, 380 nm, and ratio) measurements were recorded using a fluorescent Axiovert S100 TV inverted microscope (Carl Zeiss GmbH, Jena, Germany) equipped with a $\times 20$ water-immersion FLUAR objective (0.17 numerical aperture) with filters (BP 340/380, FT 425, and BP 500/530) and attached to a Cascade 125+ charge-coupled device camera. The cells were analyzed using MetaMorph (Molecular Devices) imaging system, and the average pixel value for each cell was measured at excitation wavelengths of 340 and 380 nm. Ca^{2+} calibration was performed as previously described.

Results

Characterization of a cohort of patients with congenital myopathy

Our cohort is composed of 11 patients from 7 unrelated families and includes 4 females (P3, P4, P6, and P11) and 7 males (P1, P2, P5, P7, P8, P9, and P10). Ages range from 8 to 60 years. Clinical summary, histopathological features, and genetic characterization of all patients are provided in Table 1. Family history reveals potentially recessive inheritance for two families (F1 and F3) and 2 families had a clear dominant transmission (F5 and F7), while P2, P5, and P9 were sporadic cases. All patients presented with a congenital myopathy involving congenital or early onset hypotonia, delayed motor milestones, and progressive muscle weakness, with prominent axial involvement in most patients. Decreased fetal movement and breech presentation suggested antenatal involvement in several patients. In addition, one patient (P5) also had periodic paralysis and loss of speech during periods of illness and stress. These symptoms improved significantly after treatment with acetazolamide, a carbonic anhydrase inhibitor known to be beneficial for some HOKPP patients [24]. All patients had mild facial involvement, four patients had ophthalmoplegia

Fig. 1 Characterization of histological features in skeletal muscle. Serial muscle sections from patients P1 (**a, c, e**) and P9 (**b, d, f**). The mesh of the intermyofibrillar network displays an “alveolar” aspect, particularly on the oxidative staining (NADH-TR: **c, d, e, f**); this appearance is also observed with ATPases reactions. Uniformity of type 1 muscle fibers is observed on ATP 9.40 staining: **a** and **b**). The same fibers on consecutive serial sections are noted with stars



and one patient had ptosis. The respiratory system is heterogeneously affected ranging from normal to severely impaired. Most of the patients had mild-to-severe swallowing issues. There was no cardiac involvement or clear involvement of other non-neuromuscular functions. Serum creatine kinase (CK) levels were within normal range in 9 patients but elevated in the 2 patients from family 7 (1000–2000 U/l range).

Morphological study has been done on muscle biopsies for individuals in six families (Fig. 1, Supplementary Figure S1). Histological analyses of the muscle biopsies of four families (F1, F2, F5, and F6) showed an alveolar aspect of the intermyofibrillar network on NADH-TR staining (Fig. 1c–f). For family F4, we noted a similar reticular

pattern of intermyofibrillar network with rare whorled fibers. Fiber size variability was present in five families (F1, F4, F5, F6, and F7) (Fig. 1, Supplementary Figure 1). Centralized or internalized nuclei were observed in five families (F1, F2, F4, F6, and F7) and core-like or focal disorganization of the structure in four families (F1, F2, F4, and F7). For patient P5 from family F4, these last features were seen in a few fibers, maybe reflecting the fact that these features appear with time as this patient was biopsied at 9 months old, while the others were biopsied in childhood or adulthood. Uniformity of type 1 (Fig. 1; and immunofluorescence assay, not shown) was observed in F1, F2, F6, and predominance of type 1 fibers in families F4 and F5 was noted. Similar to P5, the biopsy of patient P10 in

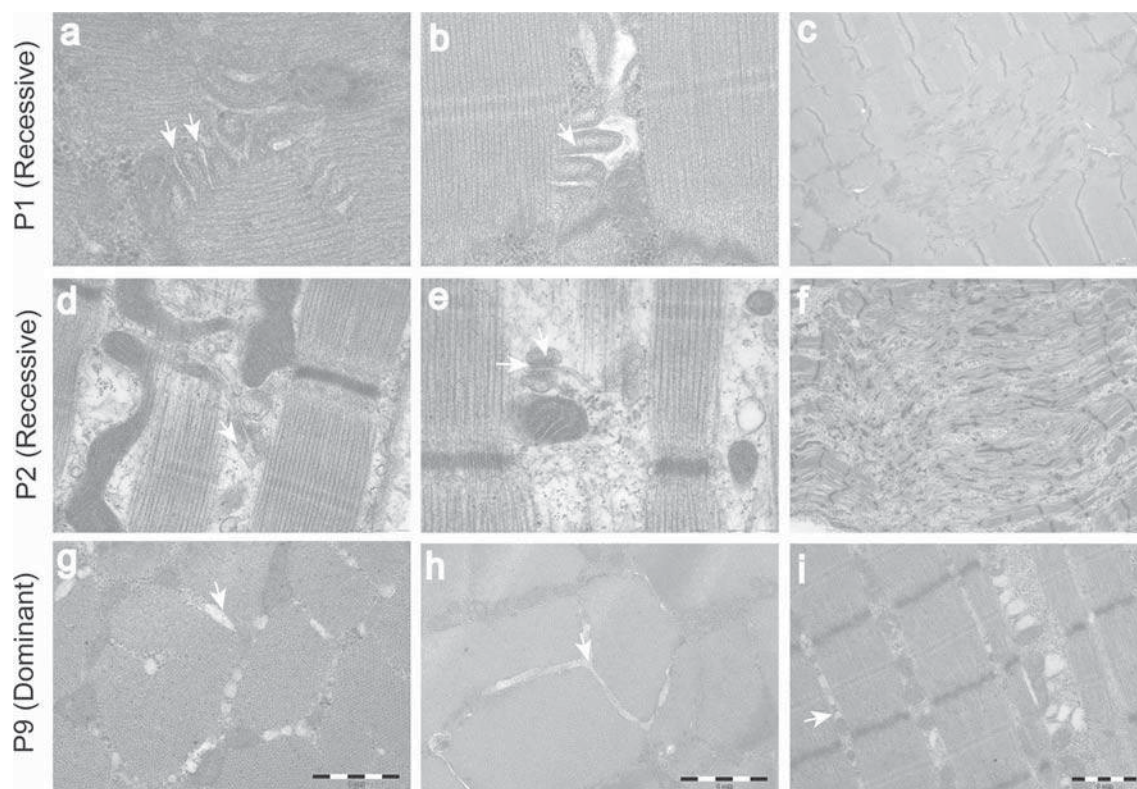


Fig. 2 Changes in muscle ultrastructure caused by *CACNA1S* mutations in patients P1 (recessive; **a–c**), P2 (recessive; **d–f**), and P9 (dominant; **g–i**). P1 biopsy shows multiple triads (*arrows*, **a**) and dilated T-tubules (*arrows*, **b**) and a few focal zones of myofibrillar

disorganization (**c**). P2 biopsy shows slight dilatation of the SR with apparently normal junctional feet connection (*arrows*, **d**, **e**) and small areas of disorganization (**f**). P9 biopsy shows numerous highly dilated SR around the myofibrils (*arrows*, **g–i**)

family F7 showed a dystrophic aspect, with mild increase in endomysial connective tissue, scattered split fibers, in addition to an increase in number of centralized nuclei. In addition, P10 showed occasional fibers with degeneration or regeneration, which is consistent with the finding of increased serum CK to levels more than 1000 IU/l.

The ultrastructure of muscles from patients P1, P2, P3, P6, P7, P9, and P10 was investigated with electron microscopy and uncovered common features, such as dilated T-tubules and SR (Fig. 2b, d, e, g–i) and focal zones of myofibrillar disorganization (Fig. 2c, f). In P1, increased frequency of triads per sarcomere has been observed (Fig. 2a). Long T-tubules and small areas of altered sarcomere striation could be seen in P2 (Fig. 2d–f). Muscle sections from P6 and P7 displayed less abnormalities and only some SR and T-tubules were dilated. However, the junctional feet between SR and T-tubules appeared normal in all patients.

The overall histological and ultrastructural findings were suggestive of a diagnosis of centronuclear or core myopathy. Exome analysis and targeted sequencing of the known related genes, including *MTM1*, *BINI1*, *DNM2*, and *RYR1*, did not reveal any pathogenic variations.

Muscle MRI or CT scan of the lower limbs was performed on nine patients (Fig. 3). Symmetric involvement of anterior and posterior compartments at the level of the thigh was seen in all, varying from mild atrophy in patients P7 and P8 to a marked atrophy in P5 and severe and extensive fatty infiltration throughout all muscle groups in patients P5 and P10. Anterior compartment muscles were slightly more involved than hamstrings in most. In some patients (P1, P2, and P9), the semitendinosus muscle was selectively more affected than the biceps femoris and semimembranosus. In patients P10 and P11, there was also relative sparing of the vastus intermedius and adductor magnus. Where available, imaging at the level of the leg showed findings ranging from mostly absence of involvement to a pattern with relative sparing of the tibialis anterior and posterior muscles as compared to soleus and gastrocnemii.

In summary, all patients display a consistent phenotype of neonatal or early onset progressive muscle weakness with facial involvement and peculiar structural alterations on the muscle biopsy, with variable extra-ocular involvement and CK elevation, suggesting a common genetic basis of the disease.

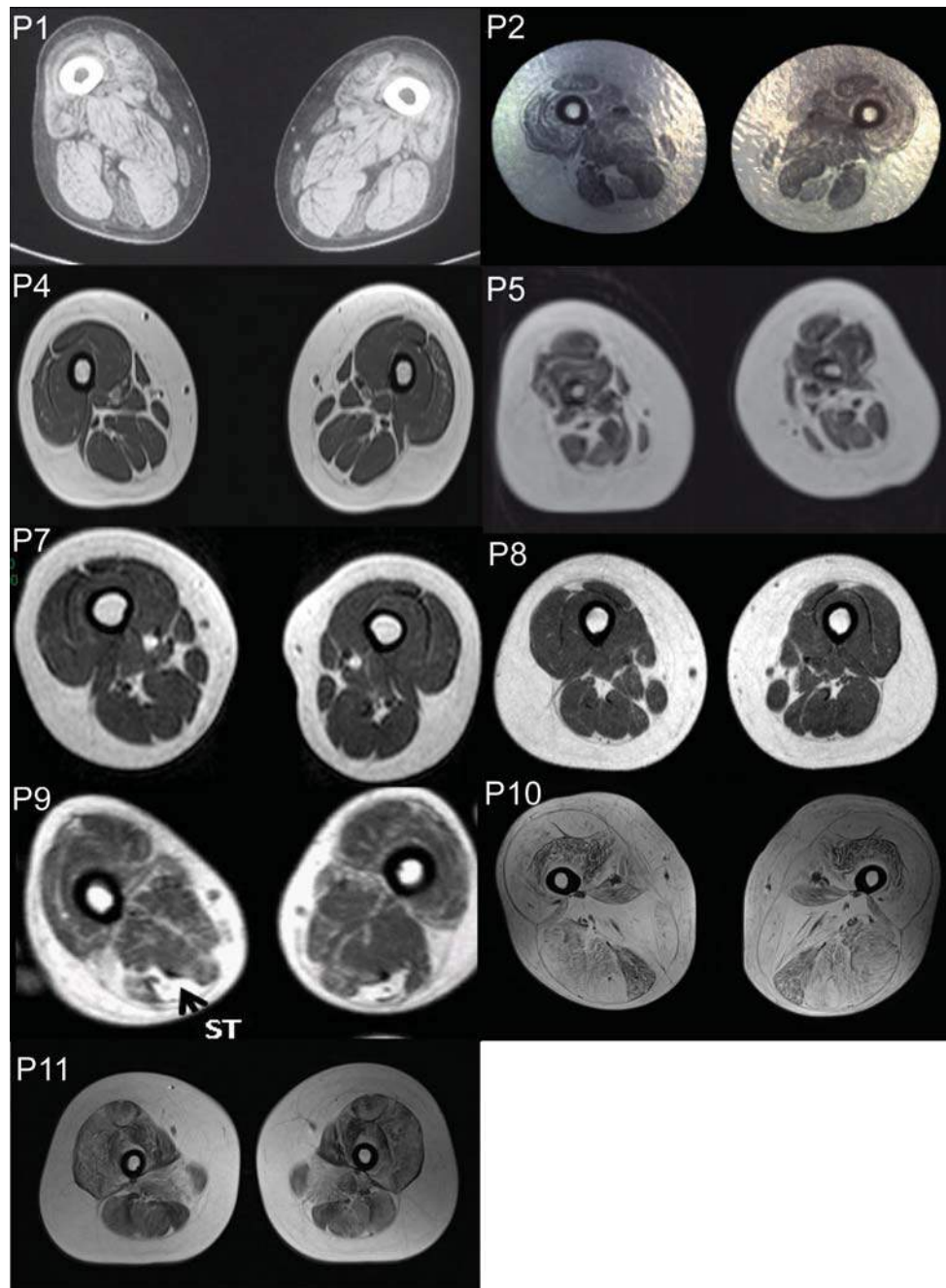


Fig. 3 CT scan (P1) and Muscle MRI of the thighs (P2, P4, P5, P7, P8, P9, P10, and P11) showing muscle involvement of nine patients. P1, P2, P4, P5, P9, P10, and P11 show more severe wasting and fatty infiltration of the anterior compartment in the thigh (vastus lateralis).

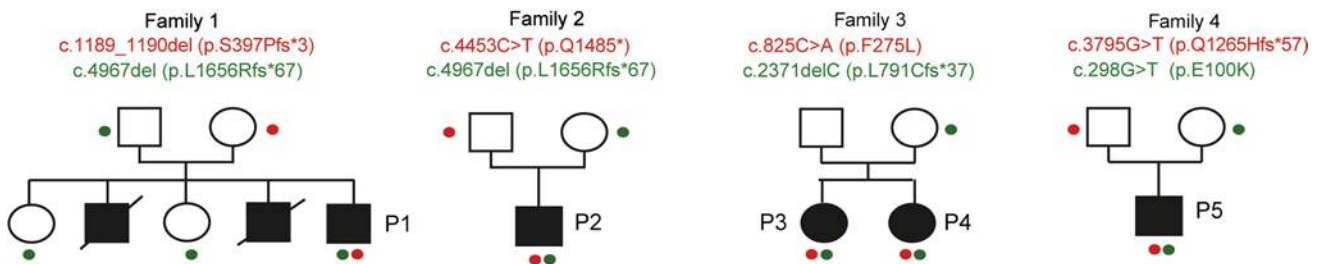
In addition, selective fatty infiltration of semitendinosus is observed in P1, P2, and P9 (*black arrow*). P7 and P8 do not show major abnormalities other than muscle wasting more prominent in the anterior compartment

Identification of dominant and recessive mutations in *CACNA1S*

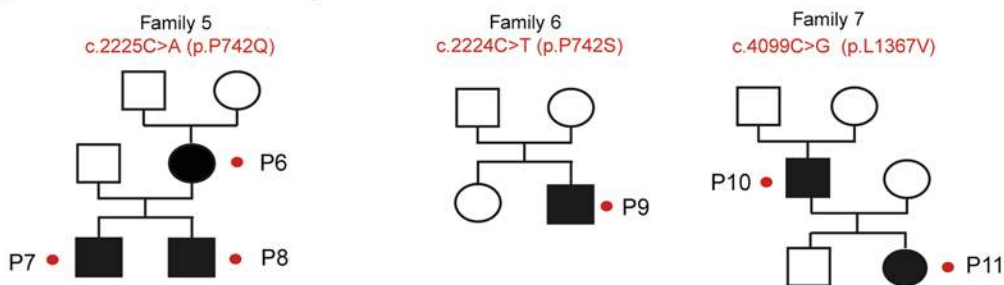
To identify the genetic cause of the disease, we performed exome sequencing on all available affected individuals, as well as one or both parents of families 1, 3, 5, and 6. With the use of different bioinformatics pipelines, we filtered and

ranked the best candidate genes and identified several rare variants in *CACNA1S*, the gene coding the alpha 1 subunit of the L-type voltage-dependent Ca^{2+} channel, and a major protein for excitation–contraction coupling in skeletal muscle. All variants were validated by Sanger sequencing in all available family members and segregation with the disease was confirmed.

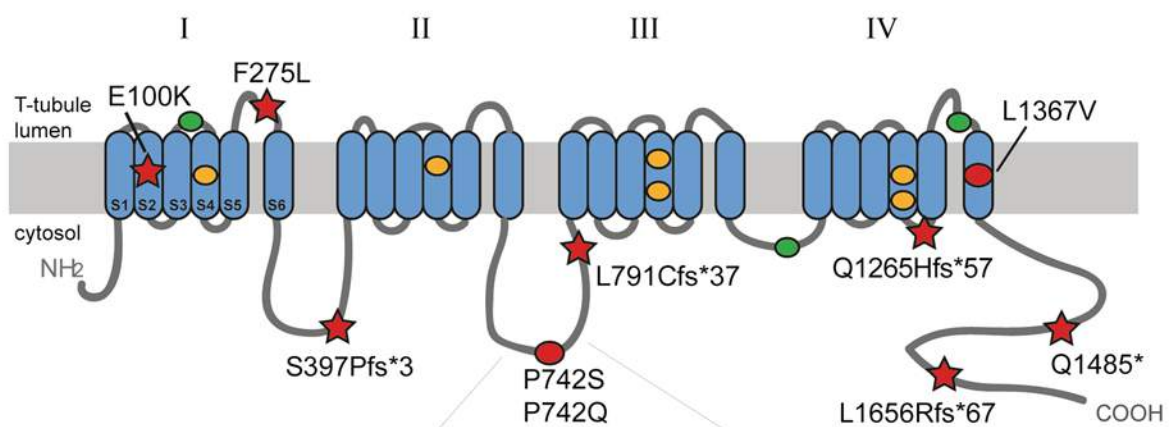
a Recessive cases



b Dominant cases, *De novo*



- c**
- ★ Recessive mutations in congenital myopathy | this study
 - Dominant mutations in congenital myopathy | this study
 - Dominant malignant hyperthermia
 - Dominant hypokalemic periodic paralysis



d

Human CACNA1S	EVKDPYPS-----ADFPGDDEEDEPEIPLSP
Human CACNA1C	EDKSPYP-----NPETTGEDEDEPEMPVGP
Human CACNA1D	EDKDPYPPCDVPVGEDEDEDEPEVPAGP
Mouse CACNA1S	EVKDPYPS-----ADFPGDDEEDEPEIPVSP
Zebrafish CACNA1Sb	EVKDPFPP-----ADFPGDDEDEDEPEIPISP
Zebrafish CACNA1Sa	EIKDPFPP-----ADFPGDDEDEDEPEIPLSP

Four families (F1–F4) displayed recessive disease segregation with compound heterozygous mutations (Fig. 4a). P1 from Family 1 has two frameshift mutations in exons 9 (p.S397Pfs*3; c.1189_1190del) and 40 (p.L1656Rfs*67;

c.4967del). P2 from Family 2 carries a non-sense mutation in exon 37 (p.Q1485*; c.4453C>T) and the same exon 40 frameshift as P1. The shared c.4967del mutation in Families 1 and 2 is likely to be from a different origin

Fig. 4 Genetic analysis of recessive and dominant families mutated in *CACNA1S*. **a** Pedigree and mutations for the four families with recessive inheritance and **b** for the three families with dominant or de novo inheritance. Mutations were screened in all depicted individuals except if indicated deceased. The presence and segregation of mutations are indicated by colored dots; if absent, the individuals do not carry any mutation supporting a de novo appearance in families 5, 6, and 7. **c** Schematic representation of *CACNA1S* showing the position of the novel mutations found in congenital myopathy (numbered), and in malignant hyperthermia or hypokalemic periodic paralysis. **d** Protein sequence alignment demonstrates the specificity of the Proline 742 in *CACNA1S* compared to other alpha 1 subunit of DHPR and the conservation of this residue in different species

considering that they do not share a common haplotype for 2 upstream microsatellites loci, the nearest being 25 kb from the gene. The two siblings P3 and P4 from Family 3 carry a missense mutation in exon 6 (p.F275L; c.825C>A) and a frameshift in exon 18 (p.L791Cfs*37; c.2371delC). P5 from Family 4 carries two predicted missense mutations in exons 30 (p.Q1265H; c.3795G>T) and 3 (p.E100 K; c.298G>A). The respective parents of the patients are carrier of one mutation each, and the 2 unaffected siblings in family 1 carry a single variant, consistent with recessive inheritance.

In the remaining 3 unrelated families, 3 novel heterozygous variants were identified in 5 patients (Fig. 4b). The affected individuals P6, P7, and P8 from family 5 carry a missense mutation in exon 16 (p.P742Q; c.2225C>A) that appears de novo in the mother and segregates in her two affected sons. Patient P9 from family 6 carries a different de novo missense affecting the same amino acid (p.P742S; c.2224C>T). Another de novo missense mutation was identified in both affected father (P10) and daughter (P11) from family 7 (p.L1367 V; c.4099C>G). None of the missense mutations were found in unaffected family members, consistent with dominant inheritance.

All variants are present on both *CACNA1S* isoforms, and affect different domains of the protein (Fig. 4c). All variants were novel with the exception of the c.825C>A (p.F275L) and c.3795G>T (p.Q1265H) variants. They were both found in recessive families 3 and 4, respectively, and are listed in a heterozygous state at very low frequency in the ExAC exome database (3×10^{-5} and 8×10^{-6} , respectively). With regard to the predicted missense changes in our recessive families, the p.F275L substitution in family 3 affects a conserved amino acid of the pore-forming loop L5, which is in close proximity to the selectivity filter. The c.3795G>T variant found in family 4 not only involves an amino-acid substitution, but is, in addition, predicted to impact on splicing, resulting in a shift of the reading frame and a premature stop codon (p.Q1265Hfs*57, outlined below). The second missense variant found in family 4 (p.E100K; c.298G>A) affects a glutamic acid that may interact with arginine 174 for the connection of

transmembrane segments in the voltage-sensing domain, as modeled in the recently resolved 3D structure of DHPR (Supplementary Fig. S2).

Concerning the missense mutations in the dominant families, proline 742 is affected by two different mutations in two unrelated families (p.P742Q and p.P742S). This residue is conserved in mouse and zebrafish, and appears to be specific for the skeletal muscle alpha 1 subunit of DHPR, as it is not conserved in other alpha 1 subunits expressed in other tissues as *CACNA1C* or *CACNA1D* (Fig. 4d). This residue is localized in the loop between domains II and III involved in DHPR-RyR1 coupling, and a previous study demonstrated that the artificial P742T mutation strongly reduced ECC [19].

Altogether, those findings indicate that mutations in *CACNA1S* cause early onset myopathy with dominant or recessive disease inheritance.

Impact of mutations on *CACNA1S* transcript and protein

In total, we identified 10 different *CACNA1S* mutations, including 3 frameshift, 1 non-sense, and 6 missense mutations, including 3 confirmed de novo mutations. The truncating variants are predicted to remove the C-terminal 217, 388, or 1476 amino acids from 1873 in the adult protein isoform. To assess if the premature stop codons lead to non-sense-mediated mRNA-decay (NMD), we extracted, reverse transcribed, and sequenced *CACNA1S* muscle RNA from patients P1 (Family 1) and P3 (Family 3). For patient P1, we detected amplicons of both alleles in comparable amounts, ruling out major mRNA-decay (Fig. 5a). In contrast, the p.L791Cfs*37 mutation in P3 leads to mRNA-decay as only the other allele, carrying the missense mutation, was detected. As mentioned above, one of the missense mutations in patient P5 (predicted protein impact p.Q1265H) is also predicted to disrupt the donor splice site of exon 30. Sequencing of *CACNA1S* RNA extracted from myotubes differentiated from P5 myoblasts indicated retention of 68 nucleotides from intron 30 leading to the frameshift p.Q1265Hfs*57 and the deletion of the last 608 amino acids (Fig. 5a). Both alleles were detected, illustrating that mRNA-decay does not occur. RNA from other patients was not available. In summary, all recessive cases described here carry at least one mutation involving a premature stop codon, although not all appear to trigger mRNA-decay.

To verify the impact of the mutations on the protein level, we performed western blot on muscle biopsies and myotubes extracts. *CACNA1S* was barely detectable by western blot in myotubes extracts from patient P1 with compound truncations (Fig. 5b). Similar results were obtained from muscle extracts of P1 (Fig. 5b). Detectable

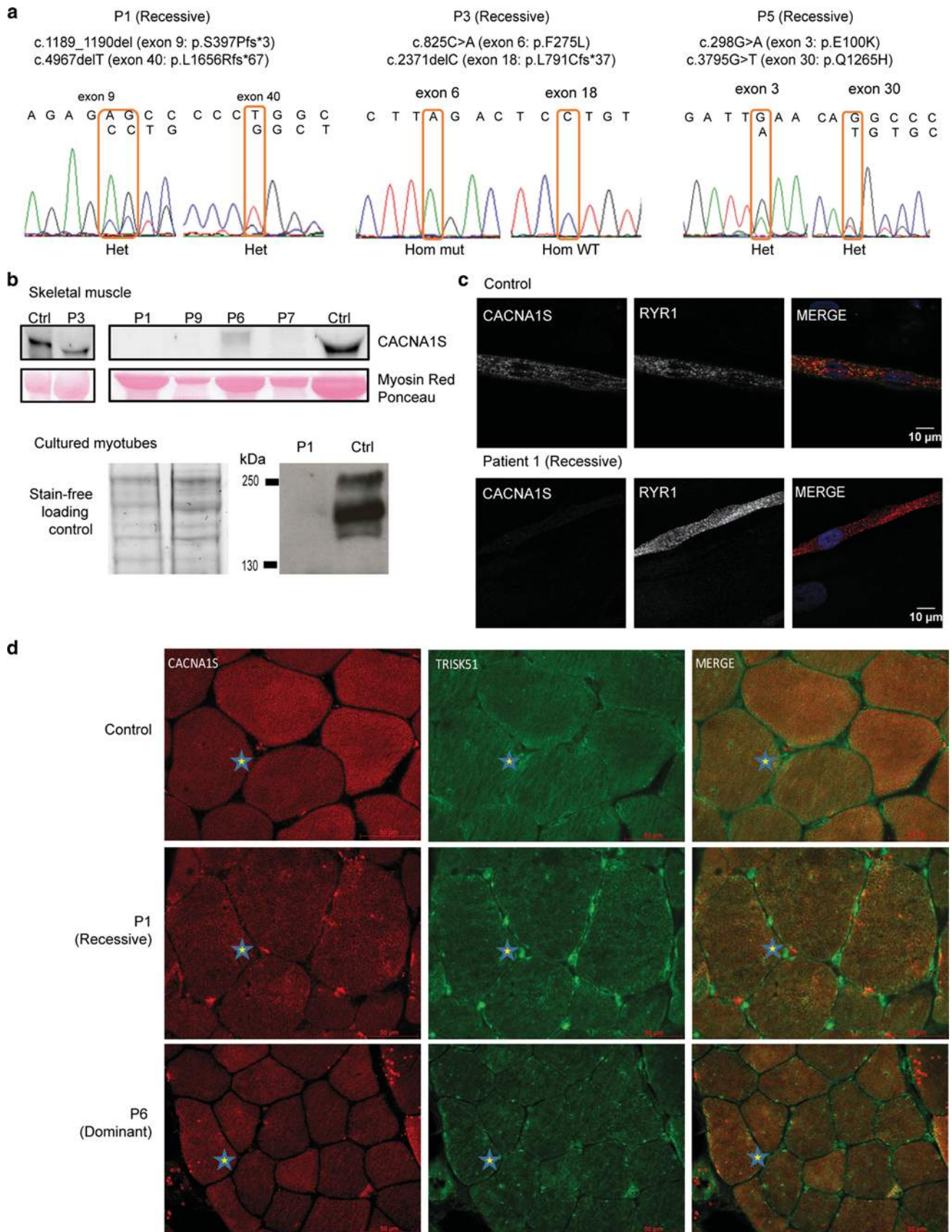


Fig. 5 Impact of the mutations on *CACNA1S* RNA and protein. **a** RNA studies of patients P1, P3, and P5. Amplification and sequencing of the mutated regions showing the presence of both alleles for P1, absence of the truncated allele for P3 (RNA decay), and a splice alteration due to the mutation c.3795G>T in P5. **b** Western Blot showing *CACNA1S* protein levels in muscle extracts (*above*) and cultured myotubes (*below*) from patients compared to controls. **c** Localization of endogenous *CACNA1S* and RyR1 in P1 differentiated myotubes. **d** Localization of the mutated *CACNA1S* and the SR marker triadin on serial sections of patients P1 and P6 muscles. The same fibers on consecutive serial sections are noted with *stars*

protein level was observed in muscle extracts from patient P3, harbouring one truncation and one missense mutation. *CACNA1S* is below the detection level of the western blot in P7 and P9 while slightly detected in P6, all dominant cases (Fig. 5b). These data support overall decreased protein stability following missense or frameshift mutations, in both dominant and recessive cases.

The subcellular localization of some of the mutated *CACNA1S* proteins was investigated in cultured myotubes from patients and in skeletal muscle. In contrast to control myotubes, a very low fluorescent signal was noted with an antibody against the N-terminal domain of *CACNA1S* in differentiated myotubes from patient P1 myoblasts, supporting western blot findings that overall *CACNA1S* is strongly reduced in this patient carrying recessive mutations (Fig. 5c). RyR1 signals appeared as longitudinally aligned dots in both control and patient myotubes, suggesting that the *CACNA1S* mutations do not impact on RyR1 localization, consistent with the previous studies showing that *CACNA1S* knock out myotubes still show triadic localization of RyR1 [31]. The muscle sections from the recessive patient P1 and the dominant patient P6 revealed decreased *CACNA1S* immunoreactivity and showed a peculiar alveolar aspect reminiscent of the observations with oxidative staining (Figs. 1, 5d). Aberrant diffuse accumulations of *CACNA1S* were also observed in the patient's muscles (Fig. 5d). Triadin (junctional SR marker) labelling appeared mildly decreased with lumps or irregular appearance in patients P1, whereas the signal was slightly decreased in patients P6 and P9 (Fig. 5d).

In conclusion, most recessive and dominant mutations we investigated in this study are associated with a decrease in *CACNA1S* protein level and an abnormal localization pattern in available mature muscle.

Physiopathological insights into *CACNA1S* myopathy

CACNA1S is the pore-forming subunit of the voltage-dependent Ca^{2+} channel (DHPR) regulating Ca^{2+} release from the SR stores. To assess the functional impact of *CACNA1S* mutations, we investigated Ca^{2+} homeostasis in myotubes from the recessive patient P1 and the dominant

patient P10 (Fig. 6). Resting cytosolic Ca^{2+} levels were similar between both patients and control myotubes, showing that the mutations do not affect resting Ca^{2+} homeostasis.

We next studied Ca^{2+} release induced by KCl depolarization. Although the dose response curves have similar shapes in patients and controls (EC_{50} 14.3 ± 8.5 for control and 13.2 ± 8.3 for patient cells; Fig. 6), the maximum level of Ca^{2+} released is 2.5 times lower in patients compared to controls. The reduction of the KCl (depolarization)-induced calcium release was not due to a reduction of the size of intracellular Ca^{2+} stores, since there was no significant difference in the total amount of calcium released caused by thapsigargin and ionomycin (Supplementary Figure 3). These results strongly suggest that the *CACNA1S* mutations impair excitation–contraction coupling due to the strong decreased content of *CACNA1S* protein.

Consistent with defects in the ECC, the patients' muscle fibers showed several defects of the triad, including dilated T-tubules and SR (Fig. 2).

Overall, these data indicate that the function of *CACNA1S* and the muscle ultrastructure are similarly altered in both recessive and dominant patients. Pathomechanistically, both mutation types are associated with altered calcium homeostasis and reduced ECC with SR dilatation and myofibrillar disorganization.

Discussion

In this study, we describe a clinical and histopathological cohort of patients with a consistent phenotype of early onset myopathy and mutations in the skeletal muscle alpha 1 subunit of DHPR, *CACNA1S*. Mutations segregated either through recessive or dominant modes of inheritance, or were found as *de novo* mutations in singletons. Two of the mutations, one dominant and one recessive, were tested functionally and both resulted in a significant decrease of EC coupling.

DHPR myopathy and DHPR-related diseases

The described 11 patients from 7 families all display severe early onset myopathy with progressive, generalized predominantly axial muscle weakness, facial involvement with or without ophthalmoplegia, elevated CK in one family, and episodes of periodic paralysis in one patient. The morphological and ultrastructural analyses revealed centralized or internalized nuclei and focal zones of sarcomeric disorganization in several patients. Taken together, this phenotype is reminiscent of findings observed in the myotubular or centronuclear myopathy (CNM) and in core myopathy, conditions in which ophthalmoplegia (an uncommon

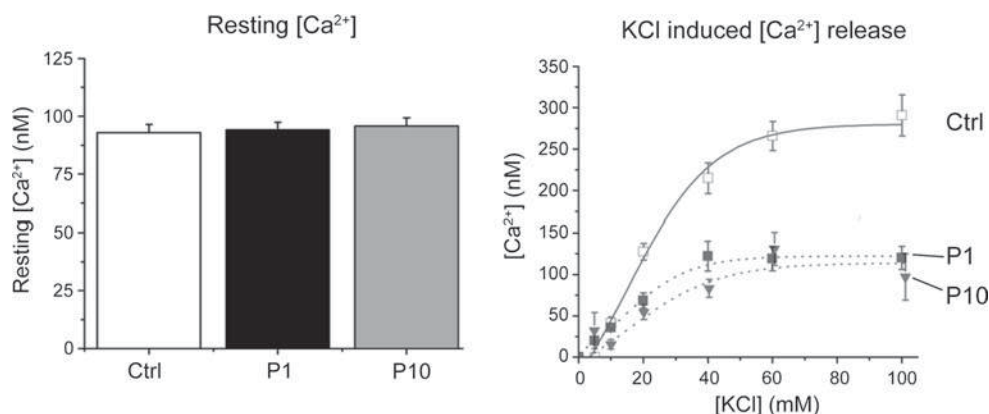


Fig. 6 Impact of recessive and dominant mutations on Ca²⁺ homeostasis. Measurements of the cytosolic Ca²⁺ concentration show no difference between patients P1 (recessive) and P10 (dominant) and controls (*left*). Results show the mean \pm SEM [Ca²⁺] measured in 186, 178, and 98 cells (control, P1, and P10, respectively). The *right*

panel shows the decreased Ca²⁺ release after depolarization by KCl in both P1 and P10 myotubes compared to control myotubes. Results show the mean \pm SEM peak Ca²⁺ release from 5 to 10 myotubes per KCl concentration

feature in other congenital myopathies) is often observed. Those myopathies are also associated with dominant and recessive mutations in *RYR1* [3, 6, 26] and the identification of *CACNA1S* mutations in patients with overlapping phenotype is not unexpected, as DHPR directly regulates the RyR1 Ca²⁺ release channel. The “alveolar” aspect of the intermyofibrillar network observed in the majority of the patients and highlighted with SR labelling both with specific antibodies or oxidative staining and appearing as a dilated SR by electron microscopy is a peculiar and possibly a histopathological hallmark for *CACNA1S* mutations.

In addition, muscle imaging recapitulates some patterns seen in CNM and congenital myopathies. While some patients show relatively mild and non-specific atrophy of muscle groups, three patients from different families had selective involvement of the semitendinosus muscle in the posterior thigh, a finding reported both in early onset CNM due to *DNM2* mutations and in *TTN*-related myopathies [11, 29, 37]. At the level of the leg, family 7 showed a differential pattern with relative preservation of muscles in the anterior compartment (tibialis anterior and posterior) as compared to the soleus and gastrocnemii, a finding which has been described in both *DNM2*- and *RYR1*-related myopathies [17]. However, in addition to such overlapping patterns, there also seems to be a wide spectrum of involvement ranging from very mild atrophy of thigh muscle groups to extensive marked fatty infiltration, suggesting that the imaging of *CACNA1S*-related myopathy is heterogeneous.

The finding of specific histological hallmarks and one of the muscle imaging patterns is of major diagnostic importance, as it can aid in directing the molecular diagnosis towards *CACNA1S* testing. Patients with centronuclear myopathies or cores myopathies without molecular

diagnosis should be reevaluated for specific hallmarks of *CACNA1S* congenital myopathy and offered *CACNA1S* testing if appropriate. Patient P10 and P11 were the only patients displaying elevated CK level; the characterization of additional families will confirm if *CACNA1S* defect leads to dystrophy under certain conditions. We believe that the gene should be included both in NGS panels for congenital muscle disorders and in filtering pipelines for whole-exome sequencing in such cases.

The association of *CACNA1S* with a congenital myopathy phenotype was recently suggested in one patient [14]. This patient displayed a similar phenotype as in our cohort, with congenital myopathy and ophthalmoplegia, and occasional internal nuclei and coarse myofibrillar architecture on muscle biopsy. He carried compound *CACNA1S* variants each inherited from a heterozygous parent, c.4947delA (p.Q1649Qfs*72) and c.3795G>T (p.Q1265H). In that report, no functional validation of the variants pathogenicity was provided, precluding a conclusion on the pathogenicity of the identified variants. Of note is that the predicted frameshift is very close to the frameshift mutation p.L1656Rfs*67 found in our recessive families 1 and 2 (Fig. 4), and we show here that the c.3795G>T change in fact leads to altered splicing in our patient P5 (Fig. 5a).

Dominant *CACNA1S* mutations have been associated with malignant hyperthermia or hypokalemic periodic paralysis [16, 25, 32]. Here, we report for the first time dominant and recessive *CACNA1S* mutations associated with a myopathy. Most *CACNA1S* mutations linked to periodic paralysis are missense changes residing in the voltage-sensing domain (transmembrane segment S4 in each transmembrane domain), while most mutations in malignant hyperthermia are missense mutations in the loop regions (Fig. 4c). In contrast, the myopathy mutations uncovered

in this study in congenital myopathy are evenly distributed in the sequence and structure of CACNA1S. Dominant mutations are either in the pore-forming domain (L1367) or in the II–III loop implicated in RYR1 coupling (P742), while recessive mutations primarily comprise truncations at different spots, or missenses in the pore-forming or voltage-sensing domains. There is thus no strict correlation between the type and location of mutations and the associated diseases, or their severity.

Noteworthy, recessive, and dominant mutations in congenital myopathy lead to similar clinical and histological phenotypes, and our functional studies demonstrated that both mutations types comparably interfere with ECC, suggesting a similar overall alteration of CACNA1S function (Fig. 5). However, ophthalmoplegia is not a common sign even if observed in several patients, CK was elevated in only one family and episodes of periodic paralysis were observed in one patient. The discovery of additional CACNA1S patients with congenital myopathies and future functional work will specify the overall clinical phenotype and its potential correlation with the position and the transmission mode of the mutations.

The fact that all dominant mutations are missense changes, while heterozygous carriers of recessive mutations are healthy, excludes haploinsufficiency as the underlying pathomechanism in the dominant cases. Instead, the dominant mutations may act through a dominant-negative manner on the WT protein. Indeed, we noted that both recessive and dominant mutations correlated with a strong decrease in overall protein level (Fig. 4), suggesting that DHPR complexes containing a mutant CACNA1S subunit form unstable or non-functional tetrads prone to degradation.

None of our patients presented with cardiac involvement. The heart-specific CACNA1C alpha 1 subunit is mutated in the Brugada syndrome (MIM#611875) characterized by shortened QT interval and high incidence of sudden death, and in the Timothy syndrome (MIM#61005) characterized by multi-organ dysfunction, including lethal arrhythmias. These findings reflect the exquisite tissue-specific expression of DHPR alpha 1 subunits, CACNA1C in heart, and CACNA1S in skeletal muscle. More generally, this is also true for the other ten different CACNA1 (alpha 1) subunits that are mutated in non-muscle diseases, such as hemiplegic migraine, ataxias, bradycardia and deafness, night blindness, or aldosteronism, in relation with their tissue-specific expression [15].

Pathophysiological mechanism

While future experimental work will be needed to decipher the detailed pathological mechanism, the published and present data suggest a sequence of events leading from the CACNA1S mutations to the pathology and

muscle disease. As both dominant and recessive mutations can lead to a rather homogeneous phenotype, we hypothesize that they both lead to a decrease in overall DHPR function in skeletal muscle. We show here that several CACNA1S mutations strongly reduced Ca²⁺ release after depolarization, while basal cytosolic Ca²⁺ and SR store Ca²⁺ levels are not altered. Of note, a previous study showed that the artificial P742T mutation, affecting the same amino acid that is mutated in our dominant families F5 (p.P742Q) and F6 (p.P742S), strongly reduced ECC, highlighting the importance of the loop between DHPR domains II and III for RyR1 activation [19]. To activate directly RyR1, we used 4-chloro-m-cresol (4-CMC) [41] and observed reduced Ca²⁺ release from the SR in patient 1 (Supplementary Fig. S3). We hypothesize that RyR1 function is impacted by the loss of CACNA1S through a feedback regulation or protein stabilization. The KCl-induced dose response curves are strikingly similar to those obtained in patients with RyR1-related central core disease (CCD) [7], although the resting calcium concentration were always higher in myotubes from RYR1 mutation bearing patients compared to controls. This would then lead to the structural defects observed on histological analysis. In most patient biopsies analyzed, the T-tubules and the SR were frequently dilated or disrupted. Some of them presented an increased frequency of triads by sarcomere. It is unclear at present whether this is an indirect effect of abnormal Ca²⁺ signal or contraction (functional role), or due to the direct alteration in CACNA1S protein (structural role). These rather specific alterations were not found in RyR1-related myopathies or in centronuclear myopathies. However, in our study, triads are still formed with visible «feet». Indeed, mice-lacking DHPR (muscular dysgenesis and mdg mouse) or RyR1 (dyspedic) form triadic junctions, with a similar architecture compared to wild type [5, 12, 31]. These data in mice thus suggest that structural defects seen in patients are not linked to a loss of DHPR but rather to altered ECC. Abnormal nuclei positioning and focal zones of myofibrillar disorganization are additional structural defects in patient muscles. The peculiar alveolar appearance of the intermyofibrillar network could be a result of the SR dilatation. Complete knock-out of CACNA1S during development is lethal in the mdg mouse [5, 28] and disease onset is antenatal or perinatal in our patients, pointing to an important role of DHPR in perinatal development. Moreover, the role of CACNA1S in adult muscle was studied by U7-mediated skipping in adult mice, revealing that decreased CACNA1S protein level was linked to muscle atrophy [30]. These data in mice are in agreement with the observation that a low level of CACNA1S has to be present in

the muscle. A decreased level lead to the muscle atrophy observed in our patients. While abnormal ECC can explain the severe muscle weakness in patients, it is possible that the concomitant structural defects contribute to the clinical phenotype.

Conclusions

Here, we have characterized the *CACNA1S* congenital myopathy as a specific entity, at the interface between the structural congenital myopathies and the triadopathies defined by alteration of the ECC. The identification of *CACNA1S* mutations in a phenotype of early onset myopathy should allow a better molecular diagnosis, genetic counseling, and prognosis. It also points to *CACNA1S* and ECC as therapeutic targets for the development of treatments that may be facilitated by the already extensive prior knowledge accumulated on DHPR. In addition, treatment by acetazolamide showed positive results on the episodes of periodic paralysis of one patient. The results of this study also expand the clinical and genetic spectra of *CACNA1S* mutations and highlight that DHPR cellular roles are important for perinatal muscle function in human.

Acknowledgements We thank Isabelle Marty for triadin antibody, John Rendu for *RYR1* molecular testing, Anne-Sophie Nicot and Clara Franzini-Armstrong for discussions, Robert Y. Carlier for analysis of MRI images, and Nicola Foulds for clinical discussions. This work was supported by the Institut National de la Santé et de la Recherche Médicale (INSERM), Centre National de la Recherche Scientifique (CNRS), University of Strasbourg, the France Génomique National infrastructure, funded as part of the Investissements d’Avenir program managed by the Agence Nationale pour la Recherche (ANR-10-INBS-09), and by Fondation Maladies Rares within the frame of the “Myocapture” sequencing project, ANR-10-LABX-0030-INRT under the frame program Investissements d’Avenir ANR-10-IDEX-0002-02, Association Française contre les Myopathies (AFM-17088), Muscular Dystrophy Association (MDA-186985), Myotubular Trust and Sparks the Children’s medical research charity grant N° 12KCL 01-MT, and the Swiss National Science Foundation grant N° 31003A-146198. T.M.P. was supported by the Diana and Steve Marienhoff Fashion Industries Guild Endowed Fellowship in Pediatric Neuromuscular Diseases. F.M. is supported by the National Institute for Health Research Biomedical Research Centre at Great Ormond Street Hospital for Children NHS Foundation Trust and University College London. The Biobank of the MRC Neuromuscular Centre and the support of the Muscular Dystrophy UK to the Dubowitz Neuromuscular Centre are also gratefully acknowledged.

Web resources ExAC Browser/Exome Aggregation Consortium (URL: <http://exac.broadinstitute.org/>). Exome Variant Server (URL: <http://evs.gs.washington.edu/EVS/>) [March, 2012]. 1000 genomes (URL: <http://www.1000genomes.org/>). Database of Single Nucleotide Polymorphisms (dbSNP Build ID: 134) (URL: <http://www.ncbi.nlm.nih.gov/SNP/>). Online Mendelian Inheritance in Man (OMIM) (URL: <http://www.omim.org/>).

References

- Al-Qusairi L, Laporte J (2011) T-tubule biogenesis and triad formation in skeletal muscle and implication in human diseases. *Skelet Muscle* 1:26. doi:10.1186/2044-5040-1-26
- Amburgey K, McNamara N, Bennett LR, McCormick ME, Acsadi G, Dowling JJ (2011) Prevalence of congenital myopathies in a representative pediatric united states population. *Ann Neurol* 70:662–665. doi:10.1002/ana.22510
- Bevilacqua JA, Monnier N, Bitoun M, Eymard B, Ferreira A, Monges S, Lubieniecki F, Taratuto AL, Laquerriere A, Claeys KG et al (2011) Recessive *RYR1* mutations cause unusual congenital myopathy with prominent nuclear internalization and large areas of myofibrillar disorganization. *Neuropathol Appl Neurobiol* 37:271–284. doi:10.1111/j.1365-2990.2010.01149.x
- Censier K, Urwyler A, Zorzato F, Treves S (1998) Intracellular calcium homeostasis in human primary muscle cells from malignant hyperthermia-susceptible and normal individuals. Effect of overexpression of recombinant wild-type and Arg163Cys mutated ryanodine receptors. *J Clin Invest* 101:1233–1242. doi:10.1172/JCI993
- Chaudhari N (1992) A single nucleotide deletion in the skeletal muscle-specific calcium channel transcript of muscular dysgenesis (mdg) mice. *J Biol Chem* 267:25636–25639
- Dowling JJ, Lawlor MW, Dirksen RT (2014) Triadopathies: an emerging class of skeletal muscle diseases. *Neurotherapeutics* 11:773–785. doi:10.1007/s13311-014-0300-3
- Ducreux S, Zorzato F, Muller C, Sewry C, Muntoni F, Quinlivan R, Restagno G, Girard T, Treves S (2004) Effect of ryanodine receptor mutations on interleukin-6 release and intracellular calcium homeostasis in human myotubes from malignant hyperthermia-susceptible individuals and patients affected by central core disease. *J Biol Chem* 279:43838–43846. doi:10.1074/jbc.M403612200
- Dulhunty AF, Karunasekara Y, Curtis SM, Harvey PJ, Board PG, Casarotto MG (2005) Role of some unconserved residues in the “C” region of the skeletal DHPR II-III loop. *Front Biosci* 10:1368–1381
- Eberl DF, Ren D, Feng G, Lorenz LJ, Van Vactor D, Hall LM (1998) Genetic and developmental characterization of *Dmca1D*, a calcium channel alpha subunit gene in *Drosophila melanogaster*. *Genetics* 148:1159–1169
- Engel AG, Franzini-Armstrong C (2004) *Myology, basic and clinical*. McGraw-Hill, New York
- Fischer D, Herasse M, Bitoun M, Barragan-Campos HM, Chiras J, Laforet P, Fardeau M, Eymard B, Guicheney P, Romero NB (2006) Characterization of the muscle involvement in dynamin 2-related centronuclear myopathy. *Brain* 129:1463–1469. doi:10.1093/brain/awl071
- Franzini-Armstrong C, Pincon-Raymond M, Rieger F (1991) Muscle fibers from dysgenic mouse in vivo lack a surface component of peripheral couplings. *Dev Biol* 146:364–376
- Geoffroy V, Pizot C, Redin C, Piton A, Vasli N, Stoetzel C, Blavier A, Laporte J, Muller J (2015) VaRank: a simple and powerful tool for ranking genetic variants. *PeerJ* 3:e796. doi:10.7717/peerj.796
- Hunter JM, Ahearn ME, Balak CD, Liang WS, Kurdoglu A, Corneveaux JJ, Russell M, Huentelman MJ, Craig DW, Carpten J et al (2015) Novel pathogenic variants and genes for myopathies identified by whole exome sequencing. *Mol Genet Genomic Med* 3:283–301. doi:10.1002/mgg3.142
- Jurkat-Rott K, Lehmann-Horn F (2004) The impact of splice isoforms on voltage-gated calcium channel alpha subunits. *J Physiol* 554:609–619. doi:10.1113/jphysiol.2003.052712

16. Jurkat-Rott K, Lehmann-Horn F, Elbaz A, Heine R, Gregg RG, Hogan K, Powers PA, Lapie P, Vale-Santos JE, Weissenbach J et al (1994) A calcium channel mutation causing hypokalemic periodic paralysis. *Hum Mol Genet* 3:1415–1419
17. Klein A, Jungbluth H, Clement E, Lillis S, Abbs S, Munot P, Pane M, Wraige E, Schara U, Straub V et al (2011) Muscle magnetic resonance imaging in congenital myopathies due to ryanodine receptor type 1 gene mutations. *Arch Neurol* 68:1171–1179. doi:10.1001/archneurol.2011.188
18. Knudson CM, Chaudhari N, Sharp AH, Powell JA, Beam KG, Campbell KP (1989) Specific absence of the alpha 1 subunit of the dihydropyridine receptor in mice with muscular dysgenesis. *J Biol Chem* 264:1345–1348
19. Kugler G, Weiss RG, Flucher BE, Grabner M (2004) Structural requirements of the dihydropyridine receptor alpha1S II–III loop for skeletal-type excitation–contraction coupling. *J Biol Chem* 279:4721–4728. doi:10.1074/jbc.M307538200
20. Kung AW, Lau KS, Fong GC, Chan V (2004) Association of novel single nucleotide polymorphisms in the calcium channel alpha 1 subunit gene (Ca(v)1.1) and thyrotoxic periodic paralysis. *J Clin Endocrinol Metab* 89:1340–1345. doi:10.1210/jc.2003-030924
21. Lu X, Xu L, Meissner G (1994) Activation of the skeletal muscle calcium release channel by a cytoplasmic loop of the dihydropyridine receptor. *J Biol Chem* 269:6511–6516
22. Malfatti E, Bohm J, Lacene E, Beuvin M, Romero NB, Laporte J (2015) A premature stop codon in MYO18B is associated with severe nemaline myopathy with cardiomyopathy. *J Neuromuscul Dis* 2:219–227. doi:10.3233/JND-150085
23. Malfatti E, Romero NB (2016) Nemaline myopathies: state of the art. *Rev Neurol (Paris)* 172:614–619. doi:10.1016/j.neurol.2016.08.004
24. Matthews E, Portaro S, Ke Q, Sud R, Haworth A, Davis MB, Griggs RC, Hanna MG (2011) Acetazolamide efficacy in hypokalemic periodic paralysis and the predictive role of genotype. *Neurology* 77:1960–1964. doi:10.1212/WNL.0b013e31823a0cb6
25. Monnier N, Procaccio V, Stieglitz P, Lunardi J (1997) Malignant-hyperthermia susceptibility is associated with a mutation of the alpha 1-subunit of the human dihydropyridine-sensitive L-type voltage-dependent calcium-channel receptor in skeletal muscle. *Am J Hum Genet* 60:1316–1325
26. Nance JR, Dowling JJ, Gibbs EM, Bonnemann CG (2012) Congenital myopathies: an update. *Curr Neurol Neurosci Rep* 12:165–174. doi:10.1007/s11910-012-0255-x
27. North KN (2011) Clinical approach to the diagnosis of congenital myopathies. *Semin Pediatr Neurol* 18:216–220. doi:10.1016/j.spn.2011.10.002
28. Pai AC (1965) Developmental genetics of a lethal mutation, muscular dysgenesis (Mdg), in the mouse. II. Developmental analysis. *Dev Biol* 11:93–109
29. Pfeffer G, Elliott HR, Griffin H, Barresi R, Miller J, Marsh J, Evila A, Vihola A, Hackman P, Straub V et al (2012) Titin mutation segregates with hereditary myopathy with early respiratory failure. *Brain* 135:1695–1713. doi:10.1093/brain/aws102
30. Pietri-Rouxel F, Gentil C, Vassilopoulos S, Baas D, Mouisel E, Ferry A, Vignaud A, Hourde C, Marty I, Schaeffer L et al (2010) DHPR alpha1S subunit controls skeletal muscle mass and morphogenesis. *EMBO J* 29:643–654. doi:10.1038/emboj.2009.366
31. Powell JA, Petherbridge L, Flucher BE (1996) Formation of triads without the dihydropyridine receptor alpha subunits in cell lines from dysgenic skeletal muscle. *J Cell Biol* 134:375–387
32. Ptacek LJ, Tawil R, Griggs RC, Engel AG, Layzer RB, Kwiecinski H, McManis PG, Santiago L, Moore M, Fouad G et al (1994) Dihydropyridine receptor mutations cause hypokalemic periodic paralysis. *Cell* 77:863–868
33. Rebeck RT, Karunasekara Y, Board PG, Beard NA, Casarotto MG, Dulhunty AF (2014) Skeletal muscle excitation–contraction coupling: who are the dancing partners? *Int J Biochem Cell Biol* 48:28–38. doi:10.1016/j.biocel.2013.12.001
34. Rezgui SS, Vassilopoulos S, Brocard J, Platel JC, Bouron A, Arnoult C, Oddoux S, Garcia L, De Waard M, Marty I (2005) Triadin (Trisk 95) overexpression blocks excitation–contraction coupling in rat skeletal myotubes. *J Biol Chem* 280:39302–39308. doi:10.1074/jbc.M506566200
35. Romero NB, Clarke NF (2013) Congenital myopathies. *Handb Clin Neurol* 113:1321–1336. doi:10.1016/B978-0-444-59565-2.00004-6
36. Sekulic-Jablanovic M, Palmowski-Wolfe A, Zorzato F, Treves S (2015) Characterization of excitation–contraction coupling components in human extraocular muscles. *Biochem J* 466:29–36. doi:10.1042/BJ20140970
37. Susman RD, Quijano-Roy S, Yang N, Webster R, Clarke NF, Dowling J, Kennerson M, Nicholson G, Biancalana V, Ilkovski B et al (2010) Expanding the clinical, pathological and MRI phenotype of DNM2-related centronuclear myopathy. *Neuromuscul Disord* 20:229–237. doi:10.1016/j.nmd.2010.02.016
38. Tang ZZ, Yarotskyy V, Wei L, Sobczak K, Nakamori M, Eichinger K, Moxley RT, Dirksen RT, Thornton CA (2012) Muscle weakness in myotonic dystrophy associated with misregulated splicing and altered gating of Ca(V)1.1 calcium channel. *Hum Mol Genet* 21:1312–1324. doi:10.1093/hmg/ddr568
39. Treves S, Pouliquin R, Moccagatta L, Zorzato F (2002) Functional properties of EGFP-tagged skeletal muscle calcium-release channel (ryanodine receptor) expressed in COS-7 cells: sensitivity to caffeine and 4-chloro-m-cresol. *Cell Calcium* 31:1–12
40. Wu J, Yan Z, Li Z, Yan C, Lu S, Dong M, Yan N (2015) Structure of the voltage-gated calcium channel Cav1.1 complex. *Science* 350:aad2395. doi:10.1126/science.aad2395
41. Zorzato F, Scutari E, Tegazzin V, Clementi E, Treves S (1993) Chlorocresol: an activator of ryanodine receptor-mediated Ca₂⁺ release. *Mol Pharmacol* 44:1192–1201

2.2.7 Publication 9: Affected female carriers of *MTM1* mutations display a wide spectrum of clinical and pathological involvement: delineating diagnostic clues (Biancalana et al. 2017)

Background

MTM1 encodes myotubularin, a ubiquitously expressed phosphoinositide phosphatase (Taylor, Maehama, and Dixon 2000). Phosphoinositides are membrane lipids with a crucial role in various cell functions including growth, cytoskeletal organization, membrane trafficking and autophagy (Vergne and Deretic 2010; Odorizzi, Babst, and Emr 2000; Cao et al. 2008). *MTM1* is located on the X chromosome, and loss-of-function mutations cause a severe form of centronuclear myopathy (CNM), affecting mainly males (XLMTM) (Laporte et al. 1996). Only a few symptomatic XLMTM females were described in the literature, allowing only a narrow view on the clinical and histological spectrum of the disorder in women (Dahl et al. 1995; Tanner et al. 1999).

Aim of the study

This publication compared new and published female XLMTM cases to assess the clinical and histological spectrum of the disorder, and to improve molecular diagnosis and disease management for affected women.

Results

We described 17 new XLMTM females and compared the clinical and histological data with the 26 previously published cases. The age of onset and the severity of the disease were highly variable, ranging from a neonatal to a milder adult-onset phenotype. The muscle weakness was asymmetric and mostly involved limb-girdle, facial, and respiratory muscles. The histological features on muscle biopsies included internalization of nuclei, necklace fibers and fatty replacement. The identified *MTM1* mutations are either truncations or missense mutations causing or predicted to cause severe phenotypes in males. Comparison of the relative X-inactivation in blood samples of seventeen XLMTM females revealed a increased prevalence of highly skewed X inactivation compared with healthy females (Amos-Landgraf et al. 2006). A direct correlation between the degree of skewing and the severity of the disease was, however, not apparent.

Conclusion

We showed that female carriers of a *MTMI* mutation can be affected and often develop a slowly progressive myopathy with specific features including asymmetric limb girdle weakness and facial weakness. Overall, this study underlines the importance to sequence *MTMI* in females with molecularly undiagnosed myopathy.

Contribution

I identified an *MTMI* splice site mutation in a woman with CNM.

Affected female carriers of *MTM1* mutations display a wide spectrum of clinical and pathological involvement: delineating diagnostic clues

Valérie Biancalana^{1,2,3,4,5} · Sophie Scheidecker¹ · Marguerite Miguet¹ · Annie Laquerrière⁶ · Norma B. Romero^{7,8} · Tanya Stojkovic⁸ · Osorio Abath Neto⁹ · Sandra Mercier^{10,11,12} · Nicol Voermans¹³ · Laura Tanner¹⁴ · Curtis Rogers¹⁵ · Elisabeth Ollagnon-Roman¹⁶ · Helen Roper¹⁷ · Célia Boutte¹⁸ · Shay Ben-Shachar¹⁹ · Xavière Lornage^{2,3,4,5} · Nasim Vasli^{2,3,4,5} · Elise Schaefer²⁰ · Pascal Laforet²¹ · Jean Pouget²² · Alexandre Moerman²³ · Laurent Pasquier²⁴ · Pascale Marcocelle^{25,26} · Armelle Magot¹² · Benno Küsters²⁷ · Nathalie Streichenberger²⁸ · Christine Tranchant²⁹ · Nicolas Dondaine¹ · Raphael Schneider^{2,3,4,5,30} · Claire Gasnier¹ · Nadège Calmels¹ · Valérie Kremer³¹ · Karine Nguyen³² · Julie Perrier¹² · Erik Jan Kamsteeg³³ · Pierre Carlier³⁴ · Robert-Yves Carlier³⁵ · Julie Thompson³⁰ · Anne Boland³⁶ · Jean-François Deleuze³⁶ · Michel Fardeau^{7,8} · Edmar Zanoteli⁹ · Bruno Eymard²¹ · Jocelyn Laporte^{2,3,4,5}

Received: 9 May 2017 / Revised: 24 June 2017 / Accepted: 2 July 2017
© Springer-Verlag GmbH Germany 2017

Abstract X-linked myotubular myopathy (XLMTM), a severe congenital myopathy, is caused by mutations in the *MTM1* gene located on the X chromosome. A majority of affected males die in the early postnatal period, whereas female carriers are believed to be usually asymptomatic. Nevertheless, several affected females have been reported. To assess the phenotypic and pathological spectra of carrier

females and to delineate diagnostic clues, we characterized 17 new unrelated affected females and performed a detailed comparison with previously reported cases at the clinical, muscle imaging, histological, ultrastructural and molecular levels. Taken together, the analysis of this large cohort of 43 cases highlights a wide spectrum of clinical severity ranging from severe neonatal and generalized weakness, similar to XLMTM male, to milder adult forms. Several females show a decline in respiratory function. Asymmetric weakness is a noteworthy frequent specific feature potentially correlated to an increased prevalence of highly skewed X inactivation. Asymmetry of growth was also noted. Other diagnostic clues include facial weakness,

Sophie Scheidecker and Marguerite Miguet contributed equally to this work.

Electronic supplementary material The online version of this article (doi:10.1007/s00401-017-1748-0) contains supplementary material, which is available to authorized users.

✉ Valérie Biancalana
valerie.biancalana@chru-strasbourg.fr

¹ Laboratoire Diagnostic Génétique, Faculté de Médecine, CHRU, Nouvel Hôpital Civil, 1 place de l'Hôpital, 67091 Strasbourg, France

² Institut de Génétique et de Biologie Moléculaire et Cellulaire, Illkirch, France

³ Centre National de la Recherche Scientifique, UMR7104, Illkirch, France

⁴ Institut National de la Santé et de la Recherche Médicale, U964, Illkirch, France

⁵ Fédération de Médecine Translationnelle de Strasbourg, Université de Strasbourg, Illkirch, France

⁶ Department of Pathology, Normandie Univ, UNIROUEN, INSERM U1245, Rouen University Hospital, F76000 Rouen, France

⁷ Center for Research in Myology, GH Pitié-Salpêtrière, Sorbonne Universités, UPMC Univ Paris 06, INSERM UMRS974, CNRS FRE3617, Paris, France

⁸ Centre de référence de Pathologie Neuromusculaire Paris-Est, Institut de Myologie, GHU Pitié-Salpêtrière, Assistance Publique-Hôpitaux de Paris, Paris, France

⁹ Departamento de Neurologia, Faculdade de Medicina da Universidade de São Paulo (FMUSP), São Paulo, Brazil

¹⁰ Service de Génétique Médicale, Unité de Génétique Clinique, CHU, Nantes, France

¹¹ Atlantic Gene Therapy Institute, University of Nantes, Nantes, France

¹² Centre de Référence des Maladies Neuromusculaires Nantes-Angers, CHU de Nantes, Nantes, France

¹³ Department of Neurology, Radboud University Medical Centre, Nijmegen, The Netherlands

ptosis and ophthalmoplegia, skeletal and joint abnormalities, and histopathological signs that are hallmarks of centronuclear myopathy such as centralized nuclei and necklace fibers. The histopathological findings also demonstrate a general disorganization of muscle structure in addition to these specific hallmarks. Thus, *MTM1* mutations in carrier females define a specific myopathy, which may be independent of the presence of an XLMTM male in the family. As several of the reported affected females carry large heterozygous *MTM1* deletions not detectable by Sanger sequencing, and as milder phenotypes present as adult-onset limb-girdle myopathy, the prevalence of this myopathy is likely to be greatly underestimated. This report should aid diagnosis and thus the clinical management and genetic counseling of *MTM1* carrier females. Furthermore, the clinical and pathological history of this cohort may be useful for therapeutic projects in males with XLMTM, as it illustrates the spectrum of possible evolution of the disease in patients surviving long term.

Keywords *MTM1* · X-linked myotubular myopathy · Centronuclear myopathy · Congenital myopathy · X inactivation

Introduction

Myotubular myopathy (XLMTM, MIM #310400) is a severe congenital myopathy linked to the X chromosome. While affected males display severe hypotonia and weakness at birth and have a very short life expectancy even with interventional care and ventilatory support, female carriers were reported to be either asymptomatic or affected through a wide spectrum of severity. The disease in females is much less characterized to date. Moreover, as affected females reach adulthood, they could potentially reveal additional symptoms that are not described in XLMTM in males. In this study, we thus aimed to better define the symptoms, the genotype–phenotype correlation and the disease progression in females with XLMTM through a thorough characterization of a large cohort of novel cases and comparison with the literature.

XLMTM is caused by mutations in the *MTM1* gene (MIM 300415) encoding the ubiquitous phosphoinositide phosphatase myotubularin (MTM1) [38]. This is the most severe form of centronuclear myopathies, a group of myopathies caused by different genes and modes of inheritance whose hallmark histological abnormalities are centrally located nuclei [2, 8, 11, 12, 15, 38, 44, 48, 52, 65], without dystrophic features. Around 500 males with XLMTM have been reported and they usually present at birth with severe

¹⁴ Department Clinical Genetics, University Hospital, Turku, Finland

¹⁵ Greenwood Genetic Center, Greenwood, SC, USA

¹⁶ Service de Génétique, Neurogénétique et Médecine Prédictive, Hôpital de la Croix Rousse, Lyon, France

¹⁷ Heartlands Hospital, Birmingham, UK

¹⁸ Pôle de psychiatrie et neurologie, CHU Grenoble, Grenoble, France

¹⁹ Sourasky Medical Center, Tel Aviv University, Tel-Aviv, Israel

²⁰ Service de Génétique Médicale, CHU de Strasbourg, Hôpital de Hautepierre, Strasbourg, France

²¹ Centre de référence de pathologie neuromusculaire Paris-Est, Groupe Hospitalier-Universitaire Pitié-Salpêtrière, Paris, France

²² National center of Expertise for Neuromuscular Disorders, University Hospital La Timone, APHM, Aix-Marseille University, Marseille, France

²³ Service de Génétique Clinique, CHRU de Lille, Hôpital Jeanne de Flandre, Lille, France

²⁴ Service de Génétique Clinique, CHU de Rennes, Hôpital Sud, Rennes, France

²⁵ Service anatomie et cytologie pathologique, Centre de compétence Breton des maladies neuromusculaires, CHRU Brest, Brest, France

²⁶ EA 4586 LNB, Université de Bretagne Occidentale, Brest, France

²⁷ Department of Pathology, Radboud University Medical Centre, Nijmegen, The Netherlands

²⁸ Hospices Civils de Lyon, Université Claude Bernard Lyon1, Institut NeuroMyogène, CNRS, UMR 5310, INSERM U1217, Lyon, France

²⁹ Neurologie, CHU de Strasbourg, Hôpital de Hautepierre, Strasbourg, France

³⁰ ICube, UMR7357, CSTB Complex Systems and Translational Bioinformatics, Faculté de Médecine, Strasbourg, France

³¹ Service cytogénétique constitutionnelle et prénatale, CHU de Strasbourg, Hôpital de Hautepierre, Strasbourg, France

³² Department of Medical Genetics, APHM, GMGF, Timone Hospital, Aix Marseille University, Marseille, France

³³ Department of Human Genetics, Radboud University Medical Centre, Nijmegen, The Netherlands

³⁴ Institut de Myologie, Laboratoire de résonance magnétique, Groupe Hospitalier-Universitaire Pitié-Salpêtrière, Paris, France

³⁵ Service de radiologie, Hôpital Raymond Poincaré, Garches, France

³⁶ CNRGH, Institut de Biologie François Jacobs, CEA, Evry, France

hypotonia, muscle weakness and respiratory insufficiency [19, 36, 45, 57, 62]. XLMTM is non-progressive and those affected males who survive several years may show additional non-muscle clinical features, the most common being liver peliosis [27, 30, 43, 59]. Atypical forms have been reported in some boys and adult men with a clinical classification based on respiratory and milestone features [30, 36, 42]. Mutations are found in all 15 exons of *MTM1* and encompass point mutations (missense, nonsense, splice site mutations), insertions, small and large deletions [10, 19, 31, 36, 37, 57, 62] and duplications [4, 45, 61]. The majority of mutations are clustered in exons 4, 8, 9, 11 and 12. Duplication has been described in some cases and a deletion of exon(s) or of the whole *MTM1* gene was reported in 7% of patients. Large deletions including part or the entire neighboring *MAMLD1* gene cause a contiguous gene syndrome with hypospadias and myotubular myopathy in males [6, 24, 32, 37].

Female carriers are usually asymptomatic but a total of 26 affected females aged 5–71 years have been reported presenting with severe neonatal form [33, 51] or moderate to mild forms [7, 18, 20, 22, 23, 25, 28, 46, 50, 55, 56]. Truncating mutations as well as missense mutations were observed scattered through the gene. Skewed X inactivation was reported in some as a potential explanation for their affected status compared to non-affected carriers, while others did not show skewing.

In this study, we reviewed the clinical, histological, imaging and molecular data from 43 affected females, including 17 new cases. We have identified consistent asymmetry in muscle involvement and have better defined the spectrum and progression of the disease, the frequency of clinical, investigation and histological findings, and discuss the clinical correlation with the type of mutation and X inactivation.

Patients and methods

Patient cohort

Data from the 43 females affected with XLMTM are summarized in Supplementary Tables 1–3. The 17 new unrelated females originated from Brazil, Finland, France, Israel, The Netherlands, UK and USA. Fifteen were from new families, while F8 is the sister of an affected male previously reported as patient HC19 [10] and patient F1 is the sister of an affected female previously reported as patient 1 by Bevilacqua and colleagues [7]. Clinical data were collected from the clinicians who referred patients for a genetic diagnosis (25 patients) or from the literature (18 patients).

Morphological studies

Muscle biopsies were performed on 14 out of the 17 new patients (Supplementary Table 1). Muscle sections were stained with hematoxylin–eosin (H&E), modified Gomori trichrome, periodic acid Schiff (PAS) and Sudan red and black. Histochemistry was performed using routine histochemical methods [21]. Ultrastructural study was carried out according to standardized protocols. Briefly, tissue samples were fixed in a 2% glutaraldehyde fixative solution, post-fixed with osmium tetroxide and embedded in resin epoxy. Semi-thin sections were stained with toluidine blue. Ultrathin sections were contrasted with uranyl acetate and lead citrate.

Molecular analysis

DNA from the 17 new patients and relatives was extracted from blood or muscle samples by standard methods.

Sequence analysis of the *MTM1* gene was performed by bi-directional sequencing of the 15 exons with flanking intronic sequences (primer sequences and PCR conditions are available on request). A search for copy number variations (deletion or duplication of exon or whole gene) was performed by MLPA analysis (multiplex ligation-dependent probe amplification) using the P309-A1-*MTM1* kit (MRC Holland) for patients F2, F3 and F4. Patient F11 was included in *MTM1* Sanger analysis due to the detection on Western blot [60] of a decreased level of myotubularin on protein extracts from lymphoblasts and muscle biopsies (manuscript in preparation). Patients F15 and F12 were diagnosed by exome sequencing in the scope of a French consortium research project (MYOCAPTURE). Exome analysis was performed using SureSelect Human all Exon 50 Mb capture library v4 (Agilent, Santa Clara, USA) and paired-end sequenced on Illumina HiSeq 2500 sequencer at the French National Center of Genotypage, Paris, France. Patient F17 was diagnosed by exome sequencing using SureSelectXT Human all Exon 50 Mb capture library (Agilent, Santa Clara, USA) on IlluminaHiSeq at BGI-EUROPE in Denmark. Patient F13 was diagnosed using a multi gene panel, MGZ laboratory, Munich, Germany. Patient F16 was diagnosed using targeted exons sequencing of a custom panel of 210 genes linked to neuromuscular diseases (SureSelect, Agilent, Santa Clara, CA) (MYOdiagHTS panel, Strasbourg, France, manuscript in preparation).

Affymetrix Cytogenetics Whole-Genome 2.7M Array was used to delineate deletion breakpoints for patient F3. DNA quantity was insufficient to perform this study for patients F2 and F4.

X-chromosome inactivation (XCI) analysis was performed using *HpaII* predigestion of DNA followed by PCR of the highly polymorphic CAG repeat of the *AR* gene

(HUMARA) [3] and the CGG repeat within the *FMR1* gene [13]. XCI with an allele ratio <80:20 was considered a random pattern, a ratio equal or greater than 80:20 was considered to be skewed and a ratio greater than 90:10 was considered to be highly skewed.

Results

Clinical, imaging, histological, ultrastructural and molecular data are summarized in Supplementary Tables 1–5 for the 43 females including 17 novel cases and 26 previously reported cases, resulting in the largest XLMTM female cohort characterized so far. The main clinical and histological findings representing the new cases are presented (Figs. 4, 5, 6, 7).

Females with XLMTM demonstrate an independently recognizable myopathy

To assess if females with XLMTM signs define a disease entity, we analyzed the familial history for XLMTM or undefined muscle disorder. The female patient was the first diagnosed case of XLMTM in 28 out of the 36 families, with 20 being sporadic cases. The diagnosis of XLMTM was previously established or suspected (based on clinical and histopathological data) in a male relative in only 8 of the 36 families (Fig. 1a; Supplementary Table 2). In four of the seven families including several affected females, there was no affected male (Fig. 1b; Supplementary Table 2). The mutation occurred de novo for the older affected females in 13 of the 19 families in which samples from parents were available for further analysis. Altogether, these findings indicate that females with XLMTM define a specific myopathy cohort, independently of the presence of male XLMTM.

Females with XLMTM are usually less severely affected than males, with overlapping clinical hallmarks

Most males with XLMTM are severely affected from birth with weakness and respiratory distress, needing respiratory and feeding support. To assess the distinctive features between male and female XLMTM, we analyzed the age of onset and severity in 43 females with XLMTM to compare with affected males.

The clinical phenotype is highly variable in age of onset and severity, in particular regarding weakness and respiratory muscle involvement (Fig. 2; Supplementary Table 3). The age of onset ranged from birth or fetal life to adulthood. Only eight of 42 females were reported to be hypotonic and have respiratory or feeding problem at birth. The pregnancy for two of these eight patients was associated with reduced fetal movements and/or polyhydramnios and was normal for two others (no data available for four patients). Most of the females affected from birth displayed generalized muscle weakness. For 30 out of 42 female patients, weakness was clinically manifest during childhood (2–14 years) with the first impairment being proximal in the lower limbs in 17 patients (delayed motor milestones, gait difficulties, difficulty with climbing stairs or raising from a squatting position) and in the upper limbs in five.

The most severely affected female in our cohort displayed similar clinical symptoms and course as an XLMTM male (F2). She was affected with severe neonatal form and died aged 18 months old. There was no family history of neuromuscular conditions. She was born eutrophic at 41 weeks of gestation, and Apgar scores were 9 and 10 at 1 and 5 min, respectively. Thirty minutes after birth, she presented with severe hypotonia and respiratory distress. Clinical examination revealed severe left facial weakness with left ptosis, stridor due to laryngomalacia and swallowing difficulties. At the age of 1.5 months, she demonstrated fluctuating and moderate axial hypotonia and a Moebius

Fig. 1 Family history of XLMTM in 36 families. **a** Families with previously diagnosed XLMTM. **b** Family history of muscular diseases

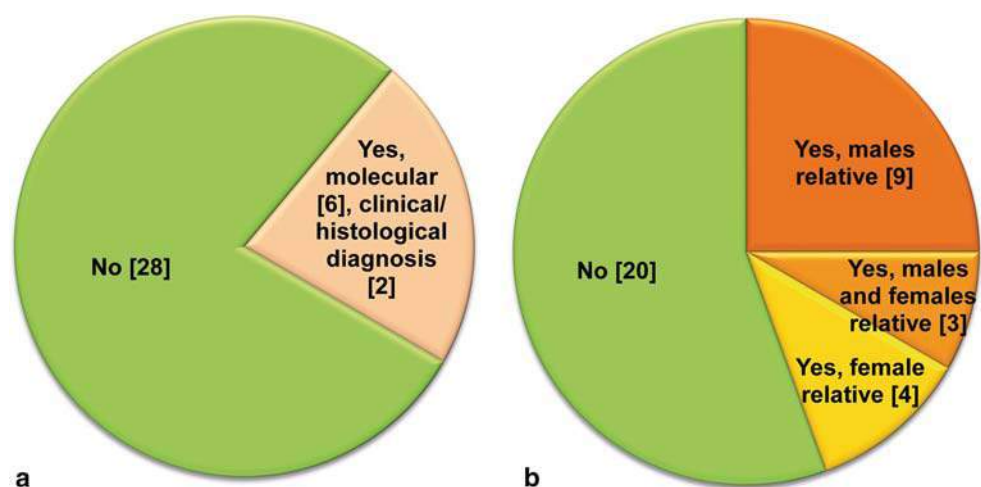
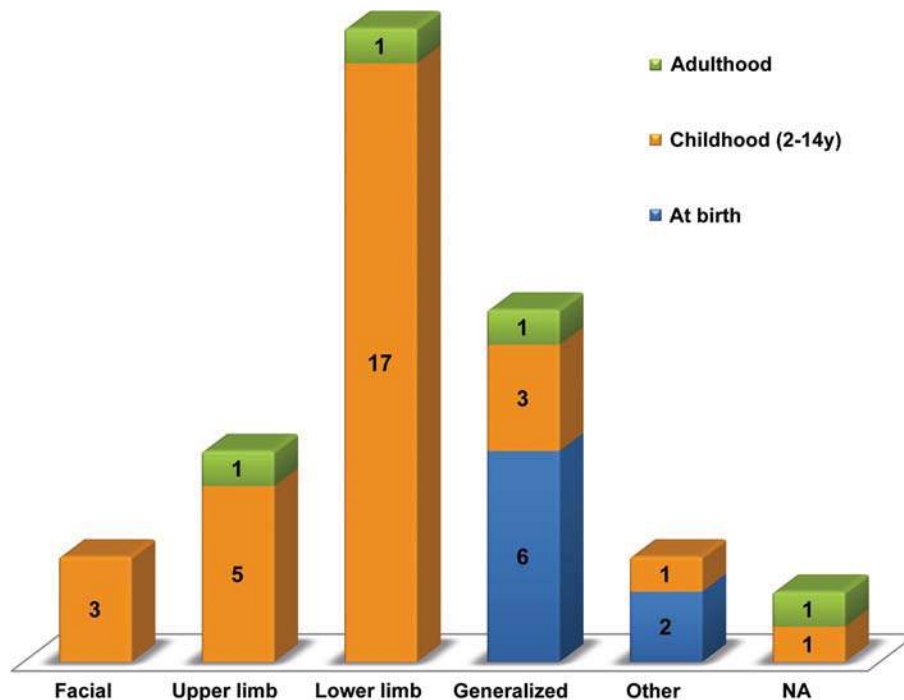


Fig. 2 Initial muscle impairment at the age of onset for 42 females with XLMTM. The initial muscle impairment reported for 42 patients (age of onset unknown for 1 patient) is presented depending on the age of onset: at birth, at childhood (2–14 years) or at adulthood. *Facial* face, ptosis; *upper limb* arm weakness; *lower limb* delayed motor milestones, gait difficulty, difficulty in climbing stairs or in standing from a squatting position; *generalized* hypotonia at birth \pm facial involvement; *Other* feeding difficulties; *NA* not available



syndrome diagnosis was initially considered. From the age of 2.5 months, she had recurrent episodes of respiratory distress and a congenital myasthenic syndrome was considered with the findings of axial hypotonia, absent deep tendon reflexes and worsening of the facial weakness. Quadriceps wasting was noted at age 15 months and a muscle biopsy was performed showing multiple anomalies (see below). The child was subsequently treated with anticholinesterase drugs (pyridostigmine) with a very transient improvement. She started walking with support at the age of 18 months, but died from an acute bronchopneumonia shortly after.

In all other cases, there was a slowly progressive course, with limb weakness being the major sign, sometimes predominating in the pelvic girdle and spreading to distal muscles. Several of the 43 patients showed significant difficulties in standing from a seated position and/or in climbing stairs and/or running. Eight patients were never able to walk ([18, 33], F2) or run ([23, 28, 50, 51], F16): seven had lost the ability to walk independently, with three patients needing a cane at ages 40, 50 and 77 years (F11 patient from [46], F10) and four needing a wheelchair at ages 13, 32, 53 and 66 years (F4, F3, F17, the mother in [29]). Pelvic floor weakness with urinary incontinence was reported in seven cases (at the ages of 6, 27, 35, 35, 52, 55 and 79 years, respectively). Neck flexor weakness was reported in 12 cases.

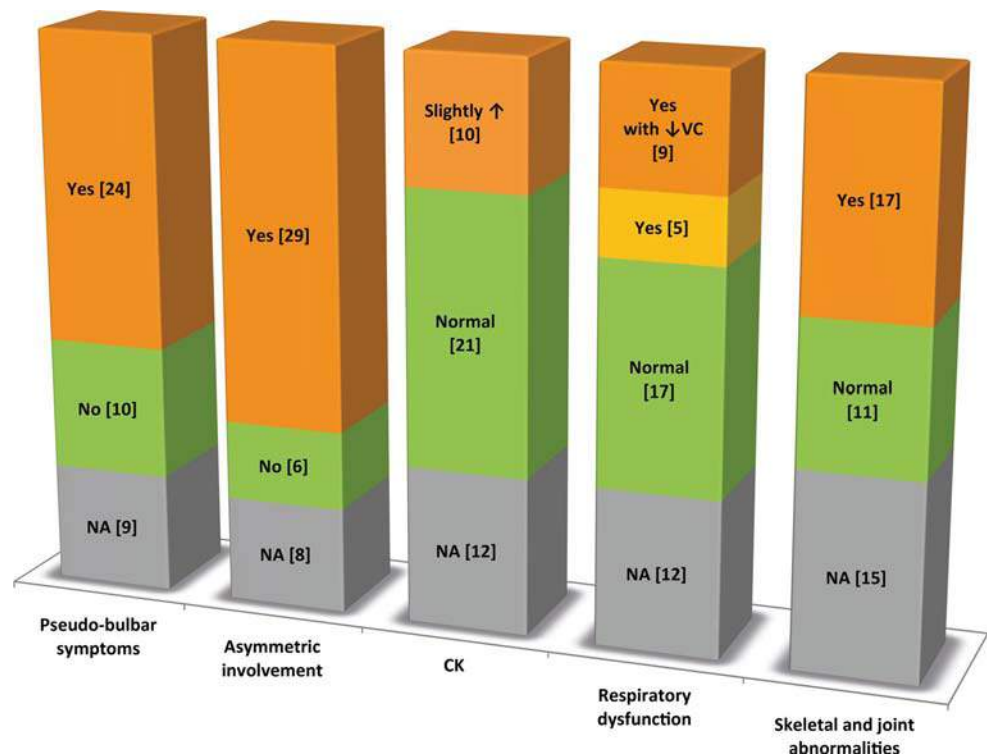
The frequency of additional clinical signs in this cohort of 43 females is summarized in Fig. 3. Bulbar or

pseudo bulbar symptoms were reported for 24 patients including facial weakness, limitation of extra-ocular movements, ophthalmoparesis, uni- or bilateral ptosis and dysarthria, whereas no such involvement was noted for ten patients. Respiratory muscle involvement was noted for 14 out of 33 patients, with a decrease in forced vital capacity in nine patients (at 37–83% of age and sex-matched predicted values). Severe restrictive respiratory dysfunctions with a hemidiaphragmatic paresis led to death of the oldest patient [46] at 84 years of age. Serum CK (creatin kinase) levels were normal in 21 patients and slightly elevated in 10 patients, supporting the finding that disease is not dystrophic. Skeletal and joint abnormalities were observed in 17 out of 28 cases, including kyphoscoliosis, scoliosis, joint hyperlaxity, joint contractures of the lower extremities, foot deformities and hand and/or facial contractures.

Five of the patients were reported to be overweight.

Overall, while a few females presented with similar onset to the male XLMTM (with fetal involvement and/or neonatal generalized weakness) with one case with an identical course (F2), the vast majority of females with XLMTM had later onset and were less severely affected than males with XLMTM. Affected females with XLMTM display similar facial signs as males with XLMTM, namely facial weakness, ophthalmoparesis and ptosis, and these appear to be important clues for diagnosis.

Fig. 3 Frequency of clinical and investigation signs in the cohort of 43 females with XLMTM. The numbers in *brackets* indicate the number of patients for each item. ↑ Elevated, ↓VC decreased vital capacity, CK creatine kinase, NA not available



Females with XLMTM frequently show a pattern of asymmetric involvement

At all ages, a consistent and striking feature was asymmetric symptoms, seen in 29 out of 35 patients. These included muscle weakness and wasting, especially of the arm, leg, and calf (Fig. 4). Hemidiaphragm elevation and asymmetric scapular winging were also noted.

There was also consistent asymmetry of facial involvement, notably asymmetric ptosis and facial weakness; examples are given for four patients of different ages in Fig. 4a–d. These asymmetries were mainly on a left–right axis.

Asymmetric involvement has been previously reported in several cases (Supplementary Table 1 and 3) and Drouet et al. reported two females with unilateral weakness [20]. In addition to asymmetric weakness, skeletal asymmetry was noted in some patients. For example, patient F5 has a right hand smaller than her left hand (Fig. 4d) and patient F13 has a lower limb length discrepancy. Grogan et al. reported females of two unrelated families with asymmetric weakness, hemidiaphragm elevation, and arms and fingers of different sizes when comparing the right and left sides [25].

Both our large cohort of novel cases and the descriptions of those in the literature highlight the frequency of asymmetric muscle involvement in females with XLMTM and suggest skeletal defects are a primary symptom of the disorder.

Imaging investigations highlight general and asymmetric muscle involvement

We next assessed whether imaging confirms the clinical symptoms, including asymmetry, and whether this yields additional diagnostic clues. Magnetic resonance imaging (MRI) findings for six newly described patients and nine previously reported patients [7, 20, 33, 46, 50, 51] are summarized in Supplementary Table 4 and representative images are depicted in Fig. 5 for several of the novel cases, including whole body MRI.

For patient F14, whole body MRI demonstrated asymmetric fatty involvement of the muscles, which predominates in the left side of the upper and lower limbs. In the lower limbs, the fatty involvement involves the anterior and posterior part of the legs: the soleus is near normal in the right side, whereas the left soleus muscle showed a moderate fatty infiltration (Fig. 5a). In the thigh and the pelvis, the asymmetric distribution of the fatty infiltrates is obvious, with gracilis, sartorius, biceps femoris, quadriceps and glutei muscles (minimus, medius and maximus) demonstrating almost complete fatty involvement (Fig. 5b, c). In the upper limbs, the fatty involvement predominates in the deltoid muscles, infra and supraspinatus and subscapularis muscles, with the left side showing the most evident fatty infiltration (Fig. 5e). Asymmetric fatty involvement is also noted in the neck extensors, while facial muscles are spared.

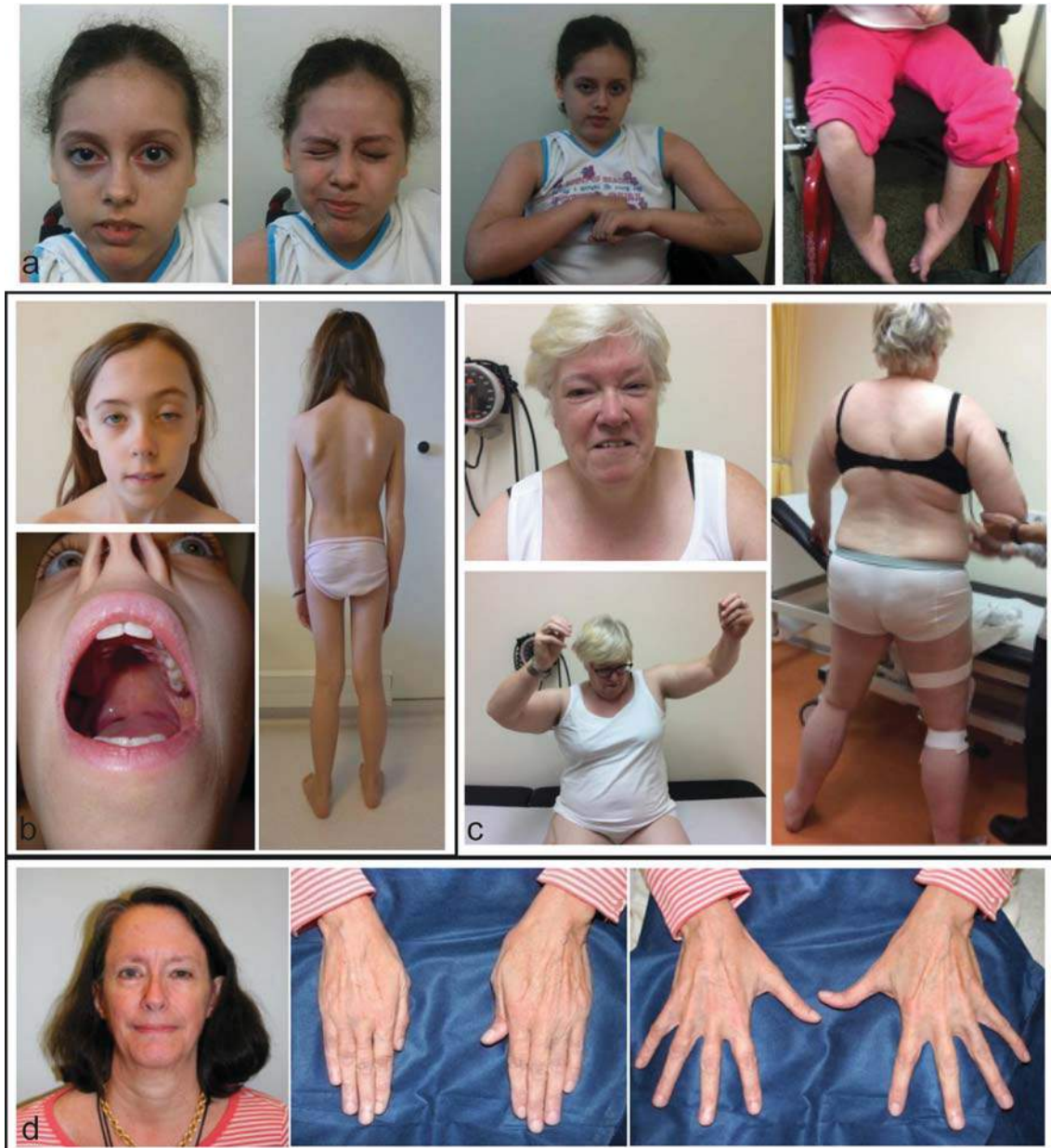


Fig. 4 Facial and general muscle weakness and asymmetric involvement. **a** Patient F4 presenting with facial asymmetry (*left weaker*), deficit in arm elevation and retractions. **b** Patient F16 presenting with left side ptosis, facial asymmetry, high arched palate, reduced mus-

cle bulk and scapula winging. **c** Patient F17 presenting with left side ptosis, deficit in arm elevation and needing support for standing. **d** Patient F5 presenting with mild left ptosis. *Right hand smaller than left hand*

Several of these features are found in other patients (Fig. 5 and Supplementary Table 4). For patient F17, there is severe atrophy and fatty infiltration of paraspinial, gluteal and psoas muscles and the upper leg muscles, while the lower leg muscles are less severely affected (Fig. 5g–n). The more proximal muscles (obturatorius, piriformis and transverse abdominal) are relatively spared. For patient F13, prominent fatty infiltration of the muscles of the lower limbs was noted, both at the

thighs and legs (Fig. 5o–q). All the muscles of the thighs were affected, but the right semimembranosus and the left vastus intermedius were slightly less affected. The anterior compartments of the legs were more affected, while the gastrocnemius and soleus were nearly spared. For patient F16, muscle involvement with clear asymmetry was noted mainly for the distal muscles, including involvement of the left tibialis anterior and the right peroneus (Fig. 5s–u). In the thighs, the anterior and posterior

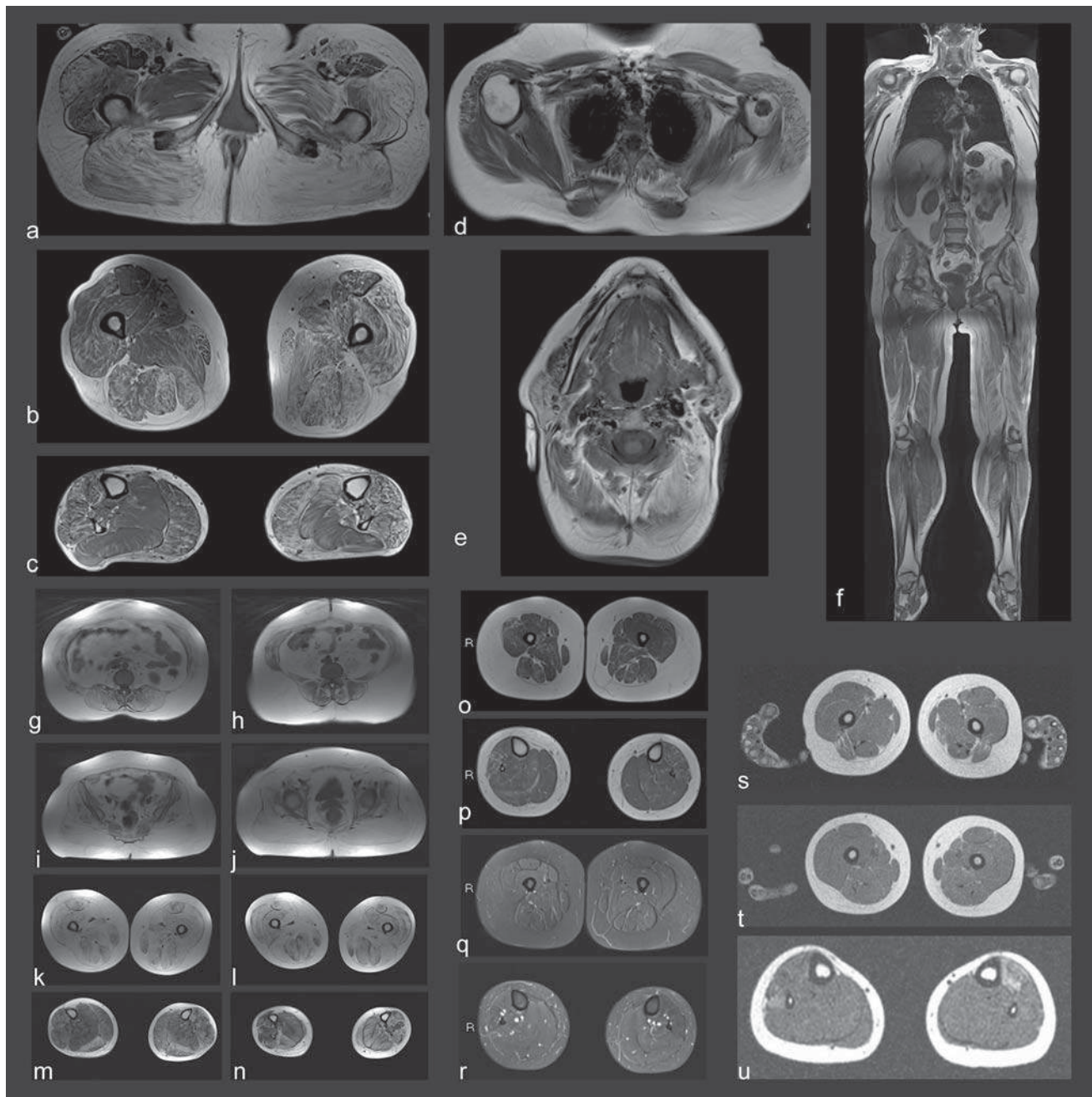


Fig. 5 Representative magnetic resonance imaging (MRI) in four patients. Whole body muscles magnetic resonance imaging (WB MRI). Patient F14: T1 axial sequences of the proximal lower limb (a), thigh (b), lower limb (c), proximal upper leg (d), neck (e) and

whole body muscles (f). Patient F17: T1 axial sequences (g, h), hip girdle (i, j), upper (k, l) and lower limb muscles (m, n). Patient F13: T1 axial and STIR sequences of the thigh (o, q) and leg (p, r). Patient F16: T1 axial sequences of the thigh (s, t) and calf (u)

muscles were affected, especially visible on the left in the vastus externus and adductor magnus.

Taking both the novel reported cases and previous reports (Supplementary Table 4), these data confirm a general involvement of muscles and often highlight an asymmetric pattern correlating with the asymmetric muscle weakness observed on clinical assessment.

Histological and ultrastructural features are similar in males and females with XLMTM

Biopsies were available for 38 patients, including one that was not interpretable due to massive fatty replacement. Variation in myofiber diameter with atrophic round fibers was reported in 25 cases, type 1 fiber predominance in 17

cases, and endomysial fibrosis and/or fatty replacement in 20 cases (Fig. 6; Supplementary Table 1 and 5). There was no fiber necrosis or inflammatory change. Abnormally positioned nuclei varied from a few scattered to numerous non-peripheral nuclei in all interpretable biopsies. Six biopsies were described with internalized nuclei, 19 biopsies with central nuclei, and 12 biopsies had both. Necklace

fibers and radial sarcoplasmic strands (RSS), as previously reported in adult XLMTM patients and also in patients with DNM2-related dominant centronuclear myopathy, were described in 11 and 3 out of the biopsies, respectively. Necklace fibers display a basophilic ring underneath the sarcolemma that is strongly reactive with PAS and oxidative reactions.

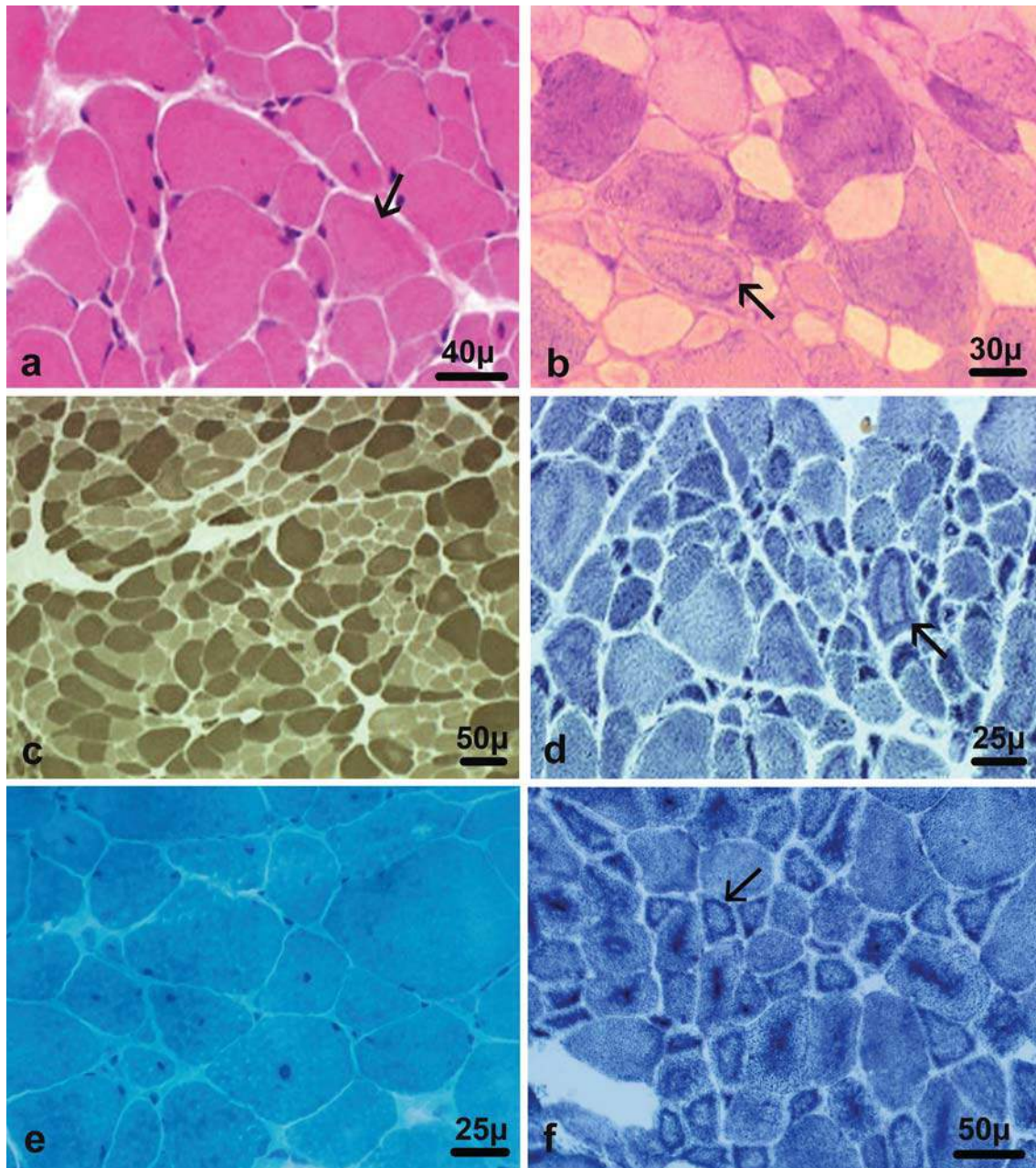


Fig. 6 Histological features in females with XLMTM. Muscle biopsies from patient F2 (a–d) and F4 (e, f). **a** A necklace fiber displaying a basophilic ring located underneath the sarcolemma (arrow) (hematoxylin and eosin staining). **b** A necklace fiber strongly reacting with PAS (arrow). **c** Type I predominance with small type I (light) and II (dark) fibers (myosin adenine triphosphatase preincubated at

pH 9.4 technique). **d** A necklace fiber strongly reactive for oxidative reactions (arrow) (nicotinamide adenine dinucleotide-tetrazolium reductase technique). **e** Numerous centralized nuclei and fiber size heterogeneity (Gomori trichrome stain). **f** Necklace fibers strongly reactive for oxidative reactions (arrow) (nicotinamide adenine dinucleotide-tetrazolium reductase technique)

At the ultrastructural level, internal nuclei may display an altered shape (Fig. 7). There were a range of signs of myofibrillar disruption from focal loss of myofibrils to fibers with complete disorganization of the myofibrillar network. Z disk streaming was also common. Necklaces form

a clear ring devoid of organelles under the sarcolemma and are associated with an oblique orientation of the myofibrils.

Overall, the histopathology and ultrastructural defects in females with XLMTM appear very similar to those seen in males with XLMTM, albeit necklace fibers are

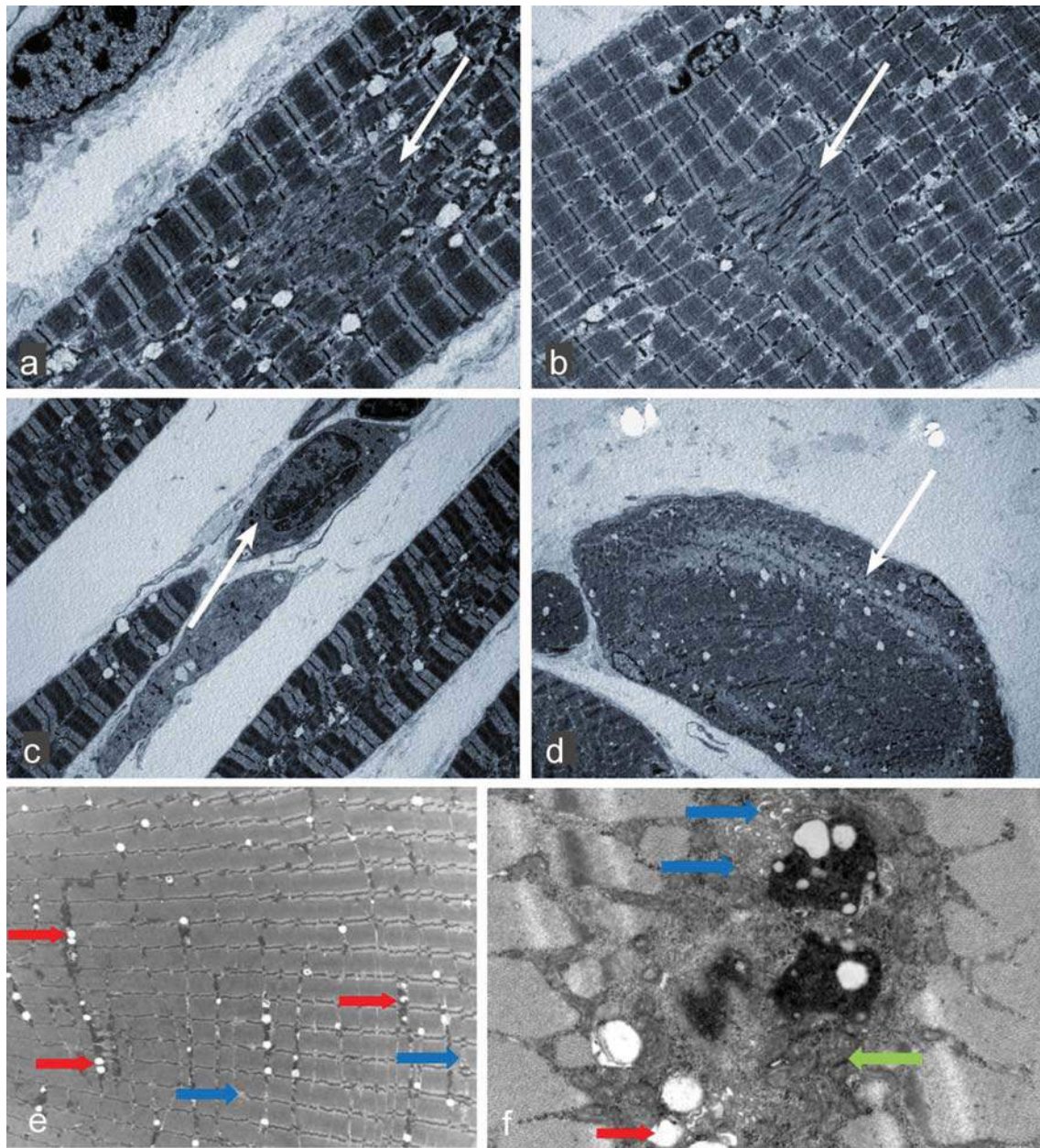


Fig. 7 Ultrastructural defects in females with XLMTM. Electron microscopy for muscles from patient F2 (a–d) and F11 (e–g). **a** Focal loss of myofibrils in a small muscle fiber (*arrow*) (OM $\times 5000$). **b** Z disk streaming running over two sarcomeres (*arrow*) (OM $\times 6000$). **c** Internalized nuclei in an atrophic fiber with a complete disorganization of the myofibrillar network (*arrow*) (OM $\times 4000$). **d** Ultrastruc-

tural pattern of a necklace, forming a clear ring devoid of organelles under the sarcolemma, with an oblique arrangement of the myofibrils (*arrow*) (OM $\times 4000$), **e**, **f** Muscle fibers showing internalized nuclei, cisternae (*blue arrow*), vacuoles (*red arrow*) and material accumulation (*green arrow*)

mainly found in adult patients and are less observed in neonatal affected males.

Most *MTM1* mutations in females were associated with a severe phenotype in males

Females with XLMTM are usually more mildly affected than males. We explored if there was a correlation between the type of mutation and the phenotypic severity. First, we analyzed the *MTM1* gene through approaches including Sanger sequencing, targeted and exome sequencing, MLPA and DNA microarray to delineate the genetic defects. Analysis of *MTM1* revealed four new heterozygous mutations in the 17 new female patients reported: an in-frame deletion encompassing exons 9 and 10, the intronic mutation c.1644+1G>A predicted to disrupt the donor splice site of exon 14 and two stop gain c.548G>A (p.Trp183*) and c.1601G>A (p.Trp534*) (Supplementary Table 1). Patients F3, F4 and F17 were heterozygous carriers of a large deletion of the whole *MTM1* gene and the neighboring *MTMR1* gene. For patient F3, comparative genomic hybridization (CGH) study delineated the deletion with a minimum size of 595,302 bp (from genomic position chrX: 150,443,004–151,038,095; hg38) and a maximum size of 597,756 bp (from genomic position chrX: 150,442,220–151,039,765;hg38) encompassing *MAMLD1*, *MTM1*, *MTMR1*, *CD99L2* and *HMGB3* genes. For patient F17, exome analysis delineated a 474,391 bp deletion (from genomic position chrX: 150,512,003–150,986,191; hg38) encompassing *MTMR1* and *CD99L2*, as well as part of *MAMLD1* and *HMGB3*.

Genotype–phenotype correlation in males has established that some mutations are more likely to be associated with a mild or moderate phenotype, probably being compatible with a residual normal function of the mutated myotubularin. Conversely, severely affected males tend to have an undetectable or a marked reduction in the protein level [39]. Twenty of the 29 mutations present in this cohort of 43 affected females have previously been found in male patients, with 16 being reported in association with a severe form of the disease, 3 predominantly with a severe form but occasionally with a mild/moderate form (c.109C>T, c.614C>T, c.1262G>A), and 1 (c.1354-1G>A) described once in a moderate case [30] and also found once in a severe case (Biancalana, unpublished observation). Among the ten mutations described only in females, nine are in-frame or out-of-frame deletions, truncations or splicing mutations predicted to be associated with a severe phenotype in males, and one is a missense mutation (c.1115T>A) which has been shown to lead to a reduced protein level. Thus, females with XLMTM in this cohort do not have specific *MTM1* mutations compared with males, but rather

harbor mutations usually associated with a severe phenotype in males with XLMTM, while these females display a milder phenotype.

Enhancement of skewed X chromosome inactivation in females with XLMTM

The difference in severity between males with XLMTM and females is not explained by the type of mutation. In a female heterozygous for an X-linked recessive mutation, half of the cells on average should have a normal level of the gene product, while the other half would express the mutated allele. However, skeletal muscle fibers are syncytia formed from the fusion of different myoblasts. It was shown at least in mice that different nuclei from single myofibers have random X-chromosome inactivation (XCI), predicting that each fiber would have about 50% expression level [66]. A skewed X-inactivation pattern favoring the mutated X chromosome has been hypothesized to be a determinant of the variability of the phenotype observed in females with XLMTM, but several reports did not confirm a skewed XCI in affected females (Supplementary Table 1). To better evaluate XCI as a determinant of the phenotype severity in females, we compared the disease onset versus the XCI pattern (random, skewed and highly skewed; see “Patients and methods”). Unfortunately, the test could not determine which X chromosome was preferentially active. XCI studies were informative in 32 out of 43 patients. Evidence of skewed XCI (80:20–90:10) or highly skewed XCI ($\geq 90:10$) was identified in 15.6 and 18.75% of patients aged <55 years, respectively, whereas in the general adult population the ratio was around 14 and 4%, respectively [5]. This enhancement in XCI among females with XLMTM is significant for the highly skewed group ($p < 0.025$) and is even more significant when considering that for the six patients with highly skewed XCI, the ratio was in fact >95:5 (found in only 1.7% of the normal population). In conclusion, there is an increased prevalence of highly skewed X inactivation in the cohort of females affected by XLMTM.

Discussion

We have described or reviewed the clinical, morphological and molecular data obtained from 43 X-linked myotubular myopathy female carriers from 36 unrelated families. To date, only 26 manifesting female carrier cases have been reported in the literature. Analyzing our data on 17 new affected females and those previously reported (see Supplementary Table 1), we were able to establish several specific observations. Females with XLMTM often present with a myopathy, independently of the presence of affected males

in the family. This myopathy can be highly heterogeneous in terms of onset and severity and shares several clinical features with male XLMTM including similar facial involvement. However, females with XLMTM frequently display asymmetric involvement and specific histological features develop with age, as necklace fibers. While they usually have a milder phenotype than males with XLMTM, females share *MTM1* mutations associated with severe cases in males, potentially due to the fact that they can express a normal allele from the non-mutated X chromosome.

Assessing the full clinical spectrum and frequency of females with XLMTM

XLMTM female carriers were previously considered to be usually non-affected or mildly affected. However, including the novel cases characterized in this study, 43 females from 36 unrelated families were reported to show signs of muscle involvement, with several presenting with muscle, respiratory or skeletal involvement significantly impacting on their daily life. Nevertheless, this cohort is not likely to represent accurately the spectrum of involvement, as several recruitment biases may exist. Females with XLMTM may be recognized either because they are severely affected (they are the proband) or are mildly affected and evaluated following the identification of males with XLMTM in the family. Those females from the 12 “female families” include some who are mildly affected, suggesting that an unknown proportion of females with XLMTM may have never come to clinical attention without a prior XLMTM diagnosis in their relatives (i.e., patient F1). It is also likely that some XLMTM manifesting females are not diagnosed because the *MTM1* gene is not suspected as the cause of their symptoms, particularly in the absence of suggestive histology. The proportion of reported manifestation of females with XLMTM compared with all diagnosed patients is around 6%, but this figure is not homogeneous across countries. For example, this proportion is increased in France with around 13% of XLMTM French patients being female (19 females of the present cohort). This variation suggests that there is likely to be a lack of consideration of the diagnosis in females and strongly suggests that the frequency of females with XLMTM is underestimated. Thorough characterization and comparison of females with XLMTM in large cohorts, as attempted in this report, should increase awareness and provide diagnostic clues to better recognize this myopathy.

Clinical spectrum and asymmetric involvement in females with XLMTM

Females with XLMTM present usually with a progressive pattern of limb-girdle myopathy, possibly associated with

respiratory muscle and/or skeletal involvement. The impairment may be as severe as in a severe male neonatal form which may be responsible for death within the first months, as observed in patient F2, ranging to a milder form occurring mostly during childhood but impacting daily life significantly. Many carriers were considered as non-affected in childhood, but were never athletic at school. Females with XLMTM display similar facial features as affected males, with facial weakness, ophthalmoplegia and ptosis being important diagnostic clues. The predominant proximal and lower leg involvement pattern observed on MRI or CT scan for most of the 15 female patients reviewed in this study is similar to the only two observations reported for affected males [7, 47].

In this analysis of a large patient cohort, we found recurrent asymmetric involvement that is also underlined in MRI analyses. This asymmetry may involve limb and facial muscle weakness and also skeletal development in several cases (this study, [20, 25]). We and others found a strong bias in the XCI in affected females, but this was not always consistent with the severity of the symptoms. Such an asymmetric weakness in manifesting carrier females is indeed described in other X-linked diseases such as Duchenne muscular dystrophy [54, 58], suggesting that a distinct X-chromosome inactivation ratio in different muscles could be responsible for this asymmetry, leading to greater expression of the mutated gene on one side of the body. It was not possible to directly investigate several muscles from the same patient for XCI, but such a study would help delineate a correlation with asymmetric features. Similarly, the skeletal asymmetry may be caused by differential expression of normal *MTM1* in the body, as *MTM1* is suspected to be linked to skeletal growth, given that males with XLMTM deficient in myotubularin often show features of overgrowth at birth. However, a mildly affected XLMTM male presenting with muscle asymmetry has been described [7] and this clearly could not be linked to XCI. Further observations are needed to establish the prevalence of asymmetry in males.

In females, asymmetric involvement detected through clinical and/or imaging investigations is another diagnostic clue to suggest undertaking *MTM1* genetic testing.

Muscle biopsy features which may be an indication for *MTM1* sequencing and XLMTM diagnosis

Muscle biopsy is routinely used to direct the molecular diagnosis of congenital myopathies. In females with XLMTM, abnormal nuclei internalization and centralization is similar to that observed in males with XLMTM. Necklace fibers were observed in nearly one-third (11 out of 37) of females with XLMTM for whom muscle biopsies were interpretable, confirming this is a prevalent histological marker in milder XLMTM, particularly in manifesting carriers [7],

although they can also be present in severe cases as in patient F2 [1, 26]. However, this marker is not exclusive for XLMTM, being described in other forms of centronuclear myopathy due to mutations in *DNM2* [14, 41].

Fatty replacement and/or fibrosis, as described in males with XLMTM, was also observed in 20 out of 38 biopsies. Such a gradual replacement of contractile tissue with non-contractile connective tissue or fat is described in congenital myopathies, in particular in severe, advanced or chronic cases. The fibrosis in XLMTM may be the result of a replacement of fibers which disappear and are not regenerated due to a defect in the number of satellite cells in the muscle of the patients [52].

Overall, the presence of centralized nuclei and/or necklace fibers is a strong diagnostic clue for XLMTM in females. Nevertheless, several females with XLMTM have non-informative muscle biopsies that show dystrophic features.

The genotype is a suggestive, but not a reliable predictor of clinical prognosis for females with XLMTM

Nearly all *MTM1* mutations detected in females with XLMTM are described in or predicted to be associated with a severe phenotype in males. It is possible that mutations associated with a mild or moderate phenotype in males are not associated with a phenotype in females due to the *MTM1* expression from the non-mutated X chromosome, but a clinical evaluation of females carrying such mutations is needed to assert this hypothesis.

A non-random XCI pattern has been proposed as an explanation for the development of symptoms in manifesting carriers without chromosomal translocations [63]. The skewed X inactivation observed in muscle for patient F2 correlated with previous reports showing a similar bias in females with a severe phenotype [33, 34]. We found here an increased prevalence of highly skewed XCI in the females with XLMTM, but there is no clear correlation between the XCI ratio and the phenotype. Thus, XCI cannot be a reliable molecular diagnostic test for clinical prognosis. Several factors prevent us from drawing correlations from XCI studies including the small number of described manifesting females, the difficulty in defining a classification of the phenotypic severity, the difficulty of defining which chromosome is predominantly active, the fact that XCI varies with age and that the XCI ratio can differ between tissues and hence the results from lymphocytes may not reflect the status in muscle. Moreover, XCI studies have not been performed in asymptomatic *MTM1* carrier females to assess potential correlation with disease severity. Thus, while skewed XCI is noted in several females with XLMTM, it

does not correlate with disease severity but is potentially the molecular basis of the asymmetric muscle involvement.

Benefits of XLMTM diagnosis in affected females

Identifying the genetic cause of the disease allows appropriate care and management. A female affected with XLMTM benefits from specific care, in particular respiratory monitoring and close follow-up during and after pregnancy (F11 and F14 were reported to worsen after a pregnancy). A study of respiratory muscle function in a cohort of ten surviving males with XLMTM has shown that the respiratory muscle function declines over time [53], suggesting that females are at risk of a gradual deterioration of respiratory function.

Genetic counseling would inform affected women of the risk of occurrence of a severely affected male and the possibility of prenatal diagnosis. When a de novo mutation arises in a female child, with no evidence of parental origin, both parents should be made aware of the risk of recurrence due to possible germinal mosaicism [64].

Females with XLMTM survive longer than most male patients. A study of affected females may thus yield crucial information on the minimal dosage of myotubularin needed to minimize symptoms and also guide future therapeutic development by documenting disease evolution and complications as targets for management. Moreover, several therapeutic proof of concepts recently reported in animal models may represent potential therapies for females with XLMTM [16, 17, 35, 40, 49].

Conclusion

The diagnosis of XLMTM should be suspected in a female presenting with a myopathy, despite the absence of a family history and/or the presence in a muscle biopsy of some dystrophic features, particularly if facial weakness and asymmetric involvement are noted. The diagnosis of XLMTM affected females is likely to increase with the increasing use of massively parallel sequencing in a diagnostic setting ([50], this study). The occurrence of large heterozygous deletions in 4 of the 17 newly described patients underlines the importance of searching for copy number variations in the *MTM1* gene [9]. Systematic long-term clinical assessment of heterozygous female relatives of any XLMTM male would allow a better ascertainment of the clinical spectrum and frequency of involvement in XLMTM carrier females. As more than 500 males have been reported to date in the literature, around 425 of their mothers were heterozygous carriers (85% of mother of affected males are carriers) as well as their other female relatives.

Acknowledgements We thank the patients and their families. Because facial features are part of the clinical picture, patients have kindly consented to the use of their clinical photographs without masking their faces. MRI images of patients F13 and F16 were kindly provided, respectively, by Dr Milja Holstila, Finland, and Dr Florence Caillon, France, and muscle biopsy from patient F3 was managed by Cardiobiotec Biobanck, Lyon, France. We thank Claire FEGER and Nadine KEMPF for technical assistance. This work was supported by the Institut National de la Santé et de la Recherche Médicale (INSERM), Centre National de la Recherche Scientifique (CNRS), University of Strasbourg, the France Génomique National infrastructure, funded as part of the Investissements d’Avenir program managed by the Agence Nationale pour la Recherche (ANR-10-INBS-09), and Fondation Maladies Rares within the frame of the “Myocapture” sequencing project, ANR-10-LABX-0030-INRT under the frame program Investissements d’Avenir ANR-10-IDEX-0002-02, Fondation pour la Recherche Médicale (DBI20131228569) and AFM (AFM-16992) and CREGEMES for the MYOdiagHTS Project.

Authors’ contributions VB and JL directed the study; VB, SS and MM performed the study; VB analyzed the data; all the others authors contributed materials; VB and JL wrote the manuscript.

Compliance with ethical standards

Conflict of interest The authors have no conflicts of interest.

Statement of human rights All procedures performed in studies involving human participants were in accordance with the ethical standards of the institutional and/or national research committee and with the 1964 Helsinki Declaration and its later amendments or comparable ethical standards.

Informed consent Informed consent was obtained from all individual participants included in the study. Additional informed consent was obtained from patients F4, F5, F16 and F17 for whom identifying photographic information is included in this article.

References

1. Abath Neto O, Silva MR, Martins CA, Oliveira AS, Reed UC, Biancalana V, Pesquero JB, Laporte J, Zanoteli E (2016) A study of a cohort of X-linked myotubular myopathy at the clinical, histologic, and genetic levels. *Pediatr Neurol* 58:107–112
2. Agrawal PB, Pierson CR, Joshi M, Liu X, Ravenscroft G, Moghadaszadeh B, Talabere T, Viola M, Swanson LC, Haliloglu G et al (2014) SPEG interacts with myotubularin, and its deficiency causes centronuclear myopathy with dilated cardiomyopathy. *Am J Hum Genet* 95:218–226
3. Allen RC, Zoghbi HY, Moseley AB, Rosenblatt HM, Belmont JW (1992) Methylation of HpaII and HhaI sites near the polymorphic CAG repeat in the human androgen-receptor gene correlates with X chromosome inactivation. *Am J Hum Genet* 51:1229–1239
4. Amburgey K, Lawlor MW, Del Gaudio D, Cheng YW, Fitzpatrick C, Minor A, Li X, Aughton D, Das S, Beggs AH et al (2013) Large duplication in MTM1 associated with myotubular myopathy. *Neuromuscul Disord* 23:214–218
5. Amos-Landgraf JM, Cottle A, Plenge RM, Friez M, Schwartz CE, Longshore J, Willard HF (2006) X chromosome-inactivation patterns of 1,005 phenotypically unaffected females. *Am J Hum Genet* 79:493–499
6. Bartsch O, Kress W, Wagner A, Seemanova E (1999) The novel contiguous gene syndrome of myotubular myopathy (MTM1), male hypogonadism and deletion in Xq28: report of the first familial case. *Cytogenet Cell Genet* 85:310–314
7. Bevilacqua JA, Bitoun M, Biancalana V, Oldfors A, Stoltenburg G, Claeys KG, Lacene E, Brochier G, Manere L, Laforet P et al (2009) “Necklace” fibers, a new histological marker of late-onset MTM1-related centronuclear myopathy. *Acta Neuropathol* 117:283–291
8. Bevilacqua JA, Monnier N, Bitoun M, Eymard B, Ferreira A, Monges S, Lubieniecki F, Taratuto AL, Laquerriere A, Claeys KG et al (2011) Recessive RYR1 mutations cause unusual congenital myopathy with prominent nuclear internalization and large areas of myofibrillar disorganization. *Neuropathol Appl Neurobiol* 37:271–284
9. Biancalana V, Beggs AH, Das S, Jungbluth H, Kress W, Nishino I, North K, Romero NB, Laporte J (2012) Clinical utility gene card for: centronuclear and myotubular myopathies. *Eur J Hum Genet*. doi:10.1038/ejhg.2012.91
10. Biancalana V, Caron O, Gallati S, Baas F, Kress W, Novelli G, D’Apice MR, Lagier-Tourenne C, Buj-Bello A, Romero NB et al (2003) Characterisation of mutations in 77 patients with X-linked myotubular myopathy, including a family with a very mild phenotype. *Hum Genet* 112:135–142
11. Bitoun M, Maugendre S, Jeannet PY, Lacene E, Ferrer X, Laforet P, Martin JJ, Laporte J, Lochmuller H, Beggs AH et al (2005) Mutations in dynamin 2 cause dominant centronuclear myopathy. *Nat Genet* 37:1207–1209
12. Bohm J, Biancalana V, Malfatti E, Dondaine N, Koch C, Vasli N, Kress W, Strittmatter M, Taratuto AL, Gonorazky H et al (2014) Adult-onset autosomal dominant centronuclear myopathy due to BIN1 mutations. *Brain* 137(12):3160–3170
13. Carrel L, Willard HF (1996) An assay for X inactivation based on differential methylation at the fragile X locus, FMR1. *Am J Med Genet* 64:27–30
14. Casar-Borota O, Jacobsson J, Libelius R, Oldfors CH, Malfatti E, Romero NB, Oldfors A (2015) A novel dynamin-2 gene mutation associated with a late-onset centronuclear myopathy with necklace fibres. *Neuromuscul Disord* 25:345–348
15. Ceyhan-Birsoy O, Agrawal PB, Hidalgo C, Schmitz-Abe K, DeChene ET, Swanson LC, Soemedi R, Vasli N, Iannaccone ST, Shieh PB et al (2013) Recessive truncating titin gene, TTN, mutations presenting as centronuclear myopathy. *Neurology* 81:1205–1214
16. Childers MK, Joubert R, Poulard K, Moal C, Grange RW, Doering JA, Lawlor MW, Rider BE, Jamet T, Daniele N et al (2014) Gene therapy prolongs survival and restores function in murine and canine models of myotubular myopathy. *Sci Transl Med*. doi:10.1126/scitranslmed.3007523
17. Cowling BS, Chevremont T, Prokic I, Kretz C, Ferry A, Coirault C, Koutsopoulos O, Laugel V, Romero NB, Laporte J (2014) Reducing dynamin 2 expression rescues X-linked centronuclear myopathy. *J Clin Invest* 124:1350–1363
18. Dahl N, Hu LJ, Chery M, Fardeau M, Gilgenkrantz S, Nivelon-Chevallier A, Sidaner-Noisette I, Mugneret F, Gouyon JB, Gal A et al (1995) Myotubular myopathy in a girl with a deletion at Xq27–q28 and unbalanced X inactivation assigns the MTM1 gene to a 600-kb region. *Am J Hum Genet* 56:1108–1115
19. de Gouyon BM, Zhao W, Laporte J, Mandel JL, Metznerberg A, Herman GE (1997) Characterization of mutations in the myotubularin gene in twenty six patients with X-linked myotubular myopathy. *Hum Mol Genet* 6:1499–1504
20. Drouet A, Ollagnon-Roman E, Streichenberger N, Biancalana V, Cossee M, Guilloton L, Petiot P (2008) Unilateral presentation of X-linked myotubular myopathy (XLMTM) in two out

- of three female carriers in a family with no affected male. *Rev Neurol (Paris)* 164:169–176
21. Dubowitz V, Sewry CA, Oldfors A (2013) *Muscle biopsy: a practical approach*, 4th edn. Saunders Elsevier, London
 22. Fattori F, Maggi L, Bruno C, Cassandrini D, Codemo V, Catteruccia M, Tasca G, Berardinelli A, Magri F, Pane M et al (2015) Centronuclear myopathies: genotype-phenotype correlation and frequency of defined genetic forms in an Italian cohort. *J Neurol* 262:1728–1740
 23. Flex E, De Luca A, D'Apice MR, Buccino A, Dallapiccola B, Novelli G (2002) Rapid scanning of myotubularin (MTM1) gene by denaturing high-performance liquid chromatography (DHPLC). *Neuromuscul Disord* 12:501–505
 24. Fukami M, Wada Y, Miyabayashi K, Nishino I, Hasegawa T, Nordenskjöld A, Camerino G, Kretz C, Buj-Bello A, Laporte J et al (2006) CXorf6 is a causative gene for hypospadias. *Nat Genet* 38:1369–1371
 25. Grogan PM, Tanner SM, Orstavik KH, Knudsen GP, Saperstein DS, Vogel H, Barohn RJ, Herbelin LL, McVey AL, Katz JS (2005) Myopathy with skeletal asymmetry and hemidiaphragm elevation is caused by myotubularin mutations. *Neurology* 64:1638–1640
 26. Gurgel-Giannetti J, Zanoteli E, de Castro Concentino EL, Abath Neto O, Pesquero JB, Reed UC, Vainzof M (2012) Necklace fibers as histopathological marker in a patient with severe form of X-linked myotubular myopathy. *Neuromuscul Disord* 22:541–545
 27. Hagiwara SI, Kubota M, Sakaguchi K, Hiwatari E, Kishimoto H, Kagimoto S (2013) Fatal hepatic hemorrhage from peliosis hepatitis with X-linked myotubular myopathy: a case report. *J Pediatr Gastroenterol Nutr* 60(5):e45–e46
 28. Hammans SR, Robinson DO, Moutou C, Kennedy CR, Dennis NR, Hughes PJ, Ellison DW (2000) A clinical and genetic study of a manifesting heterozygote with X-linked myotubular myopathy. *Neuromuscul Disord* 10:133–137
 29. Hedberg C, Lindberg C, Mathe G, Moslemi AR, Oldfors A (2011) Myopathy in a woman and her daughter associated with a novel splice site MTM1 mutation. *Neuromuscul Disord* 22:244–251
 30. Herman GE, Finegold M, Zhao W, de Gouyon B, Metzenberg A (1999) Medical complications in long-term survivors with X-linked myotubular myopathy. *J Pediatr* 134:206–214
 31. Herman GE, Kopacz K, Zhao W, Mills PL, Metzenberg A, Das S (2002) Characterization of mutations in fifty North American patients with X-linked myotubular myopathy. *Hum Mutat* 19:114–121
 32. Hu LJ, Laporte J, Kress W, Kioschis P, Siebenhaar R, Poustka A, Fardeau M, Metzenberg A, Janssen EA, Thomas N et al (1996) Deletions in Xq28 in two boys with myotubular myopathy and abnormal genital development define a new contiguous gene syndrome in a 430 kb region. *Hum Mol Genet* 5:139–143
 33. Jungbluth H, Sewry CA, Buj-Bello A, Kristiansen M, Orstavik KH, Kelsey A, Manzur AY, Mercuri E, Wallgren-Pettersson C, Muntoni F (2003) Early and severe presentation of X-linked myotubular myopathy in a girl with skewed X-inactivation. *Neuromuscul Disord* 13:55–59
 34. Kristiansen M, Knudsen GP, Tanner SM, McEntagart M, Jungbluth H, Muntoni F, Sewry C, Gallati S, Orstavik KH, Wallgren-Pettersson C (2003) X-inactivation patterns in carriers of X-linked myotubular myopathy. *Neuromuscul Disord* 13:468–471
 35. Kutchukian C, Lo Scudato M, Tourneur Y, Poulard K, Vignaud A, Berthier C, Allard B, Lawlor MW, Buj-Bello A, Jacquemond V (2016) Phosphatidylinositol 3-kinase inhibition restores Ca²⁺ release defects and prolongs survival in myotubularin-deficient mice. *Proc Natl Acad Sci USA* 113:14432–14437
 36. Laporte J, Biancalana V, Tanner SM, Kress W, Schneider V, Wallgren-Pettersson C, Herger F, Buj-Bello A, Blondeau F, Liechti-Gallati S et al (2000) MTM1 mutations in X-linked myotubular myopathy. *Hum Mutat* 15:393–409
 37. Laporte J, Guiraud-Chaumeil C, Vincent MC, Mandel JL, Tanner SM, Liechti-Gallati S, Wallgren-Pettersson C, Dahl N, Kress W, Bolhuis PA et al (1997) Mutations in the MTM1 gene implicated in X-linked myotubular myopathy. ENMC International Consortium on Myotubular Myopathy. European Neuro-Muscular Center. *Hum Mol Genet* 6:1505–1511
 38. Laporte J, Hu LJ, Kretz C, Mandel JL, Kioschis P, Coy JF, Klauck SM, Poustka A, Dahl N (1996) A gene mutated in X-linked myotubular myopathy defines a new putative tyrosine phosphatase family conserved in yeast. *Nat Genet* 13:175–182
 39. Laporte J, Kress W, Mandel JL (2001) Diagnosis of X-linked myotubular myopathy by detection of myotubularin. *Ann Neurol* 50:42–46
 40. Lawlor MW, Armstrong D, Viola MG, Widrick JJ, Meng H, Grange RW, Childers MK, Hsu CP, O'Callaghan M, Pierson CR et al (2013) Enzyme replacement therapy rescues weakness and improves muscle pathology in mice with X-linked myotubular myopathy. *Hum Mol Genet* 22:1525–1538
 41. Liewluck T, Lovell TL, Bite AV, Engel AG (2010) Sporadic centronuclear myopathy with muscle pseudohypertrophy, neutropenia, and necklace fibers due to a DNMT2 mutation. *Neuromuscul Disord* 20:801–804
 42. McEntagart M, Parsons G, Buj-Bello A, Biancalana V, Fenton I, Little M, Krawczak M, Thomas N, Herman G, Clarke A et al (2002) Genotype-phenotype correlations in X-linked myotubular myopathy. *Neuromuscul Disord* 12:939–946
 43. Motoki T, Fukuda M, Nakano T, Matsukage S, Fukui A, Akiyoshi S, Hayashi YK, Ishii E, Nishino I (2013) Fatal hepatic hemorrhage by peliosis hepatitis in X-linked myotubular myopathy: a case report. *Neuromuscul Disord* 23(11):917–921
 44. Nicot AS, Toussaint A, Tosch V, Kretz C, Wallgren-Pettersson C, Iwarsson E, Kingston H, Garnier JM, Biancalana V, Oldfors A et al (2007) Mutations in amphiphysin 2 (BIN1) disrupt interaction with dynamin 2 and cause autosomal recessive centronuclear myopathy. *Nat Genet* 39:1134–1139
 45. Oliveira J, Oliveira ME, Kress W, Taipa R, Pires MM, Hilbert P, Baxter P, Santos M, Buermans H, den Dunnen JT et al (2012) Expanding the MTM1 mutational spectrum: novel variants including the first multi-exonic duplication and development of a locus-specific database. *Eur J Hum Genet* 21:540–549
 46. Penisson-Besnier I, Biancalana V, Reynier P, Cossee M, Dubas F (2007) Diagnosis of myotubular myopathy in the oldest known manifesting female carrier: a clinical and genetic study. *Neuromuscul Disord* 17:180–185
 47. Quijano-Roy S, Carlier RY, Fischer D (2011) Muscle imaging in congenital myopathies. *Semin Pediatr Neurol* 18:221–229
 48. Romero NB (2010) Centronuclear myopathies: a widening concept. *Neuromuscul* 20:223–228
 49. Sabha N, Volpatti JR, Gonorazky H, Reifler A, Davidson AE, Li X, Eltayeb NM, Dall'Armi C, Di Paolo G, Brooks SV et al (2016) PIK3C2B inhibition improves function and prolongs survival in myotubular myopathy animal models. *J Clin Invest* 126:3613–3625
 50. Savarese M, Musumeci O, Giugliano T, Rubegni A, Fiorillo C, Fattori F, Torella A, Battini R, Rodolico C, Pugliese A et al (2016) Novel findings associated with MTM1 suggest a higher number of female symptomatic carriers. *Neuromuscul Disord* 26:292–299
 51. Schara U, Kress W, Tucke J, Mortier W (2003) X-linked myotubular myopathy in a female infant caused by a new MTM1 gene mutation. *Neurology* 60:1363–1365

52. Shichiji M, Biancalana V, Fardeau M, Hogrel JY, Osawa M, Laporte J, Romero NB (2013) Extensive morphological and immunohistochemical characterization in myotubular myopathy. *Brain Behav* 3:476–486
53. Smith BK, Renno MS, Green MM, Sexton TM, Lawson LA, Martin AD, Corti M, Byrne BJ (2016) Respiratory motor function in individuals with centronuclear myopathies. *Muscle Nerve* 53:214–221
54. Soltanzadeh P, Friez MJ, Dunn D, von Niederhausern A, Gurvich OL, Swoboda KJ, Sampson JB, Pestronk A, Connolly AM, Florence JM et al (2010) Clinical and genetic characterization of manifesting carriers of DMD mutations. *Neuromuscul Disord* 20:499–504
55. Sutton II, Winer JB, Norman AN, Liechti-Gallati S, MacDonald F (2001) Limb girdle and facial weakness in female carriers of X-linked myotubular myopathy mutations. *Neurology* 57:900–902
56. Tanner SM, Orstavik KH, Kristiansen M, Lev D, Lerman-Sagie T, Sadeh M, Liechti-Gallati S (1999) Skewed X-inactivation in a manifesting carrier of X-linked myotubular myopathy and in her non-manifesting carrier mother. *Hum Genet* 104:249–253
57. Tanner SM, Schneider V, Thomas NS, Clarke A, Lazarou L, Liechti-Gallati S (1999) Characterization of 34 novel and six known MTM1 gene mutations in 47 unrelated X-linked myotubular myopathy patients. *Neuromuscul Disord* 9:41–49
58. Tasca G, Monforte M, Iannaccone E, Laschena F, Ottaviani P, Silvestri G, Masciullo M, Mirabella M, Servidei S, Ricci E (2012) Muscle MRI in female carriers of dystrophinopathy. *Eur J Neurol* 19:1256–1260
59. Terlizzi JP, Azizi R, Chow MD, Underberg-Davis S, Noshier JL, Stafford PW, Pierre J (2013) Peliosis hepatis in a child with myotubular myopathy: successful treatment using hepatic artery embolization. *J Pediatr Surg* 48:e9–e12
60. Tosch V, Vasli N, Kretz C, Nicot AS, Gasnier C, Dondaine N, Oriot D, Barth M, Puissant H, Romero NB et al (2010) Novel molecular diagnostic approaches for X-linked centronuclear (myotubular) myopathy reveal intronic mutations. *Neuromuscul Disord* 20:375–381
61. Trump N, Cullup T, Verheij JB, Manzur A, Muntoni F, Abbs S, Jungbluth H (2012) X-linked myotubular myopathy due to a complex rearrangement involving a duplication of MTM1 exon 10. *Neuromuscul* 22:384–388
62. Tsai TC, Horinouchi H, Noguchi S, Minami N, Murayama K, Hayashi YK, Nonaka I, Nishino I (2005) Characterization of MTM1 mutations in 31 Japanese families with myotubular myopathy, including a patient carrying 240 kb deletion in Xq28 without male hypogonadism. *Neuromuscul Disord* 15:245–252
63. Viggiano E, Ergoli M, Picillo E, Politano L (2016) Determining the role of skewed X-chromosome inactivation in developing muscle symptoms in carriers of Duchenne muscular dystrophy. *Hum Genet* 135:685–698
64. Vincent MC, Guiraud-Chaumeil C, Laporte J, Manouvrier-Hanu S, Mandel JL (1998) Extensive germinal mosaicism in a family with X linked myotubular myopathy simulates genetic heterogeneity. *J Med Genet* 35:241–243
65. Wilmshurst JM, Lillis S, Zhou H, Pillay K, Henderson H, Kress W, Muller CR, Ndondo A, Cloke V, Cullup T et al (2010) RYR1 mutations are a common cause of congenital myopathies with central nuclei. *Ann Neurol* 68:717–726
66. Wu H, Luo J, Yu H, Rattner A, Mo A, Wang Y, Smallwood PM, Erlanger B, Wheelan SJ, Nathans J (2014) Cellular resolution maps of X chromosome inactivation: implications for neural development, function, and disease. *Neuron* 81:103–119

2.2.8 Publication 10: Sarcomeric disorganization and nemaline bodies in muscle biopsies of patients with *EXOSC3*-related type 1 pontocerebellar hypoplasia (Pinto et al. 2018)

Background

Pontocerebellar hypoplasia, type 1B (PCH1B) is due to recessive *EXOSC3* mutations. The main clinical features include neonatal hypotonia, progressive microcephaly, global developmental delay and respiratory insufficiency (Eggen, Barth, and Baas 1993). The severity of the disease is variable, and the severe form of PCH1B usually causes premature death within the first two years of life. The frequently encountered mutation causing severe PCH1B is the *EXOSC3* c.92G>C p.(Gly31Arg) founder mutation (Schwabova et al. 2013).

Aim of the study

Our study aimed to characterize three new patients with severe PCH1B at the clinical, histological and genetic level.

Results

We reported three unrelated patients with severe neonatal hypotonia and feeding difficulties. The patients died prematurely from respiratory failure or multi-organ failure at nine days, seven months and four years of age. Brain MRI showed pontocerebellar hypoplasia or atrophy. Histological and ultrastructural studies of muscle biopsies revealed mixed hallmarks of spinal muscular atrophy and congenital myopathy such as nemaline rods and sarcomeric disorganization. The homozygous *EXOSC3* c.92G>C p.(Gly31Arg) mutation was identified in all three patients.

Conclusion

We showed that patients with *EXOSC3*-related pontocerebellar hypoplasia display histological signs of congenital myopathy on muscle biopsy, suggesting a possible role for *EXOSC3* in muscle development.

Contribution

I identified the *EXOSC3* mutation in one patient, referred to our laboratory for a severe undefined myopathy.

REFERENCES

1. Bolduc V, Marlow G, Boycott KM, Saleki K, Inoue H, Kroon J, *et al*. Recessive mutations in the putative calcium-activated chloride channel Anoctamin 5 cause proximal LGMD2L and distal MMD3 muscular dystrophies. *Am J Hum Genet* 2010;86(2):213–221.
2. Liewluck T, Milone M. Untangling the complexity of limb-girdle muscular dystrophies. *Muscle Nerve* 2018;58(2):167–177.
3. Tsutsumi S, Kamata N, Vokes TJ, Maruoka Y, Nakakuki K, Enomoto S, *et al*. The novel gene encoding a putative transmembrane protein is mutated in gnathodiaphyseal dysplasia (GDD). *Am J Hum Genet* 2004;74(6):1255–1261.
4. Penttila S, Palmio J, Suominen T, Raheem O, Evila A, Muelas Gomez N, *et al*. Eight new mutations and the expanding phenotype variability in muscular dystrophy caused by ANO5. *Neurology* 2012;78(12):897–903.
5. Hicks D, Sarkozy A, Muelas N, Koehler K, Huebner A, Hudson G, *et al*. A founder mutation in anoctamin 5 is a major cause of limb-girdle muscular dystrophy. *Brain* 2011;134(Pt 1):171–182.
6. Milone M, Liewluck T, Winder TL, Pianosi PT. Amyloidosis and exercise intolerance in ANO5 muscular dystrophy. *Neuromuscul Disord* 2012;22(1):13–15.
7. Liewluck T, Winder TL, Dimberg EL, Crum BA, Heppelmann CJ, Wang Y, *et al*. ANO5-muscular dystrophy: clinical, pathological and molecular findings. *Eur J Neurol* 2013;20(10):1383–1389.
8. van der Kooij AJ, Ten Dam L, Frankhuizen WS, Straathof CS, van Doorn PA, de Visser M, *et al*. ANO5 mutations in the Dutch limb girdle muscular dystrophy population. *Neuromuscul Disord* 2013;23(6):456–460.
9. Wahbi K, Behin A, Becane HM, Leturcq F, Cossee M, Laforet P, *et al*. Dilated cardiomyopathy in patients with mutations in anoctamin 5. *Int J Cardiol* 2013;168(1):76–79.
10. Witting N, Duno M, Petri H, Krag T, Bundgaard H, Kober L, *et al*. Anoctamin 5 muscular dystrophy in Denmark: prevalence, genotypes, phenotypes, cardiac findings, and muscle protein expression. *J Neurol* 2013;260(8):2084–2093.
11. Liewluck T, Milone M. Characterization of isolated amyloid myopathy. *Eur J Neurol* 2017;24(12):1437–1445.
12. Askanas V, Engel WK, Alvarez RB. Enhanced detection of Congo-red-positive amyloid deposits in muscle fibers of inclusion body myositis and brain of Alzheimer's disease using fluorescence technique. *Neurology* 1993;43(6):1265–1267.
13. Penisson-Besnier I, Saint-Andre JP, Hicks D, Sarkozy A, Croue A, Hudson J, *et al*. Myopathy caused by anoctamin 5 mutations and necrotizing vasculitis. *J Neurol* 2012;259(9):1988–1990.
14. Joshi PR, Glaser D, Dressel C, Kress W, Weis J, Deschauer M. Anoctamin 5 muscular dystrophy associated with a silent p.Leu115Leu mutation resulting in exon skipping. *Neuromuscul Disord* 2014;24(1):43–47.
15. Bohlega S, Monies DM, Abulaban AA, Murad HN, Alhindi HN, Meyer BF. Clinical and genetic features of anoctaminopathy in Saudi Arabia. *Neurosciences (Riyadh)* 2015;20(2):173–177.
16. Savarese M, Di Fruscio G, Tasca G, Ruggiero L, Janssens S, De Bleecker J, *et al*. Next generation sequencing on patients with LGMD and nonspecific myopathies: findings associated with ANO5 mutations. *Neuromuscul Disord* 2015;25(7):533–541.
17. Sarkozy A, Hicks D, Hudson J, Laval SH, Barresi R, Hilton-Jones D, *et al*. ANO5 gene analysis in a large cohort of patients with anoctaminopathy: confirmation of male prevalence and high occurrence of the common exon 5 gene mutation. *Hum Mutat* 2013;34(8):1111–1118.

SARCOMERIC DISORGANIZATION AND NEMALINE BODIES IN MUSCLE BIOPSIES OF PATIENTS WITH EXOSC3-RELATED TYPE 1 PONTOCEREBELLAR HYPOPLASIA

MIGUEL M. PINTO, MD,^{1†} SOLEDAD MONGES, MD,^{2†} EDOARDO MALFATTI, PHD,³ FABIANA LUBIENIECKI, MD,² XAVIÈRE LORNAGE, MS,⁴ LAURA ALIAS, PHD,⁵ CLÉMENCE LABASSE, BS,³ ANGÉLINE MADELAINE, BS,³ MICHEL FARDEAU, MD,³ JOCELYN LAPORTE, PHD,⁴ EDUARDO F. TIZZANO, PHD,⁶ and NORMA B. ROMERO, PHD³

¹Neurology Department, Hospital de Egas Moniz, Centro Hospitalar de Lisboa Ocidental, Lisbon, Portugal

²Neuropediatric and Neuropathology Departments, National Pediatric Hospital J-P-Garrahan, Buenos Aires, Argentina

³Unité de Morphologie Neuromusculaire, Institut de Myologie, Sorbonne University, INSERM UMR 974, Groupe Hospitalier Universitaire La Pitié-Salpêtrière, 75013, Paris, France

⁴Department of Translational Medicine and Neurogenetics, IGBMC (Institut de Génétique et de Biologie Moléculaire et Cellulaire), INSERM U1258, CNRS UMR7104, Université de Strasbourg, Illkirch, France

⁵Department of Genetics, Hospital Sant Pau and CIBERER, Barcelona, Spain

⁶Department of Clinical and Molecular Genetics and Rare Diseases Division, Hospital Vall d'Hebron and CIBERER, Barcelona, Spain

Accepted 15 July 2018

Additional supporting information may be found in the online version of this article.

Abbreviations: CK, creatine kinase; H&E, hematoxylin and eosin; MRI, magnetic resonance imaging scan; mGT, modified Gömöri trichrome technique; PCH, pontocerebellar hypoplasia; RRP40, ribosomal RNA-processing protein 40; SMA, spinal muscular atrophy.

Key words: congenital hypotonia, EXOSC3 gene, nemaline bodies, non-5q spinal muscular atrophy, sarcomeric disorganization, Type 1 pontocerebellar hypoplasia

Funding: This work was supported by the France Génomique National infrastructure, funded as part of the «Investissements d'Avenir» program managed by the Agence Nationale pour la Recherche (ANR-10-INBS-09), and by Fondation Maladies Rares within the frame of the “Myocapture” sequencing project.

Conflicts of Interest: The authors have nothing to disclose.

Acknowledgments: Eduardo Tizzano is a recipient of a grant from Fundación Privada Daniel Bravo Andreu. Laura Alias is supported by CIBERER.

[†]These authors contributed equally to this work.

Correspondence to: N. B. Romero; e-mail: nb.romero@institut-myologie.org

© 2018 Wiley Periodicals, Inc.

Published online 19 July 2018 in Wiley Online Library (wileyonlinelibrary.com). DOI 10.1002/mus.26305

Short Reports

ABSTRACT: *Introduction:* Mutations in the EXOSC3 gene are responsible for type 1 pontocerebellar hypoplasia, an autosomal recessive congenital disorder characterized by cerebellar atrophy, developmental delay, and anterior horn motor neuron degeneration. Muscle biopsies of these patients often show characteristics resembling classic spinal muscle atrophy, but to date, no distinct features have been identified. *Methods:* Clinical data and muscle biopsy findings of 3 unrelated patients with EXOSC3 mutations are described. *Results:* All patients presented with a severe congenital cognitive and neuromuscular phenotype with short survival, harboring the same point mutation (c.92G>C; p.Gly31Ala). Muscle biopsies consistently showed variable degrees of sarcomeric disorganization with myofibrillar remnants, Z-line thickening, and small nemaline bodies. *Conclusions:* In this uniform genetic cohort of patients with EXOSC3 mutations, sarcomeric disruption and rod structures were prominent features of muscle biopsies. In the context of neonatal hypotonia, ultrastructural studies might provide early clues for the diagnosis of EXOSC3-related pontocerebellar hypoplasia.

Muscle Nerve 59:137–141, 2019

Pontocerebellar hypoplasia (PCH) is a group of rare autosomal recessive developmental disorders,

MUSCLE & NERVE January 2019 137

characterized by psychomotor delay, progressive microcephaly, cerebellar atrophy, and variable brainstem involvement.¹ At least 10 subtypes of PCH have been recognized. PCH type 1 is a particularly severe subgroup that includes early anterior horn motor neuron degeneration, encompassing the phenotypic spectrum of spinal muscular atrophy (SMA) plus disorders.^{2,3} Clinically, it presents with a variable degree of generalized congenital weakness and hypotonia, respiratory failure, feeding difficulties, and contractures, as well as cerebellar and brainstem signs that are usually recognized later.^{1,4} The age of onset among PCH1 patients may range from antenatal detection with polyhydramnios and fetal akinesia, to a presentation within the first months of life with mild hypotonia and delayed milestones.¹⁻³ Life expectancy is severely reduced, but survival beyond the age of 10 years has been reported.^{1,5,6}

Recently, *EXOSC3* gene mutations were shown to underlie approximately 30–50% of PCH1 cases in some cohorts,^{1,2} being particularly prevalent in patients from Romani pedigrees.^{3,4} They have not been associated with other PCH subtypes. *EXOSC3* encodes the human exosome component 3 protein, also known as ribosomal RNA-processing protein 40 (RRP40), a key element on RNA exosome complex. It has been shown to play a critical role in RNA processing and is hypothesized to potentially influence gene expression.^{5,7} To date, single point mutations and deletions have been identified,¹⁻⁴ and some reports showed a tendency for a more severe phenotype with poor neurological outcomes and early death in patients harboring the c.92G>C (p.Gly31Ala) mutation.^{1,3-6}

Previous histochemical analysis of muscle biopsies from PCH1 patients harboring different *EXOSC3* mutations have shown neurogenic aspects such as marked type grouping and round atrophic fibers resembling those seen in *SMN1*-associated SMA.^{4,5} However, no particular myofibrillar alterations have been described. Here we report three unrelated patients harboring the same *EXOSC3* mutation showing remarkably similar and distinctive ultrastructural findings in muscle biopsies.

MATERIALS AND METHODS

We searched Unité de Morphologie Neuromusculaire pathology records for genetically determined *EXOSC3*-mutated PCH1 patients who have undergone diagnostic muscle biopsies. Clinical information was obtained through medical record review. *EXOSC3* mutation analysis, amplification primers and conditions as well as sequencing methods were performed according to Wan *et al.*² and Biancheri *et al.*⁵ Muscle biopsies were analyzed through conventional histochemical techniques, and ultrastructural studies performed according to international standards (see Supplementary Material, which is available online).

RESULTS

Patient 1 was a male, born of nonconsanguineous French parents with Romani ancestry. The pregnancy was complicated by polyhydramnios and limited fetal mobility. After a term birth with slightly low birth weight but normal head circumference, the examination showed a severe areflexic hypotonia with ventilator-dependent respiratory insufficiency and feeding difficulties. Brain magnetic resonance imaging (MRI) revealed severe PCH and a thin corpus callosum. Atrioventricular dissociation and occasional complete blocks were noted. The patient died on the 9th day of life from respiratory failure.

Patient 2 was a female, born of consanguineous Romani parents living in Argentina, with severe congenital hypotonia, an absent suck reflex and respiratory difficulties resulting in early respiratory infections, atelectasis and dependence on mechanical ventilation. At 5 months of age, examination displayed slight microcephaly, profound muscle weakness with arreflexia, tongue fasciculations, strabismus, and nystagmus. Creatine kinase (CK) levels were normal. A progressive pontocerebellar atrophy with moderate cerebral cortical atrophy was noted in sequential brain MRIs. The patient remained bedridden and ventilator-dependent until the age of 4 years, when she died from respiratory failure.

Patient 3 was a female born to Argentinian consanguineous parents of Hungarian Romani ancestry. She presented with generalized congenital hypotonia, swallowing difficulties, and laryngeal stridor requiring intensive care unit management. The examination showed mild microcephaly, partial eye contact with brief fixation, nystagmus but no strabismus, and severe areflexic hypotonia. CK levels were normal. Electrodiagnostic testing was indicative of a motor neuron disorder. At age 4 months, a brain MRI revealed severe PCH. The patient continued to demonstrate severe generalized weakness requiring permanent mechanical ventilation, and remained poorly attentive. She died at the age of 7 months due to multi-organ failure.

None of the patients presented with contractures at birth. All tested negative for *SMN1* deletions or mutations. No mutations were found in the congenital myopathy-related genes *RYR1*, *ACTA1*, *TPM2*, *TPM3*, and *TNNT1* in patient 1. *EXOSC3* gene screening or exome sequencing revealed the same homozygous c.92G>C (p.Gly31Ala) missense mutation in exon 1 in all patients.

Quadriceps muscle biopsies were performed on day 9 in patient 1, in month 7 in patient 2, and in month 1 in patient 3. In patient 1, hematoxylin and eosin (H&E) stain revealed great variability of fiber size diameter with numerous round small fibers distributed randomly through the fascicles, a few normal sized fibers, and rare large fibers. No type

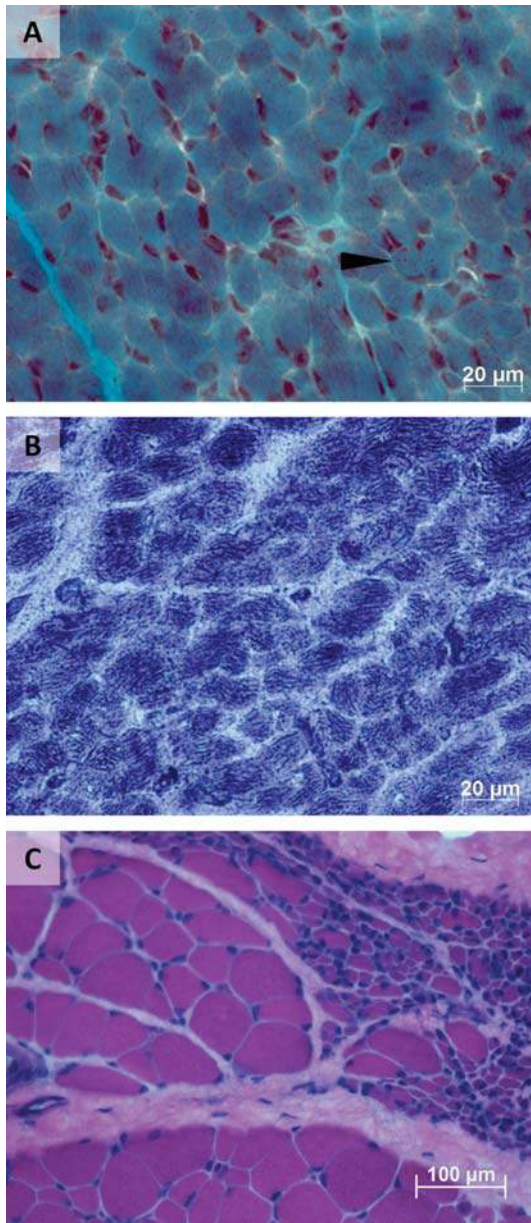


FIGURE 1. (A) mGT stains from a quadriceps muscle biopsy of patient 1 revealing small fuchsinophilic inclusions in some fibers, suggesting nemaline bodies (arrowhead). The fibers demonstrate a remarkably homogenous small diameter. (B) With nicotinamide adenine dinucleotide (NADH) oxidative stain, mild subsarcolemmal internal structure disorganization is shown in patient 1. (C) H&E stain from quadriceps muscle biopsy of patient 2 showing complete fascicle atrophy and some large fibers resembling SMA pathology. No inclusions were observed in mGT stains from patients 2 and 3. [Color figure can be viewed at wileyonlinelibrary.com]

grouping was observed. Modified Gömöri trichrome (mGT) stain revealed discrete reddish inclusions resembling small rods in roughly 10% of the fibers with very small diameter (Fig. 1A). Oxidative stains showed a few fibers with mild subsarcolemmal myofibrillar disorganization, but no peripheral halos as usually seen in SMA biopsies (Fig. 1B). Patients

2 and 3 displayed complete fascicle atrophy, few large fibers, and a marked type grouping, highly suggesting a neurogenic process (Fig. 1C).

In all patients, electron microscopy revealed numerous fibers with striking sarcomeric disorganization, involving the entire section of the fiber or affecting predominantly subsarcolemmal regions, producing a caps-like aspect (Fig. 2A). Most areas were composed of tangles of disordered sarcomeres with Z-line thickening and absent mitochondrion (Fig. 2B,C). In the most extensively affected regions, only sarcomeric remnants were observed, consisting of small fragments of thickened Z material bound to thin filaments (Fig. 2D). Small nemaline bodies with random orientation and typical cross-sectional square structure were often observed (Fig. 2E). Rare subsarcolemmal areas were composed solely of disorganized thin filaments where Z-line material was absent. These findings were more evident in patients 1 and 2. No major basal membrane detachment was observed, except for a small area in one single fiber in patient 1 (Fig. 2F).

DISCUSSION

We present 3 unrelated PCH1 patients sharing the same *EXOSC3* mutation and describe their common features of profound sarcomeric disorganization with numerous small rods. Our patients displayed the typical phenotype consistently reported for other *EXOSC3*-related PCH1 patients, namely the cognitive and neuromuscular signs at birth and progressive deterioration. Of interest, although the severe phenotype associated with the c.92G>C mutation was observed in all our patients, the most striking signs were exhibited by patient 1, accounting for the previously recognized *EXOSC3* phenotypic variability³ and suggesting that other factors may affect clinical severity.

PCH1 patients show histopathological features of muscle fibers atrophy and type grouping, resembling those of SMA with *SMN1* mutations.^{4,5} Muscles of SMA patients usually show global preservation of internal architecture, but mild to moderate denervation-related disorganization and reduction of sarcomeric structures in the smallest atrophic fibers have been demonstrated in a cohort of genetically uncharacterized SMA patients.⁸ Two of our patients demonstrated histopathology similar to SMA patients, but patient 1 also showed reddish inclusions on mGT staining, suggesting nemaline rods. Electron microscopy confirmed the presence of Z-line material thickening, compatible with small nemaline bodies. At least 1 previous report of a patient with a clinical diagnosis of PCH1 showed Z-line abnormalities and nemaline bodies in few muscle fibers, but the patient was genetically uncharacterized.⁹ Furthermore, mild widening of the Z-line material and small rods have been described in one patient from a pathologic cohort of PCH2

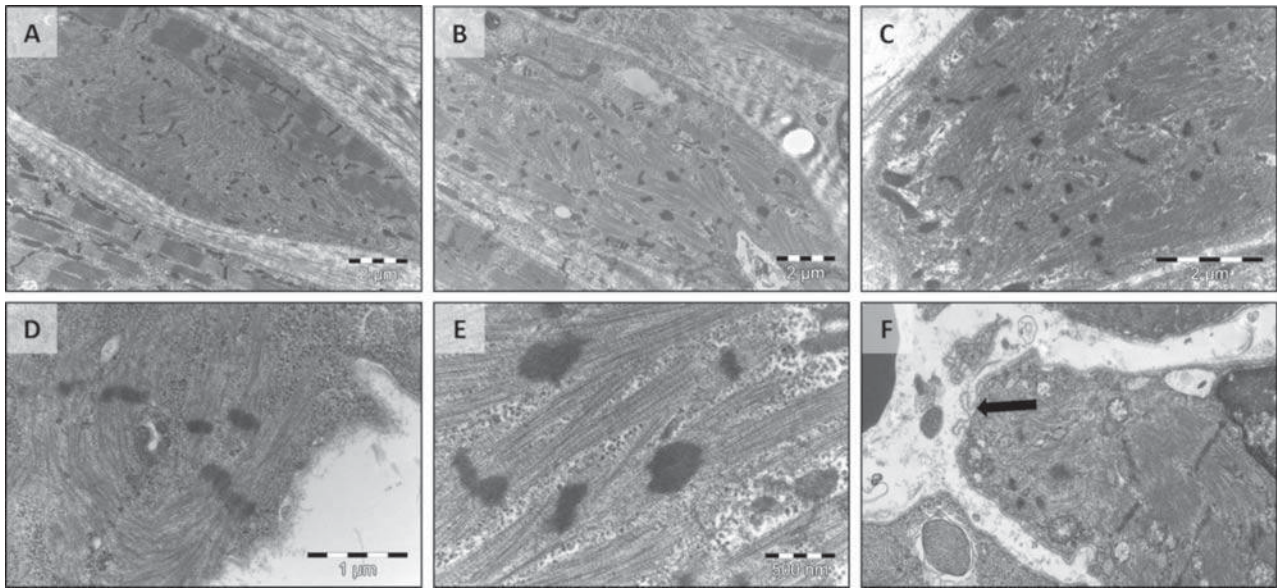


FIGURE 2. Electron microscopy studies revealing variable degrees of sarcomeric disorganization in all patients, either assuming a capsular position (A) or involving the great majority of single muscle fibers (B,C). Tangles of sarcomeric fragments with thickened Z-line and attached thin filaments were observed (D,E) sometimes forming nemaline bodies (E). No basal membrane detachment was observed, except for a small area in 1 fiber (F, arrow). Patient 1, panels D and F; patient 2, panels A, B, and E; patient 3, panel C.

patients.¹⁰ Although our patients demonstrated different and more severe pathology, in particular sarcomeric segment remnants and Z-line thickening (Fig. 2D,E), these findings could suggest that sarcomeric disruption itself might not be specific for a PCH diagnosis.

Nemaline bodies, however, are almost exclusively associated with congenital myopathies, namely with nemaline myopathies,¹¹ but are nonspecific because they can rarely occur as a secondary phenomenon in other miscellaneous disorders such as myofibrillar myopathy,¹² mitochondrial disorders,¹³ human immunodeficiency virus-related myopathy,¹⁴ and sporadic late-onset nemaline myopathy.¹⁵ Nevertheless, the presence of nemaline bodies in genetically determined childhood-onset myopathies other than nemaline myopathies is exceptionally rare. To date, there is insufficient evidence to associate *EXOSC3* mutations with typical nemaline myopathies, but our findings suggest that their screening might be adequate in early-onset hypotonic patients with nemaline bodies, particularly when central nervous system involvement and motor neuron degeneration are apparent.

This report systematically describes sarcomeric disruption and rod structures as distinctive features of muscle biopsies from three *EXOSC3*-mutated patients. While deemed consistent through our uniform genetic cohort, further studies are needed to assess their reproducibility and specificity. Because *SMN1*-associated SMA is the main differential diagnosis in the context of neonatal hypotonia, and given that a definitive diagnosis may be delayed until pontocerebellar atrophy signs are recognized, muscle biopsy is an important resource in

the diagnostic evaluation, and ultrastructural study may provide early clues to a diagnosis of PCH1.

Ethical Publication Statement: We confirm that we have read the Journal's position on issues involved in ethical publication and affirm that this report is consistent with those guidelines.

REFERENCES

- Rudnik-Schoneborn S, Senderek J, Jen JC, Houge G, Seeman P, Puchmajerova A, *et al.* Pontocerebellar hypoplasia type 1: clinical spectrum and relevance of *EXOSC3* mutations. *Neurology* 2013;80:438–446.
- Wan J, Yourshaw M, Mamsa H, Rudnik-Schoneborn S, Menezes MP, Hong JE, *et al.* Mutations in the RNA exosome component gene *EXOSC3* cause pontocerebellar hypoplasia and spinal motor neuron degeneration. *Nat Genet* 2012;44:704–708.
- Eggers VR, Barth PG, Niermeijer JM, Berg JN, Darin N, Dixit A, *et al.* *EXOSC3* mutations in pontocerebellar hypoplasia type 1: novel mutations and genotype-phenotype correlations. *Orphanet J Rare Dis* 2014;9:23.
- Schwabova J, Brozkova DS, Petrak B, Mojzisova M, Pavlickova K, Haberlova J, *et al.* Homozygous *EXOSC3* mutation c.92G→C, p.G31A is a founder mutation causing severe pontocerebellar hypoplasia type 1 among the Czech Roma. *J Neurogenet* 2013;27:163–169.
- Biancheri R, Cassandrini D, Pinto F, Trovato R, Di Rocco M, Mirabelli-Badenier M, *et al.* *EXOSC3* mutations in isolated cerebellar hypoplasia and spinal anterior horn involvement. *J Neurol* 2013;260:1866–1870.
- Zanni G, Scotton C, Passarelli C, Fang M, Barresi S, Dallapiccola B, *et al.* Exome sequencing in a family with intellectual disability, early onset spasticity, and cerebellar atrophy detects a novel mutation in *EXOSC3*. *Neurogenetics* 2013;14:247–250.
- Gillespie A, Gabunilas J, Jen JC, Chanfreau GF. Mutations of *EXOSC3*/Rrp40p associated with neurological diseases impact ribosomal RNA processing functions of the exosome in *S. cerevisiae*. *RNA* 2017;23:466–472.
- Zalneraitis EL, Halperin JJ, Grunnet ML, Russman BS, Peress N. Muscle biopsy and the clinical course of infantile spinal muscular atrophy. *J Child Neurol* 1991;6:324–328.
- Salman MS, Blaser S, Buncic JR, Westall CA, Heon E, Becker L. Pontocerebellar hypoplasia type 1: new leads for an earlier diagnosis. *J Child Neurol* 2003;18:220–225.
- Barth PG, Ryan MM, Webster RI, Aronica E, Kan A, Ramkema M, *et al.* Rhabdomyolysis in pontocerebellar hypoplasia type 2 (PCH2). *Neuromuscul Disord* 2008;18:52–58.
- Romero NB, Clarke NF. Congenital myopathies. *Handb Clin Neurol* 2013;113:1321–1336.

12. Claeys KG, Fardeau M, Schröder R, Suominen T, Tolksdorf K, Behin A, *et al.* Electron microscopy in myofibrillar myopathies reveals clues to the mutated gene. *Neuromuscul Disord* 2008;18:656–666
13. Lamont PJ, Thorburn DR, Fabian V, Vajsar J, Hawkins C, Saada Reisch A, *et al.* Nemaline rods and complex I deficiency in three infants with hypotonia, motor delay and failure to thrive. *Neuropediatrics* 2004;35:302–306.
14. Dalakas MC, Pezeshkpour GH, Flaherty M. Progressive nemaline (rod) myopathy associated with HIV infection. *N Engl J Med* 1987;317:1602–1603.
15. Chahin N, Selcen D, Engel AG. Sporadic late onset nemaline myopathy. *Neurology* 2005;65:1158–1164.

2.2.9 Publication 11: Discordant manifestations in Italian brothers with GNE myopathy (Dotti et al. 2018)

Background

In eukaryotic cells, glycoproteins and glycolipids can be modified by a process called sialylation, by which sialic acids groups are added to their terminal positions on oligosaccharide chains. Sialylation was shown to regulate a high number of cellular processes including cell adhesion and signaling (Varki 1997). *GNE* encodes the UDP-N-acetylglucosamine 2-epimerase / N-acetylmannosamine kinase, an enzyme involved in the sialic acid biosynthetic pathway (Keppler et al. 1999) (Keppler et al. 1999). Dominant *GNE* gain-of function mutations cause sialuria, a disease characterized by the accumulation of free sialic acid (Seppala, Lehto, and Gahl 1999), while recessive *GNE* loss-of-function mutations cause a distal adult-onset vacuolar myopathy also called Nonaka myopathy (Eisenberg et al. 2001).

Aim of the study

The aim of the study was to identify the genetic cause of the disease in two brothers with vacuolar myopathy.

Results

The patients presented with distal muscle weakness, spreading to more proximal muscles at later stages. The clinical course of the disease was however strikingly more severe for the younger brother, who was wheelchair-bound five years after the start of the disease, while the elder brother remained ambulant 12 years after the disease onset. The muscle biopsies revealed features of vacuolar myopathy. Both patients carried compound heterozygous *GNE* missense mutations.

Conclusion

The progression of *GNE*-related myopathy can be rapid or slow, and our study illustrates and highlights the intrafamilial variability of the disorder.

Contribution

I analyzed the exome sequencing data of the two brothers and identified the *GNE* mutations. Given the clinical heterogeneity, I compared both exomes for additional variants that might modulate the disease severity and potentially explain the phenotypic difference between both affected brothers. I did not identify any obvious modifier.



Letter to the Editor

Discordant manifestations in Italian brothers with GNE myopathy



ARTICLE INFO

Keywords:

GNE myopathy
 UDP-*N*-acetyl-glucosamine 2-epimerase/*N*-acetylmannosamine kinase
 Italy
 Exome sequencing
 Rimmed vacuoles
 Clinical discordance

Dear Sirs,

GNE myopathy (MIM 605820) is an autosomal recessive genetic disease provoked by biallelic mutations in the *GNE* gene, which encodes the bifunctional enzyme uridine diphosphate (UDP)-*N*-acetylglucosamine (GlcNAc) 2-epimerase/*N*-acetylmannosamine (ManNAc) kinase [1]. GNE deficiency causes abnormal sialylation of glycoproteins possibly leading to muscle degeneration. GNE myopathy is particularly frequent in Japan, Middle Eastern Jewish population, Iran, United States and Bulgaria where recurrent mutations are encountered due to a founder effect. Nevertheless global prevalence is reported to be 0,1 index case for 100,000 [2]. To date more than 167 causative mutations have been reported, and patients from Europe are usually compound heterozygous for mutations in different regions of the gene [3].

Foot drop, often unilateral, starting in the second or third decade of life, is the first sign and is followed by the involvement of the posterior thigh compartment. However, teenage onset (second decade) is rare, GNE myopathy being considered an adult onset myopathy. Upper extremities can show finger flexors weakness and successively proximal muscles weakness. Full-blown phenotype consists of a scapuloperoneal syndrome. Sparing of quadriceps strength and trophism is pathognomonic of this disorder. Nevertheless, variable quadriceps involvement is reported in 5% of cases and the recognition of phenotypic variants is frequent [4]. As a general rule quadriceps sparing is not unique to GNE myopathy as it has also been reported in patients affected by a non-GNE related myopathy [5].

Most of the GNE patients become wheelchair-bound within 12 years in average [6]. CK levels are usually normal or mildly elevated.

Muscle biopsies typically show the presence of rimmed vacuoles, and electron microscopy studies confirm the presence of autophagic material associated with tubulofilamentous inclusions of 18–21 nm in diameter found both inside nuclei or next to autophagic material [6]. Rimmed vacuoles, although characteristic, are not exclusive of GNE myopathy, and inflammatory infiltrates have been rarely reported in GNE myopathy, which create confusion with sporadic Inclusion-Body-Myopathy.

Here we report on two Italian brothers with an age difference of 8 years presenting highly discordant clinical features associated with GNE myopathy.

P1 is the elder brother and reported lower limbs distal weakness from age 32 causing stumbling episodes. Examination at 37 years of age showed bilateral foot-drop, waddling gait, distal lower limb (MRC 3) and milder proximal upper limb weakness (MRC 4). Muscle MRI of lower limbs revealed fibro-fatty substitution of the posterior thigh compartment with quadriceps sparing (Fig. 1A), and of the anterior leg compartment involving preferentially tibialis anterior muscles. Examination at 44 years of age revealed severe leg weakness (MRC 2), and milder arm weakness (MRC 3-4). Gait remained possible with a cane. Serum CK kinase level was normal. Electromyography showed discrete myopathic features on proximal muscles. Nerve conduction studies, as well as respiratory and cardiac functions were normal.

P2 was firstly referred to another center at age 25 due to leg weakness and atrophy. An initial diagnosis of polymyositis was done based on a muscle biopsy presenting mild endomysial inflammatory infiltrates (not shown). A therapy with corticoids was started, without any improvement. Serum CK level were normal and myositis antibodies were negative. Due to progression of his symptoms extending to the proximal muscle of the lower limbs, the patient was referred to our center. Clinical examination at 27 years revealed bilateral foot-drop with stepping gait and scapular winging with deltoid and bicipital muscles weakness quoting MRC 3; quadriceps muscle strength was normal and there was severe weakness of tibialis anterior muscles quoting MRC 3. EMG showed a myopathic pattern predominant in the distal muscles of the lower limbs, and in the proximal muscles of the upper limbs. MRI of lower limbs performed at 29 years revealed diffuse fatty infiltration of hamstring muscle with respect of quadriceps muscle (Fig. 1B). In legs there was fatty infiltration of tibialis anterior muscles and to a lesser extent of gastrocnemius. The course was progressive with loss of ambulation at 30 years. A recent examination at 36 years showed a wheelchair-bound patient. Arm elevation was severely reduced to 30° and diffuse weakness of both proximal (biceps and triceps) and distal muscles of upper limbs (wrist flexors and extensors) quoting

<https://doi.org/10.1016/j.jns.2018.01.002>

Received 20 October 2017; Received in revised form 13 December 2017; Accepted 3 January 2018

Available online 05 January 2018

0022-510X/ © 2018 Elsevier B.V. All rights reserved.

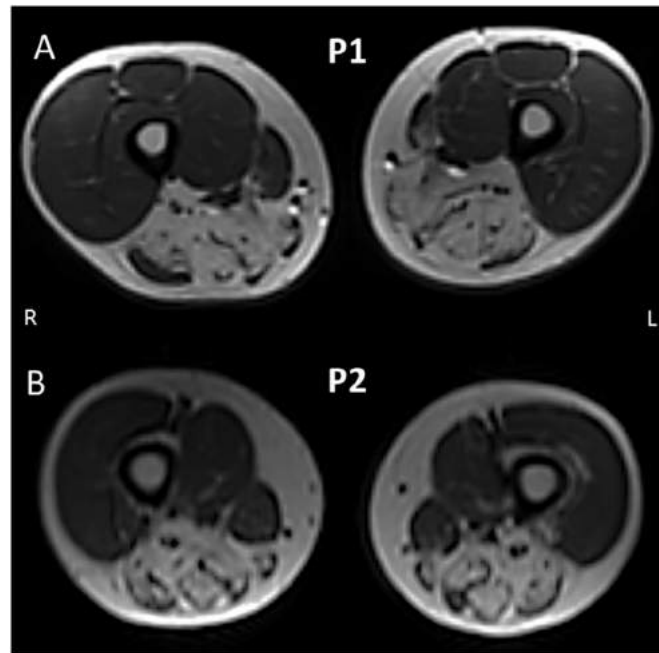


Fig. 1. Muscle MRI studies from P1 and P2. (A) and (B) presence of a diffuse fatty degeneration of all posterior thigh compartment muscles.

MRC 2 was found. There was hand weakness and atrophy and finger weakness. In contrast, quadriceps muscle strength was almost completely respected (MRC 4). ROTs were absent. Severe contractures of elbow, wrist, fingers, knees and ankles were found. Cardiac workup including EKG and echocardiography was normal.

Both patients underwent a deltoid muscle biopsy performed at 37 years in P1 and 32 in P2. Muscle samples disclosed the presence of rimmed vacuoles in about 5% of fibers. The vacuoles were single or multiple (Fig. 2A). There was no difference in the amount of connective tissue content. In contrast P2 showed greater fiber size variation with the presence of small groups of atrophic fibers, often vacuolated (Fig. 2B). By electron microscopy the vacuoles contained different compartments filled with autophagic material, cellular debris, and myelinic structures (Fig. 2C).

Exome sequencing was performed for both siblings and revealed two compound heterozygous mutations in *GNE*. The first one affecting the kinase domain p.(Tyr706His) (NM_01128227.2(GNE):c.2116T > C) and the second located in the epimerase domain p.(Arg277Gln) (NM_001128227.2(GNE):c.830G > A). Segregation studies were available only in the mother that harbored the p.(Arg277Gln) at heterozygous state. Both mutations were previously reported as pathogenic [7,8]. The p.(Arg277Gln), originally reported as p.(Arg246Gln) has previously been described in *GNE* patients from Bahamas, Taiwan, and Italy [9]. Further analysis of the exome data revealed different heterozygous sequence variants in known myopathy genes in both siblings. P1 exclusively carried variants in *SLC22A5* p.(Val481Ile), *SGCD* p.(Lys32Glu), and *DNAJB6* p.(Phe114Asp), while P2 was found to harbor variants in *COL6A2* p.(Arg380Cys), *CHRNA1* p.(Glu286Gly), and *DYSF* p.(Ser1558Phe) and p.(Arg1620His). These variants of unknown significance might contribute to the phenotypic variability within the family.

The particularity of this *GNE* family consists in discordant clinical manifestations among the two brothers with P2 being wheelchair bound at 30 years after 5 years from disease onset. Age at onset differed of 7 years but both patients started with ankle dorsiflexion weakness at age 32 in P1, and 25 in P2. The distribution of weakness was similar in both patients spreading to proximal muscles of lower limbs and successively upper limb girdle. Hand and finger weakness was evident only in P2 and appeared at the same time as the shoulder involvement. In contrast, P1 conserved

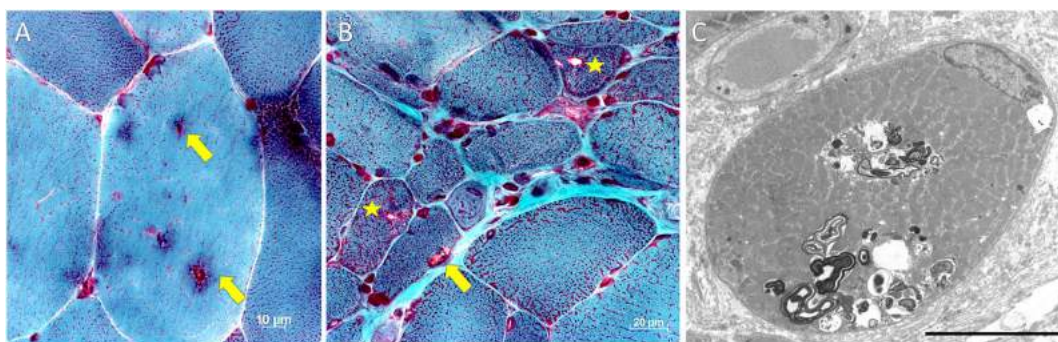


Fig. 2. Muscle morphological studies from P1 and P2. (A) Deltoid muscle biopsy at 37 years frozen section stained with Gomori trichrome technique. Rimmed vacuoles at different stage of formation (indicated by yellow arrows). (B) Deltoid muscle biopsy at 32 years; frozen section stained with Gomori trichrome technique. Significant variation of the fibers size diameter. Clusters of atrophic fibers, some of them mildly angulated. Atrophic fibers showed cytoplasmic (indicated by yellow stars) or subsarcolemmal (indicated by an arrow) rimmed vacuoles. (C) Electron microscopy from P2. Cross section showing a myofiber harbouring subsarcolemmal and cytoplasmic vacuolization. The vacuoles contained different compartments filled with autophagic material, cellular debris, and pseudo-myelinic structures. Scale bar correspond to 10 μm. (For interpretation of the references to colour in this figure legend, the reader is referred to the web version of this article.)

normal hand strength and fine fingers movements allowing him to perform wood carving activities, his principal occupation.

Another major difference was the presence of contractures. Severe contractures of ankles, elbows, wrists, and fingers were present in P2, while P1 only showed elbow contractures.

GNE myopathy can have a rapid or slow progression [10,11] but interfamilial clinical discordance has been rarely reported. Ro et al. [11] described phenotypic variability in two siblings where the elder brother presented slow disease progression with tibialis anterior weakness and unaffected quadriceps, while the younger sister showed prominent proximal weakness leading to loss of gait in a four years' time period. Interestingly, the two Italian sisters reported by Stober et al. [9] carrying the p.(Arg277Trp) missense mutation affecting the same amino acid at position 277 in our patients p.(Arg277Gln), showed clinical variability with one patient wheelchair-bound at 34 years of age and the other still ambulant late in life.

A recent study demonstrated that sialic acid deficiency is associated with oxidative stress leading to muscle atrophy and weakness in GNE myopathy [12]. Unknown epigenetic or environmental factors could be responsible for a different response to oxidative stress responsible for the clinical discordance in our patients.

As a whole clinician must be alerted about GNE myopathy intrafamilial clinical discordance both for prognostic advice and patients enrollment in future clinical trials.

Acknowledgements

We thank patients and families, Guy Brochier, Raphaël Schneider and Elodie Boeuf for technical assistance. This study was supported by Institut National de la Santé et de la Recherche Médicale (INSERM), Centre National de la Recherche Scientifique (CNRS), University of Strasbourg, France Génomique (ANR-10-INBS-09) and Fondation Maladies Rares within the frame of the “Myocapture” project, Association Française contre les Myopathies (AFM), Fondation pour la Recherche Médicale (DBI20131228569), Assistance Publique-Hôpitaux de Paris (AP-HP), and Association Institut de Myologie (AIM).

References

- [1] I. Eisenberg, et al., Physical and transcriptional map of the hereditary inclusion body myopathy locus on chromosome 9p12-p13, *Eur. J. Hum. Genet.* 9 (7) (2001) 501–509.
- [2] J.A. Urtizberea, A. Behin, GNE myopathy, *Med. Sci. (Paris)* 31 (2015) 20–27 Spec No. 3.
- [3] M. Cerino, et al., Novel pathogenic variants in a French cohort widen the mutational spectrum of GNE myopathy, *J. Neuromuscul. Dis.* 2 (2) (2015) 131–136.
- [4] Z. Argov, et al., Hereditary inclusion body myopathy: the middle eastern genetic cluster, *Neurology* 60 (9) (2003) 1519–1523.
- [5] A. Broccolini, et al., Analysis of NCAM helps identify unusual phenotypes of hereditary inclusion-body myopathy, *Neurology* 75 (3) (2010) 265–272.
- [6] I. Nishino, N. Carrillo-Carrasco, Z. Argov, GNE myopathy: current update and future therapy, *J. Neurol. Neurosurg. Psychiatry* 86 (4) (2015) 385–392.
- [7] D. Darvish, P. Vahedifar, Y. Huo, Four novel mutations associated with autosomal recessive inclusion body myopathy (MIM: 600737), *Mol. Genet. Metab.* 77 (3) (2002) 252–256.
- [8] I. Eisenberg, et al., Mutations spectrum of GNE in hereditary inclusion body myopathy sparing the quadriceps, *Hum. Mutat.* 21 (1) (2003) 99.
- [9] A. Stober, et al., Novel missense mutation p.A310P in the GNE gene in autosomal-recessive hereditary inclusion-body myopathy/distal myopathy with rimmed vacuoles in an Italian family, *Neuromuscul. Disord.* 20 (5) (2010) 335–336.
- [10] H. Mizusawa, et al., Rimmed vacuolar distal myopathy: a clinical, electrophysiological, histopathological and computed tomographic study of seven cases, *J. Neurol.* 234 (3) (1987) 129–136.
- [11] L.S. Ro, et al., Phenotypic variability in a Chinese family with rimmed vacuolar distal myopathy, *J. Neurol. Neurosurg. Psychiatry* 76 (5) (2005) 752–755.
- [12] A. Cho, et al., Sialic acid deficiency is associated with oxidative stress leading to muscle atrophy and weakness in GNE myopathy, *Hum. Mol. Genet.* 26 (16) (2017) 3081–3093.

Maria-Teresa Dotti^a, Alessandro Malandrini^a, Xavière Lornage^b, Andrea Mignarri^a, Teresa Anna Cantisani^c, Johann Bohm^b, Jocelyn Laporte^b, Edoardo Malfatti^{d,e,*}

^a Neurology and Neurometabolic Unit, Department of Medicine, Surgery, and Neurosciences, University of Siena, Siena, Italy

^b Department of Translational Medicine and Neurogenetics, Institut de Génétique et de Biologie Moléculaire et Cellulaire (IGBMC), Inserm U964, CNRS UMR7104, Strasbourg University, Illkirch, France

^c Neurophysiopathology Unit, Azienda Ospedaliera di Perugia, Perugia, Italy

^d Unité de Morphologie Neuromusculaire, Institut de Myologie, GHU La Pitié-Salpêtrière, Paris, France

^e Centre de référence de Pathologie Neuromusculaire Paris-Est, Institut de Myologie, GHU La Pitié-Salpêtrière, Assistance Publique-Hôpitaux de Paris, Paris, France

E-mail address: e.malfatti@institut-myologie.org

* Corresponding author at: Institut de Myologie, GHU La Pitié-Salpêtrière, Paris 75013, France.

2.3 Mutations in novel genes

To date, 35 congenital myopathy genes have been described (<http://www.musclegenetable.fr>). Next generation sequencing panels provide a rapid and accurate analysis of known myopathy genes but failed to identify the causative genes in many patients, suggesting that myopathy genes remain to be discovered. We therefore performed exome sequencing on molecularly undiagnosed patients.

The identification, validation and characterization of novel myopathy genes allows the establishment of novel diagnosis protocols to improve genetic counseling and provides the possibility of prenatal or pre-implantation diagnosis. Moreover, novel myopathy genes highlight new pathways relevant for muscle structure and function and represent potential therapeutic targets.

2.3.1 Publication 12: Recessive *MYPN* mutations cause cap myopathy with occasional nemaline rods (Lornage et al. 2017)

Background

Cap myopathy is a rare congenital myopathy characterized by the peripheral accumulation of Z-line remnants and thin filaments in muscle fibers (Fidzianska et al. 1981). The patients usually present with hypotonia at birth and subsequently develop a slowly progressive weakness of facial, respiratory, and limb muscles. Causative mutations have been identified in *TPM2*, *TPM3*, *ACTA1* and *NEB*, all coding for thin filament proteins (De Paula et al. 2009; Ohlsson et al. 2008; Piteau et al. 2014; Hung et al. 2010; Kiiski et al. 2019; Lehtokari et al. 2007; Tajsharghi et al. 2007). The exact molecular mechanisms underlying cap myopathy are unknown, but the occurrence of the disease may be related to defects in muscle maturation (Fidzianska 2002) and/or actin-binding (Marttila et al. 2012).

Aim of the study

The aim of the study was to identify the genetic cause of the disease in two families with molecularly undiagnosed cap myopathy.

Results

We described three patients from two unrelated families with an early-onset myopathy. The clinical course of the disease was slowly progressive with predominant weakness of the limb-girdle and distal muscles. The muscle biopsies showed numerous peripherally-placed and well-delimited structures corresponding to caps, as well as rods in about 2% of the fibers. To investigate the genetic cause of the disease, exome sequencing was performed and revealed homozygous *MYPN* mutations in all affected individuals. *MYPN* encodes the Z-line protein myopalladin, implicated in sarcomere integrity (Bang et al. 2001). The patients from family 1 carried a homozygous nonsense mutation (c.2653C>T p.(Arg885*)), and analysis of muscle extracts by reverse transcription and western blot demonstrated a strong reduction of the mRNA and protein levels. The patient from family 2 harbored a homozygous splice site mutation (c.3158+1G>A). Minigene experiments revealed the absence of wild-type transcript and the appearance of two abnormally spliced mRNAs containing premature stop codons resulting from the activation of two cryptic donor sites. In summary, both *MYPN* mutations impair mRNA stability and presumably lead to nonsense mediated mRNA decay. Accordingly, immunofluorescence detected significantly less myopalladin signals on patient muscle sections

compared to controls, and the residual myopalladin was found to accumulate in the caps together with its interacting partner alpha-actinin-2.

Conclusion

Dominant *MYPN* mutations were previously reported in patients with cardiomyopathy (Purevjav et al. 2012; Duboscq-Bidot et al. 2008; Meyer et al. 2013) and our results show that specific *MYPN* mutations cause congenital cap myopathy through a different mode of inheritance.

Contribution

I identified the *MYPN* mutations in both families, verified the segregation, performed the quantitative and functional experiments, and wrote the publication with other authors.

Recessive *MYPN* Mutations Cause Cap Myopathy with Occasional Nemaline Rods

Xavière Lornage, MS,^{1,2,3,4}
 Edoardo Malfatti, MD PhD,^{5,6,7}
 Chrystel Chéraud, MD,^{1,2,3,4}
 Raphaël Schneider, MS,^{1,2,3,4,8}
 Valérie Biancalana, PhD,^{1,2,3,4,9}
 Jean-Marie Cuisset, MD,¹⁰
 Matteo Garibaldi, MD,^{6,11,12}
 Bruno Eymard, MD, PhD,^{5,7}
 Michel Fardeau, MD,^{5,6,7}
 Anne Boland, PhD,¹³
 Jean-François Deleuze, PhD,¹³
 Julie Thompson, PhD,⁸
 Robert-Yves Carlier, MD, PhD,^{14,15}
 Johann Böhm, PhD,^{1,2,3,4}
 Norma B. Romero, MD, PhD,^{5,6,7} and
 Jocelyn Laporte, PhD^{1,2,3,4}

Congenital myopathies are phenotypically and genetically heterogeneous. We describe homozygous truncating mutations in *MYPN* in 2 unrelated families with a slowly progressive congenital cap myopathy. *MYPN* encodes the Z-line protein myopalladin implicated in sarcomere integrity. Functional experiments demonstrate that the mutations lead to mRNA defects and to a strong reduction in full-length protein expression. Myopalladin signals accumulate in the caps together with alpha-actinin. Dominant *MYPN* mutations were previously reported in cardiomyopathies. Our data uncover that mutations in *MYPN* cause either a cardiac or a congenital skeletal muscle disorder through different modes of inheritance.

ANN NEUROL 2017;00:000–000

Congenital myopathies define a clinically and genetically heterogeneous group of muscle diseases characterized by neonatal or early onset hypotonia and/or muscle weakness with structural defects on the muscle biopsy.^{1,2} Cap myopathy is a rare congenital myopathy, characterized by the presence of peripherally placed, well-delimited areas resembling a cap in muscle fibers. Caps are filled with thin filaments and segments of Z-lines.³ Although causative mutations in *TPM2*, *TPM3*, and *ACTA1* have been associated with cap myopathy,^{4–7} several patients are still devoid of genetic diagnosis,

precluding familial counseling and better patient health care. In an effort to identify additional implicated genes, we discovered recessive mutations in *MYPN* (myopalladin) in patients with congenital cap myopathy with occasional rods.

Myopalladin is a sarcomeric 145 kDa protein located at the Z-line, with homology to palladin and myotilin.^{8,9} It binds to the EF hand region of alpha-actinin, to the SH3 domain of nebulin, and to the cardiac ankyrin repeat protein.^{9,10} Heterozygous mutations in *MYPN* were reported in dilated, restrictive, or hypertrophic cardiomyopathies (Mendelian Inheritance in Man #615248) without skeletal muscle involvement.^{11–13}

Patients and Methods

Patients

We describe 3 adult patients with cap myopathy from 2 unrelated families of different ethnic backgrounds. Patients 1 and 3 underwent open muscle biopsy of the deltoid muscle at 34 and 44 years, respectively. Sample collection was performed with written informed consent from the patients, according to the Declaration of Helsinki. DNA storage and usage was

From the ¹Institute of Genetics and Molecular and Cellular Biology, Illkirch, France; ²National Institute of Health and Medical Research, Illkirch, France; ³National Center for Scientific Research, Illkirch, France; ⁴Strasbourg Federation of Translational Medicine, University of Strasbourg, Illkirch, France; ⁵Sorbonne Universities, Pierre and Marie Curie University, National Institute of Health and Medical Research, National Center for Scientific Research, Center for Research in Myology, Pitié-Salpêtrière Hospital, Paris, France; ⁶Unit of Neuromuscular Morphology, Institute of Myology, Pitié-Salpêtrière Hospital, Paris, France; ⁷Reference Center for Neuromuscular Pathology Paris-East, Institute of Myology, Pitié-Salpêtrière Hospital, Public Hospital Network of Paris, Paris, France; ⁸Department of Computer Science, ICube, National Center for Scientific Research, Strasbourg, France; ⁹Diagnostic Genetic Laboratory, New Civil Hospital, Regional University Hospital Center, Strasbourg, France; ¹⁰Department of Neuropediatrics, Reference Center for Neuromuscular Diseases, Roger-Salengro Hospital, Regional University Hospital Center, Lille, France; ¹¹Unit of Neuromuscular Diseases, Department of Neurology, Mental Health, and Sensory Organs, Faculty of Medicine and Psychology, Sapienza University of Rome, Rome, Italy; ¹²Neuromuscular Diseases Centre, Department of Clinical Neurosciences, University Hospital of Nice, Nice, France; ¹³National Genotyping Center, Genomics Institute, Office of Atomic Energy and Alternative Energies, Evry, France; ¹⁴Department of Radiology, Neurolocomotor Division, Raymond Poincaré Hospital, University Hospitals Paris-Ile-de-France West, Public Hospital Network of Paris, Garches, France; and ¹⁵Versailles Saint-Quentin-en-Yvelines University, Versailles, France.

Address correspondence to Dr J. Laporte, IGBMC, 1 rue Laurent Fries, 67404 Illkirch, France. E-mail: jocelyn@igbmc.fr

Received Dec 23, 2016, and in revised form Jan 27, 2017 and Feb 13, 2017. Accepted for publication Feb 13, 2017.

View this article online at wileyonlinelibrary.com. DOI: 10.1002/ana.24900

institutional review board approved (DC-2012-1693). Because facial features are part of the clinical picture, Patients 1 and 2 have kindly consented to use of their clinical photographs

without masking of their faces. Patient 3 was seen in 1993 and not available to give consent, so facial features are masked to prevent identification.

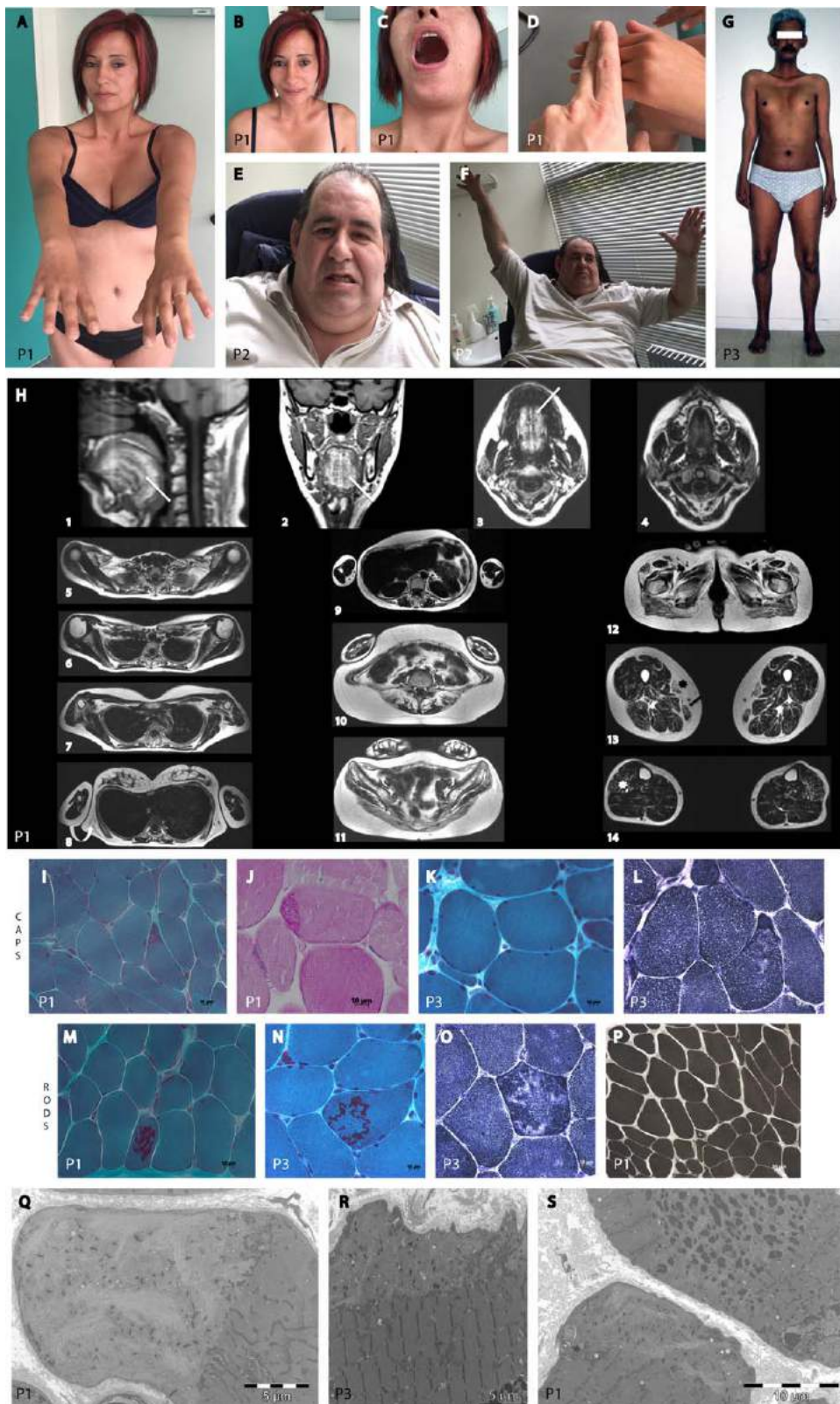


FIGURE 1.

TABLE. Clinical Features of Patients with MYPN Mutations

Characteristic	Family 1, Patient 1	Family 1, Patient 2	Family 2, Patient 3
Gender	F	M	M
Age at onset	Birth	3 months	Early childhood
Initial symptoms	Mild hypotonia, swallowing difficulties, lower limb contractures	Swallowing difficulties, delayed motor development	Upper limb weakness
Disease course	Slowly progressive	Progressive (wheelchair-bound at age 49 years)	Slowly progressive
Age at examination	34	50	44
Clinical features	Asymmetric facial weakness; shoulder, hip-girdle, axial, and milder tibial muscle weakness; neck extensors and flexors (MRC 4), proximodistal weakness (3–4), finger extensor (2)	Severe asymmetric facial weakness; severe asymmetric shoulder, hip-girdle, and axial muscle weakness; severe finger extensors and flexors; radial and interosseous hand muscles (MRC 3), pelvic girdle (1–2), distal leg muscles (1–2)	Facial, shoulder, hip-girdle, axial, severe finger extensors and flexors and tibial muscles weakness; neck flexors (MRC 2), abdominal muscle (2–3), proximodistal weakness (2–3)
Respiratory involvement	Reduced forced expiratory volume 57% and NIV; recurrent respiratory infections	Recurrent respiratory infections	Reduced vital capacity 46%
Cardiac examination	Normal	Mild cardiac involvement: asynchronous myocardial contraction, mild thickening of heart muscle, tachycardia	Normal
EMG	Myopathic	Myopathic	Myopathic

EMG = electromyography; F = female; M = male; MRC = Medical Research Council scale for muscle strength; NIV = noninvasive ventilation.

FIGURE 1: Characterization of patients. Clinical features: (A–D) Patient 1. (A) Pectus excavatum, shoulder girdle asymmetric amyotrophy, and weakness with deficit in arm elevation. (B) Elongated face, ptosis of left eye, tubular nose, and asymmetric facial weakness. (C) High-arched palate. (D) Finger extensors weakness. (E, F) Patient 2. (E) Severe facial weakness, elongated face, low-set ears, and tubular nose. (F) Asymmetric deficit in arm elevation, marked obesity. (G) Patient 3 with elongated face, tubular nose, low-set ears, pectus excavatum, amyotrophy of shoulder girdle and pectoral muscles, and atrophic legs. (H) Whole body magnetic resonance imaging of Patient 1 with Dixon method (iterative decomposition of water and fat with echo asymmetry and least-squares estimation). At the head level (1–4), fatty infiltrations of the tongue are visible (*white arrows*), whereas masticatory muscles are normal. At the scapular girdle level (5–7), muscles are thin and slightly atrophic without fatty infiltrations. At the trunk level (8–11), major fatty infiltrations of the latissimus dorsi (*curved arrow*) and an asymmetric deformity of the chest with a shrunken space between sternum and spine are seen. Rotator and extensor muscles of the back at the lumbar area (10, 11) are either infiltrated with fat or atrophic. At the pelvic girdle level (12), muscles are thin and infiltrated with fat. At the thigh level (13), slight atrophy and fatty infiltration are visible, and the sartorius (*black asterisk*) and the gracilis (*black arrow*) are the most atrophic and fat-infiltrated muscles. At the level of the lower leg (14), fatty infiltrations are especially seen in the peroneus muscles (*white asterisk*). Light microscopy: (I–L) Caps and (M–O) rods in Patient 1 and Patient 3 muscles. Caps are intensively stained with modified Gomori trichrome (mGT) (I,K), periodic acid–Schiff (J), and nicotinamide adenine dinucleotide–tetrazolium reductase (NADH-TR) techniques (L). Presence of cytoplasmic fuchsinophilic inclusions corresponding to rods with mGT staining (M, N); areas containing rods are devoid of oxidative NADH-TR activity (O). (P) Adenosine triphosphatase pH9.4 demonstrates type 1 fiber uniformity. (Q–S) Electron micrographs from Patient 1 and Patient 3 muscles showing well-delimited caps filled with thin filaments, sarcomere fragments, and cellular debris. (S) Presence of a fiber containing a cap next to a fiber with cytoplasmic rods.

Morphological Analysis

For histochemical techniques, 10 μm-thick cryostat sections were used. Photographs were obtained with a Zeiss AxioCam

HRC linked to a Zeiss Axioplan Bright Field Microscope and processed with Axio Vision 4.4 software (Carl Zeiss, Oberkochen, Germany). Antimyopalladin (gift of Dr Labeit⁹ and anti-

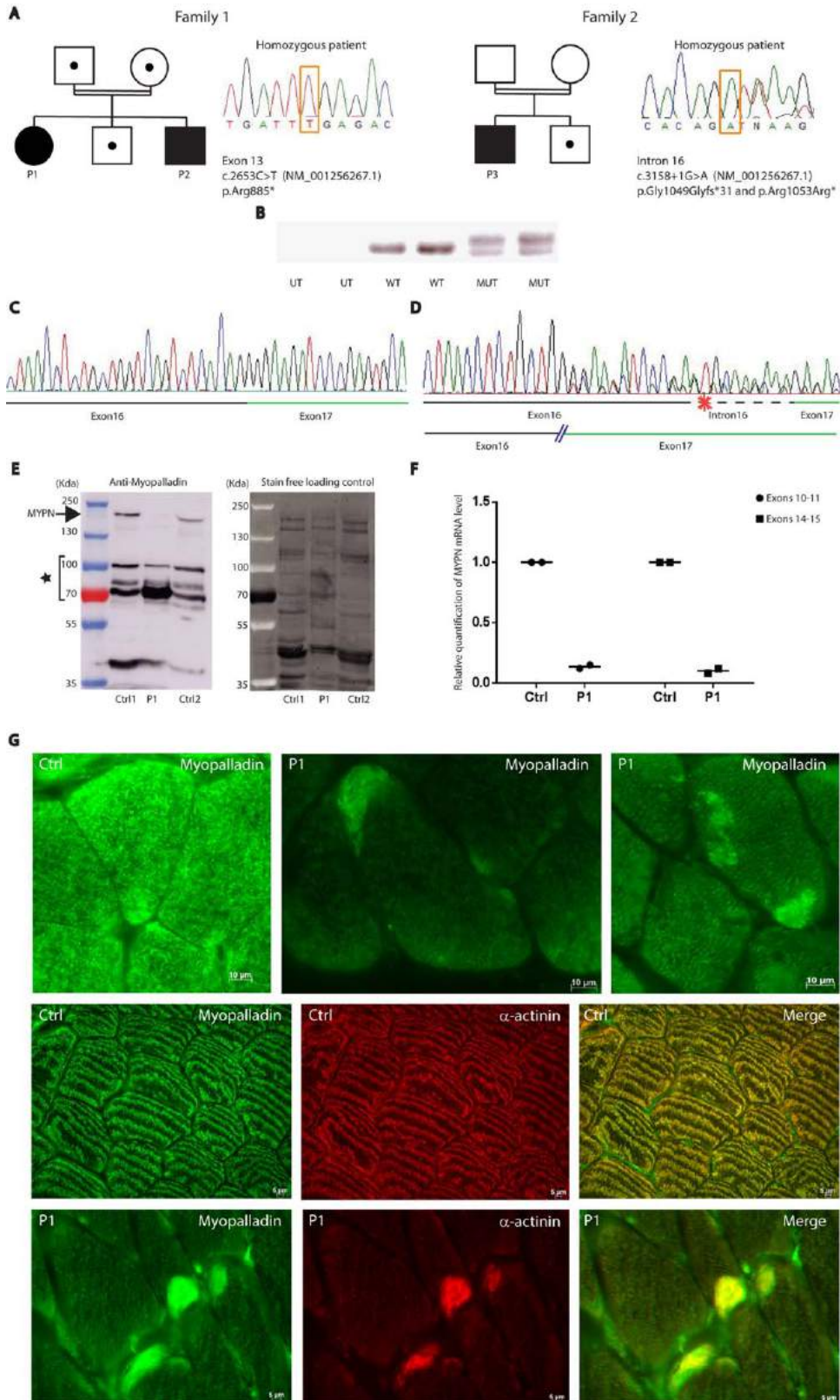


FIGURE 2.

alpha-actinin (EA-53; Sigma, Saint Louis, MO) antibodies were used for immunohistochemistry.

Exome Sequencing

Exome sequencing was performed for Patients 1 and 3 with the SureSelect Human All Exon 50Mb Capture Library v5 (Agilent, Santa Clara, CA) and paired-end sequenced on a HiSeq 2500 (Illumina, San Diego, CA). Confirmation of variants and segregation was performed by Sanger sequencing. No pathogenic variants were detected in any genes previously linked to muscular diseases.

Splicing Studies

A genomic DNA fragment encompassing *MYPN* exons 15 to 17 was amplified and cloned into pcDNA3.1 (Invitrogen, Carlsbad, CA) and the Patient 3 c.3158 + 1G>A mutation affecting the exon 16 donor site was introduced by site-directed mutagenesis (Stratagene, San Diego, CA). Wild-type and mutant constructs were transfected by Lipofectamine 3000 (Thermo Fisher Scientific, Waltham, MA) into COS-1 and HeLa cells. Total RNA was extracted after 24 hours and analyzed by reverse transcriptase polymerase chain reaction (RT-PCR).

Quantitative PCR

RNA was extracted from deltoid muscle samples of Patient 1 and age-matched controls using the Precellys 24 homogenizer (Bertin Technologies, Montigny-le-Bretonneux, France). Relative expression of *MYPN* was measured with SYBR Green PCR Master Mix (Qiagen, Hilden, Germany) on a LightCycler 480 Real-Time PCR System (Roche, Basel, Switzerland) using human *MYPN*- and *HPRT1*-specific primer sets.

Western Blot

Myopalladin was detected in total muscle protein extracts of Patient 1 with an antibody targeting its N-terminus (ab57853; Abcam, Cambridge, MA). Immunoblots were

visualized using the SuperSignal West Pico Chemiluminescent Substrate (Thermo Fisher Scientific) on an Amersham Imager 600 (GE Healthcare Life Sciences, Chicago, IL). Loading was verified with the stain-free technique (trichloroethylene, Sigma).

Results

Common Clinical Findings in *MYPN* Patients

A clinical summary is provided in the Table. Patients 1 and 2 from Family 1 are siblings born to healthy consanguineous French parents as previously described,¹⁴ and Patient 3 from Family 2 was born to consanguineous African parents from Mauritania. Initial symptoms were neonatal hypotonia and swallowing difficulties for Patients 1 and 2, and upper limb weakness from early childhood for Patient 3. Patients 1 and 2 showed asymmetric facial weakness. All patients displayed skeletal deformities and progressive limb girdle, axial, and distal weakness involving finger flexors and extensors, and tibialis anterior muscles (Fig 1A–G). Serum creatine kinase levels were normal, and electromyography was myopathic in all patients. Patients 1 and 3 had respiratory involvement. Cardiac workup including electrocardiography (EKG) and echocardiography were normal for Patients 1 and 3. In Patient 2, EKG revealed sinus tachycardia, increased QRS duration, and left axis deviation, and echocardiography at 48 years disclosed asynchronous myocardial contraction, mild thickening of heart muscle, and anterior pericardial detachment interpreted as consequences of hypertensive state.

Whole body magnetic resonance imaging of Patient 1 revealed a globally thin muscle bulk, and prominent fatty infiltrations in the tongue, latissimus dorsi, pelvic

FIGURE 2: *MYPN* mutations, segregation, and impact. (A) Pedigree from consanguineous Families 1 and 2 and chromatophograms. Patients 1 and 2 are homozygous for the c.2653C>T (p.Arg885*) nonsense mutation in exon 13, and Patient 3 is homozygous for the c.3158 + 1G>A essential splice site mutation in intron 16 (p.Gly1049Glyfs*31 and p.Arg1053Arg*1). Unaffected relatives are heterozygous (dots); neither parent from Family 2 was available for sequencing. (B) Because muscle from Patient 2 was unavailable for RNA extraction, minigene constructs harboring the mutation found in Patient 2 were transfected in COS-1 cells, and the reverse transcriptase polymerase chain reaction (RT-PCR) product from exons 15 to 17 was migrated on an agarose gel. MUT = c.3158 + 1G>A construct; UT = untransfected; WT = wild-type construct. The wild-type fragment was detectable in cells expressing the wild-type construct, whereas 2 abnormal fragments were found in cells expressing the mutant minigene. (C, D) Sanger sequencing of control amplicon (C) and of mutated amplicons (D) confirmed the disruption of the canonical donor site in Patient 2 and the usage of 2 cryptic donor sites producing 2 aberrant RNA species containing either a shorter exon 16 leading to a frameshift (p.Gly1049Glyfs*31), or part of intron 16 encompassing an in-frame stop codon (p.Arg1053Arg*). No wild-type RNA was detected for the mutant. Similar results were obtained after construct transfection in HeLa cells (not shown). (E) Left: Western blot showing myopalladin level (arrow) in muscle extracts from Patient 1 compared to age-matched controls, detected with an anti-N-terminal antibody (epitope aa 61-171). Full-length myopalladin (around 145 kDa) is strongly decreased in the patient. The star indicates unspecific signals or uncharacterized shorter myopalladin isoforms similar in both control and patient. Right: Total proteins labeled with the stain-free technique were used as a loading control. (F) Relative quantification of myopalladin mRNA level from Patient 1 muscle by quantitative RT-qPCR using primers located in 5' (exons 10–11) and in 3' (exons 14–15) of the mutation. The level of myopalladin mRNA is decreased to 10% in both cases (2 independent experiments). (G) Upper panels: Immunostaining with an anti-myopalladin N-terminal antibody shows a homogeneous striated pattern of myopalladin at the Z-line in the control (left) and decreased striated pattern and significant accumulation inside the caps (middle) and rods (right) in Patient 1 muscle. Middle panels: Coimmunostaining of myopalladin and alpha-actinin in control muscle. Myopalladin and alpha-actinin colocalize at the Z-line. Bottom panels: Coimmunostaining of myopalladin and alpha-actinin in Patient 1 muscle. Alpha-actinin concentrates in the caps.

girdle, lower limbs (especially sartorius, gracilis, and peroneus), and extensor muscles of the dorsal and lumbar areas (see Fig 1H).

Biopsies from MYPN Patients Display Caps and Rods

Morphological investigations of muscle by light and electron microscopy revealed subsarcolemmal caps in 5 to 10% of the fibers. Caps were intensively stained with modified Gomori trichrome (mGT), periodic acid–Schiff, and nicotinamide adenine dinucleotide–tetrazolium reductase (see Fig 1I–L), and did not stain with adenosine triphosphatase and succinate dehydrogenase (not shown), suggesting that they lack mitochondria. In about 2% of myofibers, mGT staining uncovered fuchsinophilic inclusions consistent with clusters of cytoplasmic rods disposed in a rosette/garland fashion. Areas containing rods were devoid of oxidative activity (see Fig 1M–O). Marked type 1 fiber predominance or uniformity and mild fiber size variability, common features associated with congenital myopathies, were also observed in all patients (see Fig 1P).

Electron microscopy demonstrated the presence of peripherally placed and well-demarcated caps (see Fig 1Q, R) containing accumulated thin filaments, Z-line fragments, and cellular debris. Clusters of cytoplasmic rods harboring the typical Z-line lattice structure were also identified (see Fig 1S).

Exome Sequencing Identified MYPN Mutations

By exome sequencing, we identified homozygous *MYPN* mutations in both families: a c.2653C>T (p.Arg885*) nonsense mutation in Family 1 and the c.3158 + 1G>A mutation affecting the essential donor splice site of exon 16 in Family 2. Each variant is listed once in the ExAC database at the heterozygous state (0.00082%). Both variants were homozygous in all affected family members and heterozygous in the available healthy family members (Fig 2A).

The impact of the c.3158 + 1G>A variant on splicing was tested through a minigene experiment. In contrast to cells transfected with the wild-type minigene, the inclusion of the variant causes the appearance of 2 splice products revealing the disruption of the canonical donor site and the usage of 2 cryptic donor sites producing 2 aberrant RNA species (see Fig 2B–D). One cryptic site resides within exon 16 and generates a frameshift from amino acid 1049 (p.Gly1049Glyfs*31), and the other site located in intron 16 leads to the inclusion of an intronic sequence containing an in-frame stop codon p.Arg1053Arg*.

To assess the impact of the p.Arg885* nonsense mutation of Family 1 on protein stability and to verify the potential presence of a 885-amino-acid myopalladin fragment,

we performed Western blot analysis of muscle extracts from Patient 1. We observed a strong reduction of full-length 1,320-amino-acid myopalladin and no signal corresponding to the putative 885aa fragment (see Fig 2E). Moreover, *MYPN* muscle RNA was found strongly reduced to around 10% of the normal level by quantitative RT-PCR, strongly suggesting nonsense-mediated mRNA decay as the cause of decreased full-length protein (see Fig 2F).

Z-Line Proteins Accumulate in the Caps

Immunolabeling of Patient 1 muscles revealed decreased Z-line staining and accumulations of myopalladin inside the caps and rods (see Fig 2G), suggesting the presence of either remaining truncated myopalladin concentrated at the caps or uncharacterized myopalladin isoforms devoid of the mutated sequence. Coimmunostaining of myopalladin and its binding partner alpha-actinin demonstrated colocalization at the Z-line in control muscle and decreased Z-line staining of alpha-actinin that accumulates within the caps in the patient (see Fig 2G). The intermediate filament desmin also intensively labeled the caps (not shown).

Discussion

Here we describe a new cap myopathy due to recessive *MYPN* mutations and resulting in myopalladin deficiency. Our patients presented with a slowly progressive condition involving asymmetric weakness, an unusual feature in congenital myopathies. Myopalladin and its interactor, the Z-line marker alpha-actinin, were found accumulated in both caps and rods, supporting an important role of myopalladin in the structural maintenance of Z-line and sarcomere.^{9,10}

Our patients are clinically and histologically similar to cap myopathy caused by tropomyosin genes mutations.¹⁵ *TPM1* mutations are associated with familial hypertrophic cardiomyopathy, and mutations in *TPM2* and *TPM3* cause cap and nemaline myopathies.^{7,16,17} We hereby show that similarly to tropomyosin-related disorders, mutations in *MYPN* can cause either a cardiomyopathy or a congenital cap myopathy. Recently, biallelic *MYPN* mutations have been reported in a childhood-onset, slowly progressive nemaline myopathy with intranuclear rods.¹⁸ All our patients presented typical caps as main histologic lesion and occasional rods disposed in a peculiar rosette/garland fashion in the myofiber cytoplasm. Intranuclear rods were not observed. We therefore propose *MYPN* as a new gene responsible for cap myopathy. Dominant *MYPN* mutations were previously linked to cardiomyopathies, and the p.Arg885* variant was also reported in 1 patient with hypertrophic cardiomyopathy at the heterozygous state.¹³ Our patients

and their heterozygous family members failed to show overt cardiomyopathy at the age of examination. The minimal cardiac alterations observed in Patient 2 seem to be related to obesity and hypertension, but an incomplete penetrance of the p.Arg885* mutation cannot be excluded. Functional analyses of *MYPN*-related cardiomyopathy mutations in transfected rat cardiomyocytes and in a knockin Q526X *Mypn* mouse suggested a dominant-negative effect rather than a haploinsufficiency as the underlying mechanism.^{11,19}

In conclusion, our findings reveal that mutations in *MYPN* cause recessive congenital cap myopathy.

Acknowledgment

This study was supported by the National Institute of Health and Medical Research, National Center for Scientific Research, University of Strasbourg, France Genomics (ANR-10-INBS-09) and Rare Diseases Foundation within the frame of the Myocapture project, French Association against Myopathies, Foundation for Medical Research (DBI20131228569), Public Hospital Network of Paris, French Society of Neurology, and Association Institute of Myology.

We thank the patients and families; M. Ney, G. Brochier, and M. T. Bui for technical assistance; and C. Wallgren-Pettersson for *NEB* exclusion.

Author Contributions

E.M., J.B., N.B.R., and J.L. conceived and designed the study; X.L., E.M., C.C., R.S., V.B., J.-M.C., M.G., B.E., M.F., A.B., J.-F.D., J.T., and R.-Y.C. acquired and analyzed the data; X.L., E.M., and J.L. wrote the manuscript. X.L. and E.M. contributed equally.

Potential Conflicts of Interest

Nothing to report.

References

1. Ravenscroft G, Laing NG, Bonnemann CG. Pathophysiological concepts in the congenital myopathies: blurring the boundaries, sharpening the focus. *Brain* 2015;138(pt 2):246–268.

2. Romero NB, Clarke NF. Congenital myopathies. *Handb Clin Neurol* 2013;113:1321–1336.
3. Fidzianska A, Badurska B, Ryniewicz B, Dembek I. "Cap disease": new congenital myopathy. *Neurology* 1981;31:1113–1120.
4. De Paula AM, Franques J, Fernandez C, et al. A TPM2 mutation causing cap myopathy. *Neuromuscul Disord* 2009;19:685–688.
5. Ohlsson M, Quijano-Roy S, Darin N, et al. New morphologic and genetic findings in cap disease associated with beta-tropomyosin (TPM2) mutations. *Neurology* 2008;71:1896–1901.
6. Ohlsson M, Fidzianska A, Tajsharghi H, Oldfors A. TPM3 mutation in one of the original cases of cap disease. *Neurology* 2009;72:1961–1963.
7. Marttila M, Lehtokari VL, Marston S, et al. Mutation update and genotype-phenotype correlations of novel and previously described mutations in TPM2 and TPM3 causing congenital myopathies. *Hum Mutat* 2014;35:779–790.
8. Otey CA, Rachlin A, Moza M, et al. The palladin/myotilin/myopalladin family of actin-associated scaffolds. *Int Rev Cytol* 2005;246:31–58.
9. Bang ML, Mudry RE, McElhinny AS, et al. Myopalladin, a novel 145-kilodalton sarcomeric protein with multiple roles in Z-disc and I-band protein assemblies. *J Cell Biol* 2001;153:413–427.
10. Ma K, Wang K. Interaction of nebulin SH3 domain with titin PEVK and myopalladin: implications for the signaling and assembly role of titin and nebulin. *FEBS Lett* 2002;532:273–278.
11. Duboscq-Bidot L, Xu P, Charron P, et al. Mutations in the Z-band protein myopalladin gene and idiopathic dilated cardiomyopathy. *Cardiovasc Res* 2008;77:118–125.
12. Meyer T, Ruppert V, Ackermann S, et al. Novel mutations in the sarcomeric protein myopalladin in patients with dilated cardiomyopathy. *Eur J Hum Genet* 2013;21:294–300.
13. Purevjav E, Arimura T, Augustin S, et al. Molecular basis for clinical heterogeneity in inherited cardiomyopathies due to myopalladin mutations. *Hum Mol Genet* 2012;21:2039–2053.
14. Cuisset JM, Maurage CA, Pellissier JF, et al. 'Cap myopathy': case report of a family. *Neuromuscul Disord* 2006;16:277–281.
15. Schreckenbach T, Schroder JM, Voit T, et al. Novel TPM3 mutation in a family with cap myopathy and review of the literature. *Neuromuscul Disord* 2014;24:117–124.
16. Piteau SJ, Rossiter JP, Smith RG, MacKenzie JJ. Congenital myopathy with cap-like structures and nemaline rods: case report and literature review. *Pediatr Neurol* 2014;51:192–197.
17. Malfatti E, Schaeffer U, Chapon F, et al. Combined cap disease and nemaline myopathy in the same patient caused by an autosomal dominant mutation in the TPM3 gene. *Neuromuscul Disord* 2013;23:992–997.
18. Miyatake S, Mitsuhashi S, Hayashi YK, et al. Biallelic mutations in *MYPN*, encoding myopalladin, are associated with childhood-onset, slowly progressive nemaline myopathy. *Am J Hum Genet* 2017;100:169–178.
19. Huby AC, Mendsaikhan U, Takagi K, et al. Disturbance in Z-disk mechanosensitive proteins induced by a persistent mutant myopalladin causes familial restrictive cardiomyopathy. *J Am Coll Cardiol* 2014;64:2765–2776.

2.3.2 Publication 13: *ACTN2* mutations cause “Multiple structured Core Disease” (MsCD) (Lornage et al. 2019)

Background

Core myopathy is histologically characterized by the focal absence of oxidative activity in the muscle fibers. Three subtypes of core myopathy have been described so far. Central core disease (CCD) is characterized by well-delimited areas with absence of oxidative activity and running along all the length of the fiber. Multiminicore disease (MmD) is defined by poorly-delimited cores spanning only to a limited zone of the longitudinal fiber axis, and dusty core disease (DucD) is recognizable by the presence of cores surrounded by a reddish-purple material on modified Gomori trichrome staining (Dubowitz and Pearse 1960; Engel, Gomez, and Groover 1971; Garibaldi et al. 2019).

Aim of the study

The aim of the study was to identify the genetic cause of the disease in two families with a new form of core myopathy.

Results

We studied two patients with neonatal hypotonia and a progressive disease course involving muscle weakness and respiratory distress. The morphological and ultrastructural analyses of muscle biopsies revealed a distinctive pattern with the presence of small structured cores and jagged Z-lines, that we termed “Multiple structured-Core Disease” (MsCD). Exome sequencing of both affected individuals identified heterozygous mutations in *ACTN2*, encoding alpha-actinin-2, an actin-crosslinking protein localized at the Z-line and specifically expressed in skeletal muscle and heart. Alpha-actinin-2 is composed of three main domains, an N-terminal actin-binding domain, an elongated rod composed of four spectrin repeats, and a C-terminal part composed of two EF-hands domains (Ribeiro Ede et al. 2014). The missense mutation identified in patient 1 and the in-frame deletion detected in patient 2 reside in close proximity within the rod domain. Functional analyses were performed on the missense mutation and showed that alpha-actinin-2 p.(Leu727Arg) localized to the Z-line in differentiated myotubes, and retained its ability to dimerize in transfected cells. Modelling of the disease was performed in zebrafish and mice by exogenous expression of the wild-type (control) or mutated protein. Mutant zebrafish were smaller than controls, and showed altered myofiber architecture and motor deficits. AAV-transduced murine muscles developed muscle weakness, core myopathy and Z-line defects, similar to the defects observed in the patient biopsies. Taken together, the

experiments in the animal models confirmed the pathogenicity of the mutation at the histological and physiological level.

Conclusion


Alpha-actinin-2 deficiency has been shown to lead to sarcomeric defects in both skeletal muscle and heart in zebrafish (Gupta et al. 2012), thereby highlighting the crucial role of alpha-actinin-2 in striated muscles. Dominant *ACTN2* mutations have previously been described in patients with dilated and hypertrophic cardiomyopathies (Chiu et al. 2010), and our results show that distinct *ACTN2* mutations are the cause of MsCD.

Contribution

I identified the *ACTN2* missense mutation and verified the segregation in the family members. I also performed all functional experiments in the cell and mouse models, and wrote the publication with other authors.



ACTN2 mutations cause “Multiple structured Core Disease” (MsCD)

Xavière Lornage^{1,2,3,4} · Norma B. Romero^{5,6,7} · Claire A. Grosogoeat⁸ · Edoardo Malfatti^{6,7,9} · Sandra Donkervoort¹⁰ · Michael M. Marchetti⁸ · Sarah B. Neuhaus¹⁰ · A. Reghan Foley¹⁰ · Clémence Labasse^{6,7} · Raphaël Schneider^{1,2,3,4} · Robert Y. Carlier^{11,12} · Katherine R. Chao¹³ · Livija Medne¹⁴ · Jean-François Deleuze¹⁵ · David Orlikowski¹⁶ · Carsten G. Bönnemann¹⁰ · Vandana A. Gupta⁸ · Michel Fardeau^{5,6,7} · Johann Böhm^{1,2,3,4} · Jocelyn Laporte^{1,2,3,4} 

Received: 23 October 2018 / Revised: 17 January 2019 / Accepted: 18 January 2019 / Published online: 30 January 2019
© Springer-Verlag GmbH Germany, part of Springer Nature 2019

Abstract

The identification of genes implicated in myopathies is essential for diagnosis and for revealing novel therapeutic targets. Here we characterize a novel subclass of congenital myopathy at the morphological, molecular, and functional level. Through exome sequencing, we identified de novo *ACTN2* mutations, a missense and a deletion, in two unrelated patients presenting with progressive early-onset muscle weakness and respiratory involvement. Morphological and ultrastructural analyses of muscle biopsies revealed a distinctive pattern with the presence of muscle fibers containing small structured cores and jagged Z-lines. Deeper analysis of the missense mutation revealed mutant alpha-actinin-2 properly localized to the Z-line in differentiating myotubes and its level was not altered in muscle biopsy. Modelling of the disease in zebrafish and mice by exogenous expression of mutated alpha-actinin-2 recapitulated the abnormal muscle function and structure seen in the patients. Motor deficits were noted in zebrafish, and muscle force was impaired in isolated muscles from AAV-transduced mice. In both models, sarcomeric disorganization was evident, while expression of wild-type alpha-actinin-2 did not result in muscle anomalies. The murine muscles injected with mutant *ACTN2* displayed cores and Z-line defects. Dominant *ACTN2* mutations were previously associated with cardiomyopathies, and our data demonstrate that specific mutations in the well-known Z-line regulator alpha-actinin-2 can cause a skeletal muscle disorder.

Keywords ACTN2 · Alpha-actinin-2 · Congenital myopathy · Core myopathy · Z-line · Nemaline myopathy

Introduction

Congenital myopathies are a group of heterogeneous genetic diseases usually associated with neonatal or early-onset hypotonia and muscle weakness, and they are characterized by distinctive alterations on muscle biopsies [13, 33, 40]. Although approximately 30 causative genes are known to date (www.muscle.genetable.fr), nearly half of the patients

with congenital myopathies do not have a molecular diagnosis despite routine access to next-generation sequencing, suggesting the implication of yet unidentified genes. The identification of novel causative genes is a prerequisite to understand the pathophysiological mechanisms underlying muscle dysfunction, and can suggest new and alternative therapeutic targets.

Congenital myopathies are classified into distinct subgroups based on characteristic histopathological features on muscle biopsies. Most patients fall into one of the three main groups encompassing centronuclear myopathy with numerous fibers containing internal or centralized nuclei, nemaline myopathy showing protein aggregates or rod inclusions, and core myopathy with fiber areas devoid of oxidative activity [40, 42]. Central core disease (CCD) is characterized by well-delimited cores running along the longitudinal myofiber axis, while multimincore disease (MmD) typically displays multiple, poorly defined, small cores spanning only a limited zone on the longitudinal axis of the muscle fiber [9, 12, 14].

Xavière Lornage and Norma B. Romero contributed equally to this work
Claire A. Grosogoeat and Edoardo Malfatti contributed equally to this work

Johann Böhm and Jocelyn Laporte contributed equally to this work

Electronic supplementary material The online version of this article (<https://doi.org/10.1007/s00401-019-01963-8>) contains supplementary material, which is available to authorized users.

✉ Jocelyn Laporte
jocelyn@igbmc.fr

Extended author information available on the last page of the article

Here we describe a peculiar form of core myopathy with ultrastructural Z-line alterations caused by mutations in *ACTN2*, encoding alpha-actinin-2 (MIM*102573).

ACTN1, *ACTN2*, *ACTN3*, and *ACTN4* form an evolutionary conserved gene family with different tissue-specific expression pattern [32]. *ACTN3* is expressed in skeletal muscle and *ACTN2* is expressed in both skeletal and cardiac muscle. *ACTN3* deficiency is common in humans and influences athletic performances [35], and dominant mutations in *ACTN2* have been reported to cause dilated or hypertrophic cardiomyopathy (MIM #612158 [6]).

Alpha-actinin-2 is one of the major components of the Z-line. It is active as a dimer, allosterically regulated by phosphoinositides [5, 38], and is essential for the integrity of the contractile apparatus through a multitude of interactions. Notably, it binds and crosslinks actin filaments, and anchors many cytoskeletal and sarcomeric proteins such as myopalladin [1], myotilin [41], muscle LIM protein [31], and the giant proteins titin [11, 26] and nebulin [34]. Moreover, alpha-actinin-2 is believed to make a link between the sarcomere and the membrane through interactions with vinculin [30], integrins [36], and the dystrophin complex [21]. Alpha-actinin-2 is also involved in the regulation of ion channels [8, 28], gene expression [23], and signalling cascades [39, 46], making it a multitasking protein with a central role in skeletal muscle physiology. Indeed, alpha-actinin-2 deficiency in the zebrafish was shown to result in sarcomeric defects, confirming its crucial role for the formation and/or maintenance of sarcomeres [19].

This report describes *ACTN2* mutations as the cause of a congenital myopathy with numerous structured cores and jagged Z-lines as the main and specific histological hallmark, and we evidence our findings by functional investigations in cell and animal models. Exogenous expression of mutant alpha-actinin-2 in mice and zebrafish induced muscle weakness and a histopathology corresponding to the unique structural aberrations characterizing the patient biopsies. The implication of *ACTN2* in a skeletal muscle disease and the peculiar histopathology define an additional class of core myopathy.

Materials and methods

DNA sampling

Sample collection was performed with written informed consent from patients P1 and P2 according to the declaration of Helsinki and its later amendments. DNA storage and usage was approved by the institutional review board (DC-2012-1693 and 12-N-0095).

MRI

Whole-body MRI in P1 was performed on a 3T magnet system using the Dixon method to obtain T1- and T2-weighted scans. Images were then post-processed with multiplanar reconstructions and 3D volume rendering. Analysis was performed for a selection of 100 muscles manifesting atrophy and fatty infiltrations as described previously [4]. 3D volume rendering images allowed a global analysis in horizontal position. Lower extremity MRI in P2 was performed on a 3T Siemens Magnetom Verio system using the Dixon method to obtain T1 and STIR-weighted scans.

Exome sequencing and analysis

Library preparation and exome capture were performed with the SureSelect Human All Exon 50 Mb Capture Library v5 (Agilent, Santa Clara, USA) for P1 and his healthy family members, and with the Nextera Rapid Capture (Illumina, San Diego, USA) for P2 and her healthy parents, and samples were paired-end sequenced on a HiSeq 2500 (Illumina). Sequence data were aligned to the GRCh37/hg19 reference genome, and variants were filtered considering their frequency in gnomAD (<http://gnomad.broadinstitute.org/>) and in our in-house database containing 1550 exomes and genomes. The mutations were numbered according to GenBank NM_001103.3 and NP_001094.1 with +1 corresponding to the A of the ATG translation initiation codon. Confirmation of variants and segregation was performed by Sanger sequencing. P1 was heterozygous and P2 homozygous for the common p.(Arg577*) *ACTN3* variation.

Morphological studies

For P1, open deltoid muscle and radial muscle biopsies were, respectively, obtained at 9 and 45 years of age. Conventional histological and histochemical techniques on 10 µm cryostat sections encompassed haematoxylin and eosin (H&E), Gomori trichrome (GT), nicotinamide adenosine dinucleotide–tetrazolium reductase (NADH-TR), succinate dehydrogenase (SDH), and myosin adenosine triphosphatase (ATPase pH 9.4) reactions. Digital photographs were obtained with a Zeiss AxioCam HRc linked to a Zeiss Axioplan Bright Field Microscope and processed with the Axio Vision 4.4 software (Zeiss, Oberkochen, Germany).

For P2, open muscle biopsy of the quadriceps was obtained at 19 years of age. Digital photographs were obtained with a Zeiss AxioCam MRc5 linked to a Zeiss Imager Bright Field Microscope and processed with the AxioVision software (Zeiss).

Murine tibialis anterior muscles were sampled in isopentane cooled in liquid nitrogen, and transversal or longitudinal

cryosections (8 μm) were fixed and stained with H&E, SDH, and GT. Images were acquired with the Hamamatsu NanoZoomer 2HT slide-scanner (Hamamatsu, Hamamatsu city, Japan).

Electron microscopy

The P1 patient biopsies were fixed with glutaraldehyde (2.5%, pH 7.4), post fixed with osmium tetroxide (2%), dehydrated, and embedded in resin (EMBed-812, Electron Microscopy Sciences, Hatfield, USA). Ultra-thin sections were stained with uranyl acetate and lead citrate, and observed using a Philips CM120 electron microscope (Philips, Amsterdam, Netherlands) and photo-documented using a Morada camera (Soft Imaging System, Münster, Germany). EM was not available for P2.

Murine TA muscles were fixed in 4% PFA and 2.5% glutaraldehyde in 0.1 M phosphate buffer (pH 7.2) overnight at 4 °C and processed as previously described [7]. Images were recorded on a Philips CM12 electron microscope (Philips).

Three dpf zebrafish larvae were fixed in formaldehyde-glutaraldehyde-picric acid in cacodylate buffer overnight at 4 °C, followed by osmication and uranyl acetate staining. Subsequently, embryos were dehydrated in a series of ethanol washes and embedded in TAAB Epon (Marivac Ltd., Halifax, Canada). Sections (95 nm) were cut with a Leica UltraCut microtome (Leica, Wetzlar, Germany), picked up on 100- μm Formvar-coated copper grids, and stained with 0.2% lead citrate. Sections were viewed and imaged with a Philips Tecnai BioTwin Spirit electron microscope (Philips) at the Harvard Medical School Electron Microscopy Core.

Cell culture, transfection, and differentiation

The pEGFP-ACTN2 construct was a kind gift from Johannes Hell (Addgene plasmid #52669) [20]. The patient's mutation was introduced by site-directed mutagenesis using the QuikChange II kit (Stratagene, San Diego, USA). C2C12 cells were transfected with wild-type and mutant constructs using Lipofectamine 3000 (Thermo Fisher Scientific, Waltham, USA), and fixed after 24 h. For differentiation, cells were plated on a BD Matrigel™ Basement Membrane Matrix (Becton–Dickinson, Franklin Lakes, USA) 24 h before transfection, and serum-free differentiation medium was applied on confluent cells. Myotubes were fixed at day 8, and immunolabelling was performed as described below.

Immunolocalization

For immunohistochemistry, transverse muscle sections were frozen in isopentane, and longitudinal sections were fixed at 4 °C in 4% PFA for 24 h and incubated overnight in 30% sucrose at 4 °C. Myoblasts and myotubes were fixed during

20 min in 4% PFA. Permeabilization was performed with PBS-Triton 0.2% and saturation with FCS 10% in PBS. Following primary and secondary antibodies were used: rabbit anti-alpha-actinin-2 (ab68167, Abcam, Cambridge, UK), mouse anti-vinculin (V9131, Sigma, St. Louis, USA), Alexa Fluor 488 or 594 goat anti-mouse or anti-rabbit antibodies (Invitrogen, Carlsbad, USA). Images were taken using a SP5-UV confocal microscope (Leica).

Protein studies

For western blot, total muscle lysates were prepared in a buffer containing 50 mM Tris, 100 mM NaCl, 1 mM EGTA, 0.5% NP-40, 0.5% Triton-X100, 0.1% SDS, 1 mM DTT, 1 mM PMSF, and a mix of protease inhibitors (Complete EDTA-free, Roche, Basel, Switzerland). For human muscles, 50 μg of protein extracts were loaded on a 10% SDS-PAGE gel. For murine muscles, 5 μg of protein extracts were loaded on 4–15% Mini-PROTEAN®TGX™ precast protein gel (Biorad, Hercules, USA). Following primary and secondary antibodies were used: rabbit anti-alpha-actinin-2 (ab68167, Abcam), rabbit anti-alpha-actinin-3 (ab68204, Abcam), mouse anti-actin (homemade), mouse anti-beta-tubulin (homemade), mouse anti-GAPDH (MAB374, Millipore, Burlington, USA), and horseradish peroxidase (Jackson immunoresearch Europe, Cambridgeshire, UK). Membranes were revealed with the Supersignal west pico kit (ThermoFisher Scientific), and all immunoblots were visualized on an Amersham Imager 600 (GE Healthcare Life Sciences, Chicago, USA).

Domain predictions and 3D protein modeling

Alpha-actinin-2 protein domains were annotated using InterPro [15] and the scheme was designed using IBS (Illustrator for Biological Sequences) [27]. The crystal structure data of human alpha-actinin-2 was obtained from the PDB database (4D1E) [38]. Molecular graphics and analyses were performed with the UCSF Chimera package. Chimera is developed by the Resource for Biocomputing, Visualization, and Informatics at the University of California, San Francisco (supported by NIGMS P41-GM103311) [37]. Structure was edited by adding arginine rotamers from the Dunbrack library [10].

Zebrafish experimentation

Zebrafish (*Danio rerio*) from the wild-type Tuebingen line were bred and maintained according to standard procedures [45]. Embryos were collected by natural spawning, staged by hours (hpf) or days (dpf) post fertilization [24], and raised at 28.5 °C in egg water. All animal works were performed with approval from the Institute animal care and user committee.

For mRNA overexpression, full-length human *ACTN2* cDNA optimized for expression in zebrafish was synthesized by Eurofins and cloned into a pCSDest destination vector (created by Nathan Lawson) using Gateway technology (Invitrogen). Mutagenesis to incorporate the substitution was performed using the GENEART kit (Invitrogen). Wild-type and mutant mRNA was synthesized in vitro using mMessage mMachine SP6 kit (Ambion, Austin, USA). We titrated the mRNA (50–250 ng) and injected 100–200 pg into embryos at the 1-cell stage, and subsequent phenotypic analyses were performed at 3 dpf.

For western blot, zebrafish larvae were homogenized in buffer containing Tris–Cl (20 mM, pH 7.6), NaCl (50 mM), EDTA (1 mM), Nonidet P-40 (0.1%) with complete protease inhibitor cocktail (Roche Applied Sciences, Indianapolis, USA). Primary antibodies were rabbit anti alpha-actinin-2 (4B3, Sigma) and mouse anti- β -actin (A5441, Sigma) [2]. Protein bands were quantified using Quantity One software (Biorad). Zebrafish swimming behavior was quantified using the Daniovision activity monitoring system (Noldus, Leesburg, USA). Single mRNA-injected larvae or uninjected controls were placed into 24-well plates. After a 10-min acclimation to the dark, larvae were stimulated by light exposure for 20 min. Swimming behavior was recorded over the entire 20 min period with an infrared light source and total distance travelled was quantified. Three independent trials were performed with larvae from different clutches, examining > 300 larvae within each group.

Whole-mount phalloidin staining for filamentous actin was performed on 3 dpf zebrafish larvae as described previously [3]. Briefly, larvae were fixed overnight in 4% PFA at 4 °C, then washed 2 × 10 min in PBS, 2 × 10 min in PBS-T (0.1% Tween-20), 1 × 60 min in PBS-TR (2% Triton X), and 2 × 5 min in PBS-T. Larvae were blocked in PBS-T containing 5% goat serum for 1 h at RT, and incubated with Alexa Fluor 488 phalloidin (A12379, Invitrogen) overnight at 4 °C. Larvae were washed 4 × 15 min in PBS-T before being mounted in 70% glycerol and visualized using a UltraVIEW VoX spinning disk confocal microscope (Perkin Elmer, Waltham, USA).

Mouse experimentation

C57B6/J mice were purchased at 3 weeks of age from Charles River (L'Arbresle, France), and housed in a temperature-controlled room and in ventilated cages. Experiments were conducted on males according to the French and European legislation on animal care and experimentation.

ACTN2 cDNA was cloned into the plasmid pAAV-MCS (Stratagene, La Jolla, USA) containing the CMV immediate early enhancer and promoter, the human growth hormone poly-adenylation signal and the AAV serotype 2 inverted terminal repeats (ITRs). An empty vector without

ACTN2 cDNA was used as control. pAAV expressing plasmids were co-transfected with pHelper (Stratagene) and pAAV2/9 packaging plasmid (PENN vector core) into a HEK293T-derived cell line using Polyethylenimine transfection reagent. AAV serotype 9 vectors were harvested 48 h after transfection from cell lysate treated with 100 U/mL Benzonase (Merck, Darmstadt, Germany). They were purified by iodixanol gradient ultracentrifugation, dialyzed and concentrated using AMICON Ultra-15 100 K in DPBS supplemented with 0.5 mM MgCl₂. Viral titers were determined by Q-PCR using the LightCycler480 SYBR Green I Master (Roche).

AAV injections were performed in 15 male C56B6/J mice. They were anesthetized by intraperitoneal injection of ketamine (20 mg/mL), and tibialis anterior muscles were injected with 20 μ L wild-type, mutant, or control AAV2/9 (5×10^{12} VG/mL). Mice were analyzed 4 weeks post injection as it was shown to be an adequate timing for AAV expression and appearance of morphological defects in skeletal muscle [7].

For in situ muscle force measurements, mice were anesthetized intraperitoneally with pentobarbital (50 mg/kg), and the distal tibialis anterior tendon was attached to the force transducer (Aurora Scientific, Aurora, Canada). The absolute maximal force was measured after tetanic stimulation of the sciatic nerve with a pulse frequency from 25 to 125 Hz. The specific maximal force was calculated by dividing the maximal force through the tibialis anterior muscle weight.

Results

Clinical description

P1 is the third child born to healthy non-consanguineous parents. First concerns arose during the neonatal period with moderate hypotonia and sucking difficulties. Cardiomegaly and heart failure were diagnosed at the age of 2 months, and disappeared by the age of 6 months following treatment with corticosteroids and digitalins. Subsequent cardiac follow-up was normal. The patient achieved independent ambulation from 20 months of age. He was examined at 9 years of age by one of us (MF) and followed for 38 years at the Myology Institute (Paris). At 9 years of age, the patient presented with diffuse muscle atrophy and extraocular muscle weakness. He underwent Achilles tendon release surgery at age 14 years, and a dorsal kyphoscoliosis was surgically corrected at 16 years of age. The patient lost ambulation at the age of 17 years. At the age of 35 years, respiratory insufficiency with a vital capacity reduced to 37% required night ventilation, which was later replaced by a tracheostomy. The last clinical examination at the age of 45 years revealed generalized atrophy, bilateral ptosis, ophthalmoparesis,

P1 at 45 years of age



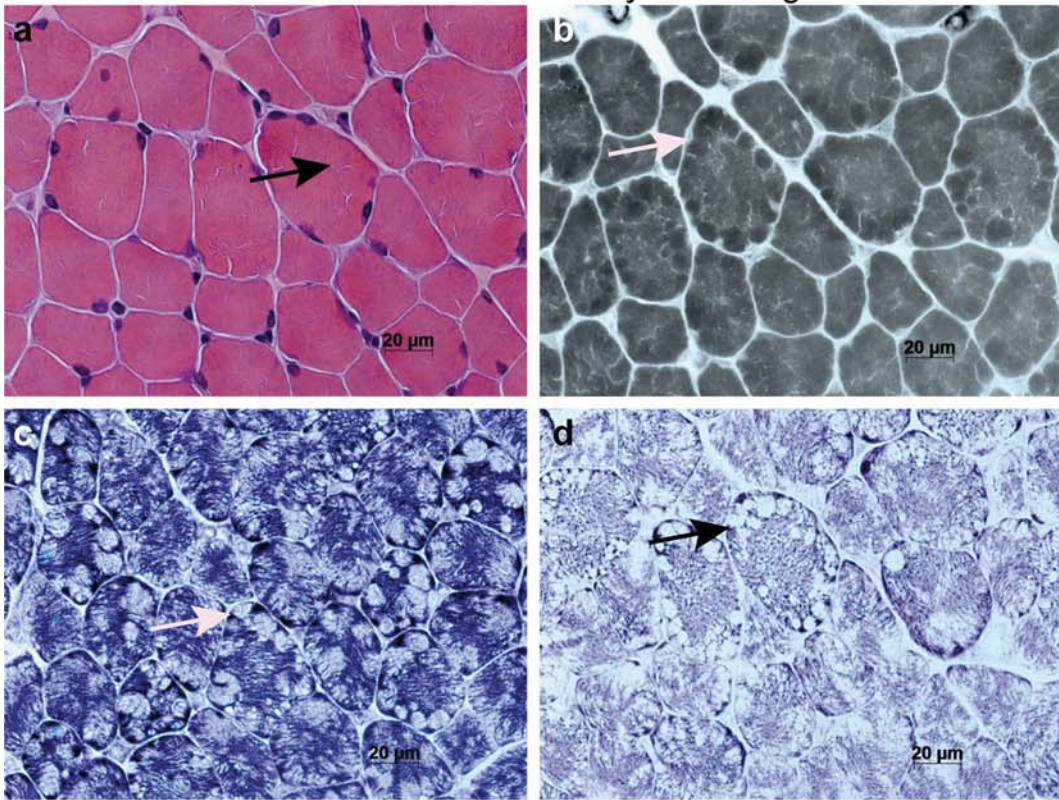
Fig. 1 Photographs of P1. **a** Mild bilateral ptosis. **b** High-arched palate. **c** Upper extremity hypotrophy and pectus excavatum. **d** Residual arm flexors force. **e** Profound leg weakness

mild facial weakness, nasal speech and high-arched palate (Fig. 1a, b). There was profound proximal and distal muscle weakness (2–3/5 MRC grade), and axial weakness of neck flexor and extensor (2/5 MRC grade) (Fig. 1c–e). Contractures of elbows, knees, and ankles were also noted, and deep tendon reflexes were absent. Creatine kinase (CK) levels were repeatedly within the normal range. Whole-body MRI revealed a significant involvement of the tongue, temporal muscles, lateral pterygoids and masseters with preservation of the medial pterygoids (supplementary Fig. S1a–s).

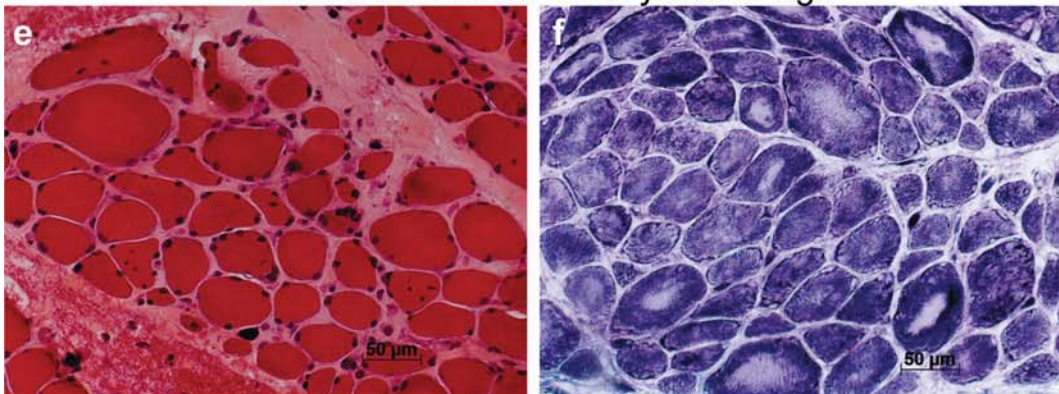
P2 is the first child born to healthy non-consanguineous parents. Neonatal and infancy periods were unremarkable, and initial concerns arose when the patient was unable to jump or run as fast as her peers at the age of 7 years. By 13 years of age she noticed difficulty ascending stairs, by 24 years of age she began using a walker, by 27 years of age she has been using a wheelchair for long distances, and by 32 years of age she noticed upper extremity proximal weakness. CK levels were repeatedly within the normal range. Examination at the age of 40 revealed symmetric, bilateral facial weakness with a transverse smile and

minimal forehead movement, and a mildly high-arched palate. Ptosis or ophthalmoparesis were not noted. There was atrophy of the deltoids, the quadriceps, and the distal gastrocnemius muscles, with reduced strength in neck flexion, arm abduction, hip flexion, and hip extension (2/5 MRC grade), as well as in hip adduction (3/5 MRC grade). She was able to take steps independently with marked swaying (lateral leaning toward the leading leg). Deep tendon reflexes were reduced throughout the bilateral upper and lower extremities. There was evidence of spinal rigidity, mild thoracic scoliosis and mild contractures of the shoulders (on external rotation). Pulmonary function testing revealed a forced vital capacity (FVC) of 68% predicted upright and 65% predicted supine. Echocardiogram was normal. Lower extremity muscle MRI revealed atrophy, fatty infiltration and increased T1 signal throughout the muscles of the upper leg with relative sparing of the center of the rectus femoris muscles (Supplementary Fig. S1t, u). In the lower leg muscles, there was strikingly increased T1 signal of the soleus muscle bilaterally and the central portion of the medial gastrocnemius muscle on

P1 deltoid muscle at 9 years of age



P1 radialis muscle at 45 years of age



P2 quadriceps muscle at 19 years of age

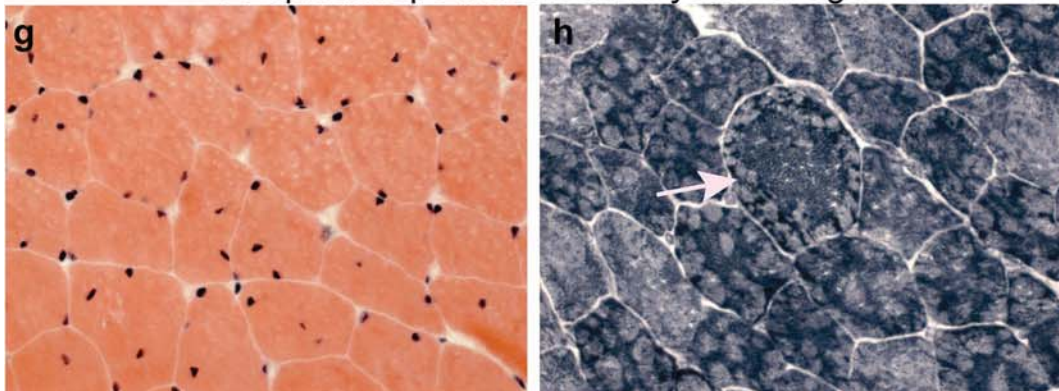


Fig. 2 Skeletal muscle histopathology of P1 at 9 and 45 years, and P2 at 19 years of age. P1 transversal muscle sections from the deltoid biopsy performed at 9 years of age (**a–d**) and from the radialialis muscle biopsy performed at 45 years of age (**e, f**). **a** HE staining reveals fiber size variability, centralized nuclei, and cores (black arrow). **b** ATP staining (pH 9.4) shows type 1 fiber predominance. The subsarcolemmal cores appear slightly darker (arrow). **c, d** NADH and SDH reactions unravel numerous small cores in a circular arrangement beneath the sarcolemma (arrows). **e** HE staining confirms fiber size variability and nuclear internalization, and reveals an increase of connective tissue. **f** NADH shows numerous muscle fibers with well-delimited cores and a diffuse structural disorganisation in several fibers. P2 transversal sections from the quadriceps biopsy performed at 19 years of age (**g, h**). **g** HE staining revealed internalized nuclei. **h** NADH reactions demonstrated several small cores mainly located at the periphery of the fibers

the left with evidence of fatty infiltration of the remaining muscles.

In summary, P1 and P2 presented with an early-onset and progressive myopathy clinically manifesting with significant muscle atrophy, facial weakness, contractures, and respiratory involvement, with a more severe disease progression and ocular involvement for P1.

Histochemical analyses revealed a unique circular arrangement of numerous small cores

P1 was biopsied twice at the age of 9 and 45 years, and P2 was biopsied at the age of 19 years. Histological analyses of the P1 deltoid muscle biopsy performed at 9 years of age revealed fiber size variability, type 1 fiber predominance, and single fibers with centralized nuclei (Fig. 2a, b). Oxidative NADH-TR and SDH reactions uncovered an exceptional aspect of the intermyofibrillar network with numerous small cores often in apposition to each other, and sometimes forming a circular arrangement beneath the sarcolemma (Fig. 2a–d; arrows). These cores also appeared slightly darker on ATPase stain (Fig. 2b; arrow). Analysis of the P1 radialialis muscle biopsy performed at 45 years of age confirmed marked fiber size variability and type 1 fiber predominance (95%), and also disclosed increased connective tissue (Fig. 2e, Supplementary Fig. S2a). Oxidative enzyme reactions revealed the presence of “cores” with sharp edges in type 1 fibers. Many fibers exhibited a diffuse structural disorganisation (Fig. 2f, Supplementary Fig. S2b), and scattered atrophic fibers were also observed (Fig. 2e, Supplementary Fig. S2a).

Histochemical analyses of the P2 quadriceps muscle biopsy performed at the age of 19 revealed striking similarities to the P1 deltoid muscle biopsy including the presence of internalized nuclei and numerous and peripheral small cores (Fig. 2g, h). Some protein aggregates were also observed (Supplementary Fig. S2c).

Taken together, P1 and P2 presented with similar clinical and histopathological features, and the remarkable arrangement of contiguous and subsarcolemmal cores was indicative of a new class of core myopathies.

Ultrastructural studies reveal jagged Z-lines with spiky edges

Electron microscopy of the P1 deltoid muscle biopsy performed at the age of 9 years uncovered numerous structured cores extending over a large number of sarcomeres, and spanning almost the whole width and length of the fibers. Within the cores, the Z-lines manifested a particular zigzag appearance to a greater or lesser extent. Centralized or internalized nuclei were also observed (Fig. 3a).

Ultrastructural analysis of the P1 radialialis muscle biopsy performed at the age of 45 confirmed the presence of structured cores containing abnormal Z-lines. The jagged Z-lines gradually become serrated and merge into spiky edges of significant amplitude resembling a saw blade (Fig. 3b,c). The A and M bands were unaltered, and only the M band appeared slightly less marked (Fig. 3c). We also observed a number of fibers with internalized or pyknotic nuclei, as well as areas with sarcomeric bifurcation (Fig. 3b, c; arrow). On transverse muscle sections, numerous fibers showed areas of dispersed Z-line material (Supplementary Fig. S3), demonstrating a disruption of the myofibrillar organisation with preservation of the double square lattice of the Z-line [25]. Cross-sections through the sarcomere illustrated the normal regular distribution of the filaments forming a hexagonal lattice (Fig. 3d).

Identification of de novo *ACTN2* mutations

To identify the genetic cause of the muscle disorder, we performed exome sequencing on DNA samples from both index patients P1 and P2 and their unaffected family members (Fig. 4a, b). Following filtering and ranking of the datasets through our in-house bioinformatics pipeline [17], no pathogenic mutation in known muscle disorder genes was detected. Instead, we identified two de novo mutations in exon 18 of *ACTN2*: a heterozygous missense mutation in P1 (c.2180T>G, p.Leu727Arg), and a heterozygous in-frame deletion of 33 nucleotides in P2 [c.2194_2226del; p.(Ala732_Ile742del)]. None of the mutations were listed in the public gnomAD database quoting human DNA variants from almost 140,000 exomes and genomes, or in our in-house database containing more than 1500 exomes. The presence of the mutations in the patients and the absence of the mutations in the healthy family members were confirmed by Sanger sequencing.

ACTN2 encodes alpha-actinin-2, which is composed of two actin-binding calponin-homology domains, a

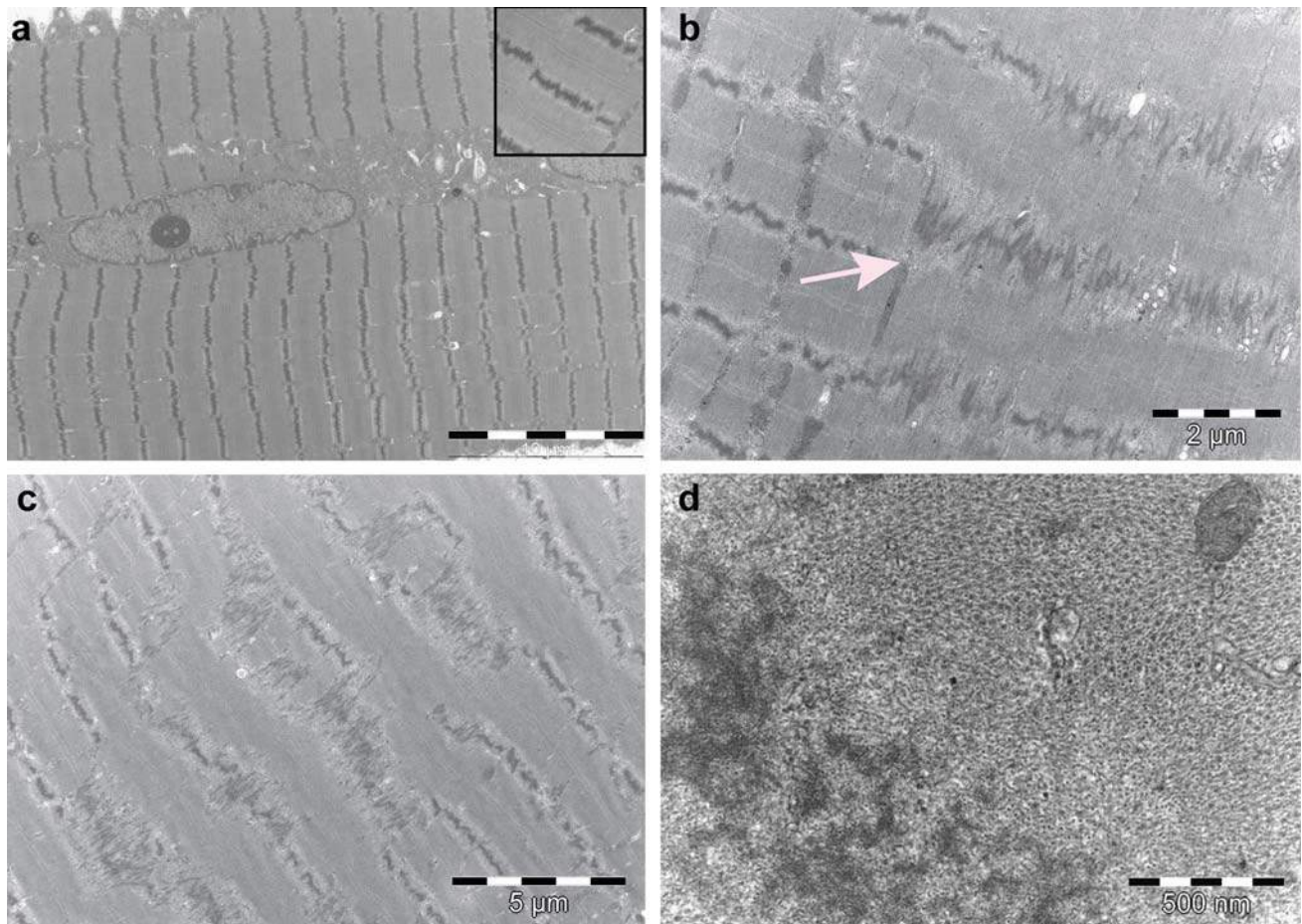


Fig. 3 Progressive ultrastructural muscle alterations of patient P1. Longitudinal muscle sections of the deltoid biopsy (**a**) and the radialis biopsy (**b**, **c**), and transversal sections of the radialis biopsy (**d**). **a** The muscle fiber is fully occupied with structured cores, one next to the other, which extend almost along the full length of the fibers. Electron microscopy of the cores shows centralized nuclei and Z-lines

with zigzag appearance (zoom on the top right corner). **b**, **c** Bifurcation and transition of zigzag Z-lines towards jagged Z-lines with sharp edges resembling a saw blade in contiguous myofibrils (arrow). **d** High-magnification image showing the scattering of Z-line material at different points. Note, however, the normal regular distribution of filaments which forms a typical hexagonal lattice

rod domain of four spectrin repeats in tandem, and two Ca^{2+} -binding EF-hands (Fig. 4c). The p.Leu727Arg substitution and the p.(Ala732_Ile742del) deletion affect conserved amino acids in the fourth spectrin repeat, and neither the nucleotide transversion nor the 33 nucleotides deletion is predicted to impact on splicing. Heterozygous *ACTN2* mutations were previously associated with cardiomyopathy [6, 18, 31, 44] (Fig. 4c). None of the eight reported cardiomyopathy mutations were found to reside within the fourth spectrin repeat, and none approximates the Leu727 and Ala732 to Ile742 residues on the resolved protein structure (Fig. 4c). In silico replacement of leucine 727 by arginine suggests that the arginine most probably interferes with neighboring amino acids, leading to steric hindrance (Fig. 4d). Arginine is also likely to alter the hydrophobic environment constituted by leucine 727 and

the surrounding residues. The deletion from alanine 732 to isoleucine 742 is predicted to shorten a helix in the fourth spectrin repeat and may impact on the orientation of the structure. Moreover, as the p.(Ala732_Ile742)del deletion was identified after the completion of the following functional experiments, cell and animal work were focused on the p.Leu727Arg missense mutation.

The p.Leu727Arg mutation does not impact on alpha-actinin-2 stability, dimerization, and localization

To assess if the identified p.Leu727Arg mutation impacts on the alpha-actinin-2 level in the patient muscle, we performed immunoblotting. Western blot on muscle extracts revealed a comparable alpha-actinin-2 band of the expected size around

100 kDa in the P1 patient muscle and age-matched controls (Fig. 5a, supplementary Fig. S4), demonstrating that the *ACTN2* missense mutation has no major effect on splicing and does not significantly alter protein stability. We next assessed the potential impact of the p.Leu727Arg mutation on alpha-actinin-2 homodimerization. In transfected HeLa cells, wild-type alpha-actinin-2 comparably immunoprecipitated with wild-type and mutant alpha-actinin-2, demonstrating that the identified *ACTN2* mutation does not interfere with the protein dimerization properties (Supplementary Fig. S5).

Alpha-actinin-2 and alpha-actinin-3 are both expressed in human skeletal muscle, and it was previously shown that alpha-actinin-3 deficiency is compensated by *ACTN2* upregulation in both human and mouse [29, 35]. To investigate if the identified p.Leu727Arg mutation influences *ACTN3* expression, we probed alpha-actinin-3 through western blot on P1 muscle extracts. In contrast to the controls, no signal was detectable in the patient's muscle (Fig. 5b). *ACTN3* is, however, exclusively expressed in type 2 muscle fibers in humans, and the histopathological findings of type 1 fiber predominance in our patient most probably accounts for the absence of alpha-actinin-3 in the biopsy as P1 is heterozygous for the common *ACTN3* p.(Arg577*) variation.

Finally, we assessed a potential impact of the p.Leu727Arg mutation on the intracellular alpha-actinin-2 localization in transfected cells. In differentiated C2C12 muscle cells, both wild-type and mutant alpha-actinin-2 were found to form a striated pattern consistent with a Z-line localization (Fig. 5c). We also observed a normal co-localization of the known alpha-actinin-2 interactor vinculin and actin in myoblasts, at the focal adhesion and stress fibers, respectively (Supplementary Fig. S6a,b).

Taken together, our protein studies suggest that the p.Leu727Arg mutation does not significantly impact on *ACTN2* mRNA splicing, and does not affect the stability or the intracellular localization of alpha-actinin-2.

The p.Leu727Arg mutation severely impairs zebrafish muscle structure and function

Alpha-actinin-2 human leucine 727 is highly conserved in all vertebrate species. To evaluate the physiological impact of the alpha-actinin-2 p.Leu727Arg mutation on skeletal muscle structure and function, we performed overexpression experiments in the zebrafish model. *ACTN2* wild-type mRNA-injected fish were indistinguishable from uninjected controls. In contrast, injection of mutant human *ACTN2* mRNA into 1-cell zebrafish embryos resulted in smaller myotome and dorsal curvature (phenotype scored in Fig. 6a, b). Western blot analysis showed equal levels of wild-type and p.Leu727Arg alpha-actinin-2 in zebrafish larvae (3dpf) (Supplementary Fig. S7). While healthy developing

zebrafish embryos typically hatch from their protective chorions by 2–2.5 dpf ($97.2 \pm 1\%$), only a small fraction of p.Leu727Arg-injected zebrafish hatched from their chorion ($12.6 \pm 7\%$, $p < 0.05$) and required manual dechoriation for imaging. Hatching defects were also reported in other zebrafish models of muscle diseases and reflect early motor defects [43]. Birefringence assays on axial skeletal muscles of live zebrafish embryos showed a reduction in birefringence only in zebrafish injected with p.Leu727Arg mRNA (Fig. 6a). The motor function was quantified by measuring the total distance travelled by control, wild-type and mutant mRNA-injected fish. Zebrafish expressing p.Leu727Arg alpha-actinin-2 displayed a significant reduction in the total swimming distance (724.6 ± 83.3 mm) in comparison to the wild-type injected fish (2489.2 ± 119.1 mm) or uninjected controls (2411.4 ± 94.7 mm), demonstrating a mutational impact on muscle function (Fig. 6c).

We also examined the skeletal muscle architecture of the injected zebrafish. Whole-mount immunostaining with phalloidin revealed a close proximity of adjacent myofibers in the controls, whereas p.Leu727Arg-injected zebrafish exhibited gaps between overall smaller myofibers (Fig. 7a). To identify potential ultrastructural defects in subcellular compartments of skeletal muscle, we performed transmission electron microscopy at 3 dpf. Longitudinal muscle sections showed significant myofibrillar disarray lacking normal actin–myosin organization in p.Leu727Arg-injected zebrafish as compared to the highly organized myofibrillar structure in *ACTN2* wild-type injected or uninjected control zebrafish (Fig. 7b). In accordance with the findings on the patient muscle biopsies, the myofibers of p.Leu727Arg-injected fish showed areas with abnormal Z-lines.

The p.Leu727Arg mutation induces structured cores and causes muscle weakness in mice

To further validate and characterize the impact of the alpha-actinin-2 p.Leu727Arg mutation on muscle function at later stages of muscle development and in a different model, we performed AAV-mediated *ACTN2* overexpression in 3-week-old mice and analyzed muscle force and muscle structure 4 weeks post injection. Tibialis anterior muscles injected with wild-type or mutant human *ACTN2* showed a twofold increased alpha-actinin-2 level as compared to control muscles injected with empty AAV (Fig. 8a), while the alpha-actinin-3 and actin levels remained unchanged (Supplementary Fig. S8a,b). Using a force transducer, we detected a significantly reduced maximal and specific force of p.Leu727Arg-injected tibialis anterior compared to muscles injected with empty AAV or wild-type *ACTN2*, respectively (Fig. 8b–d).

Immunofluorescence on longitudinal tibialis anterior sections demonstrated an abnormal Z-line organization

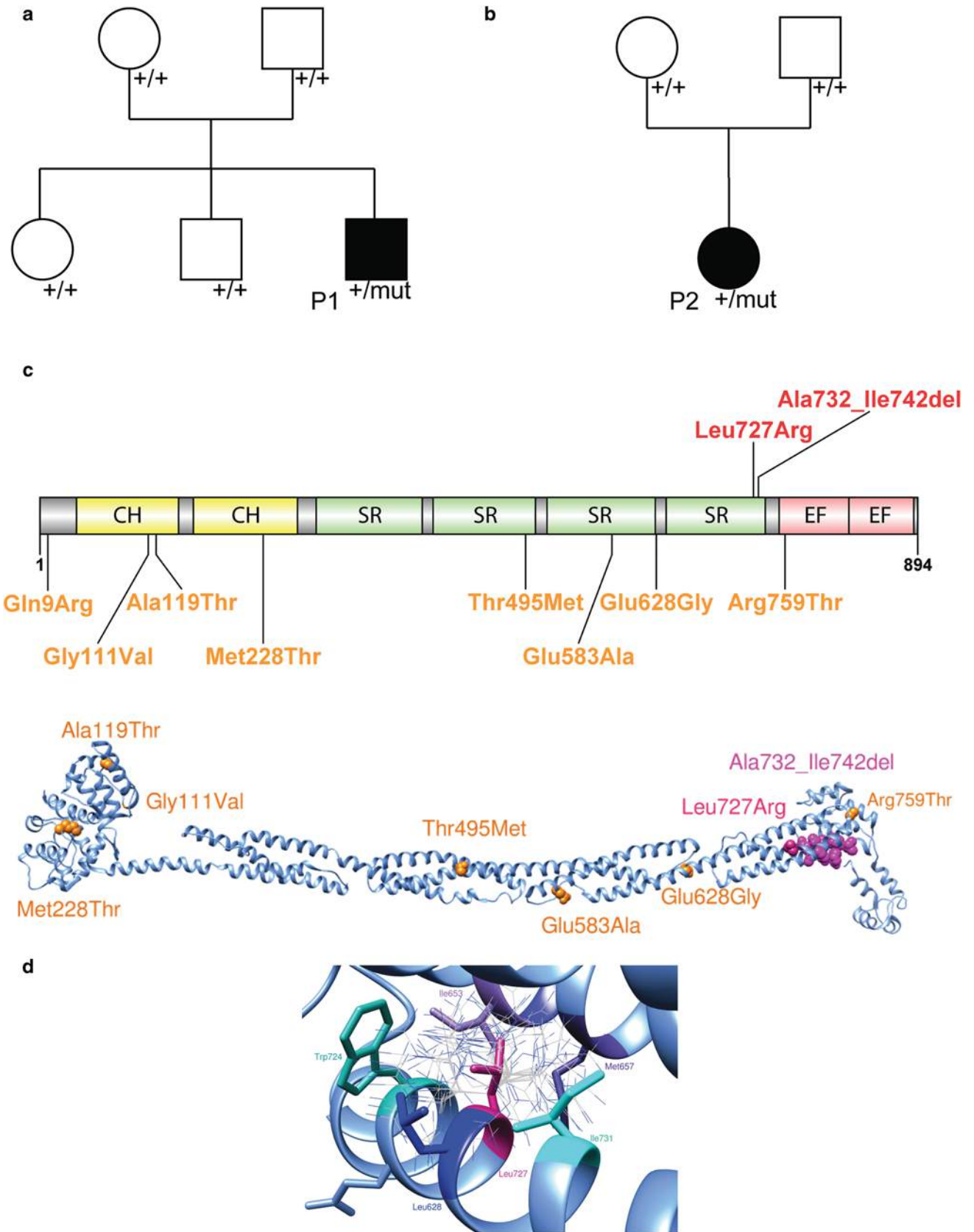


Fig. 4 *ACTN2* mutations. **a, b** Pedigrees of the families with *de novo* *ACTN2* missense mutations. **c** Representation of alpha-actinin-2 domains and structure (PDB 4D1E) showing the position of the novel mutations (in pink or red) and of the mutations previously described in cardiomyopathies (in orange). **d** Prediction of the replacement of leucine 727 (in pink) by arginine in the 3D structure of alpha-actinin-2. All rotamers (possible conformations) of arginine at position 727 were added to the wild-type structure to illustrate the potential interference with the neighboring residues. Neighboring hydrophobic residues are in cyan

in muscles injected with mutant *ACTN2* (Fig. 8e). Histochemical analyses on transversal muscle sections from mice expressing mutant *ACTN2* revealed the presence of cores (Fig. 9a, b, Supplementary Fig. S9), while none of these features were observed in the AAV-empty and AAV-*ACTN2* wild-type injected controls. We further investigated the muscle structure by electron microscopy, and we

detected an abnormal Z-line architecture in tibialis anterior expressing p.Leu727Arg alpha-actinin-2 but not in the controls (Fig. 10). The Z-lines in p.Leu727Arg injected tibialis anterior were enlarged with a zigzag appearance, and were sometimes split (Fig. 10d), in accordance to zebrafish muscles expressing the p.Leu727Arg alpha-actinin-2 and to the histopathological observations on the patient's biopsies.

In summary, the mouse and zebrafish models recapitulated the structural defects observed in the P1 biopsies with strikingly jagged Z-lines, and both animal models manifested muscle weakness, representing the main clinical feature in the patients with *ACTN2* mutations.

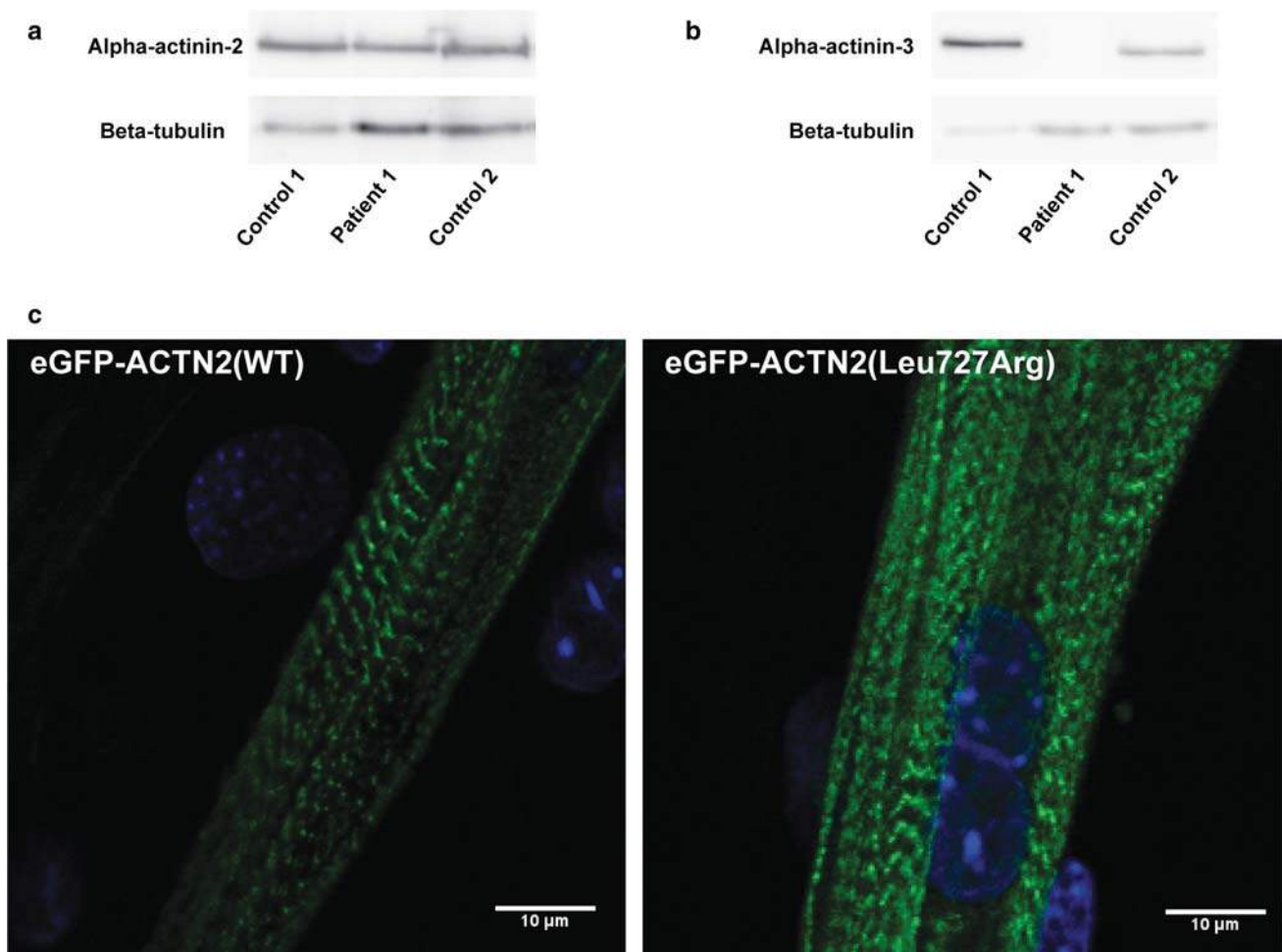


Fig. 5 Impact of the *ACTN2* p.Leu727Arg mutation on protein stability and localization. **a** SDS-PAGE of age-matched controls and patient muscle protein extracts probed with antibodies against alpha-actinin-2 and anti-beta-tubulin showed bands of similar size and signal intensity. **b** SDS-PAGE of age-matched controls and patient

P1 muscle protein extracts revealed with antibodies against alpha-actinin-3 and beta-tubulin showed strong reduction of alpha-actinin-3 in the patient's biopsy. **c** Comparable localization of eGFP-alpha-actinin-2 wild-type and mutant in transfected and differentiated C2C12 myotubes (day 8 after start of differentiation)

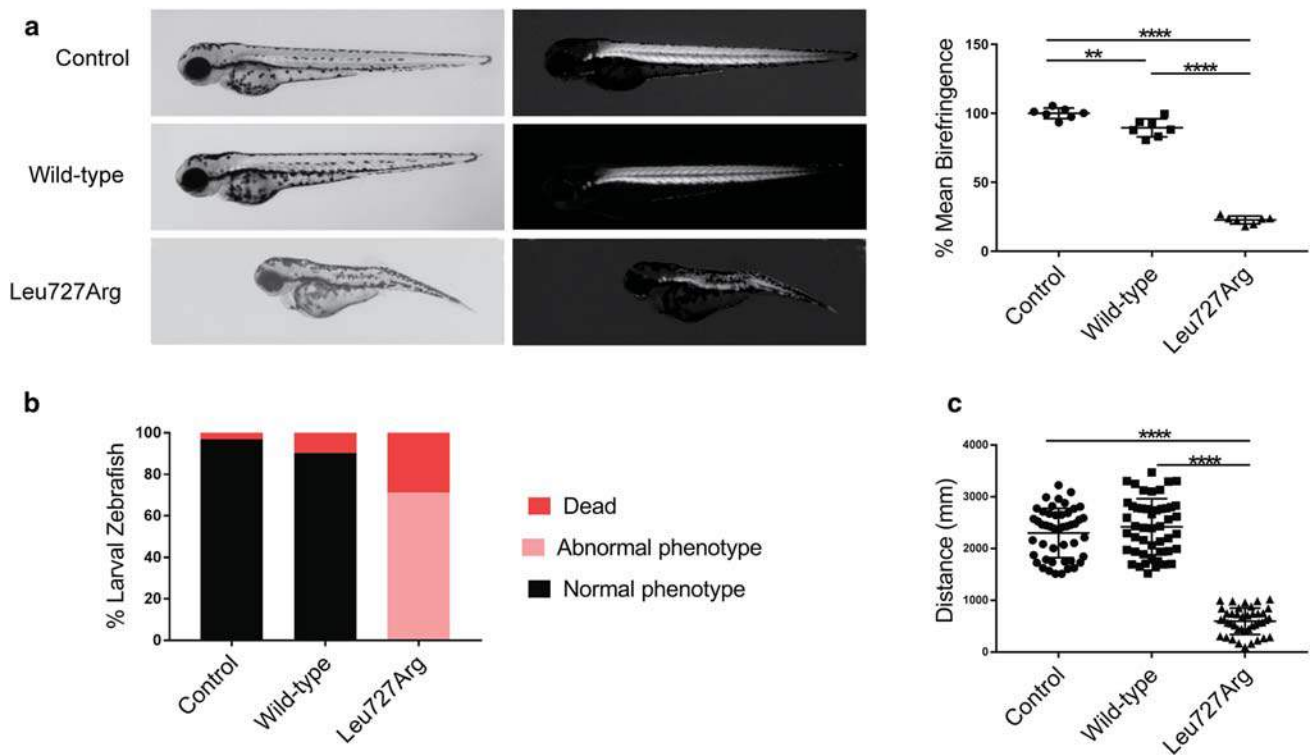


Fig. 6 Expression of p.Leu727Arg ACTN2 in zebrafish results in functional and morphological defects. **a** Representative zebrafish larvae injected with 100–200 pg of p.Leu727Arg ACTN2 mRNA exhibit structural muscle defects at 3 dpf. Imaging under polarized light revealed highly reduced birefringence in p.Leu727Arg zebrafish as compared to controls, reflecting an impaired muscle integrity and indicating an abnormal organization of the muscle. **b** Distribution of normal and abnormal (smaller myotome and dorsal curvature) phenotype in zebrafish larvae injected with p.Leu727Arg or

wild-type ACTN2 mRNA. **c** Quantification of the distance travelled by p.Leu727Arg or control zebrafish larvae at 3 dpf. The plots display the individual values obtained for each animal, their mean and standard deviation. Normal distribution of the data was assessed with the Shapiro–Wilk normality test. Groups were compared using either one-way ANOVA followed by Bonferroni’s post hoc comparison test (**a**) or using non parametric tests (**c**) (Kruskal–Wallis followed by Dunn’s post hoc test), ** $p < 0.01$; **** $p < 0.0001$

Discussion

This study describes a congenital myopathy characterized by multiple structured cores and distinctive jagged-Z-lines in muscle fibers caused by dominant *ACTN2* mutations. We provide clinical, histological, ultrastructural, and genetic data, and evidence the pathogenicity of the missense mutation through muscle function experiments in zebrafish and mouse models.

A unique core myopathy: clinical, histological, and ultrastructural hallmarks

Both patients presented with early-onset muscle weakness and a progressive course of disease resulting in partial or complete loss of ambulation. P1 presented with a more severe disease progression with an additional ocular involvement. Clinical heterogeneity has frequently been described in patients with congenital myopathies and may relate to the genetic background or non-genetic environmental effects.

Muscle biopsies from both patients revealed a highly similar picture with type 1 fiber predominance and multiple structured cores forming a circular arrangement beneath the sarcolemma. Predominance of type 1 fibers is a frequent feature in congenital myopathies and may contribute to the muscle weakness in combination with the overall reduced expression of alpha-actinin-3, a fiber type 2-specific muscle function modifier. A detailed ultrastructural comparison of both P1 biopsies performed in childhood and adulthood suggested a progression of the lesions, as the degree of Z-line jaggings was distinctively more pronounced in the second biopsy and taking an aspect of a saw blade. In CCD, structured or unstructured cores are usually unique with a central or eccentric position. In some cases, two or even three cores may coexist in the same fiber, but never contiguously. It should be noted that abnormal or multiple sarcoplasmic reticular triads are frequently found at their periphery [40]. In MmD, the cores are boundless, smaller, encompassing only a few sarcomeres, and the disorganized filaments present a rather transversal orientation. Minicores can also be

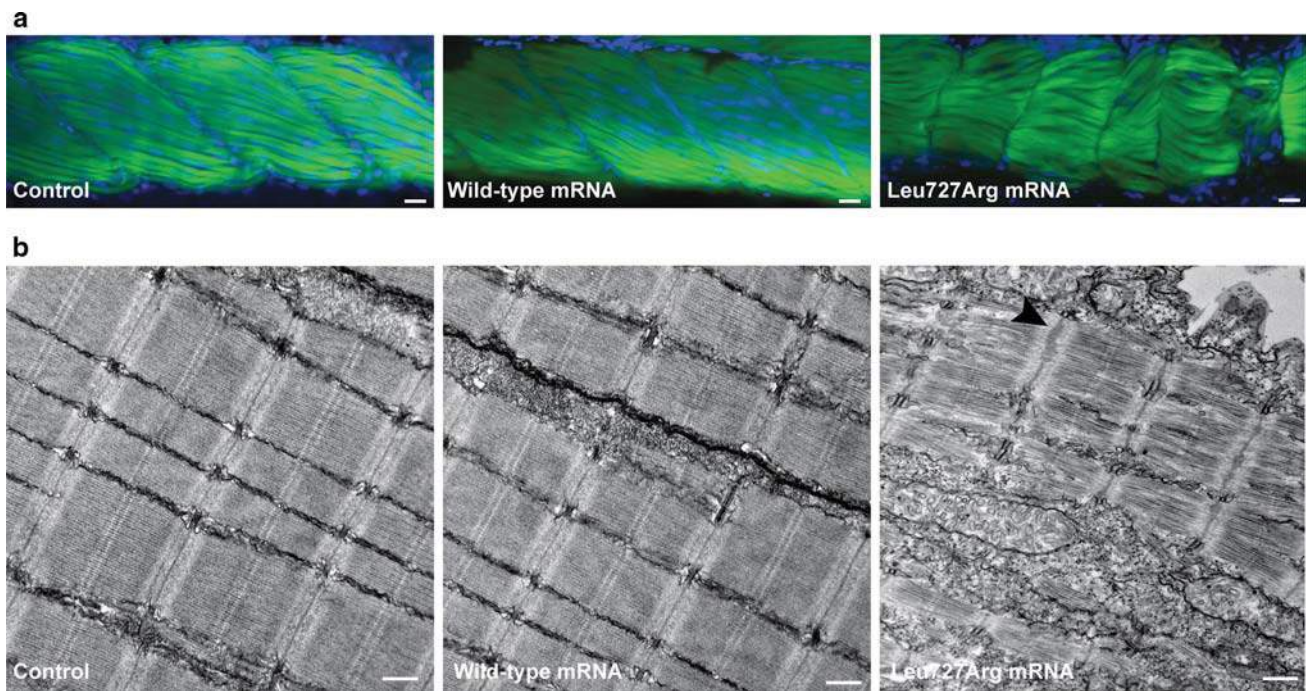


Fig. 7 Expression of p.Leu727Arg in zebrafish results in skeletal muscle disorganization. **a** Whole-mount phalloidin staining demonstrates smaller somites with profound spacing between adjacent myofibers in p.Leu727Arg-injected zebrafish larvae (3dpf). Scale bar:

2 μ m. **b** Ultrastructural evaluation by transmission electron microscopy at 3 dpf shows extensive sarcomeric disorganization and Z-line jaggings (arrowhead) in p.Leu727Arg-injected zebrafish larvae. Scale bar: 500 nm

found in healthy muscle following reactive exercise [16] or after muscle injury, and they are only considered as pathogenic if found in great numbers and exclusively in type I fibers. Taking into account the unique histopathology of multiple structured and contiguous cores in the biopsy of our patients, we propose the term “Multiple structured Core Disease” (MsCD) to describe this novel entity in the group of core myopathies.

ACTN2 mutations: cardiomyopathy vs myopathy

Alpha-actinin-2 is expressed in skeletal and cardiac muscle [2], and heterozygous *ACTN2* mutations have previously been associated with hypertrophic or dilated cardiomyopathy, without any reported motor or skeletal muscle involvement. To date, eight mutations were reported, and all are missense mutations affecting conserved amino acids [6, 18, 31, 44]. The mutations are evenly distributed and found in the calponin-homology domains, as well as in some spectrin repeats and in the EF-hands. The spectrin domain mutations p.Thr495Met and p.Glu628Gly were found in spectrin domains 2 and 3, respectively. A subset of the cardiomyopathy-related *ACTN2* mutations has been investigated experimentally. The very N-terminal p.Gln9Arg mutation was shown to disrupt the interaction with the muscle LIM protein, and the calponin-homology domain mutations

p.Gly11Val and p.Ala119Thr interfered with actin binding [22]. The resolved protein structure of alpha-actinin-2 shows that none of the cardiomyopathy-related mutations affect residues in close proximity to the myopathy-related alpha-actinin-2 mutations described here. Moreover, leucine 727 and alanine 732 to isoleucine 742 reside within the same alpha-helix and replacement by arginine or deletion of 11 amino acids may have different chemical and/or structural impacts compared to the cardiomyopathy mutations, and thereby underlies the diverging pathomechanisms resulting in either skeletal muscle or a cardiac disorder. We can, however, not exclude that the myopathy-related p.Leu727Arg or p.(Ala732_Ile742del) mutations might also result in cardiac involvement at later stages or on a different genetic background. It should be noted that P1 manifested cardiac insufficiency in the neonatal period that disappeared by the age of 6 months following symptomatic treatment.

Insight into the pathogenesis

Through exome sequencing, we identified the de novo *ACTN2* c.2180T>G (p.Leu727Arg) and c.2194_2226del (p.(Ala732_Ile742del)) mutations as the genetic cause of MsCD. *ACTN2* is highly expressed in skeletal muscle, and the identified mutations are not listed in the SNP databases. The pathogenicity of the *ACTN2* mutations can be inferred

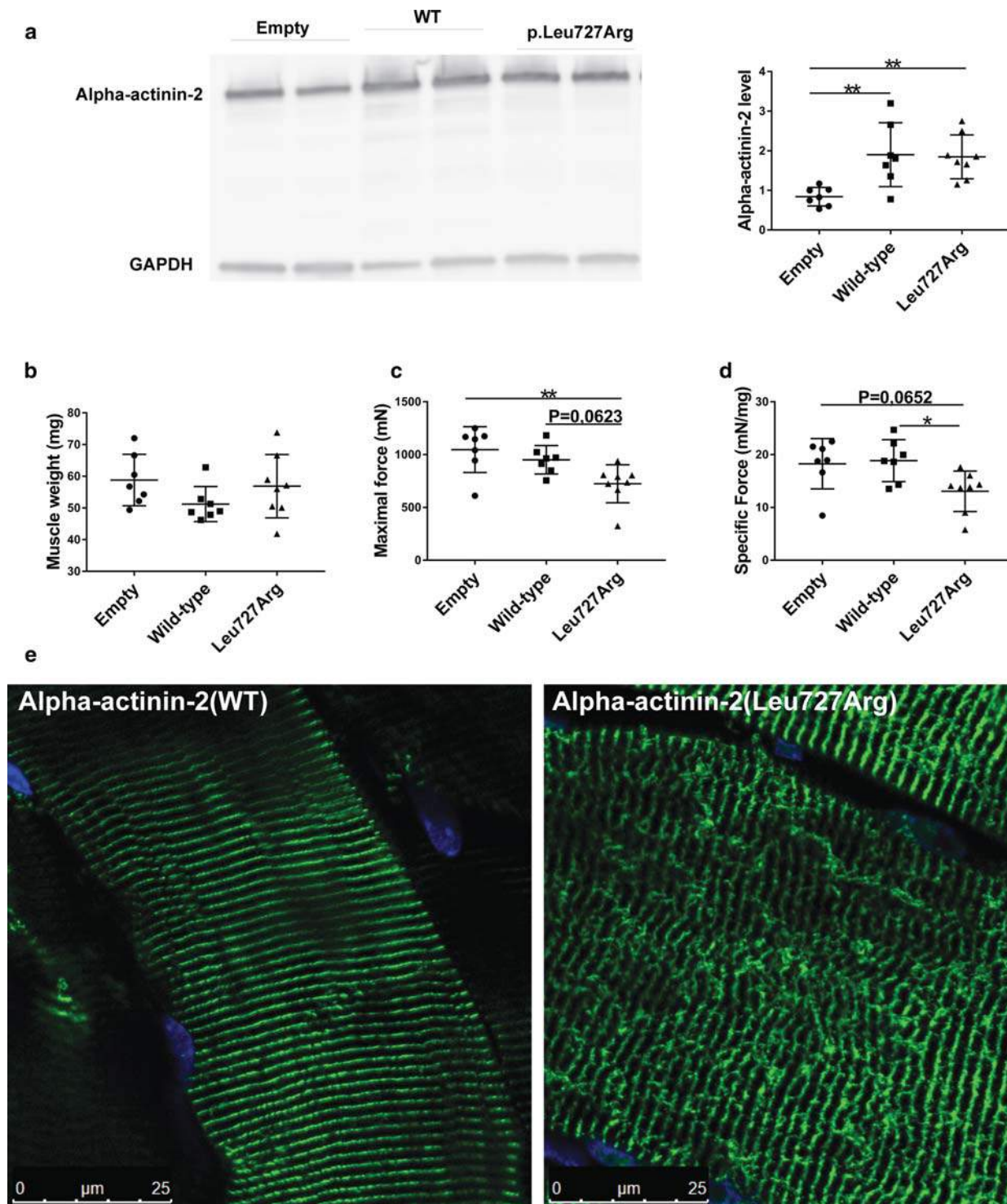


Fig. 8 Functional and structural defects in mouse tibialis anterior with the p.Leu727Arg ACTN2. **a** SDS-PAGE of tibialis anterior muscle extracts probed with antibodies against alpha-actinin-2 and beta-tubulin. Quantification of alpha-actinin-2 overexpression shows a twofold overexpression in the muscles injected with AAV encoding the wild-type or p.Leu727Arg alpha-actinin-2. **b** Weight of tibialis anterior muscles is similar for all tested conditions. **c** Maximal and **d** specific muscle force of tibialis anterior expressing the p.Leu727Arg mutation is reduced. **e** Longitudinal tibialis anterior muscle sections

stained for alpha-actinin-2 reveals proper localization at the Z-line of both wild-type and mutant proteins but abnormal Z-line organization in the mutant-injected muscle. The plots display the individual values obtained for each animal, their mean and standard deviation. Normal distribution of the data was assessed (Shapiro–Wilk normality test). Groups were compared using either one-way ANOVA followed by Bonferroni's post hoc comparison test (**a**, **c**, **d**) or using non-parametric tests (**b**) (Kruskal–Wallis followed by Dunn's post hoc test), $*p < 0.05$; $**p < 0.01$

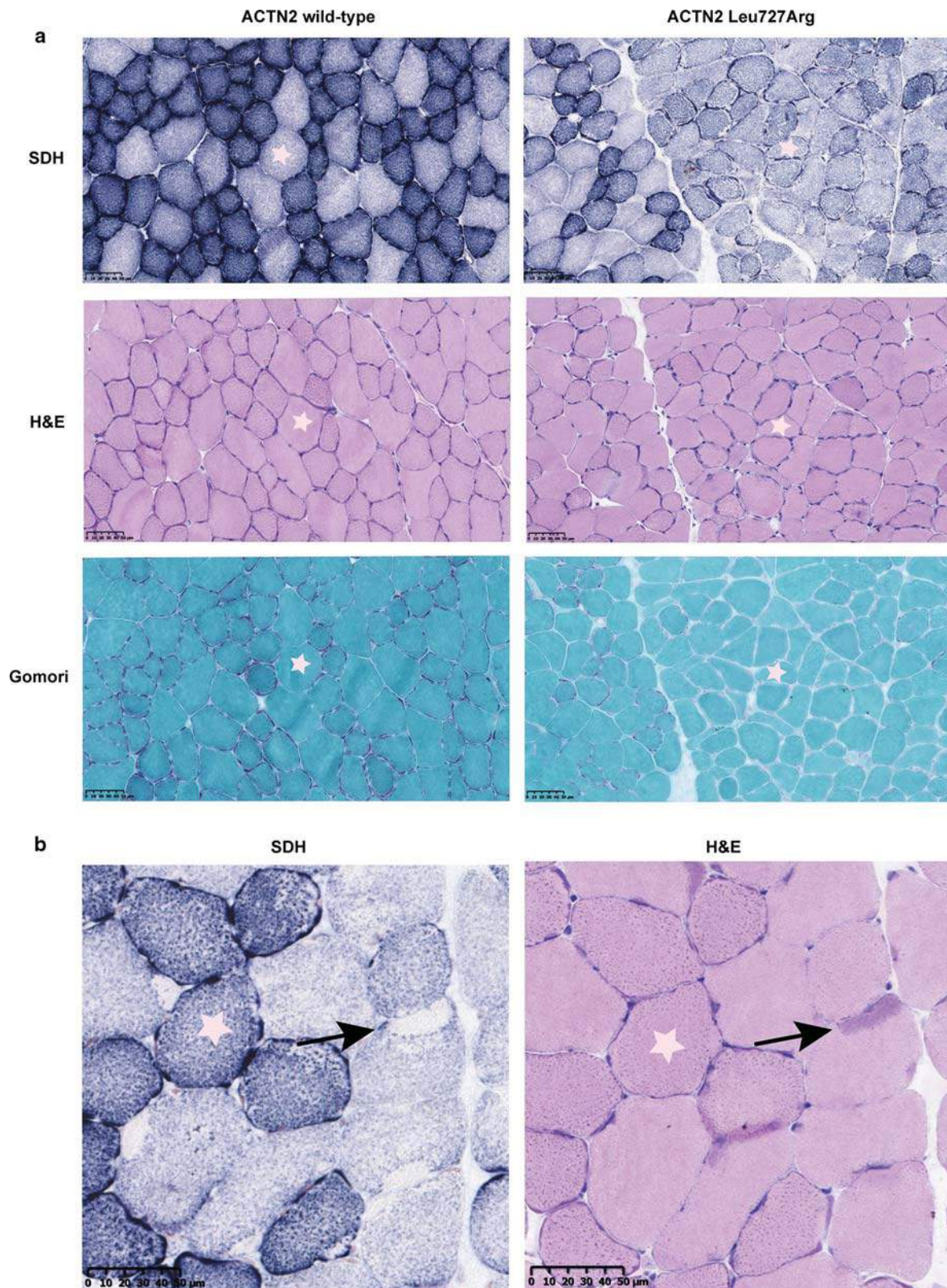


Fig. 9 Characterization of histological features in mouse tibialis anterior muscles. **a** Transversal sections (serial sections) showing large disorganized regions (SDH) in muscle expressing the p.Leu727Arg mutation. **b** Transversal sections (serial sections) of the muscles

expressing the p.Leu727Arg mutation. Some cores revealed with SDH staining are stained darker with H&E (arrows). The stars show the corresponding fibers in the different panels

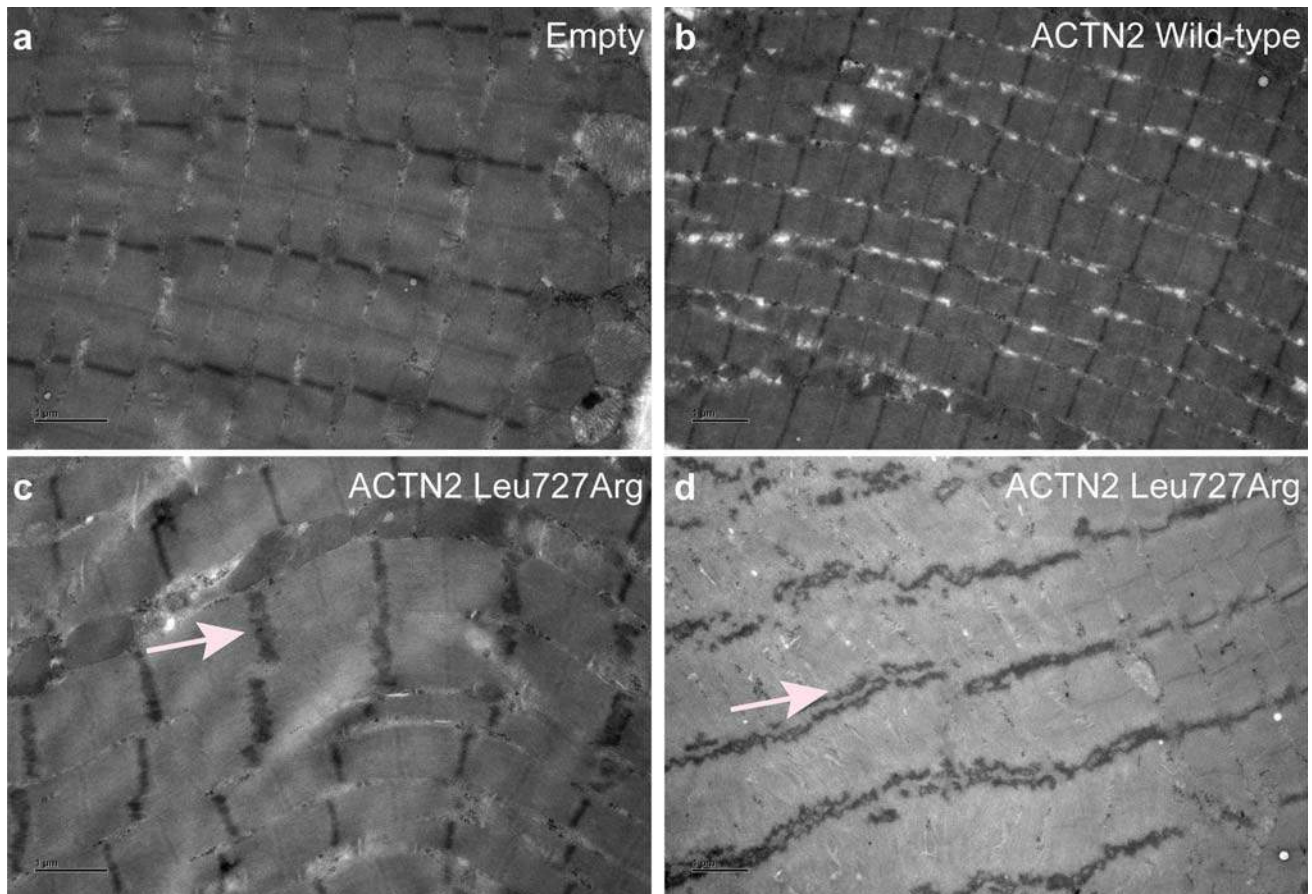


Fig. 10 Muscle ultrastructural defects caused by mutated *ACTN2* overexpression in mice. Longitudinal sections from tibialis anterior muscles from injected mice. **a** Control mouse muscle injected with empty AAV. **b** Ultrastructure of muscle overexpressing alpha-

actinin-2 wild-type is similar to control muscles. **c** Zigzagging appearance of the Z-lines in muscles overexpressing the p.Leu727Arg *ACTN2* mutation (arrow). **d** Split Z-line in muscle overexpressing the mutation (arrow)

from the patient analyses and our animal experimentation results. It has previously been shown that alpha-actinin-2 deficiency results in sarcomeric defects in zebrafish [19], demonstrating the essential role of alpha-actinin-2 in the integrity of the contractile apparatus in skeletal muscle. Here we exogenously expressed human p.Leu727Arg *ACTN2*, and the injected zebrafish manifested both functional and structural muscle defects including abnormal Z-lines. We also performed AAV-mediated human *ACTN2* overexpression in murine tibialis anterior, and the muscles injected with the p.Leu727Arg construct developed less force than the controls and displayed cores and jagged Z-lines. Taken together, the animal models recapitulated the major muscle features of human *ACTN2*-related myopathy at both the clinical and the histological level. Moreover, both animal models provide faithful tools to investigate further therapeutic approaches. Our cell experiments disclosed that the Z-line protein alpha-actinin-2 p.Leu727Arg forms a striated pattern as expected and still binds the tested interactors. The abnormal Z-line

architecture observed in the P1 muscle biopsy and in the animal models, however, demonstrates that the p.Leu727Arg mutation impacts on the integrity of the Z-line, potentially through untested or unknown function/interactors. The disease progression might thereby result from the accumulative mechanical stress acting on the Z-line over time, leading to the abnormal Z-line architecture, and representing the main reason for the progressive muscle weakness observed in the patients.

Conclusions

Here we describe a unique congenital myopathy at the clinical, histological, morphological, and genetic level. We identified the first *ACTN2* mutations associated with multiple structured Core disease (MsCD), characterized by unique and distinctive histological features including numerous

contiguous structured cores and jagged Z-lines with spiky edges, and we demonstrated pathogenicity in zebrafish and mouse. This work provides insight into pathogenic alterations of the Z-line architecture and will improve the molecular diagnosis for patients with rare muscle disorders.

Acknowledgements We thank the families for their participation in the study. We also thank Valentina Lionello, Loïc Talide, Suzie Buono, Coralie Spiegelhalter, Bruno Weber and Pascale Koebel for technical assistance, Jahannaz Dastgir, Katherine Meilleur, Neal Busis, Lauren Elman, Xilma Ortiz-Gonzalez, and Henry Wessel for their help with patient care, and Susana Quijano-Roy, Christopher Mendoza and Gilberto Averion for their help in clinic. We also would like to thank the Exome Aggregation Consortium and the groups that provided exome variant data for comparison. A full list of contributing groups can be found at <http://exac.broadinstitute.org/about>.

Author contributions NBR, CB, JB, JL conceived and designed the study. XL, CAG, SD, MMM, SN, ARF, CL, KRC, LM, JFD performed the experiments. XL, NBR, EM, SD, SN, ARF, RS, RYC, CB, VAG, MF analyzed the data. XL, NBR, MF, JB, JL wrote the manuscript with input from the other coauthors.

Funding This study was supported by the grant ANR-10-LABX-0030-INRT, a French State fund managed by the Agence Nationale de la Recherche under the frame program Investissements d’Avenir ANR-10-IDEX-0002-02. This work was funded by the Institut National de la Santé et de la Recherche Médicale (INSERM), Centre National de la Recherche Scientifique (CNRS), University of Strasbourg, GIS IBSA maladies rares, the France Génomique National infrastructure funded as part of the Investissements d’Avenir program managed by the Agence Nationale pour la Recherche (ANR-10-INBS-09) and by Fondation Maladies Rares within the frame of the “Myocapture” sequencing project, the Fondation pour la Recherche Médicale, and the Association Française contre les Myopathies. The work performed at the NIH was supported by intramural funds from the NIH National Institute of Neurological Disorders and Stroke. Sequencing analysis was provided by the Broad Institute of MIT and Harvard Center for Mendelian Genomics and was funded by the National Human Genome Research Institute, the National Eye Institute and the National Heart, Lung and Blood Institute grant UM1 HG008900 to Daniel MacArthur and Heidi Rehm.

Compliance with ethical standards

Conflict of interest None of the authors reports conflicts of interest.


References

- Bang ML, Mudry RE, McElhinny AS, Trombitas K, Geach AJ, Yamasaki R et al (2001) Myopalladin, a novel 145-kilodalton sarcomeric protein with multiple roles in Z-disc and I-band protein assemblies. *J Cell Biol* 153:413–427
- Beggs AH, Byers TJ, Knoll JH, Boyce FM, Bruns GA, Kunkel LM (1992) Cloning and characterization of two human skeletal muscle alpha-actinin genes located on chromosomes 1 and 11. *J Biol Chem* 267:9281–9288
- Bennett AH, O’Donohue MF, Gundry SR, Chan AT, Widrick J, Draper I et al (2018) RNA helicase, DDX27 regulates skeletal muscle growth and regeneration by modulation of translational processes. *PLoS Genet* 14:e1007226. <https://doi.org/10.1371/journal.pgen.1007226>
- Carlier R (2014) MNM et IRM musculaire/corps entier: apport au diagnostic et au suivi. In: AFM-Téléthon, Société Française de Myologie SFM (eds) Les Cahiers de Myologie, pp 22–32
- Chan Y, Tong HQ, Beggs AH, Kunkel LM (1998) Human skeletal muscle-specific alpha-actinin-2 and -3 isoforms form homodimers and heterodimers in vitro and in vivo. *Biochem Biophys Res Commun* 248:134–139
- Chiu C, Bagnall RD, Ingles J, Yeates L, Kennerson M, Donald JA et al (2010) Mutations in alpha-actinin-2 cause hypertrophic cardiomyopathy: a genome-wide analysis. *J Am Coll Cardiol* 55:1127–1135. <https://doi.org/10.1016/j.jacc.2009.11.016>
- Cowling BS, Toussaint A, Amoasii L, Koebel P, Ferry A, Davignon L et al (2011) Increased expression of wild-type or a centronuclear myopathy mutant of dynamin 2 in skeletal muscle of adult mice leads to structural defects and muscle weakness. *Am J Pathol* 178:2224–2235. <https://doi.org/10.1016/j.ajpath.2011.01.054>
- Cukovic D, Lu GW, Wible B, Steele DF, Fedida D (2001) A discrete amino terminal domain of Kv1.5 and Kv1.4 potassium channels interacts with the spectrin repeats of alpha-actinin-2. *FEBS Lett* 498:87–92
- Dubowitz V, Pearse AG (1960) Oxidative enzymes and phosphorylase in central-core disease of muscle. *Lancet* 2:23–24
- Dunbrack RL Jr (2002) Rotamer libraries in the 21st century. *Curr Opin Struct Biol* 12:431–440
- Eilertsen KJ, Kazmierski ST, Keller TC 3rd (1997) Interaction of alpha-actinin with cellular titin. *Eur J Cell Biol* 74:361–364
- Engel AG, Gomez MR, Groover RV (1971) Multicore disease. A recently recognized congenital myopathy associated with multifocal degeneration of muscle fibers. *Mayo Clin Proc* 46:666–681
- Fardeau M (1982) Congenital Myopathies. In: Mastaglia F, Walton J (eds) Skeletal muscle pathology, 2nd edn. Churchill Livingstone, Edinburgh, pp 237–281
- Ferreiro A, Estournet B, Chateau D, Romero NB, Laroche C, Odent S et al (2000) Multi-minicore disease—searching for boundaries: phenotype analysis of 38 cases. *Ann Neurol* 48:745–757
- Finn RD, Attwood TK, Babbitt PC, Bateman A, Bork P, Bridge AJ et al (2017) InterPro in 2017—beyond protein family and domain annotations. *Nucleic Acids Res* 45:D190–D199. <https://doi.org/10.1093/nar/gkw1107>
- Friden J, Sjöstrom M, Ekblom B (1983) Myofibrillar damage following intense eccentric exercise in man. *Int J Sports Med* 4:170–176
- Geoffroy V, Pizot C, Redin C, Piton A, Vasli N, Stoetzel C et al (2015) VaRank: a simple and powerful tool for ranking genetic variants. *PeerJ* 3:e796. <https://doi.org/10.7717/peerj.796>
- Girolami F, Iascone M, Tomberli B, Bardi S, Benelli M, Marseglia G et al (2014) Novel alpha-actinin 2 variant associated with familial hypertrophic cardiomyopathy and juvenile atrial arrhythmias: a massively parallel sequencing study. *Circ Cardiovasc Genet* 7:741–750. <https://doi.org/10.1161/CIRCGENETICS.113.000486>
- Gupta V, Discenza M, Guyon JR, Kunkel LM, Beggs AH (2012) alpha-Actinin-2 deficiency results in sarcomeric defects in zebrafish that cannot be rescued by alpha-actinin-3 revealing functional differences between sarcomeric isoforms. *FASEB J* 26:1892–1908. <https://doi.org/10.1096/fj.11-194548>
- Hall DD, Dai S, Tseng PY, Malik Z, Nguyen M, Matt L et al (2013) Competition between alpha-actinin and Ca(2)(+)-calmodulin controls surface retention of the L-type Ca(2)(+) channel Ca(V)1.2. *Neuron* 78:483–497. <https://doi.org/10.1016/j.neuron.2013.02.032>
- Hance JE, Fu SY, Watkins SC, Beggs AH, Michalak M (1999) alpha-actinin-2 is a new component of the

- dystrophin-glycoprotein complex. *Arch Biochem Biophys* 365:216–222. <https://doi.org/10.1006/abbi.1999.1172>
22. Haywood NJ, Wolny M, Rogers B, Trinh CH, Shuping Y, Edwards TA et al (2016) Hypertrophic cardiomyopathy mutations in the calponin-homology domain of ACTN2 affect actin binding and cardiomyocyte Z-disc incorporation. *Biochem J* 473:2485–2493. <https://doi.org/10.1042/BCJ20160421>
 23. Huang SM, Huang CJ, Wang WM, Kang JC, Hsu WC (2004) The enhancement of nuclear receptor transcriptional activation by a mouse actin-binding protein, alpha actinin 2. *J Mol Endocrinol* 32:481–496
 24. Kimmel CB, Ballard WW, Kimmel SR, Ullmann B, Schilling TF (1995) Stages of embryonic development of the zebrafish. *Dev Dyn* 203:253–310. <https://doi.org/10.1002/aja.1002030302>
 25. Landon D (1982) Skeletal muscle—normal morphology, development and innervation. In: Walton J, Mastaglia F (eds) *Skeletal muscle pathology*. Churchill Livingstone, Edinburgh, pp 1–87
 26. Linke WA, Ivemeyer M, Labeit S, Hinssen H, Ruegg JC, Gautel M (1997) Actin-titin interaction in cardiac myofibrils: probing a physiological role. *Biophys J* 73:905–919. [https://doi.org/10.1016/S0006-3495\(97\)78123-2](https://doi.org/10.1016/S0006-3495(97)78123-2)
 27. Liu W, Xie Y, Ma J, Luo X, Nie P, Zuo Z et al (2015) IBS: an illustrator for the presentation and visualization of biological sequences. *Bioinformatics* 31:3359–3361. <https://doi.org/10.1093/bioinformatics/btv362>
 28. Lu L, Timofeyev V, Li N, Rafizadeh S, Singapuri A, Harris TR et al (2009) Alpha-actinin2 cytoskeletal protein is required for the functional membrane localization of a Ca²⁺-activated K⁺ channel (SK2 channel). *Proc Natl Acad Sci USA* 106:18402–18407. <https://doi.org/10.1073/pnas.0908207106>
 29. MacArthur DG, Seto JT, Chan S, Quinlan KG, Raftery JM, Turner N et al (2008) An Actn3 knockout mouse provides mechanistic insights into the association between alpha-actinin-3 deficiency and human athletic performance. *Hum Mol Genet* 17:1076–1086. <https://doi.org/10.1093/hmg/ddm380>
 30. McGregor A, Blanchard AD, Rowe AJ, Critchley DR (1994) Identification of the vinculin-binding site in the cytoskeletal protein alpha-actinin. *Biochem J* 301(Pt 1):225–233
 31. Mohapatra B, Jimenez S, Lin JH, Bowles KR, Coveler KJ, Marx JG et al (2003) Mutations in the muscle LIM protein and alpha-actinin-2 genes in dilated cardiomyopathy and endocardial fibroelastosis. *Mol Genet Metab* 80:207–215
 32. Murphy AC, Young PW (2015) The actinin family of actin cross-linking proteins—a genetic perspective. *Cell Biosci* 5:49. <https://doi.org/10.1186/s13578-015-0029-7>
 33. Nance JR, Dowling JJ, Gibbs EM, Bonnemann CG (2012) Congenital myopathies: an update. *Curr Neurol Neurosci Rep* 12:165–174. <https://doi.org/10.1007/s11910-012-0255-x>
 34. Nave R, Furst DO, Weber K (1990) Interaction of alpha-actinin and nebulin in vitro. Support for the existence of a fourth filament system in skeletal muscle. *FEBS Lett* 269:163–166
 35. North KN, Yang N, Wattanasirichaigoon D, Mills M, Eastale S, Beggs AH (1999) A common nonsense mutation results in alpha-actinin-3 deficiency in the general population. *Nat Genet* 21:353–354. <https://doi.org/10.1038/7675>
 36. Otey CA, Pavalko FM, Burrige K (1990) An interaction between alpha-actinin and the beta 1 integrin subunit in vitro. *J Cell Biol* 111:721–729
 37. Pettersen EF, Goddard TD, Huang CC, Couch GS, Greenblatt DM, Meng EC et al (2004) UCSF Chimera—a visualization system for exploratory research and analysis. *J Comput Chem* 25:1605–1612. <https://doi.org/10.1002/jcc.20084>
 38. Ribeiro Ede A Jr, Pinotsis N, Ghisleni A, Salmazo A, Konarev PV, Kostan J et al (2014) The structure and regulation of human muscle alpha-actinin. *Cell* 159:1447–1460. <https://doi.org/10.1016/j.cell.2014.10.056>
 39. Robison AJ, Bass MA, Jiao Y, MacMillan LB, Carmody LC, Bartlett RK et al (2005) Multivalent interactions of calcium/calmodulin-dependent protein kinase II with the postsynaptic density proteins NR2B, densin-180, and alpha-actinin-2. *J Biol Chem* 280:35329–35336. <https://doi.org/10.1074/jbc.M502191200>
 40. Romero NB, Clarke NF (2013) Congenital myopathies. *Handb Clin Neurol* 113:1321–1336. <https://doi.org/10.1016/B978-0-444-59565-2.00004-6>
 41. Salmikangas P, Mykkanen OM, Gronholm M, Heiska L, Kere J, Carpen O (1999) Myotilin, a novel sarcomeric protein with two Ig-like domains, is encoded by a candidate gene for limb-girdle muscular dystrophy. *Hum Mol Genet* 8:1329–1336
 42. Sewry CA, Wallgren-Pettersson C (2017) Myopathology in congenital myopathies. *Neuropathol Appl Neurobiol* 43:5–23. <https://doi.org/10.1111/nan.12369>
 43. Smith SJ, Wang JC, Gupta VA, Dowling JJ (2017) A novel early onset phenotype in a zebrafish model of merosin deficient congenital muscular dystrophy. *PLoS One* 12:e0172648. <https://doi.org/10.1371/journal.pone.0172648>
 44. Theis JL, Bos JM, Bartleson VB, Will ML, Binder J, Vatta M et al (2006) Echocardiographic-determined septal morphology in Z-disc hypertrophic cardiomyopathy. *Biochem Biophys Res Commun* 351:896–902. <https://doi.org/10.1016/j.bbrc.2006.10.119>
 45. Westerfield M (2007) *The Zebrafish Book: a guide for the laboratory use of Zebrafish (Danio rerio)*, City
 46. Wyszynski M, Lin J, Rao A, Nigh E, Beggs AH, Craig AM et al (1997) Competitive binding of alpha-actinin and calmodulin to the NMDA receptor. *Nature* 385:439–442. <https://doi.org/10.1038/385439a0>

Publisher's Note Springer Nature remains neutral with regard to jurisdictional claims in published maps and institutional affiliations.

Affiliations

Xavière Lornage^{1,2,3,4} · Norma B. Romero^{5,6,7} · Claire A. Grosogeat⁸ · Edoardo Malfatti^{6,7,9} · Sandra Donkervoort¹⁰ · Michael M. Marchetti⁸ · Sarah B. Neuhaus¹⁰ · A. Reghan Foley¹⁰ · Clémence Labasse^{6,7} · Raphaël Schneider^{1,2,3,4} · Robert Y. Carlier^{11,12} · Katherine R. Chao¹³ · Livija Medne¹⁴ · Jean-François Deleuze¹⁵ · David Orlikowski¹⁶ · Carsten G. Bönnemann¹⁰ · Vandana A. Gupta⁸ · Michel Fardeau^{5,6,7} · Johann Böhm^{1,2,3,4} · Jocelyn Laporte^{1,2,3,4} 

¹ Institut de Génétique et de Biologie Moléculaire et Cellulaire (IGBMC), 1, rue Laurent Fries, BP 10142, 67404 Illkirch, France

² INSERM U1258, 67404 Illkirch, France

³ CNRS, UMR7104, 67404 Illkirch, France

- ⁴ Université de Strasbourg, 67404 Illkirch, France
- ⁵ Université Sorbonne, UPMC Univ Paris 06, INSERM UMRS974, CNRS FRE3617, Center for Research in Myology, GH Pitié-Salpêtrière, 47 Boulevard de l'hôpital, 75013 Paris, France
- ⁶ Centre de référence de Pathologie Neuromusculaire Paris-Est, Institut de Myologie, GHU Pitié-Salpêtrière, Assistance Publique-Hôpitaux de Paris, 75013 Paris, France
- ⁷ Neuromuscular Morphology Unit, Myology Institute, GHU Pitié-Salpêtrière, 75013 Paris, France
- ⁸ Division of Genetics, Brigham and Women's Hospital, Harvard Medical School, Boston, MA 02115, USA
- ⁹ Neurology Department, Raymond-Poincaré teaching hospital, Centre de référence des maladies neuromusculaires Nord/Est/Ile-de-France, AP-HP, 92380 Garches, France
- ¹⁰ Neuromuscular and Neurogenetic Disorders of Childhood Section, National Institute of Neurological Disorders and Stroke, National Institutes of Health, Bethesda, MD 20892, USA
- ¹¹ Neurolocomotor Division, Department of Radiology, Raymond Poincaré Hospital, University Hospitals Paris–Ile-de-France West, Public Hospital Network of Paris, 92380 Garches, France
- ¹² Versailles Saint-Quentin-en-Yvelines University, 78000 Versailles, France
- ¹³ Center for Mendelian Genomics, Program in Medical and Population Genetics, Broad Institute of MIT and Harvard, Boston, MA 02115, USA
- ¹⁴ Division of Human Genetics, The Children's Hospital of Philadelphia, Philadelphia, PA 19104, USA
- ¹⁵ Centre National de Recherche en Génomique Humaine (CNRGH), Institut de biologie François Jacob, CEA, 91000 Evry, France
- ¹⁶ CIC 1429, INSERM, AP-HP, Hôpital Raymond Poincaré, 92380 Garches, France

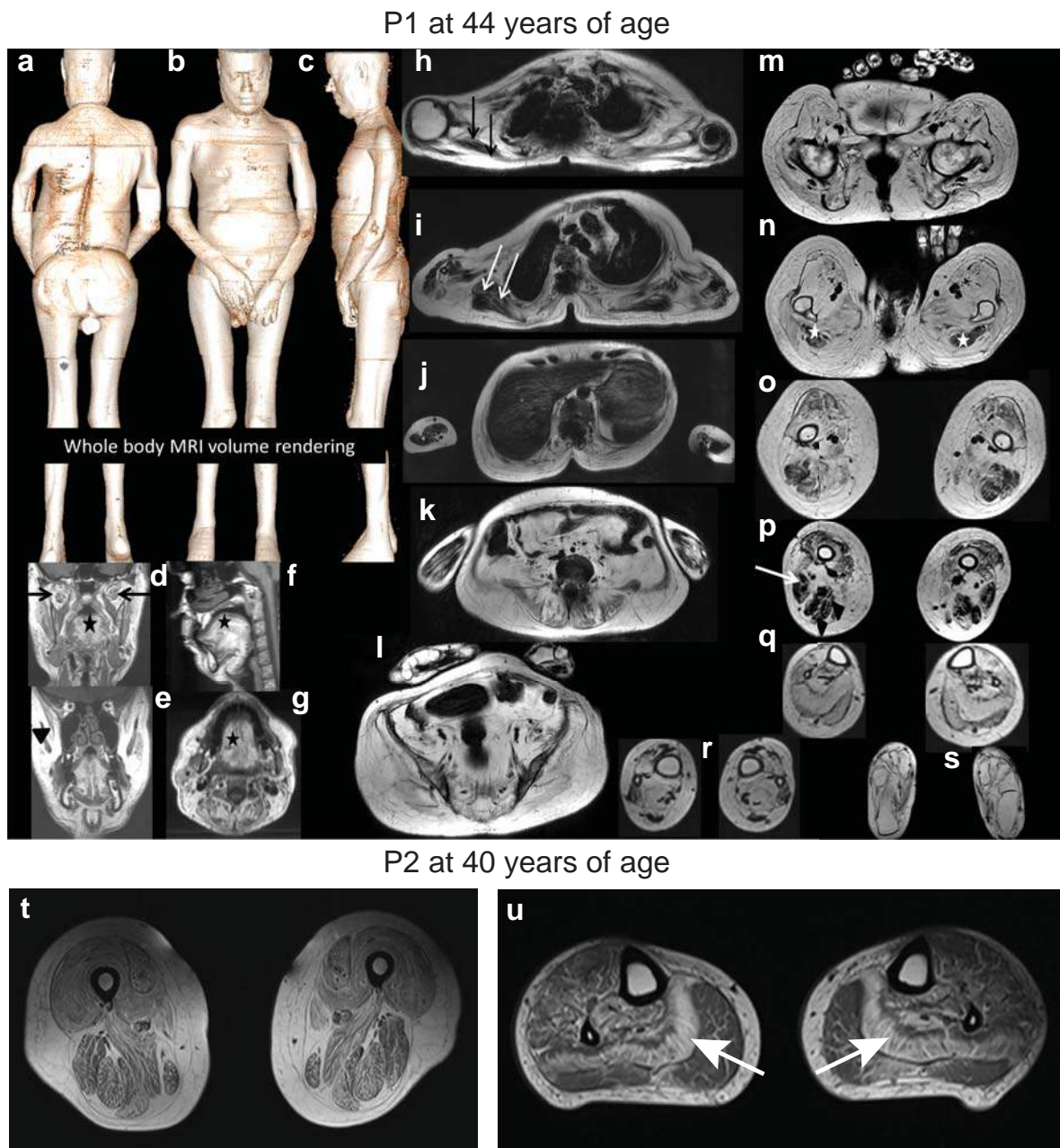
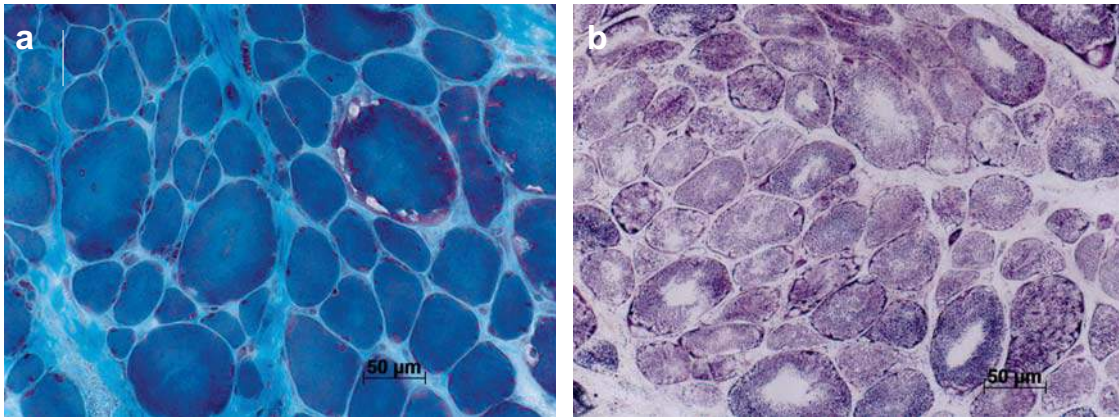


Fig. S1 MRI images of P1 and P2. Whole body MRI was performed for patient P1 (a-s) and lower extremity MRI was performed for patient P2 (t,u). **a-c** 3D volume rendering demonstrating thoracic lordosis, rigid spine, and muscle atrophy. **d-g** T1-weighted images at the face level revealed fatty infiltration of the tongue (black stars), the temporal (arrow head), and the lateral pterygoid (black arrows), while **h-m** scapular girdle supra (double black arrows) and infra spinatus (double white arrows) are better preserved. **n-p** Posterior compartment of the thigh is more preserved and particularly semitendinosus (white star), semi-membranous (double arrowheads) and short head of the biceps femoris (white arrow). **t** Abnormal muscle signal in most muscles demonstrating a generalized muscle atrophy and diffuse fatty infiltration with milder involvement of the hamstrings and of the biceps femoris. The gracilis muscle exhibits relatively less abnormal signal when compared to the sartorius muscles. **u** Selective and bilateral involvement of the soleus muscle (white arrows).

P1 Radialis muscle at 45 years of age



P2 quadriceps muscle at 19 years of age

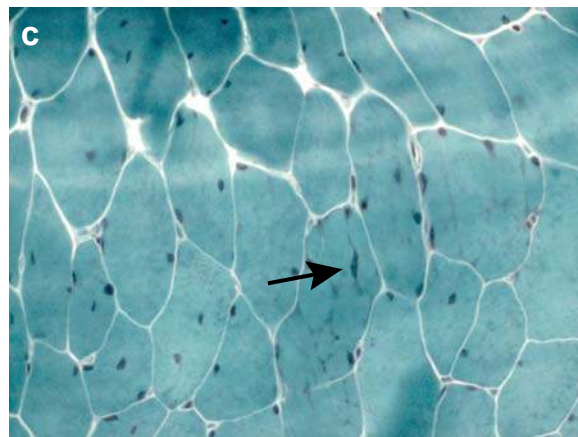


Fig. S2 Skeletal muscle histopathology of P1 at 45 years and of P2 at 19 years of age. **a** Gomori Trichrome stain revealed fibrosis and **b** oxidative SDH reaction disclosed many fibers with diffuse structural disorganization. **c** Gomori Trichrome stain showed the presence of few fibers with dark blue aggregates.

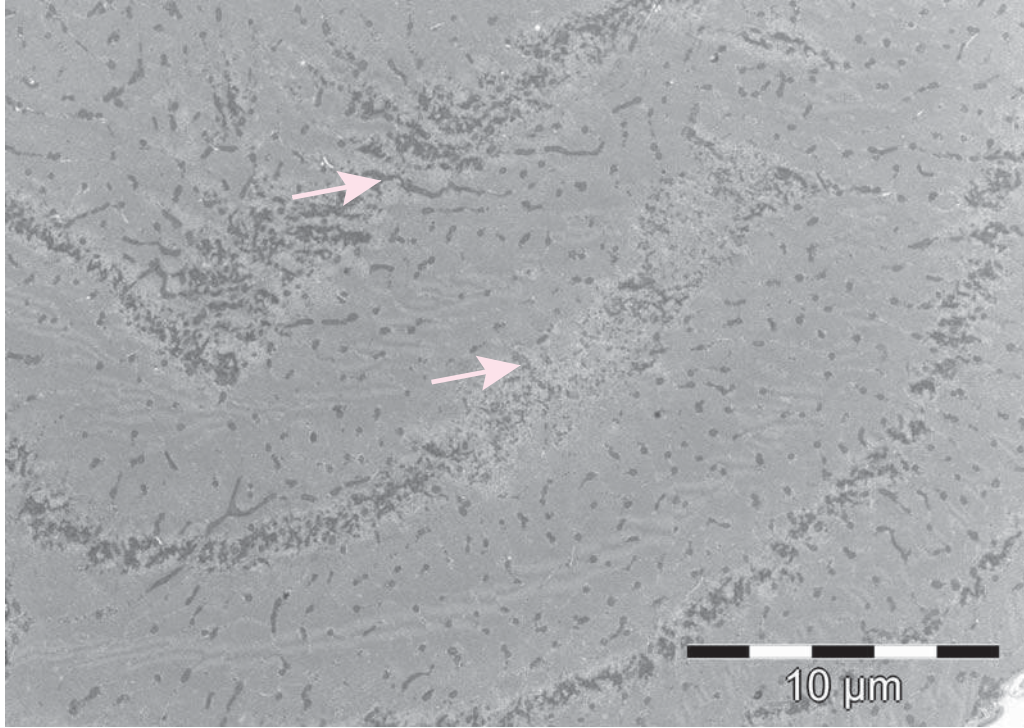


Fig. S3 Skeletal muscle ultrastructure of P1 at 45 years of age. Transverse muscle sections revealed areas of myofibrillar disorganization containing Z-line material dispersed along the myofibrils (arrows).

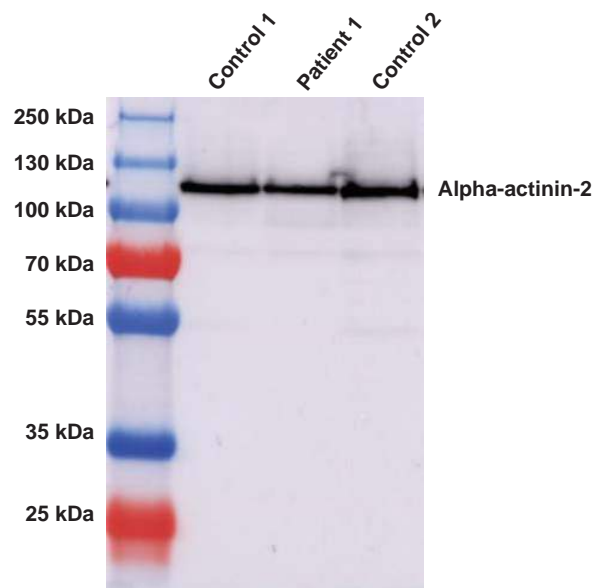


Fig. S4 Impact of the *ACTN2* p.Leu727Arg mutation on protein stability and weight. Full SDS-Page of muscle protein extracts of P1 and age-matched controls probed with antibodies against alpha-actinin-2.

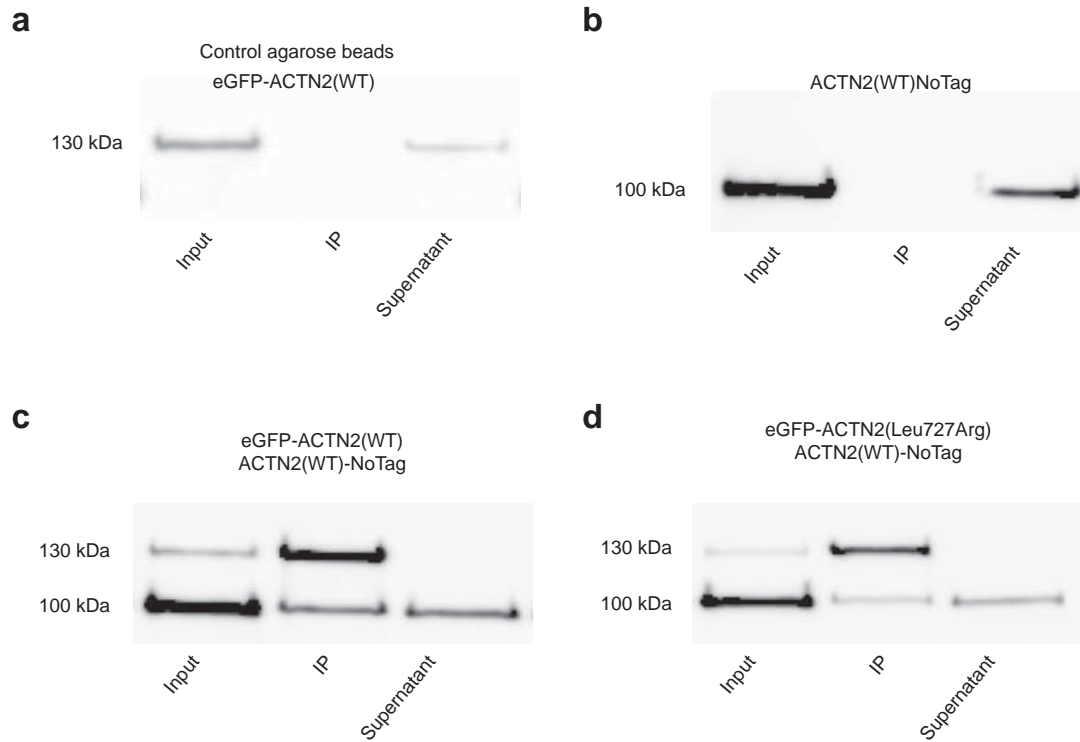


Fig. S5 Impact of p.Leu727Arg mutation on alpha-actinin-2 dimerization. Immunoprecipitation of eGFP-alpha-actinin-2 was performed with ChromoTek GFP-Trap beads or control agarose beads. **a,b** Control conditions showed that eGFP-alpha-actinin-2 does not bind to control agarose beads and that untagged alpha-actinin-2 does not bind to the GFP-Trap beads. **c,d** Coexpression of wild-type and mutant alpha-actinin-2 followed by immunoprecipitation demonstrated that the mutation does not interfere with the protein dimerization properties.

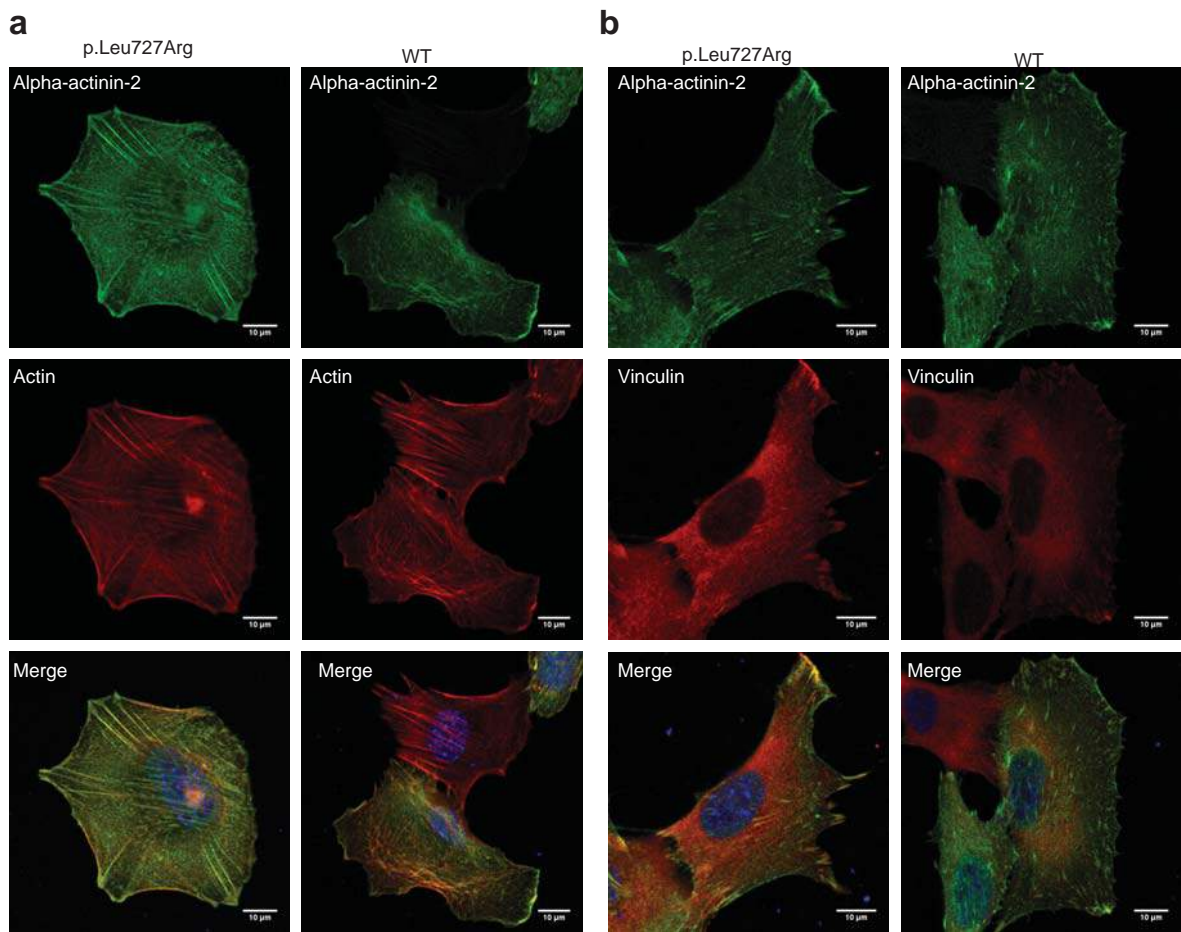


Fig. S6 Impact of the p.Leu727Arg mutation on alpha-actinin-2 interactors. **a** Phalloïdin stain marked the actin stress fibers and the presence of the p.Leu727Arg alpha-actinin-2 did not interfere with actin localization. **b** Vinculin was found at the focal adhesions and the localization in presence of mutated alpha-actinin-2 was similar to the control condition

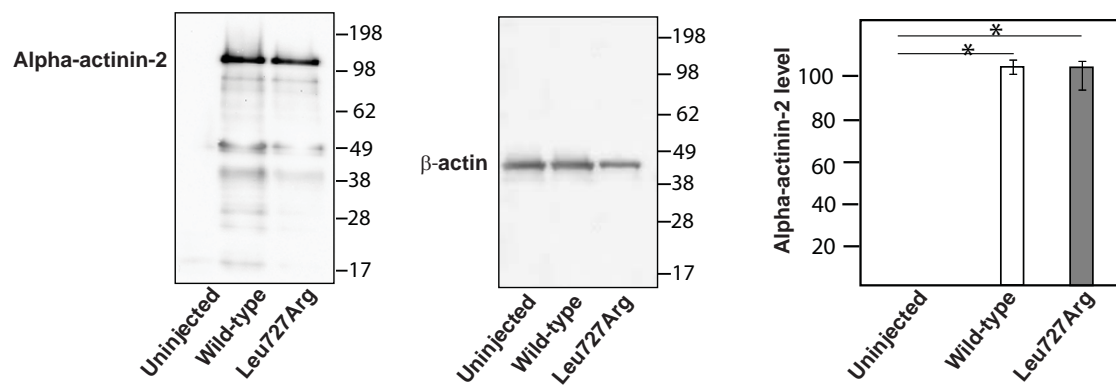


Fig. S7 Expression of human wild-type and mutant alpha-actinin-2. Alpha-actinin-2 was detected at the expected size of 100 kDa and at comparable signal intensity in wild-type and mutant mRNA-injected zebrafish.

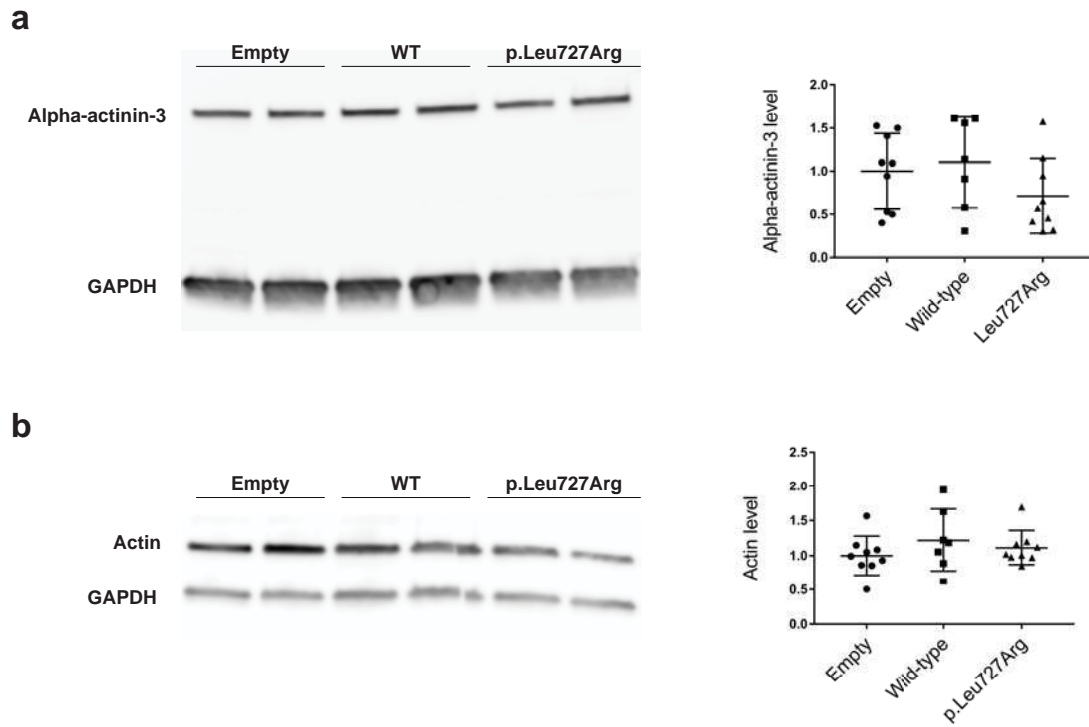
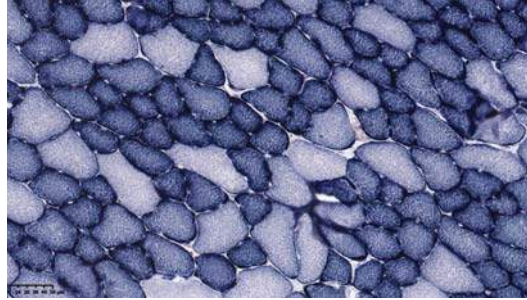


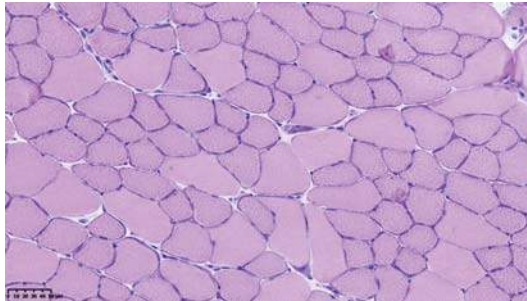
Fig. S8 Impact of the overexpression of alpha-actinin-2 in mouse skeletal muscle on the level of alpha-actinin-3 and actin. **a** SDS-Page and quantification of alpha-actinin-3 showed that the protein level is similar in muscles expressing wild-type or p.Leu727Arg alpha-actinin-2. **b** SDS-Page and quantification revealed comparable actin level in wild-type or p.Leu727Arg.

AAV-Empty

SDH



H&E



Gomori

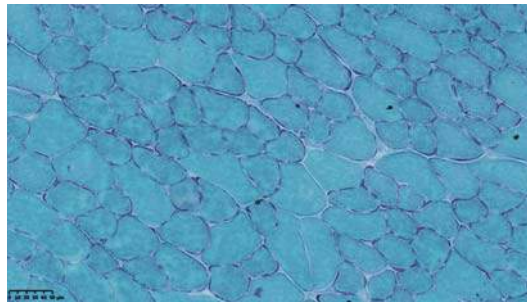


Fig. S9 Histology of control murine muscles injected with empty AAV vector. No major impact on muscle structure and no signs of inflammation were noted.

2.3.3 Investigation of the pathogenicity of the *ACTN2* c.302A>G p.(Asn101Ser) mutation

Introduction

We recently reported two families with Multiple structured Core Disease (MsCD) caused by dominant *ACTN2* mutations (Lornage et al. 2019). MsCD is characterized by early-onset muscle weakness, respiratory involvement and multiple structured-cores on muscle biopsy. Within the MYOCAPTURE project, I identified another *ACTN2* mutation in a family with different clinical and histological features. I performed functional analyses to assess the impact of the mutation, and preliminary results are presented and discussed in the following paragraphs. Except otherwise stated, the materials and methods are similar to those previously published (Lornage et al. 2019).

Clinics and histology

The family has seven affected members over two generations exhibiting severe distal retractions, sensory troubles, muscle cramps, and increased muscle fatigability (**Fig R2a**). Two patients also manifested a cardiomyopathy. Muscle biopsies were performed for all affected family members and histological analyses showed nemaline rods as the main hallmark.

Exome sequencing identified an *ACTN2* mutation

To identify the genetic cause of the muscle disease, we performed exome sequencing of all family members. Filtering and ranking of the datasets were performed using our in-house bioinformatics pipeline, and we identified a dominant *ACTN2* mutation, which was not present in the public gnomAD database. The *ACTN2* c.302A>G p.(Asn101Ser) missense mutation was found in all affected members, either at the heterozygous or at the homozygous state (**Fig R2a**). The presence and segregation of the *ACTN2* mutation was verified by Sanger sequencing. *ACTN2* encodes alpha-actinin-2, a protein composed of two actin-binding domains, a rod domain comprising four spectrin repeats, and two EF-hands (**Fig R2b**). The *ACTN2* c.302A>G p.(Asn101Ser) mutation affects a residue located in the actin-binding domain. Heterozygous *ACTN2* mutations were previously reported in patients with cardiomyopathy (Chiu et al. 2010; Girolami et al. 2014; Mohapatra et al. 2003) and in patients with MsCD (Lornage et al. 2019). On the resolved 3D protein structure, the Asn101 residue is located in close proximity to Ala119, mutated in cardiomyopathy (**Fig R2c,d**).

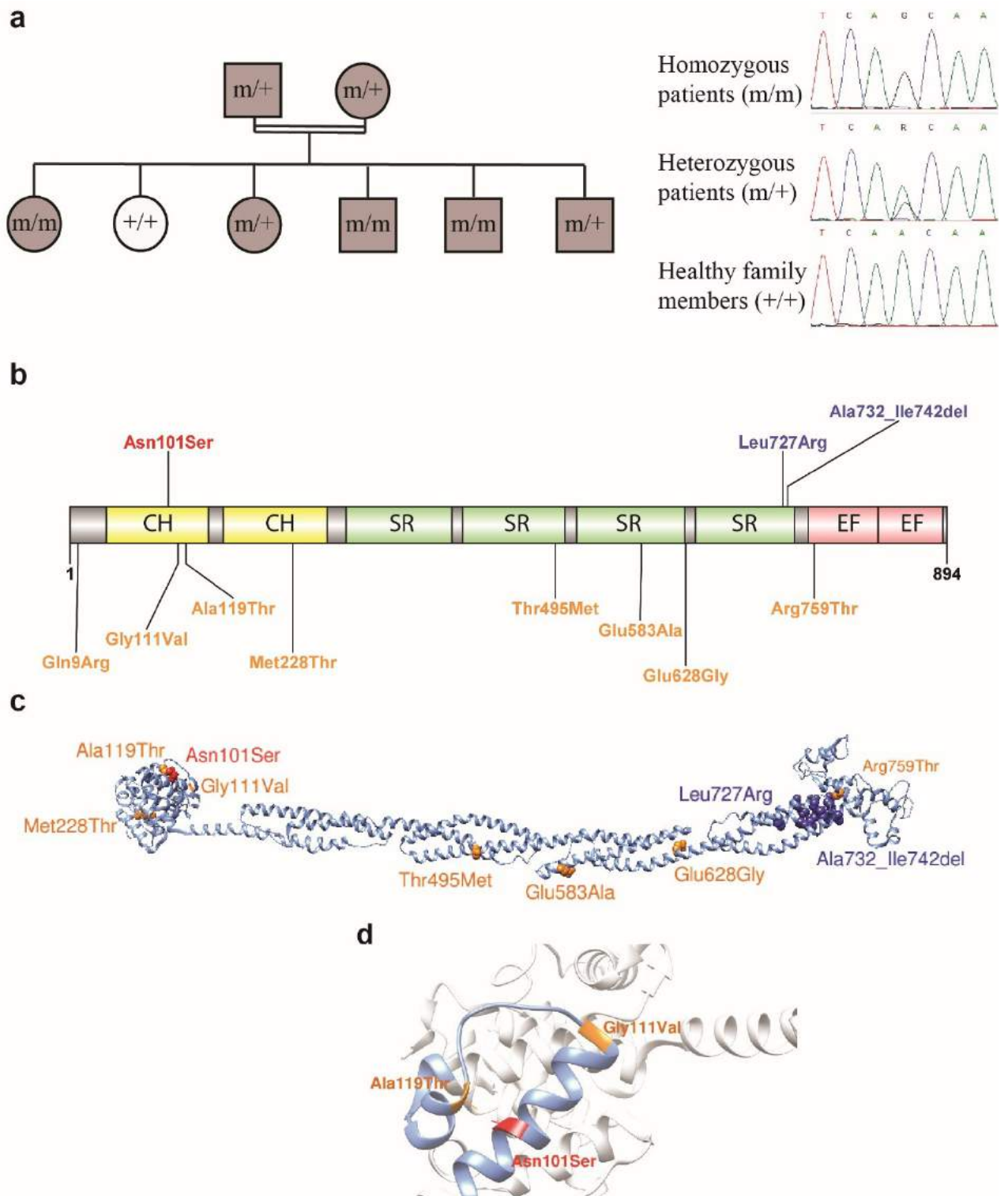


Fig R2: *ACTN2* mutation and segregation, and localization of the affected residue
a Pedigree of the family with *ACTN2* c.302A>G p.(Asn101Ser) missense mutation and chromatopherograms. **b,c** Representation of alpha-actinin-2 domains (b) and resolved protein structure (c) showing the position of the novel mutation (in pink), of the previously-reported myopathy mutations (in blue) and of the cardiomyopathy mutations (in orange). Protein domains highlighted in yellow: calponin homology domains, in green: spectrin repeats, and in pink: EF-hand domains. **d** Replacement of the asparagine 101 by a serine on the 3D protein structure and zoom.

Mutant Asn101Ser alpha-actinin-2 forms a striated pattern in C2C12 myotubes

In order to assess the impact of the *ACTN2* c.302A>G p.(Asn101Ser) mutation on the alpha-actinin-2 localization, I performed experiments in the cell model. I transfected C2C12 myoblasts with constructs coding for eGFP-tagged wild-type or Asn101Ser alpha-actinin-2 and differentiated the myoblasts into myotubes. Comparison of the intracellular organization of wild-type and mutant alpha-actinin-2 revealed a similar striated pattern of wild-type and mutant proteins presumably corresponding to the Z-line (**Fig R3**).

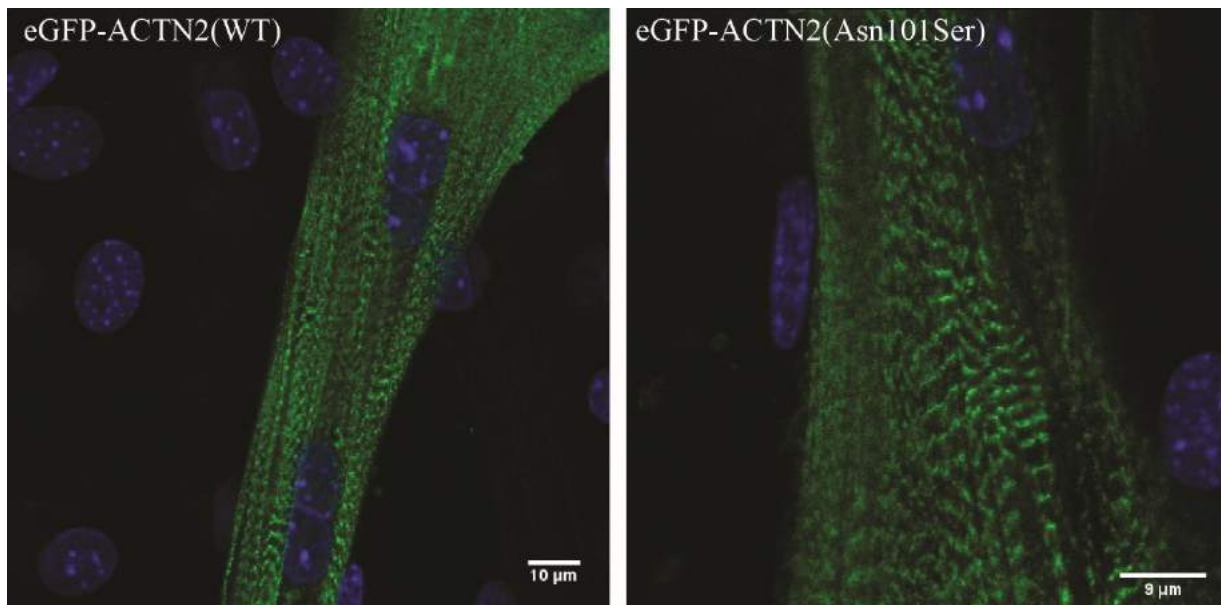


Fig R3: Impact of the *ACTN2* c.302A>G p.(Asn101Ser) mutation on alpha-actinin-2 localization

Transfected and differentiated C2C12 showed a comparable localization of wild-type and mutant eGFP-tagged alpha-actinin-2.

Mutant Asn101Ser alpha-actinin-2 shows a reduced ability to bind actin

In skeletal muscle, alpha-actinin-2 is located at the Z-line and binds actin filaments through its N-terminal calponin homology domains (**Fig R2b**) (Maruyama and Ebashi 1965; Hemmings, Kuhlman, and Critchley 1992). To compare the ability of wild-type and mutant alpha-actinin-2 to bind actin, I performed pull-down experiments in transfected C2C12 cells. Immunoprecipitation using eGFP-tagged wild-type alpha-actinin-2 as a bait revealed the presence of actin in the precipitated fraction, confirming that alpha-actinin-2 and actin interact. The Leu727Arg MsCD eGFP-alpha-actinin-2 mutant was similarly able to bind actin. In contrast, mutant Asn101Ser eGFP-alpha-actinin-2 did not immunoprecipitate actin, showing that the mutant has a reduced ability to bind actin and demonstrating that the asparagine to serine substitution at position 101 interferes with actin recruitment (**Fig R4a**). I next investigated whether the impaired interaction between Asn101Ser alpha-actinin-2 and actin

impacts on the intracellular localization and organization of actin. In C2C12 cells exogenously expressing alpha-actinin-2, fluorescent phalloidin revealed F-actin filaments. Actin fibers of comparable organization were also observed in C2C12 cells expressing mutant Asn101Ser alpha-actinin-2, indicating that the Leu101Ser mutation does not significantly disturb the intracellular actin localization (**Fig R4b**).

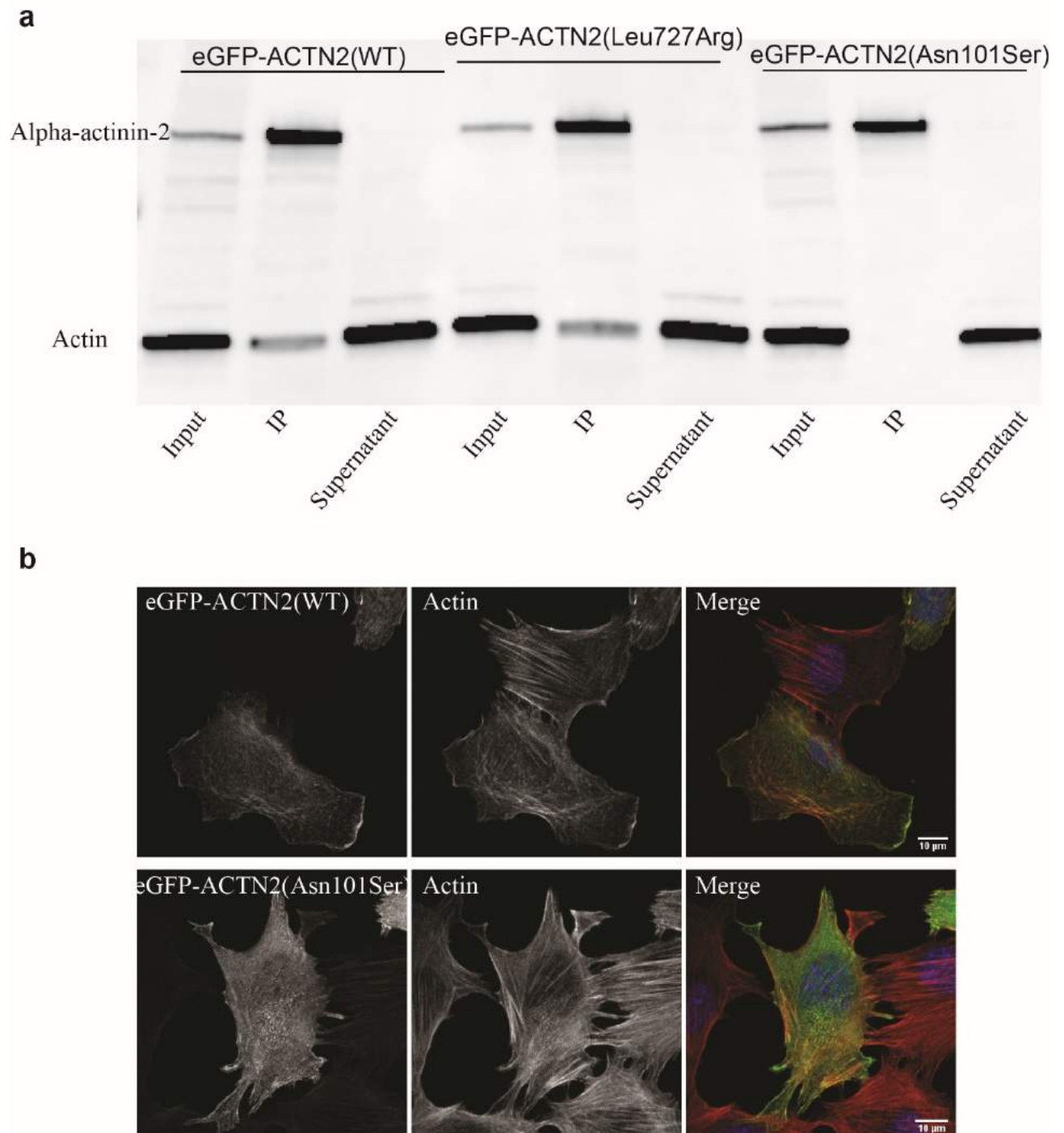


Fig R4: Impact of the Asn101Ser mutation on actin recruitment and localization

a Immunoprecipitation experiments showed that actin is efficiently bound by wild-type and Leu727Arg alpha-actinin-2, but not by the mutant Asn101Ser. **b** C2C12 myoblasts transfected with wild-type or mutant alpha-actinin-2 exhibited a comparable actin fiber organization.

Mutant Asn101Ser alpha-actinin-2 dimerizes with the wild-type

Alpha-actinin-2 is active as an antiparallel homodimer assembling predominantly via the rod domain (**Fig 2b**) (Ribeiro Ede et al. 2014; Sjoblom, Salmazo, and Djinovic-Carugo 2008). In order to investigate the ability of Asn101Ser alpha-actinin-2 to dimerize with the wild-type, I performed immunoprecipitation experiments. In co-transfected HeLa cells, GFP-tagged wild-type alpha-actinin-2 precipitated untagged wild-type alpha-actinin-2, and the same result was obtained with GFP-tagged wild-type alpha-actinin-2 and untagged mutant Asn101Ser alpha-actinin-2. This result demonstrates that the Asn101Ser mutation does not impair the interaction with wild-type alpha-actinin-2 or the ability of the protein to form stable homodimers (**Fig 5**).

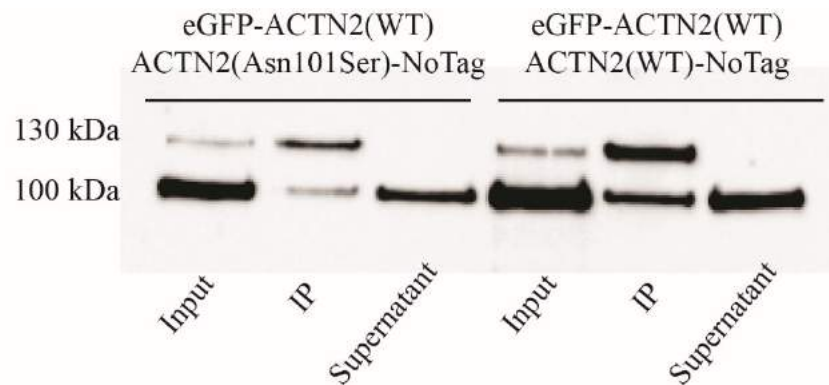


Fig R5: Impact of the Asn101Ser mutation on alpha-actinin-2 dimerization

Immunoprecipitation experiments showed that eGFP-tagged wild-type alpha-actinin-2 is efficiently bound by untagged wild-type (right) and Asn101Ser alpha-actinin-2 (left).

AAV-mediated intramuscular expression of Asn101Ser alpha-actinin-2 does not generate functional or histological defects

Alpha-actinin-2 is highly conserved across species with an asparagine residue at position 101 in human and mouse. To assess the physiological effect of the Asn101Ser alpha-actinin-2 mutation on muscle structure and function, we performed virus-mediated overexpression experiments in the mouse model. AAV2/9 coding for wild-type or mutant alpha-actinin-2 were injected into the tibialis anterior (TA) muscles of three-week-old wild-type mice. An empty AAV was used as control. The exogenous alpha-actinin-2 expression was verified by western blot, and I observed a two to three fold increased protein level in muscles injected with wild-type or mutant alpha-actinin-2 compared with injected control (**Fig R6a**). Four weeks post injection, I analyzed the impact of the mutation on TA function and structure. To assess muscle function, I performed *in situ* muscle force measurements of the injected TAs. The maximal force after electrical stimulation was similar in muscles exogenously expressing wild-type and Asn101Ser alpha-actinin-2, and calculation of the specific force by taking into account the TA

weight confirmed that wild-type and Asn101Ser injected TAs were comparably able to generate force (**Fig R6b-d**). Histochemical analyses on transversal TA sections from mice expressing the Leu101Ser alpha-actinin-2 mutant showed that the organization of the myofibers was maintained. Rods, typically observed in patients with nemaline myopathy, were not seen (**Fig R7**). Overall, the AAV-mediated alpha-actinin-2 overexpression of the Asn101Ser mutant in the TA of mice did not measurably impair the muscle contractibility or structure.

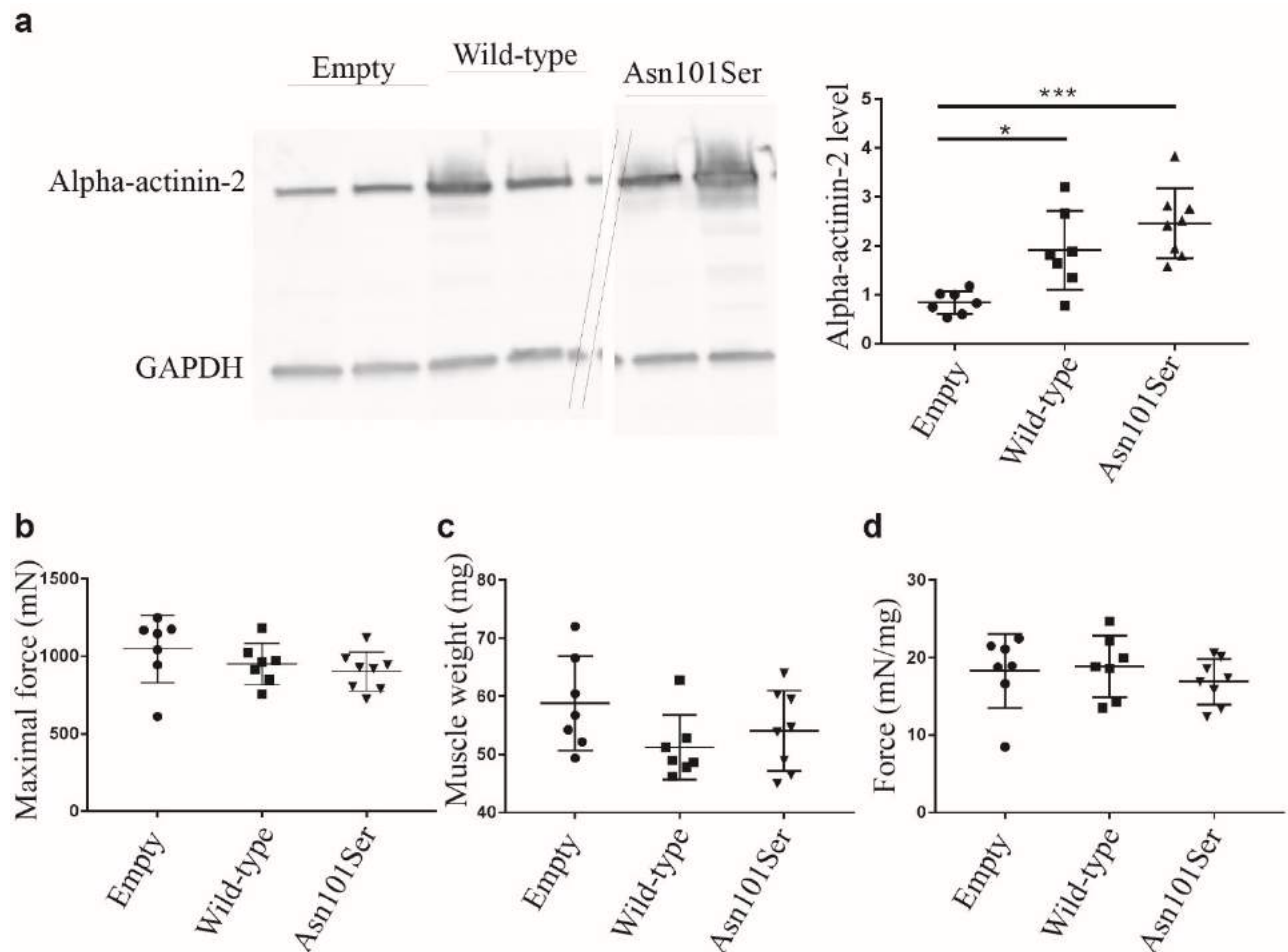


Fig R6: Impact of the AAV-mediated Asn101Ser alpha-actinin-2 expression on the TA alpha-actinin-2 level and muscle force

a SDS-PAGE and quantification demonstrated a two to threefold increase in alpha-actinin-2 level in muscles injected with AAVs encoding wild-type or mutant alpha-actinin-2 compared to empty controls. **b** Force transducing experiments revealed a similar TA maximal force in muscles expressing wild-type or mutant alpha-actinin-2. **c,d** TA muscles injected with AAVs coding for wild-type or Asn101Ser alpha-actinin-2 showed a comparable TA weight and specific force. The plots display the individual values obtained for each animal, their mean and standard deviation. Normal distribution of the data was assessed with the Shapiro-Wild normality test. Groups were compared using one-way ANOVA followed by Tukey's post hoc comparison test.

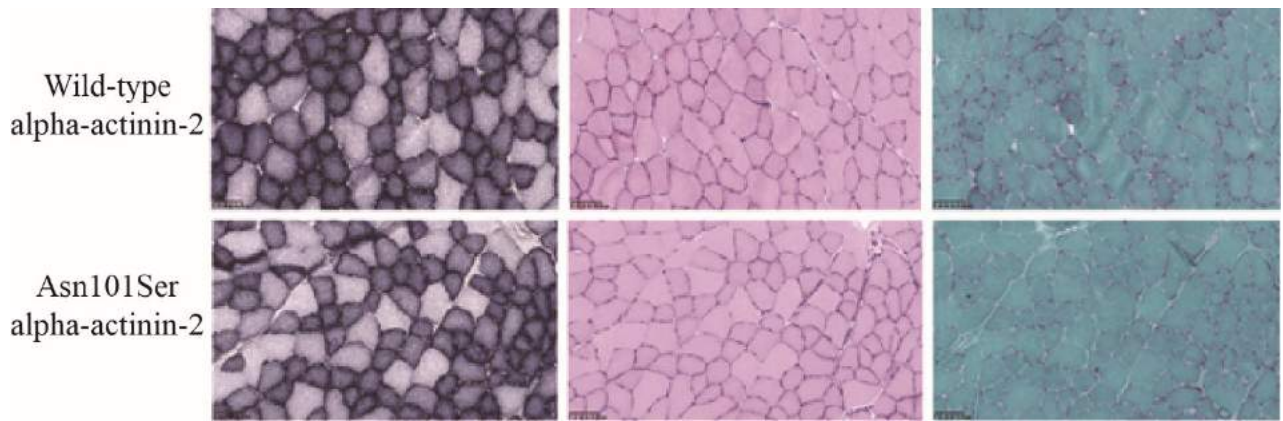


Fig R7: Impact of intramuscular AAV-mediated Asn101Ser alpha-actinin-2 expression on TA muscle histology

Transversal sections of AAV-injected TA muscles were stained with succinate dehydrogenase (SDH), hematoxylin eosin (HE) or modified Gomori trichome (mGT). The overall muscle structure was comparable in TAs expressing wild-type or Asn101Ser alpha-actinin-2.

Systemic and early AAV-mediated expression of Asn101Ser alpha-actinin-2 generates muscle weakness in mice

We showed that injections of an AAV coding for Asn101Ser alpha-actinin-2 in the TA of three-week-old mice had no measureable impact on TA structure and function, potentially indicating that the Asn101Ser alpha-actinin-2 mutation has not effect on skeletal muscle maintenance. To investigate a potential pathogenic effect of the Asn101Ser mutation on earlier developmental stages, I systemically injected one-day-old mice with AAVs coding for wild-type, Leu727Arg and Asn101Ser alpha-actinin-2, and an empty AAV was used as a control. All mice were analyzed at twelve weeks of age. The maximal force after electrical stimulation was similar in muscles exogenously expressing wild-type and mutant alpha-actinin-2. However the specific force, calculated by taking into account the TA weight, was reduced for Leu727Arg and Asn101Ser alpha-actinin-2 mutants compared to wild-type and empty controls (**Fig R8**). Histochemical analyses on transversal TA sections from mice expressing wild-type or Asn101Ser alpha-actinin-2 revealed a comparable overall muscle structure and fiber distribution. Noteworthy, expression of Leu727Arg alpha-actinin-2 induced the formation of cores, thereby confirming the pathogenicity of the Leu727Arg MsCD mutation (**Fig R9**). Overall, the systemic AAV-mediated Asn101Ser alpha-actinin-2 expression did not significantly impact on the TA muscle structure, but interfered with proper force generation of TA.

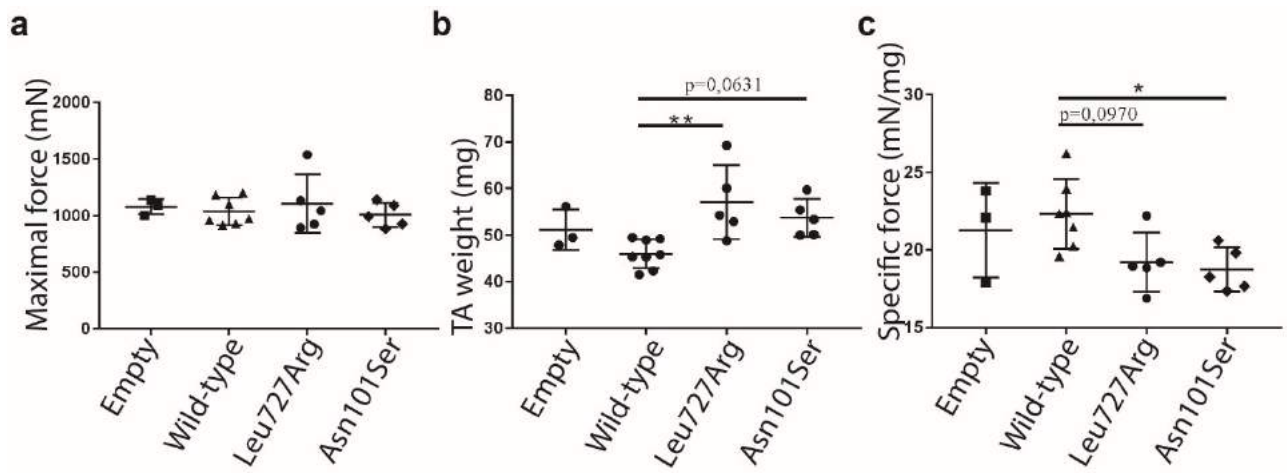


Fig R8: Impact of systemic AAV-mediated Asn101Ser alpha-actinin-2 expression on TA muscle force

a The maximal force values were comparable in TAs injected with AAV encoding wild-type or mutant alpha-actinin-2. **b** The TA weight was mildly increased in muscles expressing Leu727Arg and Asn101Ser alpha-actinin-2. **c** Specific muscle force was lower in mice exogenously expressing Leu727Arg and Asn101Ser mutant alpha-actinin-2 compared to wild-type and empty controls. The plots display the individual values obtained for each animal, their mean and standard deviation. Normal distribution of the data was assessed with the Shapiro-Wild normality test. Groups were compared using one-way ANOVA followed by Tukey's post hoc comparison test.

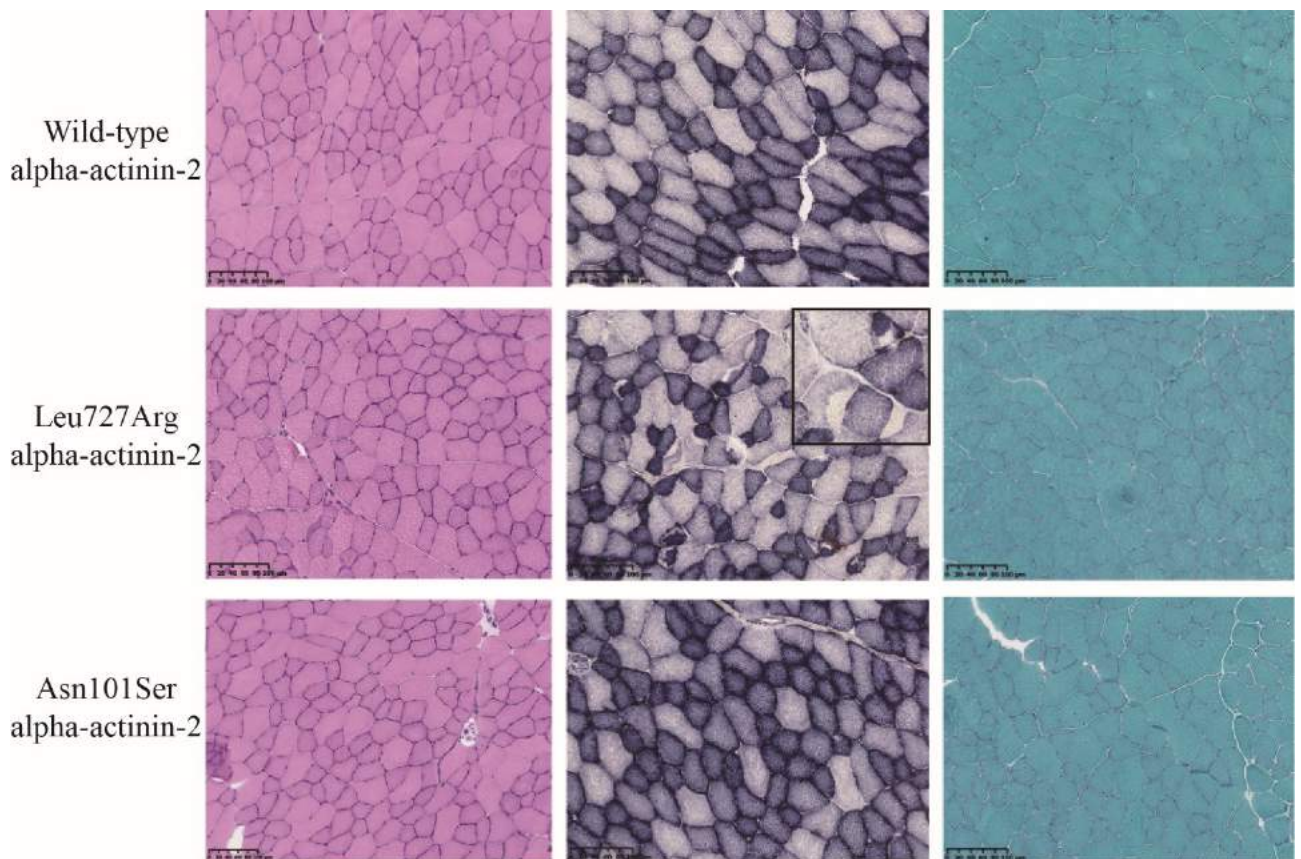


Fig R9: Impact of the systemic injection of an AAV encoding Asn101Ser alpha-actinin-2 on TA muscle histology

Transversal TA sections of systemically AAV-injected mice, stained with SDH, HE or mGT. The muscle structure of TAs expressing wild-type and Asn101Ser mutant alpha-actinin-2 was comparable. Oxidative staining revealed cores (inset) in muscles exogenously expressing Leu727Arg alpha-actinin-2, but not in muscles expressing Asn101Ser or wild-type alpha-actinin-2.

Normal heart weight and structure in mice exogenously expressing Asn101Ser alpha-actinin-2

AAV2/9 has been shown to efficiently transduce heart muscle, and I investigated if the systemically injected mice develop a cardiomyopathy as described in the patients. Mouse models of cardiomyopathy mostly exhibit a heart hypertrophy and an increased cardiac fibrosis. Heart weight was normal in mice expressing the Asn101Ser alpha-actinin-2, and histological analyses did not reveal signs of fibrosis (**Fig R10**). Overall, the systemic AAV-mediated alpha-actinin-2 overexpression of the Asn101Ser mutant did not measurably impair heart size and structure of twelve-week-old mice.

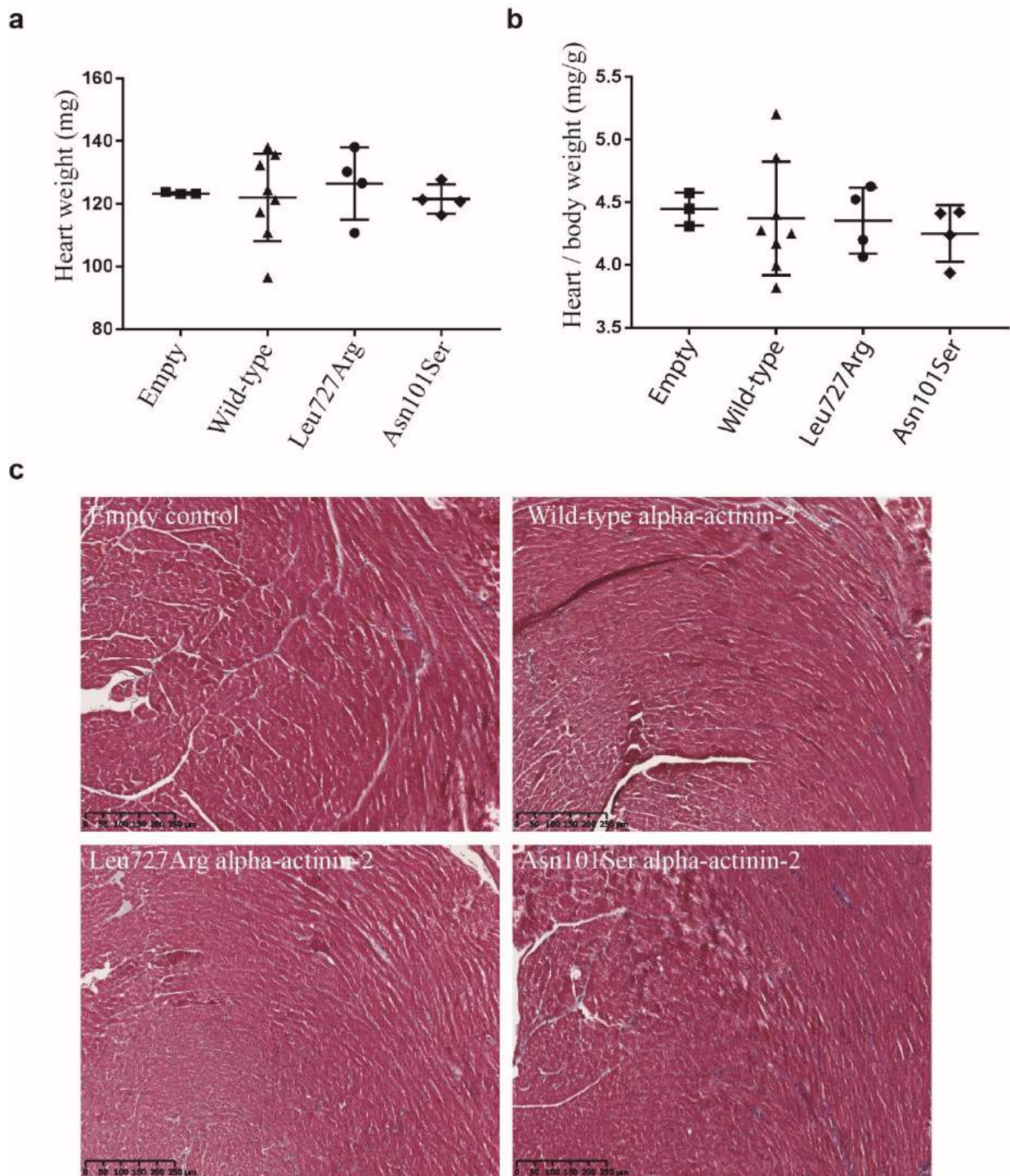


Fig R10: Normal heart weight and structure in mice systemically expressing Asn101Ser alpha-actinin-2

a Heart weight and **b** normalized heart weight of mice expressing wild-type or mutant alpha-actinin-2 were similar and did not reveal cardiac hypertrophy. **c** Masson trichome stain of heart sections showed a conserved structure in mice expressing Asn101Ser alpha-actinin-2 and did not reveal signs of fibrosis.

Conclusion and perspectives

In this study, I investigated the pathogenicity of an *ACTN2* mutation identified in a family with nemaline myopathy and cardiomyopathy. The *ACTN2* c.302A>G p.(Asn101Ser) mutation

affects a conserved amino-acid located in the actin-binding domain of alpha-actinin-2 and resides in close proximity to the *ACTN2* p.(Ala119Thr) cardiomyopathy mutation. In transfected cells, IP experiments showed a reduced ability of the Asn101Ser alpha-actinin-2 mutant to bind actin, and this defect was also observed for two cardiomyopathy mutations located in the actin-binding domain (p.(Ala119Thr) and p.(Gly111Val)) (Haywood et al. 2016). This strongly suggests that the *ACTN2* c.302A>G p.(Asn101Ser) mutation most likely accounts for the cardiomyopathy in the family described here. Further experiments are needed to confirm the causality of the Asn101Ser mutation, possibly thorough characterization of the actin-binding and bundling properties of the Asn101Ser alpha-actinin-2 mutant using an actin binding protein spin-down assay. In order to determine if the mutant exerts a dominant-negative effect on the wild-type, this assay should also be performed on a mix of wild-type and Asn101Ser alpha-actinin-2. Noteworthy, our study on mice systemically expressing Asn101Ser alpha-actinin-2 mutant did not reveal any structural cardiac anomalies. In the studied family, cardiomyopathy occurs with adult onset, and further investigations on our mice at later ages would be required. Histological analyses on heart sections could be complemented by electrocardiography and heart rate monitoring.

We also showed that the Asn101Ser mutant induces a mild muscle weakness in systemically injected mice, demonstrating the pathogenicity of the mutation. However, histological stains of muscle sections did not reveal nemaline rods, and further histological and ultrastructural investigations are necessary to fully conclude on the structural integrity of the injected muscles.

DISCUSSION

2.4 *MYPN* and *ACTN2* – two novel congenital myopathy genes

2.4.1 *MYPN* mutations in human disease

Common mutational and clinical pattern for *MYPN*-related congenital myopathy

In total, nine patients from seven unrelated families with recessive *MYPN* mutations have been reported to date (Miyatake et al. 2017; Merlini et al. 2019; Lornage et al. 2017). The identified mutations were evenly distributed on the gene and encompassed essential splice site mutations, nonsense mutations and small frameshift deletions (**Fig D1**). Protein studies were performed in all but one family, and showed that the mutations lead to the absence of full-length myopalladin. Minigene experiments with the mutation identified in the remaining family (**F6 in Table D1**) revealed two transcripts predicted to undergo nonsense-mediated mRNA decay, thereby demonstrating a similar mutational impact in all families. Comparison of the clinical features of all published *MYPN* cases reveals a common phenotype characterized by an early-onset and slowly-progressive muscle weakness primarily and firstly affecting the neck and distal muscles, and becoming more diffuse at later stages of the disease. All tested patients also exhibited a respiratory involvement with variable reduction of their vital capacity (**Table D1**).

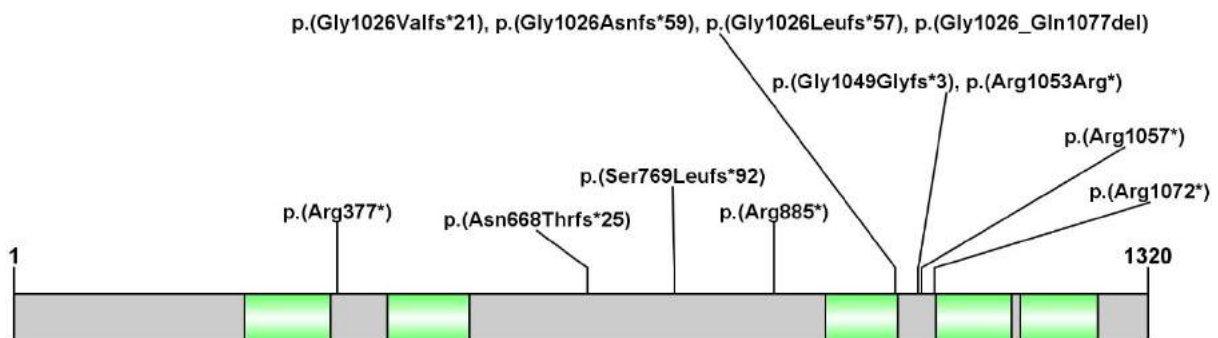


Fig D1: Myopalladin protein domains and reported mutations

*Representation of myopalladin domains showing the position of all mutations. The Ig-like domains involved in protein-protein interactions are represented in green. Two splice site mutations were identified and both generate multiple transcript containing premature stop codons. For the c.3076-2A>C *MYPN* mutation, four splice products were detected (p.(Gly1026Valfs*21), p.(Gly1026Asnfs*59), p.(Gly1026Leufs*57), p.(Gly1026_Gln1077del)), and for the c.3158+1G>A mutation, two splice products were detected (p.(Arg1053Arg*), p.(Gly1049Glyfs*3)).*

Family	Patient	Mutation	Onset	Muscle weakness	Muscle histology	Respiration	Other features	Reference
1	3	c.1129C>T p.(Arg377*)	Childhood	Distal lower limb and neck muscle weakness	Type 1 fiber predominance, nemaline bodies	NA	-	Miyatake et al., 2017
2	1	c.2003delA p.(Asn668Thrfs*25)	Childhood	Diffuse muscle weakness	Type 1 fiber predominance, nemaline bodies, intranuclear rods	VC 39,9 %	High-arched palate, cardiopathy	Miyatake et al., 2017
3	II.2	c.2304delC p.(Ser769Leufs*92)	Neonatal	Axial, distal, and facial muscle weakness, neck flexor weakness, hanging big toe	Type 1 fiber predominance, internal nuclei	VC 51 %	Pes cavus, mild ptosis, contractures, cardiopathy	Merlini et al., 2019
	II.3		Adulthood	Distal muscle weakness, neck flexor, big toes extensor weakness	NA	VC 93 %	-	
4	P1	c.2653C>T p.(Arg885*)	Neonatal	Axial, distal, limb-girdle, and facial muscle weakness, neck flexor weakness	Type 1 fiber predominance, caps, rods	VC 57%	Pectus excavatum, pes cavus, high-arched palate, ptosis	Lormage et al., 2017
	P2		Childhood	Axial, distal, limb-girdle, and facial muscle weakness, neck flexor weakness	Type 1 fiber predominance, caps, rods	NA	Low-set ears, cardiopathy	
5	2	c.3076-2A>C	Childhood	Distal lower limb, neck, and facial muscle weakness	Type 1 fiber predominance, nemaline bodies	NA	-	Miyatake et al., 2017
6	P3	c.3158+1G>A	Childhood	Axial, distal, limb-girdle, and facial muscle weakness, neck flexor weakness	Type 1 fiber predominance, caps, rods	VC 46%	Low-set ears, pectus excavatum	Lormage et al., 2017
7	P4	c.3169C>T p.(Arg1057*) c.3214C>T p.(Arg1072*)	Childhood	Axial, distal, limb-girdle, and facial muscle weakness	Type 1 fiber predominance, nemaline bodies, intranuclear rods	VC 84%	-	Miyatake et al., 2017

Table D1: Genetic, histological and clinical features of patients with *MYPN* mutations

All families have been numbered according to the mutation position. NA: not assessed; NIV: non-invasive ventilation; VC: vital capacity. Homozygous mutations are bold. The *c.3076-2A>C* and *c.3158+1G>A* splice site mutations cause the appearance of multiple transcripts containing premature stop codons.

Histopathological heterogeneity of *MYPN*-related myopathy

Muscle biopsies from eight *MYPN* patients revealed marked type 1 fiber predominance, a common feature observed in congenital myopathies. Based on the additional histological hallmarks, the patients were classified into two main groups with either nemaline rods or caps on muscle sections (**Table D1**). Overlapping histological features of cap myopathy and nemaline myopathy have been previously documented in patients with *TPM2*, *TPM3* and *NEB* mutations, suggesting that cap structures and nemaline rods arise from the same physiological muscle defects (Malfatti et al. 2013; Tajsharghi et al. 2007; Piteau et al. 2014). The biopsied muscle may also account for the differences in muscle histopathology. For patients with nemaline rods as main histological hallmark, the biceps brachii muscle was sampled, while muscle biopsies from patients with cap myopathy originated from either the quadriceps or the deltoid muscles (**Table D2**).

Family	Patient	Sampled muscle	Muscle histology	Reference
1	3	Biceps brachii	Nemaline rods	Miyatake et al., 2017
2	1	UNK	Nemaline rods, intranuclear rods	Miyatake et al., 2017
3	II.2	Quadriceps	Aspecific	Merlini et al., 2019
	II.3	ND	ND	
4	P1	Quadriceps / deltoid	Caps	Lornage et al., 2017
	P2	Quadriceps	Caps	
5	2	Biceps brachii	Nemaline rods	Miyatake et al., 2017
6	P3	Deltoid	Caps	Lornage et al., 2017
7	4	Biceps brachii	Nemaline rods, intranuclear rods	Miyatake et al., 2017

Table D2: Myopalladin myopathy patients, biopsied muscles and main histological defects
Comparison of the main histological defects on biopsies from all published MYPN patients. ND: not done; UNK: unknown.

Progression of the lesions over time

Our patient F4-P1 had a first deltoid muscle biopsy at the age of five years which was interpreted as normal. Two subsequent muscles biopsies from the quadriceps muscle at age 16 and from the deltoid muscle at age 34 revealed caps and occasional rods. Her brother (patient F4-P2) had four deltoid muscle biopsies between the age of five and 15 years, and none revealed histological anomalies. A fifth muscle quadriceps muscle biopsy performed at age 30 years finally revealed caps. This was also reported for patients with *TPM2*-, *NEB*- or *ACTA1*-related cap/rod myopathy, who also had successive muscle biopsies until the diagnosis was reached (Tajsharghi et al. 2007; Piteau et al. 2014; Hung et al. 2010). The presence of either rod, caps or both may depend on the biopsied muscle and on the age of the patient at the time of biopsy. This observation highlights the fact that the biopsy may not be informative, and that panel screening could be considered at first intention to provide a molecular diagnosis to patients with clinically diagnosed myopathy. Moreover, it demonstrates that the muscle weakness precedes the appearance of detectable histological and ultrastructural lesions, suggesting that the caps or rods are not the cause of the muscle weakness *per se*, but rather a consequence of muscle malfunction.

MYPN mutations: myopathy vs cardiomyopathy

In total, 23 different dominant *MYPN* mutations have been reported in patients with dilated, hypertrophic or restrictive cardiomyopathy (Zhao et al. 2015; Chami et al. 2014; Meyer et al. 2013; Hertz et al. 2016; Nunn et al. 2016; Duboscq-Bidot et al. 2008; Purevjav et al. 2012). The mutations encompassed 20 missense, two nonsense and one frameshift mutation (**Table D3**). A subset of the reported mutations were frequent in the gnomAD database, contesting their

causality, and potentially requiring an additional molecular analysis of the affected individuals. The missense mutations associated with cardiomyopathy were evenly distributed on the gene, indicating that they might have similar pathogenic effect (**Fig D2**).

Mutation	Type	gnomAD FREQ	References
p.(Tyr20Cys)	missense	264 het	Purevjav et al., 2012 and Nunn et al., 2016
p.(Ile83fs*105)	frameshift	NP	Duboscq-Bidot et al., 2008
p.(Arg115Cys)	missense	NP	Chami et al., 2014
p.(Lys153Arg)	missense	3 het	Purevjav et al., 2012
p.(Ile213Val)	missense	1 het	Purevjav et al., 2012
p.(Ala217Glu)	missense	NP	Purevjav et al., 2012
p.(Asp221Val)	missense	38 het / 1 hom	Hertz et al., 2016
p.(Tyr339Phe)	missense	NP	Purevjav et al., 2012
p.(Val410Ala)	missense	40 het / 1 hom	Purevjav et al., 2012
p.(Glu529*)	nonsense	NP	Purevjav et al., 2012 and Huby et al., 2015
p.(Ala611Thr)	missense	NP	Purevjav et al., 2012
p.(Glu630Lys)	missense	2 het	Zhao et al., 2015
p.(Pro841Thr)	missense	NP	Purevjav et al., 2012
p.(Ala882Thr)	missense	5 het	Purevjav et al., 2012
p.(Arg885*)	nonsense	2 het	Purevjav et al., 2012
p.(Phe954Leu)	missense	NP	Purevjav et al., 2012
p.(Arg955Trp)	missense	133 het	Meyer et al., 2013
p.(Pro961Leu)	missense	NP	Meyer et al., 2013
p.(Arg1088His)	missense	1 het	Duboscq-Bidot et al., 2008
p.(Leu1161Ile)	missense	980 het / 14 hom	Purevjav et al., 2012
p.(Pro1112Leu)	missense	865 het / 4 hom	Purevjav et al., 2012 and Duboscq-Bidot et al., 2008
p.(Val1195Met)	missense	86 het	Duboscq-Bidot et al., 2008
p.(Ala1265Pro)	missense	NP	Purevjav et al., 2012

Table D3: MYPN cardiomyopathy mutations, type of mutations and frequency

23 different MYPN cardiomyopathy mutations were reported, and all but three are missense mutations. A subset of the reported mutations is listed with high frequency in the gnomAD database. gnomAD FREQ: frequency in the gnomAD database; Het: heterozygous; Hom: homozygous; NP: not present.

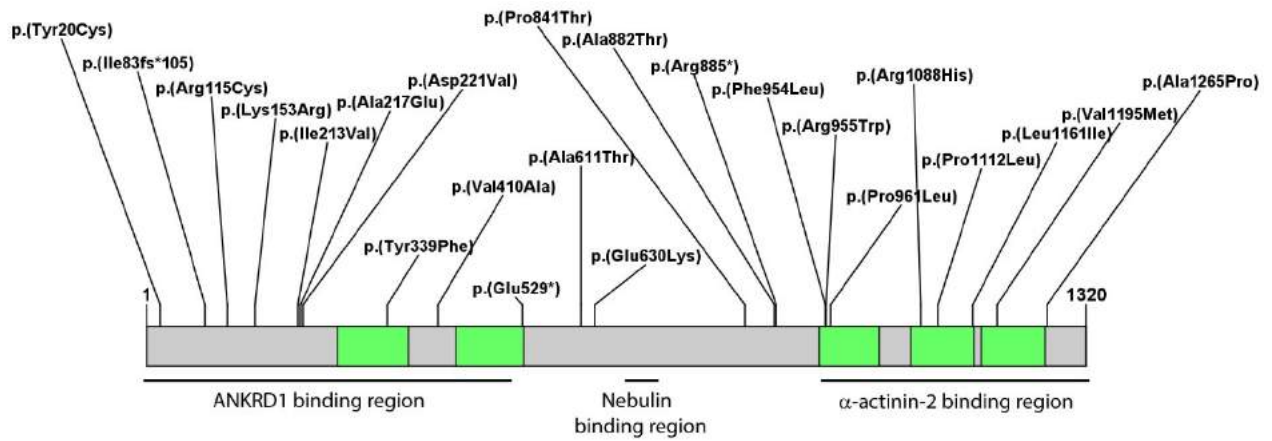


Fig D2: Myopalladin protein domains and reported cardiomyopathy mutations

Representation of myopalladin domains as predicted by the ScanProsite tool. The regions interacting with ANKRD1, nebulin and alpha-actinin-2 are highlighted. In green: Ig-like domains.

Myopalladin has a dual function in skeletal muscle and heart: it participates in the assembly of the I-band and Z-disk in the sarcoplasm through binding to alpha-actinin-2 and nebulin (skeletal muscle) or nebulin (heart), and it also regulates muscle gene expression in the nucleus by interaction with the transcription factor ANKRD1 (Ankyrin repeat protein). Functional experiments were performed for four *MYPN* cardiomyopathy mutations. Exogenous expression of the Glu529* and Pro1112Leu myopalladin mutant in rat cardiomyocytes induced sarcomeric disorganization and premature cell death. Additionally, *in vivo* experiments in mice showed that the Tyr20Cys myopalladin mutant perturbed nuclear shuttling of myopalladin and exhibited a reduced affinity for ANKRD1, and the Glu529* mutant caused an overall reduced level and a delocalization of ANKRD1 in heart (Duboscq-Bidot et al. 2008; Purevjav et al. 2012; Huby et al. 2014). In summary, the *MYPN* cardiomyopathy mutations appear to directly or indirectly interfere with ANKRD1 binding, and this suggests that the abnormal regulation of ANKRD1 target genes contributes to the pathomechanism underlying the disorder.

Noteworthy, three patients with *MYPN*-related myopathy and homozygous truncating mutations also presented with a cardiomyopathy, while heterozygous carriers in the family were healthy. As suggested by Miyatake et al., an explanation to the different mutation types and their involvement in either a cardiac or a skeletal muscle disease or both could be the following:

- Heterozygous *MYPN* gain-of-function mutations cause cardiomyopathy.
- Compound heterozygous or homozygous loss-of-function mutations cause congenital myopathy with full penetrance and might be associated with a mild cardiomyopathy with incomplete penetrance.
- Heterozygous loss-of-function mutations do not cause a phenotype.

Overall, our patients confirm the causality of *MYPN* mutations in human disorders and demonstrated that homozygous loss-of-function mutations give rise to myopathy. A better understanding of the pathomechanisms of the *MYPN*-related myopathy is however necessary for the development of targeted therapies. The creation and characterization of a *Mypn* knock-out mouse model would contribute to better understand the disease development, and could serve as a tool to assess the efficacy of therapeutic approaches by AAV-mediated *MYPN* gene replacement.

2.4.2 *ACTN2* mutations in human disease

ACTN2 mutations cause two distinct skeletal muscle diseases

To date, a total of six unrelated families with dominant *ACTN2* mutations have been reported in the literature (Lornage et al. 2019; Savarese et al. 2019) (**Table D4**). We described two individuals with *de novo* *ACTN2* mutations and both patients suffered from a slowly progressive childhood-onset myopathy with respiratory involvement affecting distal, proximal, axial, and facial muscles. Creatine kinase levels were within the normal range. The muscle biopsies revealed type-1 fiber uniformity and multiple structured cores in muscle fibers. Ultrastructural analyses of these cores revealed an overall preservation of the myofilament organization, and we termed this new core myopathy “Multiple structured Core Disease” (MsCD) (Lornage et al. 2019). Savarese et al. reported four families carrying *ACTN2* missense mutations, and suffering from an adult-onset muscular dystrophy causing quadriceps hypertrophy and/or myalgia at early stages of the disease and subsequently involving distal lower leg followed by proximal muscle weakness. The creatine kinase levels ranged from a normal level to a ten-fold elevation. Muscle biopsies were available for two individuals and showed fiber size variability, fibrosis, multiple internalized nuclei and uneven oxidative staining. The most affected individual additionally displayed autophagic vacuoles, cytoplasmic bodies and protein aggregates (p62, TDP-43, myotiline). Given the dystrophic features observed on muscle biopsies, the authors ranked this disease into a new class of muscular dystrophy that they called “Actininopathy” (Savarese et al. 2019).

Family	Patient	Mutation	Onset	Muscle weakness	Muscle histology	Other features	Reference
1	F4 II:1	c.392T>C p.(Leu131Pro)	Adulthood	Distal and proximal lower limb muscle weakness	ND	Ambulant with a walker, calf hypertrophy, mildly elevated CK levels	Savarese et al., 2019
	F4 III:1		Adulthood	Distal and proximal lower limb muscle weakness, abdominal and neck flexor weakness	ND	Uses two sticks for ambulation	Savarese et al., 2019
2	9 patients from F1	c.1459T>C p.(Cys487Arg)	Adulthood	Distal lower limb and proximal muscle weakness, foot drop	Available for 2 patients. Fiber size variation, multiple internal nuclei, fibrosis, areas with reduced oxidative activity, vacuoles (1/2), cytoplasmic bodies (1/2), p62 and TDP-43 protein aggregates (1/2).	Myalgia, hypertrophic quadriceps. Mildly elevated CK levels	Savarese et al., 2019
3	5 patients from F2	c.1459T>C p.(Cys487Arg)	Adulthood	Distal lower limb and proximal muscle weakness	ND	Hypertrophic quadriceps, mildly elevated CK levels	Savarese et al., 2019
4	F3 I:1	c.1459T>C p.(Cys487Arg)	Adulthood	Proximal lower limb and ankle dorsiflexion weakness	ND	Gait difficulties, mildly elevated CK level, cardiomyopathy	Savarese et al., 2019
	F3 II:1		Adulthood	Wrist extensor and ankle dorsiflexion weakness	ND	Muscle atrophy in forearms	
5	P1	c.2180T>G p.(Leu727Arg)	Neonatal	Proximal, axial, distal and facial muscle weakness	Type 1 fiber predominance, numerous cores, internalized nuclei	Tracheostomy, scoliosis, contractures, VC 35%	Lomage et al., 2019
6	P2	c.2194_2226del p.(Ala732_Ile742del)	Childhood	Proximal, axial and facial muscle weakness	Type 1 fiber predominance, numerous cores, internalized nuclei	Scoliosis, contractures, VC 65%	Lomage et al., 2019

Table D4: Genetic, histological and clinical features of patients with ACTN2 mutations

All families have been numbered according to the mutation position. ND not done; VC vital capacity; CK creatine kinase. All mutations were heterozygous.

While MsCD is an early-onset muscle disease with no clinical or histological signs of dystrophy, actininopathy patients presented with an adult-onset muscle weakness, mildly elevated creatine kinase level and histological signs of dystrophy. Furthermore, MsCD patients exhibited characteristic structured cores located at the periphery of the fibers, and these histological anomalies were not seen in the biopsy of actininopathy patients.

MsCD and actininopathy are both caused by heterozygous *ACTN2* mutations. The MsCD mutations encompass one missense and one in-frame deletion affecting amino acids located in the fourth spectrin repeat (p.(Leu727Arg), p.(Ala732_Ile742del)), whereas the two actininopathy missense mutations (p.(Leu131Pro), p.(Cys487Arg)) respectively affect a residue located in the actin-binding domain, and a residue of the second spectrin repeat, and none of them approximated the residues affected in MsCD (**Fig D4**). Taken together, the different clinical and histological features, and the distant localization of the MsCD and actininopathy *ACTN2* mutations suggest that both diseases are two distinct myopathies. The identification and thorough description of additional *ACTN2* patients is necessary to precisely characterize MsCD and actininopathy, and to finally conclude on the potential nosological distinction or overlap of both disorders.

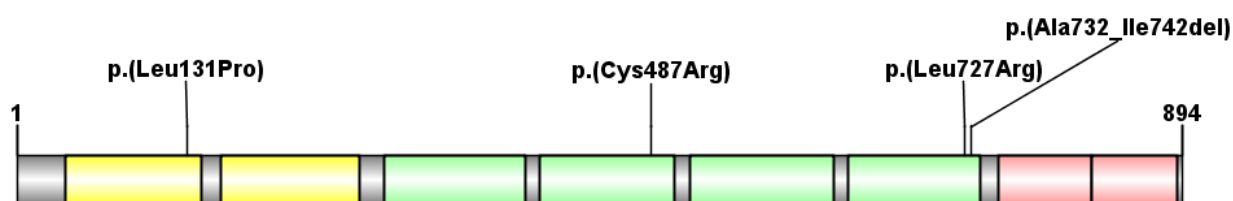


Fig D4: Alpha-actinin-2 protein domains and mutations

Position of the alpha-actinin-2 myopathy mutations. The actiniopathy mutations (*p.(Leu131Pro)*, *p.(Cys487Arg)*) affect residues located in the first calponin homology domain and in the first spectrin repeat. Both *MsCD* mutations affect residues located in the fourth spectrin repeat. Protein domains highlighted in yellow: calponin homology domains; in green: spectrin repeats; and in pink: EF-hand domains.

Specific *ACTN2* mutations cause cardiomyopathy

Eight different *ACTN2* mutations have been reported in patients with dilated or hypertrophic cardiomyopathy followed by ventricular dilatation at later stages (**Table D5**) (Chiu et al. 2010; Bagnall et al. 2014; Girolami et al. 2014; Haywood et al. 2016; Theis et al. 2006; Mohapatra et al. 2003). Six mutations were found in familial cases and segregated in a dominant fashion in the affected individuals. All were missense mutations and half of them were listed in the public gnomAD database. The age at diagnosis/onset ranged from four to 75 years of age and the severity of the disease varied considerably within the families. Four *ACTN2* mutations were found in the actin-binding domain, three in the second and third spectrin repeats of the elongated rod and one in the EF-hand (**Fig D5**). All mutations caused similar phenotypes, and the absence of an obvious mutational hotspot suggests that the mutations have the same pathogenic effect on heart physiology.

Mutation	gnomAD FREQ	Type	Family history	Age at diagnosis	Disease	Reference
<i>p.(Gln9Arg)</i>	180 het	Missense	Father died from acute-onset idiopathic dilated cardiomyopathy at 42 years of age	7 years	Dilated cardiomyopathy	Mohapatra et al., 2003
<i>p.(Gly111Val)</i>	16 het / 1 hom	Missense	No	31 years	Hypertrophic cardiomyopathy	Theis et al., 2006
<i>p.(Ala119Thr)</i>	NP	Missense	Multiple affected members in two unrelated families	Between 25 at 75 years	Hypertrophic cardiomyopathy, dilated cardiomyopathy	Haywood et al., 2016
<i>p.(Met228Thr)</i>	NP	Missense	Eleven affected members and seven clinically unaffected carriers	From four years	Hypertrophic cardiomyopathy, arrhythmia	Girolami et al., 2014 Bagnall et al., 2014 Chiu et al., 2010
<i>p.(Thr495Met)</i>	198 het / 1 hom	Missense	Four families including two with multiple affected members	Between 15 and 32 years	Hypertrophic cardiomyopathy	Theis et al., 2006 Chiu et al., 2010
<i>p.(Glu583Ala)</i>	6 het	Missense	Three affected members over two generations	65 years	Hypertrophic cardiomyopathy	Chiu et al., 2010
<i>p.(Glu628Gly)</i>	NP	Missense	Two affected members over two generations, one healthy carrier	Between 16 and 44 years	Hypertrophic cardiomyopathy	Chiu et al., 2010
<i>p.(Arg759Thr)</i>	NP	Missense	No	17 years	Hypertrophic cardiomyopathy	Theis et al., 2006

Table D5: *ACTN2* cardiomyopathy mutations, frequency, and segregation

Eight *ACTN2* cardiomyopathy mutations were reported, and all are missense mutations. Half of them are not present in the *gnomAD* database. Six mutations were found in familial cases, and the age at diagnosis varied between 4 and 75 years of age. *gnomAD*: frequency in the *gnomAD* database; *Het*: heterozygous; *Hom*: homozygous; *s NP*: not present.

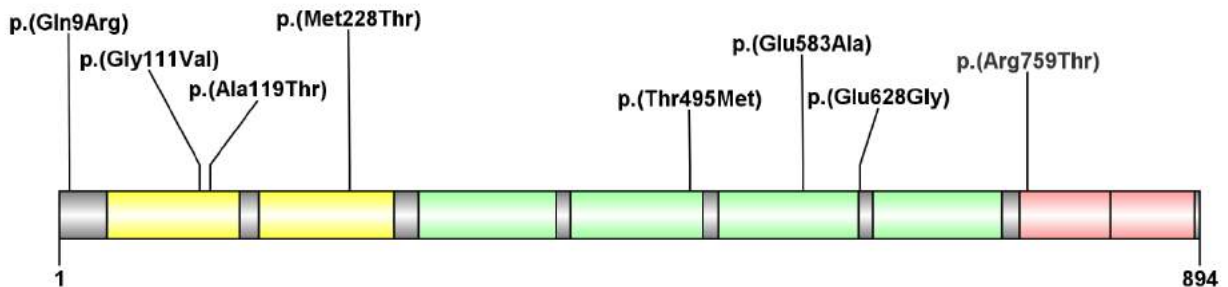


Fig D5: Alpha-actinin-2 protein domains and cardiomyopathy mutations

Position of the alpha-actinin-2 cardiomyopathy mutations. Four mutations are in the calponin homology domains, three in the spectrin repeats and one in the EF-hand. Protein domains highlighted in yellow: calponin homology domains; in green: spectrin repeats; in pink: EF-hand domains.

Physiopathological mechanisms of the *ACTN2* mutations

Heterozygous *ACTN2* missense mutations were reported in two groups of diseases, myopathies and cardiomyopathies. Patients with myopathy did not exhibit a cardiac phenotype, and conversely, individuals with *ACTN2*-related cardiomyopathy had no skeletal muscle weakness, suggesting that the mutations involve tissue-specific pathomechanisms. Alpha-actinin-2 belongs to a family of four actin-binding proteins sharing around 80% homology with each other (Kao 2015). Alpha-actinin-2 and alpha-actinin-3 are both expressed in skeletal muscle, and experiments in the zebrafish model showed that they are spatially and temporarily differentially expressed (Mills et al. 2001). While *ACTN3* loss-of-function mutations are commonly found in the general population and do not cause a myopathy (MacArthur et al. 2007; North et al. 1999), *ACTN2* knockdown in zebrafish leads to sarcomeric defects in skeletal muscle and heart (Gupta et al. 2012). In striated muscles, alpha-actinin-2 can be found in the sarcoplasm or in the nucleus, where it enhances the activity of transcription factors (Huang et al. 2004). In the sarcoplasm, alpha-actinin-2 is a cytoskeletal protein located at the Z-disks, and forms dynamic antiparallel homodimers crosslinking actin filaments. The alpha-actinin-2 dimers can be found in two conformations allosterically regulated by PIP2 and TTN (Ribeiro Ede et al. 2014). Moreover, alpha-actinin-2 forms a platform for the binding of other proteins such as sarcomeric-cytoskeletal proteins (PDLIM3, PDLIM1, LDB3, MYPN, TTN, CSRP3, ACTIN, ACTN3, MYOZ1), membrane-cytoskeletal proteins (VCL, DMD) and signaling proteins (GNE, KV1.5) (**Fig D6**) (Klaavuniemi, Kelloniemi, and Ylanne 2004; Xia et al. 1997; Au et al. 2004; Faulkner et al. 1999; Zhou et al. 1999; Atkinson et al. 2001; Ribeiro Ede et al.

2014; Sorimachi et al. 1997; Joseph et al. 2001; Bang et al. 2001; Hance et al. 1999; Takada et al. 2001; Harazi et al. 2017; Maruoka et al. 2000; Seto et al. 2011).

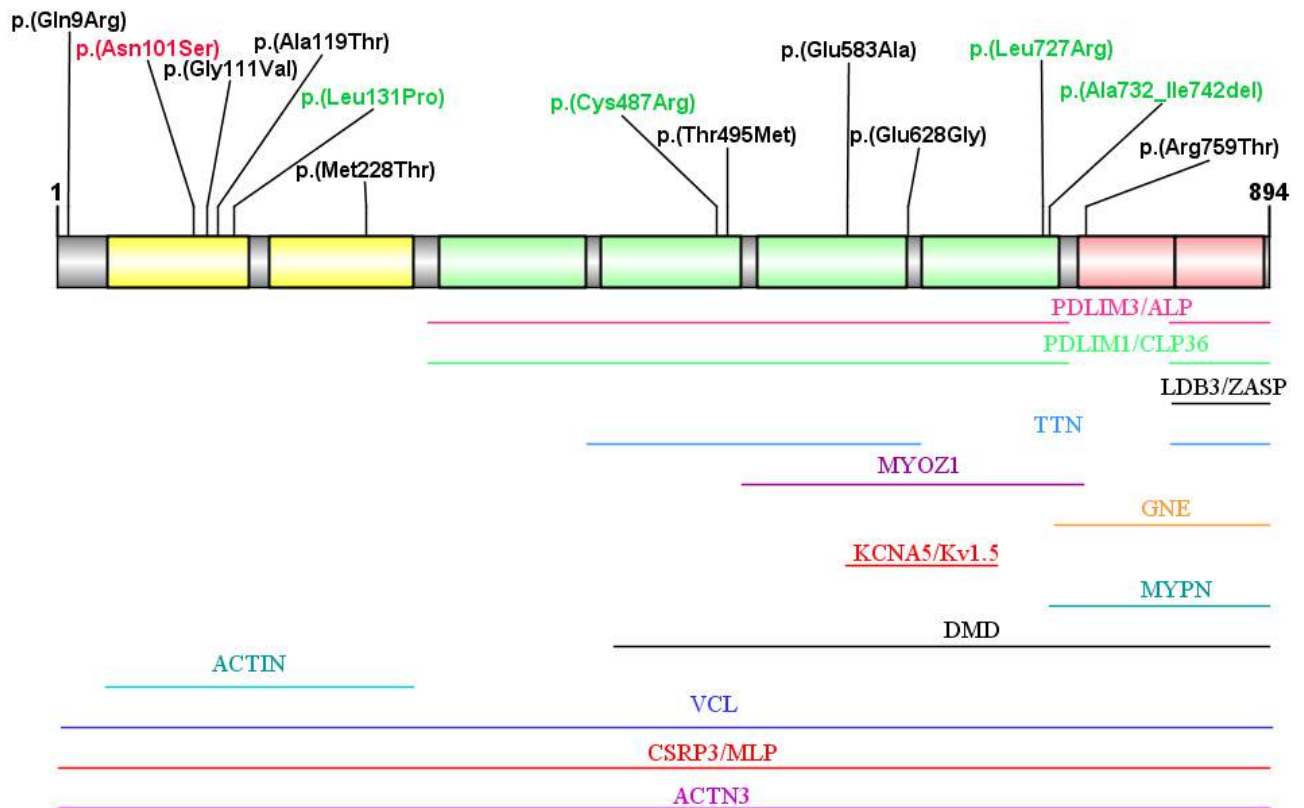


Fig D6: Alpha-actinin-2 protein domains, mutations and known interactors

The interacting regions are highlighted. Some partners have two binding sites on alpha-actinin-2 and some alpha-actinin-2 domains are able to bind different proteins. The exact interaction region of alpha-actinin-2 with VCL and CSRP3 has not been determined. Two names are indicated, if both are widely used in the literature. The cardiomyopathy mutations are highlighted in black, the myopathy mutations in green and the mutation leading to a cardiac and skeletal muscle phenotype in red. Protein domains highlighted in yellow: calponin homology domains; in green: spectrin repeats; and in pink: EF-hand domains.

The physiological mechanism underlying the *ACTN2*-related diseases was studied for three cardiomyopathy mutations located in the actin-binding domain: p.(Gln9Arg), p.(Gly111Val), and p.(Ala119Thr). The p.(Gly9Arg) mutation induced abnormal elongation of transfected C2C12, disrupted the interaction with CSRP3, and perturbed alpha-actinin-2 nuclear localization (Mohapatra et al. 2003). CSRP3 regulates myogenesis suggesting that the p.(Gly9Arg) mutation impacts on the myogenic differentiation (Arber, Halder, and Caroni 1994). According to the GTex database, *CSRP3* mRNA is highly expressed in heart and barely in skeletal muscle, explaining the pure cardiac phenotype observed in patients with the p.(Gln9Arg) mutation. Moreover, *CSRP3* mutations were previously reported associated with cardiomyopathies and one mutation was shown to abolish the interaction with alpha-actinin-2.

This highlights that the alpha-actinin-2/CSRP3 interaction is crucial for cardiac development and/or physiology. The Gly111Val and Ala119Thr alpha-actinin-2 cardiomyopathy mutants showed decreased thermal stability, reduced binding to F-actin *in vitro*, and exogenous expression of wild-type or mutant alpha-actinin-2 into rat cardiomyocytes revealed a reduced integration of the mutant into the Z-disks (Haywood et al. 2016). Alpha-actinin-2 plays a crucial role for the structural integrity and organization of the Z-discs, and a reduced incorporation of the alpha-actinin-2 mutants into Z-discs could potentially lead to reduced force transmission in cardiac muscles. Furthermore, two alpha-actinin-2 cardiomyopathy mutations (p.(Glu583Ala), p.(Glu628Gly)) affect residues located in the KCNA5-binding region (**Fig D6**). KCNA5 is a potassium channel mainly expressed in heart and mutated in patients with atrial fibrillation, a type of arrhythmia that can lead to heart failure or sudden death (Yang et al. 2009; Olson et al. 2006). Overall, the functional investigations on different *ACTN2* cardiomyopathy mutations have demonstrated a predominant impact on the interaction with heart-specific proteins, thereby explaining the absence of skeletal muscle phenotype.

Other *ACTN2* myopathy mutations were shown to cause either MsCD or actininopathy, two skeletal muscle diseases without any cardiac involvement. The MsCD mutations (p.(Leu727Arg), p.(Ala732_Ile742del)) are located in close proximity to each other in the fourth spectrin repeat, a region mediating the interaction with MYOZ1 (**Fig D6**). Both mutations are predicted to significantly impact on the structure of the region (Lornage et al. 2019) and this might prevent the interaction with MYOZ1, a Z-line protein mainly expressed in skeletal muscle (Takada et al. 2001). The two actininopathy missense mutations (p.(Leu131Pro), p.(Cys487Arg)) are located in a different region, indicating that the different skeletal muscle phenotypes of MsCD and actininopathy arise from a mutation-specific impact.

Muscle biopsies from patients with MsCD revealed a strong type 1 fiber predominance. A difference between type 1 and type 2 fibers is the expression level of alpha-actinin-3, a protein highly similar to alpha-actinin-2 in sequence and structure, and exclusively expressed in type 2 muscle fibers. As a consequence of the type 1 fiber predominance in MsCD patients, alpha-actinin-3 was not detectable in the muscle extracts (Lornage et al. 2019). In contrast, the type 1 fiber predominance was less pronounced in the actininopathy patients indicating that there might be a residual expression of alpha-actinin-3. Given the high similarity between both proteins, alpha-actinin-3 might compensate for the abnormal activity of the mutant alpha-actinin-2, and thus explain the milder phenotype of actininopathy patients compared with MsCD patients.

In section 2.3.3 of this thesis, I described a novel *ACTN2* c.302A>G p.(Asn101Ser) mutation causing both a cardiac and a skeletal muscle disease. Functional experiments demonstrated that the substitution of asparagine to serine at position 101 diminished the interaction with actin in transfected C2C12 cells. A similar observation was made for the p.(Gly111Val) and p.(Ala119Thr) cardiomyopathy mutations (Haywood et al. 2016), indicating that alpha-actinin-2 binding to actin is crucial for cardiac development and/or physiology. Since the cardiomyopathy mutations p.(Gly111Val) and p.(Ala119Thr) are not associated with a myopathy phenotype, the impaired interaction with actin does most likely not account for the myopathy in patients carrying the *ACTN2* c.302A>G p.(Asn101Ser) mutation. Another myopathy mutation also resides in the actin-binding domain, and the impact of both p.(Asn101Ser) and p.(Leu131Pro) mutations on skeletal muscle dysfunction remains to be determined.

In summary, the exact molecular mechanisms impacted by the reported *ACTN2* myopathy mutations are barely understood, and this is mainly due to the complexity of the physiological role of alpha-actinin-2 in heart and skeletal muscle. Both MsCD mutations are located in the fourth spectrin repeat and our results suggest that mutations destabilizing the fourth spectrin repeat structure are likely to cause MsCD. A better understanding of alpha-actinin-2 function is necessary to assess the pathophysiological mechanisms of the mutations, and this could be done through a detailed characterization of alpha-actinin-2 isoforms, which might have specific functions in development and maintenance of skeletal muscle and heart. The reasons why some mutations give rise to a pure cardiac phenotype, a pure skeletal muscle phenotype, or a combination of both, are still elusive, and the comparison of the alpha-actinin-2 interactome in skeletal muscle and heart will provide new insights. Additionally, identifying the precise alpha-actinin-2 residues bound by specific interactors is crucial to have a better overview of the organization of the Z-line. One of the main challenges will be to distinguish whether the interactions with specific proteins occur simultaneously or if they are consecutive and this will necessitate *in vitro* and structural studies. All these experiments should provide a more precise overview of the alpha-actinin-2 function and of the Z-line organization, which are required for understanding the pathomechanisms of *ACTN2* mutations.

2.4.3 *ACTN2*- and *MYPN*-related myopathies: conclusion

Myopalladin and alpha-actinin-2 are two sarcomeric proteins interacting with each other, and both are able to translocate into the nucleus to activate transcription factors. *MYPN* and *ACTN2* are specifically and highly expressed in skeletal muscle and heart, suggesting relevant functions

in both tissues, and mutations in these genes were previously linked to cardiomyopathies. We discovered that *MYPN* and *ACTN2* mutations can also give rise to pure skeletal muscle diseases, or to a skeletal muscle disease with associated cardiomyopathy.

We showed that homozygous *MYPN* loss-of-function mutations cause cap myopathy. Alpha-actinin-2 strongly accumulated in the caps, suggesting that myopalladin is required for proper targeting or maintenance of alpha-actinin-2 at the Z-line. We also demonstrated that specific *ACTN2* mutations cause MsCD, a disease clinically and histologically different from cap myopathy. The *ACTN2* MsCD mutations did not affect residues located in the myopalladin-binding domain and they potentially interfere with binding to MYOZ1 (**Fig D6**). Overall, the results showed that mutations in *MYPN* and *ACTN2* respectively cause cap myopathy and MsCD through different physiopathological mechanisms.

2.5 MYOCAPTURE: contributions and future prospects

2.5.1 Global analysis of the MYOCAPTURE project

Through the MYOCAPTURE project, we exome-sequenced a total of 657 patients from 258 unrelated families. As depicted in **Fig D7a**, the analyzed patients and families were classified into four distinct categories depending on the results of the molecular analysis.

- **Diagnosed:** In 23% of the families, we successfully identified the causative gene, and the segregation of the mutations with the disease was confirmed. Among the diagnosed patients, we discovered mutations in known as well as in new congenital myopathy genes. To conclude on the pathogenicity of the mutations in known myopathy genes, we evaluated the accordance of the genetic data with the clinical and histopathological picture. Thorough examination of a subset of patients revealed additional clinical and histopathological features that were not yet described in the literature. We reported our observations in diverse case reports to expand the mutational spectrum, histological anomalies and clinical presentation associated with a given gene, and to highlight the clinical and histological heterogeneity of congenital myopathies (Publications 1-11). In case we identified mutations in a novel myopathy gene, we confirmed the causality of the mutations through functional experiments in the cell and/or animal models (Publications 12-13). For all patients carrying mutations in known and new myopathy genes, we provided the molecular diagnosis to the clinician. Since the mutations were identified within the frame of a research project, the confirmation by an accredited diagnostic laboratory is required.

- **Likely**: In 16% of the families, we identified the causative gene and confirmed the segregation of the mutations, but single elements are still required to unambiguously validate the causality of the mutations. For patients with mutations in known genes, the comparison of the genetic, histopathological and clinical data is still ongoing. For patients with mutations in novel genes, further functional experiments are necessary to assess the impact of the mutation on protein function and muscle physiology.
- **Candidate**: Exome analysis of each individual reveals 700 rare variants, and the main challenge is the unambiguous identification of the disease-causing mutations. In 16% of the cases, results of the bioinformatics analyses highlighted several genes. Since congenital myopathies are considered to be monogenic disorders, further genetic investigations are necessary for molecular diagnosis. The first step is the verification of the segregation of all candidate variations in additional family members, potentially followed by functional experiments.
- **No diagnosis**: In 45% of the families, we did not obtain a diagnosis or candidate gene. The re-analysis of unsolved cases by using complementary strategies is ongoing, and takes into account new and additional information on genes and proteins in muscle physiology.

The diagnosed families or those with a likely candidate gene represent 39% of the cases. This result is in line with another whole-exome sequencing analysis of 60 Australian families with muscular dystrophy, where the diagnostic success rate was 45% (Ghaoui et al. 2015). In the MYOCAPTURE project, the success rate correlates with the number of exomes per family (**Fig D7b**). A pathogenic mutation was identified in around 20% of the singletons, and the same diagnosis rate was obtained by sequencing the index patient and one of his parents. The success rate however increased to 60% in case of trios, encompassing the index patient and both healthy parents. The significantly increased success rate of trios versus singletons was previously highlighted in the literature (Ghaoui et al. 2015; Wright, FitzPatrick, and Firth 2018). This can partially be explained by the fact that a comparison of the list of variants in the exomes of the index patient and the healthy parents enables the identification of compound heterozygous mutations and of *de novo* mutations, which occur during early embryonic development. The low diagnosis rate obtained for families with four or more family members may rely on the fact that not all individuals were clinically examined, resulting in an unclear health status and a potentially wrong assignment in the pedigree. Re-analyzing the index patients of these large families, independently of the other family members, might help to confine the number of candidate genes.

All these results point out that the simultaneous sequencing of trios provides a rapid and reliable molecular diagnosis in most cases. The high number of candidate genes remains challenging for the molecular diagnosis of singletons, and for large families with several affected members, the health status of every individual needs to be carefully evaluated by the same clinician. This is of particular relevance for the design of future sequencing projects and the recruitment of patients and families.

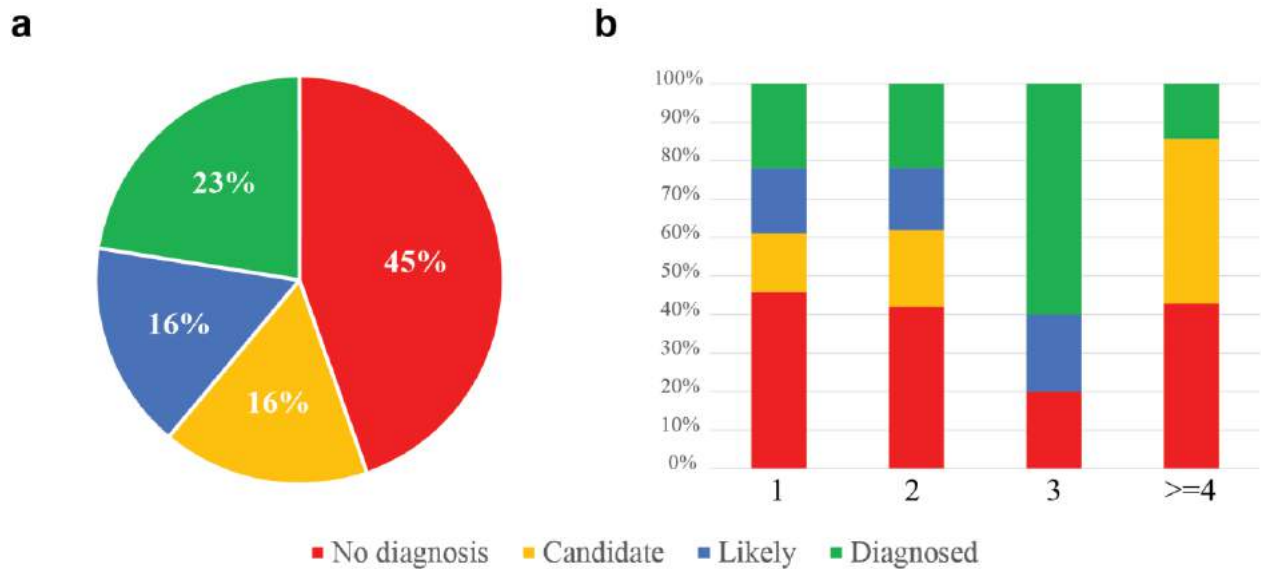


Fig D7: Overall diagnostic rate for families included in MYOCAPTURE

a Overview of the MYOCAPTURE results showing the proportion of families with or without diagnosis, or with likely or candidates genes. **b** Correlation between success rate and number of exomes per family.

2.5.2 Significance of the MYOCAPTURE project

MYOCAPTURE is an exome sequencing project encompassing 1000 patients and relatives. As congenital myopathies are clinically and histologically heterogeneous, the description of several patients with mutations in the same gene is required to characterize the hallmarks of the disease. We created a homemade database optimized to screen for mutations in the same gene in the entire MYOCAPTURE cohort, and the high number of patients enrolled in the project increases the likelihood of having multiple families with the same disorder. This approach successfully led to the identification of pathogenic mutations in genes not previously related to congenital myopathies.

Overall, the MYOCAPTURE project has delivered an efficient bioinformatics pipeline for exome sequencing data analysis, and the obtained results are of medical and scientific relevance.

Efficient bioinformatics tools adaptable to other Mendelian diseases

Through the MYOCAPTURE project, we created and validated a novel bioinformatics pipeline for human genomic variant analysis and prioritization. To identify candidate genes, we used an in-house system for high-throughput variant filtering and ranking embedding a mutation prediction tool. In addition to commonly used strategies such as coverage, quality, polymorphism databases as gnomAD, or pathogenicity predictions, we considered additional parameters such as muscle expression, biological pathways, and protein interactions. The prioritization of the candidate genes took into account the known protein functions described in the literature, as well as databases on animal models. Overall, the MYOCAPTURE project delivered an efficient tool for the analysis of exome sequencing data, and this pipeline could be easily adapted to any other Mendelian disease.

Medical and scientific impact of the molecular diagnosis

The identification and characterization of novel genes implicated in myopathies, and the recognition of new phenotypes associated with known myopathy genes have a strong impact on the diagnosis and development of therapies. The molecular diagnosis enables genetic counselling, including prenatal and preimplantation diagnosis, and the knowledge on the known genes can promote the identification of drug targets and biomarkers, and the inclusion of the patients into existing or prospective clinical studies on the natural history of the disease, a prerequisite for clinical trials.

The novel myopathy genes discovered through the MYOCAPTURE project contribute to a better understanding of skeletal muscle function and structure, and the recently discovered myopathy genes affecting enzymes with unknown function in skeletal muscle highlight novel pathways required for healthy muscle physiology (Vasli et al. 2017; O'Grady et al. 2016).

2.5.3 Future prospects: identification of the missing myopathy genes

Reanalysis of the exomes through a candidate-based approach

The MYOCAPTURE project significantly facilitated the discovery of novel disease genes underlying diverse myopathies. However, no candidate gene was identified in 45% of the patients, and a reanalysis of the unsolved exomes using complementary strategies is necessary to uncover the pathogenic mutations. An alternative approach to the analysis of families on an individual basis, is the gene-by-gene analysis. However, the subsequent analysis of 20000 genes is time consuming, and a restricted list of candidate genes would significantly reduce the data volume and facilitate the discovery of the most likely myopathy genes. To establish the list of

the best candidates, I crossed the data of genes associated with myopathies or with other muscle diseases, with data of genes associated with animal models manifesting myopathic features.

Comparison of the genes mutated in myopathies, dystrophies, and cardiomyopathies revealed a significant genetic overlap between these disorders. From the genes mutated in dystrophies, 21% were shown to also cause myopathy (14/66), and 10% of the cardiomyopathy genes are also mutated in myopathies (12/103). Such a superposition of the genetic spectrum is not a coincidence, and is barely observed for diseases that do not primarily affect striated muscles, such as motor and sensory neuropathies (**Fig D8**). It is therefore conceivable that dystrophy and cardiomyopathy genes expressed in skeletal muscle might also be mutated in myopathies.

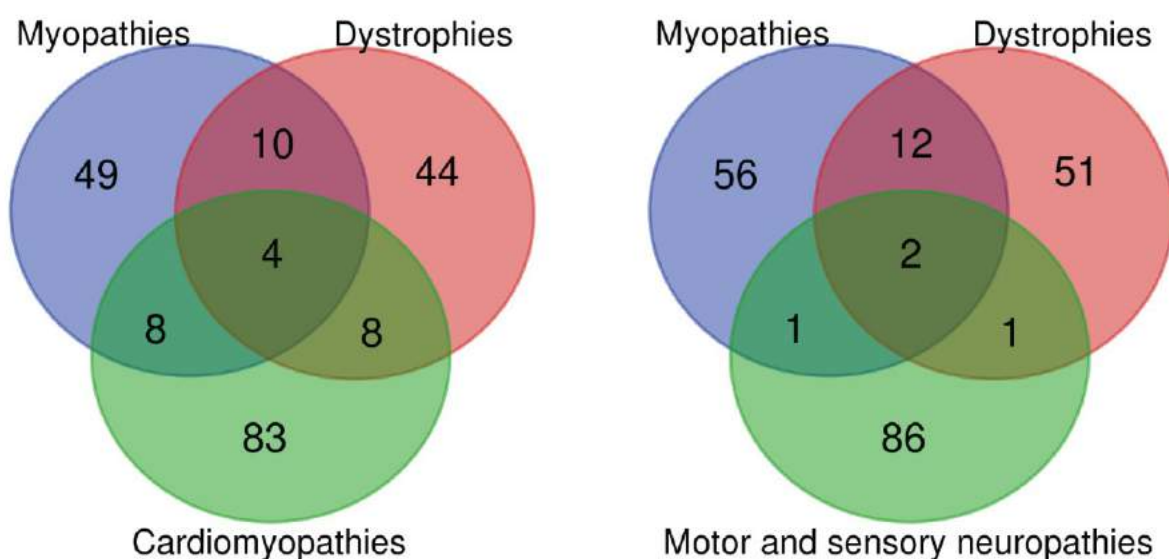


Fig D8: Venn diagram showing the genetic overlap between different neuromuscular diseases. The diagrams show the genetic overlap between the genes mutated in myopathies, dystrophies, and either cardiomyopathies or motor and sensory neuropathies. The list of genes was downloaded from the GeneTable (<http://www.muscle.genetable.fr/>). Myopathy genes encompass genes mutated in congenital myopathies, distal myopathies and other myopathies (categories 3, 4 and 5 of the GeneTable). The dystrophy genes encompass genes mutated in muscular dystrophies and congenital muscular dystrophies (categories 1 and 2 of the GeneTable).

More generally, all genes with abundant expression in skeletal muscle are necessarily important for the physiology, and mutations in these genes are likely to impair muscle function or structure and to cause myopathies. From the 50 most expressed genes in adult skeletal muscle, more than 40% were associated with a skeletal muscle disorder (21/50). Most of these causative genes are specifically expressed in striated muscle, highlighting their crucial role in muscle physiology (**Table D7**). One third of the 50 most expressed genes in skeletal muscle also belong to the 50 genes with highest expression in cardiac muscle (18/50), thereby confirming the functional

overlap between both tissues. Considering the expression level in skeletal muscle and heart, following genes may be analysed in for patients with yet undiagnosed myopathies: *ATP5B*, *CKM*, *COX6A2*, *EEF1A2*, *MYH1*, *RP11-45AG.2*, *SLN*, *TNNC2*, *MYOZ1*, *NRAP*, *MYLFPG* and *TNNC1*, the latter being already linked to cardiomyopathies.

Over the last decade, many mouse models were generated and phenotyped, and most faithfully reproduced human diseases (Meehan et al. 2017). I assembled genes for which mouse models manifest a myopathy or other myopathic features, and compared the implication of these genes in human myopathies or other neuromuscular diseases (NMD). From the 62 genes giving rise to a myopathy in mice, eight were reported as implicated in human myopathies, 17 were linked to other NMDs, and nine have been associated to both; myopathies and another NMD. For impaired contractility, fiber atrophy, and fiber size variability, similar observations were made with 51 to 66% of the murine genes previously reported to be associated with a human myopathy or another neuromuscular disease (**Fig D9**).

The significant overlap between murine and human myopathy genes highlights that genes associated with myopathic features in mice and not yet linked to a human muscle disorder, are also likely to be also mutated in human congenital myopathies and other NMDs.

50 most expressed genes in skeletal muscle	Heart expression	Striated muscle specific expression	Skeletal muscle disease	Heart disease
ACTA1	Red	X	X	
ACTN2	Red	X	X	X
ALDOA	Red	X	X	
ATP2A1		X	X	
ATP5B	Red			
CA3		X		
CKM	Red	X		
COX6A2	Red	X		
CRYAB	Red		X	X
DES	Red		X	X
EEF1G	Pink			
EEF2	Red			
EEF1A2	Pink	X		
ENO3	Pink	X	X	
FHL1	Pink	X	X	
GAPDH	Red			
HSPB1	Red			
KLHL41	Pink	X	X	
MB	Red	X	X	X
MT1X	Pink			
MTATP6P1	Red			
MYBPC1		X	X	
MYH1		X	X	
MYH7	Pink	X	X	X
MYL1		X	X	X
MYL2	Red	X	X	X
MYLPF		X		
MYOZ1	Pink	X		
NRAP	Pink	X		
PDK4	Pink			
PDLIM3	Pink			
PYGM	Pink	X	X	
RP11-451G4.2		X		
RPL13A	Red			
RPLP1	Pink			
RPS11	Pink			
RPS15	Pink			
RPS18	Pink			
RPS25	Pink			
SLN		X		
STAC3		X	X	
TCAP	Red	X	X	X
TNNC1	Red	X		X
TNNC2		X		
TNNI2		X	X	
TNNT1	Pink	X	X	
TNNT3	Pink	X	X	
TPM2	Pink		X	
TPT1	Red			
YBX3				

Table D7: Correlation between gene expression and involvement in muscle and cardiac diseases
List of 50 genes with highest expression in skeletal muscle, expression in heart and involvement in diseases. The expression data were extracted from GTex, a database gathering exome sequencing data from adults. In red: top 50 most expressed genes in heart. In pink: expressed genes in heart.

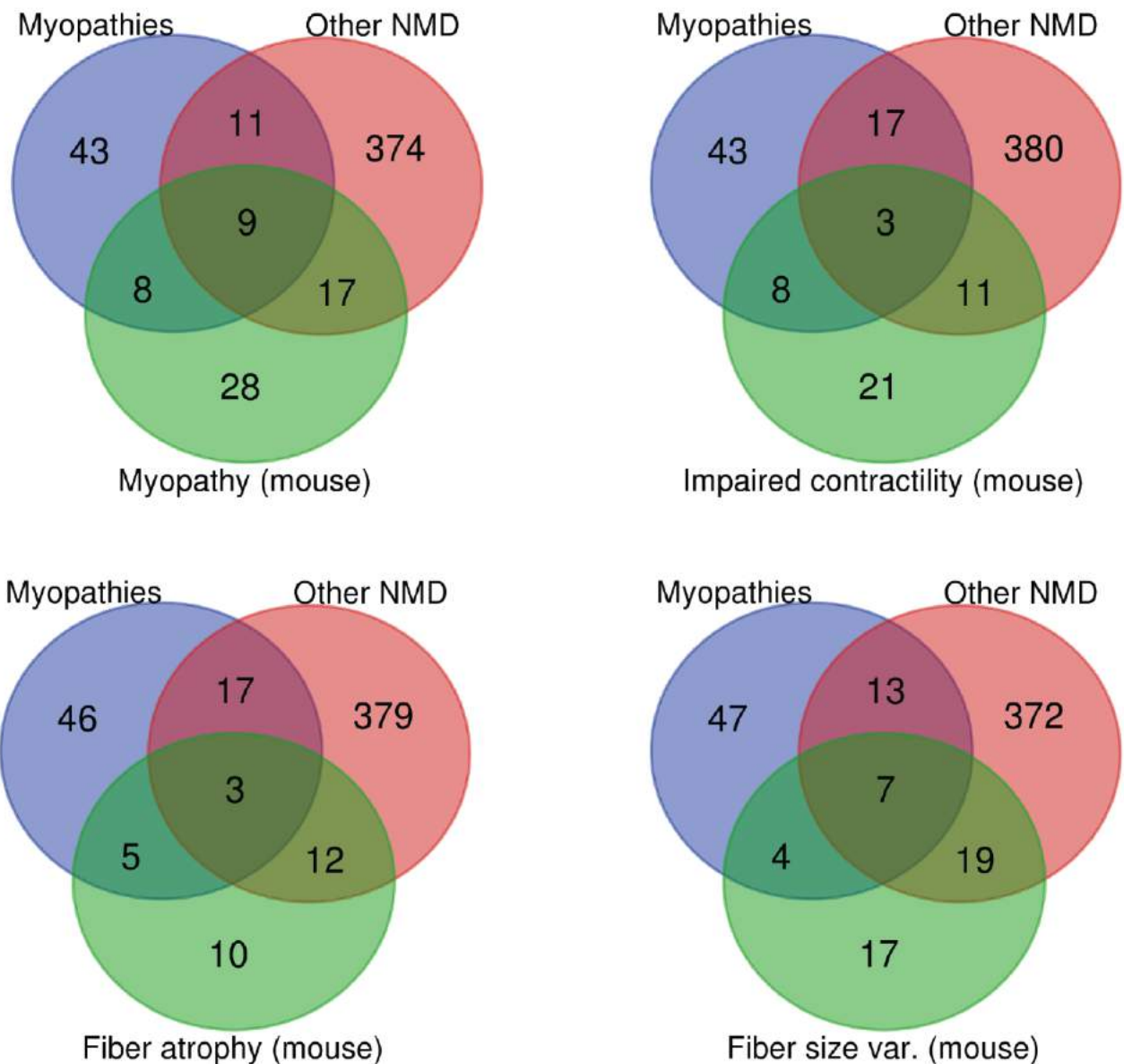


Fig D9: Venn diagram showing the genetic overlap between human diseases and mouse models. The list of human genes was downloaded from the GeneTable (<http://www.musclegenetable.fr/>). Myopathy genes encompass genes classified into the “congenital myopathies”, “distal myopathies” and “other myopathies” (categories 3, 4, and 5), and other neuromuscular diseases corresponds to all other neuromuscular diseases except “hereditary cardiomyopathies”. The Mouse Genome Informatics (<http://www.informatics.jax.org/>) was used to identify which mouse models cause a myopathy or features of myopathy. NMD: neuromuscular disease.

Taken together, all genes mutated in other NMDs than congenital myopathies, as well as genes with high expression in skeletal muscle, and all genes associated with myopathic features in mouse models represent excellent candidate genes for congenital myopathies and may explain the yet unsolved cases. The extraction and combination of data from different sources highlighted a total 153 candidate genes, and a careful re-analysis of the exomes with particular

attention to the presence of mutations in these 153 genes represents a straightforward approach to identify disease-causing mutations in the undiagnosed MYOCAPTURE families (**Table D8**).

AARS2	CALM2	EEF1A2	JUP	MIB1	MYOZ1	RBM20	SYNC	TRIM72
ABCC9	CALR3	EEF2	KCNA5	MRPL3	MYOZ2	RP11-45.	SYNE1	TSFM
ACTC1	CAMKMT	EYA4	KCND3	MRPL44	NDUFAF1	RPL13A	SYNM	VCL
ACTG1	CASQ2	FKTN	KCNE1	MTATP6P1	NEXN	RYR2	SYPL2	VEGF1
ADARB1	CKM	FLNA	KCNE2	MTMR14	NPPA	SCN1B	TAZ	VMS1
AKAP9	CKMT2	FOXJ3	KCNE3	MTO1	NRAP	SCN2B	TCAP	VMS2
ALPK3	COL14A1	GAA	KCNH2	MURC	NUP155	SCN3B	TECRL	VMS3
ANK1	COX15	GAPDH	KCNJ11	MYF5	PDK2	SCN4B	TFAM	WASF1
ANK2	COX6A2	GATAD1	KCNJ2	MYH1	PKP2	SCN5A	TGFB3	XK
ANKRD1	CSRP3	GFOT1	KCNJ5	MYH4	PLAA	SCO2	TMEM43	ZFP106
APOBEC2	CTNNA3	GJA5	KCNQ1	MYH5	PLN	SDHA	TMPO	
APP	DM15	GPD1L	LAMA4	MYH6	PRDM16	SGCD	TNNC1	
ATP5B	DMD	HCN4	LAMC1	MYL1	PRKAG2	SLC2A4	TNNC2	
BARX2	DOLK	HIRA	LMNA	MYL2	PRNP	SLC6A8	TNNI3	
CACNA1C	DSC2	HSPB1	MAML1	MYL3	PSEN1	SLN	TNNT2	
CACNB1	DSG2	ILK	MBNL1	MYL4	PSEN2	SNTA1	TPM1	
CACNB2	DSP	JPH1	MBNL2	MYLFPG	PTCD2	SRL	TPT1	
CALM1	DTNA	JPH2	MEOX2	MYLK2	RAF1	SSPN	TRDN	

Table D8: List of 153 candidate myopathy genes

These genes were identified based on their involvement in other muscular or heart diseases, their expression in skeletal muscle, and available mouse models of myopathy.

Analysis of the patients by additional unbiased approaches

More than 50% of the MYOCAPTURE families are still awaiting molecular diagnosis, and a variety of reasons account for the incomplete detection rate of disease-causing mutations through exome sequencing. This approach specifically targets the coding sequences of the human genome, and therefore solely uncovers sequence variants in the exons and adjacent intronic regions, while deep intronic mutations escape detection. Furthermore, single exons as GC-rich regions and yet undescribed exons are not captured or targeted by exome sequencing. Besides, a subset of genes contain highly similar repetitive exons, challenging the exact mapping and annotation of these exons and the unambiguous identification of mutations (Lehtokari et al. 2014; Muenzen, Monroy, and Finseth 2019). Exome sequencing data are suitable for the search of deletions, insertions and duplications larger than 1 000 nucleotides, collectively referred to as copy number variations (CNVs) (Zarrei et al. 2015; Valipakka et al. 2017). CNV detection software mostly use a strategy based on the comparison of the sequencing depth of individual neighboring exons (Pounraja et al. 2019). However, the overall depth of exome sequencing is often heterogeneous, complicating accurate CNV detection and generating numerous false positives (Karakoc et al. 2011; Straver et al. 2017). Pathogenic

CNVs are frequently encountered in myopathy patients (Valipakka et al. 2017), and an efficient analysis of the CNVs is necessary to increase the diagnostic rate of MYOCAPTURE.

In contrast to exome sequencing, genome sequencing generates a homogeneous coverage and sequencing depth of coding and non-coding regions. It is therefore a suitable approach to infer potential CNVs, to detect coding variations in exons that were poorly covered by exome sequencing, and to identify deep intronic or intergenic variations that were not targeted by exome sequencing. However, genome sequencing uncovers a confusing number of rare and unique non-coding variants of uncertain significance, and only concurrently performed RNA sequencing can indicate which genomic region most probably contains the disease-causing non-coding mutation (Shiraishi et al. 2014). Abnormal expression or splicing of genes observed with RNA sequencing would highlight the gene presumably carrying the pathogenic mutation, and genome sequence comparison of affected and healthy family members would help to prioritize the most likely sequence aberrations segregating with the disease within the selected region.

This concurrent and complementary RNA/genome sequencing approach would enable the detection of following mutation types with impact on muscle gene expression:

- **Intronic mutations impacting on splicing:** genomic regions encoding aberrant RNA transcripts lacking entire or partial exons, exon extensions or inclusions due to activation of non-canonical splice sites will be screened for rare and unique variants segregating with the disease. Prediction software as NNSplice could be used to estimate the impact of the selected variants on splicing.
- **Structural mutations:** small genomic insertions and deletions can potentially be detected by exome sequencing, but not other structural mutations as inversions. Structural mutations are likely to impact on gene expression, and a strong reduction or total absence of muscle transcripts can be spotted by RNA sequencing and compared with genomic variants. Genome sequencing produces uniform sequences of coding and non-coding regions, and therefore allows the detection of the exact breakpoints.
- **Allele-specific expression:** the complete absence or the biased expression of a single gene copy can result from specific heterozygous mutations. To detect such allele imbalances, we will compare the status of every RNA mutation with the genome data, and extract variants appearing homozygous on RNA sequences and heterozygous on genome sequences.
- **Mosaic mutations:** sequencing of muscle RNA allows the detection of tissue-specific mutations that arise during early embryonic development and specifically affect skeletal

muscle, and therefore escape detection by exome sequencing on DNA from blood or saliva DNA samples (D'Amico et al. 2017).

Taken together, specific types of mutations barely detectable by exome sequencing can explain the unsolved MYOCAPTURE cases, and a combination of additional next generation sequencing approaches such as genome and RNA sequencing will lead to the discovery of novel causative mutations and genes in the congenital myopathy families.

3 FRENCH SUMMARY

Identification et validation fonctionnelle de nouveaux gènes impliqués dans les myopathies

I) Etat de l'art

Les myopathies congénitales sont des maladies musculaires génétiques sévères qui débutent généralement à la naissance ou dès l'enfance par une forte faiblesse musculaire (hypotonie) et qui ont un impact important sur la qualité de vie des patients. Outre la faiblesse musculaire, de nombreux autres signes cliniques sont fréquemment associés aux myopathies congénitales, comme une insuffisance respiratoire et une atteinte cardiaque qui peuvent mettre en danger la survie des myopathes. Ces maladies se caractérisent par divers défauts structuraux de la fibre musculaire squelettique qui permettent de classer les myopathies en différents groupes. Les trois sous-classes principales sont les myopathies centronucléaires (CNM) qui se distinguent par la présence anormale de noyaux centraux dans la fibre, les myopathies némalines (NM) caractérisées par des agrégats de protéines et des bâtonnets, et les myopathies à cores qui se repèrent par la présence de zones sans mitochondrie dans la fibre musculaire (CCD) (**Fig S1**).

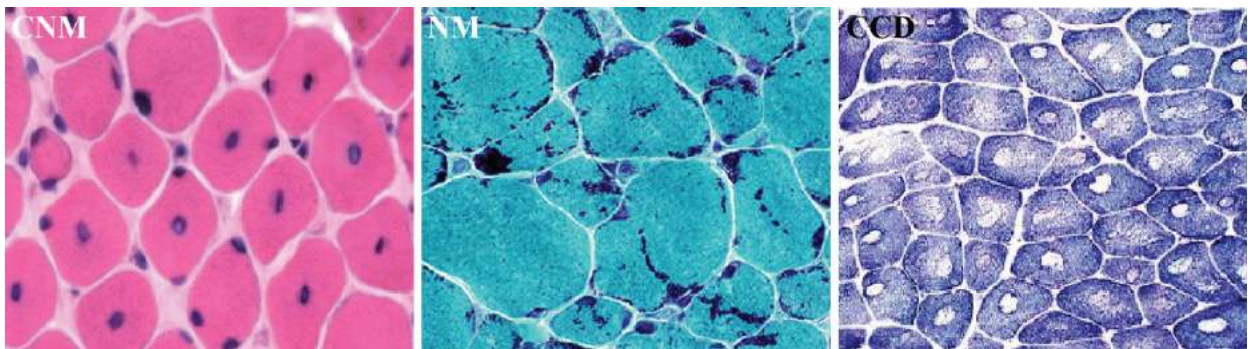


Fig S1 : Caractéristiques histologiques des principales classes de myopathies congénitales
Biopsies musculaires en coupe transversale vues au microscope. Les patients avec une myopathie centronucléaire (CNM) présentent un nombre élevé de noyaux centraux révélés en coloration H&E. Les patients souffrant d'une myopathie à némaline (NM) présentent des agrégats de protéines qui apparaissent bleu foncé en coloration de Gomori, tandis que les fibres musculaires de patients avec CCD ont des zones dépourvues d'activité oxydative SDH.

Les myopathies congénitales sont des maladies génétiques. Une trentaine de gènes ont été rapportés comme mutés dans les myopathies congénitales. Cependant, seulement la moitié des patients portent une mutation dans l'un de ces trente gènes. Ces chiffres laissent supposer qu'un

certain nombre de gènes impliqués dans les myopathies congénitales ne sont pas décrits à ce jour.

Afin d'identifier de nouveaux gènes associés à des myopathies, nous avons séquencé les exomes de patients myopathes qui ne disposaient pas de diagnostic moléculaire et pour lesquels les causes génétiques fréquentes de myopathie ont été exclues. J'ai analysé les exomes de ces patients et validé les mutations identifiées en utilisant des outils de biologie moléculaire et cellulaire ainsi que des modèles animaux.

II) Principaux résultats

Les mutations identifiées peuvent être classifiées en trois groupes selon les gènes touchés :

- Gènes déjà décrits comme mutés dans les myopathies avec des données cliniques et histologies compatibles ;
- Gènes déjà décrits comme mutés dans les myopathies mais identifiés chez des patients avec de nouveaux phénotypes ;
- Nouveaux gènes de myopathie.

a. Identification de mutations dans des gènes connus

Les mutations identifiées dans les gènes connus touchent de très grands gènes (*NEB*, *TTN*, *RYR1*, *GNE*), qui n'étaient auparavant pas criblés en routine (Abath Neto et al. 2017; Avila-Polo et al. 2018). La description de cas additionnels permet d'établir des corrélations entre le type et localisation des mutations, la sévérité de la maladie et les défauts histopathologiques observés.

b. Identification de mutations dans des gènes connus associées à de nouveaux phénotypes

J'ai identifié et caractérisé des mutations associées à de nouveaux phénotypes dans les gènes *SCN4A*, *HSPB8*, *EXOSC3*, *SPEG*, *CASQ1*, *HNRNPDL*, *EXOSC3* and *GNE* (Mercier et al. 2017; Echaniz-Laguna et al. 2017; Pinto et al. 2018; Lornage et al. 2018; Bohm et al. 2018; Berardo et al. 2019; Dotti et al. 2018). Ces résultats permettent de souligner l'hétérogénéité clinique et histologique des myopathies congénitales et ainsi d'élargir le spectre phénotypique de ces maladies.

c. Identification et validation de mutations dans de nouveaux gènes de myopathie

**i. Les mutations dans *MYPN* causent une myopathie à caps
(Lornage et al. 2017)**

J'ai identifié des mutations récessives dans le gène *MYPN* chez deux familles non-apparentées souffrant d'une myopathie à cap (agrégats protéiques localisés à la périphérie de la fibre). Les patients sont atteints depuis la naissance d'une faiblesse musculaire touchant les muscles des ceintures et les muscles distaux. Les biopsies musculaires ont démontré la présence de structures anormales et bien délimitées à la périphérie de la fibre appelées caps (**Fig S2**). *MYPN* code pour une protéine appelée myopalladine localisée à la ligne Z et nécessaire pour la maintenance du sarcomère, unité contractile du muscle.

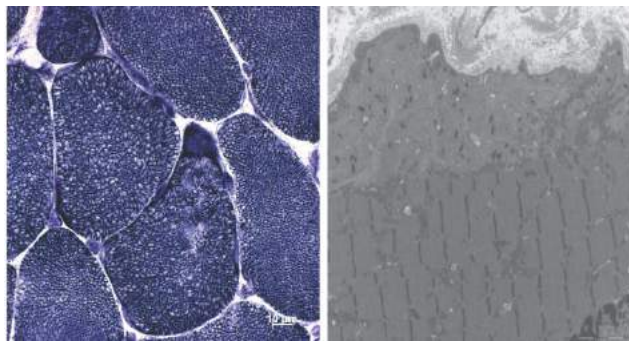


Fig S2 : Caractéristiques histologiques des patients souffrant d'une myopathie liée au gène *MYPN*

Coupe transversale d'une biopsie musculaire colorée grâce à la réaction NADH et révélant des agrégats en périphérie de la fibre (à gauche). L'étude ultrastructurale de ces agrégats révèle qu'ils sont principalement composés d'une accumulation de filaments contractiles (à gauche).

Les patients de la famille 1 portent une mutation non-sens homozygote (c.2653C>T p.(Arg885*)) et l'analyse des extraits musculaires par transcription inverse et western blot a permis de démontrer une très forte réduction au niveau de l'ARN messager (ARNm) et de la protéine (**Fig S3**). Le patient de la famille 2 est porteur homozygote d'une mutation touchant un site essentiel d'épissage de l'exon 16 (c.315811G>A), et l'analyse de cette mutation par minigène a révélé l'absence de transcrit sauvage, suggérant que les mutations identifiées dans les deux familles activent le mécanisme de dégradation des ARNm non-sens (**Fig S4**). En résumé, mes travaux ont permis de montrer que les mutations récessives de *MYPN* causent une myopathie à cap.

**ii. Les mutations dans *ACTN2* causent une myopathie à cores
(Lornage et al. 2019)**

J'ai identifié une mutation hétérozygote *de novo* dans *ACTN2* chez un patient avec une myopathie congénitale non étiquetée. Le patient est atteint d'une maladie qui a débutée dans

l'enfance avec une faiblesse musculaire et une atteinte oculaire (ptose). La biopsie musculaire a montré des défauts en coloration oxydative qui correspondent à des cores, ainsi qu'une uniformité de fibres de type 1 (**Fig S3**). *ACTN2* code pour une protéine appelée alpha-actinin-2 localisée à la ligne Z, et qui est spécifiquement exprimée dans le muscle squelettique et le cœur.

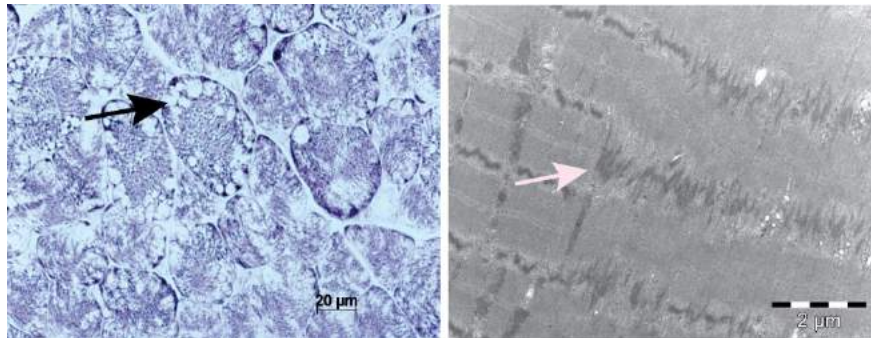


Fig S3 : Caractéristiques histologiques des patients souffrant d'une myopathie liée au gène *ACTN2*

Coupe transversale d'une biopsie musculaire colorée grâce à la réaction NADH et révélant des régions dépourvues d'activité oxydative en périphérie de la fibre (flèche noire à gauche). L'étude ultrastructurale de coupes longitudinales de ces cores révèle qu'ils sont composés de myofibrilles comportant des désorganisations majeures de la ligne Z (à droite).

La mutation identifiée est un faux-sens touchant un acide-aminé conservé au cours de l'évolution (c.2180T>G p.(Leu727Arg)). Les analyses fonctionnelles chez le poisson zèbre ont montré que l'expression de la mutation conduit à des défauts morphologiques et fonctionnels : les poissons sont plus petits, ont un myotome courbé et bougent moins (**Fig S4**). De plus, leurs myofibrilles sont désorganisées.

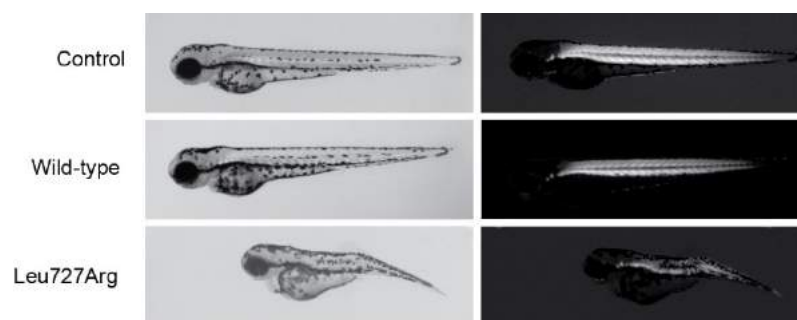


Fig S3 : Morphologie des poissons exprimant l'alpha-actinine-2 humaine sauvage et mutée
Les poissons zèbres exprimant l'alpha-actinin-2 mutée ont un myotome plus court et courbé (panel de gauche) et une birefringence anormale.

J'ai aussi reproduit la maladie dans un modèle murin en utilisant un vecteur viral pour exprimer la protéine mutée dans le muscle. Contrairement à l'expression de l'alpha-actinine-2 humaine sauvage, qui ne génère pas de phénotype, l'expression de l'alpha-actinine-2 humaine

Leu727Arg conduit à une faiblesse musculaire chez les souris. De plus, l'analyse de coupes histologiques de muscles de souris exprimant l'alpha-actinine-2 mutée a montré la présence de cores, semblables à ceux trouvés chez les patients, et a également révélé des défauts de la ligne Z (**Fig S4**). Cette étude a ainsi permis de valider l'implication du gène *ACTN2* dans les myopathies à cores et suggère qu'il est nécessaire de séquencer ce gène chez les patients atteints de myopathie à cores.

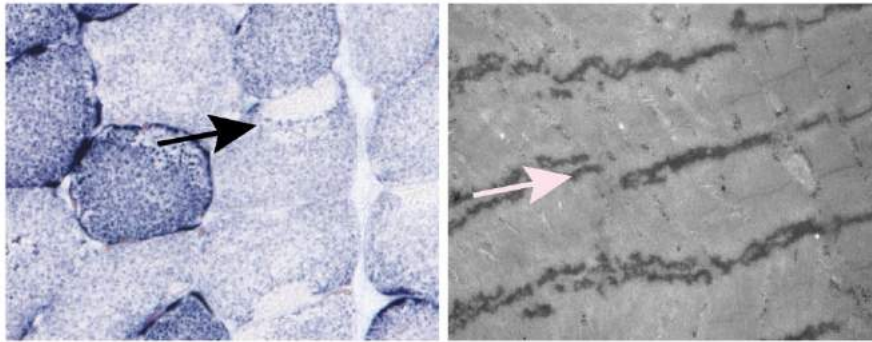


Fig S3 : Caractéristiques histologiques des muscles de souris exprimant l'alpha-actinine-2 mutée

Coupe transversale d'un muscle de souris exprimant l'alpha-actinin-2 mutée (à gauche). Les réactions oxydative révèlent des cores dépourvus d'activité en périphérie de la fibre (flèche noire à gauche). L'étude ultrastructurale de ces cores en coupe longitudinale révèle qu'ils sont composés de myofibrilles comportant des désorganisations majeures de la ligne Z (à droite).

III) Conclusion

Notre étude a permis pour la première fois d'étudier l'implication des gènes *MYPN* et *ACTN2* dans les myopathies congénitales. J'ai communiqué à propos de mes résultats en France et à l'étranger auprès d'un public de neurologues pour les informer de l'avancée de nos recherches et des nouveaux gènes caractérisés. Mon travail a donc un impact direct sur la prise en charge des patients et sur le diagnostic.

D'une manière plus fondamentale, ce projet a permis de décrire de nouveaux gènes et de nouvelles voies de signalisation moléculaires et cellulaires nécessaires pour le développement normal du muscle et pour sa physiologie. L'ensemble de ces résultats offre de nouvelles pistes thérapeutiques pour le traitement des myopathies.

4 REFERENCES

- Abath Neto, O., C. A. M. Moreno, E. Malfatti, S. Donkervoort, J. Bohm, J. B. Guimaraes, A. R. Foley, P. Mohassel, J. Dastgir, D. X. Bharucha-Goebel, S. Monges, F. Lubieniecki, J. Collins, L. Medne, M. Santi, S. Yum, B. Banwell, E. Salort-Campana, J. Rendu, J. Faure, U. Yis, B. Eymard, C. Cheraud, R. Schneider, J. Thompson, X. Lornage, L. Mesrob, D. Lechner, A. Boland, J. F. Deleuze, U. C. Reed, A. S. B. Oliveira, V. Biancalana, N. B. Romero, C. G. Bonnemann, J. Laporte, and E. Zanuteli. 2017. 'Common and variable clinical, histological, and imaging findings of recessive RYR1-related centronuclear myopathy patients', *Neuromuscul Disord*, 27: 975-85.
- Acakpo-Satchivi, L. J., W. Edelmann, C. Sartorius, B. D. Lu, P. A. Wahr, S. C. Watkins, J. M. Metzger, L. Leinwand, and R. Kucherlapati. 1997. 'Growth and muscle defects in mice lacking adult myosin heavy chain genes', *J Cell Biol*, 139: 1219-29.
- Ackerman, M. J., and D. E. Clapham. 1997. 'Ion channels--basic science and clinical disease', *N Engl J Med*, 336: 1575-86.
- Agrawal, P. B., R. S. Greenleaf, K. K. Tomczak, V. L. Lehtokari, C. Wallgren-Pettersson, W. Wallefeld, N. G. Laing, B. T. Darras, S. K. Maciver, P. R. Dormitzer, and A. H. Beggs. 2007. 'Nemaline myopathy with minicores caused by mutation of the CFL2 gene encoding the skeletal muscle actin-binding protein, cofilin-2', *American Journal of Human Genetics*, 80: 162-7.
- Agrawal, P. B., C. R. Pierson, M. Joshi, X. Liu, G. Ravenscroft, B. Moghadaszadeh, T. Talabere, M. Viola, L. C. Swanson, G. Haliloglu, B. Talim, K. S. Yau, R. J. Allcock, N. G. Laing, M. A. Perrella, and A. H. Beggs. 2014. 'SPEG interacts with myotubularin, and its deficiency causes centronuclear myopathy with dilated cardiomyopathy', *American Journal of Human Genetics*, 95: 218-26.
- Al-Qusairi, L., N. Weiss, A. Toussaint, C. Berbey, N. Messaddeq, C. Kretz, D. Sanoudou, A. H. Beggs, B. Allard, J. L. Mandel, J. Laporte, V. Jacquemond, and A. Buj-Bello. 2009. 'T-tubule disorganization and defective excitation-contraction coupling in muscle fibers lacking myotubularin lipid phosphatase', *Proc Natl Acad Sci U S A*, 106: 18763-8.
- Alazami, A. M., A. Y. Kentab, E. Faqeih, J. Y. Mohamed, H. Alkhalidi, H. Hijazi, and F. S. Alkuraya. 2015. 'A novel syndrome of Klippel-Feil anomaly, myopathy, and characteristic facies is linked to a null mutation in MYO18B', *Journal of Medical Genetics*, 52: 400-4.
- Ambaradar, S., R. Gupta, D. Trakroo, R. Lal, and J. Vakhlu. 2016. 'High Throughput Sequencing: An Overview of Sequencing Chemistry', *Indian J Microbiol*, 56: 394-404.
- Amburgey, K., N. McNamara, L. R. Bennett, M. E. McCormick, G. Acsadi, and J. J. Dowling. 2011. 'Prevalence of congenital myopathies in a representative pediatric united states population', *Annals of Neurology*, 70: 662-5.
- Amos-Landgraf, J. M., A. Cottle, R. M. Plenge, M. Friez, C. E. Schwartz, J. Longshore, and H. F. Willard. 2006. 'X chromosome-inactivation patterns of 1,005 phenotypically unaffected females', *American Journal of Human Genetics*, 79: 493-9.
- Anoussamy, M., C. Lilien, T. Gidaro, E. Gargaun, V. Che, U. Schara, A. Gangfuss, A. D'Amico, J. J. Dowling, B. T. Darras, A. Daron, A. Hernandez, C. de Lattre, J. M. Arnal, M. Mayer, J. M. Cuisset, C. Vuillerot, S. Fontaine, R. Bellance, V. Biancalana, A. Buj-Bello, J. Y. Hogrel, H. Landy, and L. Servais. 2019. 'X-linked myotubular myopathy: A prospective international natural history study', *Neurology*, 92: e1852-e67.

- Arber, S., G. Halder, and P. Caroni. 1994. 'Muscle LIM protein, a novel essential regulator of myogenesis, promotes myogenic differentiation', *Cell*, 79: 221-31.
- Atkinson, R. A., C. Joseph, G. Kelly, F. W. Muskett, T. A. Frenkiel, D. Nietlispach, and A. Pastore. 2001. 'Ca²⁺-independent binding of an EF-hand domain to a novel motif in the alpha-actinin-titin complex', *Nat Struct Biol*, 8: 853-7.
- Au, Y., R. A. Atkinson, R. Guerrini, G. Kelly, C. Joseph, S. R. Martin, F. W. Muskett, A. Pallavicini, G. Faulkner, and A. Pastore. 2004. 'Solution structure of ZASP PDZ domain; implications for sarcomere ultrastructure and enigma family redundancy', *Structure*, 12: 611-22.
- Avila-Polo, R., E. Malfatti, X. Lornage, C. Cheraud, I. Nelson, J. Nectoux, J. Bohm, R. Schneider, C. Hedberg-Oldfors, B. Eymard, S. Monges, F. Lubieniecki, G. Brochier, M. Thao Bui, A. Madelaine, C. Labasse, M. Beuvin, E. Lacene, A. Boland, J. F. Deleuze, J. Thompson, I. Richard, A. L. Taratuto, B. Udd, F. Leturcq, G. Bonne, A. Oldfors, J. Laporte, and N. B. Romero. 2018. 'Loss of Sarcomeric Scaffolding as a Common Baseline Histopathologic Lesion in Titin-Related Myopathies', *J Neuropathol Exp Neurol*, 77: 1101-14.
- Avila, G., J. J. O'Brien, and R. T. Dirksen. 2001. 'Excitation--contraction uncoupling by a human central core disease mutation in the ryanodine receptor', *Proc Natl Acad Sci U S A*, 98: 4215-20.
- Bagnall, R. D., L. K. Molloy, J. M. Kalman, and C. Semsarian. 2014. 'Exome sequencing identifies a mutation in the ACTN2 gene in a family with idiopathic ventricular fibrillation, left ventricular noncompaction, and sudden death', *BMC Med Genet*, 15: 99.
- Bang, M. L., R. E. Mudry, A. S. McElhinny, K. Trombitas, A. J. Geach, R. Yamasaki, H. Sorimachi, H. Granzier, C. C. Gregorio, and S. Labeit. 2001. 'Myopalladin, a novel 145-kilodalton sarcomeric protein with multiple roles in Z-disc and I-band protein assemblies', *J Cell Biol*, 153: 413-27.
- Barone, V., V. Del Re, A. Gamberucci, V. Polverino, L. Galli, D. Rossi, E. Costanzi, L. Toniolo, G. Berti, A. Malandrini, G. Ricci, G. Siciliano, G. Vattedi, G. Tomelleri, E. Pierantozzi, S. Spinozzi, N. Volpi, R. Fulceri, R. Battistutta, C. Reggiani, and V. Sorrentino. 2017. 'Identification and characterization of three novel mutations in the CASQ1 gene in four patients with tubular aggregate myopathy', *Human Mutation*, 38: 1761-73.
- Behin, A., E. Salort-Campana, K. Wahbi, P. Richard, R. Y. Carlier, P. Carlier, P. Laforet, T. Stojkovic, T. Maisonobe, A. Verschueren, J. Franques, S. Attarian, A. Maues de Paula, D. Figarella-Branger, H. M. Becane, I. Nelson, D. Duboc, G. Bonne, P. Vicart, B. Udd, N. Romero, J. Pouget, and B. Eymard. 2015. 'Myofibrillar myopathies: State of the art, present and future challenges', *Rev Neurol (Paris)*, 171: 715-29.
- Berardo, A., S. DiMauro, and M. Hirano. 2010. 'A diagnostic algorithm for metabolic myopathies', *Curr Neurol Neurosci Rep*, 10: 118-26.
- Berardo, A., X. Lornage, M. Johari, T. Evangelista, C. Cejas, F. Barroso, A. Dubrovsky, M. T. Bui, G. Brochier, M. Saccoliti, J. Bohm, B. Udd, J. Laporte, N. B. Romero, and A. L. Taratuto. 2019. 'HNRNPDL-related muscular dystrophy: expanding the clinical, morphological and MRI phenotypes', *Journal of Neurology*.
- Biancalana, V., S. Scheidecker, M. Miguët, A. Laquerriere, N. B. Romero, T. Stojkovic, O. Abath Neto, S. Mercier, N. Voermans, L. Tanner, C. Rogers, E. Ollagnon-Roman, H. Roper, C. Boutte, S. Ben-Shachar, X. Lornage, N. Vasli, E. Schaefer, P. Laforet, J. Pouget, A. Moerman, L. Pasquier, P. Marcocelle, A. Magot, B. Kusters, N. Streichenberger, C. Tranchant, N. Dondaine, R. Schneider, C. Gasnier, N. Calmels, V. Kremer, K. Nguyen, J. Perrier, E. J. Kamsteeg, P. Carlier, R. Y. Carlier, J. Thompson, A. Boland, J. F. Deleuze, M. Fardeau, E. Zanolli, B. Eymard, and J. Laporte. 2017. 'Affected female carriers of MTM1 mutations display a wide spectrum of clinical and

- pathological involvement: delineating diagnostic clues', *Acta Neuropathol*, 134: 889-904.
- Bitoun, M., S. Maugenre, P. Y. Jeannet, E. Lacene, X. Ferrer, P. Laforet, J. J. Martin, J. Laporte, H. Lochmuller, A. H. Beggs, M. Fardeau, B. Eymard, N. B. Romero, and P. Guicheney. 2005. 'Mutations in dynamin 2 cause dominant centronuclear myopathy', *Nat Genet*, 37: 1207-9.
- Block, B. A., T. Imagawa, K. P. Campbell, and C. Franzini-Armstrong. 1988. 'Structural evidence for direct interaction between the molecular components of the transverse tubule/sarcoplasmic reticulum junction in skeletal muscle', *J Cell Biol*, 107: 2587-600.
- Bohm, J., V. Biancalana, E. Malfatti, N. Dondaine, C. Koch, N. Vasli, W. Kress, M. Strittmatter, A. L. Taratuto, H. Gonorazky, P. Laforet, T. Maisonobe, M. Olive, L. Gonzalez-Mera, M. Fardeau, N. Carriere, P. Clavelou, B. Eymard, M. Bitoun, J. Rendu, J. Faure, J. Weis, J. L. Mandel, N. B. Romero, and J. Laporte. 2014. 'Adult-onset autosomal dominant centronuclear myopathy due to BIN1 mutations', *Brain*, 137: 3160-70.
- Bohm, J., M. Bulla, J. E. Urquhart, E. Malfatti, S. G. Williams, J. O'Sullivan, A. Szlauer, C. Koch, G. Baranello, M. Mora, M. Ripolone, R. Violano, M. Moggio, H. Kingston, T. Dawson, C. G. DeGoede, J. Nixon, A. Boland, J. F. Deleuze, N. Romero, W. G. Newman, N. Demaurex, and J. Laporte. 2017. 'ORAI1 Mutations with Distinct Channel Gating Defects in Tubular Aggregate Myopathy', *Human Mutation*, 38: 426-38.
- Bohm, J., F. Chevessier, A. Maues De Paula, C. Koch, S. Attarian, C. Feger, D. Hantai, P. Laforet, K. Ghorab, J. M. Vallat, M. Fardeau, D. Figarella-Branger, J. Pouget, N. B. Romero, M. Koch, C. Ebel, N. Levy, M. Krahn, B. Eymard, M. Bartoli, and J. Laporte. 2013. 'Constitutive activation of the calcium sensor STIM1 causes tubular-aggregate myopathy', *American Journal of Human Genetics*, 92: 271-8.
- Bohm, J., and J. Laporte. 2018. 'Gain-of-function mutations in STIM1 and ORAI1 causing tubular aggregate myopathy and Stormorken syndrome', *Cell Calcium*, 76: 1-9.
- Bohm, J., X. Lornage, F. Chevessier, C. Birck, S. Zanotti, P. Cudia, M. Bulla, F. Granger, M. T. Bui, M. Sartori, C. Schneider-Gold, E. Malfatti, N. B. Romero, M. Mora, and J. Laporte. 2018. 'CASQ1 mutations impair calsequestrin polymerization and cause tubular aggregate myopathy', *Acta Neuropathol*, 135: 149-51.
- Bouhy, D., M. Juneja, I. Katona, A. Holmgren, B. Asselbergh, V. De Winter, T. Hochepped, S. Goossens, J. J. Haigh, C. Libert, C. Ceuterick-de Groote, J. Irobi, J. Weis, and V. Timmerman. 2018. 'A knock-in/knock-out mouse model of HSPB8-associated distal hereditary motor neuropathy and myopathy reveals toxic gain-of-function of mutant Hspb8', *Acta Neuropathologica*, 135: 131-48.
- Braun, N. M., N. S. Arora, and D. F. Rochester. 1983. 'Respiratory muscle and pulmonary function in polymyositis and other proximal myopathies', *Thorax*, 38: 616-23.
- Buono, S., J. A. Ross, H. Tasfaout, Y. Levy, C. Kretz, L. Tayefeh, J. Matson, S. Guo, P. Kessler, B. P. Monia, M. Bitoun, J. Ochala, J. Laporte, and B. S. Cowling. 2018. 'Reducing dynamin 2 (DNM2) rescues DNM2-related dominant centronuclear myopathy', *Proc Natl Acad Sci U S A*, 115: 11066-71.
- Cao, C., J. M. Backer, J. Laporte, E. J. Bedrick, and A. Wandinger-Ness. 2008. 'Sequential actions of myotubularin lipid phosphatases regulate endosomal PI(3)P and growth factor receptor trafficking', *Mol Biol Cell*, 19: 3334-46.
- Carmignac, V., M. A. Salih, S. Quijano-Roy, S. Marchand, M. M. Al Rayess, M. M. Mukhtar, J. A. Urtizbera, S. Labeit, P. Guicheney, F. Leturcq, M. Gautel, M. Fardeau, K. P. Campbell, I. Richard, B. Estournet, and A. Ferreiro. 2007. 'C-terminal titin deletions cause a novel early-onset myopathy with fatal cardiomyopathy', *Annals of Neurology*, 61: 340-51.

- Cassandrini, D., R. Trovato, A. Rubegni, S. Lenzi, C. Fiorillo, J. Baldacci, C. Minetti, G. Astrea, C. Bruno, F. M. Santorelli, and Myopathies Italian Network on Congenital. 2017. 'Congenital myopathies: clinical phenotypes and new diagnostic tools', *Ital J Pediatr*, 43: 101.
- Catteruccia, M., F. Fattori, V. Codemo, L. Ruggiero, L. Maggi, G. Tasca, C. Fiorillo, M. Pane, A. Berardinelli, M. Verardo, C. Bragato, M. Mora, L. Morandi, C. Bruno, L. Santoro, E. Pegoraro, E. Mercuri, E. Bertini, and A. D'Amico. 2013. 'Centronuclear myopathy related to dynamin 2 mutations: clinical, morphological, muscle imaging and genetic features of an Italian cohort', *Neuromuscul Disord*, 23: 229-38.
- Ceyhan-Birsoy, O., P. B. Agrawal, C. Hidalgo, K. Schmitz-Abe, E. T. DeChene, L. C. Swanson, R. Soemedi, N. Vasli, S. T. Iannaccone, P. B. Shieh, N. Shur, J. M. Dennison, M. W. Lawlor, J. Laporte, K. Markianos, W. G. Fairbrother, H. Granzier, and A. H. Beggs. 2013. 'Recessive truncating titin gene, TTN, mutations presenting as centronuclear myopathy', *Neurology*, 81: 1205-14.
- Chami, N., R. Tadros, F. Lemarbre, K. S. Lo, M. Beaudoin, L. Robb, D. Labuda, J. C. Tardif, N. Racine, M. Talajic, and G. Lettre. 2014. 'Nonsense mutations in BAG3 are associated with early-onset dilated cardiomyopathy in French Canadians', *Can J Cardiol*, 30: 1655-61.
- Chauveau, C., J. Rowell, and A. Ferreira. 2014. 'A rising titan: TTN review and mutation update', *Human Mutation*, 35: 1046-59.
- Chiu, C., R. D. Bagnall, J. Ingles, L. Yeates, M. Kennerson, J. A. Donald, M. Jormakka, J. M. Lind, and C. Semsarian. 2010. 'Mutations in alpha-actinin-2 cause hypertrophic cardiomyopathy: a genome-wide analysis', *J Am Coll Cardiol*, 55: 1127-35.
- Colombo, I., M. Scoto, A. Y. Manzur, S. A. Robb, L. Maggi, V. Gowda, T. Cullup, M. Yau, R. Phadke, C. Sewry, H. Jungbluth, and F. Muntoni. 2015. 'Congenital myopathies: Natural history of a large pediatric cohort', *Neurology*, 84: 28-35.
- Cortese, A., M. Laura, C. Casali, I. Nishino, Y. K. Hayashi, S. Magri, F. Taroni, C. Stuardi, P. Saveri, M. Moggio, M. Ripolone, A. Prella, C. Pisciotto, A. Sagnelli, A. Pichiecchio, M. M. Reilly, E. Buratti, and D. Pareyson. 2018. 'Altered TDP-43-dependent splicing in HSPB8-related distal hereditary motor neuropathy and myofibrillar myopathy', *Eur J Neurol*, 25: 154-63.
- Cui, H., Y. Kong, and H. Zhang. 2012. 'Oxidative stress, mitochondrial dysfunction, and aging', *J Signal Transduct*, 2012: 646354.
- D'Amico, A., F. Fattori, G. Tasca, S. Petrini, F. Gualandi, A. Bruselles, V. D'Oria, M. Verardo, R. Carrozzo, M. Niceta, B. Udd, A. Ferlini, M. Tartaglia, and E. Bertini. 2017. 'Somatic mosaicism represents an underestimated event underlying collagen 6-related disorders', *Eur J Paediatr Neurol*, 21: 873-83.
- Dahl, N., L. J. Hu, M. Chery, M. Fardeau, S. Gilgenkrantz, A. Nivelon-Chevallier, I. Sidaner-Noisette, F. Mugneret, J. B. Gouyon, A. Gal, and et al. 1995. 'Myotubular myopathy in a girl with a deletion at Xq27-q28 and unbalanced X inactivation assigns the MTM1 gene to a 600-kb region', *American Journal of Human Genetics*, 56: 1108-15.
- Davis, M. R., E. Haan, H. Jungbluth, C. Sewry, K. North, F. Muntoni, T. Kuntzer, P. Lamont, A. Bankier, P. Tomlinson, A. Sanchez, P. Walsh, L. Nagarajan, C. Oley, A. Colley, A. Gedeon, R. Quinlivan, J. Dixon, D. James, C. R. Muller, and N. G. Laing. 2003. 'Principal mutation hotspot for central core disease and related myopathies in the C-terminal transmembrane region of the RYR1 gene', *Neuromuscul Disord*, 13: 151-7.
- De Cid, R., R. Ben Yaou, C. Roudaut, K. Charton, S. Baulande, F. Leturcq, N. B. Romero, E. Malfatti, M. Beuvin, A. Vihola, A. Criqui, I. Nelson, J. Nectoux, L. Ben Aim, C. Caloustian, R. Olasso, B. Udd, G. Bonne, B. Eymard, and I. Richard. 2015. 'A new

- titinopathy: Childhood-juvenile onset Emery-Dreifuss-like phenotype without cardiomyopathy', *Neurology*, 85: 2126-35.
- De Paula, A. M., J. Franques, C. Fernandez, N. Monnier, J. Lunardi, J. F. Pellissier, D. Figarella-Branger, and J. Pouget. 2009. 'A TPM3 mutation causing cap myopathy', *Neuromuscul Disord*, 19: 685-8.
- de Winter, J. M., D. Buck, C. Hidalgo, J. R. Jasper, F. I. Malik, N. F. Clarke, G. J. Stienen, M. W. Lawlor, A. H. Beggs, C. A. Ottenheijm, and H. Granzier. 2013. 'Troponin activator augments muscle force in nemaline myopathy patients with nebulin mutations', *Journal of Medical Genetics*, 50: 383-92.
- de Winter, J. M., and C. A. C. Ottenheijm. 2017. 'Sarcomere Dysfunction in Nemaline Myopathy', *J Neuromuscul Dis*, 4: 99-113.
- Dlamini, N., N. C. Voermans, S. Lillis, K. Stewart, E. J. Kamsteeg, G. Drost, R. Quinlivan, M. Snoeck, F. Norwood, A. Radunovic, V. Straub, M. Roberts, A. F. Vrancken, W. L. van der Pol, R. I. de Coo, A. Y. Manzur, S. Yau, S. Abbs, A. King, M. Lammens, P. M. Hopkins, S. Mohammed, S. Treves, F. Muntoni, E. Wraige, M. R. Davis, B. van Engelen, and H. Jungbluth. 2013. 'Mutations in RYR1 are a common cause of exertional myalgia and rhabdomyolysis', *Neuromuscul Disord*, 23: 540-8.
- Donner, K., M. Ollikainen, M. Ridanpaa, H. J. Christen, H. H. Goebel, M. de Visser, K. Pelin, and C. Wallgren-Pettersson. 2002. 'Mutations in the beta-tropomyosin (TPM2) gene--a rare cause of nemaline myopathy', *Neuromuscul Disord*, 12: 151-8.
- Dotti, M. T., A. Malandrini, X. Lornage, A. Mignarri, T. A. Cantisani, J. Bohm, J. Laporte, and E. Malfatti. 2018. 'Discordant manifestations in Italian brothers with GNE myopathy', *Journal of the Neurological Sciences*, 386: 1-3.
- Dowling, J. J., M. W. Lawlor, and R. T. Dirksen. 2014. 'Triadopathies: an emerging class of skeletal muscle diseases', *Neurotherapeutics*, 11: 773-85.
- Dreyfuss, G., M. J. Matunis, S. Pinol-Roma, and C. G. Burd. 1993. 'hnRNP proteins and the biogenesis of mRNA', *Annu Rev Biochem*, 62: 289-321.
- Duboscq-Bidot, L., P. Xu, P. Charron, N. Neyroud, G. Dilanian, A. Millaire, V. Bors, M. Komajda, and E. Villard. 2008. 'Mutations in the Z-band protein myopalladin gene and idiopathic dilated cardiomyopathy', *Cardiovasc Res*, 77: 118-25.
- Dubowitz, V., and A. G. Pearse. 1960. 'Oxidative enzymes and phosphorylase in central-core disease of muscle', *Lancet*, 2: 23-4.
- Durham, W. J., P. Aracena-Parks, C. Long, A. E. Rossi, S. A. Goonasekera, S. Boncompagni, D. L. Galvan, C. P. Gilman, M. R. Baker, N. Shirokova, F. Protasi, R. Dirksen, and S. L. Hamilton. 2008. 'RyR1 S-nitrosylation underlies environmental heat stroke and sudden death in Y522S RyR1 knockin mice', *Cell*, 133: 53-65.
- Echaniz-Laguna, A., X. Lornage, B. Lannes, R. Schneider, G. Bierry, N. Dondaine, A. Boland, J. F. Deleuze, J. Bohm, J. Thompson, J. Laporte, and V. Biancalana. 2017. 'HSPB8 haploinsufficiency causes dominant adult-onset axial and distal myopathy', *Acta Neuropathol*, 134: 163-65.
- Eggen, V. R. C., P. G. Barth, and F. Baas. 1993. 'EXOSC3-Related Pontocerebellar Hypoplasia.' in M. P. Adam, H. H. Ardinger, R. A. Pagon, S. E. Wallace, L. J. H. Bean, K. Stephens and A. Amemiya (eds.), *GeneReviews((R))* (Seattle (WA)).
- Eisenberg, I., N. Avidan, T. Potikha, H. Hochner, M. Chen, T. Olender, M. Barash, M. Shemesh, M. Sadeh, G. Grabov-Nardini, I. Shmilevich, A. Friedmann, G. Karpati, W. G. Bradley, L. Baumbach, D. Lancet, E. B. Asher, J. S. Beckmann, Z. Argov, and S. Mitrani-Rosenbaum. 2001. 'The UDP-N-acetylglucosamine 2-epimerase/N-acetylmannosamine kinase gene is mutated in recessive hereditary inclusion body myopathy', *Nat Genet*, 29: 83-7.
- Emery, A. E. 2002. 'The muscular dystrophies', *Lancet*, 359: 687-95.

- Endo, Y., S. Noguchi, Y. Hara, Y. K. Hayashi, K. Motomura, S. Miyatake, N. Murakami, S. Tanaka, S. Yamashita, R. Kizu, M. Bamba, Y. Goto, N. Matsumoto, I. Nonaka, and I. Nishino. 2015. 'Dominant mutations in ORAI1 cause tubular aggregate myopathy with hypocalcemia via constitutive activation of store-operated Ca(2)(+) channels', *Human Molecular Genetics*, 24: 637-48.
- Engel, A. G., M. R. Gomez, and R. V. Groover. 1971. 'Multicore disease. A recently recognized congenital myopathy associated with multifocal degeneration of muscle fibers', *Mayo Clin Proc*, 46: 666-81.
- Evila, A., M. Arumilli, B. Udd, and P. Hackman. 2016. 'Targeted next-generation sequencing assay for detection of mutations in primary myopathies', *Neuromuscul Disord*, 26: 7-15.
- Faulkner, G., A. Pallavicini, E. Formentin, A. Comelli, C. Ievolella, S. Trevisan, G. Bortoletto, P. Scannapieco, M. Salamon, V. Mouly, G. Valle, and G. Lanfranchi. 1999. 'ZASP: a new Z-band alternatively spliced PDZ-motif protein', *J Cell Biol*, 146: 465-75.
- Ferreiro, A., B. Estournet, D. Chateau, N. B. Romero, C. Laroche, S. Odent, A. Toutain, A. Cabello, D. Fontan, H. G. dos Santos, C. A. Haenggeli, E. Bertini, J. A. Urtizbera, P. Guicheney, and M. Fardeau. 2000. 'Multi-minicore disease--searching for boundaries: phenotype analysis of 38 cases', *Annals of Neurology*, 48: 745-57.
- Ferreiro, A., N. Monnier, N. B. Romero, J. P. Leroy, C. Bonnemann, C. A. Haenggeli, V. Straub, W. D. Voss, Y. Nivoche, H. Jungbluth, A. Lemainque, T. Voit, J. Lunardi, M. Fardeau, and P. Guicheney. 2002. 'A recessive form of central core disease, transiently presenting as multi-minicore disease, is associated with a homozygous mutation in the ryanodine receptor type 1 gene', *Annals of Neurology*, 51: 750-9.
- Fidzianska, A. 2002. "'Cap disease"--a failure in the correct muscle fibre formation', *Journal of the Neurological Sciences*, 201: 27-31.
- Fidzianska, A., B. Badurska, B. Ryniewicz, and I. Dembek. 1981. "'Cap disease": new congenital myopathy', *Neurology*, 31: 1113-20.
- Fleischer, S., and M. Inui. 1989. 'Biochemistry and biophysics of excitation-contraction coupling', *Annu Rev Biophys Biophys Chem*, 18: 333-64.
- Fontaine, B., J. Vale-Santos, K. Jurkat-Rott, J. Reboul, E. Plassart, C. S. Rime, A. Elbaz, R. Heine, J. Guimaraes, J. Weissenbach, and et al. 1994. 'Mapping of the hypokalaemic periodic paralysis (HypoPP) locus to chromosome 1q31-32 in three European families', *Nat Genet*, 6: 267-72.
- Franzini-Armstrong, C., and J. W. Kish. 1995. 'Alternate disposition of tetrads in peripheral couplings of skeletal muscle', *J Muscle Res Cell Motil*, 16: 319-24.
- Franzini-Armstrong, C., and F. Protasi. 1997. 'Ryanodine receptors of striated muscles: a complex channel capable of multiple interactions', *Physiol Rev*, 77: 699-729.
- Frontera, W. R., and J. Ochala. 2015. 'Skeletal muscle: a brief review of structure and function', *Calcif Tissue Int*, 96: 183-95.
- Garibaldi, M., J. Rendu, J. Brocard, E. Lacene, J. Faure, G. Brochier, M. Beuvin, C. Labasse, A. Madelaine, E. Malfatti, J. A. Bevilacqua, F. Lubieniecki, S. Monges, A. L. Taratuto, J. Laporte, I. Marty, G. Antonini, and N. B. Romero. 2019. "'Dusty core disease' (DuCD): expanding morphological spectrum of RYR1 recessive myopathies', *Acta Neuropathol Commun*, 7: 3.
- Ghaoui, R., S. T. Cooper, M. Lek, K. Jones, A. Corbett, S. W. Reddel, M. Needham, C. Liang, L. B. Waddell, G. Nicholson, G. O'Grady, S. Kaur, R. Ong, M. Davis, C. M. Sue, N. G. Laing, K. N. North, D. G. MacArthur, and N. F. Clarke. 2015. 'Use of Whole-Exome Sequencing for Diagnosis of Limb-Girdle Muscular Dystrophy: Outcomes and Lessons Learned', *JAMA Neurol*, 72: 1424-32.

- Ghaoui, R., J. Palmio, J. Brewer, M. Lek, M. Needham, A. Evila, P. Hackman, P. H. Jonson, S. Penttila, A. Vihola, S. Huovinen, M. Lindfors, R. L. Davis, L. Waddell, S. Kaur, C. Yiannikas, K. North, N. Clarke, D. G. MacArthur, C. M. Sue, and B. Udd. 2016. 'Mutations in HSPB8 causing a new phenotype of distal myopathy and motor neuropathy', *Neurology*, 86: 391-8.
- Girolami, F., M. Iascone, B. Tomberli, S. Bardi, M. Benelli, G. Marseglia, C. Pescucci, L. Pezzoli, M. E. Sana, C. Basso, N. Marziliano, P. A. Merlini, A. Fornaro, F. Cecchi, F. Torricelli, and I. Olivetto. 2014. 'Novel alpha-actinin 2 variant associated with familial hypertrophic cardiomyopathy and juvenile atrial arrhythmias: a massively parallel sequencing study', *Circ Cardiovasc Genet*, 7: 741-50.
- Gonorazky, H. D., J. J. Dowling, J. R. Volpatti, and J. Vajsar. 2019. 'Signs and Symptoms in Congenital Myopathies', *Seminars in Pediatric Neurology*, 29: 3-11.
- Gordon, A. M., E. Homsher, and M. Regnier. 2000. 'Regulation of contraction in striated muscle', *Physiol Rev*, 80: 853-924.
- Granzier, H., M. Helmes, O. Cazorla, M. McNabb, D. Labeit, Y. Wu, R. Yamasaki, A. Redkar, M. Kellermayer, S. Labeit, and K. Trombitas. 2000. 'Mechanical properties of titin isoforms', *Adv Exp Med Biol*, 481: 283-300; discussion 00-4.
- Gregorio, C. C., K. Trombitas, T. Centner, B. Kolmerer, G. Stier, K. Kunke, K. Suzuki, F. Obermayr, B. Herrmann, H. Granzier, H. Sorimachi, and S. Labeit. 1998. 'The NH2 terminus of titin spans the Z-disc: its interaction with a novel 19-kD ligand (T-cap) is required for sarcomeric integrity', *J Cell Biol*, 143: 1013-27.
- Gupta, V. A., G. Ravenscroft, R. Shaheen, E. J. Todd, L. C. Swanson, M. Shiina, K. Ogata, C. Hsu, N. F. Clarke, B. T. Darras, M. A. Farrar, A. Hashem, N. D. Manton, F. Muntoni, K. N. North, S. A. Sandaradura, I. Nishino, Y. K. Hayashi, C. A. Sewry, E. M. Thompson, K. S. Yau, C. A. Brownstein, T. W. Yu, R. J. Allcock, M. R. Davis, C. Wallgren-Pettersson, N. Matsumoto, F. S. Alkuraya, N. G. Laing, and A. H. Beggs. 2013. 'Identification of KLHL41 Mutations Implicates BTB-Kelch-Mediated Ubiquitination as an Alternate Pathway to Myofibrillar Disruption in Nemaline Myopathy', *American Journal of Human Genetics*, 93: 1108-17.
- Gupta, V., M. Discenza, J. R. Guyon, L. M. Kunkel, and A. H. Beggs. 2012. 'alpha-Actinin-2 deficiency results in sarcomeric defects in zebrafish that cannot be rescued by alpha-actinin-3 revealing functional differences between sarcomeric isoforms', *FASEB J*, 26: 1892-908.
- Guth, L., and F. J. Samaha. 1969. 'Qualitative differences between actomyosin ATPase of slow and fast mammalian muscle', *Exp Neurol*, 25: 138-52.
- Hackman, P., S. Marchand, J. Sarparanta, A. Vihola, I. Penisson-Besnier, B. Eymard, J. M. Pardal-Fernandez, H. Hammouda el, I. Richard, I. Illa, and B. Udd. 2008. 'Truncating mutations in C-terminal titin may cause more severe tibial muscular dystrophy (TMD)', *Neuromuscul Disord*, 18: 922-8.
- Hance, J. E., S. Y. Fu, S. C. Watkins, A. H. Beggs, and M. Michalak. 1999. 'alpha-actinin-2 is a new component of the dystrophin-glycoprotein complex', *Arch Biochem Biophys*, 365: 216-22.
- Harazi, A., M. Becker-Cohen, H. Zer, O. Moshel, S. Hinderlich, and S. Mitrani-Rosenbaum. 2017. 'The Interaction of UDP-N-Acetylglucosamine 2-Epimerase/N-Acetylmannosamine Kinase (GNE) and Alpha-Actinin 2 Is Altered in GNE Myopathy M743T Mutant', *Mol Neurobiol*, 54: 2928-38.
- Haywood, N. J., M. Wolny, B. Rogers, C. H. Trinh, Y. Shuping, T. A. Edwards, and M. Peckham. 2016. 'Hypertrophic cardiomyopathy mutations in the calponin-homology domain of ACTN2 affect actin binding and cardiomyocyte Z-disc incorporation', *Biochem J*, 473: 2485-93.

- Head, S. R., H. K. Komori, S. A. LaMere, T. Whisenant, F. Van Nieuwerburgh, D. R. Salomon, and P. Ordoukhanian. 2014. 'Library construction for next-generation sequencing: overviews and challenges', *Biotechniques*, 56: 61-4, 66, 68, passim.
- Hemmings, L., P. A. Kuhlman, and D. R. Critchley. 1992. 'Analysis of the actin-binding domain of alpha-actinin by mutagenesis and demonstration that dystrophin contains a functionally homologous domain', *J Cell Biol*, 116: 1369-80.
- Hertz, C. L., S. L. Christiansen, M. K. Larsen, M. Dahl, L. Ferrero-Miliani, P. E. Weeke, O. Pedersen, T. Hansen, N. Grarup, G. L. Ottesen, R. Frank-Hansen, J. Banner, and N. Morling. 2016. 'Genetic investigations of sudden unexpected deaths in infancy using next-generation sequencing of 100 genes associated with cardiac diseases', *Eur J Hum Genet*, 24: 817-22.
- Houmeida, A., J. Holt, L. Tskhovrebova, and J. Trinick. 1995. 'Studies of the interaction between titin and myosin', *J Cell Biol*, 131: 1471-81.
- Hsieh, C. M., S. Fukumoto, M. D. Layne, K. Maemura, H. Charles, A. Patel, M. A. Perrella, and M. E. Lee. 2000. 'Striated muscle preferentially expressed genes alpha and beta are two serine/threonine protein kinases derived from the same gene as the aortic preferentially expressed gene-1', *Journal of Biological Chemistry*, 275: 36966-73.
- Huang, S. M., C. J. Huang, W. M. Wang, J. C. Kang, and W. C. Hsu. 2004. 'The enhancement of nuclear receptor transcriptional activation by a mouse actin-binding protein, alpha actinin 2', *J Mol Endocrinol*, 32: 481-96.
- Huby, A. C., U. Mendsaikhan, K. Takagi, R. Martherus, J. Wansapura, N. Gong, H. Osinska, J. F. James, K. Kramer, K. Saito, J. Robbins, Z. Khuchua, J. A. Towbin, and E. Purevjav. 2014. 'Disturbance in Z-disk mechanosensitive proteins induced by a persistent mutant myopalladin causes familial restrictive cardiomyopathy', *J Am Coll Cardiol*, 64: 2765-76.
- Hung, R. M., G. Yoon, C. E. Hawkins, W. Halliday, D. Biggar, and J. Vajsar. 2010. 'Cap myopathy caused by a mutation of the skeletal alpha-actin gene ACTA1', *Neuromuscul Disord*, 20: 238-40.
- Huntoon, V., J. J. Widrick, C. Sanchez, S. M. Rosen, C. Kutchukian, S. Cao, C. R. Pierson, X. Liu, M. A. Perrella, A. H. Beggs, V. Jacquemond, and P. B. Agrawal. 2018. 'SPEG-deficient skeletal muscles exhibit abnormal triad and defective calcium handling', *Human Molecular Genetics*, 27: 1608-17.
- Irobi, J., K. Van Impe, P. Seeman, A. Jordanova, I. Dierick, N. Verpoorten, A. Michalik, E. De Vriendt, A. Jacobs, V. Van Gerwen, K. Vennekens, R. Mazanec, I. Tournev, D. Hilton-Jones, K. Talbot, I. Kremensky, L. Van Den Bosch, W. Robberecht, J. Van Vandekerckhove, C. Van Broeckhoven, J. Gettemans, P. De Jonghe, and V. Timmerman. 2004. 'Hot-spot residue in small heat-shock protein 22 causes distal motor neuropathy', *Nat Genet*, 36: 597-601.
- Janssen, I., S. B. Heymsfield, Z. M. Wang, and R. Ross. 2000. 'Skeletal muscle mass and distribution in 468 men and women aged 18-88 yr', *J Appl Physiol (1985)*, 89: 81-8.
- Johnston, J. J., R. I. Kelley, T. O. Crawford, D. H. Morton, R. Agarwala, T. Koch, A. A. Schaffer, C. A. Francomano, and L. G. Biesecker. 2000. 'A novel nemaline myopathy in the Amish caused by a mutation in troponin T1', *American Journal of Human Genetics*, 67: 814-21.
- Joseph, C., G. Stier, R. O'Brien, A. S. Politou, R. A. Atkinson, A. Bianco, J. E. Ladbury, S. R. Martin, and A. Pastore. 2001. 'A structural characterization of the interactions between titin Z-repeats and the alpha-actinin C-terminal domain', *Biochemistry*, 40: 4957-65.
- Joureau, B., J. M. de Winter, S. Conijn, S. J. P. Bogaards, I. Kovacevic, A. Kalganov, M. Persson, J. Lindqvist, G. J. M. Stienen, T. C. Irving, W. Ma, M. Yuen, N. F. Clarke, D. E. Rassier, E. Malfatti, N. B. Romero, A. H. Beggs, and C. A. C. Ottenheijm. 2018.

- 'Dysfunctional sarcomere contractility contributes to muscle weakness in ACTA1-related nemaline myopathy (NEM3)', *Annals of Neurology*, 83: 269-82.
- Jungbluth, H., and M. Gautel. 2014. 'Pathogenic mechanisms in centronuclear myopathies', *Front Aging Neurosci*, 6: 339.
- Jungbluth, H., C. A. Sewry, and F. Muntoni. 2011. 'Core myopathies', *Seminars in Pediatric Neurology*, 18: 239-49.
- Jungbluth, H., S. Treves, F. Zorzato, A. Sarkozy, J. Ochala, C. Sewry, R. Phadke, M. Gautel, and F. Muntoni. 2018. 'Congenital myopathies: disorders of excitation-contraction coupling and muscle contraction', *Nat Rev Neurol*, 14: 151-67.
- Jungbluth, H., C. Wallgren-Pettersson, and J. Laporte. 2008. 'Centronuclear (myotubular) myopathy', *Orphanet J Rare Dis*, 3: 26.
- Jurkat-Rott, K., F. Lehmann-Horn, A. Elbaz, R. Heine, R. G. Gregg, K. Hogan, P. A. Powers, P. Lapie, J. E. Vale-Santos, J. Weissenbach, and et al. 1994. 'A calcium channel mutation causing hypokalemic periodic paralysis', *Human Molecular Genetics*, 3: 1415-9.
- Kao, H. Y. 2015. 'The actinin family proteins: biological function and clinical implications', *Cell Biosci*, 5: 48.
- Karakoc, E., C. Alkan, B. J. O'Roak, M. Y. Dennis, L. Vives, K. Mark, M. J. Rieder, D. A. Nickerson, and E. E. Eichler. 2011. 'Detection of structural variants and indels within exome data', *Nat Methods*, 9: 176-8.
- Kepler, O. T., S. Hinderlich, J. Langner, R. Schwartz-Albiez, W. Reutter, and M. Pawlita. 1999. 'UDP-GlcNAc 2-epimerase: a regulator of cell surface sialylation', *Science*, 284: 1372-6.
- Kiiski, K. J., V. L. Lehtokari, A. K. Vihola, J. M. Laitila, S. Huovinen, L. J. Sagath, A. E. Evila, A. E. Paetau, C. A. Sewry, P. B. Hackman, K. B. Pelin, C. Wallgren-Pettersson, and B. Udd. 2019. 'Dominantly inherited distal nemaline/cap myopathy caused by a large deletion in the nebulin gene', *Neuromuscul Disord*, 29: 97-107.
- Klaavuniemi, T., A. Kelloniemi, and J. Ylanne. 2004. 'The ZASP-like motif in actinin-associated LIM protein is required for interaction with the alpha-actinin rod and for targeting to the muscle Z-line', *Journal of Biological Chemistry*, 279: 26402-10.
- Krahn, M., V. Biancalana, M. Cerino, A. Perrin, L. Michel-Calemard, J. Nectoux, F. Leturcq, C. Bouchet-Seraphin, C. Acquaviva-Bourdain, E. Campana-Salort, A. Molon, J. A. Urtizbera, F. Audic, B. Chabrol, J. Pouget, R. Froissart, J. Melki, J. Rendu, F. Petit, C. Metay, N. Seta, D. Sternberg, J. Faure, and M. Cossee. 2019. 'A National French consensus on gene lists for the diagnosis of myopathies using next-generation sequencing', *Eur J Hum Genet*, 27: 349-52.
- Kwok, A. S., K. Phadwal, B. J. Turner, P. L. Oliver, A. Raw, A. K. Simon, K. Talbot, and V. R. Agashe. 2011. 'HspB8 mutation causing hereditary distal motor neuropathy impairs lysosomal delivery of autophagosomes', *Journal of Neurochemistry*, 119: 1155-61.
- Labeit, S., D. P. Barlow, M. Gautel, T. Gibson, J. Holt, C. L. Hsieh, U. Francke, K. Leonard, J. Wardale, A. Whiting, and et al. 1990. 'A regular pattern of two types of 100-residue motif in the sequence of titin', *Nature*, 345: 273-6.
- Labeit, S., M. Gautel, A. Lakey, and J. Trinick. 1992. 'Towards a molecular understanding of titin', *EMBO J*, 11: 1711-6.
- Laing, N. G., N. F. Clarke, D. E. Dye, K. Liyanage, K. R. Walker, Y. Kobayashi, S. Shimakawa, T. Hagiwara, R. Ouvrier, J. C. Sparrow, I. Nishino, K. N. North, and I. Nonaka. 2004. 'Actin mutations are one cause of congenital fibre type disproportion', *Annals of Neurology*, 56: 689-94.
- Laing, N. G., D. E. Dye, C. Wallgren-Pettersson, G. Richard, N. Monnier, S. Lillis, T. L. Winder, H. Lochmuller, C. Graziano, S. Mitrani-Rosenbaum, D. Twomey, J. C.

- Sparrow, A. H. Beggs, and K. J. Nowak. 2009. 'Mutations and polymorphisms of the skeletal muscle alpha-actin gene (ACTA1)', *Human Mutation*, 30: 1267-77.
- Laing, N. G., S. D. Wilton, P. A. Akkari, S. Dorosz, K. Boundy, C. Kneebone, P. Blumbergs, S. White, H. Watkins, D. R. Love, and et al. 1995. 'A mutation in the alpha tropomyosin gene TPM3 associated with autosomal dominant nemaline myopathy NEM1', *Nat Genet*, 10: 249.
- Lamboley, C. R., R. M. Murphy, M. J. McKenna, and G. D. Lamb. 2013. 'Endogenous and maximal sarcoplasmic reticulum calcium content and calsequestrin expression in type I and type II human skeletal muscle fibres', *J Physiol*, 591: 6053-68.
- Lange, S., F. Xiang, A. Yakovenko, A. Vihola, P. Hackman, E. Rostkova, J. Kristensen, B. Brandmeier, G. Franzen, B. Hedberg, L. G. Gunnarsson, S. M. Hughes, S. Marchand, T. Sejersen, I. Richard, L. Edstrom, E. Ehler, B. Udd, and M. Gautel. 2005. 'The kinase domain of titin controls muscle gene expression and protein turnover', *Science*, 308: 1599-603.
- Laporte, J., L. J. Hu, C. Kretz, J. L. Mandel, P. Kioschis, J. F. Coy, S. M. Klauck, A. Poustka, and N. Dahl. 1996. 'A gene mutated in X-linked myotubular myopathy defines a new putative tyrosine phosphatase family conserved in yeast', *Nat Genet*, 13: 175-82.
- Lawal, T. A., J. J. Todd, and K. G. Meilleur. 2018. 'Ryanodine Receptor 1-Related Myopathies: Diagnostic and Therapeutic Approaches', *Neurotherapeutics*, 15: 885-99.
- Lehtokari, V. L., C. Ceuterick-de Groote, P. de Jonghe, M. Marttila, N. G. Laing, K. Pelin, and C. Wallgren-Pettersson. 2007. 'Cap disease caused by heterozygous deletion of the beta-tropomyosin gene TPM2', *Neuromuscul Disord*, 17: 433-42.
- Lehtokari, V. L., K. Kiiski, S. A. Sandaradura, J. Laporte, P. Repo, J. A. Frey, K. Donner, M. Marttila, C. Saunders, P. G. Barth, J. T. den Dunnen, A. H. Beggs, N. F. Clarke, K. N. North, N. G. Laing, N. B. Romero, T. L. Winder, K. Pelin, and C. Wallgren-Pettersson. 2014. 'Mutation update: the spectra of nebulin variants and associated myopathies', *Human Mutation*, 35: 1418-26.
- Lerche, H., R. Heine, U. Pika, A. L. George, Jr., N. Mitrovic, M. Browatzki, T. Weiss, M. Rivet-Bastide, C. Franke, M. Lomonaco, and et al. 1993. 'Human sodium channel myotonia: slowed channel inactivation due to substitutions for a glycine within the III-IV linker', *J Physiol*, 470: 13-22.
- Lornage, X., E. Malfatti, C. Cheraud, R. Schneider, V. Biancalana, J. M. Cuisset, M. Garibaldi, B. Eymard, M. Fardeau, A. Boland, J. F. Deleuze, J. Thompson, R. Y. Carlier, J. Bohm, N. B. Romero, and J. Laporte. 2017. 'Recessive MYPN mutations cause cap myopathy with occasional nemaline rods', *Annals of Neurology*, 81: 467-73.
- Lornage, X., N. B. Romero, C. A. Grosogeat, E. Malfatti, S. Donkervoort, M. M. Marchetti, S. B. Neuhaus, A. R. Foley, C. Labasse, R. Schneider, R. Y. Carlier, K. R. Chao, L. Medne, J. F. Deleuze, D. Orlikowski, C. G. Bonnemann, V. A. Gupta, M. Fardeau, J. Bohm, and J. Laporte. 2019. 'ACTN2 mutations cause "Multiple structured Core Disease" (MsCD)', *Acta Neuropathol*, 137: 501-19.
- Lornage, X., P. Sabouraud, B. Lannes, D. Gaillard, R. Schneider, J. F. Deleuze, A. Boland, J. Thompson, J. Bohm, V. Biancalana, and J. Laporte. 2018. 'Novel SPEG Mutations in Congenital Myopathy without Centralized Nuclei', *J Neuromuscul Dis*, 5: 257-60.
- Luo, M. C., Q. X. Li, W. F. Yin, W. W. Duan, F. F. Bi, N. Zhang, J. H. Liang, and H. Yang. 2011. '[Congenital myopathy with type 1 fiber predominance in two children]', *Zhongguo Dang Dai Er Ke Za Zhi*, 13: 499-502.
- Lynch, P. J., J. Tong, M. Lehane, A. Mallet, L. Giblin, J. J. Heffron, P. Vaughan, G. Zafra, D. H. MacLennan, and T. V. McCarthy. 1999. 'A mutation in the transmembrane/luminal domain of the ryanodine receptor is associated with abnormal Ca²⁺ release channel function and severe central core disease', *Proc Natl Acad Sci U S A*, 96: 4164-9.

- MacArthur, D. G., J. T. Seto, J. M. Raftery, K. G. Quinlan, G. A. Huttley, J. W. Hook, F. A. Lemckert, A. J. Kee, M. R. Edwards, Y. Berman, E. C. Hardeman, P. W. Gunning, S. Easteal, N. Yang, and K. N. North. 2007. 'Loss of ACTN3 gene function alters mouse muscle metabolism and shows evidence of positive selection in humans', *Nat Genet*, 39: 1261-5.
- Majczenko, K., A. E. Davidson, S. Camelo-Piragua, P. B. Agrawal, R. A. Manfready, X. Li, S. Joshi, J. Xu, W. Peng, A. H. Beggs, J. Z. Li, M. Burmeister, and J. J. Dowling. 2012. 'Dominant mutation of CCDC78 in a unique congenital myopathy with prominent internal nuclei and atypical cores', *American Journal of Human Genetics*, 91: 365-71.
- Malfatti, E., J. Bohm, E. Lacene, M. Beuvin, N. B. Romero, and J. Laporte. 2015. 'A Premature Stop Codon in MYO18B is Associated with Severe Nemaline Myopathy with Cardiomyopathy', *J Neuromuscul Dis*, 2: 219-27.
- Malfatti, E., U. Schaeffer, F. Chapon, Y. Yang, B. Eymard, R. Xu, J. Laporte, and N. B. Romero. 2013. 'Combined cap disease and nemaline myopathy in the same patient caused by an autosomal dominant mutation in the TPM3 gene', *Neuromuscul Disord*, 23: 992-7.
- Margulies, M., M. Egholm, W. E. Altman, S. Attiya, J. S. Bader, L. A. Bemben, J. Berka, M. S. Braverman, Y. J. Chen, Z. Chen, S. B. Dewell, L. Du, J. M. Fierro, X. V. Gomes, B. C. Godwin, W. He, S. Helgesen, C. H. Ho, G. P. Irzyk, S. C. Jando, M. L. Alenquer, T. P. Jarvie, K. B. Jirage, J. B. Kim, J. R. Knight, J. R. Lanza, J. H. Leamon, S. M. Lefkowitz, M. Lei, J. Li, K. L. Lohman, H. Lu, V. B. Makhijani, K. E. McDade, M. P. McKenna, E. W. Myers, E. Nickerson, J. R. Nobile, R. Plant, B. P. Puc, M. T. Ronan, G. T. Roth, G. J. Sarkis, J. F. Simons, J. W. Simpson, M. Srinivasan, K. R. Tartaro, A. Tomasz, K. A. Vogt, G. A. Volkmer, S. H. Wang, Y. Wang, M. P. Weiner, P. Yu, R. F. Begley, and J. M. Rothberg. 2005. 'Genome sequencing in microfabricated high-density picolitre reactors', *Nature*, 437: 376-80.
- Marttila, M., V. L. Lehtokari, S. Marston, T. A. Nyman, C. Barnerias, A. H. Beggs, E. Bertini, O. Ceyhan-Birsoy, P. Cintas, M. Gerard, B. Gilbert-Dussardier, J. S. Hogue, C. Longman, B. Eymard, M. Frydman, P. B. Kang, L. Klinge, H. Kolski, H. Lochmuller, L. Magy, V. Manel, M. Mayer, E. Mercuri, K. N. North, S. Peudenier-Robert, H. Pihko, F. J. Probst, R. Reisin, W. Stewart, A. L. Taratuto, M. de Visser, E. Wilichowski, J. Winer, K. Nowak, N. G. Laing, T. L. Winder, N. Monnier, N. F. Clarke, K. Pelin, M. Gronholm, and C. Wallgren-Pettersson. 2014. 'Mutation update and genotype-phenotype correlations of novel and previously described mutations in TPM2 and TPM3 causing congenital myopathies', *Human Mutation*, 35: 779-90.
- Marttila, M., E. Lemola, W. Wallefeld, M. Memo, K. Donner, N. G. Laing, S. Marston, M. Gronholm, and C. Wallgren-Pettersson. 2012. 'Abnormal actin binding of aberrant beta-tropomyosins is a molecular cause of muscle weakness in TPM2-related nemaline and cap myopathy', *Biochem J*, 442: 231-9.
- Maruoka, N. D., D. F. Steele, B. P. Au, P. Dan, X. Zhang, E. D. Moore, and D. Fedida. 2000. 'alpha-actinin-2 couples to cardiac Kv1.5 channels, regulating current density and channel localization in HEK cells', *FEBS Lett*, 473: 188-94.
- Maruyama, K., and S. Ebashi. 1965. 'Alpha-actinin, a new structural protein from striated muscle. II. Action on actin', *J Biochem*, 58: 13-9.
- Mayans, O., P. F. van der Ven, M. Wilm, A. Mues, P. Young, D. O. Furst, M. Wilmanns, and M. Gautel. 1998. 'Structural basis for activation of the titin kinase domain during myofibrillogenesis', *Nature*, 395: 863-9.
- Meehan, T. F., N. Conte, D. B. West, J. O. Jacobsen, J. Mason, J. Warren, C. K. Chen, I. Tudose, M. Relac, P. Matthews, N. Karp, L. Santos, T. Fiegel, N. Ring, H. Westerberg, S. Greenaway, D. Sneddon, H. Morgan, G. F. Codner, M. E. Stewart, J. Brown, N. Horner,

- Consortium International Mouse Phenotyping, M. Haendel, N. Washington, C. J. Mungall, C. L. Reynolds, J. Gallegos, V. Gailus-Durner, T. Sorg, G. Pavlovic, L. R. Bower, M. Moore, I. Morse, X. Gao, G. P. Tocchini-Valentini, Y. Obata, S. Y. Cho, J. K. Seong, J. Seavitt, A. L. Beaudet, M. E. Dickinson, Y. Herault, W. Wurst, M. H. de Angelis, K. C. K. Lloyd, A. M. Flenniken, L. M. J. Nutter, S. Newbigging, C. McKerlie, M. J. Justice, S. A. Murray, K. L. Svenson, R. E. Braun, J. K. White, A. Bradley, P. Flicek, S. Wells, W. C. Skarnes, D. J. Adams, H. Parkinson, A. M. Mallon, S. D. M. Brown, and D. Smedley. 2017. 'Disease model discovery from 3,328 gene knockouts by The International Mouse Phenotyping Consortium', *Nat Genet*, 49: 1231-38.
- Mercier, S., X. Lornage, E. Malfatti, P. Marcorelles, F. Letournel, C. Boscher, G. Caillaux, A. Magot, J. Bohm, A. Boland, J. F. Deleuze, N. Romero, Y. Pereon, and J. Laporte. 2017. 'Expanding the spectrum of congenital myopathy linked to recessive mutations in SCN4A', *Neurology*, 88: 414-16.
- Merlini, L., P. Sabatelli, M. Antoniel, V. Carinci, F. Niro, G. Monetti, A. Torella, T. Giugliano, C. Faldini, and V. Nigro. 2019. 'Congenital myopathy with hanging big toe due to homozygous myopalladin (MYPN) mutation', *Skelet Muscle*, 9: 14.
- Meyer, T., V. Ruppert, S. Ackermann, A. Richter, A. Perrot, S. R. Sperling, M. G. Posch, B. Maisch, S. Pankuweit, and Failure German Competence Network Heart. 2013. 'Novel mutations in the sarcomeric protein myopalladin in patients with dilated cardiomyopathy', *Eur J Hum Genet*, 21: 294-300.
- Michelucci, A., A. De Marco, F. A. Guarnier, F. Protasi, and S. Boncompagni. 2017. 'Antioxidant Treatment Reduces Formation of Structural Cores and Improves Muscle Function in RYR1(Y522S/WT) Mice', *Oxid Med Cell Longev*, 2017: 6792694.
- Mills, M., N. Yang, R. Weinberger, D. L. Vander Woude, A. H. Beggs, S. Eastal, and K. North. 2001. 'Differential expression of the actin-binding proteins, alpha-actinin-2 and -3, in different species: implications for the evolution of functional redundancy', *Human Molecular Genetics*, 10: 1335-46.
- Miyatake, S., S. Mitsuhashi, Y. K. Hayashi, E. Purevjav, A. Nishikawa, E. Koshimizu, M. Suzuki, K. Yatabe, Y. Tanaka, K. Ogata, S. Kuru, M. Shiina, Y. Tsurusaki, M. Nakashima, T. Mizuguchi, N. Miyake, H. Saitsu, K. Ogata, M. Kawai, J. Towbin, I. Nonaka, I. Nishino, and N. Matsumoto. 2017. 'Biallelic Mutations in MYPN, Encoding Myopalladin, Are Associated with Childhood-Onset, Slowly Progressive Nemaline Myopathy', *American Journal of Human Genetics*, 100: 169-78.
- Moghadaszadeh, B., B. E. Rider, M. W. Lawlor, M. K. Childers, R. W. Grange, K. Gupta, S. S. Boukedes, C. A. Owen, and A. H. Beggs. 2013. 'Selenoprotein N deficiency in mice is associated with abnormal lung development', *FASEB J*, 27: 1585-99.
- Mohapatra, B., S. Jimenez, J. H. Lin, K. R. Bowles, K. J. Coveler, J. G. Marx, M. A. Chrisco, R. T. Murphy, P. R. Lurie, R. J. Schwartz, P. M. Elliott, M. Vatta, W. McKenna, J. A. Towbin, and N. E. Bowles. 2003. 'Mutations in the muscle LIM protein and alpha-actinin-2 genes in dilated cardiomyopathy and endocardial fibroelastosis', *Mol Genet Metab*, 80: 207-15.
- Morgan-Hughes, J. A. 1998. 'Tubular aggregates in skeletal muscle: their functional significance and mechanisms of pathogenesis', *Current Opinion in Neurology*, 11: 439-42.
- Morrison, B. M. 2016. 'Neuromuscular Diseases', *Semin Neurol*, 36: 409-18.
- Motta-Mena, L. B., F. Heyd, and K. W. Lynch. 2010. 'Context-dependent regulatory mechanism of the splicing factor hnRNP L', *Mol Cell*, 37: 223-34.
- Muenzen, K., J. Monroy, and F. R. Finseth. 2019. 'Evolution of the Highly Repetitive PEVK Region of Titin Across Mammals', *G3 (Bethesda)*, 9: 1103-15.

- Nakhro, K., J. M. Park, Y. J. Kim, B. R. Yoon, J. H. Yoo, H. Koo, B. O. Choi, and K. W. Chung. 2013. 'A novel Lys141Thr mutation in small heat shock protein 22 (HSPB8) gene in Charcot-Marie-Tooth disease type 2L', *Neuromuscul Disord*, 23: 656-63.
- Nance, J. R., J. J. Dowling, E. M. Gibbs, and C. G. Bonnemann. 2012. 'Congenital myopathies: an update', *Curr Neurol Neurosci Rep*, 12: 165-74.
- Nicot, A. S., A. Toussaint, V. Tosch, C. Kretz, C. Wallgren-Pettersson, E. Iwarsson, H. Kingston, J. M. Garnier, V. Biancalana, A. Oldfors, J. L. Mandel, and J. Laporte. 2007. 'Mutations in amphiphysin 2 (BIN1) disrupt interaction with dynamin 2 and cause autosomal recessive centronuclear myopathy', *Nat Genet*, 39: 1134-9.
- North, K. N., and A. H. Beggs. 1996. 'Deficiency of a skeletal muscle isoform of alpha-actinin (alpha-actinin-3) in merosin-positive congenital muscular dystrophy', *Neuromuscul Disord*, 6: 229-35.
- North, K. N., C. H. Wang, N. Clarke, H. Jungbluth, M. Vainzof, J. J. Dowling, K. Amburgey, S. Quijano-Roy, A. H. Beggs, C. Sewry, N. G. Laing, C. G. Bonnemann, and Myopathies International Standard of Care Committee for Congenital. 2014. 'Approach to the diagnosis of congenital myopathies', *Neuromuscul Disord*, 24: 97-116.
- North, K. N., N. Yang, D. Wattanasirichaigoon, M. Mills, S. Easteal, and A. H. Beggs. 1999. 'A common nonsense mutation results in alpha-actinin-3 deficiency in the general population', *Nat Genet*, 21: 353-4.
- Nunn, L. M., L. R. Lopes, P. Syrris, C. Murphy, V. Plagnol, E. Firman, C. Dalageorgou, E. Zorio, D. Domingo, V. Murday, I. Findlay, A. Duncan, G. Carr-White, L. Robert, T. Bueser, C. Langman, S. P. Fynn, M. Goddard, A. White, H. Bundgaard, L. Ferrero-Miliani, N. Wheeldon, S. K. Suvarna, A. O'Beirne, M. D. Lowe, W. J. McKenna, P. M. Elliott, and P. D. Lambiase. 2016. 'Diagnostic yield of molecular autopsy in patients with sudden arrhythmic death syndrome using targeted exome sequencing', *Europace*, 18: 888-96.
- O'Grady, G. L., H. A. Best, T. E. Sztal, V. Schartner, M. Sanjuan-Vazquez, S. Donkervoort, O. Abath Neto, R. B. Sutton, B. Ilkovski, N. B. Romero, T. Stojkovic, J. Dastgir, L. B. Waddell, A. Boland, Y. Hu, C. Williams, A. A. Ruparelia, T. Maisonobe, A. J. Peduto, S. W. Reddel, M. Lek, T. Tukiainen, B. B. Cummings, H. Joshi, J. Nectoux, S. Brammah, J. F. Deleuze, V. O. Ing, G. Ramm, D. Ardicli, K. J. Nowak, B. Talim, H. Topaloglu, N. G. Laing, K. N. North, D. G. MacArthur, S. Friant, N. F. Clarke, R. J. Bryson-Richardson, C. G. Bonnemann, J. Laporte, and S. T. Cooper. 2016. 'Variants in the Oxidoreductase PYROXD1 Cause Early-Onset Myopathy with Internalized Nuclei and Myofibrillar Disorganization', *American Journal of Human Genetics*, 99: 1086-105.
- Odorizzi, G., M. Babst, and S. D. Emr. 2000. 'Phosphoinositide signaling and the regulation of membrane trafficking in yeast', *Trends Biochem Sci*, 25: 229-35.
- Oh, S. J., and M. J. Danon. 1983. 'Nonprogressive congenital neuromuscular disease with uniform type 1 fiber', *Arch Neurol*, 40: 147-50.
- Ohlsson, M., S. Quijano-Roy, N. Darin, G. Brochier, E. Lacene, D. Avila-Smirnow, M. Fardeau, A. Oldfors, and H. Tajsharghi. 2008. 'New morphologic and genetic findings in cap disease associated with beta-tropomyosin (TPM2) mutations', *Neurology*, 71: 1896-901.
- Olive, M., R. A. Kley, and L. G. Goldfarb. 2013. 'Myofibrillar myopathies: new developments', *Current Opinion in Neurology*, 26: 527-35.
- Olson, T. M., A. E. Alekseev, X. K. Liu, S. Park, L. V. Zingman, M. Bienengraeber, S. Sattiraju, J. D. Ballew, A. Jahangir, and A. Terzic. 2006. 'Kv1.5 channelopathy due to KCNA5 loss-of-function mutation causes human atrial fibrillation', *Human Molecular Genetics*, 15: 2185-91.

- Pajusalu, S., I. Talvik, K. Noormets, T. Talvik, H. Poder, K. Joost, S. Puusepp, A. Piirsoo, W. Stenzel, H. H. Goebel, T. Nikopensius, T. Annilo, M. Noukas, A. Metspalu, K. Ounap, and T. Reimand. 2016. 'De novo exonic mutation in MYH7 gene leading to exon skipping in a patient with early onset muscular weakness and fiber-type disproportion', *Neuromuscul Disord*, 26: 236-9.
- Pant, M., N. C. Bal, and M. Periasamy. 2016. 'Sarcolipin: A Key Thermogenic and Metabolic Regulator in Skeletal Muscle', *Trends Endocrinol Metab*, 27: 881-92.
- Pelin, K., P. Hilpela, K. Donner, C. Sewry, P. A. Akkari, S. D. Wilton, D. Wattanasirichaigoon, M. L. Bang, T. Centner, F. Hanefeld, S. Odent, M. Fardeau, J. A. Urtizberea, F. Muntoni, V. Dubowitz, A. H. Beggs, N. G. Laing, S. Labeit, A. de la Chapelle, and C. Wallgren-Pettersson. 1999. 'Mutations in the nebulin gene associated with autosomal recessive nemaline myopathy', *Proc Natl Acad Sci U S A*, 96: 2305-10.
- Periasamy, M., S. K. Maurya, S. K. Sahoo, S. Singh, S. K. Sahoo, F. C. G. Reis, and N. C. Bal. 2017. 'Role of SERCA Pump in Muscle Thermogenesis and Metabolism', *Compr Physiol*, 7: 879-90.
- Pfeffer, G., and P. F. Chinnery. 2013. 'Diagnosis and treatment of mitochondrial myopathies', *Ann Med*, 45: 4-16.
- Phadke, R. 2019. 'Myopathology of Congenital Myopathies: Bridging the Old and the New', *Seminars in Pediatric Neurology*, 29: 55-70.
- Pinto, M. M., S. Monges, E. Malfatti, F. Lubieniecki, X. Lornage, L. Alias, C. Labasse, A. Madelaine, M. Fardeau, J. Laporte, E. F. Tizzano, and N. B. Romero. 2018. 'Sarcomeric disorganization and nemaline bodies in muscle biopsies of patients with EXOSC3-related type 1 pontocerebellar hypoplasia', *Muscle & Nerve*.
- Piteau, S. J., J. P. Rossiter, R. G. Smith, and J. J. MacKenzie. 2014. 'Congenital myopathy with cap-like structures and nemaline rods: case report and literature review', *Pediatr Neurol*, 51: 192-7.
- Pounraja, V. K., G. Jayakar, M. Jensen, N. Kelkar, and S. Girirajan. 2019. 'A machine-learning approach for accurate detection of copy number variants from exome sequencing', *Genome Res*, 29: 1134-43.
- Protasi, F. 2002. 'Structural interaction between RYRs and DHPRs in calcium release units of cardiac and skeletal muscle cells', *Front Biosci*, 7: d650-8.
- Ptacek, L. J., R. Tawil, R. C. Griggs, A. G. Engel, R. B. Layzer, H. Kwiecinski, P. G. McManis, L. Santiago, M. Moore, G. Fouad, and et al. 1994. 'Dihydropyridine receptor mutations cause hypokalemic periodic paralysis', *Cell*, 77: 863-8.
- Purevjav, E., T. Arimura, S. Augustin, A. C. Huby, K. Takagi, S. Nunoda, D. L. Kearney, M. D. Taylor, F. Terasaki, J. M. Bos, S. R. Ommen, H. Shibata, M. Takahashi, M. Itoh-Satoh, W. J. McKenna, R. T. Murphy, S. Labeit, Y. Yamanaka, N. Machida, J. E. Park, P. M. Alexander, R. G. Weintraub, Y. Kitaura, M. J. Ackerman, A. Kimura, and J. A. Towbin. 2012. 'Molecular basis for clinical heterogeneity in inherited cardiomyopathies due to myopalladin mutations', *Human Molecular Genetics*, 21: 2039-53.
- Qualls, A. E., S. Donkervoort, J. C. Herkert, M. D'Gama A, D. Bharucha-Goebel, J. Collins, K. R. Chao, A. R. Foley, M. H. Schoots, J. D. H. Jongbloed, C. G. Bonnemann, and P. B. Agrawal. 2019. 'Novel SPEG mutations in congenital myopathies: Genotype-phenotype correlations', *Muscle & Nerve*, 59: 357-62.
- Ravenscroft, G., S. Miyatake, V. L. Lehtokari, E. J. Todd, P. Vornanen, K. S. Yau, Y. K. Hayashi, N. Miyake, Y. Tsurusaki, H. Doi, H. Saitsu, H. Osaka, S. Yamashita, T. Ohya, Y. Sakamoto, E. Koshimizu, S. Imamura, M. Yamashita, K. Ogata, M. Shiina, R. J. Bryson-Richardson, R. Vaz, O. Ceyhan, C. A. Brownstein, L. C. Swanson, S. Monnot, N. B. Romero, H. Amthor, N. Kresoje, P. Sivadorai, C. Kiraly-Borri, G. Haliloglu, B. Talim, D. Orhan, G. Kale, A. K. Charles, V. A. Fabian, M. R. Davis, M. Lammens, C.

- A. Sewry, A. Manzur, F. Muntoni, N. F. Clarke, K. N. North, E. Bertini, Y. Nevo, E. Willichowski, I. E. Silberg, H. Topaloglu, A. H. Beggs, R. J. Allcock, I. Nishino, C. Wallgren-Pettersson, N. Matsumoto, and N. G. Laing. 2013. 'Mutations in KLHL40 are a frequent cause of severe autosomal-recessive nemaline myopathy', *American Journal of Human Genetics*, 93: 6-18.
- Ribeiro Ede, A., Jr., N. Pinotsis, A. Ghisleni, A. Salmazo, P. V. Konarev, J. Kostan, B. Sjoblom, C. Schreiner, A. A. Polyansky, E. A. Gkougkoulia, M. R. Holt, F. L. Aachmann, B. Zagrovic, E. Bordignon, K. F. Pirker, D. I. Svergun, M. Gautel, and K. Djinovic-Carugo. 2014. 'The structure and regulation of human muscle alpha-actinin', *Cell*, 159: 1447-60.
- Romero, N. B., and N. F. Clarke. 2013. 'Congenital myopathies', *Handb Clin Neurol*, 113: 1321-36.
- Rossi, D., B. Vezzani, L. Galli, C. Paolini, L. Toniolo, E. Pierantozzi, S. Spinuzzi, V. Barone, E. Pegoraro, L. Bello, G. Cenacchi, G. Vattemi, G. Tomelleri, G. Ricci, G. Siciliano, F. Protasi, C. Reggiani, and V. Sorrentino. 2014. 'A mutation in the CASQ1 gene causes a vacuolar myopathy with accumulation of sarcoplasmic reticulum protein aggregates', *Human Mutation*, 35: 1163-70.
- Ryan, M. M., C. Schnell, C. D. Strickland, L. K. Shield, G. Morgan, S. T. Iannaccone, N. G. Laing, A. H. Beggs, and K. N. North. 2001. 'Nemaline myopathy: a clinical study of 143 cases', *Annals of Neurology*, 50: 312-20.
- Sambuughin, N., K. S. Yau, M. Olive, R. M. Duff, M. Bayarsaikhan, S. Lu, L. Gonzalez-Mera, P. Sivadorai, K. J. Nowak, G. Ravenscroft, F. L. Mastaglia, K. N. North, B. Ilkovski, H. Kremer, M. Lammens, B. G. van Engelen, V. Fabian, P. Lamont, M. R. Davis, N. G. Laing, and L. G. Goldfarb. 2010. 'Dominant mutations in KBTBD13, a member of the BTB/Kelch family, cause nemaline myopathy with cores', *American Journal of Human Genetics*, 87: 842-7.
- Savarese, M., P. H. Jonson, S. Huovinen, L. Paulin, P. Auvinen, B. Udd, and P. Hackman. 2018. 'The complexity of titin splicing pattern in human adult skeletal muscles', *Skelet Muscle*, 8: 11.
- Savarese, M., L. Maggi, A. Vihola, P. H. Jonson, G. Tasca, L. Ruggiero, L. Bello, F. Magri, T. Giugliano, A. Torella, A. Evila, G. Di Fruscio, O. Vanakker, S. Gibertini, L. Vercelli, A. Ruggieri, C. Antozzi, H. Luque, S. Janssens, M. B. Pasanisi, C. Fiorillo, M. Raimondi, M. Ergoli, L. Politano, C. Bruno, A. Rubegni, M. Pane, F. M. Santorelli, C. Minetti, C. Angelini, J. De Bleecker, M. Moggio, T. Mongini, G. P. Comi, L. Santoro, E. Mercuri, E. Pegoraro, M. Mora, P. Hackman, B. Udd, and V. Nigro. 2018. 'Interpreting Genetic Variants in Titin in Patients With Muscle Disorders', *JAMA Neurol*, 75: 557-65.
- Savarese, M., J. Palmio, J. J. Poza, J. Weinberg, M. Olive, A. M. Cobo, A. Vihola, P. H. Jonson, J. Sarparanta, F. Garcia-Bragado, J. A. Urtizbera, P. Hackman, and B. Udd. 2019. 'Actininopathy: A new muscular dystrophy caused by ACTN2 dominant mutations', *Annals of Neurology*, 85: 899-906.
- Schartner, V., N. B. Romero, S. Donkervoort, S. Treves, P. Munot, T. M. Pierson, I. Dabaj, E. Malfatti, I. T. Zaharieva, F. Zorzato, O. Abath Neto, G. Brochier, X. Lornage, B. Eymard, A. L. Taratuto, J. Bohm, H. Gonorazky, L. Ramos-Platt, L. Feng, R. Phadke, D. X. Bharucha-Goebel, C. J. Sumner, M. T. Bui, E. Lacene, M. Beuvin, C. Labasse, N. Dondaine, R. Schneider, J. Thompson, A. Boland, J. F. Deleuze, E. Matthews, A. N. Pakleza, C. A. Sewry, V. Biancalana, S. Quijano-Roy, F. Muntoni, M. Fardeau, C. G. Bonnemann, and J. Laporte. 2017. 'Dihydropyridine receptor (DHPR, CACNA1S) congenital myopathy', *Acta Neuropathol*, 133: 517-33.
- Schiaffino, S., and C. Reggiani. 2011. 'Fiber types in mammalian skeletal muscles', *Physiol Rev*, 91: 1447-531.

- Schwabova, J., D. S. Brozkova, B. Petrak, M. Mojzisova, K. Pavlickova, J. Haberlova, L. Mrazkova, P. Hedvicakova, L. Hornofova, M. Kaluzova, F. Fencl, M. Krutova, J. Zamecnik, and P. Seeman. 2013. 'Homozygous EXOSC3 mutation c.92G-->C, p.G31A is a founder mutation causing severe pontocerebellar hypoplasia type 1 among the Czech Roma', *J Neurogenet*, 27: 163-9.
- Seppala, R., V. P. Lehto, and W. A. Gahl. 1999. 'Mutations in the human UDP-N-acetylglucosamine 2-epimerase gene define the disease sialuria and the allosteric site of the enzyme', *American Journal of Human Genetics*, 64: 1563-9.
- Seto, J. T., M. Lek, K. G. Quinlan, P. J. Houweling, X. F. Zheng, F. Garton, D. G. MacArthur, J. M. Raftery, S. M. Garvey, M. A. Hauser, N. Yang, S. I. Head, and K. N. North. 2011. 'Deficiency of alpha-actinin-3 is associated with increased susceptibility to contraction-induced damage and skeletal muscle remodeling', *Human Molecular Genetics*, 20: 2914-27.
- Shiraishi, Y., A. Fujimoto, M. Furuta, H. Tanaka, K. Chiba, K. A. Borojevich, T. Abe, Y. Kawakami, M. Ueno, K. Gotoh, S. Ariizumi, T. Shibuya, K. Nakano, A. Sasaki, K. Maejima, R. Kitada, S. Hayami, Y. Shigekawa, S. Marubashi, T. Yamada, M. Kubo, O. Ishikawa, H. Aikata, K. Arihiro, H. Ohdan, M. Yamamoto, H. Yamaue, K. Chayama, T. Tsunoda, S. Miyano, and H. Nakagawa. 2014. 'Integrated analysis of whole genome and transcriptome sequencing reveals diverse transcriptomic aberrations driven by somatic genomic changes in liver cancers', *Plos One*, 9: e114263.
- Sjoblom, B., A. Salmazo, and K. Djinovic-Carugo. 2008. 'Alpha-actinin structure and regulation', *Cell Mol Life Sci*, 65: 2688-701.
- Sorimachi, H., A. Freiburg, B. Kolmerer, S. Ishiura, G. Stier, C. C. Gregorio, D. Labeit, W. A. Linke, K. Suzuki, and S. Labeit. 1997. 'Tissue-specific expression and alpha-actinin binding properties of the Z-disc titin: implications for the nature of vertebrate Z-discs', *J Mol Biol*, 270: 688-95.
- Statland, J. M., B. Fontaine, M. G. Hanna, N. E. Johnson, J. T. Kissel, V. A. Sansone, P. B. Shieh, R. N. Tawil, J. Trivedi, S. C. Cannon, and R. C. Griggs. 2018. 'Review of the Diagnosis and Treatment of Periodic Paralysis', *Muscle & Nerve*, 57: 522-30.
- Straver, R., M. M. Weiss, Q. Waisfisz, E. A. Sistermans, and M. J. T. Reinders. 2017. 'WISExome: a within-sample comparison approach to detect copy number variations in whole exome sequencing data', *Eur J Hum Genet*, 25: 1354-63.
- Stuart, C. A., W. L. Stone, M. E. Howell, M. F. Brannon, H. K. Hall, A. L. Gibson, and M. H. Stone. 2016. 'Myosin content of individual human muscle fibers isolated by laser capture microdissection', *Am J Physiol Cell Physiol*, 310: C381-9.
- Sun, Y., H. Chen, Y. Lu, J. Duo, L. Lei, Y. OuYang, Y. Hao, Y. Da, and X. M. Shen. 2019. 'Limb girdle muscular dystrophy D3 HNRNPDL related in a Chinese family with distal muscle weakness caused by a mutation in the prion-like domain', *Journal of Neurology*, 266: 498-506.
- Tajsharghi, H., M. Ohlsson, C. Lindberg, and A. Oldfors. 2007. 'Congenital myopathy with nemaline rods and cap structures caused by a mutation in the beta-tropomyosin gene (TPM2)', *Arch Neurol*, 64: 1334-8.
- Takada, F., D. L. Vander Woude, H. Q. Tong, T. G. Thompson, S. C. Watkins, L. M. Kunkel, and A. H. Beggs. 2001. 'Myozenin: an alpha-actinin- and gamma-filamin-binding protein of skeletal muscle Z lines', *Proc Natl Acad Sci U S A*, 98: 1595-600.
- Tang, B. S., G. H. Zhao, W. Luo, K. Xia, F. Cai, Q. Pan, R. X. Zhang, F. F. Zhang, X. M. Liu, B. Chen, C. Zhang, L. Shen, H. Jiang, Z. G. Long, and H. P. Dai. 2005. 'Small heat-shock protein 22 mutated in autosomal dominant Charcot-Marie-Tooth disease type 2L', *Hum Genet*, 116: 222-4.

- Tanner, S. M., K. H. Orstavik, M. Kristiansen, D. Lev, T. Lerman-Sagie, M. Sadeh, and S. Liechti-Gallati. 1999. 'Skewed X-inactivation in a manifesting carrier of X-linked myotubular myopathy and in her non-manifesting carrier mother', *Hum Genet*, 104: 249-53.
- Tasca, G., F. Fattori, E. Ricci, M. Monforte, V. Rizzo, E. Mercuri, E. Bertini, and G. Silvestri. 2013. 'Somatic mosaicism in TPM2-related myopathy with nemaline rods and cap structures', *Acta Neuropathol*, 125: 169-71.
- Tasfaout, H., S. Buono, S. Guo, C. Kretz, N. Messaddeq, S. Booten, S. Greenlee, B. P. Monia, B. S. Cowling, and J. Laporte. 2017. 'Antisense oligonucleotide-mediated Dnm2 knockdown prevents and reverts myotubular myopathy in mice', *Nat Commun*, 8: 15661.
- Taylor, G. S., T. Maehama, and J. E. Dixon. 2000. 'Myotubularin, a protein tyrosine phosphatase mutated in myotubular myopathy, dephosphorylates the lipid second messenger, phosphatidylinositol 3-phosphate', *Proc Natl Acad Sci U S A*, 97: 8910-5.
- Theis, J. L., J. M. Bos, V. B. Bartleson, M. L. Will, J. Binder, M. Vatta, J. A. Towbin, B. J. Gersh, S. R. Ommen, and M. J. Ackerman. 2006. 'Echocardiographic-determined septal morphology in Z-disc hypertrophic cardiomyopathy', *Biochem Biophys Res Commun*, 351: 896-902.
- Toussaint, A., B. S. Cowling, K. Hnia, M. Mohr, A. Oldfors, Y. Schwab, U. Yis, T. Maisonobe, T. Stojkovic, C. Wallgren-Pettersson, V. Laugel, A. Echaniz-Laguna, J. L. Mandel, I. Nishino, and J. Laporte. 2011. 'Defects in amphiphysin 2 (BIN1) and triads in several forms of centronuclear myopathies', *Acta Neuropathol*, 121: 253-66.
- Trimmer, J. S., S. S. Cooperman, S. A. Tomiko, J. Y. Zhou, S. M. Crean, M. B. Boyle, R. G. Kallen, Z. H. Sheng, R. L. Barchi, F. J. Sigworth, and et al. 1989. 'Primary structure and functional expression of a mammalian skeletal muscle sodium channel', *Neuron*, 3: 33-49.
- Tsujino, A., C. Maertens, K. Ohno, X. M. Shen, T. Fukuda, C. M. Harper, S. C. Cannon, and A. G. Engel. 2003. 'Myasthenic syndrome caused by mutation of the SCN4A sodium channel', *Proc Natl Acad Sci U S A*, 100: 7377-82.
- Tubridy, N., B. Fontaine, and B. Eymard. 2001. 'Congenital myopathies and congenital muscular dystrophies', *Current Opinion in Neurology*, 14: 575-82.
- Valipakka, S., M. Savarese, M. Johari, L. Sagath, M. Arumilli, K. Kiiski, A. Saenz, A. L. de Munain, A. M. Cobo, K. Pelin, B. Udd, and P. Hackman. 2017. 'Copy number variation analysis increases the diagnostic yield in muscle diseases', *Neurol Genet*, 3: e204.
- Varki, A. 1997. 'Sialic acids as ligands in recognition phenomena', *FASEB J*, 11: 248-55.
- Vasli, N., E. Harris, J. Karamchandani, E. Bareke, J. Majewski, N. B. Romero, T. Stojkovic, R. Barresi, H. Tasfaout, R. Charlton, E. Malfatti, J. Bohm, C. Marini-Bettolo, K. Choquet, M. J. Dicaire, Y. H. Shao, A. Topf, E. O'Ferrall, B. Eymard, V. Straub, G. Blanco, H. Lochmuller, B. Brais, J. Laporte, and M. Tetreault. 2017. 'Recessive mutations in the kinase ZAK cause a congenital myopathy with fibre type disproportion', *Brain*, 140: 37-48.
- Vergne, I., and V. Deretic. 2010. 'The role of PI3P phosphatases in the regulation of autophagy', *FEBS Lett*, 584: 1313-8.
- Vieira, N. M., M. S. Naslavsky, L. Licinio, F. Kok, D. Schlesinger, M. Vainzof, N. Sanchez, J. P. Kitajima, L. Gal, N. Cavacana, P. R. Serafini, S. Chuartzman, C. Vasquez, A. Mimbacas, V. Nigro, R. C. Pavanello, M. Schuldiner, L. M. Kunkel, and M. Zatz. 2014. 'A defect in the RNA-processing protein HNRPDL causes limb-girdle muscular dystrophy 1G (LGMD1G)', *Human Molecular Genetics*, 23: 4103-10.

- Voermans, N. C., M. Snoeck, and H. Jungbluth. 2016. 'RYR1-related rhabdomyolysis: A common but probably underdiagnosed manifestation of skeletal muscle ryanodine receptor dysfunction', *Rev Neurol (Paris)*, 172: 546-58.
- Vollestad, N. K., I. Tabata, and J. I. Medbo. 1992. 'Glycogen breakdown in different human muscle fibre types during exhaustive exercise of short duration', *Acta Physiol Scand*, 144: 135-41.
- Wallgren-Pettersson, C., A. H. Beggs, and N. G. Laing. 1998. '51st ENMC International Workshop: Nemaline Myopathy. 13-15 June 1997, Naarden, The Netherlands', *Neuromuscul Disord*, 8: 53-6.
- Wallgren-Pettersson, C., C. A. Sewry, K. J. Nowak, and N. G. Laing. 2011. 'Nemaline myopathies', *Seminars in Pediatric Neurology*, 18: 230-8.
- Wang, H., C. Castiglioni, A. Kacar Bayram, F. Fattori, S. Pekuz, D. Araneda, H. Per, R. Erazo, H. Gumus, S. Zorludemir, K. Becker, X. Ortega, J. A. Bevilacqua, E. Bertini, and S. Cirak. 2017. 'Insights from genotype-phenotype correlations by novel SPEG mutations causing centronuclear myopathy', *Neuromuscul Disord*, 27: 836-42.
- Wang, H., A. Schanzer, B. Kampschulte, H. S. Daimaguler, T. Logeswaran, H. Schlierbach, J. Petzinger, H. Ehrhardt, A. Hahn, and S. Cirak. 2018. 'A novel SPEG mutation causes non-compaction cardiomyopathy and neuropathy in a floppy infant with centronuclear myopathy', *Acta Neuropathol Commun*, 6: 83.
- Willig, T. N., J. Paulus, J. Lacau Saint Guily, C. Beon, and J. Navarro. 1994. 'Swallowing problems in neuromuscular disorders', *Arch Phys Med Rehabil*, 75: 1175-81.
- Wilmshurst, J. M., S. Lillis, H. Zhou, K. Pillay, H. Henderson, W. Kress, C. R. Muller, A. Ndong, V. Cloke, T. Cullup, E. Bertini, C. Boennemann, V. Straub, R. Quinlivan, J. J. Dowling, S. Al-Sarraj, S. Treves, S. Abbs, A. Y. Manzur, C. A. Sewry, F. Muntoni, and H. Jungbluth. 2010. 'RYR1 mutations are a common cause of congenital myopathies with central nuclei', *Annals of Neurology*, 68: 717-26.
- Witherspoon, J. W., and K. G. Meilleur. 2016. 'Review of RyR1 pathway and associated pathomechanisms', *Acta Neuropathol Commun*, 4: 121.
- Wright, C. F., D. R. FitzPatrick, and H. V. Firth. 2018. 'Paediatric genomics: diagnosing rare disease in children', *Nat Rev Genet*, 19: 325.
- Xia, H., S. T. Winokur, W. L. Kuo, M. R. Altherr, and D. S. Brecht. 1997. 'Actinin-associated LIM protein: identification of a domain interaction between PDZ and spectrin-like repeat motifs', *J Cell Biol*, 139: 507-15.
- Yang, Y., J. Li, X. Lin, Y. Yang, K. Hong, L. Wang, J. Liu, L. Li, D. Yan, D. Liang, J. Xiao, H. Jin, J. Wu, Y. Zhang, and Y. H. Chen. 2009. 'Novel KCNA5 loss-of-function mutations responsible for atrial fibrillation', *Journal of Human Genetics*, 54: 277-83.
- Zaharieva, I. T., M. G. Thor, E. C. Oates, C. van Karnebeek, G. Hendson, E. Blom, N. Witting, M. Rasmussen, M. T. Gabbett, G. Ravenscroft, M. Sframeli, K. Suetterlin, A. Sarkozy, L. D'Argenzio, L. Hartley, E. Matthews, M. Pitt, J. Vissing, M. Ballegaard, C. Krarup, A. Slordahl, H. Halvorsen, X. C. Ye, L. H. Zhang, N. Lokken, U. Werlauff, M. Abdelsayed, M. R. Davis, L. Feng, R. Phadke, C. A. Sewry, J. E. Morgan, N. G. Laing, H. Vallance, P. Ruben, M. G. Hanna, S. Lewis, E. J. Kamsteeg, R. Mannikko, and F. Muntoni. 2016. 'Loss-of-function mutations in SCN4A cause severe foetal hypokinesia or 'classical' congenital myopathy', *Brain*, 139: 674-91.
- Zarrei, M., J. R. MacDonald, D. Merico, and S. W. Scherer. 2015. 'A copy number variation map of the human genome', *Nat Rev Genet*, 16: 172-83.
- Zhao, Y., Y. Feng, Y. M. Zhang, X. X. Ding, Y. Z. Song, A. M. Zhang, L. Liu, H. Zhang, J. H. Ding, and X. S. Xia. 2015. 'Targeted next-generation sequencing of candidate genes reveals novel mutations in patients with dilated cardiomyopathy', *Int J Mol Med*, 36: 1479-86.

- Zhou, H., M. Brockington, H. Jungbluth, D. Monk, P. Stanier, C. A. Sewry, G. E. Moore, and F. Muntoni. 2006. 'Epigenetic allele silencing unveils recessive RYR1 mutations in core myopathies', *American Journal of Human Genetics*, 79: 859-68.
- Zhou, Q., P. Ruiz-Lozano, M. E. Martone, and J. Chen. 1999. 'Cypher, a striated muscle-restricted PDZ and LIM domain-containing protein, binds to alpha-actinin-2 and protein kinase C', *Journal of Biological Chemistry*, 274: 19807-13.

Xavière LORNAGE

Université

de Strasbourg



École Doctorale
des Sciences de la Vie
et de la Santé
STRASBOURG

Identification and functional characterization of novel genes implicated in congenital myopathies

Résumé

Les myopathies congénitales sont des maladies génétiques sévères caractérisées par une faiblesse musculaire très invalidante de début infantile. Afin d'identifier de nouvelles causes génétiques, nous avons séquencé les exomes de patients myopathes qui ne disposaient pas de diagnostic moléculaire et leur analyse a mis en évidence deux nouveaux gènes de myopathie. *MYPN* et *ACTN2* codent pour deux protéines structurales du sarcomères appelées myopalladine et alpha-actinine-2. Afin d'étudier l'impact des mutations sur la fonction de la protéine et sur la physiologie du muscle, des analyses moléculaires et fonctionnelles ont été réalisées en modèles cellulaires et animaux. Les mutations dans *MYPN* induisent une perte de la protéine, et dans les muscles de souris, l'alpha-actinine-2 mutée conduit à une faiblesse musculaire et génère des défauts structuraux similaires à ceux retrouvés chez les patients. Ces résultats ont un impact direct sur la prise en charge des patients et sur le conseil génétique, sur la compréhension de voies de signalisation fondamentales pour la physiologie musculaire, et mettent en évidence de nouvelles cibles thérapeutiques.

Mots-clés : myopathies congénitales, muscle, génétique humaine, *ACTN2*, *MYPN*.

Résumé en anglais

Congenital myopathies are severe genetic muscle diseases characterized by a disabling early-onset muscle weakness. In order to identify new genetic causes, we sequenced the exomes of molecularly undiagnosed congenital myopathy patients, and their analysis highlighted two novel myopathy genes. *MYPN* and *ACTN2* encode two structural sarcomeric proteins called myopalladin and alpha-actinin-2. To evaluate the impact of the mutations on the protein function and on muscle physiology, molecular and functional analyses were performed in cell and animal models. The *MYPN* mutations resulted in loss of myopalladin expression, and in mouse muscles, mutated alpha-actinin-2 led to muscle weakness and structural defects similar to those observed in the patient muscles. These results have a direct impact on the disease management of the patients and on genetic counselling, provide a better understanding of the signaling pathways required for muscle physiology, and highlight novel therapeutic targets.

Keywords: congenital myopathies, muscle, human genetics, *ACTN2*, *MYPN*